



HAL
open science

Stimuler la réponse immunitaire anti-sarcome en ciblant la physiologie et le métabolisme mitochondrial

Richard Miallot

► **To cite this version:**

Richard Miallot. Stimuler la réponse immunitaire anti-sarcome en ciblant la physiologie et le métabolisme mitochondrial. Immunologie. Aix Marseille Université (AMU), Marseille, FRA., 2023. Français. NNT: . tel-04575026

HAL Id: tel-04575026

<https://theses.hal.science/tel-04575026>

Submitted on 14 May 2024

HAL is a multi-disciplinary open access archive for the deposit and dissemination of scientific research documents, whether they are published or not. The documents may come from teaching and research institutions in France or abroad, or from public or private research centers.

L'archive ouverte pluridisciplinaire **HAL**, est destinée au dépôt et à la diffusion de documents scientifiques de niveau recherche, publiés ou non, émanant des établissements d'enseignement et de recherche français ou étrangers, des laboratoires publics ou privés.



Distributed under a Creative Commons Attribution - NonCommercial - NoDerivatives 4.0 International License

THÈSE DE DOCTORAT

Soutenue à Aix-Marseille Université
le 30 mars 2023 par

Richard MIALLOT

Stimuler la réponse immunitaire anti-sarcome en ciblant la physiologie et le métabolisme mitochondrial

Discipline

Biologie Santé

Spécialité

Immunologie

École doctorale

ED62 Sciences de la Vie et de la Santé

Laboratoire/Partenaires de recherche

C2VN

IS2M

CLB



Composition du jury

Laetitia LINARES

Rapporteure

IRCM

Alice CARRIER

Présidente de jury

CRCM

Sophie UGOLINI

Examinatrice

CIML

Jean-Ehrland RICCI

Rapporteur

C3M

Emmanuel CHAUTARD

Examineur

Centre Jean Perrin

Philippe NAQUET

Directeur de thèse

CIML

Affidavit

Je soussigné, Richard MIALLOT, déclare par la présente que le travail présenté dans ce manuscrit est mon propre travail, réalisé sous la direction scientifique du professeur Philippe NAQUET, dans le respect des principes d'honnêteté, d'intégrité et de responsabilité inhérents à la mission de recherche. Les travaux de recherche et la rédaction de ce manuscrit ont été réalisés dans le respect à la fois de la charte nationale de déontologie des métiers de la recherche et de la charte d'Aix-Marseille Université relative à la lutte contre le plagiat.

Ce travail n'a pas été précédemment soumis en France ou à l'étranger dans une version identique ou similaire à un organisme examinateur.

Fait à Marseille, le 1er janvier 2023

Signature :



Cette œuvre est mise à disposition selon les termes de la [Licence Creative Commons Attribution - Pas d'Utilisation Commerciale - Pas de Modification 4.0 International](https://creativecommons.org/licenses/by-nc-nd/4.0/).

Liste de publications et participations aux conférences

1) Liste des publications réalisées dans le cadre du projet de thèse :

1. Metabolic landscapes of sarcoma

Publiée dans Journal of Hematology & Oncology le 22/07/2021

<https://doi.org/10.1186/s13045-021-01125-y>

2. An OMA1 redox site controls mitochondrial homeostasis, sarcoma growth and immunogenicity

Publiée dans Life Science Alliance le 05/04/2023

<https://doi.org/10.26508/lsa.202201767>

3. The coenzyme A precursor pantethine enhances anti-tumor immunity in sarcoma

En révision dans Life Science Alliance

4. The vitamin B5 / coenzyme A axis: a target for immunomodulation?

En révision à European Journal of Immunology

2) Participations aux conférences et écoles d'été au cours de la période de thèse :

1. Institut Cancer Immunologie – Marseille, France - Poster
2. Karolinska Institute Retreat – Stockholm, Suède - Poster
3. EMBO Workshop – Sitges, Espagne - Poster
4. yEFIS Symposium – Berlin, Allemagne – Flash Talk + poster

Résumé en français

La mitochondrie est au cœur des réorientations métaboliques permettant aux cellules cancéreuses de subvenir à leurs besoins énergétiques et métaboliques croissants. Les cellules à croissance rapide privilégient la glycolyse aérobie à la respiration mitochondriale et surexploitent d'autres ressources énergétiques comme la glutamine ou le lactate. Le stress cellulaire et mitochondrial, l'hypoxie vont croître au sein des tumeurs, impactant la fonction du système immunitaire infiltrant. Nous avons étudié comment la modulation de la physiologie des mitochondries au sein des tumeurs peut en augmenter l'immunoréactivité.

Nous avons généré une cellule de sarcome murin portant une mutation d'un site senseur du stress oxydant de la protéase mitochondriale OMA1. Cette mutation abolit le clivage de la protéine fusio-gène OPA1 en situation de stress et perturbe le contrôle de qualité assuré par l'équilibre entre fusion et fission. Les cellules mutées ne forment pas de tumeurs *in vivo* et relarguent de l'ADN mitochondrial qui contribue à amplifier la réponse immunitaire anti-tumorale.

La compétition pour l'accès à l'oxygène, au glucose, aux acides aminés et à des métabolites essentiels contribue dans un contexte de stimulation chronique à l'épuisement lymphocytaire. La disponibilité en vitamine B5, précurseuse du coenzyme A, est régulée par l'activité pantéthénase Vanin1. Dans des banques de données de patients, l'expression de VNN1 dans les sarcomes est associée à un mauvais pronostic et une perte de signatures immunitaires. Afin de soutenir le métabolisme lymphocytaire, nous avons étudié l'impact de l'administration de pantéthine, substrat de l'activité Vnn1, sur la croissance de tumeurs. Ce traitement freine la croissance tumorale et amplifie le développement d'une réponse immunitaire de type 1 aboutissant à la génération d'effecteurs cytolytiques fonctionnels anti-tumoraux. En association avec une immunothérapie, la pantéthine améliore le pronostic de ces tumeurs.

Abstract

The mitochondria are at the heart of the metabolic shifts that allow cancer cells to meet their increasing energy and metabolic needs. Rapidly growing cells favor aerobic glycolysis over mitochondrial respiration and overexploit other energy resources such as glutamine or lactate. Cellular and mitochondrial stress and hypoxia will increase within tumors, impacting the function of the infiltrating immune system. We studied how modulation of mitochondrial physiology within tumors can increase their immunoreactivity.

We generated a murine sarcoma cell with a mutation in an oxidative stress sensor site of the mitochondrial protease OMA1. This mutation abolishes the cleavage of the fusogenic protein OPA1 under stress and disrupts the quality control provided by the balance between fusion and fission. Mutated cells do not form tumors *in vivo* and release mitochondrial DNA that contributes to amplify the anti-tumor immune response.

Competition for access to oxygen, glucose, amino acids and essential metabolites contributes to lymphocyte depletion in the context of chronic stimulation. The availability of vitamin B5, a precursor of coenzyme A, is regulated by Vanin1 pantetheinase activity. In patient databases, VNN1 expression in sarcoma is associated with poor prognosis and loss of immune signatures. To support lymphocyte metabolism, we studied the impact of administration of pantethine, a substrate of Vnn1 activity, on tumor growth. This treatment inhibits tumor growth and enhances the development of a type 1 immune response leading to the generation of functional anti-tumor cytolytic effectors. In combination with immunotherapy, pantethine improves the prognosis of these tumors.

À ma marraine et à toutes les personnes parties trop tôt

Remerciements

Ce n'est pas sans émotions que je remercie toutes les personnes qui ont partagé mon chemin durant toutes ces années qui m'ont conduit au doctorat aujourd'hui.

Je remercie tout d'abord ma famille. Papa, Maman, Michel merci d'avoir cru en moi et m'avoir soutenu à chaque étape de mon parcours, de notre petit village d'Auvergne, Malicorne, à Clermont-Ferrand, Lyon, Toulouse et Marseille. De m'avoir soutenu malgré les kilomètres qui nous séparaient, mon caractère, mes erreurs et le fait que vous ne compreniez pas un quart de ce que je faisais. Merci aussi d'avoir relu entièrement ce manuscrit. Merci Parrain pour ta bienveillance et l'intérêt que tu portes à mon parcours.

Merci à mes amies, mes confidentes de longues dates. Merci Alice pour ta générosité, tu es le modèle même que la persévérance et le travail peut nous emmener très loin dans la vie, d'un simple village à une thèse vétérinaire à Maisons Alfort. Merci Marion pour ces années de master, seuls contre tous, ces heures passées au téléphone, au maintien de ma motivation, aux conseils nutritionnels et sportifs, aux conseils de vie et pour m'apprendre à prendre du temps pour moi et du recul sur les choses.

Merci à ma petite famille de cœur, la Team Rocket. Il est impossible de faire tenir en quelques mots tous les remerciements que je vous dois, merci d'avoir été des piliers, des soutiens moraux pour moi malgré les événements. Merci pour tous les dépannages, les gardiennages de chat mais également l'ambiance stimulatrice et bienveillante qui m'a poussé à dépasser mes ambitions. Merci pour vos conseils scientifiques, votre expertise, quelques réactifs aussi. Merci particulièrement à Anaïs, qui m'a montré le potentiel d'un vrai capricorne de Janvier, pour ta détermination sans limite et pour ton humilité. Merci Clara pour ses moments de compassion et d'authenticité à mon égard, sans artifice. Merci à Hakim et Marie, pour leur générosité, les vendredis soir, toutes les activités que nous avons partagées et votre disponibilité. Merci Julie pour nos escapades sportives et nos sorties sur un coup de tête mais aussi pour ton regard sur la vie, afin d'apprendre à lâcher prise et improviser et enfin sur tes conseils pour la rédaction de la discussion de ma thèse. Merci Ugo pour ton accent, le divertissement et me montrer comment ajouter des numérotations de pages à un PDF. Merci Marion pour ta maturité et ta patience. Merci à Alexia, mon premier contact avec le CIML et aux discussions au détour des paillasses.

Merci aux enseignants qui m'ont forgé en tant que scientifique égayant ma curiosité et aux équipes de recherche qui m'ont accueilli le temps d'un stage. Merci Toufic Renno, Isabelle Coste et les mots puissants que vous m'aviez partagés, « Whatever it takes » car la science est une passion avant un métier. Merci à l'équipe de Thierry Levade, à Céline et à Anne pour les challenges que vous m'avez proposés et pour la réflexion sur mon orientation professionnelle.

Merci à Philippe NAQUET, de m'avoir fait confiance pour cette thèse. Merci de m'avoir accepté tel que j'étais, avec mon caractère et mon énergie. Merci de m'avoir transmis tant de connaissances et de sagesse, de conseils professionnels et personnels. Merci de toujours avoir pris du temps lorsque j'en avais besoin et d'avoir été à mon écoute. Merci de m'avoir laissé la liberté dont j'avais besoin dans mon travail et ne jamais m'avoir imposé quoique ce soit en étant toujours dans la discussion. Je suis honoré d'avoir été le dernier thésard de cette équipe.

Merci Virginie pour ta patience et ta générosité, merci de m'avoir fait grandir tant techniquement que professionnellement, de m'avoir transmis tes connaissances et d'avoir relevé tant de défis et d'expériences nouvelles avec moi. Merci de m'avoir compris, malgré mes « têtes d'anchois » et de t'être montrée toujours disponible. Merci de m'avoir également ouvert les yeux sur l'importance et la part de chaque chose.

Merci Frank pour ton regard extérieur sur mon travail, tes précieux conseils et ta générosité.

Merci à Romain, pour ta patience à m'expliquer le monde de la bioinfo, à satisfaire tous mes caprices en termes de graphisme, et d'avoir testé toutes les possibilités en ne te limitant pas seulement à ce que tu savais faire mais en allant toujours plus loin. Merci à ton énergie et à ta sympathie.

Merci à Pierre Milpied, mon parrain de thèse. Merci de m'avoir prouvé que l'on peut être chercheur et venir à vélo, chef d'équipe et père et même développer une plateforme au sein d'un institut. Merci d'avoir passé du temps avec moi sur mes projets et pour les conseils que tu m'as apportés.

Je tiens à remercier tout particulièrement le Pr BERTUCCI et le Pr BLAY pour le soutien apporter à mon projet et d'avoir accepté de contribuer à mes travaux en l'enrichissant de votre expertise clinique et de renforcer la relevance de mes travaux en y ajoutant des analyses chez l'Homme. Merci à Aurélie DUTOUR pour ta disponibilité, ta gentillesse et ton expertise sur les ostéosarcomes.

Merci aux comités de la Ligue contre le Cancer du Puy-de-Dôme, du Rhône, de la Garonne et des Bouches du Rhône, pour votre accueil chaleureux, pour toutes les expériences incroyables que vous m'avez fait vivre, les symposiums, les activités avec les patients, les stands de prévention, l'invitation à l'anniversaire des 100 ans à Paris et au soutien sur le Projet Casques de Réalité Virtuelle Appliquées au Cancer. Merci de m'avoir fait confiance et d'avoir pu acquérir de nombreuses compétences en dehors de mon parcours académique tout en renforçant mon projet professionnel.

Merci à toutes les collaborateurs et collaboratrices dont je me suis entouré. Merci encore à Anaïs, Juliane, Pierre, Noushine, Aurélie D., Jean-Charles, Laetitia S., Thi-Tien, Christophe, Yann, Angelika, Paul, Carole S., Gerlind et Vincent V.

Merci pour vos conseils : Sophie U., Vincent F., Guillaume, Rafaël Arguello, Sandrine H., Julie REBEJAC, Réjane, les Julien, Rémy, Mathieu, Magali G., Léa, Lionel C. Merci à Aymeric pour le petit code qui m'a bien servi pour à l'animalerie.

Table des matières

AFFIDAVIT	2
LISTE DE PUBLICATIONS ET PARTICIPATIONS AUX CONFERENCES	3
RESUME EN FRANÇAIS	5
ABSTRACT	6
REMERCIEMENTS	8
TABLE DES MATIERES	11
TABLE DES FIGURES	13
LISTE DES ABBREVIATIONS	14
INTRODUCTION	21
I) L'ONCOMETABOLISME	24
A) La cancérogénèse	24
1) Définition des <i>cancer hallmarks</i>	24
2) Oncogènes et gènes suppresseurs de tumeurs	26
3) Régulation de la chromatine	30
4) États métaboliques des sarcomes	31
	32
B) Reprogrammation métabolique tumorale	56
1) Hétérogénéité de l'utilisation du glucose	56
2) Les voies anaboliques dérivées de la glycolyse	58
3) Pourquoi l'Effet Warburg ?	60
4) Le lactate : un métabolite central du métabolisme tumoral	62
5) Hypoxie et vascularisation	66
II) LA MITOCHONDRIE	68
A) Hub énergétique	70
1) Mode catabolique et phosphorylation oxydative	70
2) La chaîne de transport d'électrons	72
3) Anaplérose et cataplérose	74
B) Adaptation métabolique et perception du microenvironnement tumoral	76
1) Altérations des mitochondries	76
2) ROS mitochondriaux	78
3) La fusion et fission mitochondriale comme réponse au stress	80
III) DECLENCHEMENT ET LIMITES D'UNE REponse ANTITUMORALE	81
A) Établissement de la réponse immunitaire et immunoédition	81
1) Développement tumoral et présentation antigénique	81
2) Antigénicité tumorale	84
3) Activation des cellules T et élimination de la tumeur	85

4) Équilibre et échappement	86
B) Immunométabolisme	88
1) Le métabolisme des cellules T après activation et maturation	88
2) L'épuisement des cellules T	90
3) Modifications épigénétiques lors de la différenciation et l'épuisement des cellules T	92
C) Polarisation et reprogrammation métabolique	93
D) Signaux mitochondriaux impactant l'immunogénicité tumorale	94
1) Les <i>Danger-associated molecular patterns</i> (DAMPs)	94
2) Morts immunogéniques	96
IV) LIMITES ET CONTRAINTES DE LA REPONSE ANTITUMORALE	97
A) Challenges thérapeutiques	97
1) Accessibilité et infiltration immunitaire	97
2) Le microenvironnement tumoral	97
3) Tumeurs froides – tumeurs chaudes	100
4) Microbiote	102
5) Les points de contrôle de l'immunité, immunothérapies et métabolisme	103
B) Cibler la mitochondrie	105
1) L'implication d'OMA1 et d'OPA1 dans la progression tumorale	105
2) An OMA1 redox site controls mitochondrial homeostasis, sarcoma growth and immunogenicity.	106
2) Restaurer les facteurs métaboliques limitants	132
3) Restaurer une réponse antitumorale par une reprogrammation métabolique dépendante de la voie de signalisation Vanin1.	132
4) Propriétés immunomodulatrices de la vitamine B5	133
5) The vitamin B5 / coenzyme A axis: a target for immunomodulation?	133
6) The coenzyme A precursor pantethine enhances anti-tumor immunity in sarcoma	152
VI) DISCUSSION ET PERSPECTIVES	210
A) La voie de signalisation du coenzyme A : perspective thérapeutique	211
1) Reprogrammation métabolique des cellules cancéreuses	211
2) L'expression de VNN1 a une valeur pronostique	213
3) Coenzyme A, B5 et immunoréactivité	216
4) Perspectives et limites du traitement à la pantéthine	219
B) Dynamiques mitochondriales et thérapies ciblées	220
1) OMA1 et OPA1 marqueurs pronostiques ?	220
2) Cibler les fonctions d'OPA1 et OMA1 dans un contexte tumoral	220
3) OMA1/OPA1 et l'immunité	221
4) Perspectives et limites	223
5) Conclusion	223
VII) BIBLIOGRAPHIE	224

Table des Figures

Figure 1 : Les « cancer hallmarks » en 2022 d'après Hanahan et Weinberg	23
Figure 2 : Voies de signalisation avec une mutation d'un oncogène ou d'un gène suppresseur de tumeur dans les différents types de cancer.	25
Figure 3 : Principales voies de signalisation dans les cellules cancéreuses.....	27
Figure 4 : régulations épigénétiques des histones et du génome.....	29
Figure 5 : Isoformes des enzymes glycolytiques	55
Figure 6 : Glycolyse et voies dérivées	57
Figure 7 : L'effet Warburg.....	59
Figure 8 : Implication du NADP et de l'acétyl-CoA dans le métabolisme tumoral	61
Figure 9 : La consommation de lactate dans le microenvironnement tumoral	64
Figure 10 : Voie de signalisation HIF1a	65
Figure 11 : Structure interne de la mitochondrie	67
Figure 12 : le Cycle de Krebs	69
Figure 13 : La chaîne de transport des électrons	71
Figure 14 : Anaplérose et cataplérose mitochondriales	73
Figure 15 : Production de ROS mitochondriaux à partir de la chaîne de transport d'électrons.....	77
Figure 16 : Fusion et fission mitochondriale	79
Figure 17 : Présentation antigénique et mécanistique présentation antigénique.....	81
Figure 18 : Antigénicité tumorale	83
Figure 19 : Immunoédition et mort immunogénique	85
Figure 20 : Métabolisme et fonction de l'infiltrat immunitaire	87
Figure 21 : Reprogrammation épigénétique dans les cellules T	91
Figure 22 : L'épigénétique et le métabolisme sur l'épuisement des cellules T	91
Figure 23 : Corrélation entre la charge mutationnelle et le score immunitaire.....	99
Figure 24 : Caractéristique de l'impact du microbiote sur le cancer.....	101
Figure 25 : Les points de contrôle de l'immunité ou immune checkpoints	103
Figure 26 : Reprogrammation métabolique par la cystéamine et la vitamine B5.....	210
Figure 27 : Expression de Vanin1 en contexte pathologique	212
Figure 28 : Rôle de la vitamine B5 et du coenzyme A dans l'immunométabolisme	216
Figure 29 : Bilan de l'effet thérapeutique dépendant de la voie de signalisation Vanin1	218

LISTE DES ABBREVIATIONS

A

ACAT	Acyl-CoA cholestérol acyltransférase
ADP	Adénosine diphosphate
AhR	Aryl hydrocarbon receptor
AKT	Protein kinase b
ALAS	Aminolevulinic acid synthase
ALDO	Aldo-keto reductase
ALT	Alanine aminotransférase
AMPK	AMP-activated protein kinase
ARG	Arginase
ASNS	Asparagine synthetase
AST	Aspartate aminotransférase
ATP	Adénosine triphosphate

B

BATF	Basic leucine zipper transcription factor
BCAA	Branched-chain amino acid
BCAAT	Branched-chain amino acid aminotransferase
BET	Bromodomain and extra-terminal motif

C

CAR-T	Chimeric Antigenic Receptor - T
CBP	Cyclic adenosine monophosphate response element binding protein
CCCP	Carbonylcyanure m-chlorophénylhydrazone
CD	Cluster de différenciation
CDC	Conventional dendritic cell
CEA	Carcinoembryonic antigen (Figure 17) or cysteamine
cGAS	Cyclic GMP-AMP synthase
CHD	Chromodomain helicase dna-binding
CIC	Citrate isocitrate
CMH	Complex majeur d'histocompatibilité
CoA(SH)	Coenzyme A
COASY	Coenzyme A synthase
CoQ	Coenzyme Q
CPA	Cellules présentatrices de l'antigène
CPG	Cytosine-phosphate-guanine
CRC	Chromatin remodeling complex
CS	Citrate synthase
CTLA4	Cytotoxic t-lymphocyte-associated protein 4
CXCL	Chemokine (c-x-c motif) ligand
CYT C	Cytochrome c

D

D-2HG	D-2-hydroxyglutarate
DAMP	Danger-associated molecular pattern
DDLPS	Dedifferentiated liposarcomas
DELE1	Dap3 binding cell death enhancer 1
DN3	Double negative 3 (stage of T cell maturation)
DNMT	DNA methyltransferases
DRP1	Dynamin-related protein 1
DSS	Dextran sulfate sodium
DUB	Deubiquitinating enzyme

E

EBV	Epstein–barr virus
ENO	Oxyde nitrique synthase
ERK	Extracellular signal-regulated kinases

F

FA	Fatty acids
FAD	Flavin adenine dinucleotide
FAH	Fumarylacetoacetase
FAS-L	Fas cell surface
FH	Fumarate hydratase
FOXO1	Forkhead box O1
FUS1	Fusion protein1

G

GAD	Glutamate décarboxylase
GAPDH	Glycéraldéhyde-3-phosphate déshydrogénase
GDP	Guanosine diphosphate
gGCs	γ -glutamylcysteine
GNAT	G protein subunit alpha transducin 1
GOT	Glutamate oxaloacétique transaminase
GPI	Glucose-6-phosphate isomerase
GPx	Glutathione peroxidase
GRZB	Granzyme B
GTP	Guanosine triphosphate

H

HAT	Histone acétyltransférase
HBP	Heparin binding protein
HDAC	Histone désacétylase
HER2	Human epidermal growth factor receptor-2
HERV	Human endogenous retrovirus

HIF	Hypoxia inducible factor
HK	Hexokinase
HMGB1	High mobility group box 1
HMGN1	Non-histone chromosomal protein
HPV	Human papillomavirus
HRE	Hypoxia-response element
HRX	Human tri-thorax gene
HSP	Heat shock protein
HSV1	Virus Herpes simplex de type 1
HTERT	Human Telomerase reverse transcriptase

I

IBD	Inflammatory Bowel disease
IDH	Isocitrate déshydrogénase
IDO	Indoleamine 2,3-dioxygenase
I$\kappa$$\kappa$$\beta$	Inhibitor Of Nuclear Factor Kappa B Kinase Subunit Beta
IL	Interleukine
IRF3	Interferon Regulatory Factor 3
ISWI	Imitation switch
ITAM	Immunoreceptor tyrosine-based activation motif

K

KMT	Histone lysine methyltransferases
------------	-----------------------------------

L

L2-HG	L-2-hydroxyglutarate
LAG3	Lymphocyte activation gene-3
LAGE	L-antigen 1
LDH	Lactate déshydrogénase
LKB1	Liver kinase b1
LMS	Leiomyosarcoma
LSD1	Lysine-specific demethylase 1

M

MAGE	Melanoma associated antigen
MAVS	Mitochondrial Antiviral Signaling Protein
MCA	Methylcholanthrene
MCT	Monocarboxylate transporters
MDH	Malate déshydrogénase
MDSC	Myeloid-derived
ME	Malic enzyme
MFN	Mitofusin

MICOS	Mitochondrial contact site and cristae organizing system
MMUT	Methylmalonyl-coa mutase
MT	Mitochondrial
MTOR	Mechanistic target of rapamycin
MYST	Moz, ybf2/sas3, sas2, tip60
MΦ	Macrophage

N

NAD	Nicotinamide adénine dinucléotide
NADP	Nicotinamide adénine dinucléotide phosphate
NEMO	NF-κB Essential Modulator
NFAT	Nuclear factor of activated t-cells
NK	Natural killer
NLRP3	Nod-like receptor family, pyrin domain containing 3
NOX	Nadph oxidase

O

OAA	Oxaloacétate
OGDH	2-oxoglutarate dehydrogenase
OGDO	2-oxoglutarate-dependent dioxygenases
OGFOD1	2-oxoglutarate and iron-dependent oxygenase domain containing 1
OMA1	Overlapping with the m-aaa protease
OPA1	Optic atrophy 1
OVA	Ovalbumine
OXPHOS	Oxidative phosphorylation

P

PANK	Pantothenate kinase
P3H/P4H	Prolyl 3-hydroxylation/ prolyl 4-hydroxylation
PC	Pyruvate carboxylase
PCC	Propionyl-coa carboxylase
PCK1	Phosphoenolpyruvate carboxykinase 1
PD1	Programmed cell death protein 1
PDGF	Platelet-derived growth factor
PEPCK	Phosphoénolpyruvate carboxykinase
PFK	Phosphofructokinase
PFN	Perforine
PGAM	Phosphoglycérate mutase
PGC1α	Peroxisome proliferator-activated receptor gamma coactivator 1 α
PGE	Prostaglandin e
PGK	Phosphoglycérate kinase

PHB	Poly-(beta)-hydroxybutyrate
PHD	Prolyl hydroxylase domain
PI3K	Phosphoinositide 3-kinase
PK	Pyruvate kinase
PKC	Protein Kinase C
PKM	Pyruvate kinase musculaire
PPAR	Peroxisome proliferator-activated receptor
PPC	Phosphoenolpyruvate carboxylase
PPP	Voie des pentoses phosphates
PRMT	Protein arginine n-methyltransferase
PUMA	p53 upregulated modulator of apoptosis

R

RAS	Rat sarcoma virus
RNMT	Mrna-capping methyltransferase
ROS	Reactive oxygen species

S

SAM	S-adenosylmethionine
SCFa	Short-chain fatty acids
SDH	Succinate dehydrogenase
SIRT	Sirtuines
SMVT	Sodium multivitamin transporter
SOD	Superoxide dismutase
SREBP	Sterol regulatory element-binding proteins
STING	Stimulator of interferon genes CGAMP Interactor 1
STLMS	Soft tissue leiomyosarcoma
SWI/SNF	Switch/sucrose non-fermentable

T

TCF1	T-cell factor
TCR	T-cell receptor
TDG	Thymine adn glycosylase
TEP	Tomographie à émission de positon
TET	Ten-eleven translocation (tet) methylcytosine dioxygenases
TFAMS	Mitochondrial transcription factor A
TG2	Transglutaminase tissulaire
TGF	Tumor growth factor
TILS	Tumor infiltrating lymphocytes
TIM3	T-cell immunoglobulin and mucin containing protein-3
TIS	Tumor immune signature
TLR	Toll-lie receptor
TNF	Tumor necrosis factor
TOX	Thymocyte selection-associated high mobility group box

TPI Triose-phosphate isomérase
TRAIL Tnf-related apoptosis-inducing ligand

U

UBC9 Ubiquitin conjugating enzyme
ULMS Uterine leiomyosarcoma
ULP Ubl-specific protease
UPR Unfolded protein response
UPS Undifferentiated pleomorphic sarcoma

V

VEGF Vascular endothelial growth factor
VHL Von hippel–lindau
VNN1 Vanin1

W

WHO World Health Organisation

Y

YMEL1 Yme1 like 1 ATPase

Introduction

Il y a environ 76 millions d'années, un dinosaure, le *Centrosaurus apertus*, développait un ostéosarcome dans les vastes plaines du Canada (1). Des plus grands mammifères aux invertébrés, traversant les ères glaciaires et les plus grands moments de l'Histoire, le cancer est un problème de société touchant sans distinction, les femmes, les hommes, les enfants et dont plus de 18,1 millions de personnes sont atteintes (WHO). Guérir le cancer c'est alors le combat de plusieurs millions de personnes à travers le monde et ce depuis plusieurs milliers d'années. Guérir le cancer, c'est en connaître les causes et les prévenir, comprendre son développement et son évolution pour développer des stratégies innovantes aux résultats prometteurs. Des civilisations ancestrales jusqu'à la fin du XIX^{ème} siècle, la chirurgie restera l'unique moyen de traiter les cancers, plus précise de nos jours, elle reste encore largement pratiquée. Pourtant, récidives, métastases et tumeurs liquides nécessiteront l'usage de traitements complémentaires. C'est à l'aube du XIX^{ème} siècle, qu'Emil Grubbe joint à la chirurgie l'utilisation des rayons X sur le cancer du sein. Quelques années plus tard, Marie Curie découvre le radium et c'est alors Pierre Curie qui en propose l'usage sur des tumeurs cutanées malignes, la curiethérapie était née. En Allemagne, Otto Warburg note que les cellules cancéreuses consomment fortement le glucose, produisent une quantité importante de lactate et ce même en présence d'oxygène, décrit de nos jours comme l'effet Warburg. Alors que le monde est plongé dans la sombre période des guerres mondiales, c'est d'une arme chimique redoutable, le gaz moutarde, que naîtront les premières chimiothérapies. Cibler la prolifération accrue de la cellule cancéreuse et freiner sa forte consommation de glucose sont alors les objectifs de nombreux traitements dont l'efficacité est certes présente mais dont les effets secondaires sont importants, comme par exemple la doxorubicine, le cisplatine ou le cyclophosphamide. L'essor des connaissances scientifiques permettra en période d'après-guerre le développement des premières thérapies ciblées qui visent à corriger les altérations moléculaires et protéiques présentes dans les cellules cancéreuses. L'imagerie médicale s'améliore également avec la tomographie à émission de positons, la TEP, utilisant notamment le glucose comme marqueur fluorescent consommé par les tumeurs. À la fin du XX^{ème} siècle, les chercheurs.euses s'accordent à étudier une tumeur comme un ensemble complexe d'acteurs cellulaires et moléculaires à caractère évolutif. Les nouvelles thérapies ne ciblent plus exclusivement la cellule cancéreuse, mais un ensemble d'acteurs. Le XXI^{ème} siècle est marqué par une révolution thérapeutique, le succès des immunothérapies, comme dans le mélanome. Cette thérapie vise les mécanismes de résistance développés par la cellule cancéreuse contre le système immunitaire. Ainsi, le système immunitaire, protection naturelle de l'hôte contre les agressions, se révèle être un acteur clef dans l'élimination des cellules cancéreuses. Cependant, l'efficacité des immunothérapies n'est pas universelle avec une hétérogénéité de réponses selon les types de cancer. En effet, bien que le système immunitaire joue un rôle prépondérant dans l'élimination des cellules cancéreuses, il nécessite qu'un ensemble de signaux soit réuni pour satisfaire ses fonctions. D'une part, la quantité et la nature de cet infiltrat immunitaire sont importantes, car la présence du système immunitaire, n'est pas toujours associée à un meilleur pronostic en termes de survie.

Ainsi, le meilleur moyen de lutter contre le cancer, après la prévention, est de combiner des thérapies diminuant l'agressivité des cellules cancéreuses tout en préservant et en augmentant la réponse antitumorale. D'autre part, il faut tenir compte du métabolisme tumoral.

Le métabolisme recouvre l'ensemble des réactions biochimiques qui transforment des métabolites pour satisfaire les fonctions biologiques d'une cellule, qu'elle soit cancéreuse ou immunitaire. C'est un domaine de recherche centenaire qui présente des perspectives thérapeutiques intéressantes. D'un côté, les altérations des cellules cancéreuses conduisent à une modification de l'utilisation des ressources, à une réorientation des voies métaboliques pour satisfaire la gestion du stress cellulaire et compenser les facteurs limitants comme l'oxygène, le glucose ou encore les cofacteurs des réactions métaboliques. Développer des thérapies pour contrer les adaptations d'une cellule cancéreuse à son environnement peut alors nuire à sa prolifération. De l'autre, le système immunitaire, bien que pourvu de la capacité à percevoir les altérations tissulaires et y répondre, entre en compétition métabolique directe avec les cellules cancéreuses. Ainsi, la modulation du métabolisme tumoral a le potentiel d'agir sur de multiples paramètres pouvant conduire à plusieurs bénéfices thérapeutiques. Le challenge de la modulation du métabolisme est d'agir sur la cellule cancéreuse tout en maintenant une réponse immunitaire durable et effective.

Nous allons, dans une première partie, détailler et comprendre les caractéristiques fonctionnelles et métaboliques d'une cellule cancéreuse. Nous allons ensuite comprendre comment une organelle telle que la mitochondrie joue un rôle crucial dans de nombreux processus cellulaires et comment elle est devenue une cible de choix dans les thérapies actuelles. Nous parlerons de l'immunométabolisme, son rôle dans l'activation, la maturation et l'exhaustion du système immunitaire. Enfin, nous verrons comment les altérations métaboliques sur la cellule cancéreuse peuvent polariser le système immunitaire et comment cibler l'interaction du système immunitaire et des cellules cancéreuses peut être une stratégie thérapeutique prometteuse.

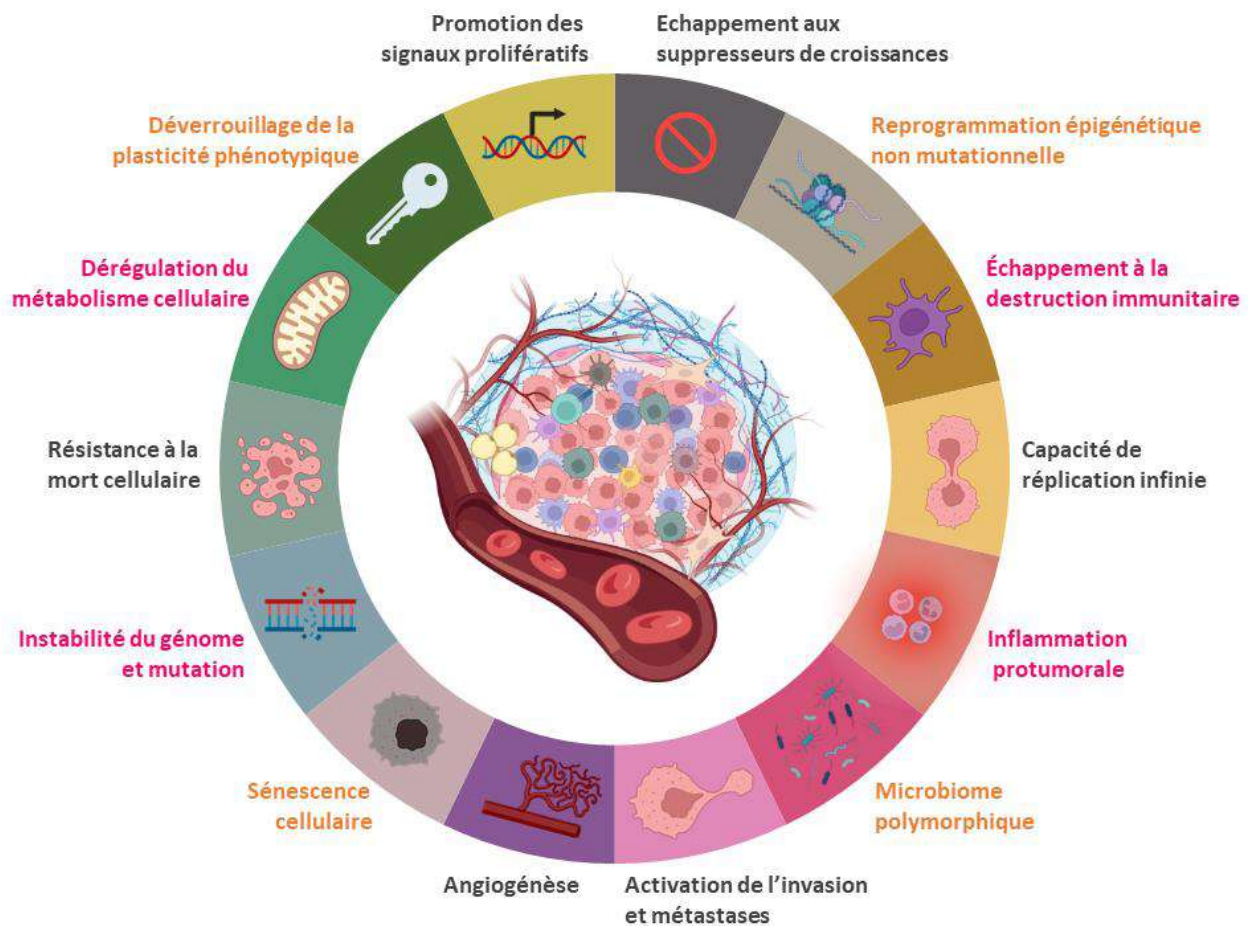


Figure 1 : Les « cancer hallmarks » en 2022 d’après Hanahan et Weinberg

Ce schéma explicatif met en perspective les 14 « cancer hallmarks » définis par Hanahan et Weinberg en 2022. Il représente l’ensemble des caractéristiques communes aux tumeurs dépendantes des cellules cancéreuses mais aussi au microenvironnement tumoral et au microbiome. Figure adaptée de la référence (2).

I) L'oncométabolisme

A) La cancérogénèse

1) Définition des *cancer hallmarks*

Le cancer regroupe un ensemble de pathologies qui se caractérise par la prolifération accrue et non contrôlée de cellules du soi. Médecine et recherche se sont efforcées de les catégoriser et d'en identifier les caractéristiques intrinsèques, appelées en anglais les cancer hallmarks. Bien que les quatre grandes catégories de cancers : les carcinomes, les mélanomes, les lymphomes/leucémies et les sarcomes restent largement utilisées, en définir les sous types reste plus complexe : deux sarcomes sont aussi différents qu'un mélanome ne l'est d'un carcinome. Doit-on les catégoriser selon le type de tissu dans lequel ils se développent, l'origine des altérations qui ont conduites à leur développement, leur infiltration par le système immunitaire, . . . Les dernières années de recherches ont permis la définition des cancer hallmarks, définissant des caractéristiques communes à tous les cancers. Leur nombre a évolué au cours du temps, reflétant la manière dont la communauté scientifique appréhende et étudie le cancer. Il y a 22 ans, Hanahan et Weinberg définissaient les caractéristiques acquises des cellules cancéreuses (indiquées par une police d'écriture grise sur la **Figure 1**) : l'échappement à l'apoptose, l'auto-suffisance vis-à-vis des facteurs de croissance, l'insensibilité aux signaux inhibiteurs de la croissance, la capacité d'invasion et de métastase, le potentiel de réplication infini et la capacité à créer de nouveaux vaisseaux, appelée néoangiogénèse (3). Il y a 11 ans, les cancer hallmarks passaient de 6 à 10. En effet, s'y ajoutent plusieurs caractéristiques favorables à la progression tumorale : l'échappement de la destruction par le système immunitaire, la dérégulation de l'énergétique cellulaire, l'instabilité du génome ainsi que l'inflammation pro-tumorale (indiquées par une police d'écriture rose sur la **Figure 1**). L'évolution notable de cette nouvelle version permet d'intégrer la notion que des paramètres externes à la cellule cancéreuse peuvent définir une tumeur comme le métabolisme et le microenvironnement tumoral (4). Enfin, l'année dernière, c'est à 14 que se portent les cancers hallmarks avec l'ajout de la modulation de la plasticité cellulaire, de la reprogrammation épigénétique non mutationnelle, du microbiome polymorphe et de la sénescence cellulaire (2) (indiquées par une police d'écriture orange sur la **Figure 1**). Ainsi, caractériser le cancer c'est avoir une vue intégrée et multidisciplinaire en étudiant l'ensemble des acteurs cellulaires et moléculaires.

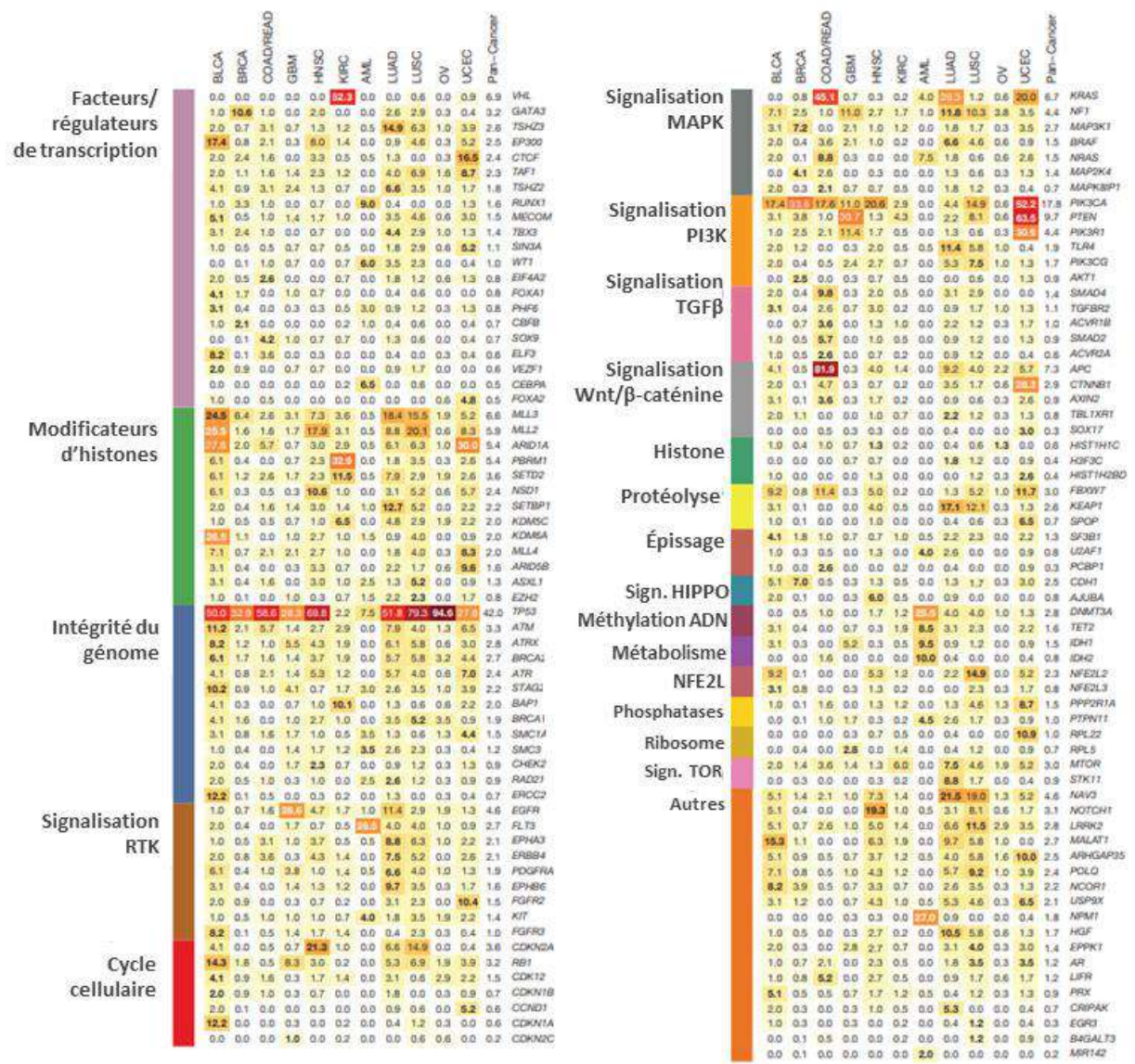


Figure 2 : Voies de signalisation avec une mutation d'un oncogène ou d'un gène suppresseur de tumeur dans les différents types de cancer.

Les 127 gènes significativement mutés dans 12 types de cancers sont regroupés ici en 20 processus cellulaires. Le pourcentage des échantillons mutés dans chaque type de tumeur et dans tous les cancers confondus est indiqué, le pourcentage le plus élevé parmi les 12 types de cancers en gras. Figure de la référence (5). Abréviation de la figure: Breast adenocarcinoma (BRCA), lung adenocarcinoma (LUAD), lung squamous cell carcinoma (LUSC), uterine corpus endometrial carcinoma (UCEC), glioblastoma multiforme (GBM), head and neck squamous cell carcinoma (HNSC), colon and rectal carcinoma (COAD, READ), bladder urothelial carcinoma (BLCA), kidney renal clear cell carcinoma (KIRC), ovarian serous carcinoma (OV) and acute myeloid leukaemia (LAML; conventionally called AML).

2) Oncogènes et gènes suppresseurs de tumeurs

Comprendre l'origine génétique, protéique ou moléculaire des altérations de la cellule cancéreuse a été essentiel pour explorer de nouvelles opportunités thérapeutiques. Rapidement, il a été mis en évidence que certains gènes régulateurs du cycle cellulaire, des voies de signalisation de croissance et de la prolifération mais aussi des gènes associés au développement embryonnaire sont préférentiellement altérés dans les cancers. Les altérations génétiques à l'origine des cancers se produisent dans deux grandes familles de gènes : les oncogènes et les gènes suppresseurs de tumeurs.

Les oncogènes sont des gènes dont la mutation seule peut être suffisante pour initier ou favoriser le processus de cancérogénèse. Il s'agit le plus souvent de proto-oncogènes, c'est-à-dire des gènes qui ont une action régulatrice positive sur le cycle cellulaire, les voies de signalisation associées aux facteurs de croissance (RTK, MAPK, PI3K, TGF β , Wnt/ β -caténine, HIPPO). Leur surexpression et/ou leur mutation conduisent à un développement malin (Figure 2).

Les gènes suppresseurs de tumeurs peuvent prévenir ou diminuer la cancérogénèse. Parmi les oncogènes et gènes suppresseurs de tumeurs les plus souvent mutés, tous types de cancers confondus, nous retrouvons : *TP53*, *CDKN2A*, *ARID1A*, *KRAS*, *PTEN*, *TERT*, *RB1*, *BRAF*, *MYC* (6). Ils peuvent être impliqués dans des voies de signalisation telles que l'intégrité du génome, la modification des histones ou l'épissage (**Figure 2**).

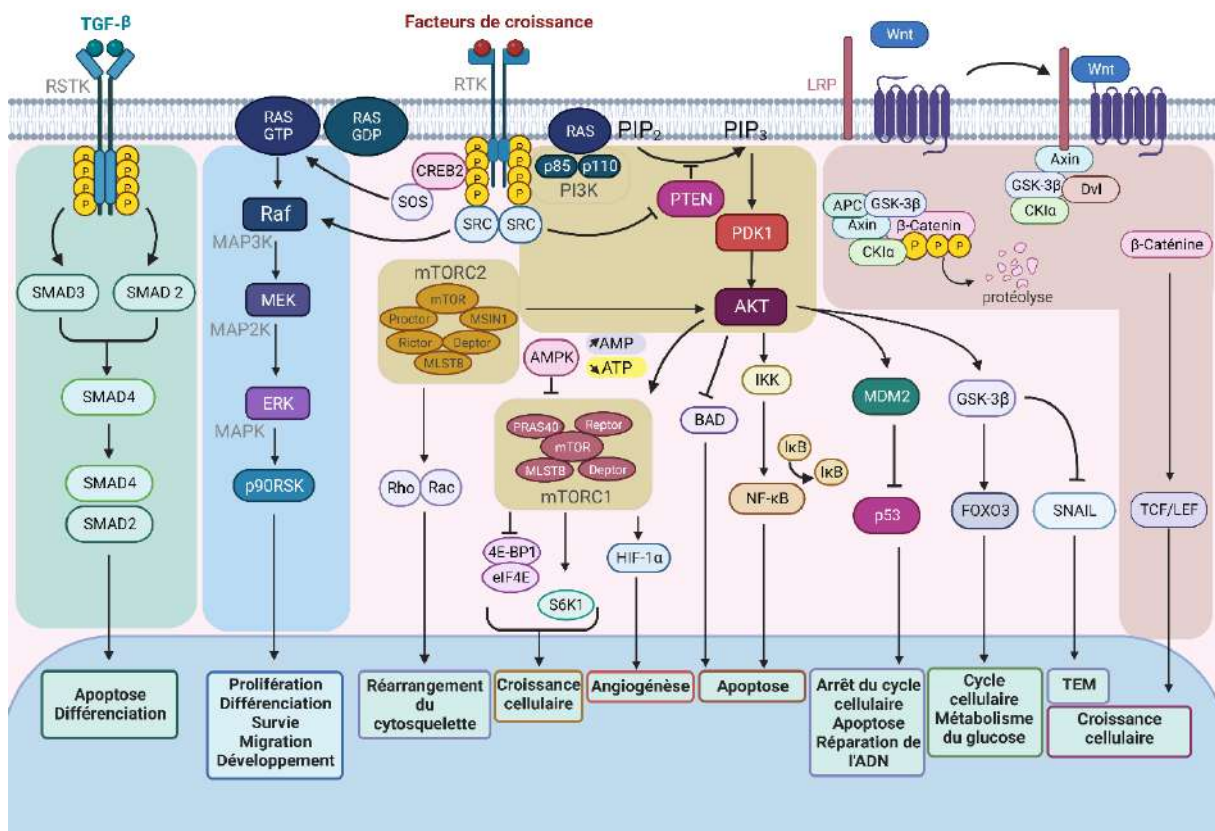


Figure 3 : Principales voies de signalisation dans les cellules cancéreuses

Ce schéma rassemble l'ensemble des voies de signalisation impliquées dans les processus tumoraux. De gauche à droite, nous retrouvons la voie de signalisation TGFβ/SMAD impliquée dans l'apoptose et la différenciation cellulaire ; la voie RAS/MAP kinases régulant la prolifération, la différenciation, la survie, la migration et le développement, la voie des RTK ou récepteurs tyrosines kinases, et notamment la voie PI3K/AKT qui régule de nombreux processus cellulaires par les nombreuses cibles d'AKT ; la voie Wnt/β-caténine régule la croissance cellulaire. La transduction de signal se fait par activation (flèches pleines), inhibition (flèches avec empâtements) ou phosphorylation (groupements phosphates en jaune). Figure adaptée de Tocris Bioscience pour News Medical Life Sciences.

Pour comprendre comment les mutations de ces gènes peuvent engendrer le processus de cancérogénèse, il faut en connaître davantage sur leurs fonctions. Physiologiquement, la liaison d'un facteur de croissance sur son récepteur va activer principalement deux voies de signalisation. La voie RAS / MAP kinases et la voie PI3K/AKT/mTOR (Figure 3). Ces voies vont activer des facteurs de transcription tels que JUN/FOS/EGR1 qui sont impliqués dans la réplication cellulaire. Ces mécanismes sont régulés par des points de restriction dont les protéines sont souvent codées par des gènes suppresseurs de tumeurs comme p53 ou PTEN (**Figure 3**). Si les mutations augmentent l'utilisation de ces voies, elles vont antagoniser les mécanismes de régulation ; au contraire si les mutations touchent des gènes suppresseurs de tumeurs comme le master régulateur p53, les processus de régulation sont perdus. Ainsi, la forte activité des facteurs de transcription codant pour les complexes du cycle cellulaire va entraîner une prolifération non contrôlée. La suractivation de ces voies est souvent observée dans l'évolution des cancers et renforce leur transformation, notamment en termes de consommation d'énergie. Les voies RAS/MAPK et PI3K/AKT/mTOR induisent notamment l'augmentation de transporteurs du glucose et le niveau d'expression des enzymes glycolytiques. La mutation d'autres gènes peut résulter en des conséquences similaires, notamment si les altérations des cellules cancéreuses touchent la prolifération cellulaire, la mobilisation des ressources énergétiques, les voies de signalisation des facteurs de croissance, la réplication et la réparation de l'ADN, la régulation des voies de mort cellulaire telle que l'apoptose ou encore la vascularisation. Les causes de surexpression de ces gènes sont très variées, d'ordre génétique comme les mutations ponctuelles, les insertions/délétions nucléotidiques, les altérations des régions non codantes (7) ou encore les variations du nombre de copies d'un gène donné (8).

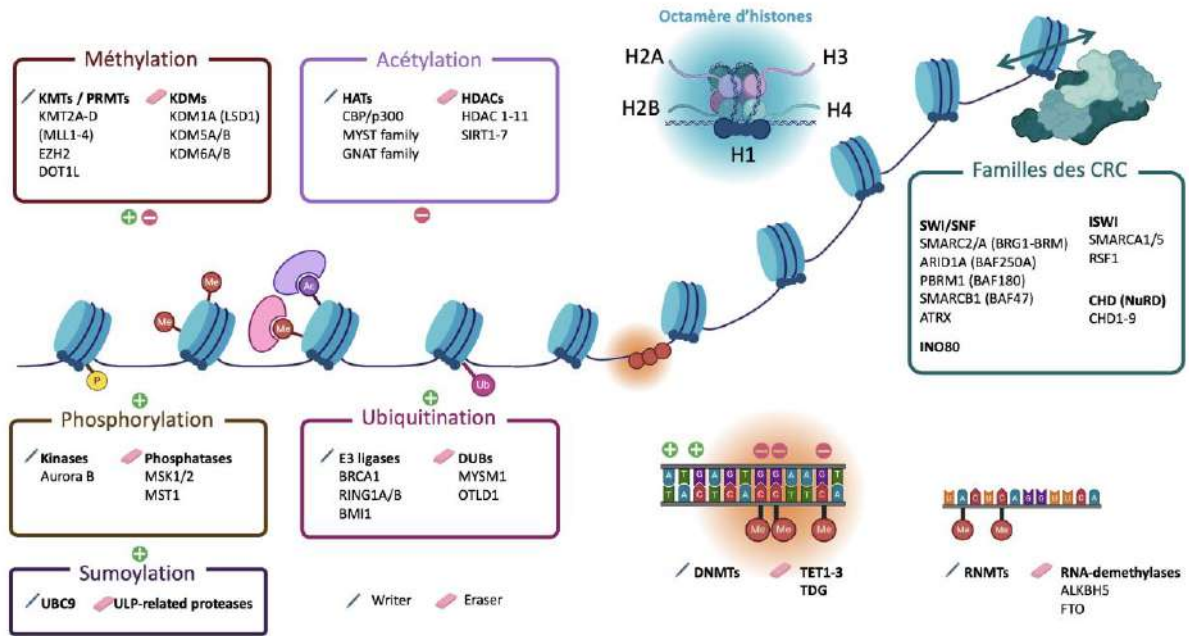


Figure 4 : régulations épigénétiques des histones et du génome

Les marques épigénétiques sur les histones, l'ADN ou l'ARN sont régularées par des « writers », les protéines qui ajoutent les marques et les « erasers », celles qui les enlèvent. On retrouve différents types de marques : méthylation, acétylation, phosphorylation, ubiquitination et sumoylation.

3) Régulation de la chromatine

Bien que largement partagées au sein des cancers, les mutations et les altérations de la séquence d'ADN ne sont pas l'unique voie de régulation de l'expression génique. En effet, la molécule d'ADN fait partie de la chromatine, un complexe constitué du matériel génétique et de protéines : les histones et les protéines non histones. On distingue deux états de la chromatine : l'hétérochromatine qui est condensée et où l'accessibilité aux séquences d'ADN est réduite et l'euchromatine, moins condensée, qui permet l'expression génique. L'unité de base de la chromatine est le nucléosome. Il est formé d'une boucle d'ADN et d'un octamère d'histones. Les régulations qui ont lieu au niveau de la chromatine porte le nom d'épigénétique. La nature des modifications épigénétiques est variée et peut se produire au niveau de la séquence d'ADN par ajout de groupe méthyl (méthylation), sur les molécules d'ARN messagers (méthylation) ou sur les histones (méthylation, acétylation, ubiquitination, phosphorylation, sumoylation) (**Figure 4**). L'ajout de ces groupements sur les différents constituants de la chromatine va moduler l'expression des gènes par des mécanismes d'encombrement stérique, de changements de charge moléculaire ou encore de modifications des interactions intramoléculaires et protéiques. Les méthylations des histones sont aussi bien associées à l'état ouvert que fermé de la chromatine selon la sous unité d'histone touchée. L'acétylation des histones est associée à une accessibilité réduite de la chromatine contrairement aux ubiquitinations, phosphorylations et sumoylations plutôt associées à l'augmentation de son accessibilité. Au niveau de la séquence génétique, plus l'ADN présentera des méthylations, moins les gènes seront actifs. Dans une autre échelle de taille, ce sont également les réarrangements intra- et interchromosomiques qui peuvent être cause de cancers, des gènes hormonaux pouvant par exemple être accolés à des gènes de croissance. C'est souvent le cas dans les sarcomes des tissus mous et les ostéosarcomes. Que ce soit par modification épigénétique ou par réarrangement chromosomique, ces processus vont altérer la fonction et la régulation des oncogènes ou des gènes suppresseurs de tumeurs. Ces réarrangements de la chromatine peuvent également mener à la formation d'oncoprotéine ou protéine de fusion dont l'expression va favoriser le développement tumoral. De nombreuses cibles thérapeutiques épigénétiques ont été développées, cependant la difficulté est de cibler l'épigénétique au sein des cellules cancéreuses sans modifier celle présente et nécessaire dans le développement de la réponse immunitaire (9).

4) États métaboliques des sarcomes

Ce chapitre a fait l'objet d'une revue, intitulée « Metabolic landscapes in sarcoma ». Dans cette revue, nous nous sommes intéressés à l'état de l'art sur les connaissances du métabolisme des sarcomes, son lien étroit avec les altérations génétiques fréquemment observées dans les sarcomes. Nous nous sommes également intéressés au lien entre état métabolique et infiltration immunitaire et à l'analyse de facteurs pronostiques à partir de banques de données humaines.

Il est important de souligner la grande disparité des mécanismes oncogéniques altérés dans le développement des sarcomes. Les sarcomes adultes présentent majoritairement des altérations génétiques complexes. En se basant sur l'analyse de données transcriptionnelles de patients, nous avons souligné que les sarcomes, comme d'autres cancers, présentent de fort taux de mutations sur les gènes associés aux voies de signalisation Ras, PI3K et Hippo. De nombreux sous types de sarcomes présentent un accroissement de la glycolyse, notamment dans les LMS, STLMS et ULMS. Au contraire, les sarcomes plus agressifs, tels que les UPS, MFS et DDLPS présentent une réduction des signatures de phosphorylation oxydative. Enfin, une signature plus discrète est présente sur la voie de signalisation de l'interconversion du pyruvate et du glucuronate. Les sarcomes pléiomorphiques non-différenciés présentent des altérations associées aux voies de signalisation PPAR/Acides gras et glycine/sérine/thréonine. Les altérations génétiques dans les ostéosarcomes touchent la synthèse des acides aminés, la glycolyse et le *shunt* pentose phosphate. Dans les sarcomes à génome complexe, les altérations sont associées à un renforcement de l'effet Warburg, qu'il s'agisse initialement d'altérations des voies Ras, PI3K, Hippo ou de la perte d'un gène suppresseur de tumeur comme p53 ou encore de la formation de protéines de fusion comme dans le sarcome d'Ewing. Nous avons également noté que l'utilisation d'autres sources énergétiques comme la glutamine ou l'arginine peuvent contribuer à la progression tumorale des sarcomes. Le métabolisme dit à un carbone (1C) est surexploité dans certains sarcomes agressifs comme le sarcome d'Ewing. Nous avons analysé comment certains facteurs limitants tels que l'oxygène ou certains cofacteurs comme la vitamine B5 contribuaient à la balance énergétique entre glycolyse et respiration mitochondriale. Enfin, nous avons dressé une synthèse des thérapies actuelles ciblant le métabolisme des sarcomes.

REVIEW

Open Access

Metabolic landscapes in sarcomas



Richard Miallot^{1*}, Franck Galland¹, Virginie Millet¹, Jean-Yves Blay² and Philippe Naquet^{1*} 

Abstract

Metabolic rewiring offers novel therapeutic opportunities in cancer. Until recently, there was scant information regarding soft tissue sarcomas, due to their heterogeneous tissue origin, histological definition and underlying genetic history. Novel large-scale genomic and metabolomics approaches are now helping stratify their physiopathology. In this review, we show how various genetic alterations skew activation pathways and orient metabolic rewiring in sarcomas. We provide an update on the contribution of newly described mechanisms of metabolic regulation. We underscore mechanisms that are relevant to sarcomagenesis or shared with other cancers. We then discuss how diverse metabolic landscapes condition the tumor microenvironment, anti-sarcoma immune responses and prognosis. Finally, we review current attempts to control sarcoma growth using metabolite-targeting drugs.

Keywords: Sarcoma, Metabolism, Microenvironment, Metabolomics, Transcriptomics, Metabolite-targeted therapies

Background

Sarcomas encompass a wide variety of tumors, with more than 170 subtypes, according to the last WHO classification. They originate from the neoplastic transformation of mesenchymal cells in connective tissues [1, 2]; 87% arise from soft tissue and 13% from bone [3, 4]. Soft tissue sarcoma (STS) presents as an indolent or aggressive disease, often only diagnosed at an advanced and/or metastatic stages. Current sarcoma classification relies on histopathology that may lead to errors in up to a quarter of cases [5]. In terms of prevalence, they represent less than 1% of adult cancers, but up to one fifth of pediatric solid malignant cancers [3]. Surgery is the standard of care for patients supplemented with chemotherapy or radiotherapy [6]. Targeted therapies remain limited to tumors with well-defined oncogenic drivers [1, 2]. Clinical trials targeting immune checkpoints show low response rates, with few responsive histotypes. Finally, biomarkers or tertiary lymphoid structures may be predictive tools for 10% of patients [7]. Consequently,

improving sarcoma typing and treatment requires the use of large-scale “omics” tools to identify the oncogenic drivers, often resulting from multiple genetic alterations in adult STS. These can include translocations, mutations or amplifications/deletions that cripple major growth and differentiation pathways [8–12].

Given the limits of current treatments, exploiting drugs targeting metabolic pathways may pave the way to effective therapy for these largely incurable diseases.

Aggressive tumors must survive in a reorganized, stressful and metabolically competitive microenvironment. This necessary adaptation exploits tumor heterogeneity and cell networks in the tumor microenvironment. Furthermore, within a given cell, plasticity depends on interconnections between various metabolic pathways to adapt growth to the available metabolites. A major trait often amplified in these tumors is the use of aerobic glycolysis, known as the Warburg effect [13], that optimizes tumor cell growth through provision of building blocks to increase biomass [14]. Since Warburg's discovery, a debate has existed about the persistence of mitochondrial activity in glycolytic tumors and its potential to be a drug target [15]. Despite the central role of mitochondria not only in cell energetics, homeostasis and stress sensing [16] but also reactive oxygen species (ROS) production [17] their contribution to oncogenic transformation

*Correspondence: miallot@ciml.univ-mrs.fr; naquet@ciml.univ-mrs.fr

¹ Centre National de la Recherche Scientifique, Institut National de la Santé et de la Recherche Médicale, Centre d'Immunologie de Marseille Luminy, Aix Marseille Univ, Marseille, France

Full list of author information is available at the end of the article



© The Author(s) 2021. **Open Access** This article is licensed under a Creative Commons Attribution 4.0 International License, which permits use, sharing, adaptation, distribution and reproduction in any medium or format, as long as you give appropriate credit to the original author(s) and the source, provide a link to the Creative Commons licence, and indicate if changes were made. The images or other third party material in this article are included in the article's Creative Commons licence, unless indicated otherwise in a credit line to the material. If material is not included in the article's Creative Commons licence and your intended use is not permitted by statutory regulation or exceeds the permitted use, you will need to obtain permission directly from the copyright holder. To view a copy of this licence, visit <http://creativecommons.org/licenses/by/4.0/>. The Creative Commons Public Domain Dedication waiver (<http://creativecommons.org/publicdomain/zero/1.0/>) applies to the data made available in this article, unless otherwise stated in a credit line to the data.

is still debated. In some STS, germline mutations affecting mitochondrial enzymes lead to the accumulation of oncometabolites that induce a pseudo-hypoxic response and alter epigenetic marks and differentiation [18]. In the tumor microenvironment, glycolytic and oxidizing cells may compete or cooperate for an optimal use and exchange of energetic metabolites. This network involves immune cells that adapt their metabolism to exert their functions in this competitive environment [19]. The purpose of this review is to link recent findings on STS genetics to the alterations of intracellular pathways affecting their tumor metabolic landscapes. Although not necessarily specific to STS, they may represent novel therapeutic opportunities.

Unsupervised omics and single cell-based analyses highlight metabolic signatures in cancer

The development of more integrated technologies with increased sensitivity and/or resolution has helped to unravel tumor genomic and metabolic complexity in situ and to bridge the gap between mouse models and patients. Several recent studies documented the power of integrated genomic or metabolomic strategies to decipher tumors complexity. An article from The Cancer Genome Atlas (TCGA) Research Network [8] combined genetic, epigenetic and transcriptomic analyses and proposed a novel classification of STS subtypes with complex genomes. In their analysis of the number and nature of copy number variations (CNVs), they identified three dominant profiles from leiomyosarcoma (LMS), myxofibrosarcoma (MFS), undifferentiated pleomorphic sarcoma (UPS) to dedifferentiated liposarcoma (DDLPS) displaying the highest level of genomic alterations. In addition to these modifications, the nature of epigenetics marks, activating pathways or immune signatures add further prognostic value. Another article exploited TCGA data to describe the relative contribution of 114 metabolic pathways to cancer progression [20]. This analysis showed that master metabolic transcriptional regulators behave as genetic drivers explaining the metabolic profiles displayed by various tumors compared to normal tissues, and help predict responsiveness to metabolism-targeting drugs. For example, alterations of specific transcriptional regulators explain the defect in polyamine biosynthesis in prostate cancer. Similarly, distinct pathways enriched in breast cancer allow the discrimination of aggressive tumors from those associated with a good prognosis. Based on this finding, metformin, a mitochondrial complex 1 inhibitor, has been proposed as a potential adjunct therapy against basal breast cancer cells, due to its unique deregulation of the Tricarboxylic Acid (TCA) cycle. In STS, this analysis highlighted the enrichment in the pentose and glucuronate

interconversion (PGI) pathway, also amplified in the Yang Huang syndrome described in the context of traditional Chinese pharmacology [21]. The PGI pathway relies on UDP-glucuronosyltransferase (UGT) enzymes that catalyze the binding of D-glucuronic acid to toxic substances or endogenous compounds such as bilirubin via glycosidic bonds, contributing to the detoxification of lipophilic compounds or glucuronides.

Exploration of the TCGA database allows one to identify more discrete signatures displayed by major STS subtypes versus other types of cancers. As shown in Fig. 1, all cancer types display abnormalities in cell cycle regulation. Most carcinomas show an enrichment in oncogenic pathways, glycolytic signatures and alterations of energetic, nucleotide, amino acid or macromolecule pathways. When considering STS as a whole, RAS, PI3K and HIPPO pathways light up, as in [8], coupled to a dominant glycolytic/OXPHOS signature. More discrete signals confirm the enhancement of the PGI pathway in STS, although this trend is not detectable when considering individually the STS subtypes. Our analysis also indicates that distinct signatures preferentially match with STS subtypes, with UPS featuring an enrichment in PPAR/fatty acids and glycine/serine/threonine pathways, whereas LMS display an enhanced OXPHOS signature. Similarly, differences in oncogenic pathway usage are apparent but it is difficult to relate these pathways to the metabolic bias in tumors.

The improvement of chromatographic and mass spectrometry (MS) analyses such as Ultra High Performance Liquid Chromatography Q-Exactive MS (UHPLC-QE MS) has allowed time to be saved in sample separation while preserving the detection capacity of a large spectrum of metabolites. In osteosarcoma (OS), studies combining state-of-the-art transcriptomic and metabolomics approaches highlighted the amplification of nucleotide and amino acid (namely alanine, aspartate, glutamate, arginine, proline, methionine) pathways, glycolysis and the pentose phosphate shunt [26, 27]. Spatially-correlated analysis, mass spectrometry imaging (MALDI-MSI) can further reveal how biomolecular ions are distributed on tissue sections, linking their molecular identification to their spatial distribution. Results from two studies [28, 29] comparing STS subtypes showed that the overexpression of acyl-CoA-binding protein and stearyl-CoA desaturase (directly involved in the processing of fatty acids) as well as MIF1, galectin 1, thioredoxin could help distinguish LMS from MFS, and predict their prognosis. To identify tumor-associated metabolites in situ, airflow-assisted desorption electrospray ionization mass spectrometry imaging (AFADESI-MSI) was used on tissues from 256 esophageal cancer (ESCA) patients [30]. This

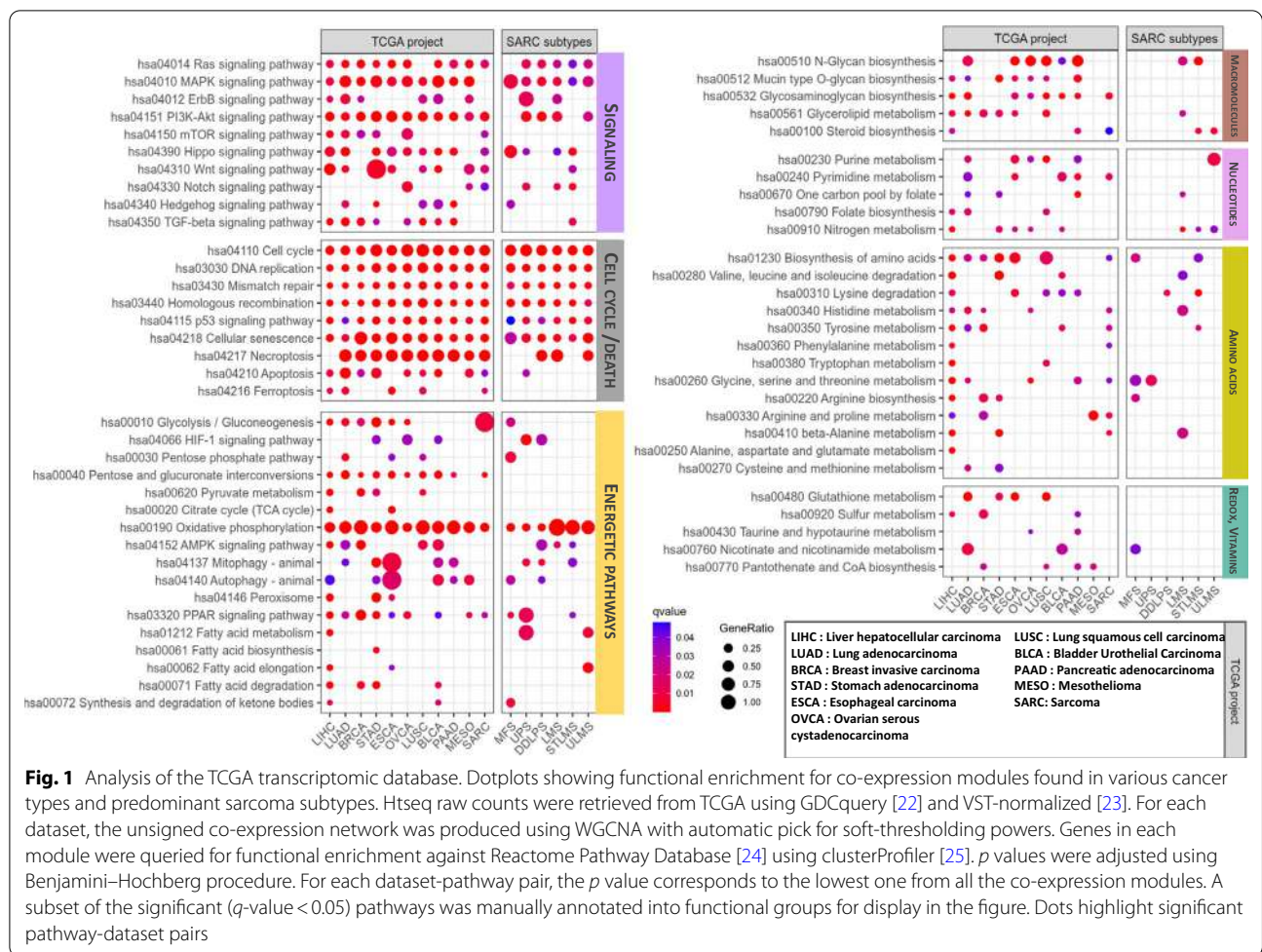


Fig. 1 Analysis of the TCGA transcriptomic database. Dotplots showing functional enrichment for co-expression modules found in various cancer types and predominant sarcoma subtypes. Htseq raw counts were retrieved from TCGA using GDCquery [22] and VST-normalized [23]. For each dataset, the unsigned co-expression network was produced using WGCNA with automatic pick for soft-thresholding powers. Genes in each module were queried for functional enrichment against Reactome Pathway Database [24] using clusterProfiler [25]. *p* values were adjusted using Benjamini–Hochberg procedure. For each dataset-pathway pair, the *p* value corresponds to the lowest one from all the co-expression modules. A subset of the significant (*q*-value < 0.05) pathways was manually annotated into functional groups for display in the figure. Dots highlight significant pathway-dataset pairs

analysis unraveled the dysregulation of several metabolic pathways affecting proline, glutamine, histidine, uridine, fatty acid and polyamine homeostasis. Among others, it identified pyrroline-5-carboxylate reductase 2 (PYCR2) and ornithine decarboxylase (ODC), rate-limiting enzymes in proline and polyamine biosynthesis, respectively, as markers of tumor proliferation. Table 1 summarizes biomarkers and metabolites linked to alterations in the activation of metabolic pathways in STS. In the future, these explorations will benefit from single-cell strategies evaluating the metabolic status of tumor versus surrounding cells. In this context, the development of novel flow cytometry-based methods to assess metabolic activity such as Met-Flow [31] or SCENITH [32] have already proven their potential to assay the metabolic status of circulating or tumor-infiltrating immunocytes.

Here, we will review and update the mechanisms that link complex oncogenic stimuli associated with various STS to metabolic alterations.

Oncogenic drivers upstream of growth pathways rewire metabolism in sarcomas

Physiologically, growth factor receptors (GFR) trigger the RAS/MAPK and PI3K/AKT/mTOR pathways and activate transcriptional regulators such as JUN/FOS/EGR1 that drive cell division (Fig. 2A). This process is temporally regulated by the co-engagement of restriction points controlled by tumor suppressor genes (TSGs) (Fig. 2B) [73]. In cancer cells, prolonged exposure to oncogenic signals strongly stimulates ERK-dependent EGR1 activation, bypassing cell cycle regulation and provoking PI3K activation that antagonizes p53-dependent tumor suppression [74] (Fig. 2B). In p53-mutated cancers, the temporal regulation of MEK/MYC/PI3K is dysfunctional and this allows cancer cells exposed to transient growth signals to proliferate, in a context of increased genomic instability. These pathways have been shown to be involved in sarcomagenesis in both human and rodent models (Fig. 2A), downstream of oncogenic GFRs or receptors involved in tissue organization and trophicity. We will highlight how various

Table 1 Biomarkers and metabolites associated with STS

	Cell processes	Biomarkers (genes or metabolites)	STS subtype	Prognosis significance	References
Signaling	RAS signaling	GLUT, HK, PFK	UPS, MFS	Poor prognosis	[33, 34]
	PI3K-AKT signaling		LMS, EWS	Poor prognosis	[35, 36]
		miR-181b	STLMS, ULMS	RFS	[8]
	GFR signaling	MDM2 amplification	DDLPS	Poor prognosis	
		IGFR1 overexpression	STLMS, EWS, MLS, ARMS, SS	Poor RFS/DSS	[8, 37, 38]
		Her4/ErbB4	OS, EWS	Poor prognosis	[38]
		Serum bFGF, VEGF	STS	Poor prognosis	[39]
	JUN signaling		DDLPS	Poor prognosis	[8]
	HIPPO pathway	Nuclear YAP/TAZ, VGLL3	UPS, MFS, MLS, RMS	Poor prognosis	[40–45]
	WNT pathway	Nuclear β -catenin/LEF1; MEG3 (lncRNA) down-regulation	EWS, OS	Poor prognosis	[46, 47]
Cell cycle/death	Cell cycle	CINSARC—67 genes	STS	Poor prognosis	[48]
		TP53, RB1, CDKN2A deficiency	LMS, UPS, MFS	Poor prognosis	[8, 49–51]
		TP53, IGAR, GLUT	LMS, UPS, MFS, EWS	Poor prognosis	
		CDCA2, KIF14, IGBP7	SS	Metastasis	[52]
	DNA replication	CDK4 amplification	DDLPS	Poor prognosis	[8]
		TOP2A	MPNST	Poor prognosis	[8]
		RRM1	OS, EWS	Good prognosis	[8]
	Transcriptional regulation	ATRX deletion	DDLPS	Poor prognosis	[8]
		DNA hypermethylation, HMGA2 amplification	DDLPS, STLMS	poor RFS/DSS	[8]
			DDLPS	Poor prognosis	[8]
Energetic pathways	Glycolysis	GLUT, ENO1, TPI1, PKG1, LDHC, lactate, pyruvate	STS	Poor prognosis	[20, 53, 54]
		<i>FBP2</i> loss	LPS, LMS, FS, UPS	Poor DSS	[55]
		Serum LDH	ULMS, EWS	Poor prognosis	[39, 51]
		<i>PKM1/2</i> isoenzymes	OS	Poor prognosis	[56]
	Pentose and glucuronate interconversions	UGT	STS	Prognosis	[20]
	Citrate cycle/OXPHOS	Downregulated metabolites	OS	Poor prognosis	[27]
		Decreased ATP Synthase subunits	OS	Poor prognosis	[56]
		SDH, FH mutations (succinate accumulation)	GIST	Poor prognosis	[57]
	Others	AMPKa, CHK1, S6, ARID1A, RBM15, MSH6, Acetyl-Tubulin	STS	Combined survival related signature	[58]
	Amino acids	Nucleotide metabolism		STS	Poor prognosis
Alanine, aspartate, glutamate		GLS	OS, KS, EWS	High risk	[27, 59, 60, 56]
Arginine, ornithine		ASS1 deficiency, ODC	OS, MFS, KS	DSS, MFS	[27, 61, 62]
Proline		PYCR2	OS, KS	DSS, MFS	[27, 63]
Serine, glycine		PHGDH, PSAT1, PSPH, SHMT2, SLC1A5, MTHFD2, MTHFD1L	EWS	DSS, MFS	[60, 64]
Tryptophane		TDO2 (low)	EWS	DSS, MFS	[65]
5 methylthioadenosine			OS	DSS, MFS	[27]

Table 1 (continued)

	Cell processes	Biomarkers (genes or metabolites)	STS subtype	Prognosis significance	References
Redox, vitamins	Pantothenate metabolism	VNN1 (low)	FS	Poor prognosis	[66]
	Redox metabolism	TXR, MIF1, GAL1, AcCoaBP	LMS (high), MFS (low)	Poor prognosis	[67]
	Hypoxia	HIF1 α , hypoxia gene signatures	EWS, OS, GIST, KS	Poor prognosis	[68–72]

activation pathways engage these metabolic programs to sustain STS cell growth and rely alternatively on various carbon sources such as glucose, amino acids or lipids (Fig. 3). We also provide an update on current clinical trials exploiting metabolic interference in Table 2.

Overactivated MAP and PI3 kinase pathways drive a Warburg effect

Both mutations and oncogene-driven overexpression of GFRs contribute to STS development. Gain-of-function mutations of the GFR KIT or PDGF-R α drive gastrointestinal stromal tumor (GIST) progression [93]. In the translocation-associated Ewing's sarcoma (EWS), myxoid liposarcomas (MLS) or alveolar rhabdomyosarcoma (ARMS), the fusion proteins EF, FUS-DDIT3 or PAX3-FOXO1, respectively, enhance IGF1R expression, a major driver of RAS/AKT/mTOR activation [37]. Hyperactivation of the RAS pathway is predictive of a high risk of disease recurrence and impaired overall survival in 30% undifferentiated pleomorphic sarcoma (UPS), a common adult STS [33, 34]. Similarly, the loss of the phosphatase PTEN induces growth-factor independent PI3K/AKT activation that sustains autonomous nutrient uptake in some LMS or MPNST [94]. Accordingly, sarcoma incidence increases in hereditary neurofibromatosis patients with carrying deletions of the RAS negative regulator genes NF1 or NF2 [49, 95]. To investigate the mechanisms of tumor progression in a mouse model, whole-exome sequencing was performed on STS induced by either KrasG12D activation/p53 deletion, 3-methylcholanthrene (MCA) or ionizing radiation [96]. Whereas CNVs were very frequent in radiation-induced STS, MCA-induced tumors showed a high mutational burden, combined with high genomic instability in the absence of p53. Candidate oncogenic drivers affecting MAPK signaling were identified either as mutations of Kras, Nf1 and Hippo effectors (Fat1/4), or as amplification of Kras and Myc in p53 deficient mice, or Met and Yap1 in radiation-induced STS. Mutations in the RAS pathway influence the prognosis of human STS such as DDLPS or pediatric embryonic rhabdomyosarcoma (ERMS) [97]. In the latter, the overactivation of p38 MAPK induces high levels of reactive oxygen species (ROS) that

increase the mutation rate [97] and may sensitize tumors to therapies enhancing oxidative stress [98, 99].

RAS- or PI3K/AKT-driven activation increases the expression of glucose importers (GLUT) and of the upstream ATP-consuming glycolytic enzymes hexokinase (HK) and phosphofructokinase (PFK), recently shown to control the glycolytic flow quantitatively [100]. The oncogenic KRAS4A isoform and to lesser extent other RAS isoforms were shown to interact with HK1 on mitochondria (Fig. 3), preventing its allosteric inhibition by glucose-6-phosphate (G6P), thereby enhancing glycolysis [101]. Hypoxia or mutations affecting the RAS pathway modulated the activity of PKM2 or PGK1, two ATP-generating enzymes in the last steps of glycolysis, thus providing them with non-metabolic pro-oncogenic functions [102]. Thus, an increase in the proportion of PKM2 dimers, lacking pyruvate kinase activity, drives PKM2 nuclear translocation where it participates in STAT3 phosphorylation and *mek5* gene transcription, driving cell growth [103]. Another study showed that activated ERK phosphorylates PGK1, promoting its association with PIN1 and its translocation into the mitochondria. There, it phosphorylates and activates pyruvate dehydrogenase kinase 1 (PDK1), an inhibitor of pyruvate dehydrogenase (PDH), the checkpoint of pyruvate entry in the TCA cycle [104] (Fig. 3). Globally, these RAS-driven effects reinforce glycolysis over mitochondrial respiration and favor glucose- and glutamine-dependent anabolism as shown in a pancreatic ductal adenocarcinoma (PDAC) model [105, 106]. Several clinical trials are currently based on drugs inhibiting PI3K, AKT, mTOR and ERK signaling in STS (Fig. 4 and Table 2).

An altered HIPPO pathway induces aerobic glycolysis in STS

Several sarcoma histiotypes re-express genes involved in developmental pathways [107–110], such as HIPPO that controls organ size. Its engagement in intercellular adhesion complexes activates the MST and LATS kinases that phosphorylate the transcriptional factors YAP1 and TAZ, promoting their degradation. In contrast, upon nuclear translocation, YAP/TAZ cooperate with mitogenic effectors and boost proliferation (Fig. 2A). HIPPO interferes with the RAS and PI3K pathways that control cell death

induction [111], acting as a tumor suppressor pathway [112]. Through cross-inhibition, MST and AKT differentially regulate the expression level of pro-apoptotic effectors (NOXA, FASL, BIM, TRAIL). In addition, ERK induces the expression of anti-apoptotic effectors (BCL2, BCL-XL, IAP, MCL1) partly via YAP/TAZ activation. Furthermore, in a PDAC model, YAP1 amplification can bypass the need for oncogenic KRAS activation [113]. The amount of translocated YAP/TAZ determines their co-activating potential for TEAD transcription factors and thereby the balance of proliferation versus cell death [40].

Loss of MST/LATS or YAP overexpression is pro-tumoral in mice [114, 115], and this pathway is often affected in MCA- or radiation-induced STS [96] and UPS [8]. In transgenic models, altering HIPPO effectors alone or in combination with other deficits augmented STS frequency [41]. An increased YAP/TAZ nuclear staining is predictive of poor survival in UPS, DDLPS and ERMS [42–45, 116]. Two studies investigated how fusion gene products mediate sarcomagenesis through alteration of the HIPPO pathway in mice. One study explored MLS that account for 5–10% STS, among which 90% tumors depend on the product of the FUS:DDIT3 translocation [44]. The authors performed a large-scale RNA interference screen and identified YAP1 as a non-redundant oncogenic driver. In MLS cell lines, FUS:DDIT3 led to a two to threefold increase in expression and co-transcriptional activity of YAP1. Co-immunoprecipitation and immunofluorescence studies revealed a physical interaction of YAP1 with FUS:DDIT3 in the nucleus. Pharmacological inhibition of YAP1 activity inhibited the growth of MLS xenografts. The other study, based on a new transgenic model, showed that doxycycline (DOX)-induced expression of YAP1 in the myogenic MYOD1 cell lineage provoked the development of ERMS through the transformation of activated satellite cells [45]. Retrieval of DOX released a YAP1-dependent differentiation block and reduced tumor formation. Transcriptional profiling of the tumors revealed that YAP1 induces pro-oncogenic effector genes and represses terminal differentiation of myoblasts. In line with these observations, an independent study found no evidence that mutant RAS isoforms were responsible for YAP overexpression in myoblasts [116]. In ARMS, the translocation product PAX3-FOXO1 suppresses HIPPO signaling through overexpression of RASSF4, which inhibits the MST1 kinase. Similarly, this

effect is linked to PAX3-FOXO1 co-localization with YAP1 in the nuclei of cancer cells. This chimeric transcription factor cooperates with YAP1/TEAD to induce downstream effectors that trigger IGFs and NF- κ B activation, and repress senescence and apoptosis in mesenchymal cells [40, 44]. Therefore, mutations of HIPPO effectors can be oncogenic in STS.

The HIPPO pathway restricts tissue growth and is connected to nutrient cues [117, 118]. Upon glucose starvation, AMPK- and LATS-kinases phosphorylate YAP resulting in its degradation [119]. Furthermore, Wang et al. showed that the phosphorylation level of YAP1 at position S61 is regulated by AMPK, itself recruited to YAP protein complexes in the cytosol of glucose-deprived cells. Addition of glucose was associated with a decrease in YAP phosphorylation and its nuclear translocation, where it interacted with TEAD transcriptional regulators to induce glycolytic genes. This glucose-sensing pathway via YAP and TAZ was required for the full deployment of glucose growth-promoting activity in breast cancer. In addition, glycolysis was required to sustain YAP/TAZ tumorigenic properties [120]. Mechanistically, phosphofructokinase (PFK1) bound to and co-activated the YAP/TAZ transcriptional cofactors TEADs (Fig. 3). In some cancers, the loss of NF2, an upstream negative regulator of HIPPO signaling, simultaneously unleashed YAP/TAZ and SMAD2/3 activation leading indirectly to the induction of aerobic glycolysis via derepression of *GLUT*, *HK2*, *LDH* and *MCT* genes [121]. Interestingly, *NF2* mutations might contribute to the maintenance of rare aggressive sarcomas [122]. This hypothesis was tested in a kidney cancer cell model bearing *NF2* mutations [123]. There, DOX-induced expression of shRNA downregulating YAP/TAZ expression provoked the regression of tumors in vivo. YAP/TAZ-depletion induced a substantial decrease in EGFR and AKT phosphorylation, associated with a reduction in glucose uptake, and a switch to glutamine anaplerosis that boosted mitochondrial respiration and ROS production. Under conditions of glucose or glutamine withdrawal, this metabolic shift favored cell death. Whereas restoration of AKT signaling by expression of a constitutively active form of AKT rescued cell proliferation, it did not prevent starvation-induced death. In vivo, YAP/TAZ^{low} tumors survived due to the engagement of a compensatory lysosome-mediated activation of MAPK signaling. By combining YAP/TAZ and MEK inhibition, tumor growth durably regressed. YAP can

(See figure on next page.)

Fig. 2 Oncogenic and tumor suppressor pathways altered in STS. **(A)** This figure highlights mutations that alter regulations of PI3K/AKT/mTOR and MAP kinase pathways in sarcoma. Colored triangles associate sarcoma subtypes (listed on the bottom right corner) with the corresponding genes alterations, either expression or loss, on the scheme. Expression or regulations of tumor suppressor genes is altered (p53, PTEN) concomitantly with increased expression of oncogenes driving malignant transformation (increase Anabolism, Warburg effect). **(B)** Panel B focuses on cell cycle alterations at the level of the p53 and RB1 tumor suppressor genes notably

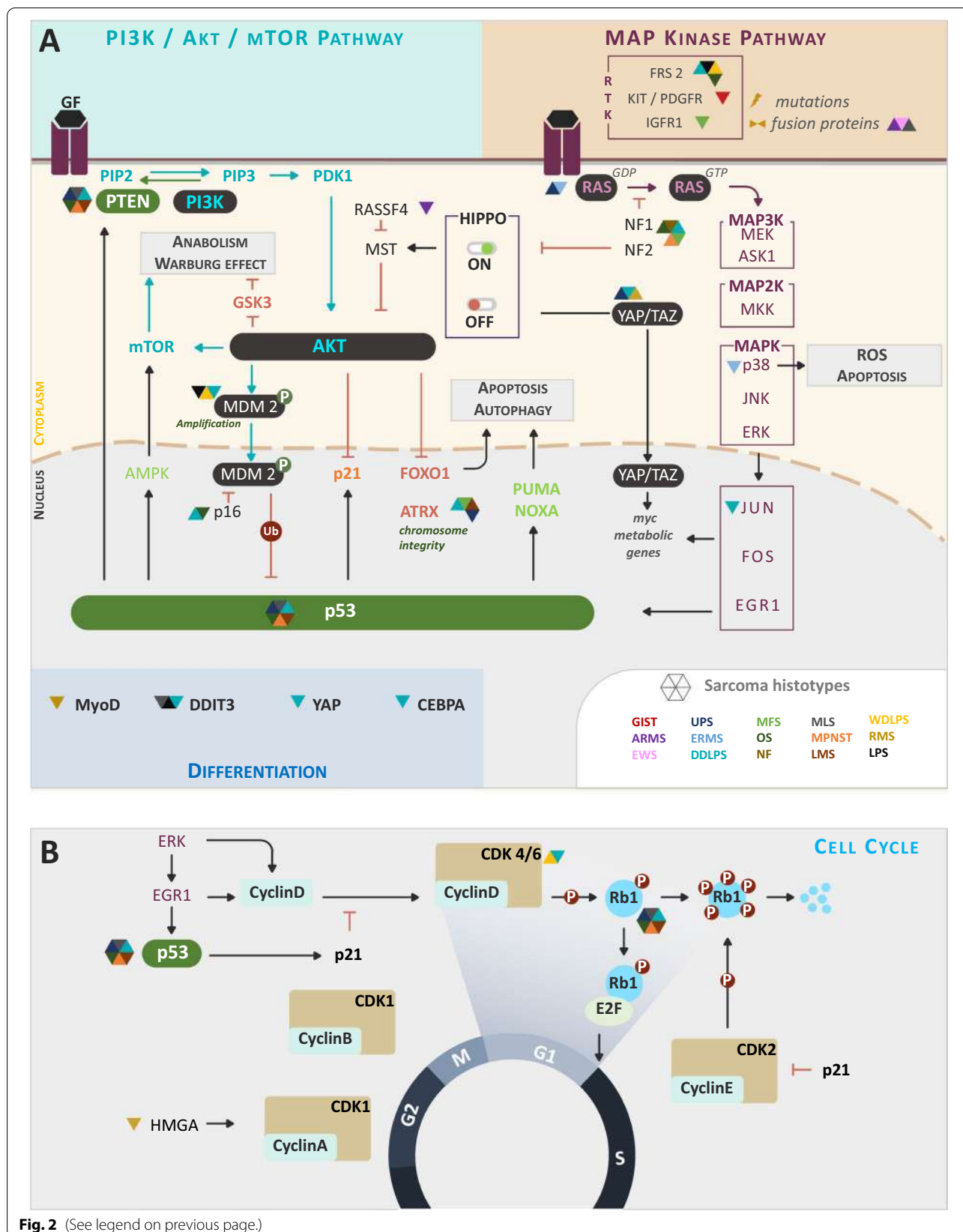


Fig. 2 (See legend on previous page.)

also induce aerobic glycolysis through a direct interaction with HIF1 α in a hypoxic environment [124, 125]. Therefore, the proglycolytic effect of YAP/TAZ engagement depends on their participation in various nuclear transcriptional complexes. In a muscle-derived UPS model, a combination of epigenetic modulators suppressed YAP1 activity and reduced sarcomagenesis through regulation of metabolism. In this case, YAP1 nuclear translocation was associated with a poor prognosis [126] and its inactivation by epigenetic modulators allowed the restoration of a clock gene-mediated unfolded protein response and muscle differentiation. It also promoted a switch toward lipid catabolism and autophagy, limiting YAP-driven UPS cell growth. The YAP/TAZ inhibitor Verteporfin is currently being tested in Ewing's sarcoma (EWS) (Fig. 4 and Table 2).

Glutamine and arginine metabolic pathways contribute to STS growth

In a UPS mouse model harboring Kras mutations and p53 deletion in the muscle [59], tumors developed in the hindlimb and metastasized in the lung, as in the human disease. Additional deletion of HIF-2 α or its binding partner aryl hydrocarbon receptor nuclear translocator (ARNT) enhanced tumor development. Use of an unbiased pan metabolomics strategy combining LC-MS and stable isotope metabolite tracing revealed a reliance on glutaminolysis for tumors, unlike muscle cells. Accordingly, glutaminase (GLS) inhibitors blocked UPS tumor growth in vivo and are the object of clinical trials in humans (Fig. 4 and Table 2). Mechanistically, GLS hydrolyses glutamine to glutamate, which is then dehydrogenated to alpha-ketoglutarate (α KG) by glutamate dehydrogenase GLUD or an aminotransferase (such as PSAT), boosting mitochondrial anaplerosis [127]. In this UPS model, tracing using C¹³- or N¹⁵-labeled glutamine demonstrated that glutamine is a carbon donor for the TCA cycle and a nitrogen donor for aspartate production from oxaloacetate. Aspartate is a crucial carbon source for purine and pyrimidine synthesis and sustains cell growth [128, 129]. Aspartate is also required for the conversion of citrullin into arginine through the activity of the rate-limiting argininosuccinate synthase 1 (ASS1) that initiates the urea cycle. This reaction generates arginine and contributes to the clearance of nitrogenous wastes. ASS1 deficiency has been observed in various cancers, including MFS, due to epigenetic silencing of its promoter [61]. Reexpression of ASS1 inhibited tumor

growth and metastases. To investigate how arginine auxotrophy induced by ASS1 deficiency contributed to the progression of tumors, another study used a pegylated arginine deiminase (ADI-PEG20) to deplete arginine pharmacologically [89]. A short-term treatment by ADI-PEG20 applied to LMS cell lines, immediately induced cell proliferation arrest and autophagy. Upon prolonged therapy, cell lines became resistant to ADI-PEG20 due to the reexpression of ASS1 that regenerated arginine. A metabolomic profiling of treated cell lines revealed a reduction in PKM2 levels. In addition, U¹³C glucose tracing studies showed that carbons were shifted away from lactate and citrate production, and reoriented toward serine/glycine synthesis. Analysis of metabolic requirements for growth showed a reduced reliance on glucose and a reinforcement in OXPHOS and glutaminolysis, as an alternative source of TCA cycle intermediates via anaplerosis. In STS, a clinical trial using ADI-PEG20 in combination with Gemcitabine and Docetaxel has been launched (Fig. 4 and Table 2). Similarly, targeting glutamine metabolism through GLS inhibition could provoke the lethality of ASS1-deficient cancers and is currently being evaluated in GIST and NF1-mutated cancers (Fig. 4 and Table 2).

Complex metabolic rewiring in Kaposi's sarcoma

Kaposi's sarcoma (KS) is caused by a lytic oncogenic herpes virus (KSHV/HHV8), infecting endothelial cell precursors in immunosuppressed individuals. Infection, which is necessary but not sufficient for the growth of KS lesions, leads to the development of a vascular neoplasm associated with cytokine dysregulation driven by the virally encoded G protein coupled receptor (vGPCR). In lytically infected cells, vGPCR induced Rac1/NOX-dependent production of ROS that activated the redox sensitive STAT3 and HIF pathways [130]. Infected cells had increased lactate production and decreased mitochondrial respiration, a phenotype in part attributable to HIF1 α activation [131]. Indeed, aerobic glycolysis favored by PKM2 induction sustains the maintenance of KS cells [132] (Fig. 3). Infected cells also exert a paracrine effect on neighboring endothelial cells. Indeed, PKM2 acts as a coactivator of HIF1 α reinforcing the production of angiogenic cytokines [131]. Among them, PDGFRA, found phosphorylated in KS-biopsies [133], plays a major oncogenic role. HIF1 α also participates in the reactivation of latently infected cells [134]. Upon transformation by KHSV, however, endothelial cells depended on glutamine

(See figure on next page.)

Fig. 3 Metabolic consequences of STS-associated molecular alterations. This scheme integrates sarcoma genetic alterations affecting tumor suppressor genes (green background) or oncogenes (black background) in the tumor metabolic network. These alterations enhance enzymatic reactions in favor of anabolic pathways by increasing the glycolytic flux (pink) and branched pathways, notably nucleotide (yellow), fatty acids (orange) and DNA/RNA synthesis at the cost of dampens mitochondrial function and TCA cycle proper functioning

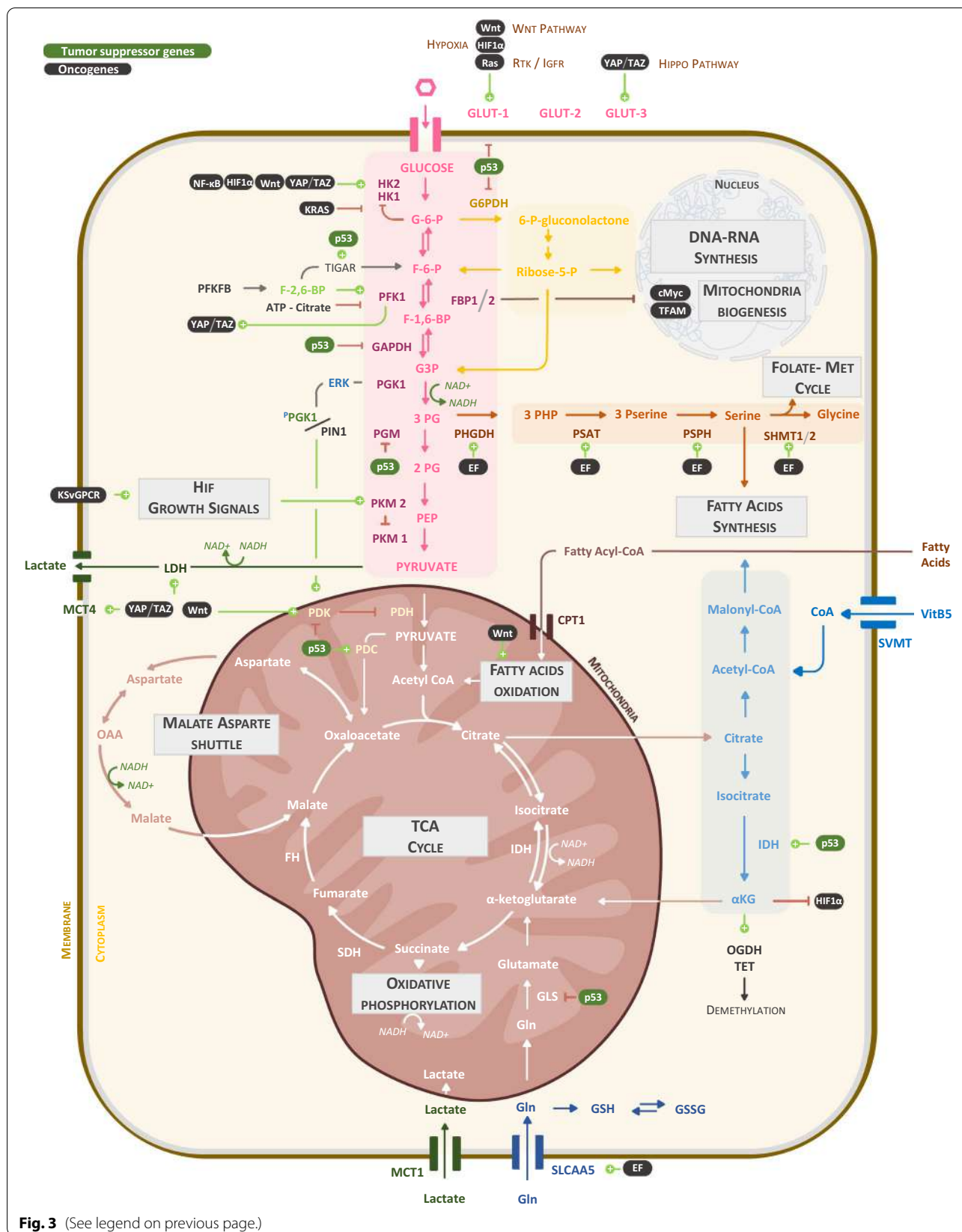
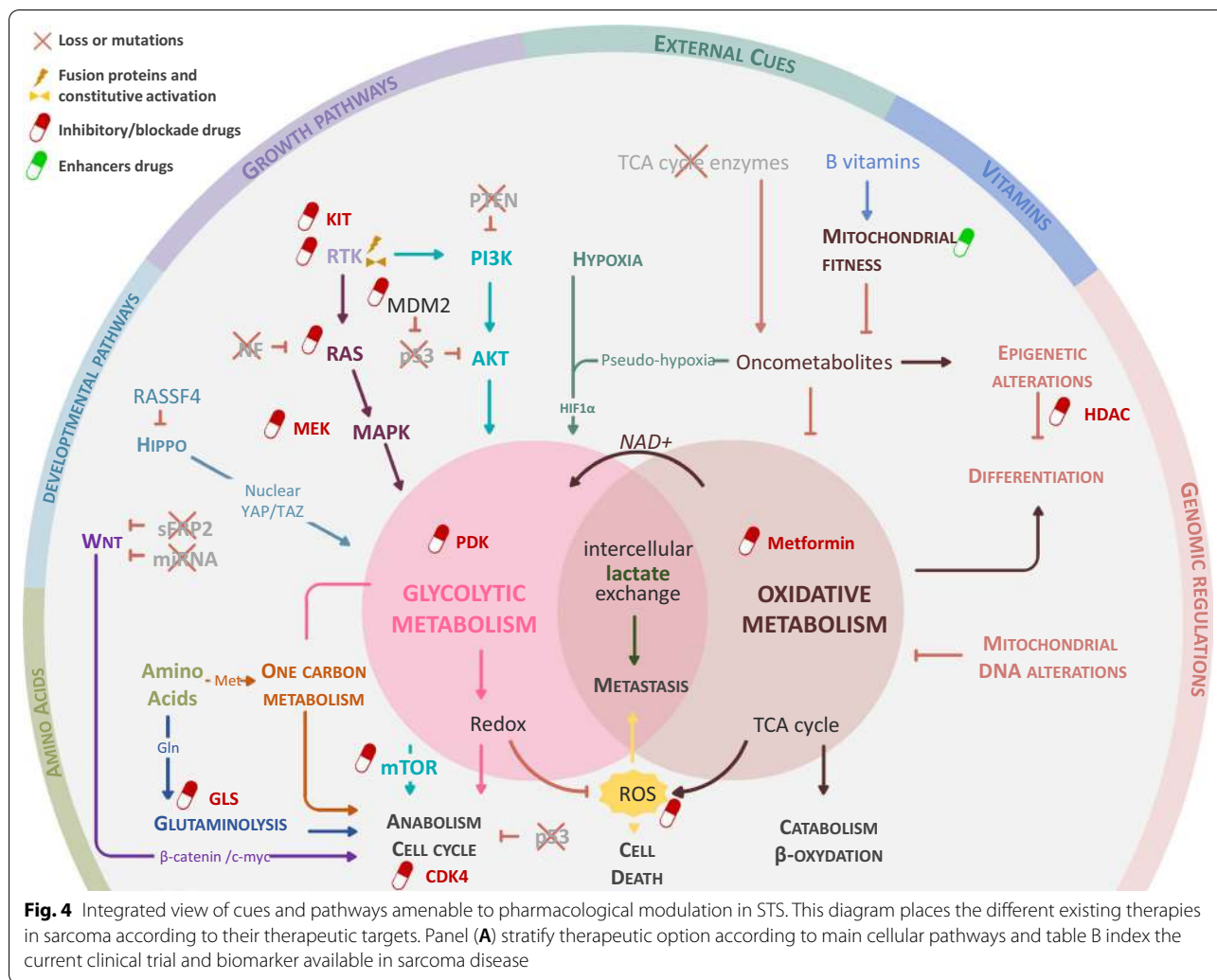


Fig. 3 (See legend on previous page.)



for proliferation. KHSV also provoked an increase in ASS1 expression, in part through the action of KHSV-encoded miRNAs [62], leading to increased arginine production. Knockdown of ASS1 inhibited cell proliferation and iNOS-dependent, arginine-derived NO production. Treatment of KS cells with a NO donor-activated STAT3 without affecting ROS cell levels. A recent article questioned the relevance of these metabolic changes by comparing 2D versus 3D cultures of KHSV-infected cells [135]. An unbiased metabolomics analysis revealed significant changes in the levels of various non-essential amino acids in 3D cultures. GST-pull down studies showed that the viral K1 protein physically interacted with and activated the pyrroline-5-carboxylate reductase PYCR leading to increased proline production. This phenotype, abrogated by PYCR depletion, promoted 3D spheroid culture and tumorigenesis in nude mice. These results highlight the complex metabolic rewiring that occurs during infection and transformation by KHSV but

also the need for appropriate in vitro culture systems to evaluate metabolic adaptation.

One carbon metabolism is overactive in aggressive STS

In Ewing’s sarcoma (EWS), the fusion protein resulting from a single translocation event between the regulatory domain of EWS and the DNA-binding domain of FLI1 behaves as a chimeric transcription factor called EF that enhances IGFR1 activation (Fig. 2A). Transcriptomic studies [60, 64] identified EF as an upstream regulator of PHGDH, PSAT, PSPH and SHMT1/2 genes involved in serine-glycine biosynthesis as well as SLC1A4/5 glutamine transporter genes (Fig. 3). Accordingly, knock-down of EF reduced the proportion of glucose-derived 3-phosphoglycerate reoriented toward serine and glycine synthesis; EWS cell lines were highly dependent on glutamine for growth and survival. Earlier work using a metabolomics approach with isotope labeling had already shown that a large proportion of glycolytic carbon was

Table 2 Clinical trials affecting metabolic pathways in STS

	Biomarker target	Therapeutic agent	Tumor type	Biomarker relevance/clinical trial phase	N° Clinical trial	References
MAPK pathways	RAF	Dabrafenib	Advanced solid tumors with BRAF mutations	Phase II	NCT02465060	[75] [A] [B]
		Vemurafenib	Relapsed or refractory advanced solid tumors with BRAF V600 mutations	Phase II	NCT03220035	
		Dabrafenib + trametinib	MULTISARC	Phase III	NCT03784014	
		Dabrafenib + trametinib	BRAF V600E- mutated rare cancers	Phase II	NCT02034110	
	MEK1/2	Binimetinib + pexidartinib	Advanced GIST	Phase I completed	NCT03158103	[A] [B] [C]
		Trametinib	Advanced solid tumors with BRAF mutations	Phase II	NCT02465060	
		Cobimetinib + MPDL3280A	Locally advanced or metastatic solid tumors	Phase I	NCT01988896	
		GDC-0941 + GDC-0973	Locally advanced or metastatic solid tumors	Phase II	NCT00996892	
		Ulixertinib	STS, OS, EWS	Phase I/II	NCT03520075	[C]
		PI3K/AKT/mTOR signaling	PIK3CA/mTOR	Samotolisib	STS GIST	Phase I/II
	Pediatric sarcoma			Phase II MATCH trial	NCT03458728 NCI MATCH EAY131-Z1F	[77] [78]
	GDC-0941		Locally advanced or metastatic solid tumors	Phase I	NCT00876109	[A]
	GDC-0980		Locally advanced or metastatic solid tumors Refractory solid tumors	Phase I	NCT00876122 NCT00854152 NCT00854126	[A]
AKT/ERK	ONC201		Desmoplastic small round cell tumor	In vitro		[C]
	GDC-0973 + GDC-0068		Locally advanced or metastatic solid tumors	Phase I	NCT01562275	[A]
mTOR	Sirolimus + pexidartinib		STS MPNST	Phase I/II	NCT02584647	[79] [80] [A]
	Rapamycin + gemcitabine		OS	Phase II completed	NCT02429973	
	nanoparticle albumin-bound rapamycin + pazopanib		Advanced nonadipocytic soft tissue sarcomas	Phase I/II trial	NCT03660930	
	Lenvatinib + everolimus		Refractory pediatric solid tumors	Phase I/II	NCT03245151	
	CCI-779		STS/GIST	Phase II	NCT00087074	
	Cixutumumab + temsirolimus		Locally advanced, metastatic, or recurrent STS or bone sarcoma	Phase II	NCT01016015	
	CP-751,871 + RAD001		Advanced sarcomas and other malignant neoplasms	Phase I	NCT00927966	
Everolimus	RAD001/progressive sarcoma	Phase II	NCT00767819			

Table 2 (continued)

	Biomarker target	Therapeutic agent	Tumor type	Biomarker relevance/clinical trial phase	N° Clinical trial	References
HIPPO	YAP/TAZ	Verteporfin	High histological grade	Reduced EWS metastatic potential		[81] [82] [83] [84]
TCA CYCLE	IDH 1	IDH 1—AG-120	Chondrosarcoma	Phase I	NCT02073994	[85]
		IDH 1—FT-2102	Advanced solid tumors	Active	NCT03684811	[86] [87]
		IDH 1—IDH305	Advanced malignancies with IDH1R132 mutations	Phase I	NCT02381886	
		IDH 1—BAY1436032	IDH1-mutant advanced solid tumors	Active	NCT02746081	
	IDH2	AG-881	Advanced solid tumors with an IDH1 and/or IDH2 mutation	Phase I	NCT02481154	
		AG-120 + nivolumab	IDH1 mutant tumors	Phase II	NCT04056910	
	TCA cycle enzymes	Devimistat	STS	FDA orphan drug designation		[D]
Amino acids	ASS1 deficiency	ADI-PEG20 + gemcitabine + docetaxel	STS, OS, EWS	Phase II	NCT03449901	[88] [89]
	PDK	DCA	FS	Mice		[90]
	GLS	CB-839—glutaminase inhibitor	GIST	Phase I completed	NCT02071862	[59]
		Telaglenastat	NF1 mutation positive MPNST	Phase II	NCT03872427	
		Telaglenastat + talazoparib	Solid tumors	Phase I + phase II	NCT03875313	
	Heparan sulfate proteoglycans	Sulfen	EWS	Zebrafish model		[91]
	NAMPT	FK866—MV87 inhibitors	FS	Mice		[92]
	Folate receptor α	Pemetrexed	STS	Phase II	NCT04605770	[C]
Lipid metabolism	CPI-613	CCS	Phase II	NCT01832857	[A] [E]	

[A] The Life Raft Group. Gisttrials. <https://gisttrials.org/iLRG/showfirstline.php>. Accessed 16 June 2021

[B] NIH U.S. National Library of Medicine. Clinicaltrial.gov. <https://clinicaltrials.gov/ct2/home>. Accessed 16 June 2021

[C] NIH. Cancer.gov. <https://www.cancer.gov/about-cancer/treatment/clinical-trials/search/?loc=0&q=sarcoma&rl=1>. Accessed 16 June 2021

[D] Rafael Pharmaceuticals, Inc. <https://rafaelpharma.com/research-and-development/cpi-613-drug>. Accessed 16 June 2021

[E] ICH GCP. Good Clinical Practice Network. <https://ichgcp.net/clinical-trials-registry/NCT04593758>. Accessed 16 June 2021

diverted into serine and glycine metabolism in melanoma; this was due to the amplification of the PHGDH gene [136], also elevated in high-risk EWS patients [100]. Serine or glycine can provide one carbon to tetrahydrofolate initiating the folate cycle. The enhancement of one-carbon metabolism, considered as an integrator of nutrient status [97], boosts the interconnected folate and methionine cycles leading to enhanced NADPH and nucleotide synthesis. NADPH regulates ROS-dependent death and methyl transfer contributes to epigenetic modifications. Knockdown of PHGDH recapitulated the

effect of anti-metabolite chemotherapies and had a major effect on cell growth and epigenetic control. Two studies investigated the sensitizing effect of methionine restriction on chemo- or radio resistant models of RAS-driven colorectal cancer and STS, respectively [137, 138]. In the FSF Kras^{G12D/+}; Tp53^{-/-} STS mouse model, tumor development was triggered by the intramuscular injection of an adenovirus carrying the FlpO recombinase. In these aggressive tumors, only the combination of diet and radiation delayed tumor growth. By combining tumor metabolomics and metabolite tracing with a time-course

analysis of data, alterations were observed for nucleotide and redox metabolisms. Interestingly, the consequences of methionine restriction could be detected at the metabolic level when applied to healthy individuals. These results indicated that a targeted dietary manipulation could improve tumor response to therapies.

Linking Wnt signaling alterations to metabolic rewiring

Physiologically, the canonical Wnt pathway participates to the maintenance of stem cell pools and cell fate, in part via the nuclear translocation of β -catenin, leading to its interaction with TCF/LEF transcription factors [139]. In a model of osteoblast differentiation, Wnt3a signaling induces aerobic glycolysis by increasing the level of glycolytic effectors (HK2, LDHA, PDK1, GLUT1). This process requires LRP5-mediated mTORC2/AKT activation but not β -catenin [140]. Other studies showed that Wnt engagement also reduced nuclear acetyl coenzyme A (AcCoA) levels and consequently impaired osteoblastic gene expression [141]. In contrast, in mature osteoblasts, Wnt-LRP5 boosted fatty acid oxidation and was required for bone mass increase [142]. In osteosarcoma (OS), Wnt participates in bone remodeling, maintenance of stem cell niches and EMT in collaboration with TGF- β and BMP signaling (reviewed in [143, 144]). In EWS, synovial sarcoma (SS), OS, and to a lesser extent in LMS [143, 145], a high level of Wnt activation, scored by the nuclear localization of β -catenin or LEF-1, is associated with a poor clinical outcome [46]. In OS, deletion of Wnt-related genes has been reported [146]. In some primary OS, the loss of the tumor suppressor RASSF1A enhanced Wnt activation through the AKT/GSK-3-Wnt/ β -catenin pathway [147]. Other studies indicated that MEG3, a long non-coding RNA downregulated in OS, controlled the expression of several tumor suppressor genes and oncogenes including *P53*, *RB*, *MYC* and *TGF- β* ; it also negatively regulated the expression of microRNA-184 (miR-184) and down-stream effectors of the Wnt/ β -catenin pathway including β -catenin, TCF4 and c-MYC [148]. Therefore, downregulation of MEG3 attenuated its tumor suppressive effect and partly resulted in the upregulation of Wnt signaling. In this model, its impact on cell metabolism relied on mTORC1-mediated activation of the S6 kinase pathway and protein synthesis. In EWS, Wnt activation was also essential for the acquisition of a metastatic phenotype and controlled a proangiogenic switch via the secretion of specific extracellular matrix (ECM) proteins called angiogenic matrix in a TGF- β -dependent context [47]. However, overexpression of sFRP2, a secreted Wnt antagonist, promoted osteosarcoma invasion and metastatic potential [149]. Therefore, Wnt participates at various stages of STS progression.

Loss of tumor suppressors affects several metabolic pathways

Tumor suppressors interrupt cell cycle and growth in a stressed environment, in part by regulating access to trophic pathways. Patients and mice carrying a hereditary defect in p53 (Li Fraumeni syndrome) or Rb1 (retinoblastoma) show a predisposition to sarcomas [49, 150]. In low/medium grade STS such as well-differentiated liposarcoma (WDLPS), the initial oncogenic event is the amplification of the p53 inhibitor MDM2. InDDLPS, MDM2 amplification synergizes with alterations affecting genes that regulate growth such as *CDK4* and *FRS2* [4], or that are required for adipocyte differentiation such as *JUN*, *DDIT3*, *PTPRQ*, *YAP1* or *CEBPA*, or with alterations of DNA methylation. More generally, in STS with complex genomes (LMS, UPS, MFS, LPS, MPNST), the accumulation of frequent somatic copy number alterations (SCNAs) and/or focal mutations of TSGs leads to the deregulation of the PI3K/AKT/mTOR axis, mitosis and chromosomal maintenance [48]. As in most cancers, the timing of occurrence of p53 mutations affects tumor progression and prognosis [8, 151–153]. Similarly, in mice, the combined loss of p53 [154] or *CDKN2A* (*Ink4/Arf*) [66] TSGs with oncogenic RAS lead to the development of undifferentiated STS. Conditional mutations in *KRAS* and p53 in muscle were sufficient to provoke high-grade STS with myofibroblastic differentiation [155].

As highlighted in Fig. 2A, p53 and AKT exert a negative feedback loop on each other, through PTEN and MDM2 regulation, respectively. Also, p53 indirectly counteracts AKT-dependent downstream effects on growth, apoptosis or metabolism [156, 157]. The tumor suppressive function of p53 depends on its role as transcription factor inducing cell cycle arrest or apoptosis via the *CDKN1A* (p21), or *PUMA* and *NOXA* effectors, respectively (Fig. 2A). However, in their absence, tumor suppression persists suggesting that additional mechanisms [158], including those with an impact on metabolism [156, 159] are also important (Fig. 3). Indeed, *GLUT* gene transcription is enhanced in STS-bearing p53 mutations [160, 161]. p53 is anti-glycolytic partly through the induction of the expression of *TIGAR* and *PARK2* regulators [162, 163]. *TIGAR* dephosphorylates fructose biphosphate (FBP) into fructose-6-phosphate (F6P), shifting glucose-6-phosphate (G6P) back toward the pentose phosphate pathway (PPP). Furthermore, the cytosolic form of p53 interacts with and inhibits G6P-dehydrogenase (G6PDH) by preventing the formation of the active dimer, therefore inhibiting PPP-dependent redox control and anabolism [164] (Fig. 3). Since *TIGAR* expression is not strictly p53-dependent, the resulting p53 effect may be difficult to predict with regards the engagement of the PPP, but it globally interferes with glycolysis. In STS, deep deletions

or more frequently amplifications of TIGAR have been documented and high TIGAR expression correlates with a better outcome [50]. *PARK2/Parkin* is an E3 ubiquitin ligase regulating the degradation of mitochondrial proteins. It cooperates with the mitochondrial serine/threonine kinase PINK1 and contributes to mitochondrial fitness [163, 165]. p53-mediated mitochondrial homeostasis also involves the quality control of mitochondrial DNA (mtDNA) and the expression of cell death regulators [166]. Finally, p53 induces the expression of pyruvate decarboxylase (PDC) that regenerates mitochondrial oxaloacetate and reinitiates the TCA cycle, and that of isocitrate dehydrogenase 1 (IDH1) that converts cytosolic citrate into α -ketoglutarate. In a KRAS driven-PDAC model, p53-dependent accumulation of cytosolic α -ketoglutarate activates aKGDD enzymes that regulate 5-hydroxymethylcytosine-producing TET enzymes, allowing tumor cell differentiation and growth control [167] (Fig. 3).

Metabolic fluxes and mitochondrial fitness in STS

Metabolite fluxes between organelles regulate the efficiency of various metabolic pathways in cells, but also contribute to the plasticity of metabolic adaptation.

Metabolic imbalances in STS

Through their evolution, most tumors tend to acquire metabolic features including an increase in nucleotide synthesis [168]. Investigations using PET-FDG uptake in STS patients confirmed the strong glycolytic bias documented in metastasized and poor prognosis STS [169, 170] such as ARMS [171] or ES [172]. However, these studies also revealed the considerable heterogeneity within a given tumor and between different tumor types, suggesting that the Warburg phenotype might be unstable and amenable to pharmacologic control [173]. Whereas the level of oxidative phosphorylation (OXPHOS) varies between tumors (Fig. 1), there is a general correlation between reduced mitochondrial activity, an epithelial-to-mesenchymal transition (EMT) gene signature and a poor prognosis [168]. Some STS tend to exhibit high levels of mitochondrial respiration compared to carcinomas (Fig. 1) [55, 174]. In vitro analysis of OS and RMS cell lines showed differences in the reliance on glycolysis versus respiration of tumors, with ARMS being in general less oxidative than OS or ERMS [175]. The equilibrium between glycolysis and mitochondrial respiration can be affected by various oncogenic alterations and/or metabolic requirements. Accordingly, the receptor tyrosine kinase Her4/ErbB4, an EGFR family member, is upregulated in several cancers including OS [176]. Exploration of xenograft models using untargeted metabolomics and ^{18}F -FDG microPET/CT scan

approaches showed that Her4 overexpression boosted glycolysis, glutaminolysis and OXPHOS in tumors. This hypermetabolic phenotype contributed to sustained growth and ATP production while conferring chemoresistance, as also shown in PDAC [177].

The crosstalk between metabolic pathways can also be altered in cancer as discussed in the following examples. Firstly, the upstream reaction committing glucose to glycolysis is catalyzed by phosphofructokinase-1 (PFK-1), itself allosterically inhibited by high ATP levels [178] (Fig. 3). Cancer cells express various PFK isoenzymes [179] such as the bifunctional 6-phosphofructo-2-kinase/fructose-2,6-bisphosphatase (PFKFB) that produces F2,6-BP, thereby overriding ATP-dependent inhibition of PFK1 [180, 181] (Fig. 3). Reciprocally, an activation of a F1,6-biphosphatase such as FBP1 enhances the gluconeogenic flow and restrains glycolysis [174]. The FBP2 isoform is frequently lost in STS including LPS, FS, LMS and UPS and lower FBP2 mRNA levels correlated with poor survival in LPS [55]. In the latter study, increasing FBP2 expression impaired sarcoma cell growth, through glycolysis inhibition and induction of mitochondrial biogenesis. The latter effect was due to FBP2 nuclear translocation where, independently of its enzymatic activity, it interacted with and inhibited c-Myc-driven transcriptional activation of TFAM, an inducer of mitochondrial biogenesis [182].

Secondly, the maintenance of glycolytic flow requires the regeneration of NAD^+ which originates from cytosolic lactate dehydrogenase (LDH) activity and from the malate aspartate shuttle between mitochondria and cytosol [183] (Fig. 2). By regulating NAD^+ levels, mitochondrial activity limits glycolysis and consequently the Warburg effect [184]. This suggests that the persistence of mitochondrial activity can be beneficial to tumors. In addition, an LDH activity has been identified in the mitochondria where it catalyzes the aerobic oxidation of lactate into pyruvate. It is thought to contribute to the maintenance or enhancement of OXPHOS in glycolytic cells [185, 186]. Pyruvate oxidation in the mitochondria depends on PDH activity, itself inhibited by PDK. The inhibition of PDK by dichloroacetate (DCA) shifts metabolism from glycolysis to glucose oxidation and boosts ROS production as well as mitochondria-dependent apoptosis in tumors [187]. This effect is exploited in EWS and other tumors where DCA synergizes with apoptosis-inducing drugs such as cisplatin. Manipulating ROS levels appears to be a promising therapeutic approach [188]. Indeed, scavenging mitochondrial ROS (mtROS) induces p53, reduces the cell transforming potential of oncogenic RAS and in some fibrosarcoma (FS) and RMS model cell lines suppresses tumor growth [17, 189].

Thirdly, the level of mitochondrial activity depends on the availability of coenzyme A (CoA) and the acetylated form, AcCoA. CoA synthesis requires the intracellular phosphorylation of pantothenate (or vitamin B5) by pantothenate kinases [190]. Reciprocally, pantothenate derives from the recycling of food-derived or cellular CoA through an extracellular degradative process involving the vanin pantetheinases [191, 192]. Interestingly, a high vanin1 (*VNN1*) level correlates with a better prognosis in STS patients [66]. Lack of *Vnn1* in *CDKN2A* deficient mice enhanced the proportion of fibrosarcomas compared to that of other cancers. In RAS-driven mouse STS lines, *Vnn1* exerted an anti-Warburg effect by enhancing CoA levels and mitochondrial activity to the detriment of glycolysis, and by maintaining cell differentiation.

Mitochondrial abnormalities disrupt the TCA cycle

Mitochondrial biogenesis depends on the transcriptional coactivator PGC1 α [193]. This process regulates the transition from myoblast growth to differentiation and requires a switch from the classical to the alternative NF- κ B activation pathway. The latter controls *PGC1 α* transcription [194], in cooperation with MyoD [195]. In RMS and OS models, an alteration in this switch leads to the induction of the pro-glycolytic HK2 isoform through the persistent activation of the classical NF- κ B pathway [196] (Fig. 3). This might also contribute to the incomplete mitochondrial biogenesis observed in a rat RMS model featuring a deficiency in respiratory potential and poor mtROS control, thereby enhancing tumorigenesis [197].

Mutations in TCA enzymes SDH [198] and FH [95], found in STS [57], are frequent in wild-type GIST without KIT or PDGFRA mutations [152]. They provoke an interruption of the TCA cycle, uncoupled from ATP production. Consequently, excess succinate diffuses in the cytoplasm where it inhibits aKGDD enzymes involved in the regulation of epigenetic modifications, DNA repair [199] or HIF degradation, rewiring cells toward glycolysis [200]. In a mouse ovarian cancer model, targeted knock-down of *Sdhb* resulted in enhanced proliferation and lead to a hypermethylated epigenome promoting EMT [198]. Using metabolic tracing and SeaHorse analysis, the authors documented an increased reliance on glutamine for cell survival and a reduced mitochondrial reserve capacity, rendering cells highly sensitive to the complex I inhibitor metformin.

Mutations in IDH1 and 2 lead to the production of 2-hydroxyglutarate [201], an inducer of HIF1 α stabilization. *HIF1 α* expression and hypoxia are associated with poor survival of sarcoma patients [68–70, 202–204].

Hypoxia regulates apoptosis resistance, cancer stemness, metastatic properties in RMS [71, 205] and is involved in ES, GIST and LPS progression [69, 70, 203, 204]. Uncoupling of electron transport chain (ETC) complexes from ATP production does not impede anaplerotic mitochondrial uptake of glutamine, transformed into glutamate via the activity of GLS to feed the reverse metabolic flow toward citrate production and anabolism [206] (Fig. 3). Accordingly, the growth of STS subtypes overexpressing GLS is sensitive to glutamine depletion in vitro and glutaminase inhibition in vivo [59].

Some components of the ETC are encoded by mtDNA. Therefore, alterations in mtDNA may lead to respiratory defects. In OS, insufficient or altered mtDNA is associated with stressed mitochondria and enhanced tumor invasiveness [207]. In an OS cell line, ethidium bromide induced-mtDNA depletion provoked a deficiency in cytochrome oxidase and OXPHOS, leading to enhanced glycolysis and EMT [208, 209]. Furthermore, mitochondrial dysfunction and loss of transmembrane potential provoked high cytosolic Ca²⁺ levels, triggering calcineurin-dependent mitochondria-to-nucleus retrograde signaling that resulted in AKT activation and glycolysis [210]. In a tunable model of mitochondrial dysfunction using cytoplasmic hybrids [57], impairment of respiration lead to NADH accumulation and cytosolic recycling into NAD⁺ by the malate deshydrogenase pathway. NAD⁺ boosted glycolysis and ATP-dependent cell migration. This suggests that glycolysis-derived ATP might be preferentially used during cell migration [211]. In conclusion, there is a high intra- and inter-tumor heterogeneity in mitochondrial activity, which can be enhanced or lost, depending on the tumor context.

Tumor metabolome impacts STS progression

Metastasis

Aerobic glycolysis induced by oncogenic or hypoxic signaling provokes changes in the tumor metabolome. Lactate excretion, hypoxia-associated hypercapnia and acidification of the extracellular milieu accelerate the degradation of the extracellular matrix and facilitate metastasis [212, 213]. Reciprocally, as shown in STS [214, 215], cancer-associated fibroblasts can produce lactate and 3-hydroxybutyrate that boost cell growth, metastasis and angiogenesis when administered to tumor-bearing mice [216–218]. Lactate uptake by tumors feeds their oxidative metabolism [212, 216, 219] and requires the importer MCT1, a marker of mitochondrial activity and stemness in cancer and a target gene of the fusion protein ASP-SCR1/TFE3 in alveolar soft part sarcoma (ASPS) [220]. The persistence of mitochondrial activity can enhance metabolic plasticity [221], mtROS-driven anoikis, metastasis [222, 223] or resistance to therapy as shown for LPS

[224]. Metabolic plasticity, required during EMT transition [225], is still incompletely documented in poorly polarized and migration-prone mesenchymal tumor cells such as sarcoma cells [226]. Indeed, hybrid epithelial/mesenchymal (E/M) phenotypes or switching from E- to N-cadherin and vimentin expression contribute to aggressiveness, metastatic properties and drug resistance [226–229]. In addition, fusion protein events and translocations, frequent in childhood STS, can regulate epithelial differentiation [230, 231]. EMT is induced by cytokines such as FGFs, PDGF, TGF- β that enhance glycolysis and TCA activity [232]. TGF- β signaling synergizes with the AKT and NF- κ B pathways, both potent drivers of glycolysis [233], but also antagonizes PDK4, thereby allowing pyruvate entry into the TCA. YB-1, an enhancer of HIF1 α translation, is overexpressed in high-risk human sarcomas and promotes EMT and metastasis [234]. Hypoxia regulates the expression of several intracellular collagen-modifying enzymes, particularly OGDH enzymes that hydroxylate proline and lysine residues, contributing to the quality of collagen folding and the stiffness of the tissue, and thereby affecting cell migration [235]. In a UPS model, HIF1 α enhances the expression of the intracellular enzyme procollagen-lysine, 2-oxoglutarate 5-dioxygenase 2 (PLOD2). Loss or overexpression of PLOD2 abrogates or restores, respectively, the metastatic potential of HIF1 α -deficient tumors and human sarcomas show elevated HIF1 α and PLOD2 expression in metastatic primary lesions [236]. Finally, HIF can enhance ECM degradation through the induction of various metalloproteases such as MMP or PLAUR, facilitating invasiveness.

Immunoreactivity

Several features including the level of infiltration of cytotoxic CD8⁺T cells or of myeloid cells, the expression of markers of immune-stimulation or -depression and the localization of these cells within the tumor, emerge as landmarks of tumor immunogenicity [8, 237–240]. STS display low mutational burden as compared to other cancer types and are generally considered to be poorly immunogenic and poorly responsive to immune checkpoint blockade [8, 241]. Synovial sarcoma, soft tissue and undifferentiated LMS are the three subtypes with the lowest CNV [8, 237] and display reduced immune infiltration, virtually devoid of lymphocytes [242–245]. In contrast, STS with several SCNAs, nucleotide and chromosome instabilities, such as undifferentiated LPS, MPNST [246–248], AS and GIST [243] and OS [244] can present high levels of lymphoid infiltration including CD8⁺ T cells. Consequently, STS display a wide range of immunophenotypes [238, 249, 250]. The metabolic rewiring imposed by tumors generates a situation

of competition for essential energetic resources. This concerns glucose, vitamins and essential amino acids (serine, leucine, methionine, etc.) leading to impairment of immune cell functions and memory [19, 251, 252]. The exchange of fatty acids is required for the survival of immunosuppressive myeloid cells [253] or Tregs [254], particularly under conditions of activation of the PI3K/AKT/mTOR axis that boosts lipogenesis [255]. Other metabolites such as extracellular nucleotides released upon cell death can induce immunosuppression via various mechanisms [256–258]. Altogether, metabolic disturbances imposed by tumor cells directly contributes to the reorganization of the microenvironment but an exhaustive analysis of the immune landscape in STS is still lacking. Techniques such as Met-Flow [31] or SCEN-ITH [32] should help dissecting the metabolic status of immunocytes.

Conclusions

Unraveling the complexity of sarcoma genetics has benefited from the development and improvement of multi-omics strategies. The phenotypic and molecular description of genomic alterations can now be complemented with the identification of prognostic mechanistic signatures in patients. The heterogeneity and scarcity of STS originally limited the description of their metabolic landscapes but PET-FDG analysis has contributed to their staging, prognostication and evaluation of their response to therapy. Several cell-autonomous pathways or environmental factors influence the degree of conversion toward aerobic glycolysis, justifying the use of drugs that antagonize these processes. Nevertheless, the classic distinctions between glycolytic and oxidative tumors must be carefully reconsidered; hybrid phenotypes may confer more adaptable behaviors to STS cells. Several important metabolic pathways associated with STS progression such as those of one carbon and arginine metabolisms, or the PGI pathway might provide novel therapeutic options in combination with conventional therapies. In addition, the development of novel animal models or 2D/3D culture systems has highlighted the metabolic plasticity of these tumors that may impact their energetic resources. However, these adaptations may have a price, rendering tumor cells more sensitive to combined therapies.

Oncogenic signals can lead to the expression of isoforms of glycolytic enzymes that display new functions tilting the balance between glycolysis and mitochondrial activity. Similarly, p53 can also act as a regulator of G6PDH activity, impacting biosynthetic pathways. Some metabolites such as α -ketoglutarate have emerged as key effectors of p53 action, whereas others behave as onco-metabolites leading to alterations of genome integrity,

metastatic behavior and therapeutic response. The balance between glycolysis, glutaminolysis and OXPHOS depends on the respective availability of key metabolites, such as amino acids, NAD⁺/NADH, lactate or VitB5, that regulate STS progression or differentiation. Metabolic studies have already shown that novel metabolite signatures will complement conventional biomarkers and help stratifying prognosis and therapeutic options. The stability of the glycolytic phenotype also depends on mitochondrial activity. Alterations of mitochondrial fitness observed in STS upon alterations of mtDNA or TCA enzymes aggravate the prognostic of tumors or can affect their chemoresistance. An unstable tumor metabolome has tumor-intrinsic or extrinsic effects causing it to be pro-metastatic or immunosuppressive. Therefore, the combination of drugs targeting different metabolic pathways should impact both tumor and immune cells in a concerted manner to reinvigorate anti-tumor immunity while tilting the balance toward cell differentiation over growth.

Abbreviations

3HB: 3-Hydroxybutyrate; AcCoA: Acetyl coenzyme A; AIDS: Acquired immunodeficiency syndrome; aKGDD: Alpha-ketoglutarate dioxygenase; ARMS: Alveolar rhabdomyosarcoma; AS: Angiosarcoma; ASPS: Alveolar soft part sarcoma; ATF6: Activating transcription factor 6; ATRX: α -Thalassemia/mental retardation syndrome x-linked; BCL2: B-cell cell/lymphoma 2; BCL-XL: B-cell lymphoma-extra large; BIM: BCL-2-interacting mediator of cell death; BLCA: Bladder urothelial carcinoma; BMP: Bone morphogenetic proteins; BRCA: Breast invasive carcinoma; CAF: Cancer-associated fibroblast; CDK4: Cyclin-dependent kinase 4; CDKN1A = p21: Cyclin-dependent kinase inhibitor 1a; CDKN2A = p16: Cyclin-dependent kinase inhibitor 2a; CEBPA: CCAAT/enhancer-binding protein alpha; CNV: Copy number variations; CS: Canine sarcoma; DCA: Dichloroacetate; DDIT3: DNA damage-inducible transcript 3; DDLPS: Dedifferentiated liposarcoma; DNMT1: DNA methyltransferase 1; ECM: Extracellular matrix; EF: EWS/FLI1 fusion protein; EGR1: Early growth response protein 1; EMT: Epithelial to mesenchymal transition; ERMS: Embryonal rhabdomyosarcoma; ESCA: Esophageal carcinoma; ETC: Electron transport chain; EWS: Ewing sarcoma; F2,6BP: Fructose-2,6-bisphosphate; FASL: Fas ligand; FBP: Fructose-biphosphate; FGFs: Fibroblast growth factors; FLI1: Friend leukemia integration 1 transcription factor; FRS2: Fibroblast growth factor receptor substrate 2; FS: Fibrosarcomas; FUS/DDIT3: Fused in sarcoma (FUS) to DNA damage inducible transcript 3 (DDIT3); G6P: Glucose-6-phosphate; GFR: Growth factor receptor; GIST: Gastrointestinal stromal tumor; GLUT: Glucose transporter; GSK: Glycogen synthase kinase; GTPase: Guanosine triphosphate hydrolase; HHV8: Human herpes virus 8; HIF: Hypoxia inducible factor; HIPPO: Hippopotamus (according to the tissue overgrowth); HK: Hexokinase; IAP: Inhibitors of apoptosis proteins; IDH1: Isocitrate dehydrogenase 1; IGF1: Insulin-like growth factor 1; IGF1R: Insulin-like growth factor 1 receptor; KRAS: Kirsten rat sarcoma viral; KS: Kaposi sarcoma; KSHV: Kaposi sarcoma-associated herpesvirus; LDH: Lactate deshydrogenase; LEF-1: Lymphoid enhancer-binding factor 1; LIHC: Liver hepatocellular carcinoma; LMS: Leiomyosarcoma; lncRNA: Long non-coding RNA; LPRS: Low-density lipoprotein receptor-related protein 5; LPS: Liposarcoma; LUAD: Lung adenocarcinoma; LUSC: Lung squamous cell carcinoma; MAPK: Mitogen-activated protein kinase; MCA: Methylcholanthrene; MCL1: Myeloid leukemia cell differentiation protein; MCT: Monocarboxylate transporter; MDH: Malate dehydrogenase; MDM2: Mouse double minute 2 homolog; MEG3: Maternally expressed 3; MEK: Mitogen-activated protein kinase; MESO: Mesothelioma; MFS: Myofibrosarcoma; MFH: Malignant fibrous histiocytoma (equivalent to UPS); miR: Micro RNA; mitROS: Mitochondrial reactive oxygen species; MLS: Myxoid liposarcoma; MMP: Matrix

metallopeptidases; MPNST: Malignant peripheral nerve sheath tumors; MSC: Mesenchymal stem cells; mtDNA: Mitochondrial DNA; mTOR: Mammalian target of rapamycin; mTORC1: Mammalian target of rapamycin complex 1; MyoD: Myoblast determination protein 1; NAD: Nicotinamide adenine dinucleotide; NADPH: Nicotinamide adenine dinucleotide phosphate; ncRNA: Non-coding RNA; NF: Neurofibromin; NFkB: Nuclear factor kappa-light-chain-enhancer of activated b; NOX: NADPH oxidase; NOXA: Phorbol-12-myristate-13-acetate-induced protein 1; OAA: Oxaloacetate; OS: Osteosarcoma; OVCA: Ovarian serous cystadenocarcinoma; OXPHOS: Oxidative phosphorylation; PARK2: Phosphatidic acid-regulated protein kinase; PAAD: Pancreatic adenocarcinoma; PDAC: Pancreatic ductal adenocarcinoma; PDC: Pyruvate decarboxylase; PDGF: Platelet-derived growth factor receptors; PDHK: Pyruvate dehydrogenase kinase; PDK: 3-Phosphoinositide-dependent protein kinase; PERK: Protein kinase r-like endoplasmic reticulum kinase; PET-FDG: Fluorine-18-fluorodeoxyglucose positron emission tomography; PFK: Phosphofruktokinase; PFKFB: 6-Phosphofruktose-2-kinase/fructose-2,6-bisphosphatase; PGC1 α : Peroxisome proliferator-activated receptor gamma coactivator 1-alpha; PGK1: Phosphoglycerate kinase 1; PHGDH: 3-Phosphoglycerate dehydrogenase; PI3K: Phosphatidylinositol-3-kinase; PKM2: Pyruvate kinase M2; PLAU: Plasminogen activator, urokinase receptor; PLOD2: Procollagen-lysine,2-oxoglutarate 5-dioxygenase 2; PPP: Pentose phosphate pathway; PSAT: Phosphohydroxythreonine aminotransferase; PSPH: Phosphoserine phosphatase; PTEN: Phosphatase and tensin homolog; PTPRQ: Protein tyrosine phosphatase receptor type q; RAC1: Phosphoserine phosphatase; RAS: Rat sarcoma oncogene; RASSF14: Ras-association domain family 1 isoform a; Rb1: Retinoblastoma protein; RMS: Rhabdomyosarcoma; ROS: Reactive oxygen species; RREB1: Ras-responsive element binding protein 1; S6K: S6 kinase; SCNAs: Somatic copy-number alterations; SHMT1/2: Serine hydroxymethyltransferase 1 and 2; SMARCB1: SWI/SNF-related, matrix-associated, actin-dependent regulator of chromatin, subfamily b, member 1; SS: Synovial sarcoma; STAD: Stomach adenocarcinoma; STS: Soft tissue sarcoma; SV: Structural variation; TA: Transit amplifying; TAZ: Transcriptional coactivator with PDZ-binding motif; TCA: Tricarboxylic acid cycle; TCF: T-cell factor; TEAD: Tea domain family member 1; TERT: Telomerase reverse transcriptase; TF: Transcription factor; TFAM: Transcription factor a mitochondrial; TGF- β : Transforming growth factor beta; TIGAR: p53-induced glycolysis regulatory phosphatase; P53: Tumor protein p53; TRAIL: TNF-related apoptosis-inducing ligand; TSC1/2: Tuberous sclerosis complex 1/2; TSG: Tumor suppressor gene; UPR: Unfolded protein response; UPS: Undifferentiated pleomorphic sarcoma; VEGF: Vascular endothelial growth factor; vGPCR: Viral encoded g protein-coupled receptor; VHL: Von Hippel-Lindau tumor suppressor; VNN1: Vanin-1; WDLS: Well-differentiated liposarcoma; WNT: Wingless/integrated; YAP1: Yes-associated protein; YB-1: Y-box binding protein 1.

Acknowledgements

We wish to thank Alice Carrier, Romain Roncagalli, Rafael Arguello and Jean Erland Ricci for their critical reading of the manuscript and Jonathan Ewbank for revising English expression. Guillaume Charbonnier performed the bioinformatics analysis of the TCGA database.

Authors' contributions

RM and PN drafted the manuscript and prepared the figures. RM, VM, FG collected the references and participated in the discussion. JYB and PN designed the review. All authors read and approved the final manuscript.

Funding

Richard Miallot is a recipient of an INCA doctoral fellowship (PLBIO19-015). Philippe Naquet is supported by institutional funding from CNRS, INSERM, and AMU, as well as grants from Fondation pour la Recherche Médicale (DEQ20140329532), ARC (PJA 20181208002) and INCA (PLBIO19-015). Jean Yves Blay is supported by funds from NetSARC, LYRIC (INCA-DGOS 4664), Lyon Recherche Innovation contre le CANCER, European Clinical trials in Rare Sarcomas (FP7-278742), and European network for Rare Adult solid Cancer.

Availability of data and materials

Data used for the bioinformatics analysis come from the publicly available TCGA database. The code to reproduce the analysis is available at GitHub (<https://github.com/guillaumecharbonnier/mw-miallot2021>).

Declarations

Ethics approval and consent to participate

Not applicable.

Consent for publication

Not applicable.

Competing interests

The authors declare that they have no competing interests.

Author details

¹Centre National de la Recherche Scientifique, Institut National de la Santé et de la Recherche Médicale, Centre d'Immunologie de Marseille Luminy, Aix Marseille Univ, Marseille, France. ²Centre Léon Bérard, Lyon 1, Lyon Recherche Innovation contre le Cancer, Université Claude Bernard, Lyon, France.

Received: 24 February 2021 Accepted: 8 July 2021

Published online: 22 July 2021

References

- Lye KL, Nordin N, Vidyadaran S, Thilakavathy K. Mesenchymal stem cells: from stem cells to sarcomas. *Cell Biol Int*. 2016;40:610–8.
- Xiao W, Mohseny AB, Hogendoorn PCW, Cleton-Jansen A-M. Mesenchymal stem cell transformation and sarcoma genesis. *Clin Sarcoma Res*. 2013;3:10.
- Burningham Z, Hashibe M, Spector L, Schiffman JD. The epidemiology of sarcoma. *Clin Sarcoma Res*. 2012;2:14.
- Italiano A, Di Mauro I, Rapp J, Pierron G, Auger N, Alberti L, et al. Clinical effect of molecular methods in sarcoma diagnosis (GENSARC): a prospective, multicentre, observational study. *Lancet Oncol*. 2016;17:532–8.
- Skubitz KM, Skubitz AP, Xu WW, Luo X, Lagarde P, Coindre J-M, et al. Gene expression identifies heterogeneity of metastatic behavior among high-grade non-translocation associated soft tissue sarcomas. *J Transl Med*. 2014;12:176.
- Grimer R, Judson I, Peake D, Seddon B. Guidelines for the management of soft tissue sarcomas. *Sarcoma*. 2010;2010:1–15.
- Thanindrataran P, Dean DC, Nelson SD, Hornicek FJ, Duan Z. Advances in immune checkpoint inhibitors for bone sarcoma therapy. *J Bone Oncol*. 2019;15:100221.
- Abeshouse A, Adebamowo C, Adebamowo SN, Akbani R, Akeredolu T, Ally A, et al. Comprehensive and integrated genomic characterization of adult soft tissue sarcomas. *Cell*. 2017;171:950–965.e28.
- Guillou L, Aurias A. Soft tissue sarcomas with complex genomic profiles. *Virchows Arch*. 2010;456:201–17.
- Penel N, Coindre J-M, Giraud A, Terrier P, Ranchere-Vince D, Collin F, et al. Presentation and outcome of frequent and rare sarcoma histologic subtypes: a study of 10,262 patients with localized visceral/soft tissue sarcoma managed in reference centers. *Cancer*. 2018;124:1179–87.
- Taylor BS, Barretina J, Maki RG, Antonescu CR, Singer S, Ladanyi M. Advances in sarcoma genomics and new therapeutic targets. *Nat Rev Cancer*. 2011;11:541–57.
- Hanahan D, Weinberg RA. Hallmarks of cancer: the next generation. *Cell*. 2011;144:646–74.
- Koppenol WH, Bounds PL, Dang CV. Otto Warburg's contributions to current concepts of cancer metabolism. *Nat Rev Cancer*. 2011;11:325–37.
- Sinkala M, Mulder N, Patrick MD. Metabolic gene alterations impact the clinical aggressiveness and drug responses of 32 human cancers. *Commun Biol*. 2019;2:1–14.
- Galluzzi L, Kepp O, Vander Heiden MG, Kroemer G. Metabolic targets for cancer therapy. *Nat Rev Drug Discov*. 2013;12:829–46.
- Galluzzi L, Kepp O, Kroemer G. Mitochondria: master regulators of danger signalling. *Nat Rev Mol Cell Biol*. 2012;13:780–8.
- Ralph SJ, Rodríguez-Enríquez S, Neuzil J, Saavedra E, Moreno-Sánchez R. The causes of cancer revisited: "Mitochondrial malignancy" and ROS-induced oncogenic transformation—why mitochondria are targets for cancer therapy. *Mol Asp Med*. 2010;31:145–70.
- Sciacovelli M, Schmidt C, Maher ER, Frezza C. Metabolic drivers in hereditary cancer syndromes. *Annu Rev Cancer Biol*. 2020;4:77–97.
- Klein Geltink RI, Kyle RL, Pearce EL. Unraveling the complex interplay between T cell metabolism and function. *Annu Rev Immunol*. 2018;36:461–88.
- Rosario SR, Long MD, Affronti HC, Rowsam AM, Eng KH, Smiraglia DJ. Pan-cancer analysis of transcriptional metabolic dysregulation using The Cancer Genome Atlas. *Nat Commun*. 2018;9:5330.
- Liu X, Zhang A, Fang H, Li M, Song Q, Su J, et al. Serum metabolomics strategy for understanding the therapeutic effects of Yin-Chen-Hao-Tang against Yanghuang syndrome. *RSC Adv*. 2018;8:7403–13.
- Colaprico A, Silva TC, Olsen C, Garofano L, Cava C, Garolini D, et al. TCGAAbiolinks: an R/Bioconductor package for integrative analysis of TCGA data. *Nucleic Acids Res*. 2016;44:e71–e71.
- Anders S, Huber W. Differential expression analysis for sequence count data. *Genome Biol*. 2010;11:R106.
- Jassal B, Matthews L, Viteri G, Gong C, Lorente P, Fabregat A, et al. The reactome pathway knowledgebase. *Nucleic Acids Res*. 2020;48:D498–503.
- Yu G, Wang L-G, Han Y, He Q-Y. clusterProfiler: an R package for comparing biological themes among gene clusters. *OMICS J Integr Biol*. 2012;16:284–7.
- Chen J, Sun M, Hua Y, Cai Z. Prognostic significance of serum lactate dehydrogenase level in osteosarcoma: a meta-analysis. *J Cancer Res Clin Oncol*. 2014;140:1205–10.
- Zhong Z, Mao S, Lin H, Li H, Lin J, Lin J-M. Alteration of intracellular metabolome in osteosarcoma stem cells revealed by liquid chromatography–tandem mass spectrometry. *Talanta*. 2019;204:6–12.
- Lou S, Balluff B, de Graaff MA, Cleven AHG, Bruijn IB, Bovée JVMG, et al. High-grade sarcoma diagnosis and prognosis: biomarker discovery by mass spectrometry imaging. *Proteomics*. 2016;16:1802–13.
- Takahashi A, Nakayama R, Ishibashi N, Doi A, Ichinohe R, Ikuyo Y, et al. Analysis of gene expression profiles of soft tissue sarcoma using a combination of knowledge-based filtering with integration of multiple statistics. *PLoS ONE*. 2014;9:e106801.
- Sun C, Li T, Song X, Huang L, Zang Q, Xu J, et al. Spatially resolved metabolomics to discover tumor-associated metabolic alterations. *PNAS*. 2019;116:52–7.
- Ahl PJ, Hopkins RA, Xiang WW, Au B, Kaliaperumal N, Fairhurst A-M, et al. Met-Flow, a strategy for single-cell metabolic analysis highlights dynamic changes in immune subpopulations. *Commun Biol*. 2020;3:1–15.
- Argüello RJ, Combes AJ, Char R, Gigan J-P, Baaziz AI, Bousiquot E, et al. SCENITH: a flow cytometry-based method to functionally profile energy metabolism with single-cell resolution. *Cell Metab*. 2020;32:1063–1075.e7.
- Serrano C, Romagosa C, Hernández-Losa J, Simonetti S, Valverde C, Moliné T, et al. RAS/MAPK pathway hyperactivation determines poor prognosis in undifferentiated pleomorphic sarcomas. *Cancer*. 2016;122:99–107.
- Dodd RD. Emerging targets in sarcoma: rising to the challenge of RAS signaling in undifferentiated pleomorphic sarcoma: RAS/MAPK levels in UPS. *Cancer*. 2016;122:17–9.
- Mora J, Rodríguez E, de Torres C, Cardesa T, Ríos J, Hernández T, et al. Activated growth signaling pathway expression in Ewing sarcoma and clinical outcome. *Pediatr Blood Cancer*. 2012;58:532–8.
- Ahmed AA, Sherman AK, Pawel BR. Expression of therapeutic targets in Ewing sarcoma family tumors. *Hum Pathol*. 2012;43:1077–83.
- Noh B-J, Jung W-W, Kim H-S, Park Y-K. Pathogenetic implications of early growth response 1 in Ewing sarcoma. *Pathology*. 2019;51:605–9.
- Machado I, López-Guerrero JA, Scotlandi K, Picci P, Lombart-Bosch A. Immunohistochemical analysis and prognostic significance of PD-L1, PD-1, and CD8+ tumor-infiltrating lymphocytes in Ewing's sarcoma family of tumors (ESFT). *Virchows Arch*. 2018;472:815–24.
- Glorie N, Baert T. Circulating Protein Biomarkers to Differentiate Uterine Sarcomas from Leiomyomas. *Anticancer Res*. 2019;39:3981–9.
- Regina C, Hettmer S. Myxoid liposarcoma: it's a Hippo's world. *EMBO Mol Med*. 2019;11(5):e10470. <https://doi.org/10.15252/emmm.2019.0470>.

41. Mohamed AD, Tremblay AM, Murray GI, Wackerhage H. The Hippo signal transduction pathway in soft tissue sarcomas. *Biochim Biophys Acta (BBA) Rev Cancer*. 2015;1856:121–9.
42. Crose LES, Galindo KA, Kephart JG, Chen C, Fitamant J, Bardeesy N, et al. Alveolar rhabdomyosarcoma-associated PAX3-FOXO1 promotes tumorigenesis via Hippo pathway suppression. *J Clin Investig*. 2014;124:285–96.
43. Fullenkamp CA, Hall SL, Jaber OI, Pakalniskis BL, Savage EC, Savage JM, et al. TAZ and YAP are frequently activated oncoproteins in sarcomas. *Oncotarget*. 2016;7:30094–108.
44. Trautmann M, Cheng Y, Jensen P, Azoitei N, Brunner I, Hüllein J, et al. Requirement for YAP1 signaling in myxoid liposarcoma. *EMBO Mol Med*. 2019;11:e9889.
45. Tremblay AM, Missiaglia E, Galli GG, Hettmer S, Urcia R, Carrara M, et al. The Hippo transducer YAP1 transforms activated satellite cells and is a potent effector of embryonal rhabdomyosarcoma formation. *Cancer Cell*. 2014;26:273–87.
46. Pedersen EA, Menon R, Bailey KM, Thomas DG, Van Noord RA, Tran J, et al. Activation of Wnt/-catenin in Ewing sarcoma cells antagonizes EWS/ETS function and promotes phenotypic transition to more metastatic cell states. *Can Res*. 2016;76:5040–53.
47. Hawkins AG, Pedersen EA, Treichel S, Temprine K, Sperring C, Read JA, et al. Wnt/ β -catenin-activated Ewing sarcoma cells promote the angiogenic switch. *JCI Insight*. 2020;5:e135188.
48. Chibon F, Lagarde P, Salas S, Pérot G, Brouste V, Tirode F, et al. Validated prediction of clinical outcome in sarcomas and multiple types of cancer on the basis of a gene expression signature related to genome complexity. *Nat Med*. 2010;16:781–7.
49. Ballinger ML, Goode DL, Ray-Coquard I, James PA, Mitchell G, Niedermayr E, et al. Monogenic and polygenic determinants of sarcoma risk: an international genetic study. *Lancet Oncol*. 2016;17:1261–71.
50. Fang P, de Souza C, Minn K, Chien J. Genome-scale CRISPR knockout screen identifies TIGAR as a modifier of PARP inhibitor sensitivity. *Commun Biol*. 2019;2:16.
51. van Maldegem AM, Hogendoorn PC, Hassan AB. The clinical use of biomarkers as prognostic factors in Ewing sarcoma. *Clin Sarcoma Res*. 2012;2:7.
52. de Necochea-Campion R, Zuckerman LM, Mirshahidi HR, Khosrowpour S, Chen C-S, Mirshahidi S. Metastatic biomarkers in synovial sarcoma. *Biomark Res*. 2017;5:1–8.
53. Benz MR, Dry SM, Eilber FC, Allen-Auerbach MS, Tap WD, Elashoff D, et al. Correlation between glycolytic phenotype and tumor grade in soft-tissue sarcomas by 18F-FDG PET. *J Nucl Med*. 2010;51:1174–81.
54. Chen H, Chen Y, Liu H, Que Y, Zhang X, Zheng F. Integrated expression profiles analysis reveals correlations between the IL-33/ST2 axis and CD8⁺ T cells, regulatory T cells, and myeloid-derived suppressor cells in soft tissue sarcoma. *Front Immunol*. 2018;9:1179.
55. Huangyang P, Li F, Lee P, Nissim I, Weljie AM, Mancuso A, et al. Fructose-1,6-bisphosphatase 2 inhibits sarcoma progression by restraining mitochondrial biogenesis. *Cell Metab*. 2020;31:174–188.e7.
56. Pillozzi S, Bernini A, Palchetti I, Crociani O, Antonuzzo L, Campanacci D, et al. Soft tissue sarcoma: an insight on biomarkers at molecular metabolic and cellular level. *Cancers*. 2021;13:3044.
57. Gaude E, Schmidt C, Gammage PA, Dugourd A, Blacker T, Chew SP, et al. NADH shuttling couples cytosolic reductive carboxylation of glutamine with glycolysis in cells with mitochondrial dysfunction. *Mol Cell*. 2018;69:581–593.e7.
58. Zhang B, Yang L, Wang X, Fu D. Identification of a survival-related signature for sarcoma patients through integrated transcriptomic and proteomic profiling analyses. *Gene*. 2021;764:145105.
59. Lee P, Malik D, Perkons N, Huangyang P, Khare S, Rhoades S, et al. Targeting glutamine metabolism slows soft tissue sarcoma growth. *Nat Commun*. 2020;11:498.
60. Sen N, Cross AM, Lorenzi PL, Khan J, Gryder BE, Kim S, et al. EWS-FLI1 reprograms the metabolism of Ewing sarcoma cells via positive regulation of glutamine import and serine-glycine biosynthesis. *Mol Carcinog*. 2018;57:1342–57.
61. Huang H-Y, Wu W-R, Wang Y-H, Wang J-W, Fang F-M, Tsai J-W, et al. ASS1 as a novel tumor suppressor gene in myxofibrosarcoma: aberrant loss via epigenetic DNA methylation confers aggressive phenotypes, negative prognostic impact, and therapeutic relevance. *Clin Cancer Res*. 2013;19:2861–72.
62. Li T, Zhu Y, Cheng F, Lu C, Jung JU, Gao S-J. Oncogenic Kaposi's sarcoma-associated herpesvirus upregulates argininosuccinate synthase 1, a rate-limiting enzyme of the citrulline-nitric oxide cycle, to activate the STAT3 pathway and promote growth transformation. *J Virol*. 2019;93:e01599–e1618.
63. Choi YM, Yeo HK, Park YW, Lee JY. Structural analysis of thymidylate synthase from Kaposi's sarcoma-associated herpesvirus with the anticancer drug raltitrexed. *PLoS ONE*. 2016;11:e0168019.
64. Tanner JM, Bensard C, Wei P, Krah NM, Schell JC, Gardiner J, et al. EWS/FLI1 is a master regulator of metabolic reprogramming in Ewing sarcoma. *Mol Cancer Res*. 2017;15:1517–30.
65. Mutz CN, Schwentner R, Kauer MO, Katschnig AM, Kromp F, Aryee DNT, et al. EWS-FLI1 impairs aryl hydrocarbon receptor activation by blocking tryptophan breakdown via the kynurenine pathway. *FEBS Lett*. 2016;590:2063–75.
66. Giessner C, Millet V, Mostert KJ, Gensollen T, Vu Manh T-P, Garibal M, et al. Vnn1 pantetheinase limits the Warburg effect and sarcoma growth by rescuing mitochondrial activity. *Life Sci Alliance*. 2018;1:e201800073.
67. Lou S, Balluff B, Cleven AHG, Bovée JVMG, McDonnell LA. Prognostic metabolite biomarkers for soft tissue sarcomas discovered by mass spectrometry imaging. *J Am Soc Mass Spectrom*. 2017;28:376–83.
68. Li Y, Zhang W, Li S, Tu C. Prognosis value of Hypoxia-inducible factor-1 α expression in patients with bone and soft tissue sarcoma: a meta-analysis. *Springerplus*. 2016;5:1–10.
69. Aryee DNT, Niedan S, Kauer M, Schwentner R, Bennani-Baiti IM, Ban J, et al. Hypoxia modulates EWS-FLI1 transcriptional signature and enhances the malignant properties of Ewing's sarcoma cells in vitro. *Can Res*. 2010;70:4015–23.
70. Jham BC, Ma T, Hu J, Chaisuparat R, Friedman ER, Pandolfi PP, et al. Amplification of the angiogenic signal through the activation of the TSC/mTOR/HIF axis by the KSHV vGPCR in Kaposi's sarcoma. *PLoS ONE*. 2011;6:e19103.
71. Kilic M, Kasperczyk H, Fulda S, Debatin K-M. Role of hypoxia inducible factor-1 alpha in modulation of apoptosis resistance. *Oncogene*. 2007;26:2027–38.
72. Merry E. Predictive and prognostic transcriptomic biomarkers in soft tissue sarcomas. *npj Precis Oncol*. 2021;5:1–8.
73. Zwang Y, Oren M, Yarden Y. Consistency test of the cell cycle: roles for p53 and EGR1. *Can Res*. 2012;72:1051–4.
74. Jones SM, Kazlauskas A. Growth-factor-dependent mitogenesis requires two distinct phases of signalling. *Nat Cell Biol*. 2001;3:165–72.
75. Liu H, Nazmun N, Hassan S, Liu X, Yang J. BRAF mutation and its inhibitors in sarcoma treatment. *Cancer Med*. 2020;9:4881–96.
76. Janku F, Hong DS, Fu S, Piha-Paul SA, Naing A, Falchook GS, et al. Assessing PIK3CA and PTEN in early-phase trials with PI3K/AKT/mTOR inhibitors. *Cell Rep*. 2014;6:377–87.
77. García-Valverde A, Rosell J, Serma G, Valverde C, Carles J, Nuciforo P, et al. Preclinical activity of PI3K inhibitor copanlisib in gastrointestinal stromal tumor. *Mol Cancer Ther*. 2020;19:1289–97.
78. Damodaran S, Zhao F, Deming DA, Mitchell EP, Wright JJ, Doyle LA, et al. Phase II study of copanlisib in patients with tumors with PIK3CA mutations (PTEN loss allowed): NCI MATCH EAY131-Z1F. *JCO Wolters Kluwer*. 2020;38:3506–3506.
79. Pollack SM, Ingham M, Spraker MB, Schwartz GK. Emerging targeted and immune-based therapies in sarcoma. *JCO*. 2018;36:125–35.
80. Babichev Y, Kabaroff L, Datti A, Uehling D, Isaac M, Al-awar R, et al. PI3K/AKT/mTOR inhibition in combination with doxorubicin is an effective therapy for leiomyosarcoma. *J Transl Med*. 2016;14:1–12.
81. Desai C, Thomason J, Kohlmeyer JL, Reisetter AC, Ahirwar P, Jahanseir K, et al. Prognostic and therapeutic value of the Hippo pathway, RABL6A, and p53-MDM2 axes in sarcomas. *Oncotarget Impact J*. 2021;12:740–55.
82. Rytlewski JD, Scalora N, Garcia K, Tanas M, Toor F, Miller B, et al. Photodynamic therapy using Hippo pathway inhibitor verteporfin: a potential dual mechanistic approach in treatment of soft tissue sarcomas. *Cancers (Basel)*. 2021;13:675.
83. Isfort I, Cyra M, Elges S, Kailayangiri S, Altvater B, Rossig C, et al. SS18-SSX-dependent YAP/TAZ signaling in synovial sarcoma. *Clin Cancer Res*. 2019;25:3718–31.

84. Bierbaumer L, Katschnig AM, Radic-Sarikas B, Kauer MO, Petro JA, Höglér S, et al. YAP/TAZ inhibition reduces metastatic potential of Ewing sarcoma cells. *Oncogenesis*. 2021;10:1–13.
85. Tap WD, Villalobos VM, Cote GM, Burris H, Janku F, Mir O, et al. Phase I study of the mutant IDH1 inhibitor ivosidenib: safety and clinical activity in patients with advanced chondrosarcoma. *J Clin Oncol*. 2020;38:1693–701.
86. Lee D, Omofoye OA, Karnati T, Graff JP, Shahlaie K. Intracranial myeloid sarcoma presentation in distant acute myeloid leukemia remission. *J Clin Neurosci*. 2021;89:158–60.
87. Cojocaru E, Wilding C, Engelman B, Huang P, Jones RL. Is the IDH mutation a good target for chondrosarcoma treatment? *Curr Mol Biol Rep*. 2020;6:1–9.
88. Bean GR, Kremer JC, Prudner BC, Schenone AD, Yao J-C, Schultze MB, et al. A metabolic synthetic lethal strategy with arginine deprivation and chloroquine leads to cell death in ASS1-deficient sarcomas. *Cell Death Dis*. 2016;7:e2406–e2406.
89. Kremer JC, Prudner BC, Lange SES, Bean GR, Schultze MB, Brashears CB, et al. Arginine deprivation inhibits the Warburg effect and upregulates glutamine anaplerosis and serine biosynthesis in ASS1-deficient cancers. *Cell Rep*. 2017;18:991–1004.
90. Rooke M, Coupland LA, Truong T, Blackburn AC. Dichloroacetate is an effective treatment for sarcoma models in vitro and in vivo. *Cancer Metab*. 2014;2:P9.
91. Vasileva E, Warren M, Triche TJ, Amatruda JF. Dysregulated heparan sulfate proteoglycan metabolism promotes Ewing sarcoma tumor growth. *bioRxiv*. 2021. <https://doi.org/10.1101/2021.05.25.445683>.
92. Travelli C, Consonni FM, Sangaletti S, Storto M, Morlacchi S, Grolla AA, et al. Nicotinamide phosphoribosyltransferase acts as a metabolic gate for mobilization of myeloid-derived suppressor cells. *Cancer Res*. 2019;79:1938–51.
93. Hirota S. Gain-of-function mutations of c-kit in human gastrointestinal stromal tumors. *Science*. 1998;279:577–80.
94. Goncalves MD, Hopkins BD, Cantley LC. Phosphatidylinositol 3-kinase, growth disorders, and cancer. *N Engl J Med*. 2018;379:2052.
95. Farid M, Ngeow J. Sarcomas associated with genetic cancer predisposition syndromes: a review. *Oncologist*. 2016;21:1002–13.
96. Lee C-L, Mowery YM, Daniel AR, Zhang D, Sibley AB, Delaney JR, et al. Mutational landscape in genetically engineered, carcinogen-induced, and radiation-induced mouse sarcoma. *JCI Insight*. 2019;4:e128698.
97. Chen X, Stewart E, Shelat AA, Qu C, Bahrami A, Hatley M, et al. Targeting oxidative stress in embryonal rhabdomyosarcoma. *Cancer Cell*. 2013;24:710–24.
98. Pal A, Chiu HY, Taneja R. Genetics, epigenetics and redox homeostasis in rhabdomyosarcoma: emerging targets and therapeutics. *Redox Biol*. 2019;25:101124.
99. Zhang M, Lincardic CM, Kirsch DG. RAS and ROS in rhabdomyosarcoma. *Cancer Cell*. 2013;24:689–91.
100. Tanner LB, Goglia AG, Wei MH, Sehgal T, Parsons LR, Park JO, et al. Four key steps control glycolytic flux in mammalian cells. *Cell Syst*. 2018;7:49–62.e8.
101. Amendola CR, Mahaffey JP, Parker SJ, Ahearn IM, Chen W-C, Zhou M, et al. KRAS4A directly regulates hexokinase 1. *Nature*. 2019;576:482–6.
102. Xu D, Shao F, Bian X, Meng Y, Liang T, Lu Z. The evolving landscape of noncanonical functions of metabolic enzymes in cancer and other pathologies. *Cell Metab*. 2021;33:33–50.
103. Gao X, Wang H, Yang JJ, Liu X, Liu Z-R. Pyruvate kinase M2 regulates gene transcription by acting as a protein kinase. *Mol Cell*. 2012;45:598–609.
104. Li X, Jiang Y, Meisenhelder J, Yang W, Hawke DH, Zheng Y, et al. Mitochondria-translocated PGK1 functions as a protein kinase to coordinate glycolysis and the TCA cycle in tumorigenesis. *Mol Cell*. 2016;61:705–19.
105. Son J, Lyssiotis CA, Ying H, Wang X, Hua S, Ligorio M, et al. Glutamine supports pancreatic cancer growth through a KRAS-regulated metabolic pathway. *Nature*. 2013;496:101–5.
106. Ying H, Kimmelman AC, Lyssiotis CA, Hua S, Chu GC, Fletcher-Sanankone E, et al. Oncogenic Kras maintains pancreatic tumors through regulation of anabolic glucose metabolism. *Cell*. 2012;149:656–70.
107. Genadry KC, Pietrobono S, Rota R, Lincardic CM. Soft tissue sarcoma cancer stem cells: an overview. *Front Oncol*. 2018;8:475.
108. Hatina J, Kripnerova M, Houfkova K, Pesta M, Kuncova J, Sana J, et al. Sarcoma stem cell heterogeneity. In: Birbrair A, editor, et al. *Stem cells heterogeneity—novel concepts*. Cham: Springer International Publishing; 2019. p. 95–118.
109. Kelleher FC, O'Sullivan H. FOXM1 in sarcoma: role in cell cycle, pluripotency genes and stem cell pathways. *Oncotarget*. 2016;7:42792–804.
110. Martins-Neves SR, Corver WE, Paiva-Oliveira DI, van den Akker BEWM, Briaire-de-Brujin IH, Bovée JVMG, et al. Osteosarcoma stem cells have active Wnt/ β -catenin and overexpress SOX2 and KLF4. *J Cell Physiol*. 2016;231:876–86.
111. Vališ K, Novák P. Targeting ERK-Hippo interplay in cancer therapy. *Int J Mol Sci*. 2020;21:3236.
112. Harvey KF, Zhang X, Thomas DM. The Hippo pathway and human cancer. *Nat Rev Cancer*. 2013;13:246–57.
113. Kapoor A, Yao W, Ying H, Hua S, Liewen A, Wang Q, et al. Yap1 Activation enables bypass of oncogenic Kras addiction in pancreatic cancer. *Cell*. 2014;158:185–97.
114. St John MA, Tao W, Fei X, Fukumoto R, Carcangiu ML, Brownstein DG, et al. Mice deficient of Lats1 develop soft-tissue sarcomas, ovarian tumours and pituitary dysfunction. *Nat Genet*. 1999;21:182–6.
115. Zhou D, Conrad C, Xia F, Park J-S, Payer B, Yin Y, et al. Mst1 and Mst2 maintain hepatocyte quiescence and suppress the development of hepatocellular carcinoma through inactivation of the Yap1 oncogene. *Cancer Cell*. 2009;16:425–38.
116. Mohamed AD, Shah N, Hettmer S, Vargesson N, Wackerhage H. Analysis of the relationship between the KRAS G12V oncogene and the Hippo effector YAP1 in embryonal rhabdomyosarcoma. *Sci Rep*. 2018;8:15674.
117. Koo JH, Guan K-L. Interplay between YAP/TAZ and Metabolism. *Cell Metab*. 2018;28:196–206.
118. Santinon G, Pocaterra A, Dupont S. Control of YAP/TAZ activity by metabolic and nutrient-sensing pathways. *Trends Cell Biol*. 2016;26:289–99.
119. Wang W, Xiao Z-D, Li X, Aziz KE, Gan B, Johnson RL, et al. AMPK modulates Hippo pathway activity to regulate energy homeostasis. *Nat Cell Biol*. 2015;17:490–9.
120. Enzo E, Santinon G, Pocaterra A, Aragona M, Bresolin S, Forcato M, et al. Aerobic glycolysis tunes YAP/TAZ transcriptional activity. *EMBO J*. 2015;34:1349–70.
121. Mota MSV, Jackson WP, Bailey SK, Vayalil P, Landar A, Rostas JW, et al. Deficiency of tumor suppressor Merlin facilitates metabolic adaptation by co-operative engagement of SMAD-Hippo signaling in breast cancer. *Carcinogenesis*. 2018;39:1165–75.
122. Agresta L, Salloum R, Hummel TR, Ratner N, Mangano FT, Fuller C, et al. Malignant peripheral nerve sheath tumor: transformation in a patient with neurofibromatosis type 2. *Pediatr Blood Cancer*. 2019;66:e27520.
123. White SM, Avantaggiati ML, Nemazany I, Di Poto C, Yang Y, Pende M, et al. YAP/TAZ inhibition induces metabolic and signaling rewiring resulting in targetable vulnerabilities in NF2-deficient tumor cells. *Dev Cell*. 2019;49:425–443.e9.
124. Chen R, Zhu S, Fan X-G, Wang H, Lotze MT, Zeh HJ, et al. High mobility group protein B1 controls liver cancer initiation through yes-associated protein-dependent aerobic glycolysis. *Hepatology*. 2018;67:1823–41.
125. Zhang X, Li Y, Ma Y, Yang L, Wang T, Meng X, et al. Yes-associated protein (YAP) binds to HIF-1 α and sustains HIF-1 α protein stability to promote hepatocellular carcinoma cell glycolysis under hypoxic stress. *J Exp Clin Cancer Res*. 2018;37:216.
126. Rivera-Reyes A, Ye S, Marino GE, Egolf S, Ciotti GE, Chor S, et al. YAP1 enhances NF- κ B-dependent and independent effects on clock-mediated unfolded protein responses and autophagy in sarcoma. *Cell Death Dis*. 2018;9:1108.
127. Altman BJ, Stine ZE, Dang CV. From Krebs to clinic: glutamine metabolism to cancer therapy. *Nat Rev Cancer*. 2016;16:619–34.
128. Birsoy K, Wang T, Chen WW, Freinkman E, Abu-Remaileh M, Sabatini DM. An essential role of the mitochondrial electron transport chain in cell proliferation is to enable aspartate synthesis. *Cell*. 2015;162:540–51.
129. Sullivan LB, Gui DY, Hosios AM, Bush LN, Freinkman E, Vander Heiden MG. Supporting aspartate biosynthesis is an essential function of respiration in proliferating cells. *Cell*. 2015;162:552–63.
130. Ma Q, Cavallin LE, Leung HJ, Chiozzini C, Goldschmidt-Clermont PJ, Mesri EA. A role for virally induced reactive oxygen species in Kaposi's sarcoma herpesvirus tumorigenesis. *Antioxid Redox Signal*. 2013;18:80–90.

131. Ma T, Patel H, Babapoor-Farrokhran S, Franklin R, Semenza GL, Sodhi A, et al. KSHV induces aerobic glycolysis and angiogenesis through HIF-1-dependent upregulation of pyruvate kinase 2 in Kaposi's sarcoma. *Angiogenesis*. 2015;18:477–88.
132. Delgado T, Carroll PA, Punjabi AS, Margineantu D, Hockenbery DM, Lagunoff M. Induction of the Warburg effect by Kaposi's sarcoma herpesvirus is required for the maintenance of latently infected endothelial cells. *Proc Natl Acad Sci*. 2010;107:10696–701.
133. Cavallin LE, Ma Q, Naipauer J, Gupta S, Kurian M, Locatelli P, et al. KSHV-induced ligand mediated activation of PDGF receptor- α drives Kaposi's sarcomagenesis. *PLoS Pathog*. 2018;14:e1007175.
134. Veeranna RP, Haque M, Davis DA, Yang M, Yarchoan R. Kaposi's sarcoma-associated herpesvirus latency-associated nuclear antigen induction by hypoxia and hypoxia-inducible factors. *J Virol*. 2012;86:1097–108.
135. Choi UY, Lee JJ, Park A, Zhu W, Lee H-R, Choi YJ, et al. Oncogenic human herpesvirus hijacks proline metabolism for tumorigenesis. *PNAS*. 2020;117:8083–93.
136. Locasale JW, Grassian AR, Melman T, Lyssiotis CA, Mattaini KR, Bass AJ, et al. Phosphoglycerate dehydrogenase diverts glycolytic flux and contributes to oncogenesis. *Nat Genet*. 2011;43:869–74.
137. Bose S, Allen AE, Locasale JW. The molecular link from diet to cancer cell metabolism. *Mol Cell*. 2020;78:1034–44.
138. Gao X, Sanderson SM, Dai Z, Reid MA, Cooper DE, Lu M, et al. Dietary methionine influences therapy in mouse cancer models and alters human metabolism. *Nature*. 2019;572:397–401.
139. Nusse R, Clevers H. Wnt/ β -catenin signaling, disease, and emerging therapeutic modalities. *Cell*. 2017;169:985–99.
140. Esen E, Chen J, Karner CM, Okunade AL, Patterson BW, Long F. WNT-LRP5 signaling induces Warburg effect through mTORC2 activation during osteoblast differentiation. *Cell Metab*. 2013;17:745–55.
141. Karner CM, Esen E, Chen J, Hsu F-F, Turk J, Long F. Wnt protein signaling reduces nuclear acetyl-CoA levels to suppress gene expression during osteoblast differentiation. *J Biol Chem*. 2016;291:13028–39.
142. Frey JL, Li Z, Ellis JM, Zhang Q, Farber CR, Aja S, et al. Wnt-Lrp5 signaling regulates fatty acid metabolism in the osteoblast. *Mol Cell Biol*. 2015;35:1979–91.
143. Danieau G, Morice S, Rédini F, Verrecchia F, Royer BL. New insights about the Wnt/ β -catenin signaling pathway in primary bone tumors and their microenvironment: a promising target to develop therapeutic strategies? *IJMS*. 2019;20:3751.
144. Fuxe J, Vincent T, Garcia de Herreros A. Transcriptional crosstalk between TGF β and stem cell pathways in tumor cell invasion: role of EMT promoting Smad complexes. *Cell Cycle*. 2010;9:2363–74.
145. Briski LM, Thomas DG, Patel RM, Lawlor ER, Chugh R, McHugh JB, et al. Canonical Wnt/ β -catenin signaling activation in soft-tissue sarcomas: a comparative study of synovial sarcoma and leiomyosarcoma. *Rare Tumors*. 2018;10:203636131881343.
146. Du X, Yang J, Yang D, Tian W, Zhu Z. The genetic basis for inactivation of Wnt pathway in human osteosarcoma. *BMC Cancer*. 2014;14:450.
147. Wang W-G, Chen S-J, He J-S, Li J-S, Zang X-F. The tumor suppressive role of RASSF1A in osteosarcoma through the Wnt signaling pathway. *Tumor Biol*. 2016;37:8869–77.
148. Li Y, Zhang S, Zhang C, Wang M. LncRNA MEG3 inhibits the inflammatory response of ankylosing spondylitis by targeting miR-146a. *Mol Cell Biochem*. 2020;466:17–24.
149. Techavichit P, Gao Y, Kurenbekova L, Shuck R, Donehower LA, Yustein JT. Secreted Frizzled-Related Protein 2 (sFRP2) promotes osteosarcoma invasion and metastatic potential. *BMC Cancer*. 2016;16:869.
150. Jacks T, Remington L, Williams BO, Schmitt EM, Halachmi S, Bronson RT, et al. Tumor spectrum analysis in p53-mutant mice. *Curr Biol*. 1994;4:1–7.
151. Barretina J, Taylor BS, Banerji S, Ramos AH, Lagos-Quintana M, DeCarolis PL, et al. Subtype-specific genomic alterations define new targets for soft-tissue sarcoma therapy. *Nat Genet*. 2010;42:715–21.
152. Blay J-Y, Ray-Coquard I. Evolving biological understanding and treatment of sarcomas. *Nat Rev Clin Oncol*. 2017;14:78–80.
153. Bui NQ. A clinico-genomic analysis of soft tissue sarcoma patients reveals CDKN2A deletion as a biomarker for poor prognosis. *Clin Sarcoma Res*. 2019;9:11.
154. Mito JK, Riedel RF, Dodd L, Lahat G, Lazar AJ, Dodd RD, et al. Cross species genomic analysis identifies a mouse model as undifferentiated pleomorphic sarcoma/malignant fibrous histiocytoma. *PLoS ONE*. 2009;4:e8075.
155. Kirsch DG, Dinulescu DM, Miller JB, Grimm J, Santiago PM, Young NP, et al. A spatially and temporally restricted mouse model of soft tissue sarcoma. *Nat Med*. 2007;13:992–7.
156. Liu J, Zhang C, Hu W, Feng Z. Tumor suppressor p53 and its mutants in cancer metabolism. *Cancer Lett*. 2015;356:197–203.
157. Simabuco FM, Morale MG, Pavan ICB, Morelli AP, Silva FR, Tamara RE. p53 and metabolism: from mechanism to therapeutics. *Oncotarget*. 2018;9:23780–823.
158. Valente LJ, Gray DHD, Michalak EM, Pinon-Hofbauer J, Egle A, Scott CL, et al. p53 efficiently suppresses tumor development in the complete absence of its cell-cycle inhibitory and proapoptotic effectors p21, Puma, and Noxa. *Cell Rep*. 2013;3:1339–45.
159. Vousden KH, Ryan KM. p53 and metabolism. *Nat Rev Cancer*. 2009;9:691–700.
160. Ahrens WA, Ridenour RV, Caron BL, Miller DV, Folpe AL. GLUT-1 expression in mesenchymal tumors: an immunohistochemical study of 247 soft tissue and bone neoplasms. *Hum Pathol*. 2008;39:1519–26.
161. Schwartzenberg-Bar-Yoseph F, Armoni M, Karnieli E. The tumor suppressor p53 down-regulates glucose transporters GLUT1 and GLUT4 gene expression. *Cancer Res*. 2004;64:2627–33.
162. Bensaad K, Tsuruta A, Selak MA, Vidal MNC, Nakano K, Bartrons R, et al. TIGAR, a p53-inducible regulator of glycolysis and apoptosis. *Cell*. 2006;126:107–20.
163. Zhang C, Lin M, Wu R, Wang X, Yang B, Levine AJ, et al. Parkin, a p53 target gene, mediates the role of p53 in glucose metabolism and the Warburg effect. *Proc Natl Acad Sci*. 2011;108:16259–64.
164. Jiang P, Du W, Wang X, Mancuso A, Gao X, Wu M, et al. p53 regulates biosynthesis through direct inactivation of glucose-6-phosphate dehydrogenase. *Nat Cell Biol*. 2011;13:15.
165. Erpapazoglou Z, Corti O. The endoplasmic reticulum/mitochondria interface: a subcellular platform for the orchestration of the functions of the PINK1–Parkin pathway? *Biochem Soc Trans*. 2015;43:297–301.
166. Kruiswijk F, Labuschagne CF, Vousden KH. p53 in survival, death and metabolic health: a lifeguard with a licence to kill. *Nat Rev Mol Cell Biol*. 2015;16:393–405.
167. Morris JP, Yashinskii JJ, Koche R, Chandwani R, Tian S, Chen C-C, et al. α -Ketoglutarate links p53 to cell fate during tumour suppression. *Nature*. 2019;573:595–9.
168. Gaude E, Frezza C. Tissue-specific and convergent metabolic transformation of cancer correlates with metastatic potential and patient survival. *Nat Commun*. 2016;7:13041.
169. Benz MR, Tchekmedyan N, Eilber FC, Federman N, Czernin J, Tap WD. Utilization of positron emission tomography in the management of patients with sarcoma. *Curr Opin Oncol*. 2009;21:345–51.
170. Wagner LM, Kremer N, Gelfand MJ, Sharp SE, Turpin BK, Nagarajan R, et al. Detection of lymph node metastases in pediatric and adolescent/young adult sarcoma: sentinel lymph node biopsy versus fludeoxyglucose positron emission tomography imaging—a prospective trial: sentinel lymph node biopsy versus PET in sarcoma. *Cancer*. 2017;123:155–60.
171. Issaq SH, Teicher BA, Monks A. Bioenergetic properties of human sarcoma cells help define sensitivity to metabolic inhibitors. *Cell Cycle*. 2014;13:1152–61.
172. Dasgupta A, Trucco M, Rainusso N, Bernardi RJ, Shuck R, Kurenbekova L, et al. Metabolic modulation of Ewing sarcoma cells inhibits tumor growth and stem cell properties. *Oncotarget*. 2017;8:77292–308.
173. Mao L, Dauchy RT, Blask DE, Dauchy EM, Slakey LM, Brimer S, et al. Melatonin suppression of aerobic glycolysis (Warburg effect), survival signalling and metastasis in human leiomyosarcoma. *J Pineal Res*. 2016;60:167–77.
174. Li B, Qiu B, Lee DSM, Walton ZE, Ochocki JD, Mathew LK, et al. Fructose-1,6-bisphosphatase opposes renal carcinoma progression. *Nature*. 2014;513:251–5.
175. Issaq SH, Mendoza A, Fox SD, Helman LJ. Glutamine synthetase is necessary for sarcoma adaptation to glutamine deprivation and tumor growth. *Oncogenesis*. 2019;8:20.

176. Han J, Zhang Y, Xu J, Zhang T, Wang H, Wang Z, et al. Her4 promotes cancer metabolic reprogramming via the c-Myc-dependent signaling axis. *Cancer Lett.* 2021;496:57–71.
177. Masoud R, Reyes-Castellanos G, Lac S, Garcia J, Dou S, Shintu L, et al. Targeting mitochondrial complex I overcomes chemoresistance in high OXPHOS pancreatic cancer. *Cell Rep Med.* 2020;1:100143.
178. Mor I, Cheung EC, Vousden KH. Control of glycolysis through regulation of PFK1: old friends and recent additions. *Cold Spring Harb Symp Quant Biol.* 2011;76:211–6.
179. Moreno-Sánchez R, Marín-Hernández A, Gallardo-Pérez JC, Quezada H, Encalada R, Rodríguez-Enríquez S, et al. Phosphofruktokinase type 1 kinetics, isoform expression, and gene polymorphisms in cancer cells. *J Cell Biochem.* 2012;113:1692–703.
180. Cabrera R, Baez M, Pereira HM. Kinetic and structural analysis of the allosteric ATP inhibition S. *J Biol Chem.* 2011;286:11.
181. Yalcin A, Telang S, Clem B, Chesney J. Regulation of glucose metabolism by 6-phosphofruktose-2-kinase/fructose-2,6-bisphosphatases in cancer. *Exp Mol Pathol.* 2009;86:174–9.
182. Scarpulla RC, Vega RB, Kelly DP. Transcriptional integration of mitochondrial biogenesis. *Trends Endocrinol Metab.* 2012;23:459–66.
183. Borst P. The malate-aspartate shuttle (Borst cycle): how it started and developed into a major metabolic pathway. *IUBMB Life.* 2020;72:2241–59.
184. Dai Z, Shestov AA, Lai L, Locasale JW. A flux balance of glucose metabolism clarifies the requirements of the Warburg effect. *Biophys J.* 2016;111:1088–100.
185. Altinok O, Poggio JL, Stein DE, Bowne WB, Shieh AC, Snyder NW, et al. Malate-aspartate shuttle promotes l-lactate oxidation in mitochondria. *J Cell Physiol.* 2020;235:2569–81.
186. Young A, Oldford C, Mailloux RJ. Lactate dehydrogenase supports lactate oxidation in mitochondria isolated from different mouse tissues. *Redox Biol.* 2020;28:101339.
187. Bonnet S, Archer SL, Allalunis-Turner J, Haromy A, Beaulieu C, Thompson R, et al. A mitochondria-K⁺ channel axis is suppressed in cancer and its normalization promotes apoptosis and inhibits cancer growth. *Cancer Cell.* 2007;11:37–51.
188. Ippolito L, Giannoni E, Chiarugi P, Parri M. Mitochondrial redox hubs as promising targets for anticancer therapy. *Front Oncol.* 2020;10:256.
189. Titova E, Shagieva G, Ivanova O, Domnina L, Domninskaya M, Strelkova O, et al. Mitochondria-targeted antioxidant SkQ1 suppresses fibrosarcoma and rhabdomyosarcoma tumour cell growth. *Cell Cycle.* 2018;17:1797–811.
190. Leonardi R, Zhang Y, Rock C, Jackowski S. Coenzyme A: back in action. *Prog Lipid Res.* 2005;44:125–53.
191. Granjeaud S, Naquet P, Galland F. An ESTs description of the new Vanin gene family conserved from fly to human. *Immunogenetics.* 1999;49:964–72.
192. Naquet P, Kerr EW, Vickers SD, Leonardi R. Regulation of coenzyme A levels by degradation: the 'Ins and Outs'. *Prog Lipid Res.* 2020;78:101028.
193. Scarpulla RC. Nuclear activators and coactivators in mammalian mitochondrial biogenesis. *Biochim Biophys Acta (BBA) Gene Struct Expr.* 2002;1576:1–14.
194. Bakkar N, Wang J, Ladner KJ, Wang H, Dahlman JM, Carathers M, et al. IKK/NF- κ B regulates skeletal myogenesis via a signaling switch to inhibit differentiation and promote mitochondrial biogenesis. *J Cell Biol.* 2008;180:787–802.
195. Shintaku J, Peterson JM, Talbert EE, Gu J-M, Ladner KJ, Williams DR, et al. MyoD regulates skeletal muscle oxidative metabolism cooperatively with alternative NF- κ B. *Cell Rep.* 2016;17:514–26.
196. Londhe P, Yu PY, Ijiri Y, Ladner KJ, Fenger JM, London C, et al. Classical NF- κ B metabolically reprograms sarcoma cells through regulation of hexokinase 2. *Front Oncol.* 2018;8:104.
197. Jahnke VE, Sabido O, Defour A, Castells J, Lefai E, Roussel D, et al. Evidence for mitochondrial respiratory deficiency in rat rhabdomyosarcoma cells. *PLoS ONE.* 2010;5:e8637.
198. Aspuria P-JP, Lunt SY, Våremo L, Vergnes L, Gozo M, Beach JA, et al. Succinate dehydrogenase inhibition leads to epithelial-mesenchymal transition and reprogrammed carbon metabolism. *Cancer Metab.* 2014;2:21.
199. Sulkowski PL, Oeck S, Dow J, Economos NG, Mirfakhraie L, Liu Y, et al. Oncometabolites suppress DNA repair by disrupting local chromatin signalling. *Nature.* 2020;582:586–91.
200. Salminen A, Kauppinen A, Kaarniranta K. 2-Oxoglutarate-dependent dioxygenases are sensors of energy metabolism, oxygen availability, and iron homeostasis: potential role in the regulation of aging process. *Cell Mol Life Sci.* 2015;72:3897–914.
201. Pollock RE, Randall RL, O'Sullivan B. *Sarcoma oncology: a multidisciplinary approach.* New York: PMPH USA; 2019.
202. Hoffmann A-C, Danenberg KD, Taubert H, Danenberg PV, Wuerl P. A three-gene signature for outcome in soft tissue sarcoma. *Clin Cancer Res.* 2009;15:5191–8.
203. Corless CL, Barnett CM, Heinrich MC. Gastrointestinal stromal tumours: origin and molecular oncology. *Nat Rev Cancer.* 2011;11:865–78.
204. Sadri N, Zhang P. Hypoxia-inducible factors: mediators of cancer progression; prognostic and therapeutic targets in soft tissue sarcomas. *Cancers.* 2013;5:320–33.
205. Das B, Tsuchida R, Malkin D, Koren G, Baruchel S, Yeger H. Hypoxia enhances tumor stemness by increasing the invasive and tumorigenic side population fraction. *Stem Cells.* 2008;26:1818–30.
206. Bott AJ, Maimouni S, Zong W-X. The pleiotropic effects of glutamine metabolism in cancer. *Cancers (Basel).* 2019;11:770.
207. Jackson M, Serada N, Sheehan M, Srinivasan S, Mason N, Guha M, et al. Mitochondrial genome and functional defects in osteosarcoma are associated with their aggressive phenotype. *PLoS ONE.* 2018;13:e0209489.
208. Srinivasan S, Guha M, Dong DW, Whelan KA, Ruthel G, Uchikado Y, et al. Disruption of cytochrome c oxidase function induces the Warburg effect and metabolic reprogramming. *Oncogene.* 2016;35:1585–95.
209. Srinivasan S, Guha M, Kashina A, Avadhani NG. Mitochondrial dysfunction and mitochondrial dynamics—the cancer connection. *Biochim Biophys Acta (BBA) Bioenerg.* 2017;1858:602–14.
210. Guha M, Srinivasan S, Ruthel G, Kashina AK, Carstens RP, Mendoza A, et al. Mitochondrial retrograde signaling induces epithelial-mesenchymal transition and generates breast cancer stem cells. *Oncogene.* 2014;33:5238–50.
211. Yizhak K, Le Dévédec SE, Rogkoti VM, Baenke F, Boer VC, Frezza C, et al. A computational study of the Warburg effect identifies metabolic targets inhibiting cancer migration. *Mol Syst Biol.* 2014;10:744.
212. Gouirand V, Guillaumond F, Vasseur S. Influence of the tumor micro-environment on cancer cells metabolic reprogramming. *Front Oncol.* 2018;8:117.
213. Kalluri R. The biology and function of fibroblasts in cancer. *Nat Rev Cancer.* 2016;16:582–98.
214. Bittner JG, Wilson M, Shah MB, Albo D, Feig BW, Wang TN. Fibroblast-conditioned media promote human sarcoma cell invasion. *Surgery.* 2009;145:42–7.
215. Bonuccelli G, Avnet S, Grisendi G, Salerno M, Granchi D, Dominici M, et al. Role of mesenchymal stem cells in osteosarcoma and metabolic reprogramming of tumor cells. *Oncotarget.* 2014;5:7575–88.
216. Bonuccelli G, Tsirigos A, Whitaker-Menezes D, Pavlides S, Pestell RG, Chiavarina B, et al. Ketones and lactate "fuel" tumor growth and metastasis. *Cell Cycle.* 2014;9:9.
217. Dai L, Qin Z, Defee M, Toole BP, Kirkwood KL, Parsons C. Kaposi sarcoma-associated herpesvirus (KSHV) induces a functional tumor-associated phenotype for oral fibroblasts. *Cancer Lett.* 2012;318:214–20.
218. De Saedeleer CJ, Copetti T, Porporato PE, Verrax J, Feron O, Sonveaux P. Lactate activates HIF-1 in oxidative but not in Warburg-phenotype human tumor cells. *PLoS ONE.* 2012;7:e46571.
219. Sotgia F, Martinez-Outschoorn UE, Lisanti MP. The reverse Warburg effect in osteosarcoma. *Oncotarget.* 2014;5:7982.
220. Goodwin ML, Jin H, Straessler K, Smith-Fry K, Zhu J-F, Monument MJ, et al. Modeling alveolar soft part sarcomagenesis in the mouse: a role for lactate in the tumor microenvironment. *Cancer Cell.* 2014;26:851–62.
221. Porporato PE. Mitochondrial metabolism and cancer. *Cell Res.* 2018;28:16.

222. Danhier P, Bański P, Payen VL, Grasso D, Ippolito L, Sonveaux P, et al. Cancer metabolism in space and time: beyond the Warburg effect. *Biochim Biophys Acta (BBA) Bioenerg.* 2017;1858:556–72.
223. Porporato PE. Metabolic changes associated with tumor metastasis, part 2: mitochondria, lipid and amino acid metabolism. *Cell Mol Life Sci.* 2016;73:1349–63.
224. Harati K, Daigeler A, Hirsch T, Jacobsen F, Behr B, Wallner C, et al. Tumor-associated fibroblasts promote the proliferation and decrease the doxorubicin sensitivity of liposarcoma cells. *Int J Mol Med.* 2016;37:1535–41.
225. Bellairs R, Van Peteghem M-C. Gastrulation: is it analogous to malignant invasion. *Am Zool.* 1984;24:563–70.
226. Sannino G, Marchetto A, Kirchner T, Grünwald TGP. Epithelial-to-mesenchymal and mesenchymal-to-epithelial transition in mesenchymal tumors: a paradox in sarcomas? *Cancer Res.* 2017;77:4556–61.
227. Chaklader M, Pan A, Law A, Chattopadhyay S, Chatterjee R, Law S. Differential remodeling of cadherins and intermediate cytoskeletal filaments influence microenvironment of solid and ascitic sarcoma. *Mol Cell Biochem.* 2013;382:293–306.
228. Kahlert UD, Joseph JV, Kruyt FAE. EMT- and MET-related processes in nonepithelial tumors: importance for disease progression, prognosis, and therapeutic opportunities. *Mol Oncol.* 2017;11:860–77.
229. Tian W, Wang G, Yang J, Pan Y, Ma Y. Prognostic role of E-cadherin and Vimentin expression in various subtypes of soft tissue leiomyosarcomas. *Med Oncol.* 2013;30:401.
230. Saito T. The SYT-SSX fusion protein and histological epithelial differentiation in synovial sarcoma: relationship with extracellular matrix remodeling. *Int J Clin Exp Pathol.* 2013;6:2272.
231. Thuault S, Hayashi S, Lagirand-Cantaloube J, Plutoni C, Comunale F, Delattre O, et al. P-cadherin is a direct PAX3–FOXO1A target involved in alveolar rhabdomyosarcoma aggressiveness. *Oncogene.* 2013;32:1876–87.
232. Hua W, ten Dijke P, Kostidis S, Giera M, Hornsveld M. TGF β -induced metabolic reprogramming during epithelial-to-mesenchymal transition in cancer. *Cell Mol Life Sci.* 2020;77:2103–23.
233. Xu W, Yang Z, Lu N. A new role for the PI3K/Akt signaling pathway in the epithelial-mesenchymal transition. *Cell Adh Migr.* 2015;9:317–24.
234. El-Naggar AM, Veinotte CJ, Cheng H, Grunewald TGP, Negri GL, Somasekharan SP, et al. Translational activation of HIF1 α by YB-1 promotes sarcoma metastasis. *Cancer Cell.* 2015;27:682–97.
235. Gilkes DM, Semenza GL, Wirtz D. Hypoxia and the extracellular matrix: drivers of tumour metastasis. *Nat Rev Cancer.* 2014;14:430–9.
236. Eisinger-Mathason TSK, Zhang M, Qiu Q, Skuli N, Nakazawa MS, Karakasha T, et al. Hypoxia-dependent modification of collagen networks promotes sarcoma metastasis. *Cancer Discov.* 2013;3:1190–205.
237. Petitprez F, Meylan M, de Reyniès A, Sautès-Fridman C, Fridman WH. The tumor microenvironment in the response to immune checkpoint blockade therapies. *Front Immunol.* 2020;11:784.
238. Thorsson V, Gibbs DL, Brown SD, Wolf D, Bortone DS, Ou Yang T-H, et al. The immune landscape of cancer. *Immunity.* 2018;48:812–830.e14.
239. Chalmers ZR, Connelly CF, Fabrizio D, Gay L, Ali SM, Ennis R, et al. Analysis of 100,000 human cancer genomes reveals the landscape of tumor mutational burden. *Genome Med.* 2017;9:34.
240. Hegde PS, Chen DS. Top 10 challenges in cancer immunotherapy. *Immunity.* 2020;52:17–35.
241. Fletcher CDM. The evolving classification of soft tissue tumours—an update based on the new 2013 WHO classification. *Histopathology.* 2014;64:2–11.
242. Cohen JE, Eleyan F, Zick A, Peretz T, Katz D. Intratumoral immune-biomarkers and mismatch repair status in leiomyosarcoma -potential predictive markers for adjuvant treatment: a pilot study. *Oncotarget.* 2018;9:30847–54.
243. D'Angelo SP, Tap WD, Schwartz GK, Carvajal RD. Sarcoma immunotherapy: past approaches and future directions. *Sarcoma.* 2014;2014:1–13.
244. van Erp AEM, Versleijen-Jonkers YMH, Hillebrandt-Roeffen MHS, van Houdt L, Gorris MAJ, van Dam LS, et al. Expression and clinical association of programmed cell death-1, programmed death-ligand-1 and CD8+ lymphocytes in primary sarcomas is subtype dependent. *Oncotarget.* 2017;8:71371–84.
245. Wedekind MF, Wagner LM, Cripe TP. Immunotherapy for osteosarcoma: where do we go from here? *Pediatr Blood Cancer.* 2018;65:e27227.
246. Dancsok AR, Setsu N, Gao D, Blay J-Y, Thomas D, Maki RG, et al. Expression of lymphocyte immunoregulatory biomarkers in bone and soft-tissue sarcomas. *Mod Pathol.* 2019;32:1772–85.
247. Feng X, Pleasance E, Zhao EY, Ng T, Grewal JK, Mohammad N, et al. Therapeutic implication of genomic landscape of adult metastatic sarcoma. *JCO Precis Oncol.* 2019;3:1–25.
248. Keung EZ, Tsai J-W, Ali AM, Cormier JN, Bishop AJ, Guadagnolo BA, et al. Analysis of the immune infiltrate in undifferentiated pleomorphic sarcoma of the extremity and trunk in response to radiotherapy: rationale for combination neoadjuvant immune checkpoint inhibition and radiotherapy. *Oncoimmunology.* 2017;7:e1385689.
249. Sautès-Fridman C, Petitprez F, Calderaro J, Fridman WH. Tertiary lymphoid structures in the era of cancer immunotherapy. *Nat Rev Cancer.* 2019;19:307–25.
250. Varn FS, Wang Y, Mullins DW, Fiering S, Cheng C. Systematic pan-cancer analysis reveals immune cell interactions in the tumor microenvironment. *Cancer Res.* 2017;77:1271–82.
251. Locasale JW. Serine, glycine and the one-carbon cycle: cancer metabolism in full circle. *Nat Rev Cancer.* 2013;13:572–83.
252. Hayward SL, Scharer CD, Cartwright EK, Takamura S, Li Z-RT, Boss JM, et al. Environmental cues regulate epigenetic reprogramming of airway-resident memory CD8+ T cells. *Nat Immunol.* 2020;21:309–20.
253. Yan D, Adeshakin AO, Xu M, Afolabi LO, Zhang G, Chen YH, et al. Lipid metabolic pathways confer the immunosuppressive function of myeloid-derived suppressor cells in tumor. *Front Immunol.* 2019;10:1399.
254. Weinberg SE, Singer BD, Steinert EM, Martinez CA, Mehta MM, Martinez-Reyes J, et al. Mitochondrial complex III is essential for suppressive function of regulatory T cells. *Nature.* 2019;565:495–9.
255. Kumagai S, Togashi Y, Sakai C, Kawazoe A, Kawazu M, Ueno T, et al. An oncogenic alteration creates a microenvironment that promotes tumor progression by conferring a metabolic advantage to regulatory T cells. *Immunity.* 2020;53:187–203.e8.
256. Choi SYC, Collins CC, Gout PW, Wang Y. Cancer-generated lactic acid: a regulatory, immunosuppressive metabolite? *J Pathol.* 2013;230:350–5.
257. Naquet P, Giessler C, Galland F. Metabolic adaptation of tissues to stress releases metabolites influencing innate immunity. *Curr Opin Immunol.* 2016;38:30–8.
258. Wang H, Franco F, Tsui Y-C, Xie X, Trefny MP, Zappasodi R, et al. CD36-mediated metabolic adaptation supports regulatory T cell survival and function in tumors. *Nat Immunol.* 2020;21:23.

Publisher's Note

Springer Nature remains neutral with regard to jurisdictional claims in published maps and institutional affiliations.

Enzymes Glycolytiques	Codés par différents gènes Epissage alternatif Modifications post-traductionnelles Régulations allostériques			
	✓	✓	✓	✓
HK	✓	✓	✓	✓
GPI	✓	✓	✓	✓
PFK1	✓	✓	✓	✓
PFK2	✓	✓	✓	
ALDO	✓	✓	✓	
TPI	✓	✓	✓	✓
GAPDH	✓	✓	✓	
PGK	✓	✓	✓	
PGAM	✓	✓	✓	✓
ENO	✓	✓	✓	
PK	✓	✓	✓	✓
LDH	✓	✓	✓	

Figure 5 : Isoformes des enzymes glycolytiques

Certaines enzymes glycolytiques présentent des isoformes issues d'un codage par différents gènes, d'un épissage alternatif, de modifications post-traductionnelles ou encore présentant une sensibilité différentielle à des mécanismes de régulation allostériques. Figure adaptée de la référence (10).

B) Reprogrammation métabolique tumorale

Les altérations génétiques, épigénétiques ou protéiques présentes dans les cellules cancéreuses vont modifier la régulation du cycle cellulaire en augmentant les capacités prolifératives, les voies de croissance mais aussi les voies énergétiques. Nous allons voir dans ce chapitre comment les altérations tumorales initient le changement du métabolisme et comment cette reprogrammation métabolique est au bénéfice de la cellule cancéreuse notamment par l'apport des blocs de construction d'une cellule fille, aussi appelés *building blocks*.

1) Hétérogénéité de l'utilisation du glucose

Les gènes associés à la glycolyse sont les plus souvent dérégulés et amplifiés dans les cancers (11,12). En plus des altérations génétiques, l'expression d'isoformes d'enzymes de la glycolyse est souvent retrouvée. Elles proviennent de la transcription de différents gènes, de formes d'épissage différentes, de modifications post-traductionnelles ou encore de régulations allostériques (**Figure 5**). Ces isoformes se distinguent de la forme sauvage par leur affinité pour leurs substrats (ex : HK), leur vitesse de catalyse (ex : PK), leur régulation allostérique (ex : PFK) et leurs fonctions régulatrices indépendantes de leur activité catalytique, notamment par translocation dans le noyau. Par exemple, la PKM2 peut augmenter la synthèse de lactate et de macromolécules une fois entrée dans le noyau. La PGK1 possède également la capacité de translocation nucléaire (13,14). L'hétérogénéité de l'utilisation du glucose permet le maintien de l'homéostasie dans l'ensemble de l'organisme, notamment l'expression d'isoformes spécifiques au sein des tissus, la garantie d'une réponse rapide en cas de stress sur la disponibilité de glucose et d'oxygène et enfin de soutenir une consommation de glucose accrue (10). Dans les tumeurs, ce sont notamment des isoformes de la PK, PFK ou encore LDH qui sont principalement trouvées.

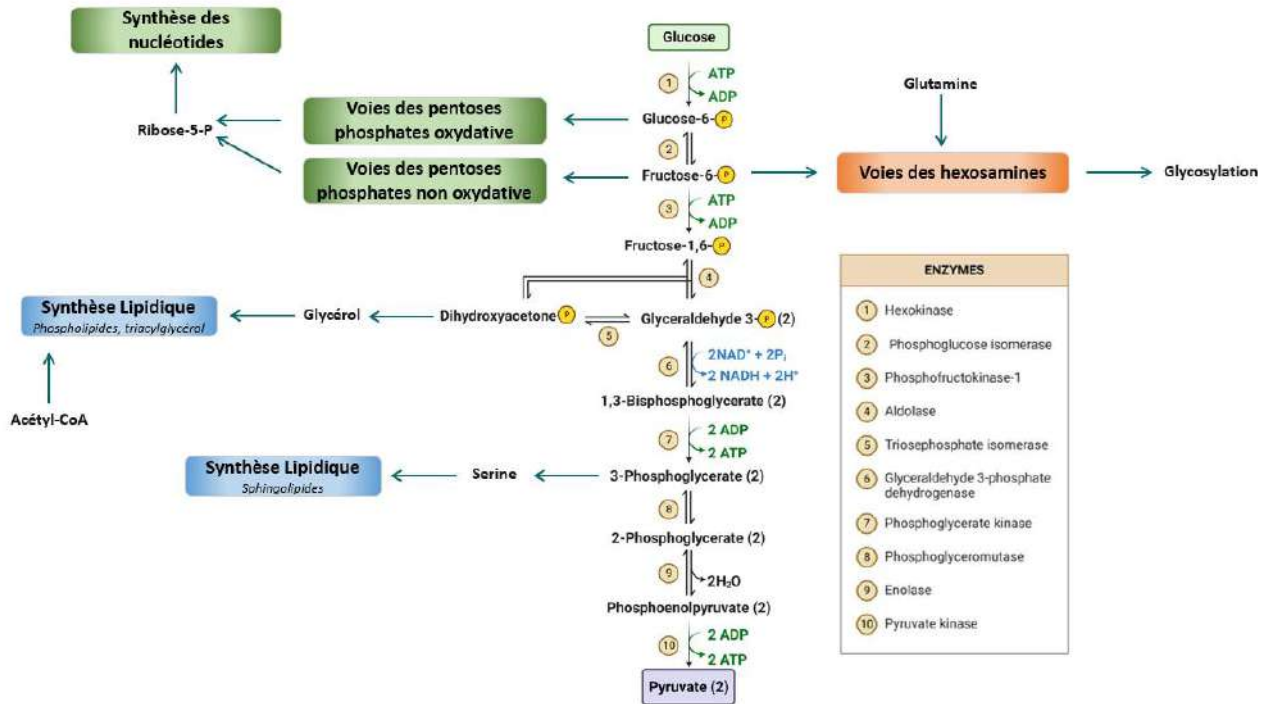


Figure 6 : Glycolyse et voies dérivées

La glycolyse désigne l'ensemble des réactions permettant la transformation de la molécule de glucose en pyruvate. Plusieurs intermédiaires de la glycolyse sont des carrefours métaboliques à l'origine des voies dérivées de la glycolyse aussi appelées voies branchées à la glycolyse que sont les voies des pentoses phosphates, la voie des hexosamines et la synthèse lipidique.

2) Les voies anaboliques dérivées de la glycolyse

Pourquoi l'augmentation de l'utilisation du glucose est-elle bénéfique au sein des tumeurs ? La réponse est la suivante. De nombreux intermédiaires de la glycolyse donnent naissance à une arborescence des voies de biosynthèse pour former des acides nucléiques, des protéines et des lipides (**Figure 6**) :

- la voie des pentoses phosphates permet la génération des riboses à partir du glucose-6-phosphate. Les riboses sont nécessaires à la formation des nucléotides, constituant des acides nucléiques et du NADPH. Le NADPH permet le maintien du glutathion à l'état réduit nécessaire à la détoxification d'espèces réactives de l'oxygène et les mécanismes de réparation moléculaire (15). Le maintien du pouvoir Redox est essentiel et déterminant pour la progression tumorale et les processus métastatiques afin d'échapper à une mort cellulaire induite par divers types de stress (ex : anoïkis).

- la voie des hexosamines est nécessaire à la glycosylation des protéines *via* l'intermédiaire fructose-6-phosphate.

- la voie de synthèse lipidique *via* la conversion du dihydroxyacétone-phosphate en glycérol alimente la synthèse des phospholipides et des triglycérides (16,17).

- la voie sérine-glycine qui enclenche le métabolisme 1C, permet la génération de glutathion, de nucléotides et d'approvisionner les mécanismes de méthylation. Elle peut contribuer à la synthèse lipidique *via* la génération de céramides qui vont permettre la synthèse des sphingolipides.

La surexpression des gènes liés à ces voies de biosynthèses dérivées de la glycolyse est fréquemment observée dans les tumeurs, notamment concernant les gènes associés à la voie des purines et des pyrimidines (11). La consommation des intermédiaires de la glycolyse en amont du cycle de Krebs va limiter l'apport de pyruvate à la mitochondrie. De même, la part plus importante de pyruvate convertie en lactate par la lactate déshydrogénase (LDH) va renforcer cet effet.

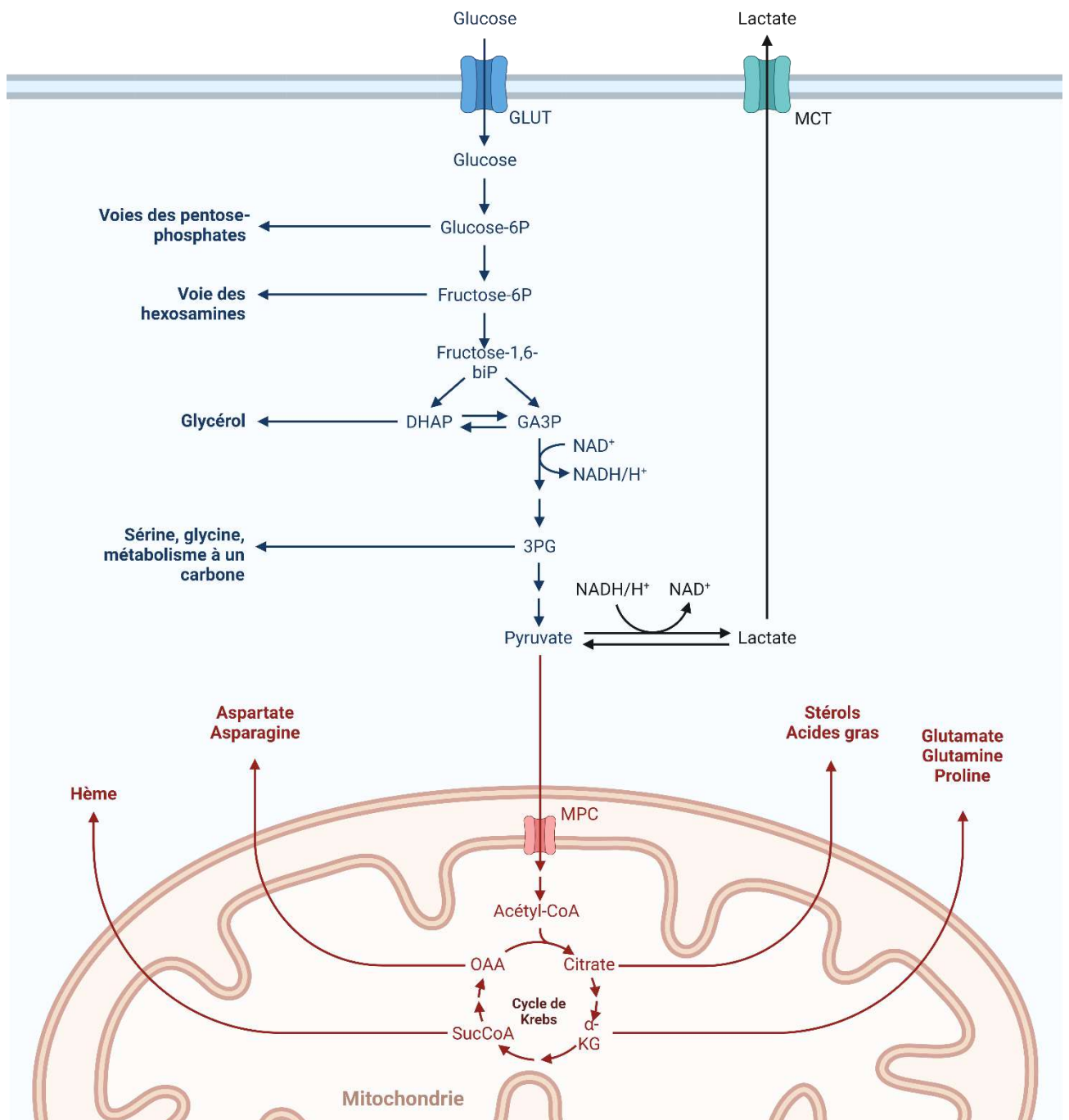


Figure 7 : L'effet Warburg

L'effet Warburg désigne l'utilisation du glucose vers une conversion en lactate en condition aérobie. Cela permet l'accumulation des intermédiaires de la glycolyse en amont et la disponibilité pour leur utilisation dans les voies dérivées de la glycolyse, la régénération de NAD⁺. Une fraction réduite de pyruvate entre dans le cycle de Krebs. Certaines intermédiaires du cycle de Krebs vont contribuer à la synthèse cellulaire, processus aussi régulé par l'import mitochondrial de métabolites par anaplérose.

3) Pourquoi l'Effet Warburg ?

L'effet Warburg désigne un état métabolique dans lequel les cellules présentent une forte consommation de glucose, une forte production de lactate et cela même si la concentration en oxygène est suffisante pour garantir la respiration mitochondriale (18). L'un des grands débats de la communauté scientifique fut de savoir, comme le postulait initialement Warburg (19), si les altérations mitochondriales parfois observées dans les cellules cancéreuses étaient à l'origine de l'effet Warburg. En effet, l'altération de l'expression de certaines enzymes mitochondriales va conduire à la réorientation des flux métaboliques. Cette réorientation des flux notamment des intermédiaires du cycle de Krebs vers les voies de biosynthèses permet d'éviter une forte production de ROS par la chaîne de transports des électrons (**Figure 7**). Pourtant, ce n'est pas seulement l'altération des voies mitochondriales qui explique la plus forte consommation de glucose et la production de lactate. D'ailleurs, les mitochondries cellules tumorales contribuent toujours au métabolisme malgré un dysfonctionnement potentiel. Plusieurs études utilisant des isotopes lourds ont prouvé que les carbones présents dans les différentes sources énergétiques comme le glucose, le lactate ou encore la glutamine peuvent se retrouver dans des intermédiaires du cycle de Krebs (20).

C'est donc un ensemble d'altérations internes et externes à la mitochondrie ainsi qu'une modification des besoins énergétiques qui vont renforcer l'effet Warburg.

Premièrement, comme nous l'avons vu dans le chapitre précédent, l'altération de l'expression d'oncogènes et des gènes suppresseurs de tumeurs va favoriser certaines voies de signalisation comme PI3K/AKT associées à la prolifération. L'activation de ces voies de signalisation va promouvoir la transcription des gènes des enzymes glycolytiques ou des régulateurs positifs ou négatives de celle-ci. Par exemple, certaines tyrosines kinases peuvent impacter la fonction de PKM2, favorisant la conversion du pyruvate vers le lactate. L'utilisation de l'effet Warburg renforce également l'apport des *building blocks*, nécessaire et limitant, pour la prolifération cellulaire (**Figure 7**).

Il est également intéressant de noter qu'en cas de forte demande énergétique, comme c'est le cas des cellules cancéreuses, la production de lactate va être favorisée malgré un apport réduit en ATP. L'apport réduit en ATP d'origine mitochondriale peut être en partie compensé par l'augmentation du flux glycolytique permettant le maintien de la prolifération cellulaire (17). En effet, bien que certaines réactions de synthèse de biomasse nécessitent de l'ATP, ce n'en est pas pour autant le substrat principal. De nombreux cofacteurs peuvent devenir limitants dans des cellules cancéreuses.

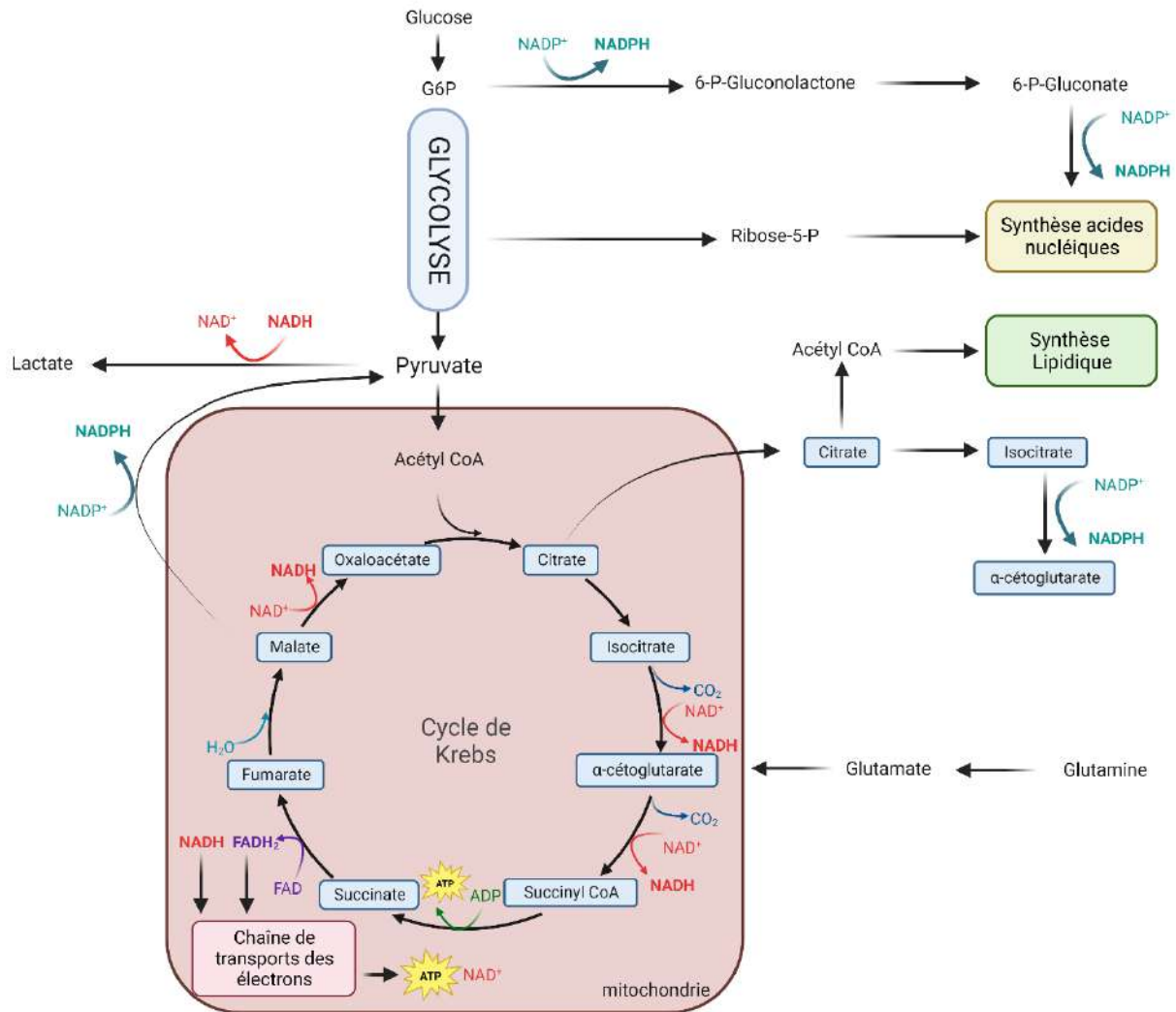


Figure 8 : Implication du NADP et de l'acétyl-CoA dans le métabolisme tumoral

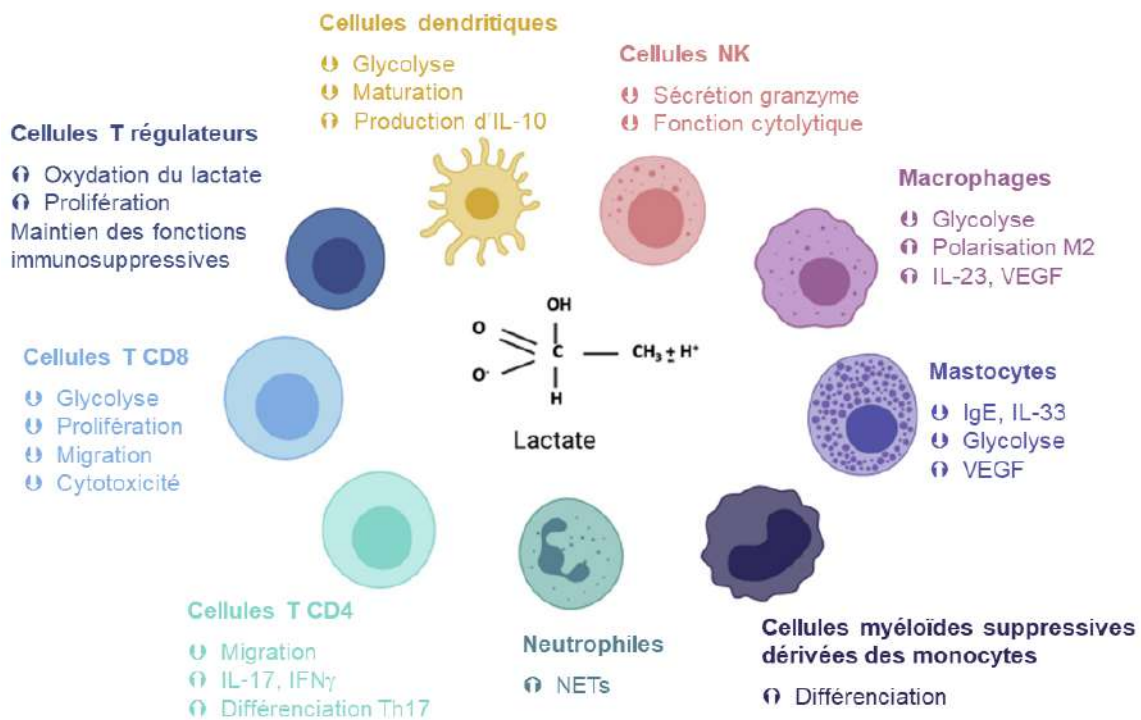
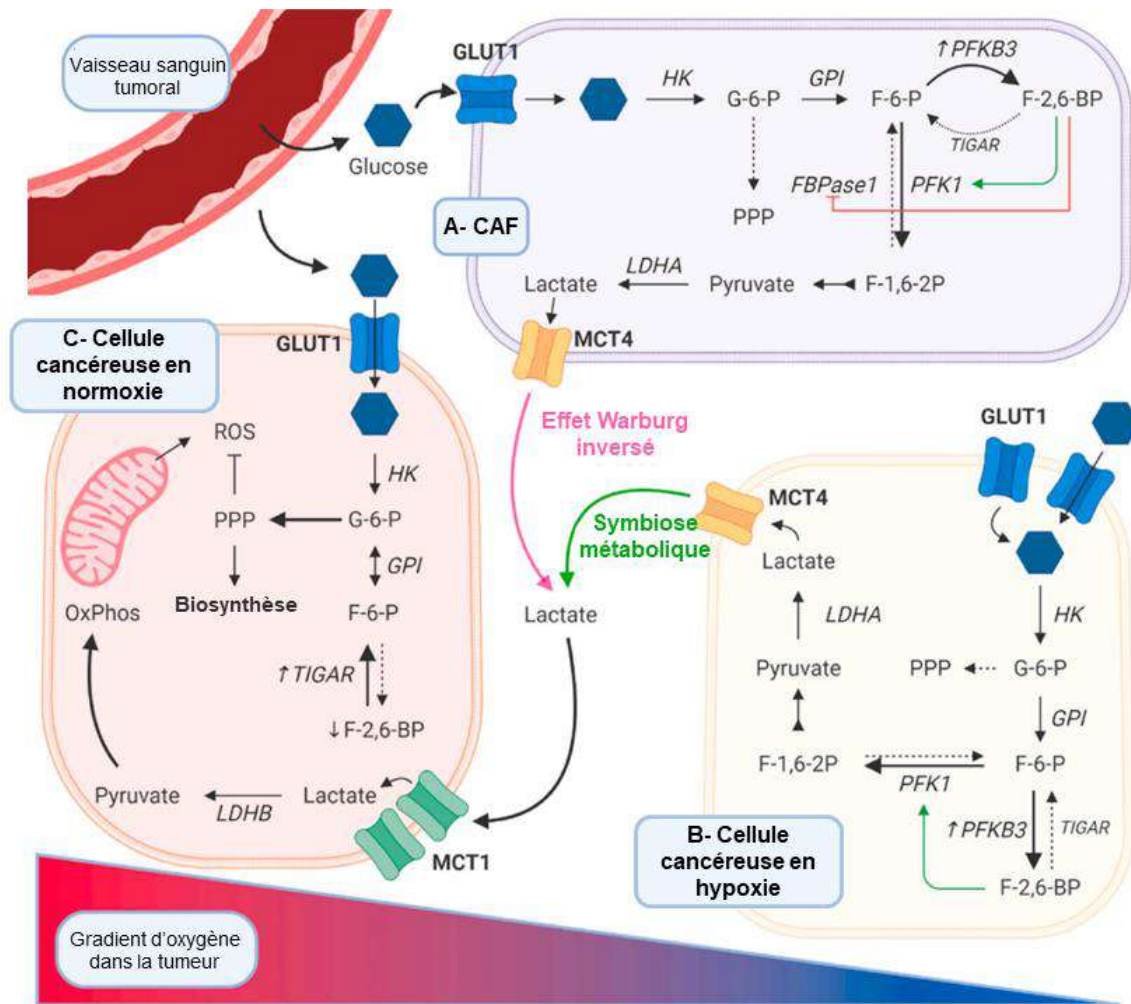
Les cofacteurs NAD, NADP et acétyl-coA interviennent dans de nombreuses réactions, la balance entre leur consommation et leur génération est finement régulée. Le NAD⁺ est produit lors de la génération de lactate et au cours des réactions de la chaîne de transports des électrons. Le NADH est généré au cours de la glycolyse, du cycle de Krebs et l'oxydation des acides gras. La conversion NADP⁺/NADPH intervient dans la voie des pentoses phosphates et le NADPH est consommé lors des réactions anaboliques et des défenses antioxydantes.

Les cellules prolifératives vont avoir besoin d'une grande quantité de NADPH et d'acétyl-CoA. En effet, une molécule de glucose suffira pour l'apport de tout l'ATP nécessaire à de multiples réactions alors que l'utilisation de plusieurs molécules de glucose ou d'autres sources de carbones seront nécessaires pour la régénération du NADPH et de l'acétyl-CoA (**Figure 8**). La glutaminolyse désigne la conversion de la glutamine en glutamate puis en alpha-cétoglutarate. L'alpha-cétoglutarate va être converti en succinate, fumarate puis malate. La malate déshydrogénase NADP⁺ spécifique va convertir le malate en pyruvate permettant la régénération d'une molécule de NADPH. Le NADPH peut être régénéré également par l'activité de la glucose-6-phosphate déshydrogénase, de la conversion de l'isocitrate en alpha-cétoglutarate ou au cours du *shunt* pentose phosphate du 6-P-gluconate vers la synthèse des acides nucléiques. (**Figure 8**).

Enfin, la mise en place de l'effet Warburg nécessite un maintien de la glycolyse forte consommatrice de NAD⁺. Plusieurs réactions cytosoliques ou mitochondriales vont participer à ce mécanisme de régénération (**Figure 8**). En effet, les tumeurs possèdent un ratio élevé de NAD⁺/NADH (21). La conversion du pyruvate en lactate va contribuer à régénérer le NAD⁺ sans faire intervenir des processus mitochondriaux. La régénération du NAD, FAD peut également provenir de la synthèse d'alanine, de la navette malate-aspartate ou encore de la voie des pentoses phosphates

4) Le lactate : un métabolite central du métabolisme tumoral

À l'état physiologique, le lactate est la source principale d'énergie dans certains organes notamment le cœur, le cerveau ou les muscles squelettiques. Au niveau du foie, il peut être converti en glucose dans un processus que l'on nomme le cycle de Cori. Le lactate joue également le rôle de navette de carbone entre différents organes, différentes cellules et donc possède également ce rôle de navette dans les tumeurs. L'export du lactate en dehors d'une cellule permet de garantir l'homéostasie cellulaire notamment par le maintien du pH intracellulaire et ainsi limiter sa toxicité cellulaire. Il est un métabolite central dans plusieurs processus biologiques, par exemple en alimentant le cycle de Krebs (22). La source principale de lactate dans les cellules cancéreuses est le pyruvate issu de la glycolyse bien que la glutamine puisse également générer le pyruvate. C'est la lactate déshydrogénase A cytosolique qui va catalyser la conversion du pyruvate. Son expression est souvent élevée dans les tumeurs et associée à un mauvais pronostic. Certaines tyrosines kinases surexprimées dans les tumeurs contribuent à la phosphorylation de la LDHA ayant pour conséquence une augmentation de son activité catalytique (23). Enfin, la LDHA peut produire un oncométabolite, le L-2-HG. Une autre isoforme, la lactate déshydrogénase B pourrait être située dans la membrane interne de la mitochondrie. Il est supposé que le lactate entre dans la mitochondrie *via* le récepteur MCT afin d'être converti en pyruvate et potentiellement alimenter le cycle de Krebs.



Ce phénomène, appelé effet Warburg inversé, décrit une situation où des cellules stromales comme les fibroblastes associés aux cellules cancéreuses présentent un métabolisme fortement glycolytique (**Figure 9**). Le lactate sécrété va être consommé par les cellules cancéreuses, entrer dans la mitochondrie et alimenter le cycle de Krebs. Les cellules cancéreuses vont présenter un métabolisme énergétique différent selon qu'elles se situent en zone de normoxie ou d'hypoxie, conduisant à une modification du fonctionnement mitochondrial. Ainsi, une symbiose métabolique peut s'instaurer entre des cellules cancéreuses en hypoxie et productrices de lactate et les cellules cancéreuses en normoxie qui peuvent utiliser le lactate comme source de pyruvate et renforcer l'utilisation de leur mitochondrie (**Figure 9**).

Le lactate présent dans le microenvironnement tumoral peut également être consommé par différentes cellules immunitaires infiltrant les tumeurs et altérer leurs fonctions (**Figure 9**) (24,25). Le lactate va notamment avoir pour effet une diminution de la glycolyse au sein des cellules dendritiques, des cellules T CD8 et des macrophages. Leur maturation et leur production cytokinique vont également être altérées. Les CD8 comme les cellules NK vont perdre leur potentiel cytotoxique. La consommation de lactate sera bénéfique pour les fonctions des cellules immunitaires immunosuppressives telles que les cellules T régulatrices, les cellules myéloïdes immunosuppressives dérivées des monocytes (MDSC) ou les mastocytes (25). Cependant, le lactate peut promouvoir dans certains cas, les fonctions cytolytiques dans les cellules T CD8 en renforçant leurs propriétés cellules souches en inhibant l'activité des histones désacétylases (26).

◀ **Figure 9 : La consommation de lactate dans le microenvironnement tumoral**

Panel haut : *Le glucose apporté par les vaisseaux sanguins présent dans les tumeurs va pouvoir être consommé par les cellules du microenvironnement tumoral. Dans les cellules cancéreuses en normoxie, le glucose va être converti en pyruvate et alimenter le métabolisme mitochondrial. Dans les fibroblastes associés au cancer (acronyme CAF en anglais) ainsi que dans les cellules cancéreuses en zone hypoxique, le glucose consommé sera converti en lactate et sécrété dans le microenvironnement tumoral. Ce dernier pourra être réutilisé par les cellules cancéreuses en normoxie par un phénomène d'effet Warburg inversé ou par symbiose métabolique.*

Panel bas : *la consommation de lactate par les différents types de cellules immunitaires infiltrant les tumeurs va avoir des conséquences variables sur leur activation, leur fonction métabolique ou encore leur maturation. La conséquence sera une diminution des fonctions des cellules immunitaires anti-tumorales et l'augmentation de la maturation et des fonctions des cellules immunosuppressives et protumorales, contribuant ainsi à la progression tumorale. Figure adaptée Caslin et al 2021.*

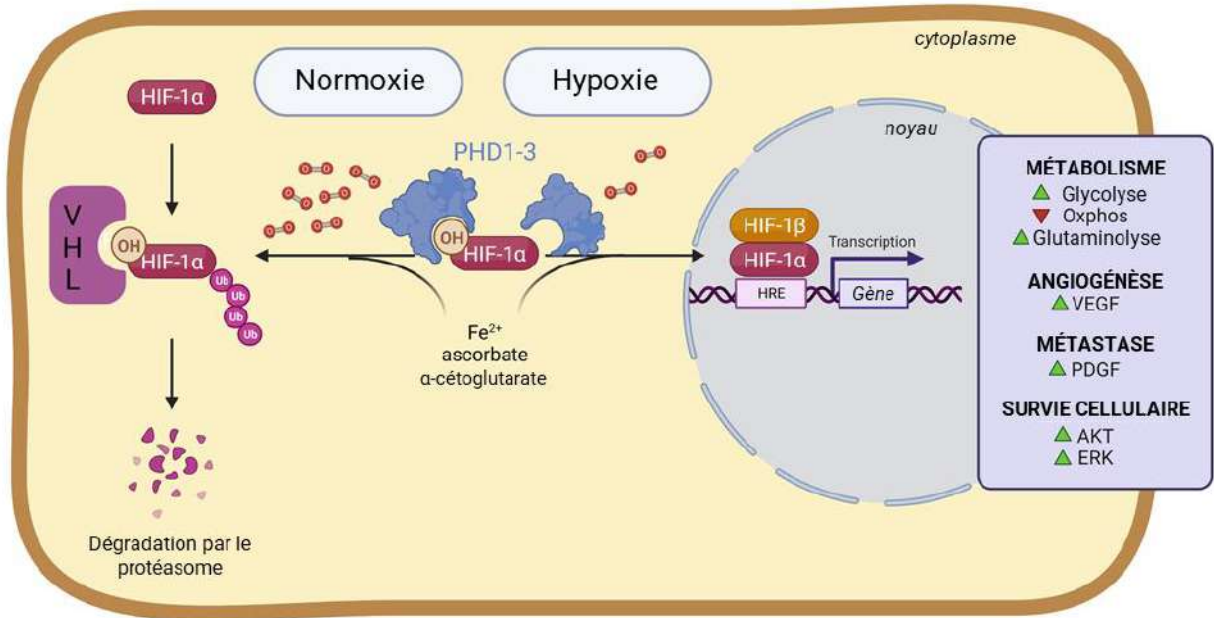


Figure 10 : Voie de signalisation HIF1 α

La perception de l'hypoxie s'effectue par la régulation du facteur de transcription HIF1 α via par hydroxylation dépendantes des prolylhydroxylases PHDs. Une fois hydroxylé, HIF1 α est ubiquitinylé par l'enzyme VHL et adressé au protéasome pour dégradation. En condition hypoxique, HIF1 α transloque dans le noyau où il se fixe sur un élément HRE sous forme de dimère avec HIF-1 β et permet la transcription de différents gènes impliqués dans le métabolisme, l'angiogénèse, le processus de métastase ou encore la survie cellulaire. Figure adaptée de la référence (27).

5) Hypoxie et vascularisation

La présence d'oxygène dans les tissus est indispensable au bon fonctionnement de différentes réactions biologiques, notamment lors de la respiration mitochondriale où il est l'accepteur final d'électrons de la chaîne respiratoire. Les cellules ont la capacité de percevoir le niveau d'oxygène dans leur environnement afin de pouvoir s'adapter. Cette capacité de mesurer le niveau d'oxygène passe par le relargage de ROS mitochondriaux et ne nécessite pas le fonctionnement de la chaîne de transports d'électrons (28,29). Les tumeurs possèdent une vascularisation anarchique ce qui contribue à la formation de zones hypoxiques. De plus, les altérations fréquentes du fonctionnement mitochondrial conduisent à l'accumulation d'espèces réactives de l'oxygène, un défaut du potentiel de membrane mitochondrial et un détournement des voies de production énergétique. Le manque d'oxygène va permettre la stabilisation d'une famille de facteurs de transcription hétérodimériques connus sous le nom de facteurs inductibles par l'hypoxie, HIFs en anglais (30). En normoxie, les prolylhydroxylases vont conduire à l'hydroxylation du facteur HIF1 α (**Figure 10**). La forme hydroxylée d'HIF1 α va être reconnue par le complexe VHL, favorisant son ubiquitination et sa dégradation par le protéasome. En condition hypoxique ou en cas d'élévation de succinate ou de L-2HG, ce processus est inactivé ; HIF1 α va pouvoir transloquer dans le noyau et induire l'expression de nombreux gènes impliqués dans le métabolisme, l'angiogenèse, l'identité, la prolifération et la différenciation cellulaire (24) (**Figure 10**). Le manque d'oxygène va non seulement modifier les propriétés intrinsèques et le métabolisme des cellules cancéreuses mais également celles de tout le microenvironnement (32).

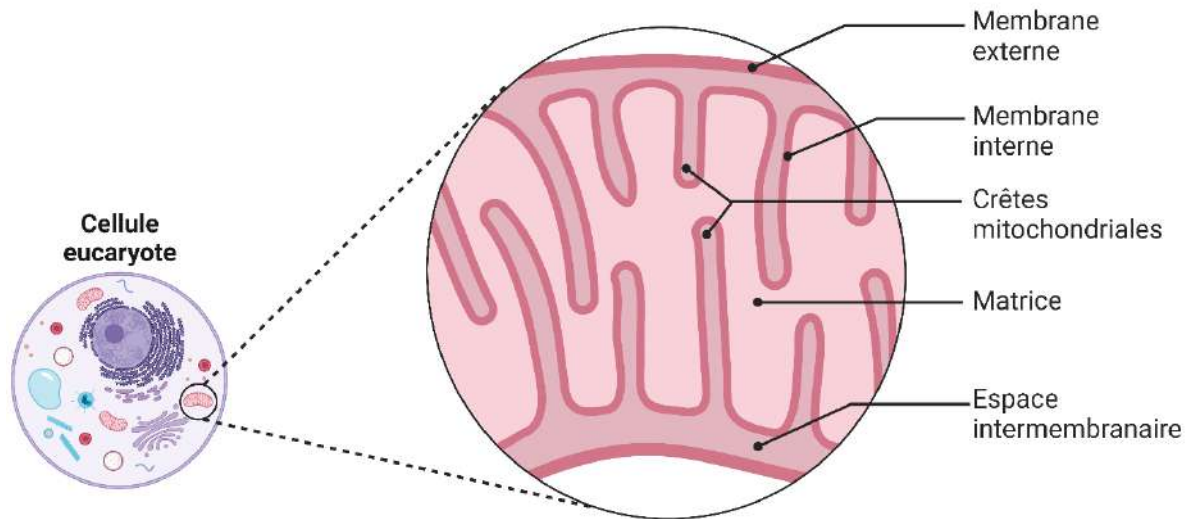


Figure 11 : Structure interne de la mitochondrie

La mitochondrie est une organelle présente dans les cellules eucaryotes. Elle est composée d'une membrane externe et d'une membrane interne séparées par l'espace intermembranaire. La membrane interne forme des replis désignés sous le terme de crêtes mitochondriales. La matrice constitue l'espace le plus interne de la mitochondrie.

II) La mitochondrie

La mitochondrie est désignée par la communauté scientifique comme le générateur énergétique de la cellule. Le spectre de processus biologiques dépendant tout ou partie de la mitochondrie est très large. C'est une organelle centrale, connectée aux autres composants cellulaires, senseur du stress cellulaire et véritable carrefour décisionnel. Ses fonctions sont hautement régulées impliquant des modifications fonctionnelles comme une réorientation des flux énergétiques, de la polarité et de la perméabilité de ces membranes mais aussi structurales. La structure de la mitochondrie est assez complexe, reflet de son origine endosymbiotique. Elle est composée d'une membrane externe et d'une membrane interne, qui délimitent respectivement l'espace intermembranaire du cytosol et la matrice de l'espace intermembranaire (33) (**Figure 11**). Les nombreux replis de la membrane interne délimitent ce qu'on appelle les crêtes mitochondriales. La taille et l'aspect des crêtes peuvent également être très différents en fonction du stress tissulaire perçu (34). Les mitochondries sont souvent représentées comme des objets individualisés, allongés et ronds. Pourtant, leur organisation peut varier d'un réseau complexe et continu à de petites mitochondries individualisées. Le passage de l'un à l'autre dépend des mécanismes de fusion et fission mitochondriale qui nécessitent l'intervention de nombreux régulateurs dont les principaux acteurs sont OMA1 et OPA1 en situation de réponse au stress.

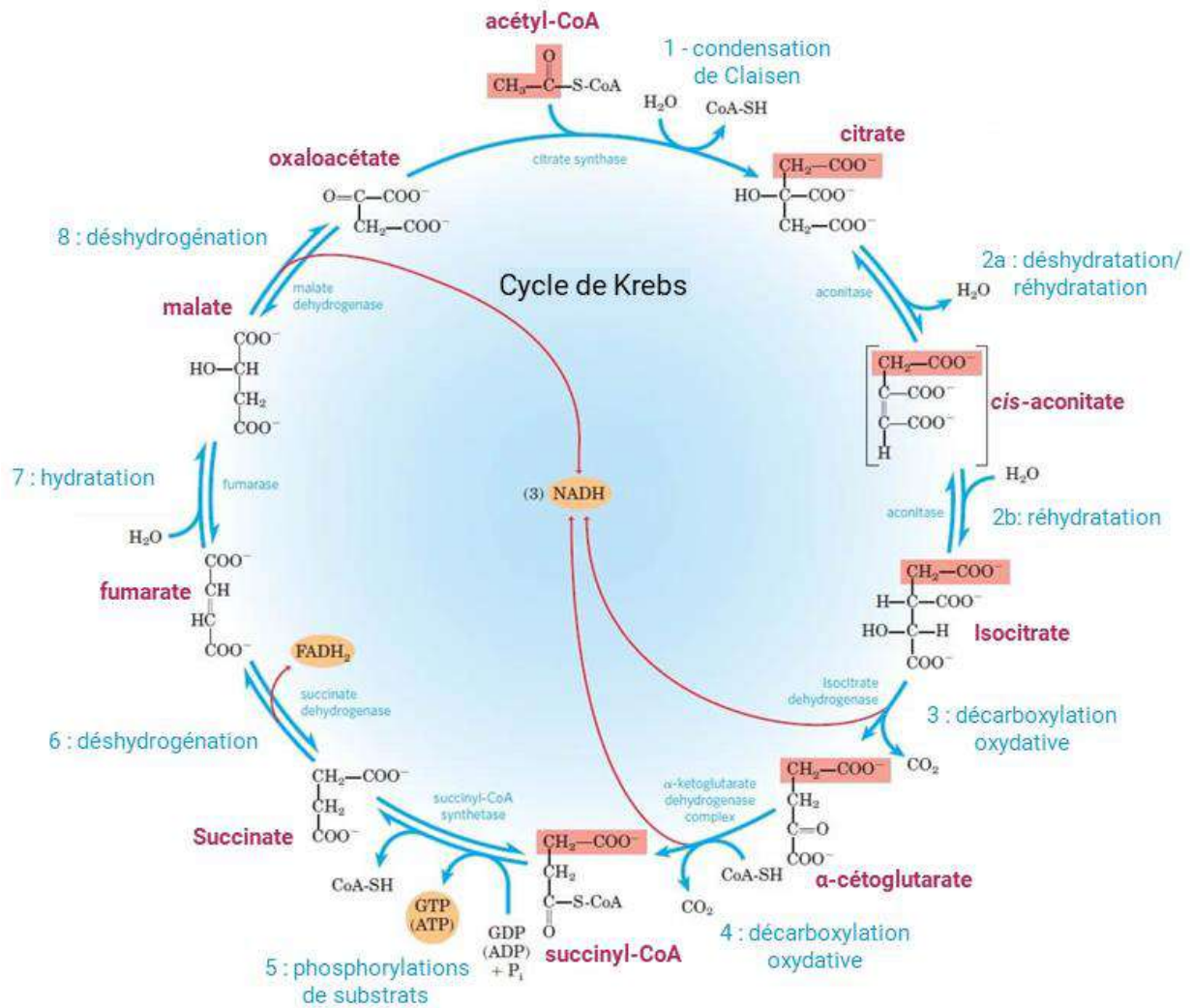


Figure 12 : le Cycle de Krebs

Le cycle de Krebs désigne un ensemble de 8 réactions enzymatiques permettant la génération de NADH et FADH₂. Figure traduite et adaptée du livre (35).

A) Hub énergétique

Nous pouvons différencier deux grands modes de fonctionnement métabolique de la mitochondrie. Un mode catabolique qui va conduire à la conversion du glucose en pyruvate alimentant le cycle de Krebs, la chaîne de transport des électrons et à la production *via* l'ATP synthase, d'une grande quantité d'ATP. Le fonctionnement anabolique quant à lui favorise l'accumulation d'intermédiaires du cycle de Krebs, favorisant leur utilisation dans les voies anaboliques. Ce sont ces processus que nous allons voir plus amplement dans les sous-parties qui suivent.

1) Mode catabolique et phosphorylation oxydative

Le catabolisme regroupe l'ensemble des processus liés à la dégradation de molécules carbonées comme le glucose ou les acides gras en une forme d'énergie utilisable par la cellule comme l'ATP. Après la conversion du glucose en pyruvate, celui-ci va entrer dans la mitochondrie et initier le cycle de Krebs (aussi appelé cycle des déshydrogénases). La première réaction est la décarboxylation du pyruvate en acétyl-CoA. Le pyruvate n'est pas la seule source d'acétyl-CoA cellulaire (**Figure 12**). Lors de la dégradation des acides gras par β -oxydation, une molécule d'acétyl-CoA sera générée à chaque cycle dégradatif. L'acétyl-CoA va être assemblé à l'oxaloacétate pour former le citrate. Par processus d'isomérisation, le citrate va devenir l'isocitrate, qui, après oxydation et décarboxylation, va donner l'alpha-cétoglutarate. Par décarboxylation oxydative, l'alpha-cétoglutarate va être converti en succinyl-CoA puis phosphorylé en succinate. Le succinate va être oxydé en fumarate, lui-même converti en malate après déshydratation. Enfin, l'oxydation du malate permet la régénération de l'oxaloacétate (**Figure 12**). L'ensemble de ces réactions vont conduire à la génération de trois molécules de NADH, une molécule de FADH₂, de l'ATP, deux protons H⁺ et une molécule de coenzymeA. C'est le couplage du cycle de Krebs à la chaîne de transport des électrons qui permettra de régénérer les cofacteurs consommés lors du cycle et de produire une grande quantité d'ATP (36).

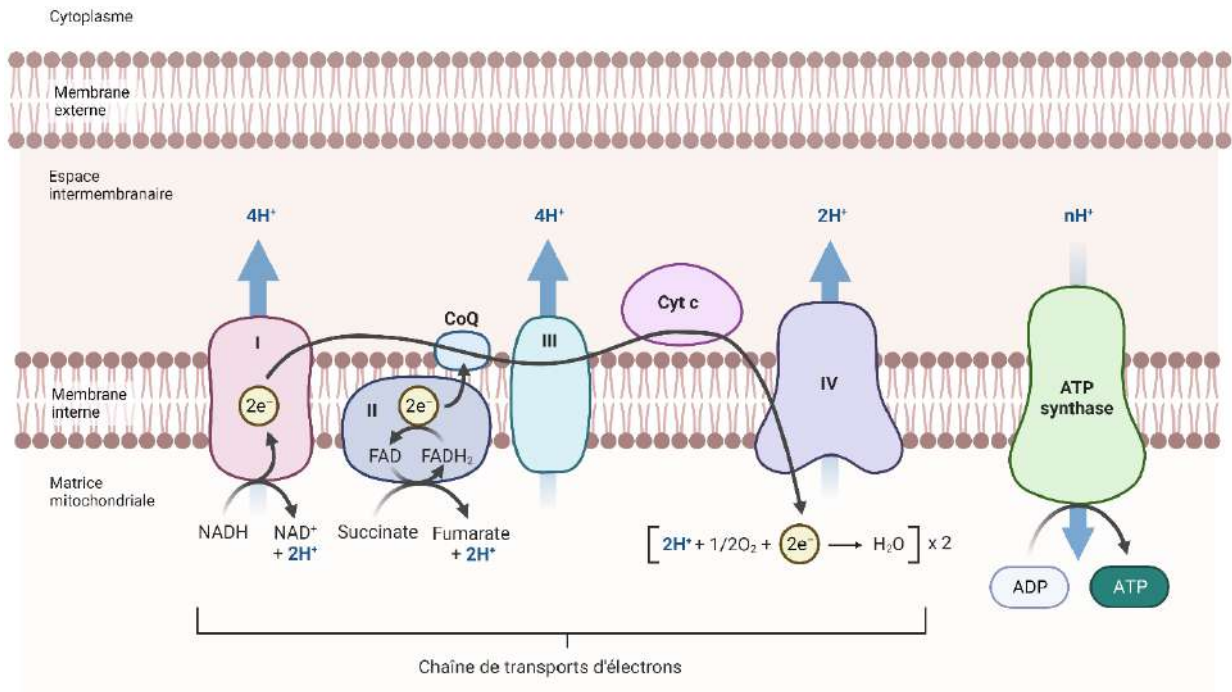


Figure 13 : La chaîne de transport des électrons

La chaîne de transport des électrons est constituée de 5 complexes protéiques insérés dans la membrane interne de la mitochondrie. Les électrons libérés lors de l'oxydation du NADH ou de la conversion du succinate en fumarate vont être conduits dans les différents complexes et résulter en la formation d'H₂O. L'ensemble permet l'établissement d'un gradient de protons H⁺ permettant l'activation de l'ATP Synthase et la production d'ATP.

2) La chaîne de transport d'électrons

La membrane interne mitochondriale possède un rôle de barrière pour les protons H^+ séparant l'espace intermembranaire, où ils s'accumulent, de la matrice mitochondriale. L'homéostasie de la mitochondrie et la production d'ATP dépendent du maintien de ce gradient de protons. La chaîne de transport des électrons joue un rôle essentiel dans le maintien de ce gradient et régule les processus de vie et de mort cellulaire. Elle est constituée de quatre complexes protéiques. Les complexes I, III et IV pompent directement les protons de la matrice mitochondriale vers l'espace intermembranaire (**Figure 13**). Les molécules de NADH produites lors des réactions du cycle de Krebs vont se fixer sur le complexe I de la chaîne de transport d'électrons. Le NADH va être oxydé en NAD^+ et libérer un proton H^+ . Ce proton va réduire la quinone présente dans le complexe I. Les électrons également libérés par la réaction vont passer successivement par plusieurs centres redox Fe-S au sein même du complexe I. L'énergie libérée par le transfert d'électrons va donner l'énergie nécessaire au complexe pour pomper des protons de la matrice vers l'espace intermembranaire. Après leurs passages successifs par plusieurs centres redox, les électrons vont être capturés par la Coenzyme Q qui va transférer ces électrons au complexe III. Le complexe II fonctionne d'une manière similaire bien que les molécules participant à la réaction d'oxydo-réduction soient différentes et qu'il ne possède pas d'activité protomotrice. Le complexe II n'est autre que l'enzyme SDH, seul enzyme du cycle de Krebs liée à la membrane mitochondriale, qui catalyse la conversion du succinate en fumarate couplée à la réduction du FAD^+ en $FADH_2$. Les électrons seront, comme pour le complexe I, acheminés vers le complexe III. Un électron va être recyclé et les autres capturés par le cytochrome c qui va les conduire au complexe IV. C'est dans ce complexe que se termine la réaction, les électrons vont être utilisés dans la conversion de l'oxygène en molécule d'eau. La réaction va utiliser quatre protons de la matrice et permettre le passage de quatre autres dans l'espace intermembranaire. Les protons contenus dans l'espace intermembranaire vont regagner la matrice mitochondriale *via* l'ATP synthase, générant ainsi une grande quantité d'ATP. L'ATP est formée par ajout d'un groupement de phosphate inorganique à l'ADP. C'est à cette réaction que l'on fait allusion lorsque que nous employons le terme de phosphorylation oxydative ou l'acronyme OXPHOS en anglais. L'étude de l'activité mitochondriale se fait *via* l'utilisation de différentes drogues qui viennent prévenir l'activité de certains complexes de la chaîne de transport d'électrons. La roténone vient inhiber le complexe I, l'antimycine le complexe III, le cyanide le complexe IV et l'oligomycine, l'ATP synthase. On parle également d'agents découplants comme le carbonylcyanure m-chlorophénylhydrazone ou CCCP, qui est un protonophore. Il va dissiper le gradient de protons, diminuant ainsi l'efficacité du complexe ATP synthase et donc, sous action prolongée, induire la mort cellulaire (37).

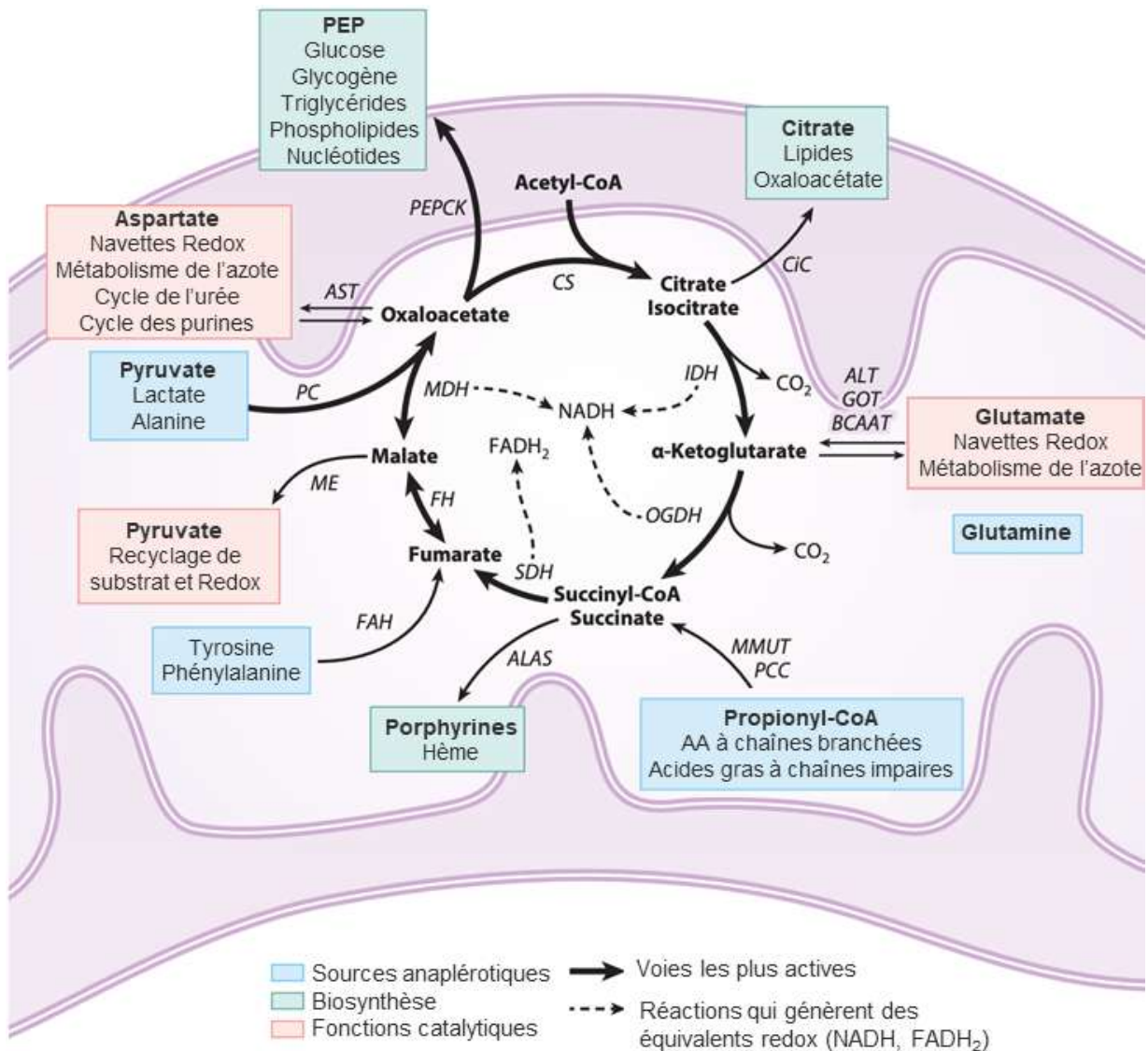


Figure 14 : Anaplrèse et cataplrèse mitochondriales

Les intermédiaires du cycle de Krebs constituent des carrefours métaboliques, leur consommation et renouvellement sont régis par les principes de cataplrèse et anaplrèse respectivement. Les sources anaplerotiques renouvèlent l'alpha-cétoglutarate, le succinate, l'oxaloacétate ou le fumarate. Les métabolites pouvant alimenter la biosynthèse sont le citrate, l'oxaloacétate et le succinate. Enfin, certains intermédiaires comme l'oxaloacétate, l'alpha-cétoglutarate et le malate peuvent intervenir dans des réactions de cataplrèse. Abréviations : ALAS : δ -aminolévulinique acide synthase; ALT : alanine aminotransférase; AST : aspartate aminotransférase; BCAAs : acides aminés à chaînes branchées; BCAAT : acides aminés à chaînes branchées aminotransférase; CiC : citrate-isocitrate transporteur; CS : citrate synthase; FAH : fumarylacétoacétate hydrolase; Fas : acides gras ; FH, fumarate hydratase; GOT : glutamique-oxaloacétique transaminase; IDH : isocitrate déshydrogénase; MDH : malate déshydrogénase; ME : enzyme malique; MMUT : méthylmalonyl-CoA mutase; OAA : oxaloacétate; OGDH : 2-oxoglutarate déshydrogénase; PC : pyruvate carboxylase; PCC : propionyl-CoA carboxylase; PEP : phosphoenolpyruvate; PEPC : phosphoenolpyruvate carboxykinase; redox : réduction-oxydation; SDH : succinate déshydrogénase; TCA, Acides tricarboxyliques. Figure traduite de la référence (38).

3) Anaplérose et cataplérose

Au-delà de leurs fonctions dans le cycle de Krebs, certains intermédiaires sont des carrefours métaboliques qui permettent de réguler les flux vers les voies de biosynthèse en jouant sur l'apport des précurseurs des réactions chimiques dans lesquelles ils sont impliqués, de la même manière que les voies de synthèse dérivées de la glycolyse. Ainsi, selon les conditions, les intermédiaires du cycle de Krebs peuvent être renouvelés par le principe d'anaplérose ou exportés par cataplérose (**Figure 14**). Ces deux modes de fonctionnement peuvent être au bénéfice de la plasticité du métabolisme tumoral. Dans des modèles génétiques où le complexe III de la chaîne de transport d'électrons est absent mais où le cycle de Krebs est fonctionnel, la croissance tumorale est favorisée, montrant que le cycle de Krebs et la chaîne de transport des électrons peuvent soutenir la progression tumorale indépendamment des réactions de phosphorylation oxydative (20,36). Comme nous l'avons vu, pour initier le cycle de Krebs, le pyruvate va entrer dans la mitochondrie et être converti en acétyl-CoA, cependant, une autre conversion est possible, celle du pyruvate en oxaloacétate, réaction anaplérotique catalysée par la pyruvate carboxylase. L'oxaloacétate peut régénérer le phosphoénolpyruvate ce qui contribue à la biosynthèse de nombreux glucides par néoglucogénèse, comme le glucose, le glycogène, les triglycérides et par les voies de synthèse dérivées de la glycolyse, la synthèse des nucléotides et des phospholipides (38–40). L'oxaloacétate peut être également renouvelé par transamination de l'aspartate ou *via* le pyruvate (provenant lui-même du lactate ou de l'alanine). La réaction de transformation d'aspartate en oxaloacétate étant réversible, ce dernier peut contribuer à la synthèse des nucléotides et des amino-acides. La glutaminolyse est un autre exemple de voie anaplérotique. En condition d'inhibition du transporteur MPC ou d'un accès restreint au glucose, la glutamine est convertie en glutamate et en ammoniacque. Le glutamate va être converti en alpha-cétoglutarate par déshydrogénation. De nombreuses études ont pu démontrer l'importance de la glutaminolyse dans la progression tumorale et plusieurs thérapies ont été développées sur l'inhibition de cette voie métabolique. Le citrate participe aux voies de synthèse des acides gras notamment par sa conversion en acétyl-CoA dans le cytosol (17). Le citrate peut également régénérer l'oxaloacétate qui sera converti en malate puis pyruvate, générant du NAD⁺. Le succinyl-CoA peut être régénéré à partir du propionyl-CoA afin de participer à la synthèse des porphyrines précurseurs des hèmes.

B) Adaptation métabolique et perception du microenvironnement tumoral

1) Altérations des mitochondries

Plusieurs altérations peuvent subvenir dans les cellules cancéreuses et entraîner le dysfonctionnement de la chaîne de transport d'électrons, le cycle de Krebs mais aussi la balance redox. Les mutations de gènes codant pour des enzymes du cycle de Krebs sont rarement observées dans les tumeurs cependant leur dérégulation peut avoir plusieurs conséquences sur le métabolisme des cellules cancéreuses. La mutation de la SDH va conduire à l'accumulation de succinate qui sera exporté dans le cytosol. La forme mutée de la FH entraîne une augmentation du fumarate et une inhibition de la SDH, complexe II de la chaîne de transports des électrons. La perte de fonction des enzymes FH peut également favoriser les réactions dépendantes de la glutamine comme source de régénération de l'alpha-cétoglutarate et du NADH. Cela va également promouvoir l'accumulation d'adénylosuccinate (41). Le fumarate peut être exporté dans d'autres compartiments cellulaires comme le noyau ou relargué dans le milieu extracellulaire pour prévenir la cellule de sa toxicité. L'IDH mitochondriale peut subir des mutations de type gain de fonction. Ces mutations vont produire un oncométabolite, le D-2-hydroxyglutarate à partir de l'alpha-cétoglutarate. Le D-2HG peut également être impliqué dans la promotion de l'hypersuccinylation.

L'accumulation du succinate, du fumarate ou du D-2HG, participe à l'inhibition de l'activité des dioxygénases dépendantes du 2-oxoglutarate (OGDOs). Les OGDOs sont une famille regroupant notamment les enzymes TET1-3, les déméthylases KDM2-7, les prolylhydroxylases (PHDs 1-3), les P3Hs, P4Hs et OGFOD1. L'altération des enzymes TETs et des KDMs change la balance entre méthylases et déméthylases favorisant les attaques par hyperméthylation au niveau de l'ADN et des histones. L'inhibition des PHDs va conduire à une stabilisation du complexe HIF. La synthèse de collagène va être impactée par l'altération des enzymes P3Hs, P4Hs. Enfin, les fonctions altérées de l'OGFOD1 vont moduler la synthèse protéique (42). Lorsque ces mutations de type gain de fonctions surviennent, l'usage d'inhibiteurs de ces enzymes est utilisé en thérapie notamment des inhibiteurs d'IDH2, d'IDH1 (43).

Enfin, les altérations du fonctionnement du métabolisme mitochondrial peuvent provenir de mutations qui touchent l'ADN mitochondrial. En effet, cette organelle possède son propre génome qui code 37 gènes chez l'Homme codant pour 13 protéines impliquées dans la production énergétique. La mutation de l'ADN mitochondrial va engendrer un défaut de fonctionnement de la chaîne de transport des électrons, une augmentation de la production de lactate et donc contribuer à la progression tumorale (44).

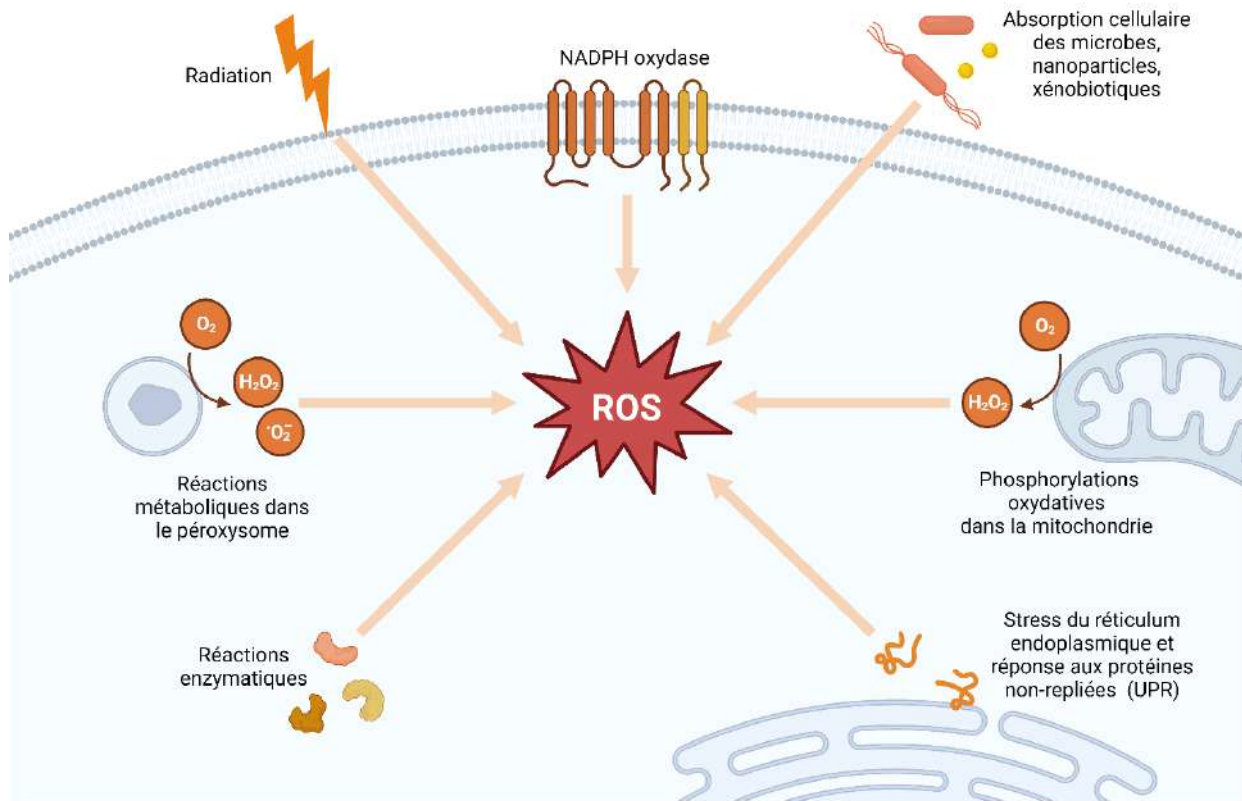


Figure 15 : Production de ROS mitochondriaux à partir de la chaîne de transport d'électrons

Les composés réactifs de l'oxygène (acronyme ROS en anglais) sont le produit de réactions enzymatiques dans les peroxysoxe, la mitochondrie, le réticulum endoplasmique ou le cytosol. La génération de ROS peut également provenir de stress extracellulaire comme les radiations ou l'absorption cellulaire microbienne.

2) ROS mitochondriaux

Les échanges dynamiques et séquentiels d'énergie au sein de la chaîne de transport d'électrons peuvent conduire à une fuite d'électrons. Ces électrons seront capturés par la molécule d'oxygène et formeront des ions superoxydes qui peuvent avoir de nombreuses conséquences au niveau du métabolisme mais également du stress cellulaire voire aboutir à la mort cellulaire. Les ions superoxydes font partie de la famille des ROS, de l'anglais *reactive oxygen species* qui signifie « espèces réactives de l'oxygène ». En effet, ces radicaux libres peuvent oxyder des lipides, des protéines ou encore l'ADN. Au cours du cycle de Krebs, de nombreuses réactions d'oxydo-réduction ont lieu. Les enzymes qui participent à ces réactions possèdent des groupements prosthétiques flavines ou un cluster Fe-S. Ces enzymes du cycle de Krebs ou de la chaîne de transports d'électrons sont impliquées dans des réactions séquentielles et n'échangeront qu'un seul électron à la fois. Ainsi, un radical libre transitoire est généré et si l'arrivée du second électron est retardée, il va être capturé par l'oxygène qui possède une plus grande affinité que les complexes protéiques pour les électrons et donc être source de ROS (45). D'autres compartiments cellulaires comme le réticulum endoplasmique, les peroxysomes, ou certaines enzymes comme les NADPH oxydases (NOXs) ou les superoxydes dismutases (SOD), peuvent être source d'une autre forme de radicaux libres qu'est l' H_2O_2 (**Figure 15**). Il est intéressant de noter que mis à part les produits dérivés de l'oxygène, d'autres types de composés existent comme les lipides hydroperoxydés : le peroxy et l'alkoxy. La génération de composés oxydants au niveau cellulaire peut également être la conséquence d'exposition à des agents environnementaux comme les rayonnements (UVs, Rayons X, radiations ionisantes) ou liés aux comportements individuels (tabac, alcool, drogues) (46–48). L'effet Warburg et les ROS sont le talon d'Achille des cellules cancéreuses. La dégradation du glucose et le pyruvate vont être détournés du cycle de Krebs et de la chaîne de transport des électrons, découplant ainsi la production énergétique du catabolisme du glucose et une modification de l'utilisation de métabolites mitochondriaux. Modifier l'usage de la mitochondrie ou altérer les flux glycolytiques va freiner la progression tumorale et cela d'une manière plus ou moins directement liée à la génération de ROS. Les ROS présents dans le microenvironnement peuvent être des facteurs de l'évolution tumorale tant par leurs rôles dans les mutations génétiques que leur potentiel d'activateur du système immunitaire.

La relation structure/fonction est au cœur de l'homéostasie mitochondriale, en effet, la grande majorité des fonctions que nous avons vu nécessitent une compartimentalisation des complexes protéiques de la chaîne de transport des électrons mais aussi de différents composés comme les protons et les électrons. La régulation de l'organisation structurale des mitochondries est essentielle pour le maintien de ses fonctions, notamment par fusion, fission et processus de mitophagie.

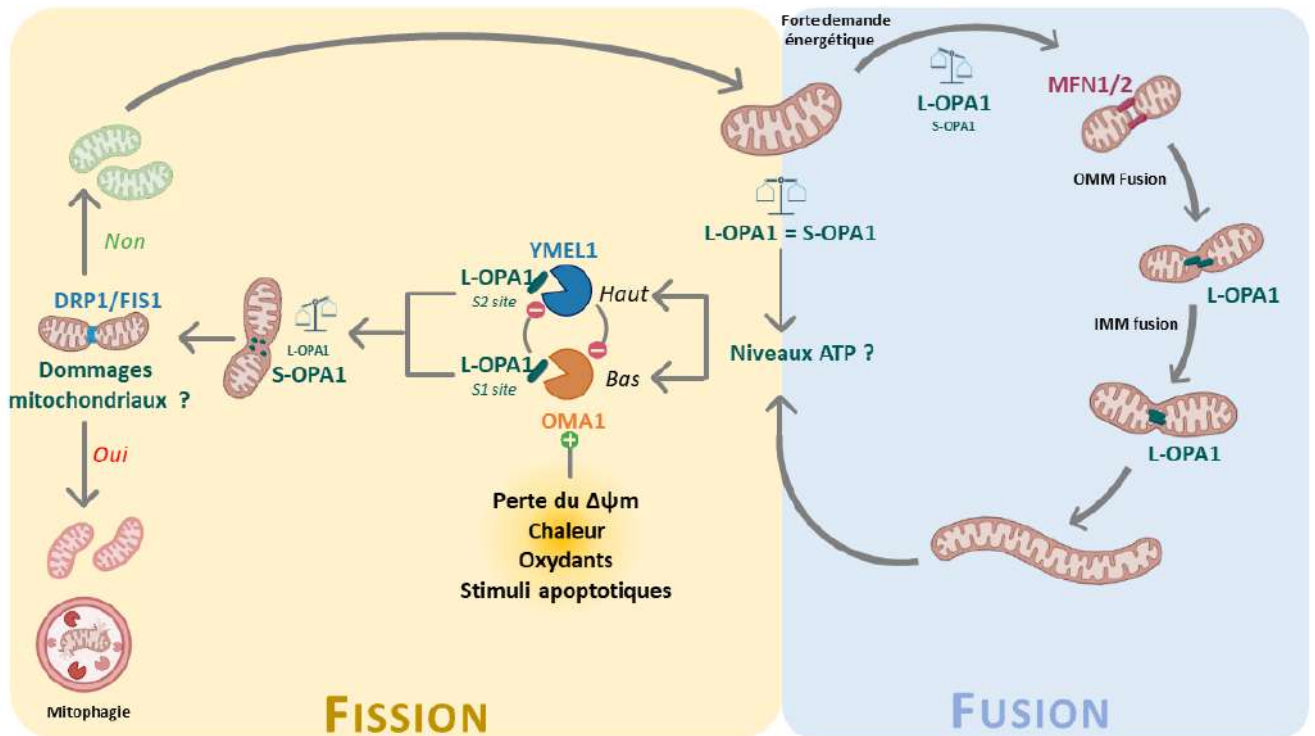


Figure 16 : Fusion et fission mitochondriale

Les processus de fusion et fission mitochondriale sont des mécanismes dynamiques étroitement régulés par la balance entre la forme longue et la forme courte d'OPA1 mais aussi par l'activation des enzymes YMEL1 et OMA1. La forme longue d'OPA1 appelée L-OPA1 est promotrice de la fusion mitochondriale. YMEL1 est activable par de hauts niveaux d'ATP et OMA1 par de bas niveaux d'ATP mais aussi une perte de potentiel mitochondrial ($\Delta\Psi_m$), la chaleur, la présence d'oxydants ou encore des stimuli apoptotiques. L'activation de ces enzymes va conduire au clivage de L-OPA1 en S-OPA1 acteur de la fission mitochondriale. Abréviations : OMM : membrane mitochondriale externe ; IMM : membrane interne mitochondriale.

3) La fusion et fission mitochondriale comme réponse au stress

La mitochondrie va subir des stress de nature variée au cours de la progression tumorale. Il peut s'agir de mutations du génome nucléaire ou mitochondrial, de la privation ou l'abondance d'un substrat métabolique, de la présence d'ions calcium et fer ou encore de facteurs environnementaux tels que certaines toxines, les chimiothérapies, les UVs ou des inhibiteurs de la chaîne de transports d'électrons. La mitochondrie dispose donc d'un spectre large de réponses au stress. Il peut s'agir de la motilité de la mitochondrie, de signalisation rétrograde vers le noyau, de l'établissement de différents points de contact avec d'autres organelles comme le réticulum endoplasmique, de la réponse UPR, de la sécrétion de vésicules mitochondriales, de processus mitophagiques ou la formation de pores. Il peut s'agir également de remodelage des crêtes mitochondriales et des processus de fusion et fission des membranes internes et externes. Ce sont ces deux derniers points que nous allons développer dans ce paragraphe. Cette dynamique de fusion/fission permet d'assurer la distribution des métabolites dérivés de la mitochondrie dans le reste de la cellule et d'exercer le contrôle qualité des mitochondries. En condition de stress ou en période de jeûne, la fission mitochondriale va être inhibée favorisant la formation d'un réseau mitochondrial interconnecté (49–51). La fragmentation mitochondriale va se produire après perception de dommage ou dépolarisation mitochondriale (52). Le processus de mitophagie éliminera les mitochondries endommagées. Si le stress persiste, cela peut conduire à l'induction de mort cellulaire par apoptose ou nécrose (53,54). La fusion des membranes externes mitochondriales est médiée par les mitofusines MFN1 et MFN2 alors que la fusion des membranes internes est médiée par la GTPase OPA1 (**Figure 16**). OPA1 est présent sous deux formes, l'une courte et l'autre longue, c'est le ratio entre ces deux formes qui régule l'équilibre entre fusion et fission mitochondriale. L'accumulation de la forme S-OPA1 survient après perception du stress, permettant la fission mitochondriale (55). Le clivage d'OPA1 est médié par les i-AAA protéases, YMEL1 sur le site S2 et la metalloendopeptidase OMA1 sur le site S1. OMA1 a été identifié historiquement chez la levure par ses fonctions similaires aux m-AAA protéases. Plusieurs stimuli ont été identifiés comme initiateurs de la fission mitochondriale, par exemple le niveau d'ATP intramitochondrial ou le potentiel de membrane à travers la membrane interne. Il a été démontré que c'est l'enzyme redox-sensible OMA1 qui catalyse le clivage d'OPA1 en condition de stress (**Figure 16**). OPA1 fait également partie du complexe protéique MICOS régulant notamment la morphologie et la dynamique des crêtes mitochondriales (56,57).

III) Déclenchement et limites d'une réponse antitumorale

Ce chapitre va aborder la réponse immunitaire antitumorale de la reconnaissance de la nature altérée d'une cellule cancéreuse à sa destruction. Nous allons discuter des changements fonctionnels et métaboliques au cours de cette réponse ainsi qu'aux adaptations multiples du système immunitaire dans un contexte de coévolution et de compétition d'accès aux ressources énergétiques. La reconnaissance et l'élimination d'une tumeur par le système immunitaire suit le concept d'immunoédition composé de trois phases distinctes, les 3 « E », référence aux termes anglais : *elimination, equilibrium* et *escape* (58,59).

A) Établissement de la réponse immunitaire et immunoédition

1) Développement tumoral et présentation antigénique

Les cellules cancéreuses vont croître de manière incontrôlée et former une masse tumorale envahissant les tissus adjacents. Ce processus va compartimenter la tumeur en fonction d'un accès différentiel aux ressources requises à la formation de nouvelles cellules. Progressivement, l'hypoxie et l'accumulation de mutations d'oncogènes et de gènes suppresseurs de tumeurs permettent la sélection de sous clones tumoraux présentant un phénotype plus agressif, par exemple par la sécrétion de molécules pro-angiogéniques, par la perte de contrôle des signaux de régulations intra- et extra-cellulaires et par un changement métabolique impliquant notamment une consommation accrue de métabolites énergétiques comme le glucose, la glutamine, le lactate, etc.

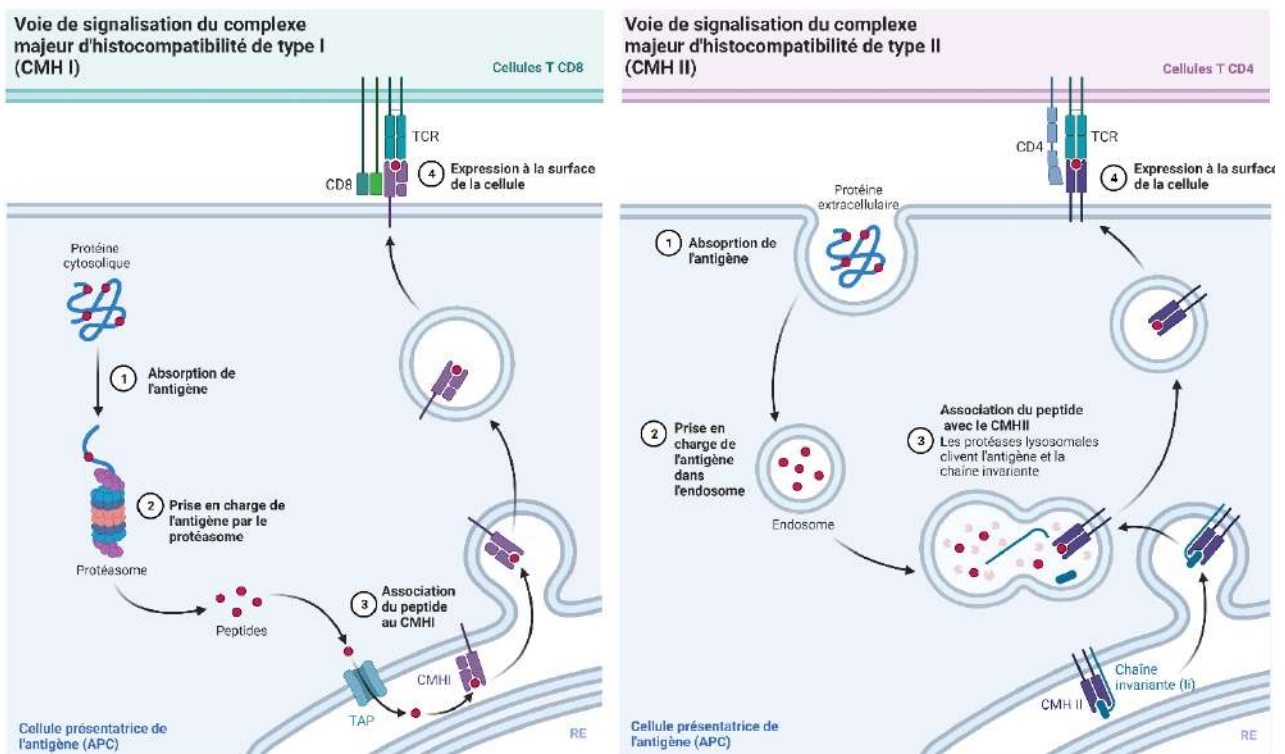


Figure 17 : Présentation antigénique et mécanisme de présentation antigénique

La reconnaissance d'une cellule altérée tumorale dépend du processus de présentation antigénique, sous forme de peptides « altérés » associés aux molécules du complexe majeur d'histocompatibilité (CMH). L'antigène va être à la fois exprimé à la surface de la cellule cancéreuse sur le CMH de type I mais aussi à la surface de cellules présentatrices d'antigènes (CPA) professionnelles comme les cellules dendritiques, les macrophages et les cellules B (60). Les CPA vont capturer les antigènes dans les tissus, les internaliser avant de les présenter sur leurs molécules du CMH de type II. Par ailleurs, les CPA ont la possibilité de réaliser une présentation antigénique dite croisée, assurant la présentation d'antigènes extracellulaires sur les molécules du CMHI, notamment par certaines sous populations de cellules dendritiques de type cDC1 (61). La présentation antigénique sur le CMHI ou le CMHII va respectivement permettre l'activation d'un lymphocyte T CD8 ou CD4 (**Figure 17**).

La présentation antigénique peut être altérée pour plusieurs raisons dans les tumeurs. Différents complexes protéiques interviennent dans le chargement des peptides sur le complexe CMH et les gènes codant pour ses acteurs peuvent être mutés dans les tumeurs. Les mutations ou perte d'hétérozygotie les plus fréquentes touchent les gènes HLA-I et le gène de la $\beta 2$ microglobuline (62,63). L'uprégulation des voies des MAPK ou de MYC, l'expression de DUX4 vont altérer l'expression des gènes associés à la présentation antigénique. L'expression de *SND1*, *MAL2* ou *ATG4B* va inhiber les processus de dégradation des protéines. Les ARNs non codant peuvent également interférer avec les ARN messagers comme mir148a-3p, mir-125a-5p ou LINK-A. Certaines régulations épigénétiques peuvent avoir lieu sur les promoteurs des gènes *HLA*, *$\beta 2M$* et *TAP1*. Toutes ces altérations vont conduire à une diminution de la présentation antigénique sur les cellules cancéreuses. D'autres types d'altérations peuvent prévenir le recrutement et les fonctions des cellules dendritiques notamment les cDC1s. Les cDC1s sont recrutées sur le site tumoral par la sécrétion des chimiokines comme CCL4 ou CCL5 par les cellules cancéreuses ou les cellules NK intratumorales. Cependant, la voie de signalisation de la β -caténine dans les cellules cancéreuses peut inhiber la sécrétion de ces chimiokines et donc réduire le nombre de cellules dendritiques infiltrant les tumeurs et par conséquent, celle des cellules T également. D'autres composés peuvent avoir des rôles similaires comme la PGE2, le VEGF, l'IL6, le TGF β et l'IL10 qui joue sur la différenciation, la maturation des cellules dendritiques et même la conversion vers un phénotype tolérogène (64,65). Le dysfonctionnement peut également affecter la capacité de présentation croisée comme par exemple en présence d'un taux élevé de lipides oxydés dans les cellules dendritiques.

◀ **Légende Figure 17 :** Les cellules présentatrices de l'antigène (APC) possèdent deux mécanismes principaux de présentation antigénique (CMH I et CMH II). Les protéines cytosoliques dégradées par le protéasome génèrent des peptides antigéniques qui seront chargés sur le complexe du CMHI via les protéines du réticulum endoplasmique TAP. Le complexe CMHI peptide sera alors exprimé à la surface par transport vésiculaire. Les protéines extracellulaires seront dégradées par la voie endosomale et les peptides générés seront présentés sur le CMHII avant d'être exprimé à la surface.

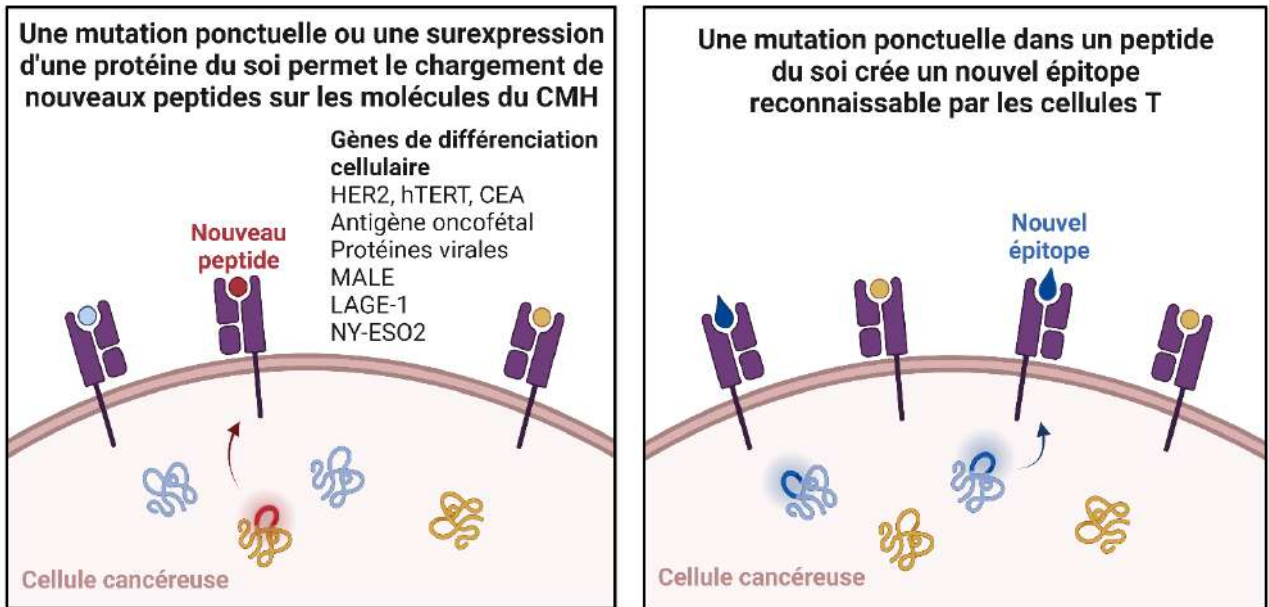


Figure 18 : Antigénicité tumorale

L'antigénicité tumorale désigne la présentation sur les complexes majeurs d'histocompatibilité de nouveaux peptides ou de nouveaux épitopes.

2) Antigénicité tumorale

L'antigénicité tumorale est définie comme l'ensemble des antigènes qu'une cellule cancéreuse va exprimer à sa surface sur son complexe majeur d'histocompatibilité de type I. Certains antigènes d'une cellule saine du corps humain peuvent être perdus par les cellules cancéreuses et d'autres de nouveau exprimés (66). On distingue 3 principaux types d'antigènes tumoraux (65). Il y a d'une part les antigènes associés à la tumeur, issus de mutations somatiques, c'est-à-dire de protéines du soi, qui sont préférentiellement exprimés pendant le processus de carcinogénèse. C'est le cas par exemple des Melanoma Associated Antigens pour le mélanome, de LAGE-1 exprimé dans le mélanome, les carcinomes du poumon à petites cellules, cancer de la vessie, de la prostate, de la tête et du cou (67)) ou encore de NY-ESO2 dans le cancer ovarien épithélial ou NY-ESO1 dans le mélanome, cancer ovarien ou cancer du col de l'utérus (68,69). C'est également à cette catégorie qu'appartiennent les antigènes de différenciation cellulaire, les antigènes surexprimés par les cellules cancéreuses (HER2, hTERT, CEA), les antigènes oncofœtaux et les antigènes associés à des protéines virales (**Figure 18**). D'autre part, on distingue les néo-antigènes ou antigènes spécifiques tumoraux ; ils sont le résultat d'anomalies intrinsèques à la cellule cancéreuse notamment de l'instabilité génomique, des variations nucléotidiques simples, insertion-délétions (indel), fusion de gènes ou encore d'anomalies de l'épissage ou de changement de cadre de lecture sous l'effet d'interruption de la traduction en cas de déficit en certains aminoacides. Ces néo-antigènes sont anormaux par nature et donc non connus du répertoire lymphocytaire. L'antigénicité peut également provenir de cibles moléculaires ayant subi des modifications post-traductionnelles telles que les glycosylations ou les phosphorylations. Ces modifications peuvent favoriser la présentation sur les complexes du CMH ou favoriser les interactions entre le récepteur des cellules effectrices le TCR et le CMH (70–72). C'est en sondant ces antigènes présentés sur le CMHI des cellules cancéreuses que les cellules immunitaires vont pouvoir déclencher une réponse antitumorale et cytotoxique.

3) Activation des cellules T et élimination de la tumeur

L'activation des cellules immunitaires suit les étapes suivantes : i) Reconnaissance du fragment antigénique tumoral sur la CPA, ii) Activation du TCR par phosphorylations successives des motifs ITAMs des régions cytoplasmiques des chaînes du CD3 et des effecteurs en aval de la signalisation du TCR, iii) Co-stimulation *via* l'interaction entre CD28 et le récepteur B7 et l'émission de signaux cytokiniques.

D'autres populations lymphocytaires comme les lymphocytes T $\gamma\delta$ ne nécessitent pas la présentation de l'antigène pour leur activation tout comme les cellules tueuses naturelles, aussi appelées cellules NK. Les cellules T $\gamma\delta$ seront capables d'avoir une activité cytotoxique après reconnaissance de phosphoantigènes sur le CMHI des cellules cancéreuses. Les cellules NK ont la capacité de reconnaître l'absence de CMHI et en présence de récepteurs activateurs avoir une activité cytolytique directe. Cette année, de Vries *et al*, a mis en évidence l'activation des cellules T $\gamma\delta$ dans un contexte d'absence de CMHI.

Une fois activés les lymphocytes T CD8 et CD4 vont sonder toutes les cellules de l'organisme à la recherche de l'antigène pour lequel ils ont été sélectionnés. Les lymphocytes T de type CD8 portent l'activité cytotoxique et les CD4 possèdent des fonctions de support, notamment des signaux cytokiniques régulatrices de la réponse primaire. Les lymphocytes T CD4 possèdent également un rôle essentiel effecteur dans la réponse tumorale (73). Lors de la phase effectrice, la production d'IFN γ , de cytokines et de chimiokines attractrices du système immunitaire (CXCL9, CXCL10, CXCL11) va augmenter dans le microenvironnement tumoral.

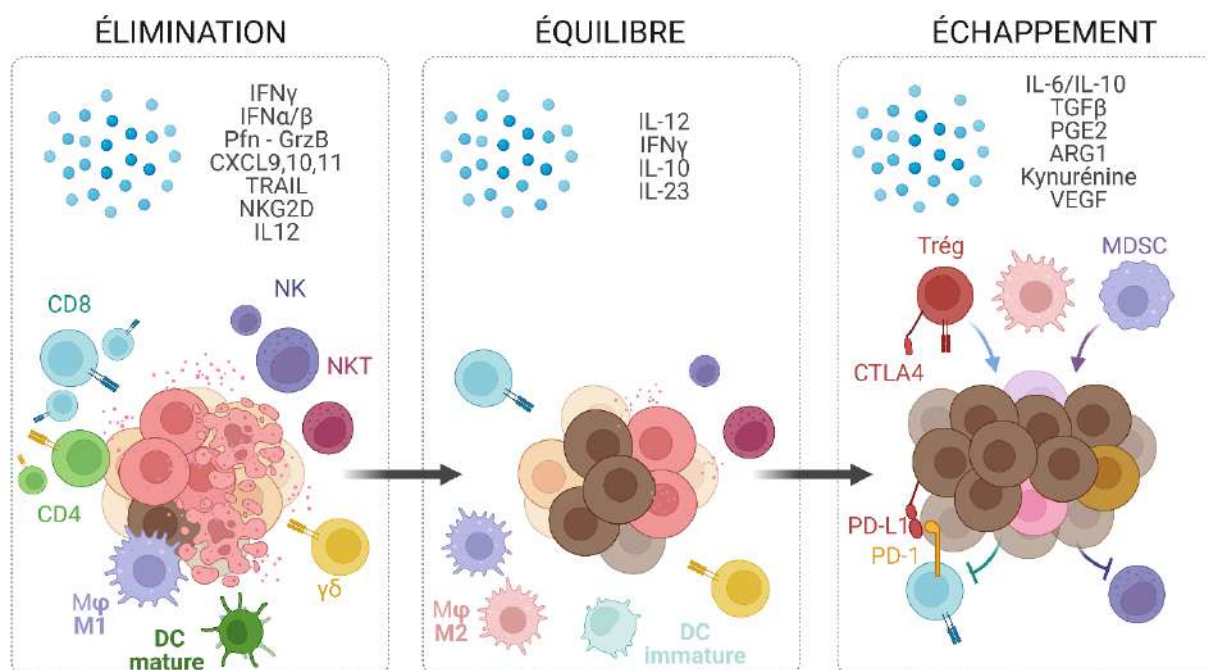


Figure 19 : Immunoédition et mort immunogénique

Après reconnaissance des antigènes tumoraux, les cellules effectrices vont éliminer les cellules tumorales par cytolyse, dépendante de molécules appartenant à la famille des granzymes, des perforines ou encore par contact direct avec la cellule tumorale *via* des récepteurs de mort membranaires. Cette phase, dite d'élimination, va permettre la destruction des cellules cancéreuses (**Figure 19**).

4) Équilibre et échappement

Lors de la progression tumorale, les différentes cellules cancéreuses qui constituent la tumeur vont accumuler de nouvelles mutations selon l'environnement direct auquel elles sont confrontées. Ceci contribue à augmenter l'hétérogénéité clonale au sein d'une tumeur. Certains clones tumoraux seront résistants aux thérapies administrées, d'autres échapperont à l'action du système immunitaire. Le terme métastase désigne la capacité d'une cellule cancéreuse à migrer du site primaire où elle s'est initialement développée, à un site distant, dans un autre organe favorable à son établissement. Ce processus complexe implique de nombreux changements morphologiques et métaboliques favorisant son échappement vis-à-vis du système immunitaire. La sélection exercée par le système immunitaire va conduire à la surreprésentation numérique de clones au phénotype plus agressif. La persistance de la masse tumorale stimule l'activation chronique du système immunitaire et donc progressivement mener à sa perte de fonction. La lyse va devenir moins efficace et les sécrétions des cellules cytokiniques vont changer. Par ailleurs, la sélection d'un clone tumoral peut également présenter un sécrétome différent du clone tumoral majoritaire déjà éliminé. L'ensemble de ces modifications va conduire à un changement dans les cellules pouvant infiltrer les tumeurs, la plupart ayant des propriétés favorables à la progression tumorale. Ces cellules de phénotype régulateur ainsi que le changement du microenvironnement cellulaire vont conduire à l'expression de points de contrôle de l'immunité. L'activation des cellules effectrices va décroître lors de la liaison de ces ligands inhibiteurs. Cette étape s'accompagne, comme nous le verrons dans une prochaine partie, d'une modification de leur état métabolique conduisant progressivement à l'épuisement cellulaire.

Certaines tumeurs, dès leur implantation, ne vont que faiblement déclencher une réponse immunitaire. C'est également dans les phases plus précoces que certaines cellules cancéreuses peuvent échapper au système immunitaire en gagnant d'autres organes par métastase.

◀ **Légende Figure 19** : *L'immunoédition comporte 3 phases distinctes interdépendantes : la phase d'élimination, d'équilibre et d'échappement. Lors de ces 3 phases, l'infiltration par le système immunitaire va évoluer vers l'enrichissement en cellules immunitaires suppressives et en cytokines promotrices de la progression tumorale au dépend d'une réponse immunitaire anti-tumorale portée par les lymphocytes T CD8 et cellules NK. DC : cellules dendritiques, M ψ : macrophages, NK : natural killer ; MDSC : cellules myéloïdes dérivées des monocytes ; Trég : T régulateur.*








Type cellulaire	Fonctions	Phénotype métabolique
Activation immunitaire ou inflammatoire		
Cellules NK 	Cytotoxicité indépendante du CMH Perforine, Granzymes FASL, TRAIL IFN γ , TNF	Glycolyse et OXPHOS
TAM inflammatoire 	Cytotoxicité indépendante du CMH TNF, IL-1 β Choc oxydatif Présentation antigénique	Glycolyse et voie des pentoses phosphates
Cellule dendritique 	Perception des DAMPs Activation des cellules T effectrices Présentation antigénique	Glycolyse
Cellules T effectrices 	Cytotoxicité spécifique d'un antigène Perforines, Granzymes FASL IFN γ , TNF	Glycolyse élevée et OXPHOS Voie des pentoses phosphates Métabolisme des acides aminés (arginine, tryptophane, sérine, leucine, glutamine, cystéine)
Cellules T mémoires 	Maintenir une réponse mémoire à long terme	OXPHOS
Immunosuppression		
Cellules myéloïdes dérivées des monocytes	IL10, TGF β Déplétion acides aminés Polyamines, kynurénine	Glycolyse et OXPHOS
TAM immunosuppresseur 	IL10 Déplétion acides aminés Polyamines, kynurénine VEGF	OXPHOS Biosynthèse des hexosamines
Cellules T régulatrices 	Séquestration de l'IL2 Diminue la costimulation des cellules présentatrices d'antigènes IL10, TGF β Adénosine	OXPHOS

Figure 20 : Métabolisme et fonction de l'infiltrat immunitaire

B) Immunométabolisme

Chaque cellule immunitaire doit être en mesure de répondre aux différentes stimulations rencontrées, acquérir des caractéristiques de cellule effectrice ou mémoire et migrer dans les tissus concernés afin de rétablir l'homéostasie. À chacune de ces étapes, le métabolisme joue un rôle crucial dans la mobilisation des différents acteurs moléculaires nécessaires au développement d'une réponse immunitaire adaptée. Dans le cas d'une tumeur, l'adaptation métabolique des cellules du système immunitaire doit soutenir leur prolifération et leur polarisation, la mise en place de nouvelles fonctions sécrétrices ou cytotoxiques dans un microenvironnement où la disponibilité des nutriments est limitée, ainsi que maintenir un ensemble de cellules mémoires. Par ailleurs, en cas de stimulation chronique dans un contexte tumoral, les transitions métaboliques vont accompagner le développement d'état d'épuisement ou d'anergie (**Figure 20**).

◀ **Légende Figure 20** : Les cellules immunitaires infiltrantes les tumeurs se divisent en deux catégories majeures contribuant à : l'activation immunitaire ou inflammatoire et l'immunosuppression. Chaque cellule du système immunitaire par ses fonctions est impliquée dans une réponse antitumorale ou au contraire soutient la progression des cellules cancéreuses ou altère les fonctions des cellules effectrices. Les sources énergétiques utilisées par ces cellules seront donc différentes selon leur fonction et auront ou non un potentiel compétitif avec les cellules cancéreuses pour les ressources, notamment le glucose. DAMPs : danger-associated molecular patterns. Figure traduite de la référence (74)

1) Le métabolisme des cellules T après activation et maturation

Le plus souvent, l'interaction des complexes du CMHI/TCR sur le CD8 ou CMHII sur les CD4 ainsi que les signaux de costimulation vont conduire à une grande mobilisation du métabolisme des cellules T. Une grande quantité d'énergie est nécessaire pour assurer l'expansion clonale ainsi que la maturation vers des stades effecteurs. Cela se traduit par une forte augmentation de la glycolyse aérobie, par augmentation des transporteurs du glucose, mais aussi du cycle de Krebs et de la respiration oxydative. Cette reprogrammation métabolique dépend de la voie PI3K/AKT/mTOR notamment *via* les facteurs de transcription Myc et HIF-1 (indépendamment de son rôle dans l'hypoxie) (75). Ce sont les gènes associés à la glycolyse et à la voie des pentoses phosphates qui seront principalement exprimés lors de l'activation des cellules T (**Figure 20**) (74). La voie des pentoses phosphates dans les cellules T est nécessaire à la synthèse des acides gras pour la production des membranes plasmiques et au maintien du potentiel redox. Si les intermédiaires de la glycolyse ne sont pas consommés en amont par la voie des pentoses phosphates ou la voie serine-glycine, ils généreront du pyruvate. Il sera converti en lactate ou pourra alimenter *via* les intermédiaires du cycle de Krebs, les voies de cataplérose. Dans un contexte tumoral où le glucose peut être limitant, les cellules T activées peuvent accuser un déficit en phosphoénolpyruvate et limiter l'activation

des facteurs de transcription NFAT, essentiels à leur activation et leur fonction. Il a été montré *in vitro* qu'une diminution de la concentration de glucose dans le milieu de culture de lymphocytes contribue à augmenter la phosphorylation oxydative atténuant la voie mTOR. Ce changement empêche l'expression des fonctions effectrices des lymphocytes qui entrent dans un état de quiescence et diminuent leur production de cytokines telles que l'IFN γ , l'IL17 ou des molécules associées à la cytotoxicité comme le granzyme B. Dans certains cas, ces changements métaboliques peuvent favoriser leur polarisation vers un phénotype régulateur. L'un des phénotypes fréquemment retrouvé dans les populations lymphocytaires infiltrantes des tumeurs (TILs) est une diminution de la masse mitochondriale suggérant que les fonctions mitochondriales peuvent être également altérées. Les mitochondries des cellules T sont productrices d'une quantité élevée de ROS et sont hypopolarisées.

Au-delà du métabolisme énergétique, l'apport d'éléments essentiels tels que les acides aminés est nécessaire pour satisfaire l'activation des cellules. Ainsi, lors de leur activation les cellules T vont consommer de la leucine, de l'arginine, de la sérine ou encore du tryptophane (74). Certains de ces composants ont également la capacité de réguler la fonction même des lymphocytes par reprogrammation métabolique, notamment le tryptophane et l'arginine qui peuvent être associés à une perte des fonctions effectrices. La glutamine est également importante pour l'anaplérose dans les cellules immunitaires en permettant l'apport d'azote pour la synthèse des acides aminés et des acides nucléiques ; ainsi une restriction peut avoir des conséquences sur l'activation et les fonctions effectrices des cellules. Enfin, les cellules auront besoin de mobiliser la synthèse des lipides membranaires *via* les facteurs de transcription SREBP1 et SREBP2.

L'un des aspects de la réponse immunitaire est lié au développement d'une réponse mémoire. Les besoins énergétiques de ce type de cellules est différent des cellules effectrices. Leurs besoins de production des cytokines et des molécules sont moindres et l'accent est mis sur leur longévité. Pour cela, les cellules mémoires vont principalement utiliser le glucose ou le glycérol pour la synthèse lipidique. L'oxydation des acides gras va permettre d'apporter les intermédiaires du cycle de Krebs. Ces cellules vont avoir une activité métabolique faible mais être en mesure d'établir une réponse immunitaire sur le long terme (75).

En ce qui concerne les autres cellules de l'immunité, leur métabolisme va être majoritairement glycolytique dans les phases d'activation bien que certaines fonctions comme la présentation antigénique puissent nécessiter une part plus importante de l'utilisation d'O₂PHOS. Certaines cellules au phénotype régulateur comme les macrophages de type M2 ou les MDSC vont présenter un métabolisme analogue aux cellules tumorales.

2) L'épuisement des cellules T

L'épuisement, ou *exhaustion* en anglais, des cellules T désigne un état de dysfonctionnement qui survient lors d'une stimulation chronique, comme par exemple dans les infections chroniques ou les cancers. Des études *in vitro* ont montré qu'une stimulation chronique en condition hypoxique induit l'épuisement des cellules T CD8. Ce mécanisme est dépendant de l'action répressive de Blimp1 sur le facteur de transcription PGC1 α , lui-même impliqué dans la biogénèse mitochondriale et l'activité antioxydante. Ainsi, les cellules CD8 T ne présentent plus de capacités d'adaptations à l'hypoxie et présentent des niveaux élevés de ROS (76). L'état d'épuisement des cellules T se traduit par une diminution de leur production cytokinique et l'augmentation de l'expression de récepteurs inhibiteurs à leur surface (77). Ces récepteurs font partie de la famille des points de contrôle immunitaire. Leur activation permet la régulation et le contrôle de la réponse immunitaire. Il est important de mentionner que l'expression de ces récepteurs n'est pas l'unique caractéristique de l'épuisement des cellules T et que cet état n'est pas non plus irréversible. En effet, bien que ces cellules soient dysfonctionnelles, elles n'en sont pas pour le moins anergiques. Elles peuvent encore produire certaines molécules effectrices, des cytokines ou encore des granzymes. On distingue alors un stade d'épuisement terminal qui va renforcer l'état d'hypo-réponse suite à la reconnaissance d'un antigène et réception des signaux de costimulation. Cet état est défini par l'expression de certains facteurs de transcriptions comme Eomesodermin (Eomes), TCF1, BATF, NFAT1, TOX et BLIMP1, susceptibles de modifier les fonctions mitochondriales et l'expression des marques épigénétiques, entraînant une déprogrammation cellulaire. Parmi ces facteurs de transcription importants, TCF1 semble jouer un rôle central dans l'orientation précoces des cellules T vers un phénotype d'épuisement terminal, la perte de son expression au profit de TIM3 définit le stade terminal d'épuisement des cellules T (78,79). Les facteurs de transcription TBET et TOX ont également été décrits comme possédant un rôle dans l'épuisement tardif des cellules T en agissant à la fois sur le transcriptome et l'épigénétique des cellules T (80,81). D'un point de vue métabolique, l'altération des fonctions mitochondriales est également une caractéristique des cellules T présentant un phénotype tardif d'épuisement. En effet, les cellules T accumulent de nombreuses mitochondries dépolarisées résultant de la diminution de leur capacité à renouveler leurs mitochondries *via* une activité mitophagique et une mitochondriogénèse insuffisante (82).

Comme nous l'avons vu, certains métabolites générés par les cellules tumorales vont modifier le microenvironnement tumoral et impacter la fonctionnalité des TILs notamment en modifiant le contrôle des marques épigénétiques.



Figure 21 : Reprogrammation épigénétique dans les cellules T

Le niveau d'expression des signatures liées à l'identité d'une cellule T évolue vers un stade d'épuisement et de stress du réticulum endoplasmique (RE). Ces transitions sont régulées par des variations de l'accessibilité à la chromatine sur des gènes donnés. Figure traduite de la référence (83).

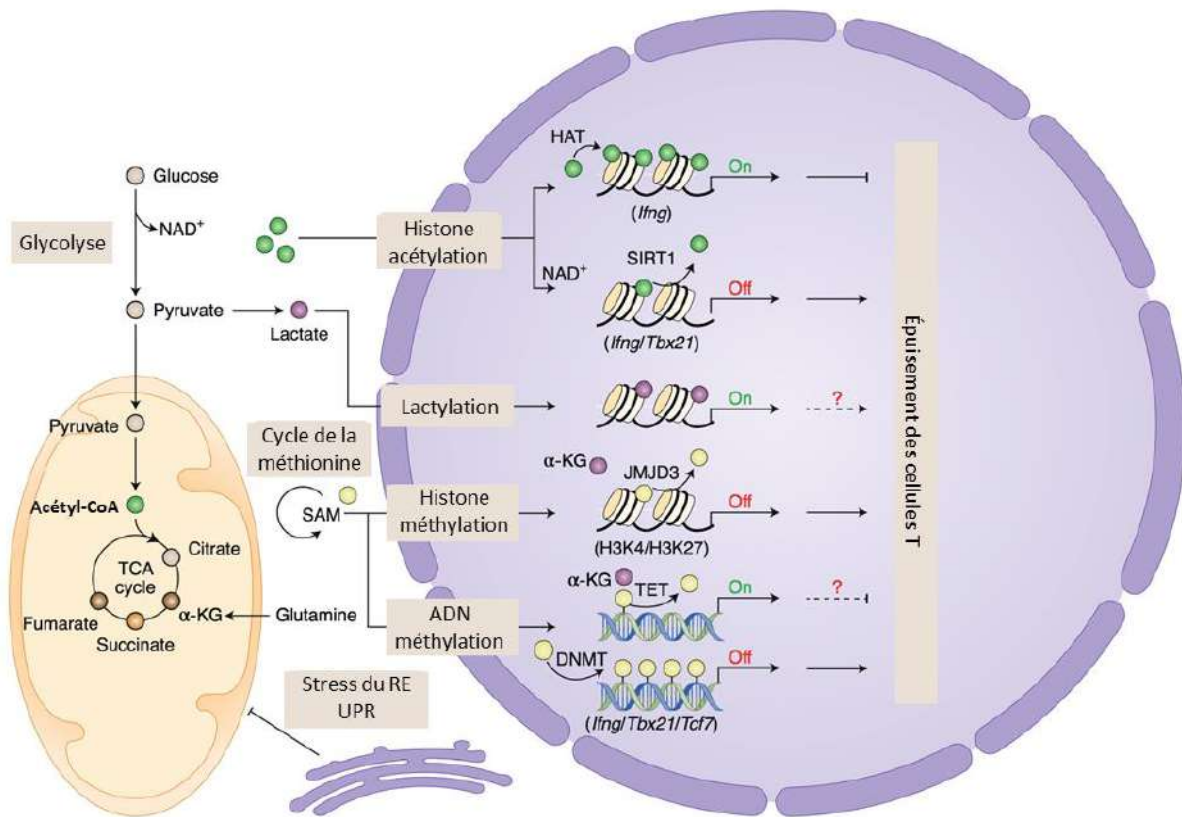


Figure 22 : L'épigénétique et le métabolisme sur l'épuisement des cellules T

Différents intermédiaires de voies métaboliques peuvent jouer un rôle régulateur épigénétique conduisant à l'épuisement des cellules. Figure traduite de la référence (83)

3) Modifications épigénétiques lors de la différenciation et l'épuisement des cellules T

Du stade naïf multipotent au stade activé et différencié, l'identité des cellules T varie et permet l'émergence de sous types cellulaires fonctionnellement distincts. Classiquement, nous distinguons quatre grandes catégories parmi les lymphocytes : les cellules T naïves, les cellules mémoires, les cellules activées ou effectrices et les cellules épuisées (84). Les cellules T naïves possèdent une grande plasticité cellulaire et peuvent conduire à de multiples stades d'activation et de différenciation. Cette plasticité diminue avec l'acquisition des fonctions effectrices et de manière plus accentuée lors de l'épuisement. Les cellules mémoires, quant à elles, présentent encore des propriétés de plasticité cellulaire afin de renouveler le pool de cellules effectrices et maintenir leur longévité. Les cellules T une fois différenciées, présentent un état plus stable avec un faible potentiel de reprogrammation. Cette plasticité cellulaire dépend du contrôle des programmes transcriptionnels et de leur stabilité notamment grâce à la mise en place de marques épigénétiques (**Figure 21**). Cette régulation est influencée par la force du signal antigénique, la spécificité et l'affinité du TCR, les stimuli environnementaux et les mécanismes de tolérance immunitaire. Les cellules naïves vont présenter un taux élevé de méthylation de l'ADN sur les îlots CpG des gènes codant pour la production de cytokines et leurs récepteurs, de molécules effectrices et de leurs régulateurs. Les cellules mémoires possèdent un degré de méthylation moindre par rapport aux cellules naïves notamment sur les gènes de l'IFN γ et l'IL2 et une capacité de déméthylation plus rapide que les cellules naïves (85). Les cellules mémoires présentent également une méthylation sur les gènes associés à la mort cellulaire comme *Noxa*, favorisant la survie de ces cellules. Durant la différenciation cellulaire, les promoteurs de l'IFN γ et de l'IL2 chez les CD4 et IFN γ , la granzyme B et la perforine chez les CD8 présentent une hyperacétylation. Plusieurs modifications d'histones notamment des triméthylations sont importantes dans ces processus. La triméthylation de H3K4 et H3K27 va respectivement permettre ou contraindre l'expression génique. Durant la différenciation des cellules T, le niveau d'H3K27m3 va diminuer au profit d'une augmentation du niveau d'H3K4m3. Ce sont les enzymes HRX qui catalysent la réaction de méthylation des histones et donc régulent l'expression des gènes associés à la différenciation cellulaire.

Les cellules T épuisées présentent une hétérochromatinisation de loci de nombreuses cytokines comme l'IFN γ et de molécules effectrices. L'ouverture d'autres régions comprenant des gènes codant par exemple pour *Pdcd1* renforcent l'état d'épuisement de ces cellules (86). Ces modifications de la chromatine sont étroitement liées à l'accumulation de différents métabolites, reflet d'un métabolisme mitochondrial défectueux. Par exemple, la disponibilité en acétyl-CoA va permettre l'acétylation des histones dans les loci des gènes de l'IFN γ ou *Tbx21*. La hausse du métabolisme 1C dans les cellules immunitaires va augmenter la production de la S-adenosylméthionine (SAM) qui est une source de groupements méthyls pour l'ADN et les histones. Le lactate peut également être impliqué dans la modification de la chromatine par un processus appelé lactylation (**Figure 22**). Ainsi, épigénétique et métabolisme jouent un rôle interconnecté dans l'épuisement des cellules T.

C) Polarisation et reprogrammation métabolique

La reprogrammation métabolique des cellules cancéreuses ainsi que leur forte demande en ressources énergétiques vont altérer les propriétés du microenvironnement. L'hypoxie et l'acidose du milieu extracellulaire vont augmenter suite aux processus suivants : la libération de protons H^+ , la production de lactate ou la formation d' HCO_3^-/H^+ par conversion du CO_2 par les carboniques anhydrases extracellulaires. Le lactate et la présence d'ions H^+ vont diminuer la transcription du facteur NFAT dans les cellules T effectrices et par conséquent diminuer leur production cytokinique, prolifération, survie et cytotoxicité.

La concentration de certains métabolites pourra devenir limitante pour assurer les fonctions biologiques de toutes les cellules en présence. Les tumeurs présentent des concentrations élevées d'adénosine, tryptophane, kynurénine, ornithine, de ROS et de potassium. Toutes ces modifications peuvent impacter directement les fonctions effectrices et régulatrices, l'activation et la polarisation du système immunitaire et donc potentiellement limiter la réponse anti-tumorale. L'hypoxie, outre son rôle dans la diminution des fonctions effectrices des cellules T, augmente l'expression d'ectonucleotidases telles que CD39 et CD73 qui vont catalyser la réaction de transformation de l'ATP extracellulaire immunostimulant en adénosine immunosuppressive dans le microenvironnement tumoral. L'adénosine va se fixer sur les récepteurs A2A et A2B exprimés par un large spectre de cellules immunitaires. La transduction du signal va inhiber les fonctions des cellules effectrices et la prolifération cellulaire. Le tryptophane sert de substrat à l'activité de l'enzyme IDO qui catalyse sa conversion en kynurénine. La kynurénine est un ligand du récepteur nucléaire Ahr sur les cellules T. Cette liaison va entraîner l'augmentation des voies de signalisation de signaux co-inhibiteurs, comme PD1 et la diminution de production d' $IFN\gamma$ mais aussi favoriser le développement de cellules T régulatrices. Les forts taux de nécroses présents dans les tumeurs engendrent des concentrations élevées de potassium pouvant directement impacter les fonctions des cellules T effectrices par une diminution de leurs capacités à consommer les nutriments présents dans le milieu extracellulaire. Cet état dysfonctionnel est également lié à une diminution de l'acétyl-CoA dans le cytoplasme (87). L'oncométabolite le L-2HG déjà évoqué précédemment peut avoir une influence sur la prolifération, l'activité de NFAT, la synthèse des polyamines et la signalisation du TCR dans les cellules T par régulations épigénétiques dépendantes des dioxygénases. Enfin, le lactate peut également influencer l'activation et le métabolisme des cellules T effectrices. La consommation de lactate par les cellules T effectrices va augmenter la proportion de NADH/NAD⁺. Le NADH va agir comme un inhibiteur des flux glycolytiques *via* son action inhibitrice sur la GAPDH. Les intermédiaires de la glycolyse situées après la GAPDH vont alors diminuer, notamment la sérine dérivée du 3-phosphoglycérate. Le manque de sérine entraîne une diminution de la prolifération des cellules T effectrices, étant requise lors de ce processus (88).

Ainsi, le métabolisme peut altérer les fonctions du système immunitaire. Pourtant, par certains aspects que nous allons détailler par la suite, il peut également initier une réponse immunitaire antitumorale, notamment par le relargage de certains composés mitochondriaux.

D) Signaux mitochondriaux impactant l'immunogénicité tumorale

Il est intéressant d'évoquer que la mitochondrie est une organelle complexe qui peut jouer un rôle dans l'immunogénicité tumorale, c'est-à-dire la capacité d'une cellule cancéreuse à déclencher une réponse immunitaire. En effet, de nombreuses études se focalisent sur le génome nucléaire comme principale source d'antigènes tumoraux, cependant, les mitochondries possèdent elles aussi un génome qui est susceptible de subir des mutations lors du processus de cancérogénèse (89) et donc être un potentiel contributeur de l'immunogénicité et de la progression tumorale. La mitochondrie est également une organelle génératrice de multiples composés susceptibles d'activer le système immunitaire.

1) Les *Danger-associated molecular patterns* (DAMPs)

Certains composés intra- et extracellulaires sont capables d'être reconnus par le système immunitaire et d'induire son activation. Ces composés sont désignés par le terme anglophone DAMPs, comprendre « motifs moléculaires associés au danger ». On retrouve différents types de DAMPs dans les tumeurs provenant de plusieurs compartiments subcellulaires, exprimés à la membrane ou libérés dans le milieu extracellulaire. La mitochondrie peut relarguer de l'ATP, de l'ADN mitochondrial ou encore des peptides formylés. Le cytoplasme des cellules peut générer également des ions K^+ , de l'ATP, des miARNs ou de l'actine F. De la même manière, le réticulum endoplasmique contient également de l'ATP, des molécules HSP et de la calréticuline. Enfin, dans le noyau, nous retrouvons les molécules HMGB1, HMGN1 ainsi que les histones qui peuvent être exportées (90). Leur présence anormale dans le milieu extracellulaire sous forme libre, à l'intérieur de petites vésicules ou d'exosomes peut déclencher une réponse inflammatoire. D'autres seront reconnus à l'intérieur des cellules. Les DAMPs seront reconnus par des récepteurs spécialisés comme les TLRs (Toll Like Receptors), les récepteurs purinergiques ou les NLR (Nod Like Receptors) cytoplasmiques. La localisation subcellulaire de certaines protéines, cytoplasmique ou mitochondriale, peut également avoir une importance sur l'immunogénicité. En effet, la comparaison de modèles cellulaires tumoraux exprimant de l'OVA ou NY-ESO1 cytoplasmique ou mitochondriale montre que la localisation mitochondriale augmente significativement la présence de lymphocytes T spécifiques de l'antigène au sein de la tumeur en comparaison à leur analogue cytoplasmique (71). La reconnaissance de ces DAMPs va conduire à la sécrétion de cytokines et chimiokines pro-inflammatoires dont certaines comme l'IL1 α ou l'IL18 dépendent de l'activation de l'inflammasome NLRP3. Certains DAMPs comme l'ATP, le succinate, les cardiolipines, des peptides formylés, l'ADN mitochondrial ou encore des molécules TFAMs peuvent également déclencher une réaction inflammatoire par des cellules non immunitaires (91). De même, ces molécules peuvent agir directement sur la progression tumorale, indépendamment de leur rôle dans l'inflammation (92).

L'adénosine, la S100 ou encore HMGB1 peuvent promouvoir les voies de signalisation immunosuppressives dans leurs cellules cibles comme les cellules T, les NKs, les MDSCs ou encore les DCs. Elles peuvent être également impliquées dans la prolifération des cellules tumorales. HMGB1 et IL1 α peuvent être promotrices de l'angiogénèse.

Il a été montré par un mécanisme encore inconnu que des cellules dendritiques peuvent capter des mitochondries endommagées, relarguées par les cellules cancéreuses dans le microenvironnement et les internaliser. Les molécules associées seront apprêtées et pourront être source de présentation antigénique (71).

D'autres processus comme la fission mitochondriale peuvent être directement liés au niveau d'expression du CMHI à la surface des cellules tumorales (93).

Enfin, les modifications épigénétiques peuvent contribuer à une diminution de l'immunogénicité tumorale par diminution de la présentation antigénique, de la génération de néo-antigènes, par régulation de la mort immunogénique ou encore de la modulation de la sécrétion de cytokines.

2) Morts immunogéniques

La mort est dite immunogénique lorsque l'activation du système immunitaire et l'efficacité de la phase d'élimination vont augmenter, permettant de retarder ou d'éviter la phase d'équilibre voire même dans les meilleurs cas, de préserver une réponse immunitaire effectrice et mémoire contre les cellules cancéreuses. La plupart des thérapies ne vont pas induire une mort immunogène (94) ; ainsi différentes stratégies thérapeutiques ont été mises en place pour essayer d'en inverser l'effet. Les chimiothérapies sont souvent associées à une immunosuppression et au développement de multiples résistances par les cellules tumorales. Cependant, de récentes études ont montré qu'en fonction du protocole thérapeutique, certaines chimiothérapies peuvent promouvoir une réponse innée et adaptative antitumorale forte, c'est le cas de la doxorubicine, de la mitoxantrone et du cyclophosphamide (95). L'usage de ces chimiothérapies en amont d'un traitement par immunothérapie peut permettre une meilleure réponse thérapeutique (96). Parmi les autres traitements pouvant induire une mort immunogénique, nous retrouvons les anthracyclines, les anticorps monoclonaux anti-EGFR, le bortezomib, l'oxaliplatine ou la thapsigargine. Ces drogues déclenchent une mort immunogénique qui sera associée à un stress du réticulum endoplasmique et à l'induction d'autophagie. Cela va aboutir au relargage d'ATP, d'HMGB1 ou à l'expression à la surface des cellules cancéreuses de protéines normalement situées dans le lumen du réticulum endoplasmique comme la calréticuline. Plusieurs modulateurs épigénétiques peuvent contribuer à une mort immunogénique par plusieurs mécanismes (97). Les inhibiteurs des DNMTs, HDACs et EZH2 régulent par exemple des composantes de la machinerie de la présentation antigénique et augmentent la réponse à l'IFN γ . D'autres, comme les inhibiteurs de BET, peuvent jouer sur l'expression de molécules de point de contrôle inhibiteur comme PD-L1 ou sur l'expression de cytokines pro-inflammatoires comme les inhibiteurs de LSD1.

IV) Limites et contraintes de la réponse antitumorale

A) Challenges thérapeutiques

1) Accessibilité et infiltration immunitaire

L'efficacité de la réponse immunitaire intra-tumorale dépend de manière critique de l'accessibilité des cellules immunitaires au sein de la masse tumorale. L'infiltration par des CPA est nécessaire à la capture de l'antigène avant leur migration dans les ganglions drainants la tumeur et l'initiation des réponses effectrice ou mémoire. Par ailleurs, la mise en jeu des fonctions effectrices cytotoxiques et notamment celles des cellules T CD8, nécessite leur pénétration au sein de la tumeur pour qu'elles exercent leur fonction cytotoxique au contact des cellules tumorales. Cependant, l'implantation de la tumeur dans un tissu peut s'accompagner d'une accessibilité limitée par le système immunitaire. Il peut s'agir de la formation d'une capsule autour de la masse tumorale (98) ou encore d'une vascularisation ectopique des tumeurs ne permettant pas la circulation, la migration et l'extravasation des cellules immunitaires de manière optimale sur le site tumoral (99). Par ailleurs, la surexpression de protéines comme l'endothéline B récepteur peut influencer l'adhésion des cellules T à l'épithélium et donc diminuer la réponse immunitaire (100).

Au-delà de l'accessibilité du système immunitaire à la tumeur, c'est aussi l'organisation spatiale de la réponse immunitaire et notamment des cellules T infiltrant la masse tumorale qui jouera une importance. Cette organisation peut être la formation de structures secondaires, tertiaires ou de niches périvasculaires. Elle est également caractérisée par différents types d'infiltrats immunitaires : diffus dans la masse tumorale, en ligne d'invasion ou dans le stroma tumoral (101). L'index de Ball-Hall permet de classer ces motifs (102).

Enfin, l'accessibilité des molécules thérapeutiques dans les tumeurs est aussi un paramètre critique. Il a été démontré que la diffusion de certaines thérapies n'est pas optimale dans les tumeurs en cause d'une vascularisation défective (103).

2) Le microenvironnement tumoral

Le microenvironnement tumoral est constitué d'acteurs cellulaires : les cellules cancéreuses, les cellules stromales incluant les fibroblastes, les cellules endothéliales, les péricytes ou encore le système immunitaire (104). La présence de ces cellules va avoir un impact direct sur la progression tumorale. Les fibroblastes peuvent participer activement à l'angiogenèse par sécrétion de VEGF, l'invasion ou encore supporter le développement des cellules souches tumorales. De nombreuses cellules stromales sous l'action de facteurs activateurs peuvent se transformer en fibroblastes associés au cancer (CAFs). Ainsi, les fibroblastes résidents, les cellules épithéliales, les cellules endothéliales, les cellules souches myéloïdes, hématopoïétiques et cancéreuses, les adipocytes, les péricytes ou encore les cellules stellaires peuvent être à l'origine des CAFs. Les facteurs favorisant l'activation des CAFs sont des facteurs de croissance : le TGF β , le PDGF, l'HGF, le FGF ; des facteurs de

transcription : NF- κ B, HSF-1 ; des cytokines : IL1, IL6 ; les ROS ; des métalloprotéinases ; des protéines de signalisation comme Wnt-3a ; ou encore des exosomes (105). Ils vont sécréter des signaux promoteurs de la mitose, de la survie, de l'invasion et des processus métastatiques et apporter également un soutien métabolique aux cellules cancéreuses. Les adipocytes peuvent posséder des fonctions similaires pro-métastatiques et soutenir le métabolisme des cellules cancéreuses. Les cellules endothéliales peuvent être impliquées dans la sécrétion paracrine de facteurs trophiques, favoriser la dissémination des cellules cancéreuses ou encore prévenir l'inflammation. Les cellules immunitaires peuvent être associées à une diminution des actions cytolytiques des cellules effectrices comme les Th2, les Treg et les B cells, les macrophages de type M2, les MDSC ou encore les neutrophiles. D'autres vont moduler différents processus protumoraux, en favorisant la polarisation vers des phénotypes régulateurs, tolérogène ou anergique. Ces mécanismes dépendent notamment de la sécrétion de cytokines telles que l'IL10, le TGF β , le M-CSF ou encore l'IL5, l'IL6, IL13, l'IL18, l'IL35. Enfin, ils peuvent contribuer à l'augmentation de processus tumoraux comme l'angiogenèse, l'inhibition de l'apoptose ou promouvoir la multiplication des cellules cancéreuses. Le microenvironnement tumoral est également composé de matrice extracellulaire dont les constituants principaux sont le collagène, la fibronectine, la laminine ou encore les acides hyaluroniques. Les tumeurs sont également associées au reste de l'organisme par la présence de vaisseaux sanguins, de fibres nerveuses et de la proximité des ganglions drainants. Elles possèdent divers mécanismes de communications comme les cytokines, les chimiokines, les acides nucléiques circulant et différentes sortes de vésicules (106). La connexion au système vasculaire, lymphatique ainsi que l'ensemble des facteurs solubles peut contribuer au développement d'une niche distante favorisant l'implantation de cellules cancéreuses métastatiques.

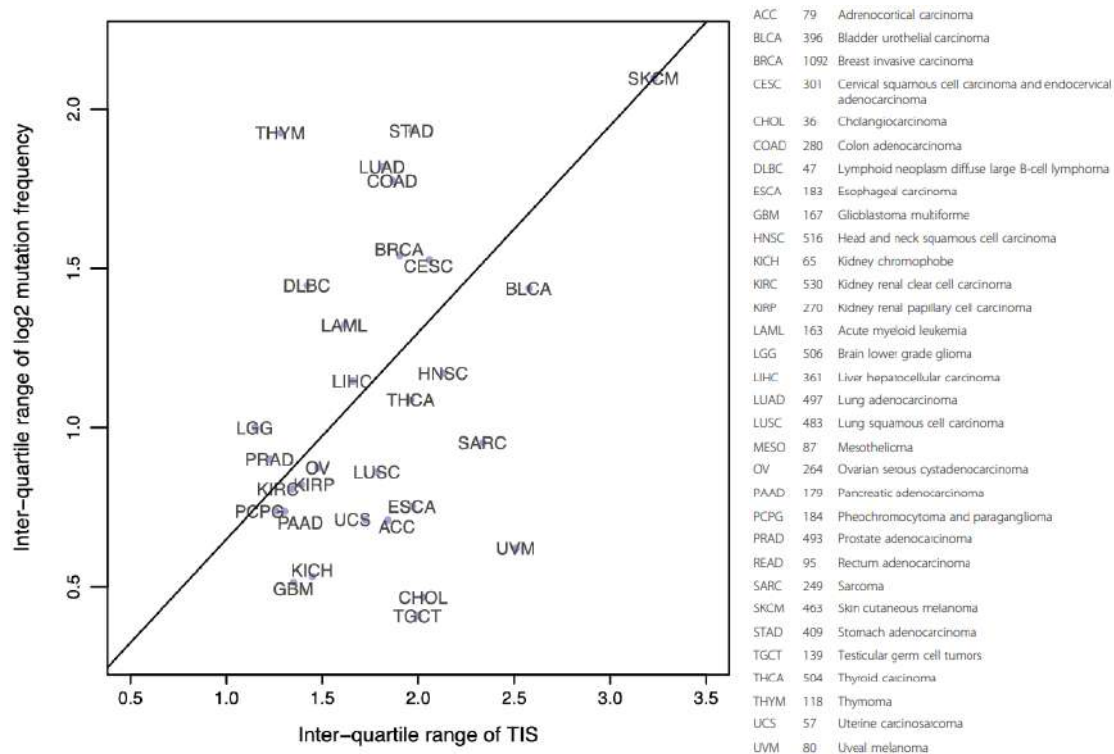


Figure 23 : Corrélation entre la charge mutationnelle et le score immunitaire

Ce diagramme de corrélation représente le rang interquartile du score immunitaire tumoral (acronyme TIS en anglais) en fonction de la charge mutationnelle. Chaque type de cancer est représenté selon ces axes. Figure traduite de la référence (6) .

3) Tumeurs froides – tumeurs chaudes

Ainsi, selon les niveaux d'antigénicité, d'immunogénicité, d'immunoédition et d'accessibilité, on peut distinguer deux catégories de tumeurs, appelées tumeurs « chaudes » et qui désignent un état inflammatoire prononcé et donc une présence forte du système immunitaire et par opposition des « tumeurs froides », véritable désert immunitaire. Les tumeurs froides sont associées à un mauvais pronostic et les tumeurs chaudes à un bon pronostic. Cependant, certaines tumeurs présentant un fort taux d'infiltration par le système immunitaire sont pourtant associées à un mauvais pronostic. Ce mécanisme est notamment dépendant des fonctions de la cyclooxygénase produisant de la prostaglandine E2, convertissant les fonctions de l'infiltrat myéloïde vers un phénotype pro-tumoral et changeant les profils cytokiniques des cellules T (107).

Les tumeurs dites « froides » sont très peu immunogéniques et associées à un défaut d'infiltration par les cellules de l'immunité. Ce sont des tumeurs agressives de mauvais pronostic. De plus, une tumeur chaude, après immunoédition ou après d'autres changements métaboliques, peut devenir une tumeur froide. C'est notamment le cas lors d'une polarisation et d'une conversion du système immunitaire par les cellules cancéreuses. Si l'on étudie l'ensemble des types de cancers, il existe un fort lien entre l'antigénicité tumorale, de forts taux de mutations, l'expression du CMHI et l'infiltration du système immunitaire et donc de réponses aux immunothérapies. Par exemple, les mélanomes présentent un taux important de mutations et un taux de réponse aux immunothérapies élevé. En opposition, certains cancers comme celui de la prostate et du pancréas sont des déserts immunitaires et ils présentent une faible charge mutationnelle (108). Cependant, certains types de cancers dérogent à la règle d'une corrélation entre charge mutationnelle et infiltration immunitaire, basée sur la *Tumor inflammation signature* (TIS) (6). Si nous prenons l'exemple du sarcome, considéré comme une tumeur froide, avec une charge mutationnelle modérée voir faible, la TIS est elle proportionnellement plus élevée. Ainsi, la présence d'une charge mutationnelle suffisante est nécessaire à une survie améliorée des patients en présence d'un infiltrat immunitaire dans les sarcomes et ostéosarcomes (109–111).

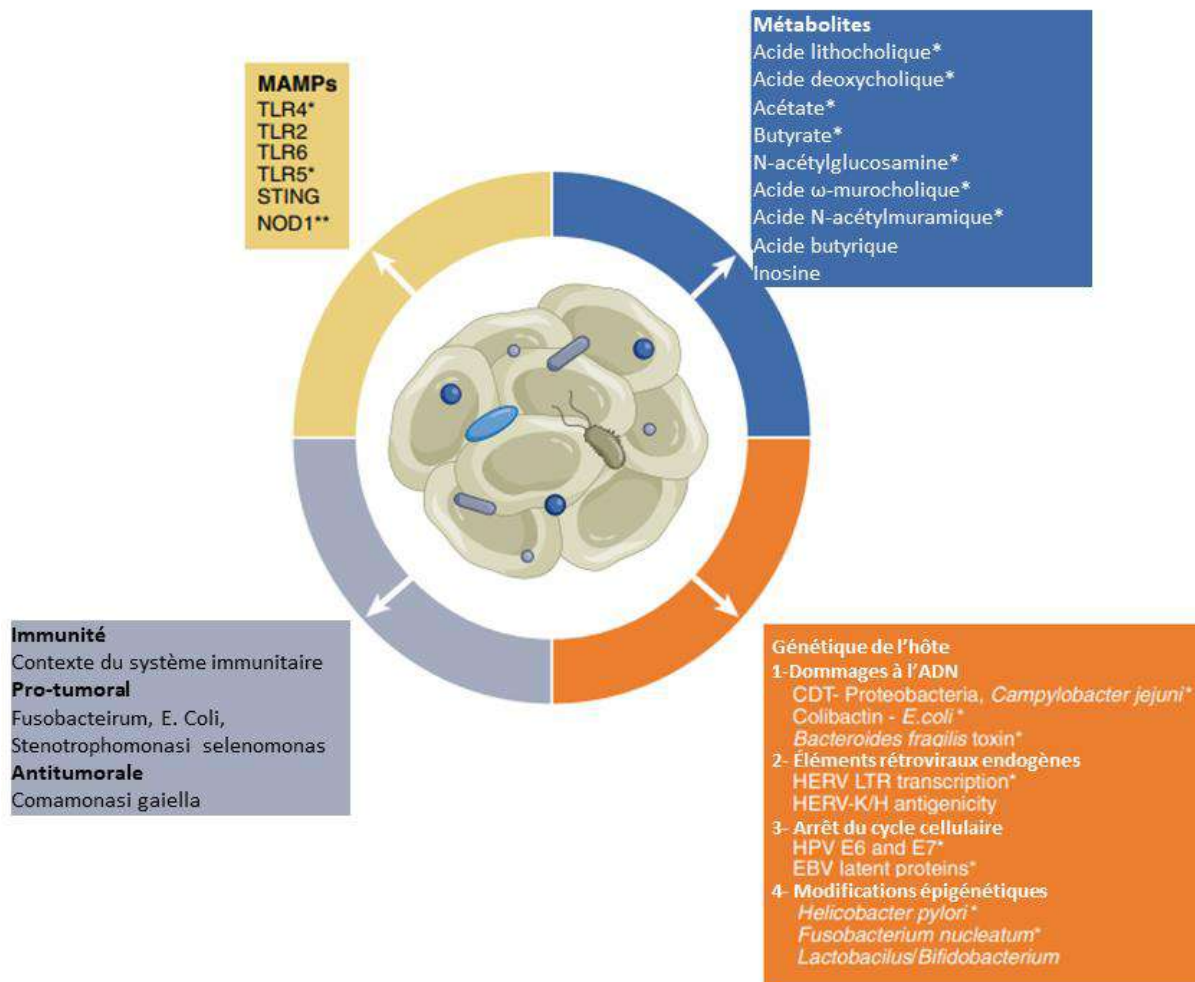


Figure 24 : Caractéristique de l'impact du microbiote sur le cancer

Le microbiote produit plusieurs composés qui peuvent influencer les réponses immunitaires. Les effets médiateurs ou mécanismes associés à une réponse antitumorale sont listés sans symbole, alors que ceux associés à un état pro-tumoral sont indiqués par un astérisque. Les effets médiateurs ou mécanismes dépendant du contexte sont indiqués par deux astérisques. Abréviations : MAMPs : de l'anglais motifs moléculaires associés aux microorganismes. Figure traduite de la référence (112).

4) Microbiote

D'un point de vue structurel, les tumeurs peuvent être considérées comme des organes à part entière (113). Ce sont des organes anormaux composés de plusieurs sous types cellulaires, ayant leur propre matrice et vascularisation et qui peuvent héberger en leur sein un microbiote telles que des bactéries. Certaines bactéries intratumorales peuvent promouvoir la résistance des tumeurs aux traitements comme par exemple une résistance à la gemcitabine (114). La nature du microbiote, intratumoral ou non, est liée à la progression tumorale. Certains composés dérivés du microbiote peuvent doper la réponse immunitaire ; c'est le cas d'acides gras à chaînes courtes (SCFa) qui vont promouvoir des réponses de type mémoire (115). Au contraire, le microbiote peut contribuer à la résistance aux immunothérapies anti-PD1 ou anti-CTLA4 (116,117).

Les organismes présents dans l'intestin peuvent moduler les réponses immunitaires par plusieurs mécanismes : compétition écologique inter-espèces, stimulation des PRR (pattern recognition receptors), modulation des hormones intestinales, modulation métabolique des ressources *via* l'apport de vitamines B et de polyamines ou induction d'une réponse immunitaire par réaction croisée d'une réponse immunitaire anti-microbiote contre une cellule cancéreuse (112).

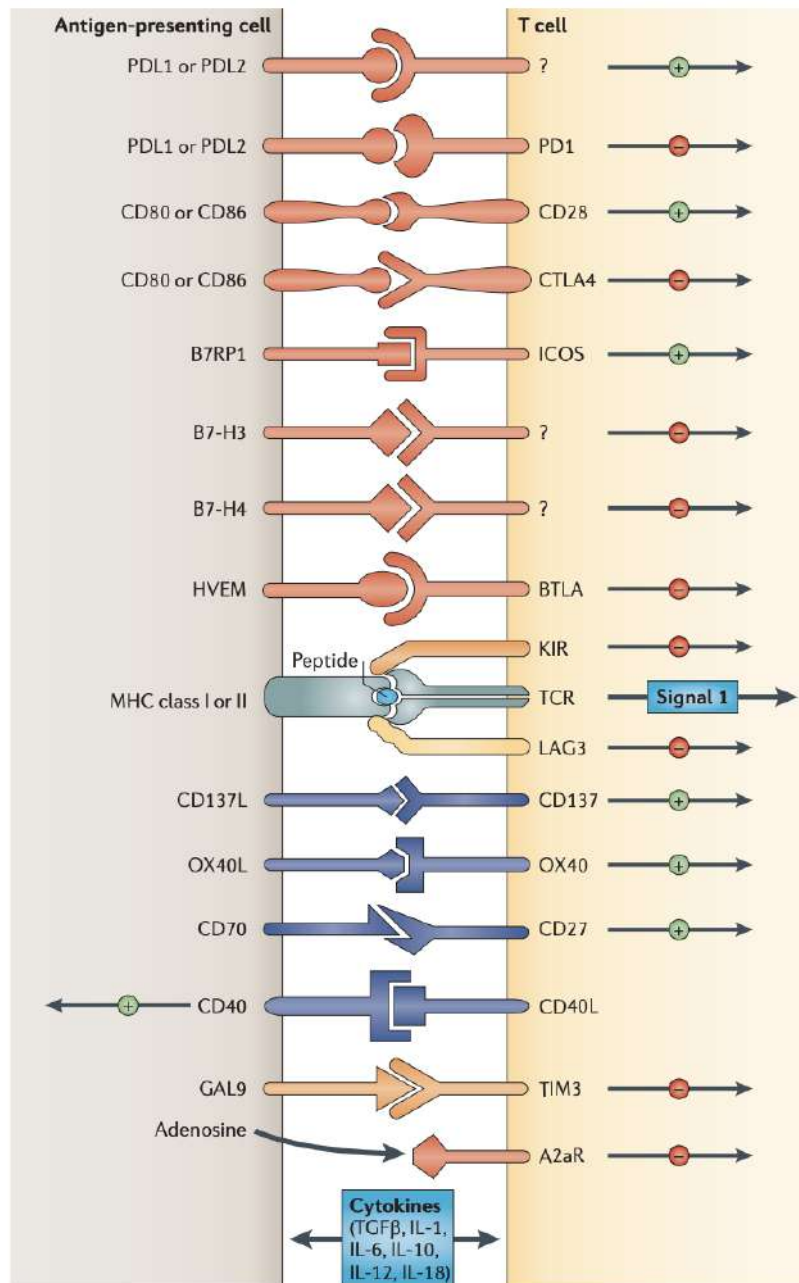


Figure 25 : Les points de contrôle de l'immunité ou immune checkpoints

Les points de contrôle de l'immunité ou immune checkpoints en anglais désigne un couple ligand récepteur entre une cellule présentatrice de l'antigène (Antigen-presenting cell en anglais) et une cellule T (T cell en anglais) impliqué dans le rétrocontrôle de l'activation cellulaire. Figure de la référence (118)

5) Les points de contrôle de l'immunité, immunothérapies et métabolisme

À l'état physiologique, les réponses immunitaires possèdent une phase de rétrocontrôle négatif sur l'activation des cellules effectrices. Celle-ci est nécessaire au bon fonctionnement de la réponse immunitaire et limite les potentielles conséquences délétères, souvent observées dans les cas d'auto-immunité. Ce système de régulation, qu'il soit

moléculaire ou cellulaire, est souvent enrichi dans un contexte tumoral. Ainsi, plusieurs ligands inhibiteurs ou compétitifs de l'activation des cellules T vont être exprimés et sécrétés sous forme de petites vésicules par les cellules tumorales. Ces couples ligands récepteurs sont appelés les points de contrôle de l'immunité. On retrouve sans en faire une liste exhaustive, les couples ligands/récepteurs suivants : PD-L1/PD1, CD80/CTLA4, GAL9/TIM3 et CMH/LAG3 parmi les plus décrits (69). Les immunothérapies cherchent à prévenir ces signaux inhibiteurs et restaurer une réponse immunitaire antitumorale. De nombreux anticorps monoclonaux bloquants ont été développés à cet usage et ont démontré une grande efficacité notamment dans le mélanome. Cependant, l'efficacité des immunothérapies possède ses limites dans les cancers métastatiques ou les tumeurs froides et peuvent présenter dans certains cas des effets secondaires de type auto-immun.

Au-delà de l'impact sur l'activation des cellules effectrices, la liaison engendre des voies de signalisation dans les deux cellules impliquées dans l'interaction. Du côté immunitaire, l'interaction va impacter l'activation des fonctions effectrices et l'expression des molécules activatrices mais également conduire l'altération métabolique de ces cellules, notamment par inhibition des processus mitochondriaux d'oxydation des acides gras et de lipolyse au détriment de la glycolyse (119,120). Ces changements vont amener les cellules immunitaires vers un état dysfonctionnel et d'épuisement irréversible. Plusieurs acteurs cellulaires et moléculaires ont été décrits pour leur implication dans ces processus avec des rôles complexes dépendant de la temporalité de la progression tumorale. C'est le cas pour la présence de cellules myéloïdes comme les macrophages associés aux tumeurs (121), du TGF β (122,123) ou encore de l'IFN γ (124)

L'expression des points de contrôle de l'immunité est étroitement liée au métabolisme et cibler ce dernier peut favoriser la réponse aux immunothérapies. Par exemple, l'augmentation de l'expression de CD36, un transporteur de lipides, peut diminuer la fonction des cellules T CD8 par peroxydation des lipides. Ainsi, l'inhibition de PD1 et de CD36 favorise l'efficacité thérapeutique (125). D'autres thérapies ont été développées ciblant :

- la glycolyse et l'effet Warburg : transporteurs du glucose, enzymes glycolytiques, métabolisme du lactate (MCT1 inhibiteurs, LDHA inhibiteurs), AMPK
- le métabolisme des lipides : inhibiteurs d'ACAT, agonistes de PPAR α , activateurs de CPT1
- la biogénèse mitochondriale : PGC1 α
- le métabolisme des acides aminés : inhibiteurs des récepteurs de la glutamine, de la méthionine, inhibiteurs d'Ahr, TG2, GAD1, ASNS
- le métabolisme de l'adénosine : inhibiteurs de CD73 et CD39, d'A2aR, CD38

Dans les précédentes parties, nous avons vu la relation étroite entre le métabolisme, son implication dans l'agressivité des cellules cancéreuses et son lien avec la réactivité du système immunitaire. Nous avons vu aussi que la mitochondrie, l'organelle énergétique y joue un rôle central et que l'altération de ses fonctions peut être génératrice de

dysfonctionnement cellulaire mais également altérer les propriétés du microenvironnement tumoral. Ainsi, cibler la mitochondrie émerge comme une opportunité thérapeutique.




B) Cibler la mitochondrie

1) L'implication d'OMA1 et d'OPA1 dans la progression tumorale

OMA1 et OPA1 sont les principaux acteurs de la fission mitochondriale en réponse à un stress, ainsi s'interroger sur leur expression dans les tumeurs est une question pertinente. La corrélation entre l'expression d'OMA1 et OPA1, la progression tumorale et la survie est assez complexe, compte tenu de l'hétérogénéité même de l'utilisation des mitochondries dans les tumeurs. Par exemple, dans le cancer ovarien, il a été montré que la voie de signalisation PHB2/OMA1/DELE1 couplée au stress du réticulum endoplasmique est associée à une meilleure réponse aux chimiothérapies (126). Dans le cancer colorectal, OMA1 contrôle une reprogrammation métabolique sous hypoxie associée à un effet pro-tumoral (127). D'une manière similaire l'inhibition d'OPA1 diminue la prolifération de cellules de cancer du sein triple négatif, leur migration et leur potentiel invasif (128). La régulation de l'activité d'OMA1 dépend d'un pont disulfure initialement découvert chez la levure. En utilisant la technologie du prime editing, nous avons inséré, dans une lignée de sarcome murin, une mutation ponctuelle dans la séquence codante d'OMA1, remplaçant l'une des cystéines constitutives du pont disulfure, par une alanine. Après avoir caractérisé les conséquences de la mutation sur la maturation d'OMA1, le clivage d'OPA1 et les processus de fusion/fission, nous nous sommes intéressés aux conséquences physiologiques, métaboliques et tumorales. Enfin, nous avons établi que la présence de cette mutation altérait la croissance de la cellule chez la souris en augmentant l'activation du système immunitaire. Cette activation est dépendante du relargage d'ADN mitochondrial par les cellules mutantes et nécessite la présence des cellules dendritiques cDC1, dotée de la capacité de cross-priming, et des cellules T CD8.



An OMA1 redox site controls mitochondrial homeostasis, sarcoma growth, and immunogenicity

Richard Miallot¹, Virginie Millet¹, Yann Groult¹, Angelika Modelska¹, Lydie Crescence², Sandrine Roulland¹, Sandrine Henri¹ , Bernard Malissen^{1,3}, Nicolas Brouilly⁴, Laurence Panicot-Dubois² , Renaud Vincentelli⁵, Gerlind Sulzenbacher⁵, Pascal Finetti⁶, Aurélie Dutour⁷, Jean-Yves Blay^{7,8}, François Bertucci⁶, Franck Galland¹, Philippe Naquet¹ 

Aggressive tumors often display mitochondrial dysfunction. Upon oxidative stress, mitochondria undergo fission through OMA1-mediated cleavage of the fusion effector OPA1. In yeast, a redox-sensing switch participates in OMA1 activation. 3D modeling of OMA1 comforted the notion that cysteine 403 might participate in a similar sensor in mammalian cells. Using prime editing, we developed a mouse sarcoma cell line in which OMA1 cysteine 403 was mutated in alanine. Mutant cells showed impaired mitochondrial responses to stress including ATP production, reduced fission, resistance to apoptosis, and enhanced mitochondrial DNA release. This mutation prevented tumor development in immunocompetent, but not nude or cDC1 dendritic cell-deficient, mice. These cells prime CD8⁺ lymphocytes that accumulate in mutant tumors, whereas their depletion delays tumor control. Thus, OMA1 inactivation increased the development of anti-tumor immunity. Patients with complex genomic soft tissue sarcoma showed variations in the level of OMA1 and OPA1 transcripts. High expression of OPA1 in primary tumors was associated with shorter metastasis-free survival after surgery, and low expression of OPA1, with anti-tumor immune signatures. Targeting OMA1 activity may enhance sarcoma immunogenicity.

occurrence of mitochondrial stress (McBride & Soubannier, 2010; Baker et al, 2014). These changes contribute to the metabolic rewiring of cancer cells toward a glycolytic phenotype, a process often driven by oncogenic alterations. Nevertheless, the preservation of mitochondrial activity is required for the metabolic plasticity of tumor cells. It contributes to NAD⁺ regeneration and to the processing of alternative carbon sources such as glutamine for anabolic pathways (Porporato, 2018).

To optimize their functionality, mitochondria undergo fusion and fission processes, allowing cells to cope with metabolic adaptations and to scavenge damaged organelles. OPA1 is necessary for inner membrane fusion (Alavi, 2019). This protein is highly expressed in metabolically demanding tissues (Gilkerson, 2018). The abundance of the L-OPA1 isoform is down-regulated by proteolytic cleavage at the S2 or S1 sites generating distinct S-OPA1 isoforms by either the constitutively expressed YMEL1 (Song et al, 2007) or the stress-regulated OMA-1 proteases, respectively (Ehses et al, 2009; Head et al, 2009). An additional YMEL1 cleavage site called S3 is involved in the production of another S-OPA1 isoform that contributes to mitochondrial elongation (Wang et al, 2021). Furthermore, the S2 site is required for OXPHOS-induced hyperfusion. The equilibrium between L-OPA1 and S-OPA1 determines the inner membrane fusion potential (Ishihara et al, 2006), whereas S-OPA1 alone contributes to the maintenance of mitochondrial DNA, respiratory complexes, and crista structure (Del Dotto et al, 2017). Upon mitochondrial depolarization or oxidative stress, the activation of OMA1 leads to the cleavage of several target proteins including OPA1 at the S1 site (Baker et al, 2014; Murata et al, 2020) and DELE1 (Fessler et al, 2020; Guo et al, 2020), provoking mitochondrial fission and integrated stress response, respectively. Then, the peripheral mitochondrial division is triggered (Kleele et al, 2021) and leads to the clearance of damaged mitochondria by mitophagy (Twig & Shirihai, 2011). Furthermore, OMA1 links mitochondrial protein

DOI 10.26508/lsa.202201767 | Received 13 October 2022 | Revised 21 March 2023 | Accepted 24 March 2023 | Published online 5 April 2023

Introduction

Mitochondria operate as major hubs regulating cell life and death. By providing energy through the electron transport chain (ETC), they also generate reactive oxygen species (ROS) that may be detrimental to tumor survival. Functional and/or structural alterations in these organelles frequently occur in cancer and witness the

¹Aix-Marseille Université, INSERM, CNRS, Centre d'Immunologie de Marseille-Luminy, Marseille, France ²Aix Marseille Université, INSERM 1263, INRAE 1260, Plateforme d'Imagerie Vasculaire et de Microscopie Intravital, C2VN, Marseille, France ³Centre d'Immunophénomique, Aix Marseille Université, INSERM, CNRS, Marseille, France ⁴Aix-Marseille Université, CNRS, IBDM, Marseille, France ⁵Aix-Marseille Université, CNRS, Architecture et Fonction des Macromolécules Biologiques, Marseille, France ⁶Laboratory of Predictive Oncology, Centre de Recherche en Cancérologie de Marseille (CRCM), Institut Paoli-Calmettes, Aix-Marseille Université, Centre National de la Recherche Scientifique (CNRS), Institut National de la Santé et de la Recherche Médicale (INSERM), Marseille, France ⁷Childhood Cancers and Cell Death Laboratory, Cancer Research Center of Lyon (CRCL), INSERM 1052, CNRS, Lyon, France ⁸Department of Medicine, Centre Léon Bérard, UNICANCER & University Lyon I, Lyon, France

Correspondence: naquet@ciml.univ-mrs.fr; miallot@ciml.univ-mrs.fr

quality control to retrograde signaling that is required for the induction of tolerance mechanisms to stress (Bohovych et al, 2016; O'Malley et al, 2020).

OMA1 maturation is a tightly regulated process allowing its integration in the inner mitochondrial membrane; both proteolytic and autocatalytic processes lead to the production of enzymatically active OMA1 protein isoforms (Baker et al, 2014; Zhang et al, 2014; Consolato et al, 2018). Interestingly, distinct regions of the OMA1 protein are involved in stress sensing. A recent report in yeast identified a redox-sensing site required for the production of active OMA1 upon mitochondrial depolarization and oxidative stress (Bohovych et al, 2019). This regulation depends on the formation of a disulfide bridge between cysteines 272 and 332 of yeast OMA1 and contributes to the organization and function of the ETC. In this model, the loss of OMA1 function results in increased ROS production and impaired retrograde signaling required for cell survival. We reasoned that by interrupting OMA1 function in cancer cells, one might interfere with the induction of stress response pathways and enhance cancer cell death. Because the above-mentioned Cys are conserved in the mammalian *oma1* gene, we decided to evaluate their contribution to the regulation of OMA1 activity and mitochondrial function in sarcoma.

Oma1 is a candidate modulator of cancer progression. Its overexpression is of poor prognosis in gastric carcinoma (Amini et al, 2020), and breast and squamous cell lung carcinoma (Alavi, 2019), but conversely associated with improved survival in lung adenocarcinoma (Alavi, 2019) and breast carcinoma (Daverey et al, 2019). In colorectal cancer, OMA1 supports metabolic reprogramming under hypoxic conditions (Wu et al, 2021). These results indicate that OMA1 involvement in cancer depends upon the context, suggesting a differential involvement of mitochondrial activity in these tumors. We previously showed that preservation of mitochondrial fitness limited mouse fibrosarcoma progression (Giessner et al, 2018). In sarcoma patients, the contribution of mitochondrial activity to tumor progression is still debated, an issue complicated by the heterogeneity of these tumors (Miallot et al, 2021). We therefore probed the involvement of the OMA1/OPA1 pathway in a mouse sarcoma model and tested whether the level of OMA1 and OPA1 expressions was associated with clinical outcome and immune variables in human soft tissue sarcomas (STS).

Results

The C403A mutation abrogates OMA1-dependent OPA1 cleavage in a mouse sarcoma model

OMA1 processing is recapitulated in Fig 1A and based on a 3D model of the mouse 59-kD pre-pro-OMA1 protein available in the AlphaFold database (<https://alphafold.ebi.ac.uk/>). This immature form undergoes further proteolysis during mitochondrial insertion (see Fig 1 legend). Upon depolarization induced by the carbonyl cyanide *m*-chlorophenyl hydrazine (CCCP) uncoupling drug, the mature 40-kD L-OMA1 isoform is autocatalytically cleaved at the C-terminal end to generate the 35-kD S-OMA1. This isoform is catalytically active on its target proteins, undergoes further C-terminus

cleavage, and is unstable (Baker et al, 2014; Zhang et al, 2014; Alavi, 2021). As shown in yeast, this activation process might involve redox changes in cysteines 272 and 332, corresponding to cysteines 403 and 461 in mouse OMA1 (Bohovych et al, 2019). Because mutation of yeast Cys332, equivalent to mouse Cys461, provoked a loss of OMA1 stability, we focused our efforts on Cys403. We addressed the contribution of these cysteines to OMA1 activation using biochemical and molecular approaches. We first produced a recombinant OMA1 protein displaying only the outer membrane domain that contains the catalytic site, coupled to the protein disulfide-isomerase DsbC to optimize the production in bacteria (Fig S1A). The recombinant OMA1 protein cleaved an artificial substrate based on a short OPA1 peptide containing the OMA1-specific cleavage site (Tobacyk et al, 2019). However, the specificity of this cleavage has been questioned (Alavi, 2022). Accordingly, the activity is only partially inhibited by the N,N,N',N'-tetrakis(2-pyridylmethyl)ethylenediamine (TPEN), a zinc chelator used as a negative control of the Zn-dependent OMA1 activity (Fig S1B). Unfortunately, the production of a protein in which Cys403 was replaced by an Ala (C403A mutant) did not lead to the production of a stable protein (Fig S1A). Because no experimental 3D structure of OMA1 is available, we took advantage of recent developments in artificial intelligence (AI) and inspected the 3D model of mouse OMA1 generated by the AlphaFold algorithm (Jumper et al, 2021), which revealed that the disulfide bridge in question is located far from the catalytic site and exposed at the protein surface (Fig 1A). It is worth mentioning that significant portions of the protein, mostly external loops, are modeled with a very low confidence level, suggesting structural disorder and plasticity. We then generated a model of the OMA1 C403A mutant using DeepMind's Colab notebook (Jumper et al, 2021). Comparison of AlphaFold models between WT and mutated OMA1 revealed that no major structural changes were induced by the C403A mutation. It should, however, be noted that the model of the OMA1 C403A mutant generated by DeepMind's Colab notebook might be biased toward the training provided by the model of native OMA1, not accounting for subtle modifications engendering major structural changes in vivo (Fig S1C).

We then mutated Cys403 into Ala in the murine fibrosarcoma cell line MCA205 by prime editing (Anzalone et al, 2019). We obtained heterozygote and homozygote 403C>A mutant clones (named C403A throughout the study) and control unedited cells (named CTRL throughout the study; Fig S1D and E for DNA sequencing profile). We performed several control experiments to validate the edition process. First, as expected, *Oma1* and *Opa1* transcript levels were unchanged in edited cell lines (Fig S1F). Furthermore, all edited lines had a comparable although not equivalent growth rate in vitro (Fig S1G). Although the experiments were performed with several independent clones (Fig S1G), we chose representative CTRL and C403A clones to illustrate our results.

We then evaluated the expression of OMA1 protein isoforms in control or CCCP-treated cells. In MCA205 sarcoma cells at a steady state, both the immature and the active S-OMA1 isoforms are detectable in total cell extracts (Fig 1B and C). In mitochondrial extracts, only L- and S-OMA1 were detected, with a predominance of the S-OMA1 isoform (Fig 1D) that may witness the presence of an endogenous mitochondrial stress associated with OMA1 autocatalysis in this tumor cell line. In C403A unstimulated total cell and

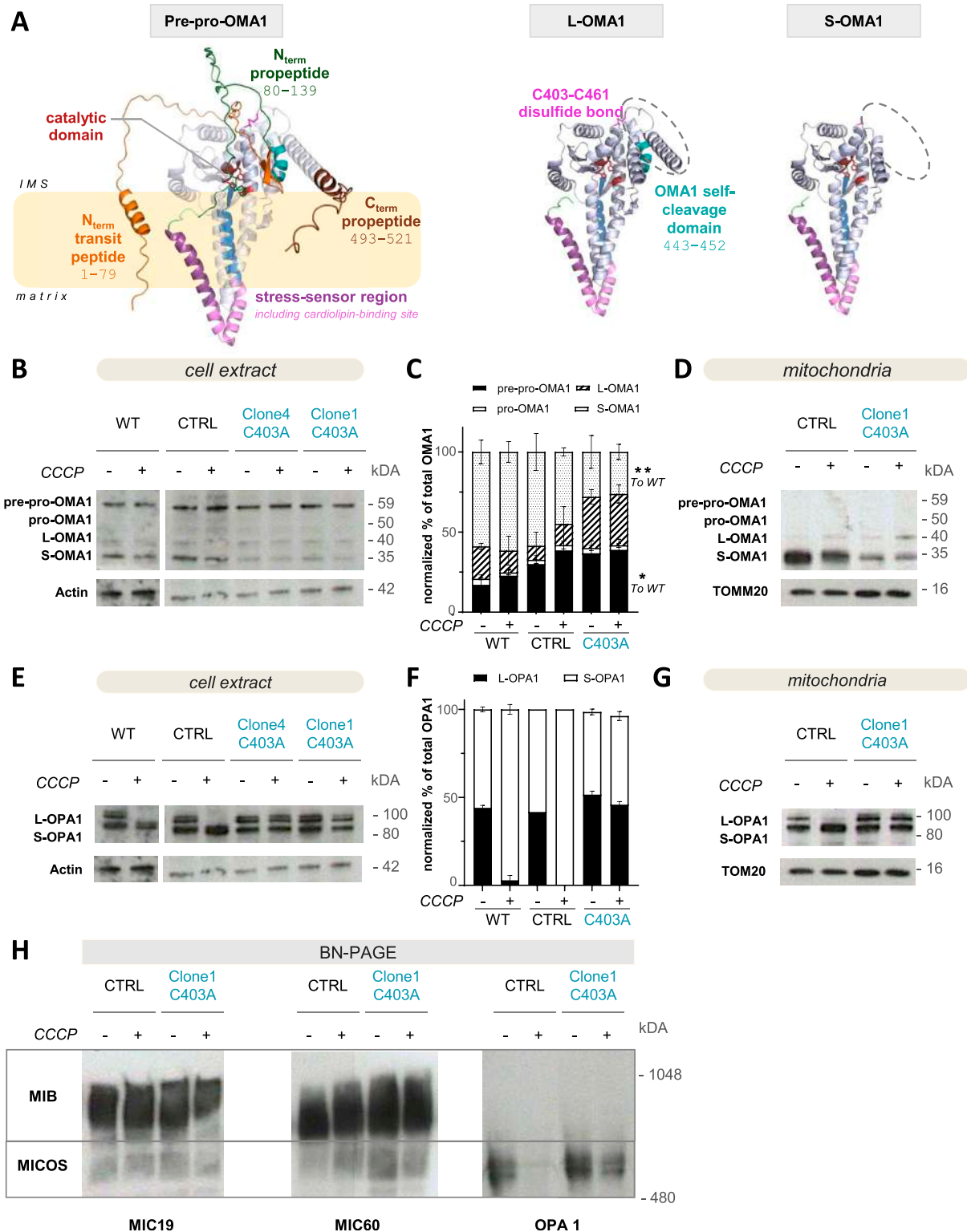


Figure 1. C403A mutation alters OMA1 maturation and catalytic activity.

(A) OMA1 model, retrieved from the AlphaFold tool, and representation of the maturation processing of OMA1. OMA1 is a mitochondrial protein with a M48 metalloendopeptidase domain facing the mitochondrial intermembrane space. It probably exists as a homo-oligomeric complex, and the activation mechanism remains incompletely understood (Levytsky et al, 2017; Alavi, 2021). The cysteine residues of interest are highlighted in pink. OMA1 maturation follows the following steps: the transit peptide in orange, facing the mitochondrial matrix from pre-pro-OMA1, is cleaved between 79L and 80S residues to obtain the pro-OMA1 form. The propeptide in dark green is then cleaved between residues 139Q and 140A and in the C-terminal region after residue 493, in brown. This process requires the AFG3L2 and YMEL1 proteases (Rainbolt et al, 2016; Consolato et al, 2018). The mature long form of OMA1 (L-OMA1) is autocatalytically cleaved into the S-OMA1 form through the cleavage of a

mitochondrial extracts, the relative proportion of S-OMA1 was significantly reduced compared with CTRL extracts (Fig 1B–D). Because OMA1 is subjected to autocatalysis, we tested whether this activity was preserved in C403A OMA1. We performed a kinetic analysis of OMA1 processing after CCCP exposure in both cell types (Fig S1H). In CTRL mitochondrial extracts, the L-OMA1 isoform progressively disappeared and 35- and 33-kD S-OMA1 isoforms progressively appeared after 1 h of treatment in agreement with the autocatalytic activity. In C403A cells, the 35-kD S-OMA1 isoform was present in reduced amounts, and at late time points, the shorter OMA1 isoforms were not detectable. This might be due to the fact that C403A cells show more signs of damage after prolonged CCCP treatment than CTRL cells. These results indicate that the C403A mutation enhances S-OMA1 instability and might affect its autocatalytic activity.

We then investigated whether the C403A mutation prevented the cleavage of the OMA1–target protein OPA1. At the steady state, the OPA1 long isoform (L-OPA1) is cleaved by YMEL1 at the S2 or S3 site into a short 80- to 90-kD isoform (S-OPA1), thereby contributing to the regulation of the homeostatic fusion/fission process (Song et al, 2007; Head et al, 2009; Wang et al, 2021). This explains the presence of comparable levels of L- and S-OPA1 isoforms under basal culture conditions of the cell line (Fig 1E). Activated S-OMA1 cleaves L-OPA1 at the S1 site to generate another short inactive S-OPA1 isoform (Song et al, 2007). We evaluated the proportion of S-OPA1 and L-OPA1 as an indicator of CCCP-induced OMA1 activation in total cell extracts. Under CCCP-induced stress, OPA1 was fully converted into S-OPA1 (Fig 1E and F). In contrast, untreated or CCCP-treated C403A cells displayed a constant proportion of S- and L-OPA1 isoforms. These results were confirmed using mitochondrial extracts (Fig 1G). Therefore, C403A OMA1 is unable to cleave its mitochondrial OPA1 substrate upon stress. Unexpectedly, extracts from both CTRL and C403A cells could cleave the reporter peptide with equivalent efficacy, and this cleavage was inhibited by TPEN (Fig S1C) (Tobacyk & MacMillan-Crow, 2021). Keeping in mind the poor specificity associated with the reporter peptide, this finding suggested that modifications induced by the C403 mutation might be preventing the engagement of OMA1 with its target proteins.

The OMA1 and OPA1 proteins are part of the mitochondrial contact site and crista organizing system (MICOS) complex that regulates crista structure (Glytsou et al, 2016; Huynen et al, 2016; Viana et al, 2021). The lack of OMA1 was shown to reduce the stability of the MICOS complex (Viana et al, 2021). BN-PAGE analysis revealed no significant changes between control and C403A cells in the proportion of the mitochondrial bridging (MIB) complex and MICOS supramolecular complexes under basal or CCCP-treated conditions, showing that the C403A mutation does not prevent their formation (Figs 1H and S1I). OPA1 could be detected in the MICOS complex, and interestingly, its proportion was reduced after CCCP

treatment of control but not C403A cells, as expected because of the lack of OMA1-mediated cleavage.

Loss of mitochondrial homeostasis in stressed OMA1 mutant cells

We evaluated the impact of the C403A OMA1 mutation on mitochondrial organization. We performed a high-resolution confocal analysis of MCA205 cells stained with MitoTracker Deep Red and reconstructed the mitochondrial network in 3D. Under basal conditions, both CTRL and C403A OMA1 cells showed a complex mix of small individual mitochondria and tubular mitochondrial networks (Fig 2A). After CCCP-induced mitochondrial membrane depolarization, CTRL cells showed an increased mitochondrial fission index in agreement with OPA1 inactivation. In contrast, the mitochondrial network and index remained unchanged in CCCP-treated C403A cells (Figs 2A and B and S2A for data on additional edited clones). Because MitoTracker Deep Red depends on transmembrane potential for uptake (Xiao et al, 2016), we confirmed our results using translocase of the outer mitochondrial membrane 20 (TOMM20) staining on fixed and permeabilized cells (Nakashima-Kamimura et al, 2005). As shown in Fig S2B, C403A cells showed a network of hypertubular mitochondria that were unaffected by CCCP treatment unlike that of CTRL cells. This result confirmed the loss of stress-induced adaptation of mitochondrial reorganization.

Because OMA1-dependent regulation is required for the maintenance of mitochondrial fitness, we scored several parameters of mitochondrial function in vitro. Despite higher basal ECAR and OCR in C403A versus CTRL cells (Fig S2C), the ATP rate index reflecting mitochondrial versus glycolytic-dependent ATP production was reduced in C403A compared with CTRL cells (Fig 2C and S2D). Overall, this indicated that whereas the lack of mitochondrial fragmentation could be associated with a relative increase in OXPHOS (Wu et al, 2021), C403A cells rather relied on glycolysis to sustain their hypermetabolic profile. Quantification of mitochondrial ROS overproduction after inhibition of complex III of the ETC complex by antimycin A showed that C403A cells had a reduced leakage of mitochondrial ROS compared with CTRL cells (Fig 2D). We then quantified mitochondrial depolarization and mass using the MitoTracker Deep Red (MDR) and MitoTracker Green (MG) probes, respectively (Xiao et al, 2016). As shown in Fig S2E, CTRL and C403A clones showed comparable levels of MDR and MG staining in culture. In vitro CCCP treatment provoked a major reduction in mitochondrial mass and polarization in both cell types. Interestingly, the MDR/MG ratio tended to increase in CTRL but to decrease in C403A cells (Fig 2E), suggesting that mitochondria from C403A cells might be more susceptible to CCCP-induced depolarization.

OMA1-deficient cells were previously shown to be resistant to apoptosis because of the reduced leakage of cytochrome c (Jiang et al, 2014; Gilkerson et al, 2021). We treated CTRL and C403A cells

second peptide approximately in the region 443–452, in turquoise (Baker et al, 2014; Zhang et al, 2014). (B, C, D, E, F, G) Western blot analysis of OMA1 (B, C, D) and OPA1 (E, F, G) proteins prepared from WT, unedited, and C403A total MCA205 cell (panels B and E) or mitochondrial extracts (panels D and G) exposed for 1 h or not to the uncoupling agent CCCP. Quantification included data obtained from analysis of two WT and four C403A samples (source data), as shown in panels C for OMA1 and F for OPA1 using actin or TOMM20 as control cell or mitochondrial protein (n = 2). Mann–Whitney test; * P < 0.05. (H) BN-PAGE analysis of native proteins prepared from CTRL and C403A cell mitochondrial extracts. MIB and MICOS complex composition was analyzed using anti-MIC60, anti-MIC19, and anti-OPA1 antibodies (n = 2). Source data are available for this figure.

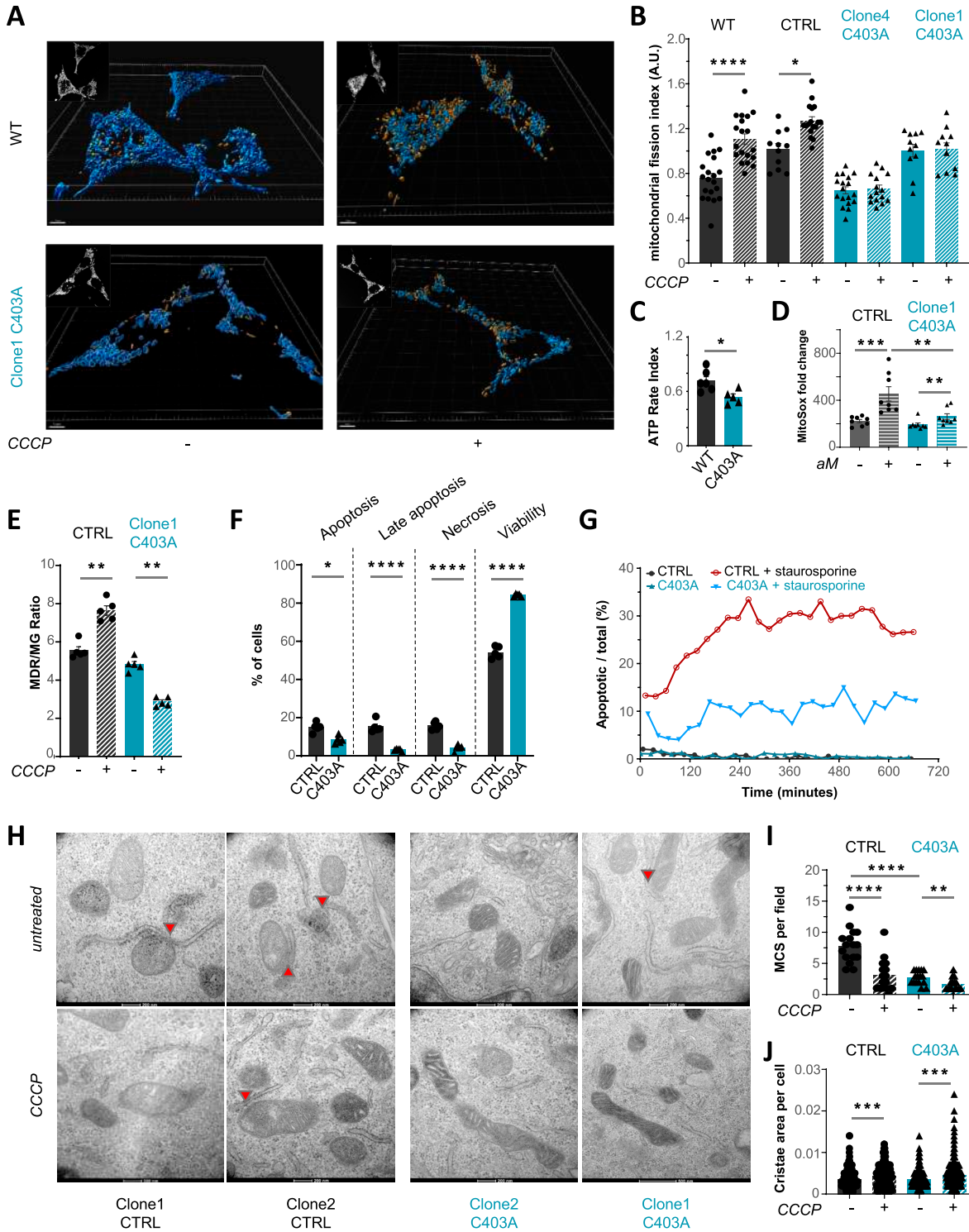


Figure 2. Evaluation of mitochondrial fitness.

(A) Untreated or CCCP-treated CTRL and C403A MCA205 cells were labeled with mitochondrial depolarization (MDR) (5 μ M), and the mitochondrial network was reconstructed by 3D modeling as described in the Materials and Methods section. Yellow and blue dots represent individual mitochondria and network, respectively. Scale bar: 5 μ m (n = 2). (B) Mitochondrial fission index was calculated in WT, CTRL, and C403A cells in the presence or the absence of CCCP stimulation (n = 2). Two-way ANOVA Tukey's multiple comparisons test was performed for statistical analysis (****P < 0.0001 and *P < 0.05). (C) ATP rate index of WT and C403A MCA205 cells was assessed using Seahorse XFp (n = 2). Mann–Whitney test; *P < 0.05. (D) Mitochondrial ROS were evaluated by flow cytometry. Data were represented as the mean fluorescent intensity of the MitoSOX probe on CTRL and C403A clones. Mann–Whitney test; ***P < 0.001 and **P < 0.01. (E) Flow cytometry quantification of MDR and mass (MG) from untreated or CCCP-treated CTRL and C403A cells. The MDR/MG ratio was calculated (n = 5). Mann–Whitney test; **P < 0.01. (F) Flow cytometry evaluation using Annexin V and SYTOX Blue staining of staurosporine-induced CTRL and C403A cell death at 24 h. (G) Quantification of apoptosis by holotomographic microscopy of CTRL

with the apoptosis-inducing agent staurosporine and quantified by flow cytometry the fraction of apoptotic cells 24 h later. As shown in Fig 2F, C403A cells were more resistant to apoptosis than CTRL cells. This result was confirmed by live-imaging holotomographic microscopy recording over the first 12 h post-CCCP treatment (Fig 2G). Similar results on apoptosis induction were obtained upon exposure to bortezomib (Fig S2F), an inducer of ER stress and cell death. In contrast, the proportion of stress-induced cell necrosis was higher in C403A than in CTRL cells (Fig S2F and G). The disorganization in the crista structure is a consequence of OMA1 deficiency (Viana et al, 2021). To define qualitative changes in mitochondrial and crista organization, we performed a transmission electron microscopy (TEM) analysis on *in vitro*-grown, untreated, or CCCP-stressed cell lines. As shown in Fig 2H, CTRL cell lines illustrated the mitochondrial distribution, electron density, and crista ultrastructure observed under untreated conditions. The number of mitochondria-ER membrane contact sites (MCS) per field of view was quantified (Fig 2I). CTRL cells showed a high proportion of well-structured mitochondria and frequent MCS, up to 8 per field. Upon CCCP treatment, mitochondrial morphology was more heterogeneous and often displayed structural abnormalities in the matrix. In edited cell lines, we observed a 60% reduction in the proportion of MCS and addition of CCCP further exaggerated the accumulation of mitochondrial alterations. We then analyzed the organization of cristae as described in Lam et al (2021). Whereas CCCP treatment reduced the area of cristae in CTRL cells, that of CCCP-treated C403A cells remained significantly larger in agreement with the loss of OMA1-induced mitochondrial fission (Figs 2J and S2H).

Grafted C403A tumor cells show impaired growth in immunocompetent mice

Metabolic rewiring of mitochondrial activity may have a significant impact on tumor growth (Giessner et al, 2018; Miallot et al, 2021). Because tumor development is often associated with mitochondrial stress (O'Malley et al, 2020), we quantified the growth of CTRL versus C403A cells in nude mice to limit the contribution of adaptive immunity. Both CTRL and C403A grafted clones developed tumors. Although interclonal variability in their growth rate was apparent, it was unrelated to their genotype (Fig 3A). In conclusion, the C403A mutation had no significant impact on their intrinsic growth potential *in vivo*.

We then quantified OMA-1 expression and proteolytic activity on its targets in tumors grown in nude mice. We performed a Western blot analysis on protein extracts from enriched CD45-negative tumor cells to monitor the expression of OMA1, OPA1, and DELE1 isoforms involved in the handling of mitochondrial and ER stress, respectively (Fessler et al, 2020). As observed with cultured cells, S-OMA1 expression was preponderant in CTRL but almost

undetectable in C403A tumor cells (Fig 3B). Similarly, the 90-kD S-OPA1 isoform predominated over the 120-kD L-OPA1 isoform in CTRL but not C403A tumors (Fig 3B and C). The situation with DELE1 was more heterogeneous between tumors, but overall, the proportion of the S-DELE1 isoform was higher in CTRL versus C403A tumor cells (Fig S3A and B for quantification). To directly test whether C403A OMA1 could contribute to the proteolysis of the 65-kD L-DELE1 into the cytosolic 56-kD S-DELE1 isoform, we exposed cultured cells to oligomycin and monitored the appearance of the S-DELE1 isoform in total cell extracts. As shown in Fig S3C, the L- and S-DELE1 isoforms were detected even in the absence of oligomycin. In C403A cells, the S-DELE1 isoform was predominant in all conditions. This suggested that in mutant tumor cells, C403A OMA1 or other proteases might be able to cleave DELE1 under basal conditions. Altogether, these results demonstrate that the C403A mutation prevents stress-induced OMA1 activation and downstream cleavage of OPA1.

We then tested the growth of various clones grafted in immunocompetent mice. Interestingly, whereas CTRL cells grew exponentially, edited cells failed to expand (Fig 3D). To test the potential of C403A cells to grow in immunocompetent mice, we combined them with CTRL cells and followed the growth of chimeric tumors containing a mix of CTRL and C403A cells. In these experiments, 3×10^5 cells of each type were injected to enhance the detection of small or slowly growing tumors (Fig 3E). Interestingly, the addition of an equivalent number of C403A to CTRL cells slowed down the growth of the latter until day 18. To quantify the relative proportion of CTRL versus C403A cells, we designed a PCR assay able to discriminate their respective contribution to mixed cultures or chimeric tumors (Fig 3F and S3D). On day 12 post-grafting, both CTRL and C403A cells were detected although CTRL cells were more abundant. On day 21, C403A cells were barely detectable in most of the tumors. These results suggest that although C403A cells could grow in immunocompetent mice, their development was rapidly impaired and delayed the growth of CTRL cells, possibly through the release of immunogenic signals.

OMA1 C403A edition induces a mitochondrial stress associated with the development of anti-tumor immune responses

Immunogenic cues may derive from increased mitochondrial stress within the tumor. We scored mitochondrial polarization and mass, ROS, and mtDNA release in CD45⁺ cells extracted from CTRL and C403A tumor masses. CD45⁺ cells from C403A tumors showed significantly reduced mitochondrial polarization and mass (Fig 4A). Whereas total ROS levels were comparable in both types of tumors (Fig 4B), the abundance of cytosolic mtDNA was higher in C403A versus CTRL CD45⁺ cells (Fig 4C). Dendritic cells but not macrophages can sense tumor mtDNA, a process leading to enhanced

and C403 cells after 12-h staurosporine stimulation (n = 2). (H, I, J) EM analysis of CTRL and C403A MCA205 cells. Cells were treated for 1 h with CCCP and fixed for TEM acquisition. Scale bars: 200 nm (n = 2). Quantification was performed on 16 independent fields obtained from CTRL and C403A MCA205 cells. (I) We scored MCS (panel I) per field in untreated or CCCP-treated conditions. (J) Additional analyses were performed to evaluate crista area (panel J). Mann-Whitney test; ****P < 0.0001, ***P < 0.001, and **P < 0.01.

Source data are available for this figure.

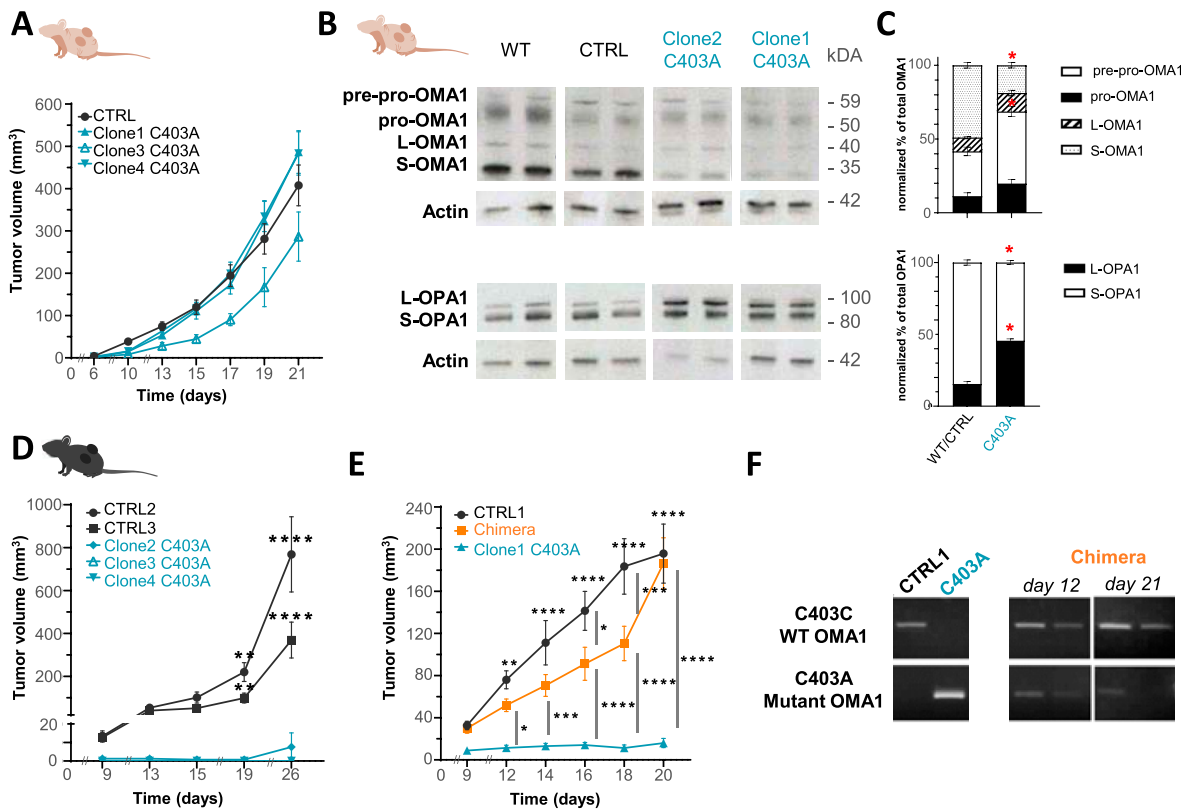


Figure 3. Growth potential of C403A and CTRL tumor cells in vivo.

(A) Tumor growth in nude mice. 10^5 WT and C403A MCA205 cells were subcutaneously grafted in the two flanks of mice, and tumor volume was quantified ($n = 10$). (B) Western blot analysis of total protein extracts from CD45-negative cells isolated from WT or C403A tumors at day 21 post-cell engraftment. (C) OMA1 and OPA1 expressions were evaluated and quantified in panel (C), as in Fig 2 ($n = 4$). (D, E) Tumor growth in C57BL/6 mice. 3×10^5 CTRL, 3×10^5 C403A, or a mix of 3×10^5 CTRL and 3×10^5 C403A MCA205 cells were grafted in the two flanks of mice, and tumor volume was quantified ($n = 10$). Two-way ANOVA with Šidák's multiple comparisons test; **** $P < 0.0001$, *** $P < 0.001$, ** $P < 0.01$, and * $P < 0.05$. (F) PCR screening to evaluate the proportion of the C403A MCA205 cell in chimera tumors at day 12 and 21 post-cell engraftment ($n = 2$). Source data are available for this figure.

cross-presentation of tumor antigen (Xu et al, 2017). Furthermore, the XCR1⁺ cDC1 cell subset cross-presents antigen and primes anti-tumor CD8⁺ cytotoxic lymphocytes (Ferris et al, 2020). To test the contribution of these processes to the control of tumor growth in immunocompetent mice, we grafted CTRL and C403A tumor cells in *Xcr1*^{DTA} mice that lack cDC1 cells (Wohn et al, 2020). As shown in Fig 4D, CTRL and C403A cells developed tumors at the same rate in these mice; furthermore, the difference in C403A tumor growth between immunocompetent (Fig 3D) and *Xcr1*^{DTA} mice (Fig 4D) confirmed the major role of DC in sensing tumor-derived stress for the initiation of immune responses.

We then characterized by flow cytometry the immune infiltrate at days 12 (Fig S3E) and 21 (Fig 4E) after grafting. The proportion of CD45⁺ cells represented around 40–60% of the tumor mass, but this proportion increased significantly in C403A compared with CTRL tumors. Among CD45⁺ cells in non-edited tumors, CD11b⁺ myeloid cells represented 40% on day 12 and up to 60% of infiltrating cells on day 21. In C403A tumors, CD11b⁻ cells were preponderant and reached 60% of the immune infiltrate. More specifically, CD8⁺, CD4⁺, and NK1.1⁺ cells predominated and were twice more abundant in edited tumors on day 21, whereas the proportion of tumor-associated macrophages was significantly reduced (Fig 4F). We

then tested whether the treatment from days 13 to 20 with an anti-CD8 mAb would rescue the growth of edited tumors. As shown in Fig 4G, the enhancing effect was only transient and most of the edited clones disappeared. This suggested that in addition to intrinsic C403A cell death, CD8⁺ T cells and probably other cytotoxic cells contributed to the control of tumor growth.

High OPA1 expression correlates with poor prognosis in sarcoma subtypes

Results obtained in the mouse model suggest that the loss of mitochondrial adaptation to stress may generate immunogenic signals that enhance anti-tumor immunity. We searched for correlations between OMA1 and OPA1 mRNA expressions and clinicopathological and immune variables in our merged cohort of complex genomic STS. It included 921 clinical samples from non-metastatic and operated primary tumors, comprising 726 samples informative for OMA1 expression and 845 for OPA1. Their characteristics are summarized in Table S1. OMA1 and OPA1 mRNA expressions were heterogeneous across the whole cohort with a range of intensities over 5 and 4 units in the log₂ scale, respectively (Fig 5A), allowing the search for correlations with other variables. No

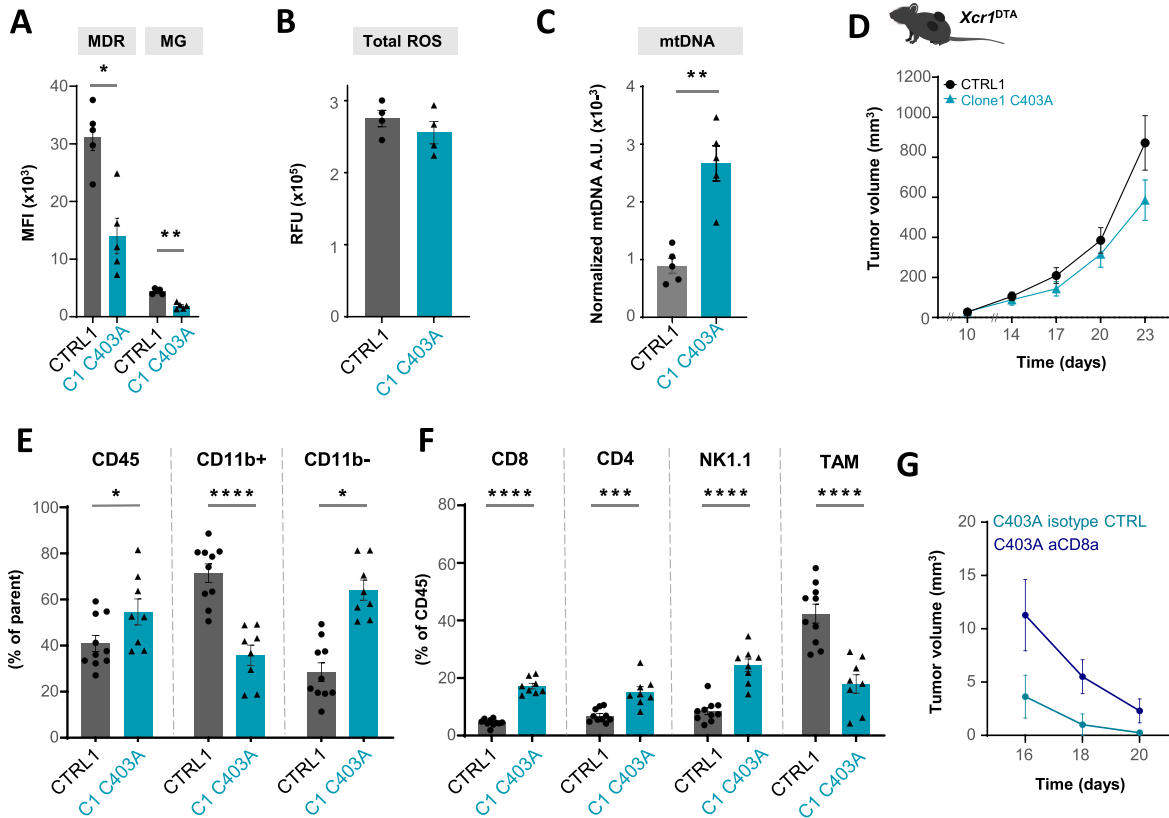


Figure 4. Evaluation of mitochondrial alterations and immune infiltrate in C403A tumors.

(A) Quantification of mitochondrial depolarization and mass by flow cytometry in CD45-negative cells from WT and C403A MCA205 tumors at day 12. Mann–Whitney test; * $P < 0.05$ and ** $P < 0.01$ ($n = 4–5$). (B, C) Relative proportion of total ROS production in CTRL and C403A tumors ($n = 4$). (C). Relative proportion of cytosolic mtDNA (Nd1) by PCR in CD45-negative cells isolated from CTRL and C403A tumors. Mann–Whitney test; ** $P < 0.01$ ($n = 5–6$). (D) Tumor growth in *Xcr1*^{DTA} mice. 3×10^5 CTRL or C403A MCA205 cells were subcutaneously grafted in the two flanks of mice, and tumor volume was quantified ($n = 8$). (E, F) Analysis of the immune infiltrate of CTRL or C403A tumors in WT mice at day 21 post-cell engraftment. Mann–Whitney test; ** $P < 0.01$ and * $P < 0.05$ ($n = 8–10$). (G) Tumor growth of C403A tumors in CD8 T cell-depleted mice after day 13 ($n = 6$). Two-way ANOVA with Sidák’s multiple comparisons test; * $P < 0.05$. Source data are available for this figure.

significant correlation existed with patients’ age and gender, and pathological grade (Table S1). Correlations were found with the pathological subtype and the tumor site, with more leiomyosarcomas (LMS) and less undifferentiated pleomorphic sarcomas (UPS) among “OMA1-high” tumors than among “OMA1-low” tumors ($P = 6.87 \times 10^{-6}$) and more LMS and less liposarcomas and myxofibrosarcomas among “OMA1-high” tumors than among “OMA1-low” tumors ($P = 9.25 \times 10^{-8}$). OPA1 expression was also associated with the Complexity INdex in SARcoma (CINSARC) risk with more “high risk” among “OMA1-high” tumors ($P = 3.53 \times 10^{-3}$). Because OMA1 regulation of activity depends on post-translational modifications, variations in OMA1 transcripts might have a modest impact on prognosis as confirmed by the analysis of metastasis-free survival (MFS) in OMA1-high or OMA1-low patients (Fig 5B). The 5-yr MFS was 48% (95% CI 40–57) in the “OMA1-high” class versus 59% (95% CI 53–67) in the “OMA1-low” class ($P = 0.062$, log-rank test; Fig 5B). In contrast, variations in OPA1 levels might ultimately tune mitochondrial fusion potential. Accordingly, the prognostic analyses (Fig 5C) showed that an “OPA1-high” status was associated with reduced MFS in univariate ($P = 1.11 \times 10^{-2}$, Wald’s test) and multivariate (hazard ratio (HR) = 1.35, 95% CI 0.96–1.91, $P = 0.089$)

analyses (Table S2), and 5-yr MFS was 48% (95% CI 40–57) in the “OPA1-high” class versus 60% (95% CI 52–69) in the “OPA1-low” class ($P = 5.48 \times 10^{-3}$, log-rank test; Fig 5C).

Then, we investigated whether OPA1 expression was associated with immune variables in our clinical samples (Fig 5D). First, we compared the composition and functional orientation of tumor-infiltrated immune cells using the 24 immune cell types defined as the immunome. Significant differences existed between “OPA1-high” and “OPA1-low” classes; “OPA1-low” tumors displayed a higher infiltrate than “OPA1-high” tumors in 12 immune cell types ($P < 0.05$) including T cells, Tem cells, Th1 cells, Th17 cells, cytotoxic cells, CD56dim NK cells, dendritic cells (DC, iDC, aDC, and pDC), macrophages, and neutrophils. Second, “OPA1-low” tumors displayed higher expression of many signatures related to antigen presentation (Table S3). Finally, “OPA1-low” samples displayed a higher immune cytolytic activity score ($P = 4.39 \times 10^{-6}$) and ICR score ($P = 1.60 \times 10^{-5}$), which reflect an anti-tumor cytotoxic immune response, than “OPA1-high” samples, and higher scores for signatures associated with response to immune checkpoint inhibitors (ICI): T cell-inflamed signature (TIS) ($P = 2.86 \times 10^{-6}$) and tertiary lymphoid structure score ($P = 5.66 \times 10^{-7}$). Altogether, these results

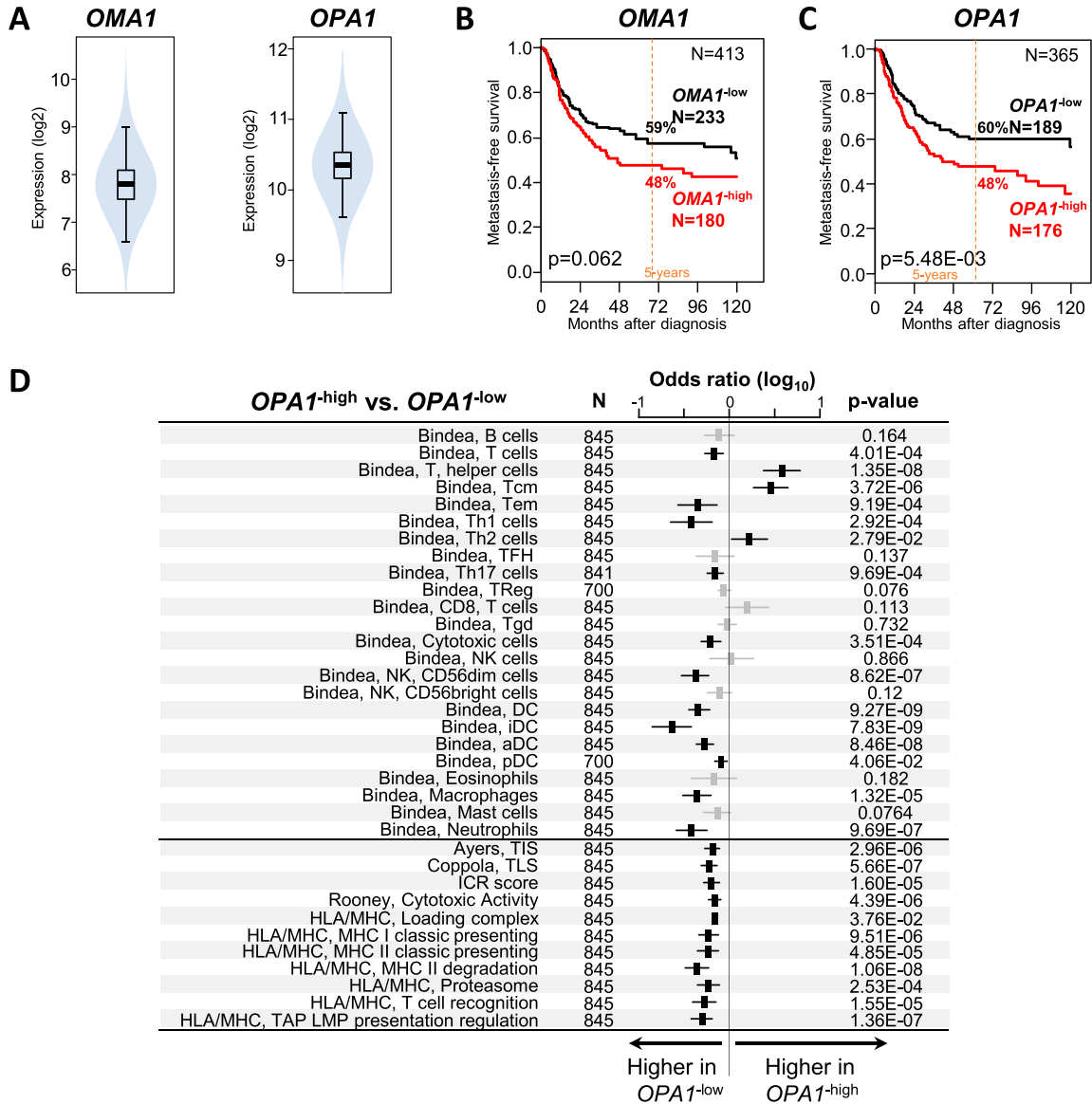


Figure 5. OMA1 and OPA1 expressions in clinical samples of STS with complex genomics.

(A) Violin plots showing the distribution of mRNA expression levels of OMA1 and OPA1 in 921 tumor samples. (B, C) Kaplan–Meier MFS curves according to OMA1 and OPA1 expressions. The P-values are for the log-rank test. (D) Correlations between OPA1 expression-based classification and immune variables. Forest plots of correlations between OPA1-high and OPA1-low expressions and immune features including the 24 Bindea’s innate and adaptive immune cell subpopulations, the TIS signature and the TLS signature associated with response to immune checkpoint inhibitors, the ICR score and the cytolytic activity score associated with anti-tumor cytotoxic immune response, and several antigen-processing signatures. The P-values are for the logit link test.

obtained in complex genomic STS reinforce the notion that variations in OMA1/OPA1 expression might condition the development of immune responses.

Discussion

Tumor development is progressively associated with mitochondrial stress that triggers several compensatory mechanisms (O’Malley et al, 2020). Preservation of mitochondrial fitness depends on the induction of cytoprotective mitochondrial proteins via the retrograde

mitochondria–nuclear signaling and on the tight balance between fusion and fission (da Cunha et al, 2015). Ultimately, damaged mitochondria are scavenged by mitophagy. Through the regulation of its proteolytic activity, the OMA1 metalloprotease is a major sensor of mitochondrial stress (Ehse et al, 2009; Baker et al, 2014). A redox molecular switch involving a disulfide bridge between two cysteines has been identified in yeast OMA1 (Bohovych et al, 2019). We confirmed in murine sarcoma cells that the mutation of cysteine 403 abrogated OMA1 proteolytic activity toward the OPA1 protein and also possibly its autocatalytic activity. Indeed, the production of the long and short OMA1 isoforms is the result of a complex interplay between

the YMEL1 and OMA proteases (Wang, MCB 21). In contrast, we could not obtain conclusive results concerning DELE1 processing by C403A OMA1. Although the role of this disulfide bridge is not fully understood, results in yeast suggest that it may participate in OMA1 stability and/or interaction with other proteins (Bohovych et al, 2019). Indeed, OMA1 participates in the stability (Viana et al, 2021) and function of the MICOS complex in the control of cell bioenergetics and intermembrane contacts (Bohovych et al, 2015; Sakowska et al, 2015; Burke, 2017; Wollweber et al, 2017; Viana et al, 2021). Furthermore, the MICOS complex is sensitive to variations in the oxidation status of several proteins including OMA1 (Bohovych et al, 2019) and MIC19 (Sakowska et al, 2015). Although we could not detect the presence of OMA1 in the complexes because of the lack of appropriate antibodies, the absence of cysteine 403 did not impair complex formation but prevented the proteolysis of OPA1 within the MICOS complex. OPA1 is positioned upstream of MICOS and regulates crista junction width (Glytsou et al, 2016) and cell death (Burke, 2017). Interestingly, the C403A mutation had a functional impact on mitochondrial organization, leading to the accumulation of abnormal cristae, depolarized mitochondria, reduced MCS, and mitochondrial ATP production.

Our results show that the C403A mutation does not impair tumor cell growth in immunodeficient mice. Growth depends on the metabolic rewiring occurring in the competitive tumor environment. C403A cells showed a preferential use of glycolysis over respiration for ATP production. In vivo, this phenotypic bias should favor the development of a Warburg phenotype that enhances tumor aggressiveness, particularly in the absence of a potent anti-tumor immunity (Giessner et al, 2018). The modalities of cell death are known to influence tumor immunogenicity (Kroemer et al, 2013). Interestingly, C403A cells, while more resistant to apoptosis induction, showed increased stress-induced cell death in vitro associated with mtDNA release in the cytosol. Because S-OPA1 contributes to the maintenance of mtDNA and cristae (Del Dotto et al, 2017), the inability to maintain a correct proportion between the L-OPA1 and S-OPA1 isoforms in C403A cells may explain this result. mtDNA is a major immunostimulating danger-associated molecular pattern, which participates in endocellular inflammasome-mediated (Nakahira et al, 2011; Tschopp, 2011; Galluzzi et al, 2012; Zhong et al, 2018) or extracellular neutrophil-mediated (Zhang et al, 2010; Oka et al, 2012) triggering of inflammation. The consequences of mtDNA release in tumor microenvironment vary depending on the nature of infiltrating immunocytes, associated with the neutrophil-mediated worsening of tumor progression (Singel et al, 2019) or, reciprocally, with the stimulation of the cross-priming potential of cDC1 cells for the development of anti-tumor cytotoxic CD8 cells (Xu et al, 2017). Our results support this latter hypothesis because over time, edited tumors were enriched in NK1.1⁺ and CD8⁺ lymphocytes, and furthermore, in the absence of cDC1 cells, C403A clones grew in immunocompetent mice. In addition, the presence of mutant tumor cells in a chimeric tumor slowed down the growth of the non-edited clones and was associated with the accumulation of an immune infiltrate.

The relevance of our findings in a mouse sarcoma model was questioned by exploring the levels of expression of the transcripts coding for OMA1 and OPA1 in a large series of STS with complex genomics, documented in various databases. Whereas the level of expression of these proteins is relatively independent from their activation status, few contradictory studies reported an association

of OMA1 levels with susceptibility to cancer (Alavi, 2019). The OPA1 protein regulates tumor growth through the modulation of angiogenesis and apoptosis, but its contribution to tumor cells themselves has not been documented (Herkenne & Scorrano, 2020). Our results in sarcoma suggest that the expression level of OMA1 and OPA1 varies significantly among sarcoma subtypes with complex genomics. This may reflect an adaptation to mitochondrial stress in tumor clones allowing the selection of the fittest variants. Furthermore, the complex functions of various OPA1 isoforms on the control of crista structure and fission would justify to complete our study with a biochemical analysis of OPA1 protein on tumor samples. The most significant observation was to show the good prognosis value of low OPA1 expression for MFS in STS and the associated presence of immune signatures linked to IFN- γ signaling, MHC expression, and infiltration by immune cells with potential anti-tumor functions. This type of signature evokes that found in the OMA1 mutant model that was developed in which stress-induced OPA1 cleavage is prevented, limiting adaptation to mitochondrial stress of tumor cells and exposing to increased immunogenic cell death. One might hypothesize that a reduced level of OPA1 could lead to a similar result under stress conditions. One report showed that the use of an OPA1 inhibitor (MYLS22) could limit tumor growth (Herkenne et al, 2020). However, in this report, the authors concluded in favor of angiogenic alterations. Because the effect of this inhibitor in vivo is not clarified, the interpretation of these results must be cautious. Based on our results, one could propose to design modulators of OMA1 or OPA1 activation targeting the redox switch or the fusiogenic function of OPA1 to enhance tumor cell fragility and immunostimulation.

Materials and Methods

Animals

8–10-wk-old female C57BL/6 and NMRI-nu mice were purchased from Janvier Laboratories. Few experiments were performed on male mice. *Xcr1*^{Cre-mTFFP1} and *Rosa*^{26LSL-DTA} (B6.129P2-Gt(ROSA)26Sor^{tm1(DTA)Lky/l}) were previously described (Voehringer et al, 2008; Wohn et al, 2020). *Xcr1*^{Cre-mTFFP1} mice were crossed to *Rosa*^{26Isl-DTA} mice in which Cre-mediated excision of a loxP-flanked transcriptional STOP element triggers the expression of diphtheria toxin fragment A (DTA), and results in the constitutive ablation of cDC1 in *Xcr1*^{DTA}. Mice were housed under a standard 12-h: 12-h light–dark cycle with ad libitum access to food and non-acid water, 22°C \pm 1°C, and 45–60% humidity, and were maintained under specific pathogen-free conditions at the animal facility of the Centre d'Immunologie de Marseille-Luminy (F1305510). Experimentations were authorized by the Ethical Committee for Animal Experimentation (#30566–2021032215496999 v2; APAFIS). Collaborative experiments using *Xcr1*^{DTA} mice (Wohn et al, 2020) were performed in B. Malissen's laboratory (#26488–2020070612584424 v2; APAFIS).

Cell lines

The MCA205 cell line was kindly provided by E Vivier at Centre d'Immunologie de Marseille-Luminy and cultured in DMEM/F-12

(Gibco) supplemented with 10% FBS (Gibco), 100 $\mu\text{g}/\text{ml}$ penicillin-streptomycin (Gibco), 2 mM of L-glutamine, and 1 mM of sodium pyruvate at 37°C with 10% CO₂. Mitochondrial stress was triggered by incubating cells in 20 μM CCCP for 1 h at 37°C. Mycoplasma status was checked using MycoAlert Lonza Detection Kit, and cells were used at low passage. For cell number quantification, 10⁵ cells were seeded at low density in a 12-well plate, and cells were harvested every 2 d with trypsin and counted with a cell counter (CASYton).

Edition of the *Oma1* gene

Mutated C403A clones were obtained using the prime editing (PE) technique as described (Anzalone et al, 2019). CTRL OMA-1 corresponds to cells that were subjected to the editing process but did not internalize the mutation. PE (#132775; Addgene) produces template-directed local sequence changes in the genome without the requirement for DSBs or exogenous donor DNA templates. We designed the pegRNA sequences using the pegFinder online tool (Chow et al, 2021) to target the desired genomic sequence. Cells were first edited using the PE2 system that edits only one DNA strand and is expected to have a maximum editing efficiency of 50%. To obtain homozygous mutants, heterozygote clones were submitted to the PE3 editing system that uses an additional sgRNA to direct SpCas9H840A to nick the non-edited DNA strand and encourages the edited strand to be used as a repair template by DNA repair factors, leading to a further increase in editing efficiency.

Plasmids expressing pegRNA were constructed by Golden Gate assembly. Sequences of sgRNA and pegRNA are listed in the Supplemental Data 1. The oligonucleotides corresponding to the pegRNA spacer, pegRNA 3' extension, and pegRNA scaffold were annealed and assembled into the Bsal-digested pU6-pegRNA-GG acceptor vector (#132777; Addgene). For the PE3 editing system, the sgRNA was cloned in the pLKO.1-puro-GFP vector (Phelan et al, 2018). All vectors for mammalian cell experiments were purified using EndoFree Plasmid Maxi Kit (QIAGEN). The pCMV-PE2 and the pU6-pegRNA-GG-acceptor were a gift from David Liu (Addgene plasmid #132775; <http://n2t.net/addgene:132775>; RRID:Addgene_132775; Addgene plasmid #132777; <http://n2t.net/addgene:132777>; RRID:Addgene_132777).

8 × 10⁵ MCA205 cells were seeded in six-well plates, and transfections were conducted when cells reached ~70% confluency after 16–20 h. Cells were transfected with jetOPTIMUS reagent (Polyplus) following the manufacturer's instructions. For PE2 experiments, cells were transfected with 2 μl of jetOPTIMUS, 1.5 μg of PE2 plasmid (#132775; Addgene), 500 ng of pegRNA plasmid (#132777; Addgene), and 200 ng of pGFP-C1 vector plasmid (Clontech). The transfected cells were collected after 72 h of culture and GFP-positive cells sorted in single clones in 96-well plates. After genomic DNA extraction (QIAGEN), clones were screened by PCR (Supplemental Data 2) for the presence of mutation. 12% of the clones were positive for the mono-allelic mutation and confirmed by sequencing (Fig S1E). For PE3, cells were transfected with 2 μl of jetOPTIMUS, 1.5 μg of PE2 plasmid, 500 ng of pegRNA plasmid, and 200 ng of pLKO-GFP-sgRNA plasmid. The transfected cells were collected after 72 h of culture and GFP-positive cells sorted in single

clones in 96-well plates. Clones were screened by PCR for the presence of mutation and the absence of WT sequence. Four of 40 clones presented the bi-allelic mutation, confirmed by sequencing.

Tumor experiments

MCA205 cells (10⁵ or 3 × 10⁵ depending on experiments) were subcutaneously grafted in the flanks of C57BL/6, *Xcr1*^{DTA}, or nude mice. For tumor growth monitoring, mice were anesthetized with 2.5% isoflurane every 2 d. Tumor size was assessed with a caliper by measuring the length (L) and width (W) of the tumor. Tumor volumes were calculated using the following formula: $(L \times W)^2/2$. A limit point was settled when tumor volume was above 1,000 mm³. Tumors were harvested between D10 and D26 post-implantation, each tumor being considered as an experimental unit referred to as n. Animals were euthanized when severe bleeding or scars were detected on the tumor implantation site or when they presented symptoms of poor health (weight loss, prostration). In vivo CD8⁺ cell depletion was achieved by injecting the purified anti-CD8 mAb (clone 53–5.8) intraperitoneally from day 13 and every 3 d at 200 μg per mouse, respectively. Rat-IgG1 anti-horseradish peroxidase (clone HRPN) was used as an isotype CTRL after the same dosage.

Tumors were mechanically and enzymatically digested using the Miltenyi Biotec gentleMACS Octo Dissociator technology. Samples were filtered through a 70- μm Cell Strainer (Becton Dickinson) to remove cell clumps and submitted to red blood cell lysis (eBioscience buffer). Cell suspensions were analyzed by flow cytometry. Alternatively, CD45-negative cells were isolated using CD45 microbeads from Miltenyi Biotec and the MultiMACS Cell24 separation on LS columns according to the manufacturer's protocols.

Analysis of OMA1 and OPA1 expressions in soft tissue sarcoma clinical samples

We analyzed our database (Bertucci et al, 2022) including clinico-pathological and normalized gene expression data of clinical STS samples gathered from 16 public data sets (Table S4). All samples were from an operative specimen of previously untreated primary tumors. The gene expression profiles had been generated using DNA microarrays or RNA sequencing. Because our mouse model represented a sarcoma with complex genomics, our analysis was limited to the 921 cases of STS with complex genomics. The most frequent pathological types were LMS and UPS, and 56% of cases were high-risk CINSARC. *OMA1* and *OPA1* mRNA expressions were analyzed as discrete variables (high versus. low) using their mean expression level of the whole series as cutoff. Based on the link we observed in our mouse model between *OMA1/OPA1* and immunity, we searched for correlations between *OPA1* tumor expression and immunity-related variables. These latter were represented by the following multigene classifiers/scores: the 24 Bindea's innate and adaptive immune cell subpopulations (Bindea et al, 2013), several antigen-processing machinery signatures (Tables S1, S2, and S4), two signatures associated with anti-tumor cytotoxic immune response (the Immunologic Constant of Rejection classifier (Bertucci et al, 2018) and the cytolytic activity score (Rooney et al, 2015)), and two metagenes associated with response to immune checkpoint inhibitors (the T cell-inflamed signature (Ayers et al, 2017) and the

tertiary lymphoid structure signature (Coppola et al, 2011)). We also applied the CINSARC signature, now recognized as the most relevant prognostic signature in STS (Chibon et al, 2010) that identifies patients as either high risk or low risk of relapse. The correlations between OMA1 or OPA1 expression-based classes and clinicopathological variables and molecular signatures were measured using Fisher's exact test or a *t* test when appropriate. The endpoint of prognostic analysis was the MFS, calculated from the date of diagnosis until the date of metastatic relapse or death from any cause, whichever occurred first. The follow-up was measured from the date of diagnosis to the date of last news for event-free patients. Survival rates were estimated using the Kaplan–Meier method and curves compared with the log-rank test. Uni- and multivariate prognostic analyses were done using the Cox regression analysis (Wald's test). The variables tested in univariate analysis were the patients' age and gender, pathological tumor type (UPS, LMS, pleomorphic liposarcomas, myxofibrosarcomas, others), pathological grade (2–3, 1), tumor site (extremities, head and neck, internal trunk, superficial trunk), CINSARC-based risk (high, low), and the OMA1- or OPA1-based classification (high, low). Multivariate analysis incorporated all variables with a *P*-value inferior to 5% in univariate analysis. The correlations between molecular immune variables and OPA1-based classification were assessed by logistic regression analysis with the *glm* function (R Statistical Package; significance estimated by specifying a binomial family for models with a logit link). All statistical tests were two-sided, and the significance threshold was 5%. Analyses were done with the survival package (version 2.43) from R software (version 3.5.2).

Flow cytometry

Cell death was evaluated using the LIVE/DEAD Fixable Blue flow cytometry, and unspecific labeling was prevented by incubation with anti-CD16/CD32 mAb in PBS/2 mM EDTA for 30 min. Cell surface antibody labeling was performed in FACS buffer for 1 h at 4°C. For intracellular staining, the Foxp3/Transcription Factor Staining Buffer Set (eBioscience) was used. Cells were analyzed on BD LSR Symphony or Fortessa (Becton Dickinson). Data analysis was done using FlowJo 10.8 software. To evaluate mitochondrial depolarization and mitochondrial mass, cells were stained with MDR (10 nM) and MitoTracker Green (100 nM) for 20 min at 37°C (Thermo Fisher Scientific) in serum-free RPMI. For staining of cultured cells, we used 100 nM MDR. CD8 and CD4 T cells were quantified within CD45⁺ CD11b⁻ NK1.1⁻ cells, and tumor-associated macrophages, within CD11b⁺ Ly6G⁻ NK1.1⁻ Ly6C^{low} MHCII⁺ CD64⁺ F4/80⁺ cells.

Annexin V/SYTOX Blue assay

3 × 10⁵ CTRL and C403A cells were seeded in a six-well plate. After 24 h of 1 μM staurosporine (used as a positive control) or 1 μM bortezomib stimulation, cells were harvested and stained for 20 min with 1 μM SYTOX Blue in PBS. Apoptotic cells were stained with Annexin PE for 20 min and immediately analyzed on FACSCalibur/Canto II. Data analysis was done using FlowJo 10.8 software.

Recombinant protein production

We produced a truncated version of OMA1 protein starting on amino acid 213 (SPVTGR ...) corresponding to the beginning of the outer membrane region. The corresponding sequence carrying or not the C403A mutation in a synthetic gene (codon optimized for *E. coli* expression) was cloned into a prokaryotic expression vector. The OMA1 fusion proteins produced in *E. coli* contain a signal sequence to export the protein to the *E. coli* periplasmic space, followed by a hexahistidine tag for purification, a protein disulfide-isomerase (DsbC) fusion to help disulfide bridge formation, and a TEV recognition sequence to allow cleavage and isolation of the OMA1 alone if necessary. The gene synthesis and cloning were outsourced (Twist Bioscience). For the production phase, the proteins were transformed in T7 express strains (NEB) and grown in 400 ml TB media for 24 h at 25°C (induction with 1 mM when O.D was at 0.8). Cells were centrifuged and frozen in purification buffer A (Tris 50 mM, NaCl 300 mM, and imidazole 10 mM, pH 8) with the addition of 0.5 mg/ml of lysozyme. After thawing, the lysed bacterial pellets were treated with DNase, sonicated (6*30 s), and centrifuged for 40 min at 20,000g. Supernatants were run on AKTA xPress on a 5-ml Nickel HisTrap FF crude column (Cytiva), washed in buffer A with 50 mM imidazole, and eluted in a buffer containing 250 mM imidazole. The eluted material was dialyzed in PBS overnight and purity-confirmed by SDS–PAGE analysis. A protein with the expected molecular weight was obtained only for the WT sequence and not the mutated version that could not be purified. The purified OMA1 protein (His–DsbC) was used for enzymatic characterization.

Structure prediction

The mouse OMA-1 amino acid sequences were obtained from ENSEMBL (ENSMUSG00000035069). With the advent of powerful AI implementations, the AlphaFold Protein Structure Database (<https://alphafold.ebi.ac.uk/>) and DeepMind's Colab notebook (Jumper et al, 2021) have been used for structure prediction. Figures representing structural renderings were generated with the PyMOL Molecular Graphics System (version 2; Schrödinger, LLC).

Electron microscopy

The cells were fixed with 2.5% glutaraldehyde in 0.1 M cacodylate buffer for 30 min. After three washes over 15 min in the same buffer, the cells were post-fixed with 1% OsO₄ in the same buffer. After three washes over 15 min in water, the cells were dehydrated in 50% ethanol for 10 min and 70% ethanol for 10 min and incubated in uranyl acetate 2% in 70% ethanol for 30 min. Dehydration was then pursued with a single bath of 95% ethanol, three baths of pure ethanol, and three baths of acetone (10 min each). The cells were then infiltrated with Epon resin in acetone (1:2, 2:2, 2:1, and pure resin, 1 h each) and pure resin overnight. The next day, the pellets were embedded in fresh pure Epon resin and cured for 48 h at 60°C. 70-nm ultrathin sections were performed on a Leica UCT Ultramicrotome (Leica) and deposited on formvar-coated slot grids. The grids were contrasted using lead citrate and observed in a FEI Tecnai G2 at 200 KeV. Acquisition was performed on a Veleta camera (Olympus).

BN-PAGE

CTRL and C403A OMA1 mutant cells were stimulated with 20 μM CCCP or DMSO control for 1 h. Mitochondria were purified using the mitochondrial isolation kit for cultured cells (89874; Thermo Fisher Scientific) according to the manufacturer's instructions. Samples were lysed in NativePAGE sample buffer with 2% digitonin. 75 μg or 20 μg of non-denatured mitochondrial proteins was prepared with NativePAGE 5% G-250 Sample Additive, separated on precast NuPAGE 3–12% Bis-Tris Mini Protein Gel, and transferred to PVDF membrane. Protein ladder was revealed with Imperial Blue staining, and membranes were immunoblotted with the indicated antibodies.

Immunoblotting

Cell lysates were prepared in ice-cold RIPA buffer, supplemented with a protease inhibitor cocktail. Samples were centrifuged at 10,000g for 5 min at 4°C and supernatants collected. Protein concentrations were determined using the Pierce BCA assay. Laemmli buffer was supplemented with β -mercaptoethanol and incubated for 5 min at 95°C. 5 μg of total proteins was loaded on a 4–12% SDS-PAGE run at 150 V and then transferred to PVDF membranes during 1 h at 100 V. Membranes were saturated in PBS/Tween/5% BSA overnight at 4°C, followed by incubation with either mouse anti-OMA-1, anti-OPA1, anti-DELE1, anti-TOM20, and anti-actin antibodies at 4°C (see Supplemental Data 1). Membranes were washed and incubated with HRP-linked goat anti-rabbit IgG or HRP-linked goat anti-mouse IgG for 1 h at RT. The antigen-antibody complex was detected using ECL, according to the manufacturer's instructions. Images were captured on autoradiography films and scanned using Samsung Digital Presenter with a 720P HD document camera with a 14 \times optical zoom and 3 \times digital zoom. Signals were quantified with ImageJ software and normalized using actin signal intensity as a reference.

Enzymatic activity

The OMA1 activity assay relies on a fluorogenic 8-mer peptide derived from the OPA1 sequence containing the OMA1 cleavage site (Ishihara et al, 2006). Using a final 200 μl reaction volume, the reagents were quickly added in the following order in a black 96-well plate: (1) OMA1 activity assay buffer (50 nM of Tris-HCl, pH 7.5, and 40 mM of KCl); (2) 5 μg of protein sample with or without 200 μM zinc chelator N,N,N',N'-tetrakis(2-pyridylmethyl)ethylenediamine (TPEN); and (3) the OPA1 fluorogenic reporter substrate (5 μM). Relative fluorescence was recorded (excitation and emission, respectively, at 320 and 405 nm) every 5 min for 30 min at 37°C using a fluorescent plate reader (TECAN). For statistical analysis, the average fluorescence of the OPA1 fluorogenic reporter substrate alone was measured (<200 relative fluorescence units).

Immunofluorescence analysis

C403A and CTRL MCA205 cells were seeded in eight-well Nunc Lab-Tek plates (Thermo Fisher Scientific) and labeled with MDR at 100 nM at 37°C in prewarmed DMEM/F-12 without phenol red for 30 min.

Airyscan imaging was performed using a commercial Zeiss confocal microscope LSM 880 equipped with an Airyscan module (Carl Zeiss AG), and images were taken with a 63 \times /1.40 NA M27 Plan-Apochromat oil objective. In this mode, the emitted light was projected onto an array of 32 sensitive GaAsP detectors, arranged in a compound eye fashion. MDR-labeled samples were excited with a 633-nm beam, and emission was recorded using BP 570–620 + LP 645 filters. Images were processed using Zen Black 2.3 software. For TOMM20 staining, cells were seeded on glass coverslips, treated with 20 μM CCCP for 45 min, then fixed in PFA 4% for 10 min, and permeabilized in PBS/3% Triton/10% DKS (donkey serum) for 30 min. Mitochondria were stained overnight using a rabbit anti-TOMM20 antibody (186734-1/500; Abcam) and revealed with Alexa Fluor 594-AffiniPure Donkey Anti-Rabbit IgG. Coverslips were prepared using DAPI-containing Fluoromount. The Airyscan processing performs filtering, deconvolution, and pixel reassignment to improve SNR. The filtering (the Wiener filter associated with deconvolution) was set to the default filter setting of 6.1 in 2D. Microscopy images were analyzed using Imaris 5.104 software. To model MDR-labeled mitochondria in 3D, we used the plugin “structure.” The threshold was positioned at the curve inflexion point. The mitochondrial volume of fragmented mitochondria varies between 0.08 and 0.53 μm^3 , and that of fused mitochondria is set over 0.53 μm^3 . To quantify fission potential, we calculated the mitochondrial fission index as $\log_{10}(\sum 0.08 \mu\text{m}^3 < V_{mit} < 0.53 \mu\text{m}^3 / \sum V_{mit} > 0.08 \mu\text{m}^3)$.

Holotomographic microscopy

The holotomographic microscopy—Nanolive CXA—allows to capture the real, kinetic response of cells without imaging-induced artifacts. CTRL and C403A cells were recorded during 16 h with an interval of 25 min in the presence or in the absence of staurosporine 1 μM diluted in DMSO (final concentration 0.1% DMSO in regular medium condition). The control condition was performed in the presence of DMSO 0.1% diluted in regular medium condition. All the captures were analyzed with the LIVE Cell Death Assay module. The results are expressed by the percentage of apoptosis over time. Experiments were performed in duplicate.

Seahorse

Agilent Seahorse XFp Real-Time ATP Rate Assay Kit was used to measure OCR and ECAR using a Seahorse XFp Extracellular Flux Analyzer. Cells were seeded at 5×10^4 cells/well for 16 h at 37°C in 10% CO₂. One hour before measurement, the cell culture medium was replaced with Seahorse DMEM, pH 7.4, supplemented with 10 mM of glucose, 1 mM of pyruvate, and 2 mM of glutamine, and the miniplate was incubated for 1 h at 37°C in a non-CO₂ incubator. Cells were stimulated with 1.5 μM of oligomycin and 0.5 μM of rotenone/antimycin A. The ATP rate index corresponds to the mitoATP production rate divided by glycoATP production rate at a given time point.

qRT-PCR analysis

Total mRNA from cells was purified using RNeasy Mini Kit (QIAGEN). For qRT-PCR analysis, 0.5 μg RNA was reverse-transcribed with the

SuperScript II RT kit (Life Technologies). Amplification was performed on a 7,500 Fast Real-Time PCR system (Applied Biosystems) using SYBR Green Master Mix (Takara) and specific primer pairs. Expression levels were normalized to the control gene actin.

Quantification of cytosolic mitochondrial DNA

To evaluate the content of cytosolic mitochondrial DNA, WT or C403A OMA1 tumors were harvested at day 12 post-cell engraftment and processed as described. Two tumors from the same mice were pooled, and CD45-negative fractions were split into two equivalent fractions and processed for total or cytosolic DNA extraction. For total DNA extraction, 50 mM NaOH was added and cells were incubated at 95°C for 15 min. The reaction was stopped by adding 1 M of Tris-HCl, pH 8. For cytosolic DNA extraction, cells were incubated with cytosolic extract buffer (150 mM NaCl, 50 mM Hepes, and 25 mg/ml digitonin) for 10 min on ice. Cells were centrifuged at 410g for 5 min. The supernatant was centrifuged at 16,000g for 10 min. The total and cytosolic extracts were then used for DNA extraction using DNA Blood & Tissue Kit. Total DNA abundance was evaluated using the Qubit assay. Nd1 (mitochondrial DNA) and POLG1 (nuclear DNA) expression was quantified using ONEGreen Fast qPCR Premix on a 7,500 Fast Real-Time PCR system (Applied Biosystems). For each gene, cycle threshold (Ct) values were obtained on cytosolic and total DNA fractions and their ratio normalized using the amount of total DNA as shown in the formula:

$$\text{formula: } \frac{\frac{Ct_{Nd1}^{\text{cytosol}}}{Ct_{Nd1}^{\text{total}}}}{\frac{Ct_{Polg1}^{\text{cytosol}}}{Ct_{Polg1}^{\text{total}}}} \times \frac{1}{\text{DNA abundance}}$$

ROS assay

Total CTRL and C403A tumors were snap-frozen, and total ROS production was evaluated using the OxiSelect In Vitro ROS Assay kit according to the manufacturer's instructions. Briefly, frozen tumors were homogenized on ice. Catalyst was added to cell lysates or hydrogen peroxide standards, mixed, and incubated for 5 min. DCFH (2', 7'-dichlorodihydrofluorescein) solution was added to each well, followed by a 45-min incubation at room temperature. Accumulation of ROS in tumors was calculated by monitoring the fluorescence intensity at excitation and emission wavelengths of 480 and 530 nm.

Statistics analysis

Sample size was designed to minimize the number of individual experimental units (mice or samples), and obtain informative results and appropriate material for downstream analysis. This represents five mice per group, and experiments were typically performed 2–3 times as stated in figure legends. Error bars represent the standard error of the mean. GraphPad Prism 9 software was used for statistical significance assessment. The Gaussian distribution was tested using the D'Agostino–Pearson omnibus normality test. When passing the normality test, a *t* test was used. Otherwise, a Mann–Whitney *U* test was used. Differences were considered to be statistically significant when *****P* < 0.0001, ****P* < 0.001, ***P* < 0.01, and * *P* < 0.05.

Supplementary Information

Supplementary Information is available at <https://doi.org/10.26508/lsa.202201767>

Acknowledgements

The INCA PLBIO19-015 grant supported R Miallot funding and the work realized in the teams of P Naquet and J-Y Blay. We thank the Cancéropôle Provence-Alpes-Côte d'Azur, the National Cancer Institute, and the CRISPR Screen Action for the support brought to the realization of this research project. We thank the core facilities involved in this project: CIML flow cytometry, CIML animal facilities, ImagImm (Roxane Fabre), the French Infrastructure for Integrated Structural Biology (FRISBI) ANR-10-INSB-05-01, and the Plateforme d'Imagerie Vasculaire et de Microscopie Intravitalité at the C2VN. The electron microscopy experiments were performed on the PiCSL-FBI core facility (IBDM, AMU-Marseille), a member of the France-BioImaging National Research Infrastructure (ANR-10-INBS-0004). BM and SH were supported by DCBIOL LabEx (grants ANR-11-LABEX-0043 and ANR-10-IDEX-0001-02 PSL).

Author Contributions

R Miallot: conceptualization, formal analysis, supervision, funding acquisition, investigation, methodology, project administration, and writing—original draft, review, and editing.
V Millet: resources, formal analysis, investigation, methodology, writing—original draft, and project administration.
Y Groult: resources, methodology, and project administration.
A Modelska: methodology.
L Crescence: methodology.
S Roulland: methodology.
S Henri: resources.
B Malissen: resources.
N Brouilly: methodology.
L Panicot-Dubois: methodology.
R Vincentelli: resources, funding acquisition, and methodology.
G Sulzenbacher: resources, data curation, funding acquisition, and methodology.
P Finetti: resources, data curation, formal analysis, supervision, methodology, and writing—original draft.
A Dutour: resources, formal analysis, methodology, and writing—original draft.
J-Y Blay: resources, data curation, funding acquisition, and methodology.
F Bertucci: resources, data curation, formal analysis, supervision, methodology, and writing—original draft.
F Galland: supervision and methodology.
P Naquet: conceptualization, supervision, funding acquisition, methodology, project administration, and writing—original draft, review, and editing.

Conflict of Interest Statement

The authors declare that they have no conflict of interest.

References

- Alavi MV (2019) Targeted OMA1 therapies for cancer. *Int J Cancer* 145: 2330–2341. doi:[10.1002/ijc.32177](https://doi.org/10.1002/ijc.32177)
- Alavi MV (2021) OMA1—an integral membrane protease? *Biochim Biophys Acta Proteins Proteom* 1869: 140558. doi:[10.1016/j.bbapap.2020.140558](https://doi.org/10.1016/j.bbapap.2020.140558)
- Alavi MV (2022) Recent advances in, and challenges of, designing OMA1 drug screens. *Pharmacol Res* 176: 106063. doi:[10.1016/j.phrs.2022.106063](https://doi.org/10.1016/j.phrs.2022.106063)
- Amini MA, Karimi J, Khodadadi I, Tavilani H, Talebi SS, Afshar B (2020) Overexpression of ROMO1 and OMA1 are potentially biomarkers and predict unfavorable prognosis in gastric cancer. *J Gastrointest Canc* 51: 939–946. doi:[10.1007/s12029-019-00330-w](https://doi.org/10.1007/s12029-019-00330-w)
- Anzalone AV, Randolph PB, Davis JR, Sousa AA, Koblan LW, Levy JM, Chen PJ, Wilson C, Newby GA, Raguram A, et al (2019) Search-and-replace genome editing without double-strand breaks or donor DNA. *Nature* 576: 149–157. doi:[10.1038/s41586-019-1711-4](https://doi.org/10.1038/s41586-019-1711-4)
- Ayers M, Lunceford J, Nebozhyn M, Murphy E, Loboda A, Kaufman DR, Albright A, Cheng JD, Kang SP, Shankaran V, et al (2017) IFN- γ -related mRNA profile predicts clinical response to PD-1 blockade. *J Clin Invest* 127: 2930–2940. doi:[10.1172/jci91190](https://doi.org/10.1172/jci91190)
- Baker MJ, Lampe PA, Stojanovski D, Korwitz A, Anand R, Tatsuta T, Langer T (2014) Stress-induced OMA1 activation and autocatalytic turnover regulate OPA1-dependent mitochondrial dynamics. *EMBO J* 33: 578–593. doi:[10.1002/emboj.201386474](https://doi.org/10.1002/emboj.201386474)
- Bertucci F, Finetti P, Simeone I, Hendrickx W, Wang E, Marincola FM, Viens P, Mamessier E, Ceccarelli M, Birnbaum D, et al (2018) The immunologic constant of rejection classification refines the prognostic value of conventional prognostic signatures in breast cancer. *Br J Cancer* 119: 1383–1391. doi:[10.1038/s41416-018-0309-1](https://doi.org/10.1038/s41416-018-0309-1)
- Bertucci F, Niziers V, de Nonneville A, Finetti P, Mescam L, Mir O, Italiano A, Le Cesne A, Blay J-Y, Ceccarelli M, et al (2022) Immunologic constant of rejection signature is prognostic in soft-tissue sarcoma and refines the CINSARC signature. *J Immunother Cancer* 10: e003687. doi:[10.1136/jitc-2021-003687](https://doi.org/10.1136/jitc-2021-003687)
- Bindea G, Mlecnik B, Tosolini M, Kirilovsky A, Waldner M, Obenauf AC, Angell H, Fredriksen T, Lafontaine L, Berger A, et al (2013) Spatiotemporal dynamics of intratumoral immune cells reveal the immune landscape in human cancer. *Immunity* 39: 782–795. doi:[10.1016/j.immuni.2013.10.003](https://doi.org/10.1016/j.immuni.2013.10.003)
- Bohovych I, Fernandez MR, Rahn JJ, Stackley KD, Bestman JE, Anandhan A, Franco R, Claypool SM, Lewis RE, Chan SSL, et al (2015) Metalloprotease OMA1 fine-tunes mitochondrial bioenergetic function and respiratory supercomplex stability. *Sci Rep* 5: 13989. doi:[10.1038/srep13989](https://doi.org/10.1038/srep13989)
- Bohovych I, Kastora S, Christianson S, Topil D, Kim H, Fangman T, Zhou YJ, Barrientos A, Lee J, Brown AJP, et al (2016) Oma1 links mitochondrial protein quality control and TOR signaling to modulate physiological plasticity and cellular stress responses. *Mol Cell Biol* 36: 2300–2312. doi:[10.1128/mcb.00156-16](https://doi.org/10.1128/mcb.00156-16)
- Bohovych I, Dietz JV, Swenson S, Zahayko N, Khalimonchuk O (2019) Redox regulation of the mitochondrial quality control protease Oma1. *Antioxid Redox Signal* 31: 429–443. doi:[10.1089/ars.2018.7642](https://doi.org/10.1089/ars.2018.7642)
- Burke PJ (2017) Mitochondria, bioenergetics and apoptosis in cancer. *Trends Cancer* 3: 857–870. doi:[10.1016/j.trecan.2017.10.006](https://doi.org/10.1016/j.trecan.2017.10.006)
- Chibon F, Lagarde P, Salas S, Pérot G, Brouste V, Tirode F, Lucchesi C, de Reynies A, Kauffmann A, Bui B, et al (2010) Validated prediction of clinical outcome in sarcomas and multiple types of cancer on the basis of a gene expression signature related to genome complexity. *Nat Med* 16: 781–787. doi:[10.1038/nm.2174](https://doi.org/10.1038/nm.2174)
- Chow RD, Chen JS, Shen J, Chen S (2021) A web tool for the design of prime-editing guide RNAs. *Nat Biomed Eng* 5: 190–194. doi:[10.1038/s41551-020-00622-8](https://doi.org/10.1038/s41551-020-00622-8)
- Consolato F, Maltecca F, Tulli S, Sambri I, Casari G (2018) m-AAA and i-AAA complexes coordinate to regulate OMA1, the stress-activated supervisor of mitochondrial dynamics. *J Cell Sci* 131: jcs213546. doi:[10.1242/jcs.213546](https://doi.org/10.1242/jcs.213546)
- Coppola D, Nebozhyn M, Khalil F, Dai H, Yeatman T, Loboda A, Mulé JJ (2011) Unique ectopic lymph node-like structures present in human primary colorectal carcinoma are identified by immune gene array profiling. *Am J Pathol* 179: 37–45. doi:[10.1016/j.ajpath.2011.03.007](https://doi.org/10.1016/j.ajpath.2011.03.007)
- da Cunha FM, Torelli NQ, Kowaltowski AJ (2015) Mitochondrial retrograde signaling: Triggers, pathways, and outcomes. *Oxid Med Cell Longev* 2015: 482582. doi:[10.1155/2015/482582](https://doi.org/10.1155/2015/482582)
- Daverey A, Levytsky RM, Stanke KM, Viana MP, Swenson S, Hayward SL, Narasimhan M, Khalimonchuk O, Kidambi S (2019) Depletion of mitochondrial protease OMA1 alters proliferative properties and promotes metastatic growth of breast cancer cells. *Sci Rep* 9: 14746. doi:[10.1038/s41598-019-49327-2](https://doi.org/10.1038/s41598-019-49327-2)
- Del Dotto V, Mishra P, Vidoni S, Fogazza M, Maresca A, Caporali L, McCaffery JM, Cappelletti M, Baruffini E, Lenaers G, et al (2017) OPA1 isoforms in the hierarchical organization of mitochondrial functions. *Cell Rep* 19: 2557–2571. doi:[10.1016/j.celrep.2017.05.073](https://doi.org/10.1016/j.celrep.2017.05.073)
- Ehse S, Raschke I, Mancuso G, Bernacchia A, Geimer S, Tondera D, Martinou J-C, Westermann B, Rugarli EI, Langer T (2009) Regulation of OPA1 processing and mitochondrial fusion by m-AAA protease isoenzymes and OMA1. *J Cell Biol* 187: 1023–1036. doi:[10.1083/jcb.200906084](https://doi.org/10.1083/jcb.200906084)
- Ferris ST, Durai V, Wu R, Theisen DJ, Ward JP, Bern MD, Davidson JT, Bagadia P, Liu T, Briseño CG, et al (2020) cDC1 prime and are licensed by CD4+ T cells to induce anti-tumour immunity. *Nature* 584: 624–629. doi:[10.1038/s41586-020-2611-3](https://doi.org/10.1038/s41586-020-2611-3)
- Fessler E, Eckl E-M, Schmitt S, Mancilla IA, Meyer-Bender MF, Hanf M, Philippou-Massier J, Krebs S, Zischka H, Jae LT (2020) A pathway coordinated by DELE1 relays mitochondrial stress to the cytosol. *Nature* 579: 433–437. doi:[10.1038/s41586-020-2076-4](https://doi.org/10.1038/s41586-020-2076-4)
- Galluzzi L, Kepp O, Kroemer G (2012) Mitochondria: Master regulators of danger signalling. *Nat Rev Mol Cell Biol* 13: 780–788. doi:[10.1038/nrm3479](https://doi.org/10.1038/nrm3479)
- Giessler C, Millet V, Mostert KJ, Gensollen T, Vu Manh T-P, Garibal M, Dieme B, Attaf-Bouabdallah N, Chasson L, Brouilly N, et al (2018) Vnn1 pantetheinase limits the Warburg effect and sarcoma growth by rescuing mitochondrial activity. *Life Sci Alliance* 1: e201800073. doi:[10.26508/lsa.201800073](https://doi.org/10.26508/lsa.201800073)
- Gilkerson R (2018) A disturbance in the force: Cellular stress sensing by the mitochondrial network. *Antioxidants* 7: 126. doi:[10.3390/antiox7100126](https://doi.org/10.3390/antiox7100126)
- Gilkerson R, De La Torre P, St Vallier S (2021) Mitochondrial OMA1 and OPA1 as gatekeepers of organellar structure/function and cellular stress response. *Front Cell Dev Biol* 9: 626117. doi:[10.3389/fcell.2021.626117](https://doi.org/10.3389/fcell.2021.626117)
- Glytsou C, Calvo E, Cogliati S, Mehrotra A, Anastasia I, Rigoni G, Raimondi A, Shintani N, Loureiro M, Vazquez J, et al (2016) Optic atrophy 1 is epistatic to the core MICOS component MIC60 in mitochondrial cristae shape control. *Cell Rep* 17: 3024–3034. doi:[10.1016/j.celrep.2016.11.049](https://doi.org/10.1016/j.celrep.2016.11.049)
- Guo X, Aviles G, Liu Y, Tian R, Unger BA, Lin Y-HT, Wiita AP, Xu K, Correia MA, Kampmann M (2020) Mitochondrial stress is relayed to the cytosol by an OMA1–DELE1–HRI pathway. *Nature* 579: 427–432. doi:[10.1038/s41586-020-2078-2](https://doi.org/10.1038/s41586-020-2078-2)
- Head B, Griparic L, Amiri M, Gandre-Babbe S, van der Blik AM (2009) Inducible proteolytic inactivation of OPA1 mediated by the OMA1 protease in mammalian cells. *J Cell Biol* 187: 959–966. doi:[10.1083/jcb.200906083](https://doi.org/10.1083/jcb.200906083)
- Herkenne S, Scorrano L (2020) OPA1, a new mitochondrial target in cancer therapy. *Aging (Albany NY)* 12: 20931–20933. doi:[10.18632/aging.104207](https://doi.org/10.18632/aging.104207)
- Herkenne S, Ek O, Zamberlan M, Pellattiero A, Chergova M, Chivite I, Novotná E, Rigoni G, Fonseca TB, Samardzic D, et al (2020) Developmental and tumor angiogenesis requires the mitochondria-shaping protein Opa1. *Cell Metab* 31: 987–1003.e8. doi:[10.1016/j.cmet.2020.04.007](https://doi.org/10.1016/j.cmet.2020.04.007)

- Huynen MA, Mühlmeister M, Gotthardt K, Guerrero-Castillo S, Brandt U (2016) Evolution and structural organization of the mitochondrial contact site (MICOS) complex and the mitochondrial intermembrane space bridging (MIB) complex. *Biochim Biophys Acta* 1863: 91–101. doi:10.1016/j.bbamcr.2015.10.009
- Ishihara N, Fujita Y, Oka T, Mihara K (2006) Regulation of mitochondrial morphology through proteolytic cleavage of OPA1. *EMBO J* 25: 2966–2977. doi:10.1038/sj.emboj.7601184
- Jiang X, Jiang H, Shen Z, Wang X (2014) Activation of mitochondrial protease OMA1 by Bax and Bak promotes cytochrome c release during apoptosis. *Proc Natl Acad Sci U S A* 111: 14782–14787. doi:10.1073/pnas.1417253111
- Jumper J, Evans R, Pritzel A, Green T, Figurnov M, Ronneberger O, Tunyasuvunakool K, Bates R, Židek A, Potapenko A, et al (2021) Highly accurate protein structure prediction with AlphaFold. *Nature* 596: 583–589. doi:10.1038/s41586-021-03819-2
- Kleele T, Rey T, Winter J, Zaganelli S, Mahecic D, Perreten Lambert H, Ruberto FP, Nemir M, Wai T, Pedrazzini T, et al (2021) Distinct fission signatures predict mitochondrial degradation or biogenesis. *Nature* 593: 435–439. doi:10.1038/s41586-021-03510-6
- Kroemer G, Galluzzi L, Kepp O, Zitvogel L (2013) Immunogenic cell death in cancer therapy. *Annu Rev Immunol* 31: 51–72. doi:10.1146/annurev-immunol-032712-100008
- Lam J, Katti P, Biete M, Mungai M, AshShareef S, Neikirk K, Garza Lopez E, Vue Z, Christensen TA, Beasley HK, et al (2021) A universal approach to analyzing transmission electron microscopy with ImageJ. *Cells* 10: 2177. doi:10.3390/cells10092177
- Levytsky RM, Bohovych I, Khalimonchuk O (2017) Metalloproteases of the inner mitochondrial membrane. *Biochemistry* 56: 4737–4746. doi:10.1021/acs.biochem.7b00663
- McBride H, Soubannier V (2010) Mitochondrial function: OMA1 and OPA1, the grandmasters of mitochondrial health. *Curr Biol* 20: R274–R276. doi:10.1016/j.cub.2010.02.011
- Miallot R, Galland F, Millet V, Blay J-Y, Naquet P (2021) Metabolic landscapes in sarcomas. *J Hematol Oncol* 14: 114. doi:10.1186/s13045-021-01125-y
- Murata D, Yamada T, Tokuyama T, Arai K, Quirós PM, López-Otín C, Iijima M, Sesaki H (2020) Mitochondrial safeguard: A stress response that offsets extreme fusion and protects respiratory function via flickering-induced Oma1 activation. *EMBO J* 39: e105074. doi:10.15252/embj.2020105074
- Nakahira K, Haspel JA, Rathinam VAK, Lee S-J, Dolinay T, Lam HC, Englert JA, Rabinovitch M, Cernadas M, Kim HP, et al (2011) Autophagy proteins regulate innate immune responses by inhibiting the release of mitochondrial DNA mediated by the NALP3 inflammasome. *Nat Immunol* 12: 222–230. doi:10.1038/ni.1980
- Nakashima-Kamimura N, Asoh S, Ishibashi Y, Mukai Y, Shidara Y, Oda H, Munakata K, Goto Y-I, Ohta S (2005) MIDAS/GPP34, a nuclear gene product, regulates total mitochondrial mass in response to mitochondrial dysfunction. *J Cell Sci* 118: 5357–5367. doi:10.1242/jcs.02645
- Oka T, Hikoso S, Yamaguchi O, Taneike M, Takeda T, Tamai T, Oyabu J, Murakawa T, Nakayama H, Nishida K, et al (2012) Mitochondrial DNA that escapes from autophagy causes inflammation and heart failure. *Nature* 485: 251–255. doi:10.1038/nature10992
- O'Malley J, Kumar R, Inigo J, Yadava N, Chandra D (2020) Mitochondrial stress response and cancer. *Trends Cancer* 6: 688–701. doi:10.1016/j.trecan.2020.04.009
- Phelan JD, Young RM, Webster DE, Roulland S, Wright GW, Kasbekar M, Shaffer AL, Ceribelli M, Wang JQ, Schmitz R, et al (2018) A multiprotein supercomplex controlling oncogenic signalling in lymphoma. *Nature* 560: 387–391. doi:10.1038/s41586-018-0290-0
- Porporato PE, Filigheddu N, Pedro JMBS, Kroemer G, Galluzzi L (2018) Mitochondrial metabolism and cancer. *Cell Res* 28: 265–280. doi:10.1038/cr.2017.155
- Rainbolt TK, Lebeau J, Puchades C, Wiseman RL (2016) Reciprocal degradation of YME1L and OMA1 adapts mitochondrial proteolytic activity during stress. *Cell Rep* 14: 2041–2049. doi:10.1016/j.celrep.2016.02.011
- Rooney MS, Shukla SA, Wu CJ, Getz G, Hacohen N (2015) Molecular and genetic properties of tumors associated with local immune cytolytic activity. *Cell* 160: 48–61. doi:10.1016/j.cell.2014.12.033
- Sakowska P, Jans DC, Mohanraj K, Riedel D, Jakobs S, Chacinska A (2015) The oxidation status of Mic19 regulates MICOS assembly. *Mol Cell Biol* 35: 4222–4237. doi:10.1128/mcb.00578-15
- Singel KL, Grzankowski KS, Khan ANMH, Grimm MJ, D'Auria AC, Morrell K, Eng KH, Hylander B, Mayor PC, Emmons TR, et al (2019) Mitochondrial DNA in the tumour microenvironment activates neutrophils and is associated with worse outcomes in patients with advanced epithelial ovarian cancer. *Br J Cancer* 120: 207–217. doi:10.1038/s41416-018-0339-8
- Song Z, Chen H, Fiket M, Alexander C, Chan DC (2007) OPA1 processing controls mitochondrial fusion and is regulated by mRNA splicing, membrane potential, and Yme1L. *J Cell Biol* 178: 749–755. doi:10.1083/jcb.200704110
- Tobacyk J, MacMillan-Crow LA (2021) Fluorescence-based assay for measuring OMA1 activity. *Methods Mol Biol* 2276: 325–332. doi:10.1007/978-1-0716-1266-8_24
- Tobacyk J, Parajuli N, Shrum S, Crow JP, MacMillan-Crow LA (2019) The first direct activity assay for the mitochondrial protease OMA1. *Mitochondrion* 46: 1–5. doi:10.1016/j.mito.2019.03.001
- Tschopp J (2011) Mitochondria: Sovereign of inflammation? *Eur J Immunol* 41: 1196–1202. doi:10.1002/eji.201141436
- Twig G, Shirihai OS (2011) The interplay between mitochondrial dynamics and mitophagy. *Antioxid Redox Signaling* 14: 1939–1951. doi:10.1089/ars.2010.3779
- Viana MP, Levytsky RM, Anand R, Reichert AS, Khalimonchuk O (2021) Protease OMA1 modulates mitochondrial bioenergetics and ultrastructure through dynamic association with MICOS complex. *iScience* 24: 102119. doi:10.1016/j.isci.2021.102119
- Voehringer D, Liang H-E, Locksley RM (2008) Homeostasis and effector function of lymphopenia-induced [L8S2Q1M6]memory-like [R8S2Q1M7] T cells in constitutively T cell-depleted mice. *J Immunol* 180: 4742–4753. doi:10.4049/jimmunol.180.7.4742
- Wang R, Mishra P, Garbis SD, Moradian A, Sweredoski MJ, Chan DC (2021) Identification of new OPA1 cleavage site reveals that short isoforms regulate mitochondrial fusion. *Mol Biol Cell* 32: 157–168. doi:10.1091/mbc.e20-09-0605
- Wohn C, Le Guen V, Voluzan O, Fiore F, Henri S, Malissen B (2020) Absence of MHC class II on cDC1 dendritic cells triggers fatal autoimmunity to a cross-presented self-antigen. *Sci Immunol* 5: eaba1896. doi:10.1126/sciimmunol.aba1896
- Wollweber F, von der Malsburg K, van der Laan M (2017) Mitochondrial contact site and cristae organizing system: A central player in membrane shaping and crosstalk. *Biochim Biophys Acta Mol Cell Res* 1864: 1481–1489. doi:10.1016/j.bbamcr.2017.05.004
- Wu Z, Zuo M, Zeng L, Cui K, Liu B, Yan C, Chen L, Dong J, Shangguan F, Hu W, et al (2021) OMA1 reprograms metabolism under hypoxia to promote colorectal cancer development. *EMBO Rep* 22: e50827. doi:10.15252/embr.202050827
- Xiao B, Deng X, Zhou W, Tan E-K (2016) Flow cytometry-based assessment of mitophagy using MitoTracker. *Front Cell Neurosci* 10: 76. doi:10.3389/fncel.2016.00076
- Xu MM, Pu Y, Han D, Shi Y, Cao X, Liang H, Chen X, Li X-D, Deng L, Chen ZJ, et al (2017) Dendritic cells but not macrophages sense tumor

mitochondrial DNA for cross-priming through signal regulatory protein α signaling. *Immunity* 47: 363–373.e5. doi:[10.1016/j.immuni.2017.07.016](https://doi.org/10.1016/j.immuni.2017.07.016)

Zhang Q, Raoof M, Chen Y, Sumi Y, Sursal T, Junger W, Brohi K, Itagaki K, Hauser CJ (2010) Circulating mitochondrial DAMPs cause inflammatory responses to injury. *Nature* 464: 104–107. doi:[10.1038/nature08780](https://doi.org/10.1038/nature08780)

Zhang K, Li H, Song Z (2014) Membrane depolarization activates the mitochondrial protease OMA1 by stimulating self-cleavage. *EMBO Rep* 15: 576–585. doi:[10.1002/embr.201338240](https://doi.org/10.1002/embr.201338240)

Zhong Z, Liang S, Sanchez-Lopez E, He F, Shalapour S, Lin X-j, Wong J, Ding S, Seki E, Schnabl B, et al (2018) New mitochondrial DNA synthesis enables NLRP3 inflammasome activation. *Nature* 560: 198–203. doi:[10.1038/s41586-018-0372-z](https://doi.org/10.1038/s41586-018-0372-z)

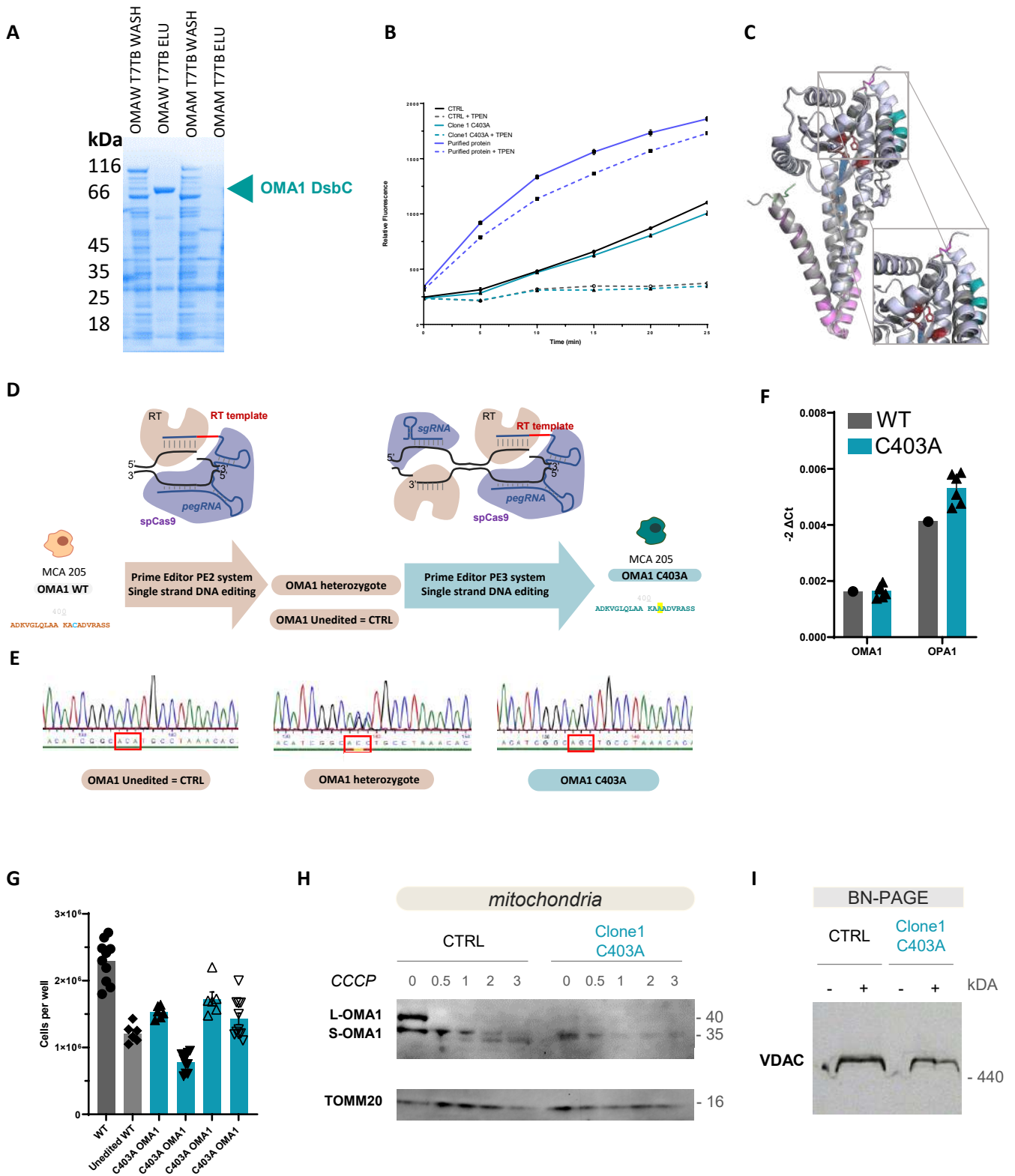


License: This article is available under a Creative Commons License (Attribution 4.0 International, as described at <https://creativecommons.org/licenses/by/4.0/>).

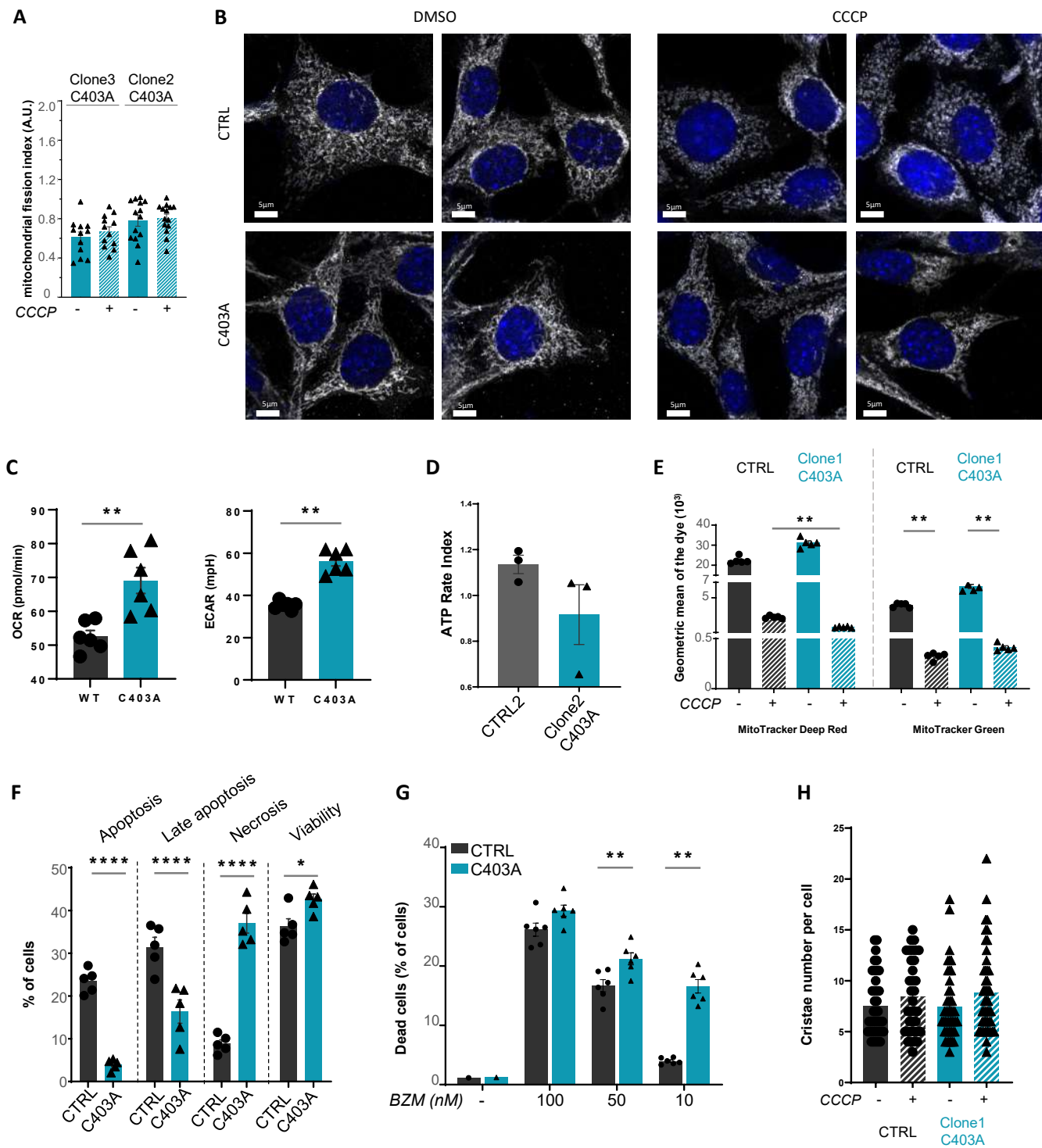
Appendix Supplementary Methods

Primer name	Sequence 5'-3'
OMA1 screening WT F	TTAACTCTGTGTTTAGGCATG
OMA1 screening WT R	TTAGTGGGGTTAGCTCACC
OMA1 screening C403A F	TTAACTCTGTGTTTAGGCAGC
OMA1 screening C403A R	TTAGTGGGGTTAGCTCACC
OMA1 WT PCR F	CATCTGCAAGGGTTCAGGCT
OMA1 WT PCR R	AACACTACAAAGAGCAGTCCAAA
OPA 1 F	TGGAAAATGGTTCGAAGTCAG
OPA1 R	CATTCCGTCTCTAGGTTAAAGCG
POLG1 F	GATGAATGGGCCTACCTTGA
POLG1 R	TGGGGTCCTGTTTCTACAGC
ND1 F	CAAACACTTATTACAACCCAAGAACA
ND1R	TCATATTATGGCTATGGGTCAGG

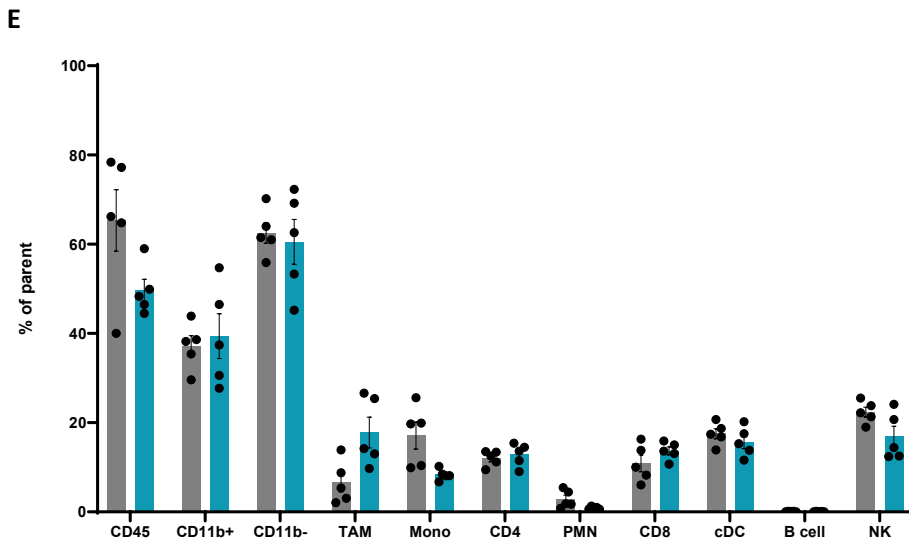
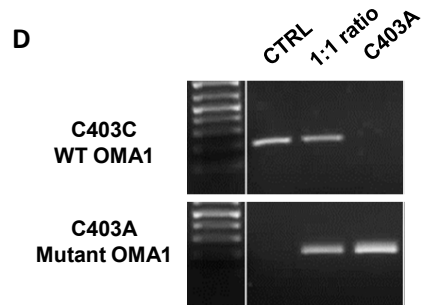
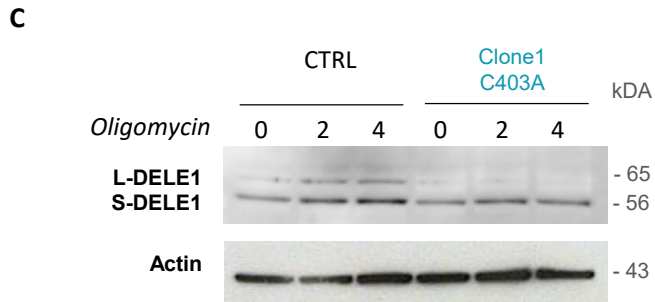
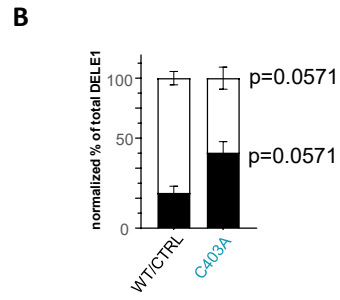
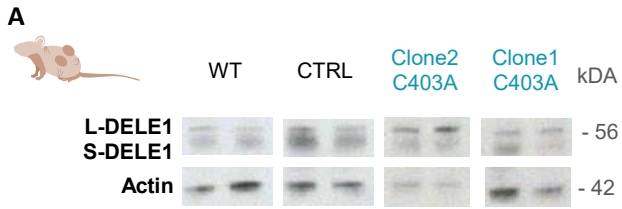
Expanded View 1



Expanded View 2



Expanded View 3



A

Table 1 : Clinicopathological characteristics of patients and samples in the whole population and according to OMA1 and OPA1-based classification

Characteristics	All patients		OMA1				OPA1			
	N	N (%)	N	low	high	p-value	N	low	high	p-value
Age (years), median (range)	484	63.94 (11-93)	468	61.86 (11-91)	62.77 (11-93)	0,519	409	62.19 (11-92.12)	59.72 (11-91)	0,118
Gender						0,474				0,886
female	262	262 (49%)	237	134 (52%)	103 (49%)		229	119 (50%)	110 (51%)	
male	270	270 (51%)	231	122 (48%)	109 (51%)		228	121 (50%)	107 (49%)	
Pathological subtype						0,000				0,000
Undifferentiated	330	330 (36%)	294	187 (47%)	107 (33%)		288	152 (36%)	136 (32%)	
Leiomyosarcoma	341	341 (37%)	289	130 (33%)	159 (49%)		312	117 (28%)	195 (46%)	
Liposarcoma	81	81 (9%)	38	15 (4%)	23 (7%)		81	53 (13%)	28 (7%)	
Myxofibrosarcoma	105	105 (11%)	59	37 (9%)	22 (7%)		100	66 (16%)	34 (8%)	
Others	58	58 (6%)	40	28 (7%)	12 (4%)		58	30 (7%)	28 (7%)	
Pathological grade						0,088				0,302
2-3	371	371 (98%)	361	204 (99%)	157 (96%)		296	167 (98%)	129 (96%)	
1	9	9 (2%)	9	2 (1%)	7 (4%)		9	3 (2%)	6 (4%)	
Tumor site						0,000				0,042
Extremity	199	199 (52%)	199	126 (61%)	73 (41%)		198	116 (57%)	82 (45%)	
Head and neck	7	7 (2%)	7	3 (1%)	4 (2%)		7	5 (2%)	2 (1%)	
Internal trunk	103	103 (27%)	103	34 (17%)	69 (39%)		103	44 (22%)	59 (33%)	
Superficial Trunk	75	75 (20%)	74	43 (21%)	31 (18%)		75	37 (18%)	38 (21%)	
CINSARC risk						0,607				0,004
Good	408	408 (44%)	364	203 (51%)	161 (49%)		368	204 (49%)	164 (38%)	
Poor	513	513 (56%)	362	194 (49%)	168 (51%)		477	215 (51%)	262 (62%)	
Follow-up (months), median (range)	433	28 (1-222)	413	28 (1-195)	25 (1-222)	0,857	365	27 (1-188)	25 (1-222)	0,663
MFS event	433	178 (41%)	413	84 (36%)	82 (46%)	0,055	365	62 (33%)	82 (47%)	0,008
5-year MFS [95%CI]	433	53% [48-59]	413	59% [53-67]	48% [40-57]	0,062	365	60% [52-69]	48% [40-57]	0,005

B

Table 2: List of soft tissue sarcoma data sets included in our analysis

Reference	Source of data	Technological platform	N° of probe sets/genes	All samples	complex STS primary tumor samples included in the present analysis
Baird K et al., Cancer Res 2005	GEO database, GSE2553	Homemade, spotted DNA/cDNA	12K	181	89
Barretina J et al., Nat Genet 2010	GEO database, GSE21124	Affymetrix, array U133 A	22K	158	79
Beck A et al., Oncogene 2010	GEO database, GSE17555	Stanford, spotted DNA/cDNA	24K	51	26
Chibon F et al., Nat. Med. 2010	GEO database, GSE21050	Affymetrix, array U133 Plus 2.0	54K	310	237
Detwiller K et al., Cancer Res 2005	GEO database, GSE2719	Affymetrix, array U133 A	22K	54	25
Gibault L et al., J Pathol 2011	GEO database, GSE23980	Affymetrix, array U133 Plus 2.0	54K	171	34
Gobble R et al., Cancer Res 2011	GEO database, GSE30929	Affymetrix, array U133 A	22K	140	20
Hadju M et al., J Pathol 2010	http://cbio.mskcc.org/public/SFT/	Affymetrix, array U133 Plus 2.0	54K	56	5
Henderson S et al., Genome Biology 2005	Array Express database, E-MEXP-353	Affymetrix, array U133 A	22K	96	15
Nakayama R et al., Modern Pathol 2007	GEO database, GSE6481	Affymetrix, array U133 A	22K	105	48
Nielsen TO et al., Lancet 2002	GEO database, GSE3443	Stanford, spotted DNA/cDNA	24K	46	21
Renner M et al., Genome Biol 2013	GEO database, GSE52392	Illumina, array Human HT-12 V3.0	48K	94	48
Skubitz et al, Cancer 2012	Masonic Cancer Center	Homemade, spotted DNA/cDNA	16K	73	71
TCGA, Cell 2017	TCGA portal, https://tcga-data.nci.nih.gov	Illumina, RNA sequencing V2	25K	265	158
West R et al., PLoS Biology 2005	http://microarray-pubs.stanford.edu/tma-portal/DTF_SFTbreast	Stanford, spotted DNA/cDNA	24K	57	14
Ylipää A et al., Cancer 2011	http://www3.mdanderson.org/~genomics/sarcoma_data_matrix_for_su pplemental.zip	Agilent, array 44K G4112A (012391)	44K	68	31
Total					921

C

MFS, Cox	Univariate			Multivariate		
	N	HR [95%CI]	p-value	N	HR [95%CI]	p-value
Age (years)	316	1.00 [0.99-1.01]	0.911			
Gender, Male vs. Female	316	1.10 [0.78-1.55]	0.589			
Pathological subtype, Leiomyosarcoma vs. Undifferentiated	433	2.45 [1.74-3.43]	2.48E-06	365	2.1 [1.41-3.11]	2.25E-04
Liposarcoma vs. Undifferentiated		2.25 [1.29-3.92]		365	2 [1.10-3.62]	2.26E-02
Myxofibrosarcoma vs. Undifferentiated		1.11 [0.61-2.02]		365	1.1 [0.55-2.18]	0.793
Others vs. Undifferentiated		1.07 [0.43-2.68]		365	1.16 [0.46-2.93]	0.753
Pathological grade, 1 vs. 2-3	275	0.00 [0.00-Inf]	0.994			
Tumor site, Head and neck vs. Extremity	283	0.00 [0.00- Inf]	0.147			
Internal trunk vs. Extremity		1.42 [0.92-2.17]				
Superficial Trunk vs. Extremity		0.71 [0.40-1.25]				
CINSARC risk, Poor vs. Good	433	1.82 [1.34-2.47]	1.13E-04	365	1.84 [1.28-2.64]	9.64E-04
OMA1 ^{high} vs. OMA1 ^{low}	413	1.33 [0.95-1.85]	0.093			
OPA1 ^{high} vs. OPA1 ^{low}	365	1.58 [1.11-2.25]	1.11E-02	365	1.35 [0.96-1.91]	0.089

A Table 3: List of genes included in the MHC/HLA gene signatures analysed

Symbol	Description	Cytoband	Entrez Gene ID	Category
HLA-A	major histocompatibility complex, class I, A	6p22.1	3105	MHC I classic presenting
HLA-B	major histocompatibility complex, class I, B	6p21.33	3106	MHC I classic presenting
HLA-C	major histocompatibility complex, class I, C	6p21.33	3107	MHC I classic presenting
PSME1	proteasome activator subunit 1	14q12	5720	Proteasome
PSME2	proteasome activator subunit 2	14q12	5721	Proteasome
PSME3	proteasome activator subunit 3	17q21.31	10197	Proteasome
PSMB8	proteasome 20S subunit beta 8	6p21.32	5696	Proteasome
PSMB9	proteasome 20S subunit beta 9	6p21.32	5698	Proteasome
PSMB10	proteasome 20S subunit beta 10	16q22.1	5699	Proteasome
TAP1	transporter 1, ATP binding cassette subfamily B member	6p21.32	6890	Loading complex
TAP2	transporter 2, ATP binding cassette subfamily B member	6p21.32	6891	Loading complex
ABCB9	ATP binding cassette subfamily B member 9	12q24.31	23457	Loading complex
HSPA5	heat shock protein family A (Hsp70) member 5	9q33.3	3309	Loading complex
CANX	calnexin	5q35.3	821	Loading complex
CALR	calreticulin	19p13.13	811	Loading complex
PDIA3	protein disulfide isomerase family A member 3	15q15.3	2923	Loading complex
TAPBP	TAP binding protein	6p21.32	6892	Loading complex
B2M	beta-2-microglobulin	15q21.1	567	Loading complex
HLA-DOA	major histocompatibility complex, class II, DO alpha	6p21.32	3111	TAP LMP presentation regulation
HLA-DOB	major histocompatibility complex, class II, DO beta	6p21.32	3112	TAP LMP presentation regulation
HLA-DMA	major histocompatibility complex, class II, DM alpha	6p21.32	3108	TAP LMP presentation regulation
HLA-DMB	major histocompatibility complex, class II, DM beta	6p21.32	3109	TAP LMP presentation regulation
HLA-DPB1	major histocompatibility complex, class II, DP beta 1	6p21.32	3115	MHC II classic presenting
HLA-DQA1	major histocompatibility complex, class II, DQ alpha 1	6p21.32	3117	MHC II classic presenting
HLA-DQB1	major histocompatibility complex, class II, DQ beta 1	6p21.32	3119	MHC II classic presenting
HLA-DRA	major histocompatibility complex, class II, DR alpha	6p21.32	3122	MHC II classic presenting
HLA-DRB1	major histocompatibility complex, class II, DR beta 1	6p21.32	3123	MHC II classic presenting
HLA-DRB3	major histocompatibility complex, class II, DR beta 3	6p21.3	3125	MHC II classic presenting
CTSS	cathepsin S	1q21.3	1520	MHC II degradation
CTSB	cathepsin B	8p23.1	1508	MHC II degradation
CTSL	cathepsin L	9q21.33	1514	MHC II degradation
LGMN	legumain	14q32.12	5641	MHC II degradation
IFI30	IFI30 lysosomal thiol reductase	19p13.11	10437	MHC II degradation
P4HB	prolyl 4-hydroxylase subunit beta	17q25.3	5034	MHC II degradation
CD1A	CD1a molecule	1q23.1	909	T cell recognition
CD1B	CD1b molecule	1q23.1	910	T cell recognition
CD1C	CD1c molecule	1q23.1	911	T cell recognition
CD1D	CD1d molecule	1q23.1	912	T cell recognition
CD1E	CD1e molecule	1q23.1	913	T cell recognition

EXPANDED VIEW FIGURE LEGENDS

Expanded View 1

A. SDS-PAGE colored with Coomassie blue staining was performed to confirm the presence of purified WT but not mutant OMA1-DsbC protein after elution.

B. Overlay of the AlphaFold-predicted structure of WT and C403A OMA1 proteins.

C. OMA1 enzymatic assay on purified OMA1 WT protein, CTRL and C403A MCA205 cells evaluated by using fluorogenic OPA1-peptide reporter.

D. Scheme of the two-step prime editing method used to obtain homozygous C403A OMA1 mutated MCA205 cell line, adapted from Anzalone et al, 2019.

E. Sequencing profile of genomic DNA reveals the presence of mono or bi-allelic C403A mutation in region of interest of OMA1.

F. OMA1 and OPA1 transcripts levels in CTRL and C403A cell lines. Actin was used for data normalization.

G. WT, CTRL or C403A OMA1 cells (1.5×10^5) were seeded and counted 3 days later.

H. Western blot analysis of mitochondrial protein extracts from CTRL and C403A MCA205 cells at different times of CCCP-stimulation using OMA1 antibody and TOMM20 as a loading control.

I. BN-PAGE analysis of native proteins prepared from CTRL and C403A mitochondrial extracts. VDAC was used as a loading control on a fraction of mitochondrial lysates.

Expanded View 2

A. Untreated or CCCP-treated C403A MCA205 clone 3 and 2 cells were labelled with MDR (5 μ M) and images from confocal microscope analysis were acquired using AiryScan. The mitochondrial network was reconstructed by 3D modeling using the Imaris technology. Yellow and blue dots represent individual mitochondria and mitochondrial network respectively. Scale bar: 5 μ m n=2.

B. Confocal microscopy analysis of CTRL and C403A MCA205 cells stained with anti-TOMM20 antibody (in white) and DAPI (in blue) after 45 min of CCCP stimulation. Images were acquired and processed using AiryScan technology. Scale bar: 5 μ m (n=10).

C. Basal oxygen consumption rate and extracellular acidification rate analysis by Seahorse of CTRL and C403A cells (n=2).

D. The ATP rate index (i.e. Ratio of the mitoATP Production Rate divided by glycoATP Production Rate) of CTRL2 and clone 2 C403A MCA205 cells was assessed using Seahorse Xfp. n=2. Mann-Whitney test; * p-value<0.05.

E. Flow cytometry quantification of mitochondrial depolarization (MDR) and mass (MG) from untreated or CCCP-treated CTRL and C403A cells. (n=5). Mann-Whitney test; **p-value < 0.01

F. Flow cytometry evaluation using Annexin V and SYTOX blue staining of bortezomib-induced CTRL and C403A cell death at 24h.

G. Flow cytometry quantification of the proportion of CTRL and C403A MCA205 dead cells after incubating for 16h with the proteasome inhibitor bortezomib (BZM) at indicated concentrations. Mann-Whitney test; **p-value < 0.01.

H. EM analysis of CTRL and C403A MCA205 cells. Cells were treated for 1 hour with CCCP and fixed for TEM acquisition. We quantified number of cristae per cell in untreated or CCCP-treated conditions.

Expanded View 3

A. Western blot analysis of total protein extracts from CD45 negative cells isolated from WT or C403A tumors at day 21 post cell engraftment. DELE1 expression was evaluated and quantified in panel **B** (n=4).

C. Western blot analysis of DELE1 in total protein extracts from CTRL and C403A MCA205 cells after different times of oligomycin (20 μ M) stimulation.

D. A PCR assay discriminating C403A mutation was used to evaluate the proportion of C403A MCA205 cells at different ratios of CTRL/C403A cells in vitro.

D. Analysis of the immune infiltrate of CTRL or C403A tumors in WT mice at day 12 post cell engraftment. Mann-Whitney test; **p-value < 0.01, * p-value<0.05. n=8-10.

Expanded View 4

A. Table 1: Clinicopathological characteristics of patients and samples in the whole population and according to OMA1 and OPA1-based classification.

B. Table 2: List of soft tissue sarcoma data sets included in our analysis.

C. Uni- and multivariate prognostic analyses for MFS. The p-values are for the Wald test.

Expanded View 5

C. Table 3: List of genes included in the MHC/HLA gene signatures analyzed.

2) Restaurer les facteurs métaboliques limitants

La demande énergétique accrue des cellules cancéreuses va induire une compétition métabolique entre les cellules présentes dans le microenvironnement. D'une manière générale, les cellules possédant des activités cytotoxiques comme les lymphocytes T CD8 et les macrophages de polarisation M1 fonctionnent d'une manière analogue aux cellules tumorales et donc entrent en compétition pour les ressources (129). Au contraire, les cellules du microenvironnement tumoral possédant une fonction de support des cellules tumorales vont avoir un métabolisme complémentaire et non compétitif des cellules tumorales. C'est par exemple le cas des cellules de types lymphocytes T régulateurs, des macrophages M2, des MDSCs et des CAFs. Lors des processus d'activation cellulaire et pour posséder une activité cytotoxique et/ou sécrétrice, les cellules immunitaires vont largement faire appel à la glycolyse (130). Ainsi dans un contexte où le glucose est limitant, les cellules T CD8 vont avoir une activité cytotoxique diminuée. De la même manière, la sécrétion de l'IFN γ par les macrophages M1 ou les lymphocytes T sera diminuée en cas de déficit en glucose. Il a été démontré que l'efficacité des inhibiteurs d'immunité checkpoints tels que les anticorps anti-PDL1 dépend en partie d'une régulation du métabolisme tumoral (14,131). Ainsi, le glucose va être le premier élément limitant dans les tumeurs, même si d'autres intermédiaires de la glycolyse comme le PEP peuvent l'être également (132).

Les cellules cancéreuses vont consommer dans le microenvironnement des acides aminés, des acides gras libres, d'autres sources énergétiques comme le lactate ou la glutamine mais également de nombreux cofacteurs nécessaires au bon fonctionnement des voies métaboliques. Bien que la plupart des ressources soient disponibles dans le microenvironnement ou disponibles après recyclage intracellulaire, certaines ressources peuvent devenir limitantes. C'est notamment le cas de la disponibilité de la vitamine B5, précurseur biosynthétique du coenzyme A. Le coenzyme A est impliqué dans plus de 300 réactions notamment d'anabolisme. Sa biodisponibilité est donc essentielle et se fait par captation de la vitamine B5 dans l'alimentation ou par recyclage intracellulaire du coenzyme A (133).

3) Restaurer une réponse antitumorale par une reprogrammation métabolique dépendante de la voie de signalisation Vanin1.

Le coenzyme A est un cofacteur essentiel et ubiquitaire dans les organismes. Il est un transporteur de groupement acyl et un activateur des fonctions carboxyl par formation de thioesters. Il est impliqué, sous forme de CoA ou acyl-CoA, dans environ 4% des réactions biochimiques cellulaires (134), notamment la glycolyse, le cycle de Krebs, la synthèse et l'oxydation des acides gras, la céto-génèse, le métabolisme des acides aminés et la synthèse de l'acétylcholine (135–138). Il peut également intervenir dans la régulation allostérique de certaines enzymes métaboliques comme la pyruvate décarboxylase, la carnitine palmitoyltransférase ou par régulation post transcriptionnelle des histones (rôle épigénétique) et d'autres protéines par acylation ou CoAlation (139–145). Parmi les formes

acylées du coenzyme A, l'acétyl-CoA est le plus abondant et représente un métabolite central au carrefour entre les voies anaboliques et cataboliques. Étant donné la grande diversité des processus biologiques centraux dans lequel il est impliqué, la régulation des pools de coenzyme A intracellulaire ainsi que son apport à la cellule est fondamental et nécessaire à son bon fonctionnement (133).

4) Propriétés immunomodulatrices de la vitamine B5

L'assimilation de la molécule de coenzyme A présent dans l'alimentation ou dérivé du microbiote va être réalisée dans l'intestin (146). Le coenzyme A va être hydrolysé par des phosphatases en pantéthine. La pantéthine ainsi que sa forme dimérique oxydée appelée pantéthine est le substrat de la réaction d'hydrolyse médiée par l'enzyme Vanin1 (147–152). Cette réaction va libérer deux composés dans la circulation sanguine, la cystéamine (CEA) et le pantothénate (Pan), plus communément appelée vitamine B5 (153,154). Dans les tissus, la cystéamine diffuse à travers la membrane plasmique alors que le pantothénate dépend du transporteur multivitamine (B5, B6, acide lipoïque) sodium-dépendant (SMVT) (155,156). La régénération du coenzyme A à partir du pantothénate nécessite l'implication de plusieurs réactions dans le cytosol et dans la mitochondrie (150,157–159). Le pantothénate est phosphorylé par les pantothénate kinases PanK, puis couplé à une molécule de cystéine par la PPC, adénylé et enfin phosphorylé par les CoASY pour reformer le coenzyme A. Chaque passage de membrane à l'intérieur de la cellule nécessite également la conversion en différents intermédiaires (3'5'ADP, phosphopantéthine) car le coenzyme A ne traverse pas les membranes (150,157–159).

La Vanin1 est exprimée par toutes les cellules de l'organisme avec une prédominance dans le foie, l'intestin grêle et les tubules proximaux du rein. Elle est retrouvée sous forme soluble dans le sang. La Vanin1 est l'une des cibles de PPAR α et de PGC-1 α qui régulent en période de jeûne la consommation, l'utilisation et le catabolisme des acides gras et la biogenèse mitochondriale (160).

L'expression de la Vanin1 et les variations dans les niveaux des métabolites cystéamine et vitamine B5 ont fait l'objet de nombreuses études dans des contextes physiologiques et pathologiques.

Cette partie était complétée par la réalisation d'une revue soumise à European Journal of Immunology.

The vitamin B5 / coenzyme A axis: a target for immunomodulation?

Miallot R, Millet V, Galland F and Naquet P

Abstract

Coenzyme A serves as a vital cofactor in numerous enzymatic reactions involved in energy production, lipid metabolism, and the synthesis of essential molecules. Dysregulation of CoA-dependent metabolic pathways can contribute to chronic diseases such as obesity, diabetes, cancer, and cardiovascular disorders. Additionally, CoA influences immune cell activation by modulating the metabolism of these cells, thereby affecting their proliferation, differentiation, and effector functions. Targeting CoA metabolism presents a promising avenue for therapeutic intervention, as it can potentially restore metabolic balance, mitigate chronic inflammation, and enhance immune cell function. This might ultimately improve the management and outcomes for these diseases. This review will more specifically focus on the contribution of pathways regulating the availability of the coenzyme A precursor Vitamin B5/pantothenate *in vivo* and modulating the susceptibility to inflammatory diseases.

Introduction

Chronic diseases exert considerable environmental constraints on tissue and immune cells recruited on the site of damage. Cells must adapt their metabolic pathways to the available resources and to their functions. One key decision concerns the balance between anabolic and catabolic pathways, a process in which coenzyme A-dependent biochemical reactions play a major role. This review will focus on the contribution of pathways regulating the level of the coenzyme A precursor vitamin B5/pantothenate *in vivo* and their involvement in T lymphocyte activation and susceptibility to inflammatory diseases. Often considered as a non-limiting metabolite, recent studies revealed that VitB5 levels regulate CoA-dependent metabolism in stressed tissues, immune cell activation and condition the severity of several chronic inflammatory or degenerative diseases, including neurodegeneration, infection and cancer.

CoA homeostasis

Regulation of pantothenate/VitB5 supply

Under homeostatic conditions, CoA levels are maintained by the constant supply of the pantothenate (Pan) precursor. Pan originates from the processing of food-derived (acyl)-CoAs derivatives in the ileum (**Fig1**) [1]. Indeed, VitB5 is synthesized by plants, mushrooms and bacteria mostly [2]. Furthermore, absorbed CoA may also derive from Pan synthesis through endosymbiotic processes in the microbiota [3][4], or from maternal origin, as shown during fly development [5]. Pan is recycled in host tissues and its urinary excretion reflects dietary intake [6]. Since CoA cannot cross membranes, it needs to be degraded prior to cellular uptake. The initial steps rely on phosphatase activities present in the gut lumen or serum leading to the production of 4'-phosphopantetheine, which is hydrolyzed into Pan by pantetheinases [6], or possibly internalized by cells [7]. In cells, Pan is taken up through the sodium-dependent multivitamin transporter (SMVT) (**Fig1**).

Regulation of CoA synthesis

The intracellular concentrations of free or acyl CoAs are regulated by the rate of synthesis from Pan controlled by the pantothenate kinases (PANK) [8] (**Fig1**). The physiological evaluation of PANK deficient mice showed the importance of maintaining CoA concentration to support oxidative metabolism, ketone production and glucose homeostasis [9],[10]. Mice lacking Pank1 and/or 2 isoforms did not exhibit gross defects in anatomy, behavior or liver organization, but presented metabolic alterations affecting blood glucose and triglyceride levels upon adaptation to fasting [10]–[12]. Indeed, the AcCoA/CoA ratio is a central integrator of the balance between anabolism and catabolism [13]. CoA and acylated forms activate carboxylic acid substrates as thioesters for energy production, fatty acid oxidation (FAO), acetylcholine (Ach) synthesis [8] (**Fig2**). Cytosolic acetyl-CoA is a major acetate donor for acetylation reactions involved in the control of protein synthesis and gene expression [14],[15] (**Fig2**). In mammalian cell cultures, Pan increases glutathione (GSH) levels and cell respiration using pyruvate as exogenous substrate, suggesting that GSH synthesis is a consequence of ATP production [16]. PANK2 and PANK4 are also substrates of the PI3K effector kinase AKT8 [17] and the PI3K-PANK4 axis regulates CoA-dependent pathways involved in lipid metabolism and cell proliferation.

Regulation of CoA degradation

CoA levels also depend on intra- and extracellular degradation pathways controlled by the Nudix (NUDT) and Vanin (VNN) hydrolases, respectively [6]. NUDT are distributed in cell organelles and adjust subcellular (acyl)-CoA levels [18]. This process regenerates 4-phosphopantetheine but not Pan (**Fig1**). The hydrolysis of pantetheine into Pan requires a pantetheinase [19] encoded by *Vnn* genes [27]. These extracellular enzymes are present in serum (VNN1 and 3) or GPI-anchored at the cell membrane [22],[23] (VNN1 and VNN2 / GPI80). In tissues, VNN1 is highly expressed at the brush border of epithelial cells in the ileum, which represents the primary site of food-derived CoA degradation and VitB5 absorption [6], and in the proximal tubules of the kidney [24],[25]. In the colon, Vnn1 is not expressed under physiological conditions but induced upon PPAR- γ activation in the context of inflammation [25]. In fasted liver, VNN1 expression by hepatocytes is induced upon PPAR α -activation [26] and contributes to the response to fasting through modulation of fatty acid oxidation [25]. Accordingly, in cultured cells, a transient VitB5-starvation led to persistent PPAR α activation, improving cell viability by increasing resistance to stress [28]. In other tissues, VNN1 expression is modulated by oxidative, mitochondrial, metabolic or xenobiotic stresses [29]–[31]. More generally, an increase in pantetheinase levels will contribute to CoA recycling and tissue tolerance to stress [32].

Regulation of immunocyte activation by (acyl)CoAs

Regulation of CD4⁺ T helper cell activity

The contribution of VitB5 has been documented in CD4⁺ Th17 and CD8⁺ T lymphocytes, but much less for other hematopoietic populations. To acquire their functionality, activated lymphocytes undergo metabolic changes that involve CoA-dependent pathways [33],[34]. Th17 cells play an important homeostatic role in the control of barriers and, under inflammatory stress, can acquire pathogenic features that contribute to the progression of immune-mediated diseases such as colitis, multiple sclerosis (MS) or infectious diseases [35].

This metabolic adaptation relies on the differential use of carbon sources such as glucose, fatty acids or amino acids to support the acquisition of cellular programs. One study showed that the pathogenic potential of Th17 cells required enhanced GLUT3-dependent glycolysis, coupled to mitochondrial oxidation of pyruvate to citrate to enhance ACLY-dependent AcCoA generation and histone acetylation [36]. This epigenetic regulation increased the production of inflammatory cytokines such as IL-17, GM-CSF or IL-2, by CD4⁺ Th17 lymphocytes involved in the pathogenesis of experimental autoimmune encephalomyelitis (EAE) or colitis. A related study showed that this glycolytic shift associated with lactate production by lymphocytes was involved in the development of EAE [37] or non-alcoholic fatty liver disease (NAFLD)-mediated damage [38]. Mechanistically, the expression of the pyruvate kinase isoform M2 (PKM2) was enhanced in pathogenic CD4⁺ lymphocytes and associated with its nuclear translocation. There PKM2 acts as a transcriptional regulator for glycolytic and cytokine (IL-17, IL-21, TNF- α) gene expression [39]. PKM2 silencing impaired CD4⁺ T lymphocyte differentiation and reduced EAE progression by antagonizing the development of proinflammatory CXCR3⁺ Th17 lymphocytes [37]. Mechanistically, the differentiation of Th17 but not that of Th2 and Tregs cells was restrained by increased CoA concentration. CoA bound PKM2 and prevented its nuclear translocation and enhancement of STAT-3 phosphorylation, IL-17 production and HIF1 α -driven glycolysis (**Fig3**). Another report used a small-molecule PKM2 activator (named TEPP-46) that induced PKM2 tetramerization and also blocked its nuclear translocation [40]. TEPP-66 administration inhibited Th1 and Th17 polarization and EAE development *in vivo*. Interestingly, dietary Pan supplementation that enhances CoA levels, reduced the severity of experimental colitis or EAE. Furthermore, low serum VitB5 levels were documented in ulcerative colitis and multiple sclerosis patients [35]. These findings position the CoA/AcCoA ratio as a potential regulator of PKM2 activity and Th17 pathogenicity.

Regulation of CD8⁺ T cell activity

Tumors represent a metabolic challenge for effector CD8⁺ T lymphocytes where the competition for nutrients impairs the maintenance of their functions. Whereas quiescent naive and memory cells rely on OXPHOS for their persistence, effector T lymphocyte activation requires a glycolytic shift coupled to a transient increase in CoA-dependent mitochondrial activity. This process depends on the expression of the mitochondrial pyruvate carrier (MPC) that allows glucose-dependent mitochondrial AcCoA production (**Fig2**). CD8⁺ T cells lacking MPC were unable to acquire anti-tumor activity [41] and deviated towards memory cell differentiation. Under these conditions, glutamine and fatty acids became the main source of citrate, regenerating cytosolic AcCoA that sustained histone acetylation, lipid synthesis and memory cell survival [42]. Similarly, acetate released by an acute catabolic stress in infections or cancers could be reimported by memory CD8⁺ T cells to boost their recall responses [43],[44]. Other metabolites or cytokines influence the balance between effector versus memory functions. Lactate uptake and oxidation in the mitochondria could partially rescue CD8⁺ tumor infiltrating lymphocytes (TILs) from metabolic collapse and loss of effector functions. IL-12 was shown to boost glucose-derived citrate export in the cytoplasm contributing to enhanced IFN- γ production by CD8⁺ T cells in nutrient-deprived conditions [45]. Mitochondrial AcCoA could also be diverted towards ketogenesis and β -hydroxybutyrate production that contributed to the epigenetic acetylation of histone H3K9 [46]. This led to the upregulation of FoxO1, PGC1s and consequently Pck1 expression that enhanced the gluconeogenic and pentose phosphate pathways resulting in an improved redox control in memory cells (Fig2).

Several subsets of CD8⁺ T cells have been defined according to their polarization and cytokine profiles [47]. St Paul *et al* showed that glucose oxidation in the TCA cycle was the main driver of IL-22-secreting CD8⁺ T cell polarization (Tc22) [48]. Tc22 development required elevated OXPHOS but not FAO. Oligomycin treatment partially abolished IL-22 production but did not affect that of IFN- γ or IL-17 by CD8⁺ Tc1 or Tc17 cells. CoA concentration was higher in Tc22 than Tc1/17 cells and addition of exogenous CoA to cell cultures induced OXPHOS, succinate production and HIF1- α / AhR-dependent Tc22 polarization in the absence of the polarizing cytokines IL-6 and TNF- α . Importantly, Tc22 exerted a powerful cytotoxic activity against tumors and Pan supplementation exacerbated the response to anti-PDL1 immunotherapy in a melanoma model. Similarly, upon pantothenate administration to sarcoma-bearing mice, tumor growth was reduced through enhancement of anti-tumor immune responses [49]. Interestingly, melanoma patients with high pantothenate levels in serum showed better efficacy of anti-PD1 therapy. Nevertheless, another report showed that succinate accumulation could block effector CD4⁺ and CD8⁺ T cell functions by inhibiting the succinyl-CoA synthase activity and interrupting the TCA cycle [50]. All these studies indicate that the relative level of CoA and AcCoA modulates lymphocyte activation and maturation. It is therefore of interest to apply these notions to pharmacological strategies.

Contribution of the VNN pathway to CoA homeostasis in tissues

Vnn1 contributes to tissue homeostasis

Vnn genes code for various pantothenase isoforms [21]. With the exception of hepatocytes and specific epithelial cell subsets such as ileal enterocytes, proximal tubular cells in kidney or some endocrine cells [32], *Vnn1* expression is not detectable in tissues under homeostatic conditions. Two studies directly demonstrated that increased VNN1 expression enhanced CoA levels and changed disease phenotypes. First, VNN1 was shown to act as a tumor suppressor gene in sarcomas [30]. VNN1 expression in a sarcoma cell line reduced the Warburg phenotype and growth rate while maintaining tumor cell differentiation through the enhancement of CoA-dependent mitochondrial activity. Secondly, *Vnn1* expression is strongly induced on all colonocytes by microbiota-driven inflammation and is a hallmark of inflammatory bowel diseases (IBD) [51]. Importantly, *Vnn1* overexpression by gut colonocytes was associated with augmented Pan and CoA levels and contributed to the maintenance of protective cell functions such as the secretion of mucus or anti-microbial peptides [52]. VNN1 overexpression also induced a dysbiosis associated with increased butyrate production, the predominant short chain fatty acid required for CoA-dependent colonocyte energetics [53]. This combined phenotype affecting host cells and microbiota led to the restoration of mitochondrial activity, colonocyte fitness and viability [52]. Altogether, it reinforced the mucosal barrier and dampened colitis severity. A VNN1-mediated cytoprotective phenotype was also observed in a type 1 diabetes model [54]. Indeed, *Vnn1*-deficient nonobese diabetic (NOD) mouse showed enhanced islet cell β -cell death and susceptibility to diabetes. Therefore VNN1 contributes to tissue tolerance to stress through local and systemic Pan regeneration [32].

Vnn1 regulates the quality of immune responses in tissues

Other studies based on the use of *Vnn1*-deficient mice suggested that the behavior of immune cells might be affected by a limited supply in Pan. However, with the exception of neutrophils

and some human myeloid cell subsets that express VNN isoforms, hematopoietic cells generally do not express *Vnn1* [55]. In a systemic sclerosis (Ssc) model, *Vnn1* expression was induced on profibrotic myofibroblasts leading to elevated Pan serum levels, a phenotype also observed in patients developing a severe form of Ssc. *Vnn1* expression was also associated with high levels of anti-topoisomerase antibodies and Th2/17 cytokines that participate to the pathology, all disease-associated phenotypes being attenuated in *Vnn1*-deficient mice [56]. In infectious models, the presence of VNN1 was generally associated with enhanced immune cell reactivity. In *Coxiella burnetii* infection, VNN1 was required for the microbicidal competence of inflammatory macrophages and the development of granulomas in the liver [57]. In schistosomiasis, the presence of VNN1 was associated with increased intestinal tissue damage due to the increased recruitment of activated neutrophils [58]. Accordingly, in a model of *Mycobacterium tuberculosis* infection, VitB5 rather enhanced the production of inflammatory cytokines and macrophage phagocytic activity. *In vivo*, this resulted in increased CD4⁺ Th1 activation and a reduction in bacterial burden [59]. Although the mechanistic links between VNN1 expression and pathogenesis were not directly defined in all models, the presence of VNN1 in inflamed tissues was associated with an enhancement of immunocyte functions, being Th1- or Th2/Th17-oriented in infectious diseases and Ssc, respectively. These results suggest that the enhanced regeneration of VitB5 might be preferentially exploited by metabolically active cells present in the tissue, boosting their CoA-dependent metabolism.

Therapeutic applications

Isolated Pan deficiency results in dermatitis, metabolic imbalance, cardiac, neurological and gastrointestinal symptoms and a generalized malaise clinically [60],[61]. Cellular absorption of Pan requires SMVT that also mediates the internalization of biotin and lipoic acid [62]. Interestingly, mild cases of SMVT deficiency due to compound heterozygous variants in *SLC5A6* are responsible for metabolic or bone defects, anemia and immunodeficiency that could be rescued by biotin, Pan and lipoate substitution [63]. Historically, pantothenate supplementation has been used to enhance wound healing by increasing epithelial cell renewal and viability. This therapy is mostly efficient as a topical administration of dexpanthenol, a stable form of Pan [64]. Its administration is followed by increased skin repair and moisturization, keratinocyte proliferation and fibroblast activation (Table 1) [65]. Accordingly, Pan has a strong effect on skin cell proliferation [65],[66]. More recently, it was shown that it contributes to enhance hair follicle development and restoration of hair growth [66].

CoA homeostasis in brain diseases

VitB5 and related compounds can also contribute to the handling of genetic deficits in enzymes participating to CoA synthesis. PANK2 deficiency induces a neurodegenerative disease linked to reduced CoA levels in brain and some peripheral cells [7]. This disease could be controlled by the administration of an allosteric PANK activator [67] or possibly acetyl-4-phospho-pantetheine [68]. A cerebral deficiency in VitB5 has been observed in neurodegenerative disorders involving myelin loss such as Huntington's (HD) [69] and Alzheimer's (AD) diseases [70]. In rat brain, cerebral Pan was predominantly localized in myelin-containing structures where it might participate to the synthesis of fatty acids required for myelin production. Therefore, pantetheine supplementation experiments were tested in various models of neurodegenerative disease and generally led to an improvement of the

pathology. In a transgenic AD model, it reduced the symptoms of glial reactivity, amyloid- β deposition and inflammation [71] and in a Parkinson disease's (PD) model, it correlated with the enhanced production of ketone bodies, a process dependent on L-3-hydroxybutyryl-CoA dehydrogenase activity [72]. Interestingly, the aminothiols cysteamine (CEA) also exerted a cytoprotective effect in PD [73] and HD [74] models, through modulation of redox metabolism and detoxication pathways [75]. The last step of CoA synthesis depends on the CoA synthetase (COASY). COASY expression is upregulated during erythropoiesis and lost in patients with myelodysplastic syndrome and ring sideroblasts (MDS-RS). This is due to mutations in the splicing factor 3B subunit 1 (SF3B1) that lead to the mis-splicing of several genes including *coasy* [76]. Interestingly, VitB5 complementation increased CoA levels in *SF3B1*mut cells and corrected erythropoiesis differentiation defects in MDS-RS primary patient cells. Pan also regulates oxidative stress, a property exploited for ionizing therapy of tumors [77]. It potentiated a radiolytic effect following irradiation through the production of reactive oxygen species derived from VitB5. Similarly, serum VNN1 improved the redox status of erythrocytes and contributed to the tolerance to malaria. Some patients with complicated forms of malaria have reduced levels of serum pantetheinase [78] and pantethine administration could protect against mouse cerebral malaria [79].

CoA homeostasis in inflammatory diseases

Diseases involving a chronic immune activation expose to restricted access to several metabolites. As already evoked, colon homeostasis is particularly dependent upon VitB5 availability. A deficit in VitB5 was recently reported in the blood / feces of IBD patients [80],[81]; accordingly, pantethine administration enhanced intestinal barrier repair and fitness in part through restoration of butyrate levels in feces [52]. Fecal short chain fatty acid levels, reduced in IBD patients [82], could simultaneously enhance colonocyte energetics and exert immunomodulatory functions [83], in part through a propionate-mediated downmodulation of IL-17 and IL-22 production by $\gamma\delta$ T cells [84]. In addition, VitB5 contributes to the regulation of Th17 immunity in IBD [35]. In addition to Pan effect on host cells, infectious agents also require Pan to sustain their metabolic activity and inhibitors of microbial PANK enzymes, called pantothenamides, are considered as potential anti-infectious drugs in parasite, bacterial or fungal infections [85]–[91]. Finally, one could speculate that the link between Pan and inflammation might also involve ACh signaling. Indeed, mitochondrial acetyl CoA is required for ACh synthesis [92]. ACh participates to the vagal cholinergic and splenic sympathetic anti-inflammatory pathways [93],[94]. Enteric neurons stimulated by vagal efferent fibers and noradrenaline-stimulated splenic lymphocytes release ACh that, through binding to the α -7-nicotinic ACh receptors on macrophages, inhibits TNF- α release [95].

Conclusion

This review highlights recent findings showing the importance of CoA homeostasis in pathology. This process depends on enzymes regulating the rate of CoA synthesis and degradation. Evidence is provided that VitB5, called an anti-stress vitamin, can become a limiting metabolite under nutrient-deprived contexts most frequently found in chronic inflammatory or cancerous diseases. Modulation of the expression of pantetheinases or VitB5 complementation in diet provide cytoprotection for tissue cells, allow the maintenance of lymphocyte effector functions and contribute to their polarization and pathogenic potential. VitB5 levels in blood or tissues could serve as a prognostic biomarker in these pathologies.

Bibliography

1. **Said HM.** Intestinal absorption of water-soluble vitamins in health and disease. *Biochemical Journal*. 2011; **437**:357–372.DOI: 10.1042/BJ20110326.
2. **Coxon KM, Chakauya E, Ottenhof HH, Whitney HM, Blundell TL, Abell C, Smith AG.** Pantothenate biosynthesis in higher plants. *Biochemical Society Transactions*. 2005; **33**:743–746.DOI: 10.1042/BST0330743.
3. **Wilson ACC, Duncan RP.** Signatures of host/symbiont genome coevolution in insect nutritional endosymbioses. *Proc. Natl. Acad. Sci. U.S.A.* 2015; **112**:10255–10261.DOI: 10.1073/pnas.1423305112.
4. **Deng P, Valentino T, Flythe MD, Moseley HNB, Leachman JR, Morris AJ, Hennig B.** Untargeted Stable Isotope Probing of the Gut Microbiota Metabolome Using ¹³ C-Labeled Dietary Fibers. *J. Proteome Res.* 2021; **20**:2904–2913.DOI: 10.1021/acs.jproteome.1c00124.
5. **Yu Y, van der Zwaag M, Wedman JJ, Permentier H, Plomp N, Jia X, Kanon B, et al.** Coenzyme A precursors flow from mother to zygote and from microbiome to host. *Molecular Cell*. 2022; **82**:2650-2665.e12.DOI: 10.1016/j.molcel.2022.05.006.
6. **Naquet P, Kerr EW, Vickers SD, Leonardi R.** Regulation of coenzyme A levels by degradation: the 'Ins and Outs'. *Progress in Lipid Research*. 2020; **78**:101028.DOI: 10.1016/j.plipres.2020.101028.
7. **Jeong SY, Hogarth P, Placzek A, Gregory AM, Fox R, Zhen D, Hamada J, et al.** 4'-Phosphopantetheine corrects CoA, iron, and dopamine metabolic defects in mammalian models of PKAN. *EMBO Molecular Medicine*. 2019; **11**:e10489.DOI: 10.15252/emmm.201910489.
8. **Leonardi R, Zhang Y-M, Rock CO, Jackowski S.** Coenzyme A: Back in action. *Progress in Lipid Research*. 2005; **44**:125–153.DOI: 10.1016/j.plipres.2005.04.001.
9. **Zhang Y-M, Chohnan S, Virga KG, Stevens RD, Ilkayeva OR, Wenner BR, Bain JR, et al.** Chemical knockout of pantothenate kinase reveals the metabolic and genetic program responsible for hepatic coenzyme A homeostasis. *Chem Biol*. 2007; **14**:291–302.DOI: 10.1016/j.chembiol.2007.01.013.
10. **Leonardi R, Rehg JE, Rock CO, Jackowski S.** Pantothenate Kinase 1 Is Required to Support the Metabolic Transition from the Fed to the Fasted State. *PLOS ONE*. 2010; **5**:e111107.DOI: 10.1371/journal.pone.0011107.
11. **Garcia M, Leonardi R, Zhang Y-M, Rehg JE, Jackowski S.** Germline Deletion of Pantothenate Kinases 1 and 2 Reveals the Key Roles for CoA in Postnatal Metabolism Waki H, ed. *PLoS ONE*. 2012; **7**:e40871.DOI: 10.1371/journal.pone.0040871.
12. **Kuo Y-M, Duncan JL, Westaway SK, Yang H, Nune G, Xu EY, Hayflick SJ, et al.** Deficiency of pantothenate kinase 2 (Pank2) in mice leads to retinal degeneration and azoospermia. *Human Molecular Genetics*. 2005; **14**:49–57.DOI: 10.1093/hmg/ddi005.
13. **Pietrocola F, Galluzzi L, Bravo-San Pedro JM, Madeo F, Kroemer G.** Acetyl Coenzyme A: A Central Metabolite and Second Messenger. *Cell Metabolism*. 2015; **21**:805–821.DOI: 10.1016/j.cmet.2015.05.014.

14. **Sabari BR, Zhang D, Allis CD, Zhao Y.** Metabolic regulation of gene expression through histone acylations. *Nat Rev Mol Cell Biol.* 2017; **18**:90–101.DOI: 10.1038/nrm.2016.140.
15. **Fernandez-Fuente G, Rigby MJ, Puglielli L.** Intracellular Citrate/acetyl-CoA flux and endoplasmic reticulum acetylation: Connectivity is the answer. *Molecular Metabolism.* 2023; **67**:101653.DOI: 10.1016/j.molmet.2022.101653.
16. **Slyshenkov VS, Dymkowska D, Wojtczak L.** Pantothenic acid and pantothenol increase biosynthesis of glutathione by boosting cell energetics. *FEBS Letters.* 2004; **569**:169–172.DOI: 10.1016/j.febslet.2004.05.044.
17. **Dibble CC, Barritt SA, Perry GE, Lien EC, Geck RC, DuBois-Coyne SE, Bartee D, et al.** PI3K drives the de novo synthesis of coenzyme A from vitamin B5. *Nature.* 2022; **608**:192–198.DOI: 10.1038/s41586-022-04984-8.
18. **Vickers SD, Shumar SA, Saporito DC, Kunovac A, Hathaway QA, Mintmier B, King JA, et al.** NUDT7 regulates total hepatic CoA levels and the composition of the intestinal bile acid pool in male mice fed a Western diet. *J Biol Chem.* 2022; **299**:102745.DOI: 10.1016/j.jbc.2022.102745.
19. **Wittwer CT, Schweitzer C, Pearson J, Song WO, Windham CT, Wyse BW, Hansen RG.** Enzymes for liberation of pantothenic acid in blood: use of plasma pantetheinase. *Am J Clin Nutr.* 1989; **50**:1072–1078.DOI: 10.1093/ajcn/50.5.1072.
21. **Granjeaud S, Naquet P, Galland F.** An ESTs description of the new Vanin gene family conserved from fly to human. *Immunogenetics.* 1999; **49**:964–972.DOI: 10.1007/s002510050580.
22. **Aurrand-Lions M, Galland F, Bazin H, Zakharyev VM, Imhof BA, Naquet P.** Vanin-1, a Novel GPI-Linked Perivascular Molecule Involved in Thymus Homing. *Immunity.* 1996; **5**:391–405.DOI: 10.1016/S1074-7613(00)80496-3.
23. **Nitto T, Inoue T, Node K.** Alternative spliced variants in the pantetheinase family of genes expressed in human neutrophils. *Gene.* 2008; **426**:57–64.DOI: 10.1016/j.gene.2008.08.019.
24. **Pitari G, Malergue F, Martin F, Philippe JM, Massucci MT, Chabret C, Maras B, et al.** Pantetheinase activity of membrane-bound Vanin-1: lack of free cysteamine in tissues of Vanin-1 deficient mice. *FEBS Letters.* 2000; **483**:149–154.DOI: 10.1016/S0014-5793(00)02110-4.
25. **Berruyer C, Pouyet L, Millet V, Martin FM, LeGoffic A, Canonici A, Garcia S, et al.** Vanin-1 licenses inflammatory mediator production by gut epithelial cells and controls colitis by antagonizing peroxisome proliferator-activated receptor γ activity. *Journal of Experimental Medicine.* 2006; **203**:2817–2827.DOI: 10.1084/jem.20061640.
26. **Rommelaere S, Millet V, Gensollen T, Bourges C, Eeckhoutte J, Hennuyer N, Baugé E, et al.** PPARalpha regulates the production of serum Vanin-1 by liver. *FEBS Letters.* 2013; **587**:3742–3748.DOI: 10.1016/j.febslet.2013.09.046.
27. **van Diepen JA, Jansen PA, Ballak DB, Hijmans A, Hooiveld GJ, Rommelaere S, Galland F, et al.** PPAR-alpha dependent regulation of vanin-1 mediates hepatic lipid metabolism. *J Hepatol.* 2014; **61**:366–372.DOI: 10.1016/j.jhep.2014.04.013.

28. **Pourcel L, Buron F, Garcia F, Delaloix M-S, Le Fourn V, Girod P-A, Mermoud N.** Transient vitamin B5 starving improves mammalian cell homeostasis and protein production. *Metabolic Engineering*. 2020; **60**:77–86.DOI: 10.1016/j.ymben.2020.03.008.
29. **Berruyer C, Martin FM, Castellano R, Macone A, Malergue F, Garrido-Urbani S, Millet V, et al.** Vanin-1 Δ/Δ Mice Exhibit a Glutathione-Mediated Tissue Resistance to Oxidative Stress. *MOL. CELL. BIOL.* 2004; **24**.
30. **Giessner C, Millet V, Mostert KJ, Gensollen T, Vu Manh T-P, Garibal M, Dieme B, et al.** Vnn1 pantetheinase limits the Warburg effect and sarcoma growth by rescuing mitochondrial activity. *Life Sci. Alliance*. 2018; **1**:e201800073.DOI: 10.26508/lisa.201800073.
31. **Ferreira DW, Goedken MJ, Rommelaere S, Chasson L, Galland F, Naquet P, Manautou JE.** Enhanced hepatotoxicity by acetaminophen in Vanin-1 knockout mice is associated with deficient proliferative and immune responses. *Biochimica et Biophysica Acta (BBA) - Molecular Basis of Disease*. 2016; **1862**:662–669.DOI: 10.1016/j.bbadis.2016.02.001.
32. **Naquet P, Pitari G, Duprè S, Galland F.** Role of the Vnn1 pantetheinase in tissue tolerance to stress. *Biochemical Society Transactions*. 2014; **42**:1094–1100.DOI: 10.1042/BST20140092.
33. **Klein Geltink RI, Kyle RL, Pearce EL.** Unraveling the Complex Interplay Between T Cell Metabolism and Function. *Annu. Rev. Immunol.* 2018; **36**:461–488.DOI: 10.1146/annurev-immunol-042617-053019.
34. **Wang A, Luan HH, Medzhitov R.** An evolutionary perspective on immunometabolism. *Science*. 2019; **363**:aar3932.DOI: 10.1126/science.aar3932.
35. **Chen C, Zhang W, Zhou T, Liu Q, Han C, Huang Z, Chen S, et al.** Vitamin B5 rewires Th17 cell metabolism via impeding PKM2 nuclear translocation. *Cell Reports*. 2022; **41**. Available at: [https://www.cell.com/cell-reports/abstract/S2211-1247\(22\)01619-9](https://www.cell.com/cell-reports/abstract/S2211-1247(22)01619-9) [Accessed January 17, 2023].DOI: 10.1016/j.celrep.2022.111741.
36. **Hochrein SM, Wu H, Eckstein M, Arrigoni L, Herman JS, Schumacher F, Gerecke C, et al.** The glucose transporter GLUT3 controls T helper 17 cell responses through glycolytic-epigenetic reprogramming. *Cell Metabolism*. 2022; **34**:516-532.e11.DOI: 10.1016/j.cmet.2022.02.015.
37. **Kono M, Maeda K, Stocton-Gavanescu I, Pan W, Umeda M, Katsuyama E, Burbano C, et al.** Pyruvate kinase M2 is requisite for Th1 and Th17 differentiation. *JCI Insight*. 2019; **4**. Available at: <https://insight.jci.org/articles/view/127395> [Accessed January 18, 2023].DOI: 10.1172/jci.insight.127395.
38. **Moreno-Fernandez ME, Giles DA, Oates JR, Chan CC, Damen MSMA, Doll JR, Stankiewicz TE, et al.** PKM2-dependent metabolic skewing of hepatic Th17 cells regulates pathogenesis of non-alcoholic fatty liver disease. *Cell Metabolism*. 2021; **33**:1187-1204.e9.DOI: 10.1016/j.cmet.2021.04.018.
39. **Jiang S.** Tetrameric PKM2 Activation Curbs CD4+ T Cell Overactivation. *Trends in Endocrinology & Metabolism*. 2020; **31**:393–395.DOI: 10.1016/j.tem.2020.04.001.
40. **Angiari S, Runtsch MC, Sutton CE, Palsson-McDermott EM, Kelly B, Rana N, Kane H, et al.** Pharmacological Activation of Pyruvate Kinase M2 Inhibits CD4+ T Cell Pathogenicity and Suppresses Autoimmunity. *Cell Metabolism*. 2020; **31**:391-405.e8.DOI: 10.1016/j.cmet.2019.10.015.

41. **Wenes M, Jaccard A, Wyss T, Maldonado-Pérez N, Teoh ST, Lepez A, Renaud F, et al.** The mitochondrial pyruvate carrier regulates memory T cell differentiation and antitumor function. *Cell Metab.* 2022; **34**:731-746.e9.DOI: 10.1016/j.cmet.2022.03.013.
42. **Lee J, Walsh MC, Hoehn KL, James DE, Wherry EJ, Choi Y.** Regulator of fatty acid metabolism, acetyl coenzyme a carboxylase 1, controls T cell immunity. *J Immunol.* 2014; **192**:3190–3199.DOI: 10.4049/jimmunol.1302985.
43. **Balmer ML, Ma EH, Bantug GR, Grählert J, Pfister S, Glatter T, Jauch A, et al.** Memory CD8(+) T Cells Require Increased Concentrations of Acetate Induced by Stress for Optimal Function. *Immunity.* 2016; **44**:1312–1324.DOI: 10.1016/j.immuni.2016.03.016.
44. **Qiu J, Villa M, Sanin DE, Buck MD, O’Sullivan D, Ching R, Matsushita M, et al.** Acetate Promotes T Cell Effector Function during Glucose Restriction. *Cell Reports.* 2019; **27**:2063-2074.e5.DOI: 10.1016/j.celrep.2019.04.022.
45. **Chowdhury S, Kar A, Bhowmik D, Gautam A, Basak D, Sarkar I, Ghosh P, et al.** Intracellular Acetyl CoA Potentiates the Therapeutic Efficacy of Antitumor CD8+ T Cells. *Cancer Res.* 2022; **82**:2640–2655.DOI: 10.1158/0008-5472.CAN-21-4052.
46. **Zhang H, Tang K, Ma J, Zhou L, Liu J, Zeng L, Zhu L, et al.** Ketogenesis-generated β -hydroxybutyrate is an epigenetic regulator of CD8+ T-cell memory development. *Nat Cell Biol.* 2020; **22**:18–25.DOI: 10.1038/s41556-019-0440-0.
47. **Paul MS, Ohashi PS.** The Roles of CD8+ T Cell Subsets in Antitumor Immunity. *Trends in Cell Biology.* 2020; **30**:695–704.DOI: 10.1016/j.tcb.2020.06.003.
48. **St. Paul M, Saibil SD, Han S, Israni-Winger K, Lien SC, Laister RC, Sayad A, et al.** Coenzyme A fuels T cell anti-tumor immunity. *Cell Metabolism.* 2021; **33**:2415-2427.e6.DOI: 10.1016/j.cmet.2021.11.010.
49. Anon. The coenzyme A precursor pantethine restrains sarcoma growth through promotion of type 1 immunity. 2022. Available at: <https://www.researchsquare.com> [Accessed January 17, 2023].DOI: 10.21203/rs.3.rs-2345803/v1.
50. **Gudgeon N, Munford H, Bishop EL, Hill J, Fulton-Ward T, Bending D, Roberts J, et al.** Succinate uptake by T cells suppresses their effector function via inhibition of mitochondrial glucose oxidation. *Cell Reports.* 2022; **40**. Available at: [https://www.cell.com/cell-reports/abstract/S2211-1247\(22\)01010-5](https://www.cell.com/cell-reports/abstract/S2211-1247(22)01010-5) [Accessed January 16, 2023].DOI: 10.1016/j.celrep.2022.111193.
51. **Gensollen T, Bourges C, Rihet P, Rostan A, Millet V, Noguchi T, Bourdon V, et al.** Functional Polymorphisms in the Regulatory Regions of the VNN1 Gene Are Associated with Susceptibility to Inflammatory Bowel Diseases: *Inflammatory Bowel Diseases.* 2013; **19**:2315–2325.DOI: 10.1097/MIB.0b013e3182a32b03.
52. **Millet V, Gensollen T, Maltese M, Serrero M, Lesavre N, Bourges C, Pitaval C, et al.** Harnessing the Vnn1 pantetheinase pathway boosts short chain fatty acids production and mucosal protection in colitis. *Gut.* 2022. Available at: <https://gut.bmj.com.proxy.insermbiblio.inist.fr/content/early/2022/09/29/gutjnl-2021-325792> [Accessed October 24, 2022].DOI: 10.1136/gutjnl-2021-325792.

53. **Donohoe DR, Garge N, Zhang X, Sun W, O'Connell TM, Bunger MK, Bultman SJ.** The microbiome and butyrate regulate energy metabolism and autophagy in the mammalian colon. *Cell Metab.* 2011; **13**:517–526. DOI: 10.1016/j.cmet.2011.02.018.
54. **Roisin-Bouffay C, Castellano R, Valéro R, Chasson L, Galland F, Naquet P.** Mouse vanin-1 is cytoprotective for islet beta cells and regulates the development of type 1 diabetes. *Diabetologia.* 2008; **51**:1192–1201. DOI: 10.1007/s00125-008-1017-9.
55. **Nitto T, Onodera K.** The Linkage Between Coenzyme A Metabolism and Inflammation: Roles of Pantetheinase. *J Pharmacol Sci.* 2013; **123**:1–8. DOI: 10.1254/jphs.13R01CP.
56. **Kavian N, Mehlal S, Marut W, Servettaz A, Giessner C, Bourges C, Nicco C, et al.** Imbalance of the Vanin-1 Pathway in Systemic Sclerosis. *The Journal of Immunology.* 2016; **197**:3326–3335. DOI: 10.4049/jimmunol.1502511.
57. **Meghari S, Berruyer C, Lepidi H, Galland F, Naquet P, Mege J-L.** Vanin-1 controls granuloma formation and macrophage polarization in *Coxiella burnetii* infection. *European Journal of Immunology.* 2007; **37**:24–32. DOI: 10.1002/eji.200636054.
58. **Martin F, Penet M-F, Malergue F, Lepidi H, Dessein A, Galland F, Reggi M de, et al.** Vanin-1^{-/-} mice show decreased NSAID- and *Schistosoma*-induced intestinal inflammation associated with higher glutathione stores. *J Clin Invest.* 2004; **113**:591–597. DOI: 10.1172/JCI19557.
59. **He W, Hu S, Du X, Wen Q, Zhong X-P, Zhou X, Zhou C, et al.** Vitamin B5 Reduces Bacterial Growth via Regulating Innate Immunity and Adaptive Immunity in Mice Infected with *Mycobacterium tuberculosis*. *Frontiers in Immunology.* 2018; **9**. Available at: <https://www.frontiersin.org/articles/10.3389/fimmu.2018.00365> [Accessed January 17, 2023].
60. **Depeint F, Bruce WR, Shangari N, Mehta R, O'Brien PJ.** Mitochondrial function and toxicity: Role of the B vitamin family on mitochondrial energy metabolism. *Chemico-Biological Interactions.* 2006; **163**:94–112. DOI: 10.1016/j.cbi.2006.04.014.
61. **Rébeillé F, Ravanel S, Marquet A, Mendel RR, Smith AG, Warren MJ.** Roles of vitamins B5, B8, B9, B12 and molybdenum cofactor at cellular and organismal levels. *Nat. Prod. Rep.* 2007; **24**:949. DOI: 10.1039/b703104c.
62. **Prasad PD, Ganapathy V.** Structure and function of mammalian sodium-dependent multivitamin transporter. *Curr Opin Clin Nutr Metab Care.* 2000; **3**:263–266. DOI: 10.1097/00075197-200007000-00004.
63. **Holling T, Nampoothiri S, Tarhan B, Schneeberger PE, Vinayan KP, Yesodharan D, Roy AG, et al.** Novel biallelic variants expand the SLC5A6-related phenotypic spectrum. *Eur J Hum Genet.* 2022; **30**:439–449. DOI: 10.1038/s41431-021-01033-2.
64. **Proksch E, de Bony R, Trapp S, Boudon S.** Topical use of dexpanthenol: a 70th anniversary article. *Journal of Dermatological Treatment.* 2017; **28**:766–773. DOI: 10.1080/09546634.2017.1325310.
65. **Björklund S, Pham QD, Jensen LB, Knudsen NØ, Nielsen LD, Ekelund K, Ruzgas T, et al.** The effects of polar excipients transcutol and dexpanthenol on molecular mobility, permeability, and electrical impedance of the skin barrier. *Journal of Colloid and Interface Science.* 2016; **479**:207–220. DOI: 10.1016/j.jcis.2016.06.054.

66. **Shin JY, Kim J, Choi Y-H, Kang N-G, Lee S.** Dexpanthenol Promotes Cell Growth by Preventing Cell Senescence and Apoptosis in Cultured Human Hair Follicle Cells. *Current Issues in Molecular Biology*. 2021; **43**:1361–1373.DOI: 10.3390/cimb43030097.
67. **Sharma LK, Subramanian C, Yun M-K, Frank MW, White SW, Rock CO, Lee RE, et al.** A therapeutic approach to pantothenate kinase associated neurodegeneration. *Nat Commun*. 2018; **9**:4399.DOI: 10.1038/s41467-018-06703-2.
68. **Srinivasan B, Baratashvili M, van der Zwaag M, Kanon B, Colombelli C, Lambrechts RA, Schaap O, et al.** Extracellular 4'-phosphopantetheine is a source for intracellular coenzyme A synthesis. *Nat Chem Biol*. 2015; **11**:784–792.DOI: 10.1038/nchembio.1906.
69. **Ismail N, Kureishy N, Church SJ, Scholefield M, Unwin RD, Xu J, Patassini S, et al.** Vitamin B5 (d-pantothenic acid) localizes in myelinated structures of the rat brain: Potential role for cerebral vitamin B5 stores in local myelin homeostasis. *Biochemical and Biophysical Research Communications*. 2020; **522**:220–225.DOI: 10.1016/j.bbrc.2019.11.052.
70. **Xu J, Patassini S, Begley P, Church S, Waldvogel HJ, Faull RLM, Unwin RD, et al.** Cerebral deficiency of vitamin B5 (d-pantothenic acid; pantothenate) as a potentially-reversible cause of neurodegeneration and dementia in sporadic Alzheimer's disease. *Biochemical and Biophysical Research Communications*. 2020; **527**:676–681.DOI: 10.1016/j.bbrc.2020.05.015.
71. **Baranger K, van Gijssel-Bonnello M, Stephan D, Carpentier W, Rivera S, Khrestchatisky M, Gharib B, et al.** Long-Term Pantethine Treatment Counteracts Pathologic Gene Dysregulation and Decreases Alzheimer's Disease Pathogenesis in a Transgenic Mouse Model. *Neurotherapeutics*. 2019; **16**:1237–1254.DOI: 10.1007/s13311-019-00754-z.
72. **Cornille E, Abou-Hamdan M, Khrestchatisky M, Nieoullon A, de Reggi M, Gharib B.** Enhancement of L-3-hydroxybutyryl-CoA dehydrogenase activity and circulating ketone body levels by pantethine. Relevance to dopaminergic injury. *BMC Neurosci*. 2010; **11**:51.DOI: 10.1186/1471-2202-11-51.
73. **Cisbani G, Drouin-Ouellet J, Gibrat C, Saint-Pierre M, Lagacé M, Badrinarayanan S, Lavallée-Bourget MH, et al.** Cystamine/cysteamine rescues the dopaminergic system and shows neurorestorative properties in an animal model of Parkinson's disease. *Neurobiology of Disease*. 2015; **82**:430–444.DOI: 10.1016/j.nbd.2015.07.012.
74. **Borrell-Pages M.** Cystamine and cysteamine increase brain levels of BDNF in Huntington disease via HSP1b and transglutaminase. *Journal of Clinical Investigation*. 2006; **116**:1410–1424.DOI: 10.1172/JCI27607.
75. **Paul BD, Snyder SH.** Therapeutic Applications of Cysteamine and Cystamine in Neurodegenerative and Neuropsychiatric Diseases. *Front. Neurol*. 2019; **10**:1315.DOI: 10.3389/fneur.2019.01315.
76. **Mian SA, Philippe C, Maniati E, Protopapa P, Bergot T, Piganeau M, Nemkov T, et al.** Vitamin B5 and succinyl-CoA improve ineffective erythropoiesis in *SF3B1* -mutated myelodysplasia. *Sci. Transl. Med*. 2023; **15**:eabn5135.DOI: 10.1126/scitranslmed.abn5135.
77. **Schittl H, Getoff N.** Radiation-Induced Antitumor Properties of Vitamin B₅ (Pantothenic Acid) and its Effect on Mitomycin C Activity: Experiments In Vitro. *oncol res*. 2006; **16**:389–394.DOI: 10.3727/000000006783980919.

78. **Rommelaere S, Millet V, Rihet P, Atwell S, Helfer E, Chasson L, Beaumont C, et al.** Serum Pantetheinase/Vanin Levels Regulate Erythrocyte Homeostasis and Severity of Malaria. *The American Journal of Pathology*. 2015; **185**:3039–3052.DOI: 10.1016/j.ajpath.2015.07.011.
79. **Penet M-F, Abou-Hamdan M, Coltel N, Cornille E, Grau GE, de Reggi M, Gharib B.** Protection against cerebral malaria by the low-molecular-weight thiol pantethine. *Proc. Natl. Acad. Sci. U.S.A.* 2008; **105**:1321–1326.DOI: 10.1073/pnas.0706867105.
80. **Santorù ML, Piras C, Murgia A, Palmas V, Camboni T, Liggi S, Ibba I, et al.** Cross sectional evaluation of the gut-microbiome metabolome axis in an Italian cohort of IBD patients. *Sci Rep*. 2017; **7**:9523.DOI: 10.1038/s41598-017-10034-5.
81. **IBDMDB Investigators, Lloyd-Price J, Arze C, Ananthakrishnan AN, Schirmer M, Avila-Pacheco J, Poon TW, et al.** Multi-omics of the gut microbial ecosystem in inflammatory bowel diseases. *Nature*. 2019; **569**:655–662.DOI: 10.1038/s41586-019-1237-9.
82. **Parada Venegas D, De la Fuente MK, Landskron G, González MJ, Quera R, Dijkstra G, Harmsen HJM, et al.** Short Chain Fatty Acids (SCFAs)-Mediated Gut Epithelial and Immune Regulation and Its Relevance for Inflammatory Bowel Diseases. *Front. Immunol.* 2019; **10**:277.DOI: 10.3389/fimmu.2019.00277.
83. **Siddiqui MT, Cresci GAM.** The Immunomodulatory Functions of Butyrate. *J Inflamm Res*. 2021; **14**:6025–6041.DOI: 10.2147/JIR.S300989.
84. **Dupraz L, Magniez A, Rolhion N, Richard ML, Da Costa G, Touch S, Mayeur C, et al.** Gut microbiota-derived short-chain fatty acids regulate IL-17 production by mouse and human intestinal $\gamma\delta$ T cells. *Cell Reports*. 2021; **36**:109332.DOI: 10.1016/j.celrep.2021.109332.
85. **Dietl A-M, Meir Z, Shadkchan Y, Osheroov N, Haas H.** Riboflavin and pantothenic acid biosynthesis are crucial for iron homeostasis and virulence in the pathogenic mold *Aspergillus fumigatus*. *Virulence*. 2018; **9**:1036–1049.DOI: 10.1080/21505594.2018.1482181.
86. **van Wyk M, Strauss E.** Development of a method for the parallel synthesis and purification of N-substituted pantothenamides, known inhibitors of coenzyme A biosynthesis and utilization. *Org. Biomol. Chem*. 2008; **6**:4348.DOI: 10.1039/b811086g.
87. **Akinnusi TO, Vong K, Auclair K.** Geminal dialkyl derivatives of N-substituted pantothenamides: Synthesis and antibacterial activity. *Bioorganic & Medicinal Chemistry*. 2011; **19**:2696–2706.DOI: 10.1016/j.bmc.2011.02.053.
88. **Spry C, Chai CLL, Kirk K, Saliba KJ.** A Class of Pantothenic Acid Analogs Inhibits *Plasmodium falciparum* Pantothenate Kinase and Represses the Proliferation of Malaria Parasites. *Antimicrob Agents Chemother*. 2005; **49**:4649–4657.DOI: 10.1128/AAC.49.11.4649-4657.2005.
89. **Pett HE, Jansen PA, Hermkens PH, Botman PN, Beuckens-Schortinghuis CA, Blaauw RH, Graumans W, et al.** Novel pantothenate derivatives for anti-malarial chemotherapy. *Malar J*. 2015; **14**:169.DOI: 10.1186/s12936-015-0673-8.
90. **Gihaz S, Gareiss P, Choi J-Y, Renard I, Pal AC, Surovsteva Y, Chiu JE, et al.** High-resolution crystal structure and chemical screening reveal pantothenate kinase as a new target for antifungal development. *Structure*. 2022; **30**:1494-1507.e6.DOI: 10.1016/j.str.2022.09.001.

91. **de Vries LE, Lunghi M, Krishnan A, Kooij TWA, Soldati-Favre D.** Pantothenate and CoA biosynthesis in Apicomplexa and their promise as antiparasitic drug targets Mitchell AP, ed. *PLoS Pathog.* 2021; **17**:e1010124.DOI: 10.1371/journal.ppat.1010124.
92. **Jope RS, Jenden DJ.** The Utilization of Choline and Acetyl Coenzyme A for the Synthesis of Acetylcholine. *J Neurochem.* 1980; **35**:318–325.DOI: 10.1111/j.1471-4159.1980.tb06267.x.
93. **Cox MA, Bassi C, Saunders ME, Nechanitzky R, Morgado-Palacin I, Zheng C, Mak TW.** Beyond neurotransmission: acetylcholine in immunity and inflammation. *J Intern Med.* 2020; **287**:120–133.DOI: 10.1111/joim.13006.
94. **Bonaz B, Sinniger V, Pellissier S.** Anti-inflammatory properties of the vagus nerve: potential therapeutic implications of vagus nerve stimulation: Anti-inflammatory effect of vagus nerve stimulation. *J Physiol.* 2016; **594**:5781–5790.DOI: 10.1113/JP271539.
95. **Wang H, Yu M, Ochani M, Amella CA, Tanovic M, Susarla S, Li JH, et al.** Nicotinic acetylcholine receptor $\alpha 7$ subunit is an essential regulator of inflammation. *Nature.* 2003; **421**:384–388.DOI: 10.1038/nature01339.

Figure 1

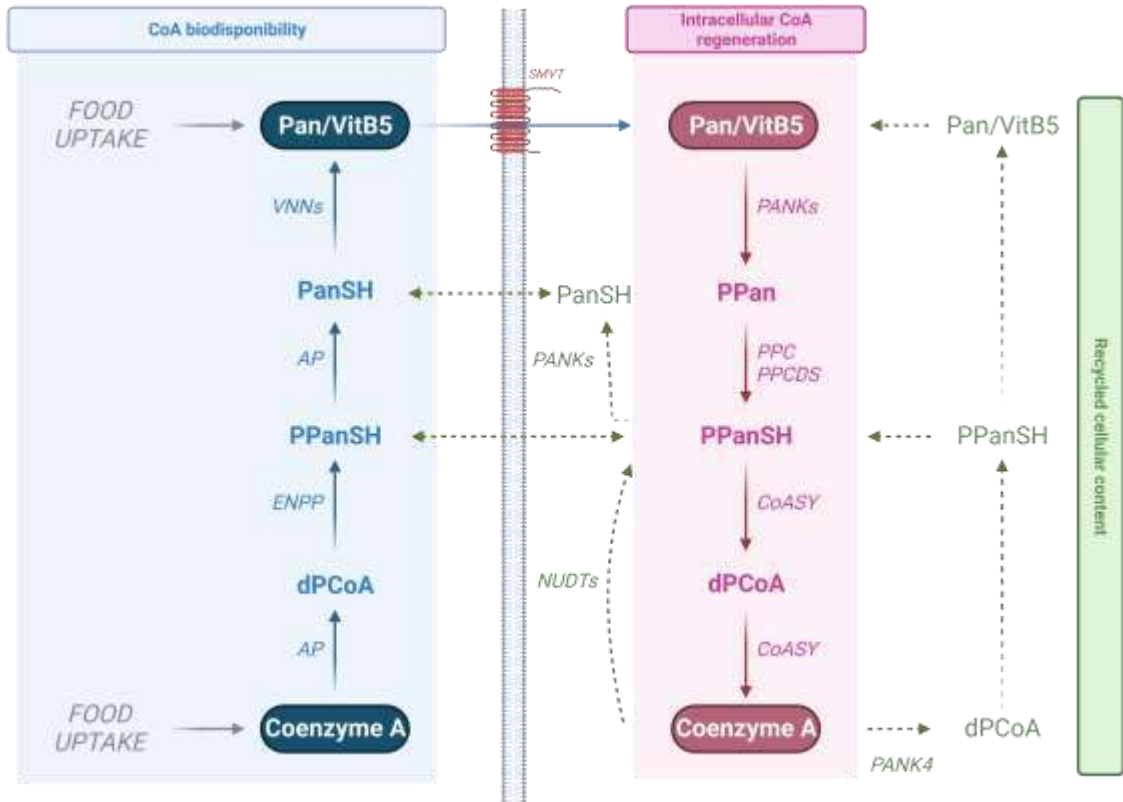


Figure 1 : Schematic overview of CoA biodisponibility, intracellular regeneration and recycled cellular content

Coenzyme A (CoA) and pantothenate (PAN) are provided by food uptake (Fig1A). CoenzymeA cannot cross the plasma membrane and is converted towards Pan via several enzymatic reactions involving AP, alkaline phosphatase; ENPP, ectonucleotide pyrophosphatase/phosphodiesterase and vanin hydrolases (Vnn). Subsequently, the Coenzyme A is converted to diphosphocoenzyme A (dPCoA), phosphopantetheine (PPanSh) and pantetheine. Pantetheine is hydrolyzed by Vnns enzymes into Pan and cysteamine (not shown). Intracellular Coenzyme A regeneration from pantothenate requires the phosphorylation of Pan by pantothenate kinases (PANK). Phosphopantothenoylcysteine synthetase (PPCS) and phosphopantothenoylcysteine decarboxylase (PPCDC) with coenzyme A synthase (CoASY) convert Phosphopantothenate (Ppan) into PPanSh, dPCoA and CoA. The recycled cellular content of intracellular CoA involves Nudix hydrolases (NUDT) enzymes and PANKs. SMVT : sodium pyruvate multitransporter.

Figure2

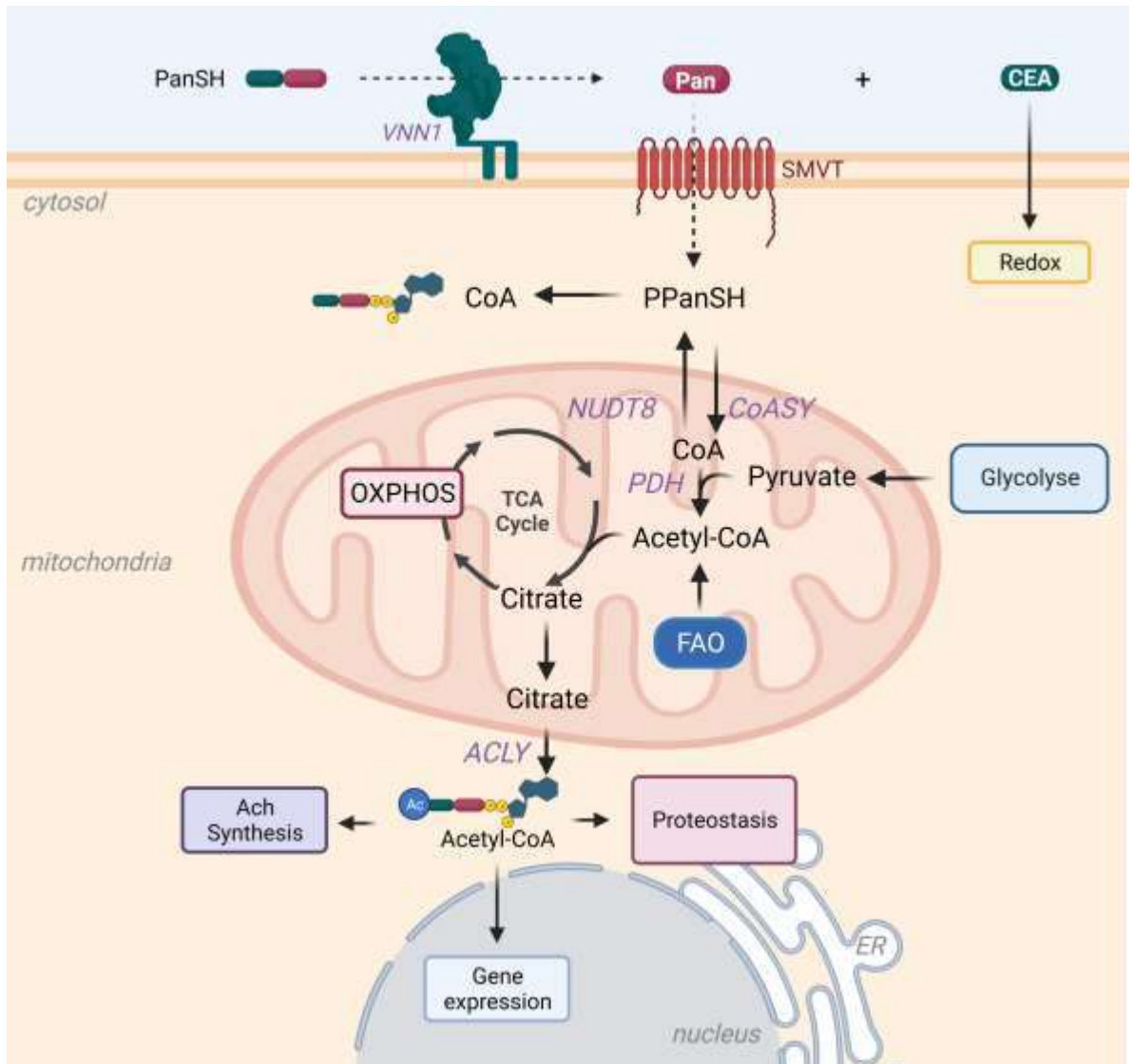


Figure 2: Schematic overview of CoA in intracellular contribution to cell processes.

B. CEA can cross the plasma membrane and regulate Redox intracellular processes. PPanSH can cross organelle membranes as mitochondrial membranes and fuels the tricarboxylic cycle (TCA cycle). TCA cycle-derived citrate can be converted by ATP Citrate Lyase (ACLY) towards Acetyl-CoA. AcetylCoA is required for Acetylcholine (Ach) synthesis, gene expression regulation in the nucleus or proteostasis in the endoplasmic reticulum (E.R). ATP : adenosine triphosphate ; ADP : adenosine diphosphate; FAO : fatty acid oxidation ; OXPHOS : oxidative phosphorylation ; VNN1 : Vanin1. PDH : pyruvate déshydrogénase. SMVT : sodium pyruvate multitransporter.

Figure 3

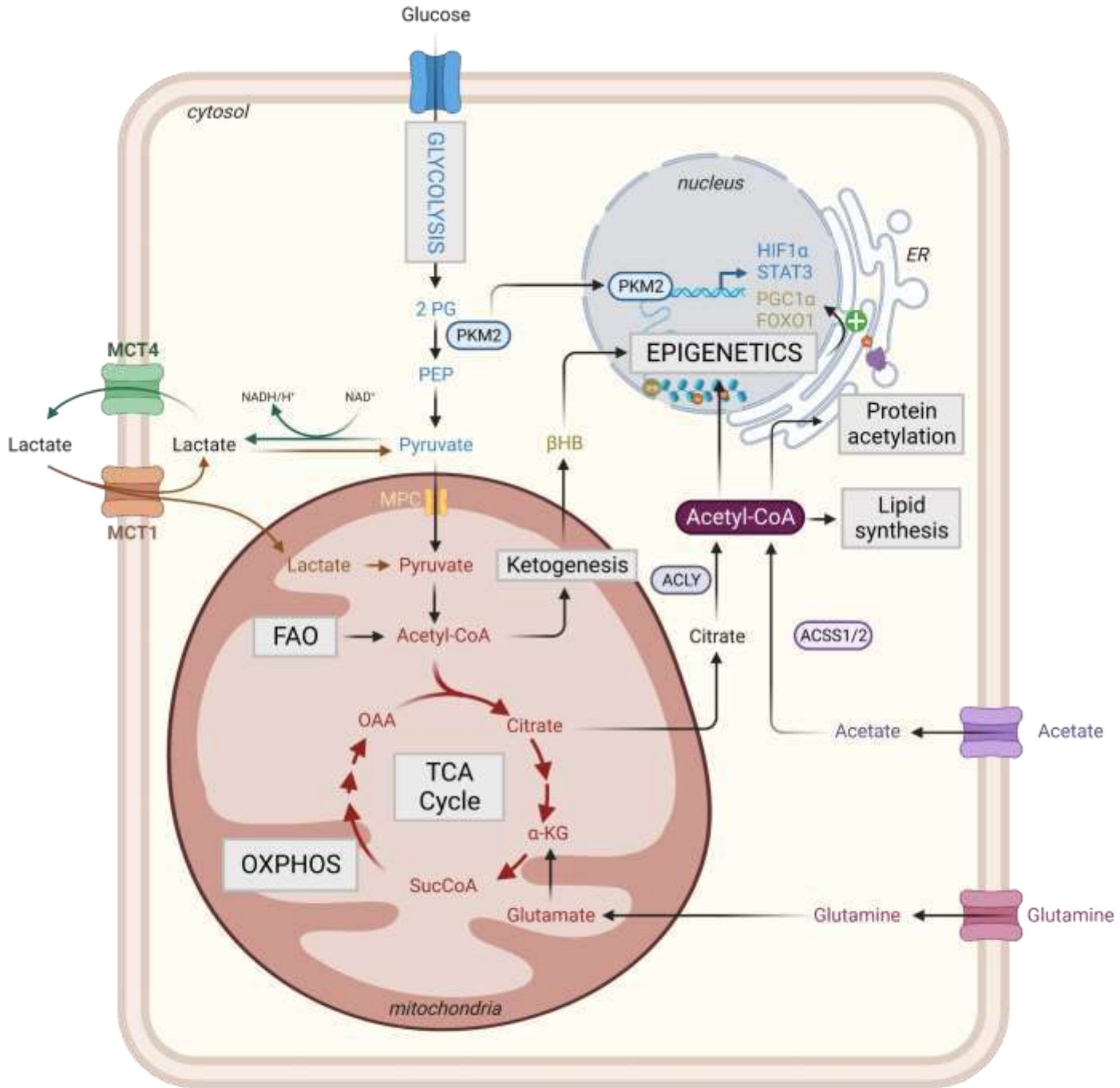


Figure 3: Involvement of CoA in intracellular processes during immune cell activation and maturation

VitB5 interaction with the glycolytic enzyme pyruvate kinase muscle isozyme 2 (PKM2) prevents its nuclear translocation resulting in the reduced transcription of downstream target genes. Lactate exchange via monocarboxylate transporters (MCT) regenerate cytosolic and mitochondrial pyruvate. Acetyl-CoA generated from pyruvate, fatty acids or lactate fuels the TCA cycle or participates to ketogenesis. β-hydroxybutyrate (βH) contributes to epigenetic regulation. Citrate and acetate can participate to epigenetic reprogramming through the generation of cytosolic acetyl-CoA. 2PG : 2phosphoglycerate; PEP: phosphoenolpyruvate; NAD : Nicotinamide adenine dinucleotide; OAA: oxaloacetate; SucCoA : succinylCoA; α-KG : alpha ketoglutarate; ACLY : ATP citrate lyase; ACSS : Acetyl-CoA synthetase. MPC : mitochondrial pyruvate carrier.

Table 1 : Pharmaceutical perspective of VitB5-related drugs

Drug	Admin. type	Mechanism of action	Lessons from preclinical animal models	Potential relevance to human diseases
D-panthenol	Topical	Increased skin permeability Keratinocyte proliferation Fibroblast activation Enhanced cell viability, Reduced of apoptosis and senescence	<i>Increased collagen production in Vnn1 pantetheinase-expressing tumors</i>	Skin damage Dermatitis Hair follicle growth
Pantethine	I.p	Reduced A β deposition, Improved behavioral alteration Production of ketone bodies Improved redox status in blood cells Increased proinflammatory cytokines and macrophage phagocytic activity Improved intestinal barrier repair and fitness Enhanced CoA metabolism Enhanced anti-tumor type I immunity	Improved prognosis in 5XFAD mouse model of Alzheimer's disease Reduction of dopaminergic neuron loss and motility disorders Reduced symptoms in cerebral malaria Enhanced granuloma formation in <i>M. tuberculosis</i> infection Improved tolerance to chronic colitis Improved immunogenicity of sarcoma	Alzheimer's disease Parkinson's disease Serum Vnn1 activity as prognosis biomarker of severe malaria Bacterial infections VNN1 prognostic biomarker in IBD Prognostic value of VNN1 in sarcoma
Pantothenate	I.p.	Improved Tc22 immunity	Improved control of melanoma and colon adenocarcinoma	Combined therapy with immune checkpoint blockade?
PANK allosteric activators	Oral	Rescues CoA synthesis	Correction of deficit in PANK-deficient mice	PKAN disease
4-P pantethine	Diet Diet	Normalization of CoA levels Reduced ROS and ox-LDL	Correction of deficit in PANK-mutant mice Reduced atherosclerotic plaque formation and endothelial injury	PKAN disease Coronary heart disease
Vnn1 inhibitors	Water	Improved Insulin sensitivity and glucose tolerance	Type 2 diabetes	Type 2 diabetes
Microbial PANK inhibitors	Soluble	Inhibition of microbial CoA production	In vitro control of microbial growth	Parasite, bacterial and fungal infections

6) The coenzyme A precursor pantethine enhances anti-tumor immunity in sarcoma

Mon équipe, dans ses précédents travaux, s'est intéressée à l'impact de la perte de Vanin1 dans un modèle murin génétiquement modifiée ayant perdu l'expression des points de contrôle du cycle cellulaire p16 et p19 (161).

Ainsi, la perte de l'expression du gène Vanin1 dans ce fond génétique prédisposé au cancer était associée à une prévalence plus importante de sarcomes (notamment de fibrosarcomes). Dans des fibroblastes murins transformés exprimant un oncogène RAS, la surexpression de Vanin1 était associée à une reprogrammation du métabolisme des cellules cancéreuses de type anti-Warburg, à une récupération de la morphologie et de la fonctionnalité des mitochondries, et notamment de leur capacité respiratoire. Ces phénotypes intracellulaires étaient couplés à un maintien de l'état de différenciation cellulaire. *In vivo*, la surexpression de Vanin1 empêchait la croissance tumorale. Une diminution de la croissance tumorale a été observée après administration de cystéamine, de pantothénate ou du dimère stable de la pantéthéine, la pantéthine accompagné au niveau transcriptomique, d'un changement du phénotype immunitaire. Les limites de ce premier modèle étaient liées d'une part à l'utilisation d'une cellule cancéreuse fabriquée *de novo* et à l'utilisation de souris Nude pour les protocoles de greffe tumorale. Il était donc nécessaire de valider ces résultats dans un modèle plus proche de la réalité expérimentale.

Compte tenu des connaissances mécanistiques apportées par cette étude et dans un but thérapeutique, nous nous sommes intéressés à l'impact de l'administration d'un précurseur du Coenzyme A, la pantéthine, à des souris portant une forme plus agressive de fibrosarcome. Nous avons évalué si la délivrance pharmaceutique de pantéthine reprogrammait le métabolisme de la cellule cancéreuse, impactait l'infiltration, la fonctionnalité, le métabolisme et l'épuisement du système immunitaire. Nous avons également étudié les différents acteurs cellulaires et moléculaires impliqués dans l'effet thérapeutique de la pantéthine et avons élargi ces observations à des modèles infectieux, des modèles de mélanomes et d'ostéosarcome afin de décrire le potentiel adjuvant de la pantéthine dans les immunothérapies actuellement utilisées en clinique.

The coenzyme A precursor pantethine enhances anti-tumor immunity in sarcoma

Richard MIALLOT¹, Virginie MILLET¹, Anais ROGER¹, Romain FENOUIL¹, Catherine TARDIVEL², Jean-Charles MARTIN², Laetitia SHINTU³, Paul BERCHARD⁴, Juliane SOUSA LANZA¹, Bernard MALISSEN^{1,5}, Sandrine HENRI¹, Sophie UGOLINI¹, Aurélie DUTOUR⁴, Pascal FINETTI⁶, François BERTUCCI^{6,7}, Jean-Yves BLAY^{4,8}, Franck GALLAND¹, Philippe NAQUET¹

1. Aix-Marseille Université, INSERM, CNRS, Centre d'Immunologie de Marseille-Luminy, Marseille (CIML), France.
2. Aix Marseille Université, INRAE, INSERM, C2VN, Marseille, France.
3. ISM2, Aix Marseille Université, CNRS, Centrale Marseille, Marseille, France.
4. INSERM 1052, CNRS 5286, Cancer Research Center of Lyon (CRCL), Childhood Cancers and Cell Death Laboratory, Lyon, France.
5. Aix Marseille Université, INSERM, CNRS, Centre d'Immunophénomique (CIPHE), Marseille, France
6. Aix-Marseille Université, INSERM, CNRS, Centre de Recherche en Cancérologie de Marseille (CRCM), Institut Paoli-Calmettes (IPC), Laboratory of Predictive Oncology, Marseille, France.
7. Institut Paoli-Calmettes, Department of Medical Oncology, Marseille, France.
8. Université Lyon I, UNICANCER Centre Léon Bérard, Department of Medicine, Lyon, France.

Abstract – 183 words

The tumor microenvironment is a dynamic network of stromal, cancer and immune cells that interact and compete for resources. Mitochondria play an essential role in the control of metabolic plasticity and contribute to tumor progression and immune cell functionality. We have previously identified the Vanin1 pathway as a tumor suppressor of sarcoma development *via* vitamin B5 and coenzyme A regeneration. Using an aggressive sarcoma cell line that lacks Vnn1 expression, we showed that the administration of pantethine, a vitamin B5 precursor, attenuates tumor growth in immunocompetent mice. Pantethine boosts anti-tumor immunity, including the polarization of myeloid and dendritic cells towards enhanced IFN γ -driven antigen presentation pathways and improved development of hypermetabolic effector CD8⁺ T cells endowed with potential anti-tumor activity. At later stages of treatment, the effect of pantethine was limited by the development of immune cell exhaustion. Nevertheless, its activity was comparable to that of anti-PD1 treatment in sensitive tumors. In humans, *VNN1* expression correlates with improved survival and immune cell infiltration in soft tissue sarcomas, but not in osteosarcomas. Pantethine could be a potential therapeutic immunoadjuvant for the development of anti-tumor immunity.

Introduction

Soft-tissue sarcomas (STSs) are heterogeneous subtypes of tumors with distinct origins and genomic profiles (Fletcher, 2014). To stratify them and define prognostic markers, large-scale approaches have revealed how histo- and genotypes are associated with distinct epigenetic, metabolic or immune traits (Abeshouse et al., 2017). A bioinformatics analysis of TCGA database centered on metabolic signatures showed that, while enhanced glycolysis was a hallmark of sarcomas, the degree of oxidative phosphorylation varied significantly amongst histotypes (Miallot et al., 2021). Mitochondrial activity conditions metabolic plasticity (Masoud et al., 2020), adaptation to stress and progression towards aggressive phenotypes (Senyilmaz and Teleman, 2015). Along this line, Vnn1 pantetheinase that regulates the generation of the coenzyme A (CoA) precursor pantothenate (Pan), also known as vitamin B5 (VitB5) (Millet et al., 2022; Naquet et al., 2020), acts as a negative regulator of spontaneous sarcoma development in a p16/p19-deficient tumor-prone mouse model (Giessner et al., 2018). In a limited set of human sarcomas, VNN1 transcript levels are associated with improved metastasis-free survival. Furthermore, in mouse models, Vnn1-expressing tumors are less aggressive and enriched in transcriptional immune signatures (Giessner et al., 2018). The development of immune responses is influenced by metabolic cues released within the tumor microenvironment (de la Cruz-López et al., 2019; Naquet et al., 2016). In a stressful context, chronically activated immune cells compete for nutrients with tumor cells (Chang et al., 2015; Klein Geltink et al., 2018; Reinfeld et al., 2021). Furthermore, hypoxic conditions can enhance the development of effector T cell responses (Doedens et al., 2013; Gropper et al., 2017) but also drive CD8⁺ T cells towards exhaustion (Scharping et al., 2021). Exhausted CD8⁺ lymphocytes display abnormal mitochondria biogenesis (Scharping et al., 2016), with a reduction in cristae structure and mitochondria/endoplasmic reticulum (ER) contacts (Yu et al., 2020). Accordingly, PGC1 α -transfection in CD8⁺ T cells enhanced the development of anti-tumor CD8⁺ tumor-infiltrating lymphocytes (TILs) (LeBleu et al., 2014). As the loss of mitochondrial fitness contributes to exhaustion (Soto-Heredero et al., 2021), pharmacological strategies modulating mitochondrial activity may induce exploitable effects on both tumor and immune cells.

Sarcomas are generally considered poorly immunogenic (Fletcher, 2014; Choi and Ro, 2021), but some respond to immunotherapy (D'Angelo et al., 2014; Tawbi et al., 2017; Eulo and Van Tine, 2022). In a recent study, among the 30% complex STSs that presented immune infiltration, the presence of B cell-containing tertiary lymphoid structures (TLS) was associated with the efficacy of anti PD1 therapy (Petitprez et al., 2020). We reasoned that strategies that exploit the immune-boosting effect of the Vnn1 pathway observed in autoimmune or infectious models (Meghari et al., 2007; Kavian et al., 2016) might enhance the development of anti-

sarcoma immunity. Indeed, provision of high VitB5 levels can be obtained *in vivo* through the administration of pantethine (Pant), a well-tolerated dimeric form of pantetheine hydrolyzed by Vnn1 in VitB5. In cancer models, *in vitro* stimulation of CD8⁺ T cells with CoA could boost the maturation of effector cells with potent anti-tumor potential (Paul and Ohashi, 2020; St. Paul et al., 2021). Furthermore, melanoma patients with high VitB5 serum levels showed a better response to anti PD1 therapy (St. Paul et al., 2021). Finally, in an ovarian cancer model, pantethine administration limited tumor growth (Penet et al., 2016). Since VNN1 expression tends to be lost in advanced sarcomas, we speculated that Pant therapy might mimic the beneficial effect of VNN1 expression on anti-tumor immune responses *in vivo*. Therefore, we tested whether VNN1 expression was associated with immune signatures in sarcomas and whether enhancing VitB5 levels *via* Pant administration could enhance anti-tumor immunity in a mouse model.

Results

High VNN1 expression in STS correlates with heightened immune response and better prognosis

We queried the TCGA database (including 206 soft tissue sarcoma STS samples) to search for VNN1-coexpressed gene modules. VNN1 expression matched MSigDB hallmarks associated with IFN γ /inflammatory responses (FigS1A). Using a CIBERSORT (<http://cibersort.stanford.edu/>) deconvolution method to link VNN1 expression with the presence of immunocyte subsets, we found a significant correlation between high VNN1 expression and the presence of immune cells that do not express VNN1 such as M1/M2 macrophages and T cells (including CD8⁺) transcripts (FigS1B). To broaden this analysis, we searched for correlations between VNN1 mRNA expression and clinicopathological and immune variables in an independent cohort of 1377 clinical STS samples (FigS1C) collected during surgery for non-metastatic primary tumors. Their characteristics are summarized in FigS1D. VNN1 expression was heterogeneous across the cohort, with a range of intensities over 20 units on the log₂ scale (Fig1A), allowing the search for correlations with tumor variables. VNN1 expression, assessed as discrete variable (high vs. low), correlated (FigS1D) with patient's age at diagnosis pathological tumor grade, and tumor site: as compared to the "VNN1-low" class, the "VNN1-high" class included older patients ($p=3.78E-08$), more grade 1 tumors ($p=5.22E-06$), and more extremity and less superficial trunk tumor sites ($p=5.20E-03$). No significant correlation was found between patient's sex, pathological tumor size, and tumor depth. We then analyzed the correlation between the VNN1 classes and immune variables (Fig1B). First, the probability of activation of the IFN α , IFN γ , and STAT3 immune pathways was higher in the "VNN1-high" class than in the "VNN1-low" class ($p<0.05$). Second, we

compared the composition and functional orientation of tumor-infiltrated immune cells between VNN1 classes using the Bindea immune cell types defined as the immunome. “VNN1-high” tumors displayed a higher infiltrate concerning 18 immune cell types ($p < 0.05$) including B cells, T cells, Tem cells, Th1 cells, TFH cells, Th17 cells, CD8⁺ T cells, $\gamma\delta$ T cells, cytotoxic cells, CD56^{dim} NK cells, dendritic cells (DC, interstitial DC, activated DC and plasmacytoid DC), eosinophils, macrophages, mast cells, and neutrophils. By contrast, “VNN1-low” tumors displayed a higher infiltrate in two immune cell types, NK cells and CD56^{bright} NK cells ($p < 0.05$). Third, “VNN1-high” samples displayed higher Immunologic Constant of Rejection (ICR) and immune cytolytic activity score, reflects of an anti-tumor cytotoxic immune response, than “VNN1-low” samples, and higher scores for signatures associated with response to immune checkpoint inhibitors (ICI): tumor inflammation signature (TIS) and TLS. Finally, “VNN1-high” samples displayed higher TILs scores using lymphoid-alone, myeloid-alone and combined signatures, and higher Antigen-Processing Molecules (APMs) score. Next, we searched for correlations between VNN1 classes and clinical outcomes. Patients with “VNN1-high” samples displayed longer MFS than those with “VNN1-low” samples (Fig1C with respective 5-year MFS equal to 66% (95%CI 60-73) vs. 61% (95%CI 54-68) (Fig1D). In the univariate prognostic analysis (Fig1D), high VNN1 expression was associated with longer metastasis-free survival (MFS), as was pathological grade 1. In multivariate prognostic analysis, VNN1 status tended towards significance (hazard ratio [HR] S=0.64, 95%CI 0.41-1.00, $p = 0.051$). Altogether, these results show heterogeneous VNN1 expression levels in STS, with high VNN1 levels positively correlated with improved immune infiltration and clinical outcome. Nevertheless, the prognostic value of VNN1 expression was not observed in a cohort of 326 patients with bone sarcoma, or in a subcohort of 94 patients with osteosarcoma (FigS2A, B).

Pantethine reduces fibrosarcoma, melanoma but not osteosarcoma growth

As a surrogate mouse model of complex sarcomas, we implanted the Vnn1^{negative} MCA205 (MCA) sarcoma cell line in immunocompetent mice to test whether systemic administration of Pant would compensate for the lack of Vnn1 in the tumor mass. Indeed, pantethine can be hydrolyzed into vitB5 and cysteamine by serum VNN activity (Fig2A). Intraperitoneal Pant administration was initiated on established tumors 10 days after cell engraftment (Fig2B). Growth reduction occurred within a few days post injection and persisted throughout the treatment period (Fig2C). A similar result was obtained by co-injecting Pan and cysteamine (CEA), the products of pantetheinase activity (FigS3A) or when using MCA cell line transfected with Vnn1 as a control of pantethine effect (FigS3B). Importantly, when Pant was administered to nude mice bearing MCA tumors, no significant growth inhibition was detected (Fig2D). This result suggested that the Pant effect might directly or indirectly regulate immune responses and possibly modulate the efficacy of ICI. As shown in Fig2E-F, administration of anti-CTLA4

or anti-PD1 mAbs inhibited MCA growth with variable efficacy and combination with Pant modestly accentuated their inhibitory effect. We then tested an osteosarcoma cell line (OsA) for which ICI alone or in combination with doxorubicin had no effect. The addition of Pant treatment did not change the behavior of this highly resistant tumor (Fig2G) or the organization of the immune infiltrate (FigS3C-D). Nevertheless, the combined therapy might enhance the extent of necrosis, despite high variability among samples (FigS3D). In the B16F10 melanoma model, which is known to be sensitive to anti PD1 therapy (36), Pant inhibited B16F10 growth to a level comparable to that obtained in MCA tumors and its effect was equivalent to that of an anti-PD1 mAb or their combination (Fig2H). In conclusion, in the MCA model, Pant efficacy relies on the immunocompetence of the recipient mouse.

Pantethine boosts myeloid cell signatures associated with antigen presentation and IFN γ signaling

To further characterize the effect of pantethine therapy on immune response, we first performed a follow-up of immune cell infiltration at different stages of MCA tumor development. As shown in Fig3A (see FigS6A for gating strategy), myeloid cells were approximately 2-fold more abundant than lymphoid cells in D13 tumor infiltrates, with the myeloid/lymphoid cell ratio evolving progressively towards an enrichment in lymphocytes after Pant administration. In Pant-treated mice, the proportion of tumor-infiltrating monocytes on day 20 (D20) was reduced, whereas that of tumor-associated macrophages (TAMs) increased (Fig3B, C). The latter subset was significantly enriched in MHCII^{high} cells (Fig3D), previously identified as having potential anti-tumor functions (Wang et al., 2011).

To further dissect myeloid cell heterogeneity, we performed single-cell RNA sequencing analysis of CD45⁺ tumor-infiltrating cells at D20 and D28 of tumor progression. We focused on the three main metaclusters corresponding to myeloid, antigen-presenting (APC) and lymphoid cells, the cluster “others” being invariant under our experimental conditions (FigS4A). Volcano plot analysis of the myeloid metacluster showed that control tumors were enriched in *Arg1* and *Bnip3*, *Pgam1*, *Ldha*, *Ddit4* transcripts (Fig3E and S4B for D20 and D28 tumors, respectively) associated with M2 polarization and tumor hypoxia (Semenza, 2013). In contrast, the *MhcII*, *Cd74*, *Cxcl9* transcripts were overexpressed in Pant samples. The myeloid (Fig3F and S4C) and APC (FigS5A, B) metaclusters were further stratified into subgroups defined by the preferential expression of specific genes (FigS4D for myeloid cells and FigS5B for APC). The density plots distinguished control from Pant-treated samples (FigS4C and S5C); Pant-treated samples showed progressive accumulation of activated TAMs (identified as mono-TAM B and C and inflammatory TAMs in Fig3G) and IFN γ -activated DC subsets (Fig3H). Gene Enrichment Analysis (GSEA) (Table 1) and Kyoto Encyclopedia of Genes and Genomes pathways (KEGG,

FigS4E) analyses confirmed that Pant samples were enriched in IFN γ -driven transcriptomic profiles associated with antigen presentation (Table1). APC from Pant tumors expressed high membrane MHC II levels (FigS5D). Furthermore, tumor sections documented 2- to 3-fold more MHC II⁺/CD8⁺ cell contacts (Fig3I and S5E). To identify the dominant chemokine profiles at the protein level, we performed a proteome analysis (Fig3J) and a cytometric bead assay (CBA) (FigS5F). Control PBS samples showed an overrepresentation of proteins associated with tissue clearance (pentraxin), extra cellular matrix (MMP9, Serpin) and endothelial cell reorganization (angiopoietin, VEGF, endostatin). Pant-treated samples contained higher levels of cytokines and chemokines associated with type 1 immunity. This included CCL2 or CXCL9 (26,27) involved in monocyte (via CCR2) or effector lymphocyte (via CXCR3) recruitment, IL2p40 (Cooper and Khader, 2007; Abdi and Singh, 2015) or Flt3-L (Cueto and Sancho, 2021), associated with M1 or DC maturation (Fig3J). Within each cluster, we did not observe major differences in the overall expression of genes previously associated with anti- or pro-tumor function (FigS5G). Altogether, Pant samples were enriched in APC subsets, highlighting IFN γ responsiveness, enhanced antigen presentation, and chemoattraction potential.

Pantethine enhances the development of effector lymphocytes

We used the CD8⁺/Treg cell ratio as a global indicator of anti-tumor lymphoid responses and OVA-MCA cells to track tumor-specific CD8⁺ T cell responses. We observed a progressive enrichment in CD8⁺ T cells from D17 to D28 (Fig4A). Pant-treated D20 samples contained 2-fold more NK/ILC, CD4⁺ in the tumor as well as OVA-specific effector CD8⁺ T cells in the tumor and draining lymph nodes (TDLNs) (Fig4B, C). CD8⁺ TILs tended to express higher levels of effector molecules such as GZMB, PRF1 or TNF α (Fig4D). In contrast, the proportion of other immune cells was comparable in lymph nodes or spleen, at steady state or in a tumor context (FigS6B-D).

The analysis of the lymphoid metacluster (FigS7A-C) confirmed the cytometry results. On D20, total CD4⁺ and CD8⁺ T cells were increased to the expense of Tregs and activated memory CD8⁺ cells (Fig4E and S7A-C). CD8⁺ T cells showed an enriched representation of pathways associated with the IFN γ response, cytotoxic function, chemokine production, and, to a lesser extent, PD1 signaling (Fig4F and Table 1). On D28, NK/ILC and Treg signatures predominated in Pant and PBS samples, respectively. Furthermore, in Pant treated samples, two-fold fewer CD4⁺ but not CD8⁺ T cells expressed CTLA4, PD1 or TIM3 molecules (Fig4G). We then scored the number of coexpressed genes associated with a cytotoxic program by each cell type. Although this analysis was limited by the total number of cells, CD8⁺ T cells derived from Pant samples expressed a higher number of cytokine or cytotoxicity genes, an argument in favor of their polyfunctionality (FigS7D). Finally, we used a global score to recapitulate the expression

levels of genes involved in the activation or exhaustion programs in CD8⁺ lymphocytes. Control and Pant samples were comparable for each cell subset, suggesting that Pant administration modifies the proportion, but not the transcriptional state, of these cells (FigS7E).

While the relative number of total NK/ILC1 was increased in the cytometry analysis, their proportion within the lymphoid metacluster was reduced in the Pant samples. Interestingly, by projecting NK *versus* ILC1 signatures (FigS7F) and applying RNA velocity analysis of the NK/ILC cluster (Fig4H), we observed an enhanced dynamic conversion of NK into ILC1 cells in control samples, whereas Pant therapy tended to reinforce NK cell signatures (Gao et al., 2017; Vienne et al., 2021), showing by GSEA an enrichment in IFN γ response (FigS7G). Taken together, our results show that Pant therapy induces a robust effector lymphocyte response.

Pantethine efficacy depends on IFN γ , cDC1, NK1.1⁺ and tumor-infiltrating CD8⁺ T cells

The development of cytotoxic CD8⁺ T lymphocytes requires antigen cross presentation by XCR1⁺ cDC1 cells and tumor-infiltrating potential, a program driven by type 1 cytokines such as IL-12 and IFN γ . We tested whether the efficacy of pantethine therapy would persist in the absence of IFN γ signaling and cDC1 cells, using IFNGR1- and *Xcr1*-deficient mice (Wohn et al., 2020). Based on the results presented in Fig2B, 2D or 5C, the volume of MCA tumors reached 200 mm³ after D20-22. As shown in Fig5A, B, the lack of *Ifngr1* or cDC1 cells led to uncontrollable growth as early as D16. Pant administration had a paradoxically enhancing effect under these conditions. Then, using *in vivo* depleting anti-NK1.1 or CD8-antibodies, we eliminated cells with cytotoxic potential (FigS8A, B). As expected, the lack of CD8⁺ or NK1.1⁺ cells boosted tumor progression after D17 and D22, respectively (Fig5C, D). Furthermore, Pant-mediated inhibition was preserved in NK1.1⁺ cell-depleted mice and was significantly reduced in CD8⁺ cell-depleted mice. This showed that the Pant inhibitory effect involved the contribution of both cell types, shown to participate in a DC/NK circuit determining the sensitivity to immunotherapy (Barry et al., 2018). As this cellular pathway is also required for the control of viral infection, we used a model of cutaneous HSV-1 infection (Srivastava et al., 2017) in which virus replication and virus-specific T cells could be monitored. Although the viral load was equivalent under both conditions (Fig5E), the proportion of central memory and effector CD8⁺ T cells in DLNs was enhanced 2-fold by Pant treatment, including virus-specific CD8⁺ T cells (Fig5F).

Former analyses showed that the levels of CXCL9 and MHC molecules regulated by IFN γ signaling were enhanced by Pant therapy (Table 1). To test whether Pant might influence antigen presentation or T cell proliferation, we injected OVA-expressing MCA cells, extracted CD11c⁺ DC from TDLNs and co-cultured them *in vitro* with CFSE-labeled OT-1 CD8⁺ T cells in the presence or absence of OVA. Both dendritic cell numbers (FigS8C) and CD8⁺ T cell

proliferation index (FigS8D) were comparable under the two conditions. We then performed immunohistochemical analysis in tumor sections that showed a higher proportion of CXCL9-dependent infiltrating CD3⁺ and CD8⁺ TILs (Marcovecchio et al., 2021) (Chow et al., 2019; Dangaj et al., 2019) in Pant samples (Fig5G, H), whereas they were in reduced numbers or confined to the periphery in control tumors. Altogether, these results confirm the boosting effect of Pant therapy on IFN γ -regulated pathways.

Pantethine therapy enhances VitB5-dependent metabolism in tumor T lymphocytes

Vnn1 pantetheinase hydrolyzes Pant in VitB5, which supports CoA synthesis (Naquet et al., 2020). We first confirmed by metabolomics analysis that these metabolites were enriched in tumor masses following Pant therapy (Fig6A). Since prolonged Pant administration might progressively induce metabolic adaptations in tissues, we performed another analysis on D28 tumors and compared the Pant effect to that induced by dichloroacetate (DCA), a compound that increases pyruvate uptake in mitochondria *via* PDK inhibition (Michelakis et al., 2008) and exerts comparable but not synergistic anti-tumor activity on MCA cells (Fig6B) and other tumors (46). The results showed that global metabolic changes were not superimposable (Fig6C). Pant enhanced the levels of metabolites associated with the stress response, and protein and nucleotide metabolism, whereas DCA enhanced carbohydrate metabolism and mitochondrial activity. Interestingly, their association had a significant effect on the production of mitochondrial energetic metabolites and biogenic amines, a phenotype confirmed by nuclear magnetic resonance analysis (Fig S9A).

We then focused our metabolic analysis on *in vitro* grown autochthonous or *ex vivo* isolated cancer cells. *In vitro*, addition of Pant slightly enhanced the production of mitochondrial reactive oxygen species (mtROS) (Fig6D). In contrast, the oxygen consumption (OCR) and extracellular acidification rates (ECAR) measured by Seahorse analysis were marginally affected (Fig6E), showing that these tumor cells have a limited spared respiratory capacity. Since chronic stress may progressively induce mitochondrial damage/repair processes in tumor cells, we comparatively evaluated mitochondrial fitness *in vivo*, by scoring using flow cytometry from D24 to D28 the mitochondrial polarization over mass ratio (MDR/MG, see methods) (Elefantova et al., 2018). As shown in Fig6F and FigS9B, depolarized mitochondria accumulated in D28 tumors in favor of increased stress, and the MDR/MG ratio evolved similarly between PBS and Pant samples. Since alterations in mitochondrial metabolism can contribute to the reinforcement of the Warburg effect (Senyilmaz and Telean, 2015; Liberti and Locasale, 2016), we tested lactate production in tumor masses (Fig6G) and quantified by qRT-PCR the expression level of transcripts associated with an increased glycolytic flow on isolated cancer cells (FigS9C). The results showed that neither lactate nor transcript levels

were modified by Pant. Altogether, Pant administration does not seem to affect mitochondrial and glycolytic activities by MCA cells.

Consequently, immune cells may be the preferential targets of Pant therapy in this model. In purified CD8⁺ lymphocytes extracted from D20 tumors, Pant administration provoked a significant increase in both OCR and ECAR, demonstrating their higher energy status (Fig6H). To follow mitochondrial fitness over time, we quantified mitochondrial polarization and mass and deduced the MDR/MG ratio in CD4⁺ and CD8⁺ T cells at different time points. Although no difference was observed in both cell subsets on D20, this ratio was lowered in D28 CD4⁺ and CD8⁺ T cells from the Pant samples (Fig6I). These results showed that Pant boosts mitochondrial metabolism *in vivo* but does not prevent the development of mitochondrial depolarization (Table 1) associated with chronic lymphocyte activation and exhaustion (Yu et al., 2020).

Discussion

Pantethine administration aimed at restoring vitB5 and mitochondrial homeostasis led to the reduced growth of an aggressive sarcoma cell line in immunocompetent mice. Pant acts predominantly *via* cysteamine-dependent redox modulation and CoA regeneration. An intrinsic tumor-suppressive effect *via* metabolic rewiring was unlikely in the MCA model, which contradicts a previous report in which the mitochondrial activity of H1 cells could be rescued by exogenous VitB5 (Giessner et al., 2018). In contrast, MCA cells originate from MCA-driven tumorigenesis, with a long evolution time *in vivo* (Vienne et al., 2021). As many aggressive tumors display mitochondrial alterations (Miallot et al., 2021), MCA cells show reduced respiratory capacity and consequently, Pant neither corrects mitochondrial fitness nor inhibits tumor growth in nude mice. It rather enhanced mtROS generation, a phenotype observed in cells with electron transport chain (ETC) deficiencies (Zorov et al., 2014), and envisaged as a therapeutic strategy for embryonal rhabdomyosarcoma (ERMS) (Chen et al., 2013) to induce cell death or immunostimulation *via* damage-associated molecular pattern (DAMP) release (Rongvaux, 2018; Porporato, 2018). Therefore, we suspected that metabolic changes induced by Pant could boost anti-tumor immunity. In Pant-treated mice, tumor-associated myeloid and lymphoid cells displayed signatures of IFN γ -driven activation. The contribution of mitochondrial activity to antigen recognition and the efficacy of immunotherapy is still debated (Jones and Divakaruni, 2020; Harel et al., 2019; Yin and O'Neill, 2021; Bonifaz et al., 2014). In macrophages, CoA administration enhances acetyl-CoA-mediated epigenetic activation of pro-inflammatory gene transcription and boosts TAM anti-tumor activity in breast cancer (Timblin et al., 2022). Although dendritic cells require enhanced mitochondrial activity for the acquisition of antigen-presenting capacity *in vitro*, we failed to detect any Pant-mediated

enhancement in OVA presentation to OT1 T cells by cDC1 extracted from Pant-treated mice. *In vivo*, Pant therapeutic efficacy requires the presence of IFN γ signaling, cDC1, and NK1+ and CD8+ TILS. Indeed, cDC1 cells cross present antigens (Broz et al., 2014; Brewitz et al., 2017; Dorner et al., 2009) and, through cooperation with Th1 cytokine-producing NK or CD4+ Th1 cells (Wohn et al., 2020; Barry et al., 2018), prime anti-tumor CD8+ T cell responses. Interestingly, perturbation of fatty acid oxidation or mitochondrial clearance increases the development of cDC2 at the expense of cDC1 cells (Kratchmarov et al., 2018). Furthermore, CD8+ DC boost mitochondrial energy production to maintain cross presentation or IL-12 production (63). Interestingly, tumors from Pant-treated mice showed increased IL12p40 and CXCL9 production involved in Th1 effector cell priming and recruitment via the CXCR3 axis (Chow et al., 2019). Mitochondrial activity is also essential for T lymphocyte activation, cytokine production, and differentiation (Chang et al., 2013; Sena et al., 2013; Almeida et al., 2021; van der Windt and Pearce, 2012), in part through mtROS (Sena et al., 2013; Phan et al., 2016; Kamiński et al., 2012; Ma et al., 2019). Accordingly, they were two-three-fold more infiltrated by CD4+ or CD8+ effector T cells, in which the simultaneous expression of Th1 cytokines and cytolytic activity markers was enhanced, an argument in favor of their polyfunctionality. In the D20 Pant-treated samples, CD8+ T cells showed a hypermetabolic profile with simultaneous enhancement of ECAR and OCR. Accordingly, TLR-induced IFN γ production by CD8+ T cells depends on mitochondrial ATP (Salerno et al., 2016). ETC complexes 1 and 2 are differentially required for Th1 cell proliferation and epigenetic remodeling *versus* the maintenance of terminal effector functions, respectively (Bailis et al., 2019). Interestingly, velocity index analyses suggested that the identity of the effector innate or adaptive lymphocytes was reinforced by Pant therapy. Our results indicate that Pant, through its effect on mitochondrial fitness, may enhance the functionality of anti-tumor cells and/or their ability to migrate within the tumor mass. They extended recent findings showing that, *in vitro*, addition of CoA could enhance the production of effector memory CD8+ T cells that upon *in vivo* injection rejected a tumor (St. Paul et al., 2021). In this study, pantothenate administration also enhanced the efficacy of anti-PDL1 therapy in the MC38 model, a situation that was at the limit of detection using the MCA and B16 models treated with anti-PD1 or CTLA4 therapy.

Several explanations may explain the incomplete effect of Pant administration. First, pro-tumor cells may also be activated by Pant. Accordingly, in the absence of cDC1 or IFN γ signaling, Pant enhanced tumor growth. Indeed, CoA- and its acylated forms have a strong impact on fatty acid oxidation and mitochondrial activity that participate in pro-tumorigenic type 2 immunity through the regulation of macrophage (Jha et al., 2015) and Treg functions (Field et al., 2020). Second, chronic activation of lymphocytes commonly leads to cell exhaustion (Yang et al., 2020; Blank et al., 2019) and expression of inhibitory PD1 or TIM3 molecules. This

phenotype is correlated with long-lived effector cells that survive the contraction phase of the immune response, but develop various dysfunctions and mitochondrial alterations (Scharping et al., 2016; Blank et al., 2019), in part induced by inhibitory molecules such as PD1 (Wei et al., 2018; Bengsch et al., 2016; Chowdhury et al., 2018). Our results indicated that PD1 / TIM3 expression was lower in CD4⁺ but not CD8⁺ T cells from Pant-treated tumors than in control situation. Furthermore, mitochondrial depolarization was more important in CD8⁺ T cells from Pant-treated mice, likely because of the higher activation level at various stages of tumor development. Although the difference between the control and Pant samples was not detected at the transcriptional level for each cell subset, the progressive loss of functionality might limit Pant efficiency and explain the lack of synergy with anti-PD1 therapy. Indeed, Pant and anti-PD1 therapies were equally effective or ineffective on B16 melanoma or osteosarcoma cell lines, respectively, possibly because they converge on similar metabolic pathways (Chamoto et al., 2017).

Pant administration mimics the biological effects linked to the overexpression of Vnn1 pantetheinase *in vivo* (Giessner et al., 2018; Millet et al., 2022). More generally, Vnn1 is involved in tissue tolerance to stress (Naquet et al., 2014). Therefore, we tested whether VNN1 expression in human sarcomas might be correlated with enhanced survival and/or development of anti-tumor responses. VNN1 expression was variable in complex genomic sarcomas and inversely correlated with their severity. However, when detected, its expression positively correlated with improved prognosis and the presence of immune signatures recapitulating the phenotypes observed in the mouse model. Conversely, in human bone sarcomas, VNN1 expression does not correlate with prognosis, and Pant does not control tumor growth. This phenotype may be related to the fact that loss of mtDNA is often found associated with aggressive osteosarcomas (Jackson et al., 2019), whereas its enhanced release can boost cDC1-dependent immune responses in MCA tumors (Miallot et al., 2023).

In conclusion, our results extend the former observation that vitB5 is a limiting metabolite in many tumors, and that this defect participates in the impairment of anti-tumor immunity. Pantetheine may present a therapeutic interest in the context of immune enhancement prior to surgery or in vaccine programs.

Material & Methods

Animals

Female 8-10 weeks old C57BL/6 and nude mice were purchased from Janvier Laboratories. *Xcr1*^{DTA} and OT-I (ovalbumin-specific TCR-transgenic mice) mice obtained from B. Malissen's laboratory have been previously described (34,73,74). *Ifngr1*^{KO} mice were purchased from CNRS (UMR 7355). Mice were housed under a standard 12-h:12-h light–dark cycle with ad

libitum access to food and non-acid water, 22°C +/- 1°C, 45–60% humidity and maintained under specific pathogen-free conditions at animal facility of the CIML (F13-055-10). For the osteosarcoma murine model, 5 weeks old BALB/cByj mice were purchased from Charles River Laboratories and housed at CRCL animal facilities under the same conditions as mentioned previously. All experiments were conducted in accordance with institutional committees and the French and European guidelines for animal care. The experiments were approved by the Ethical Committee for Animal Experimentation.

Cell lines

The MCA205 mouse fibrosarcoma cell line (SCC173), the OVA-expressing cells (a kind gift from Laurence Zitvogel, Institut Gustave Roussy, Villejuif, France) and the B16F10 melanoma cell line (ATCC-CRL-6475) were cultured in Dulbecco's modified Eagle's medium F-12 (Thermo Fisher) supplemented with 10% fetal bovine serum (FBS, Gibco), 100 units/mL penicillin-streptomycin (Gibco), 2 mM of L-glutamine and 1 mM of sodium pyruvate at 37°C with 10% CO₂. Murine OsA K7M2 (ATCC – CRI-2836) was cultured in complete DMEM and maintained for 2 weeks before mouse cell engraftment. Mycoplasma status was evaluated using the MycoAlert Lonza Detection kit and cells were used at low passage.

Treatments

For drug treatment mice were injected intraperitoneally (*i.p.*) starting at day 10 post cell engraftment. D-pantethine (1g/Kg) was administered every day and dichloroacetate (1g/Kg) every 2 days. Cysteamine and pantothenate were administered *i.p.* at 120 mg/kg and 500 mg/kg, respectively. For all experiments, control PBS vehicle was used. All reagents were purchased from Sigma-Aldrich. For osteosarcoma experiment, mice were treated with doxorubicine (0.75mg/Kg - Baxter) or NaCl vehicle two days a week. The anti-CTLA4 (BioXcell, clone 9H10, 100 µg/injection/mouse), anti-PD1 antibodies (BioXcell, clone RMP1-14, 200 µg/injection/mouse) and isotype control mAbs (BioXcell, InVivoMab polyclonal Syrian hamster IgG and InVivoMab rat IgG2a, clone2A3) were injected 4 times at 3-day intervals *i.p.*

Tumor experiments

A total of 10⁵ MCA 205 cells or OVA-expressing MCA205 were subcutaneously and bilaterally grafted into the flanks of C57BL/6, nude mice, *XCR1*^{DTA} mice and *Ifngr1*^{KO} mice. 3.10⁵ B16F10 were injected intradermally and bilaterally in C57BL/6 mice. Murine OsA K7M2 was injected into the tibia of BALB/cByj mice. Mice were anesthetized with 2.5% isoflurane every two days and tumor growth was scored using a caliper by measuring the length (L) and width (W) of the tumor and volumes were calculated using the following formula: $(L \times W)^2 / 2$. A limit point was set when the tumor volume was > 1500 mm³ or when symptoms of poor health were detected

(weight loss, prostration, bleeding, and scars). Tumors were harvested between D10-D28 post cell engraftment, and each tumor was considered as an experimental unit referred to as *n*. Tumors were mechanically and enzymatically digested using Miltenyi Biotech GentleMACS Octo Dissociator technology. The samples were filtered through a 70µm Cell Strainer (Becton Dickinson) and subjected to red blood cells lysis (eBioscience). The cell suspensions were analyzed using flow cytometry. Alternatively, CD45⁻ cells, CD8a⁺ naïve T cells and CD8⁺ TILs were isolated using microbeads from Miltenyi Biotech and MultiMACS™ Cell24 separation on LS columns according to the manufacturer's protocols. The inguinal TDLNs were collected between D14 and D28 post-cell engraftment, scratched on a 70µm Cell Strainer and analyzed by flow cytometry. Spleen samples were processed as described for the lymph nodes. For osteosarcoma experiments, the tumors were harvested, fixed in PFA 4%, included in paraffin for subsequent histological analysis.

LC-MS

Metabolomics experiments to detect VitB5-related metabolites were performed by Metabolon (USA). All dried polar extracts from the samples were reconstituted with 200µL of acetonitrile/water (50:50; v:v). The samples were separated using high-performance liquid chromatography (UPLC) Ultimate 3000 (Thermo Scientific), coupled to a high-resolution mass spectrometer (HRMS). The Q-Exactive Plus quadrupole-orbitrap hybrid was equipped with an electrospray ionization source (H-ESI II). The chromatographic separation was performed on a binary solvent system using a reverse phase C18 column (Hypersil Gold, Thermo Scientific, 100mm X 2.1mm, 1.9µm) at 40°C with a flow rate of 0.4 mL min⁻¹ and a HILIC column (Merk, SeQuant® ZIC®-HILIC, 150 mm x 2.1 mm, 5µm, 200 Å) at 25°C with a flow rate of 0.25 mL min⁻¹. The injection volume for both columns was 5µL. The chromatographic separation was performed on a binary solvent system at a flow rate of 0.4 mL min⁻¹ using a reverse phase C18 column (Hypersil Gold, Thermo Scientific, 100mm X 2.1mm, 1.9µm) at 40°C. The mobile phase consisted of a combination of solvents A (0.1% formic acid in water, v/v) and B (0.1% formic acid in acetonitrile, v/v). The injection volume was 5µL. The following gradient conditions were used: 0 to 1 min, isocratic 100% A; 1 to 11 min, linear from 0 to 100% B; 11 to 13 min, isocratic 100% B; 13 to 14 min, linear from 100% to 0% B; 14 to 16 min, isocratic 100% A. The separated molecules were analyzed in both the positive and negative ionization modes in the same run. The mass spectra were collected using a resolving power 35 000 Full Width at Half Maximum (FWHM) for the theoretical mass-to-charge ratio (*m/z*) of 200. Full-scan mass spectra were acquired in the *m/z* range of 80–1000. The ionization source parameters for positive and negative ion modes were as follows: capillary temperature 320 °C, spray voltage 3.5 kV, sheath gas 30 (arbitrary units), auxiliary gas 8 (arbitrary units), probe heater temperature 310 °C and S-Lens RF level was set at 55 V. MS/MS experiments were performed

using Higher energy Collision induced Dissociation (HCD) and the Normalized Collision Energy (NCE) applied was ramped from 10 to 40%. To ensure good repeatability of the analysis, a quality control sample (QC) was formed by pooling a small aliquot of each biological sample. The QC sample was analyzed intermittently (because of the small number of samples, QC was analyzed one out of every three samples) for the duration of the analytical study to assess the variance observed in the data throughout the sample preparation, data acquisition and data pre-processing steps. The mobile phase for HILIC column separation consisted of a combination of solvent A (100% water, 16mM ammonium formate) and solvent B (100% acetonitrile 0.1% formic acid). The following gradient conditions were used: 0 to 2 min, isocratic 97% B; 2 to 10 min, linear from 97 to 70% B; 10 to 15 min, linear 70 to 10% B; 15 to 17 min, isocratic 10% B; 17 to 18 min linear from 10 to 97% B; from 18 to 22 min isocratic 97% B. The separated molecules were analyzed in both the positive and negative ionization modes in the same run. The mass acquisition parameters were the same as those used for the C18 columns. The repeatability of the analysis was ensured by analyzing the quality control sample (QC) intermittently (one out of every five samples).

NMR

Samples of thawed tissue (approximately 15 mg) were placed into a 30 μ L disposable insert, in which 10 μ L of D₂O was added to provide a field-lock signal. The disposable insert was then inserted into a 4-mm ZrO₂ HRMAS rotor for HRMAS NMR spectral acquisition. All NMR experiments were carried out on a Bruker Avance III spectrometer operating at 400MHz for the ¹H frequency equipped with a ¹H/¹³C/³¹P HRMAS probe. Spectra were obtained at 278 K with a spin rate of 4 kHz. To attenuate the NMR signals of macromolecules, the Carr-Purcell-Meiboom-Gil (CPMG) NMR sequence with an overall spin echo time of 150 ms was employed, preceded by a water presaturation pulse during a relaxation delay of 2 s. For each sample, 256 free induction decays (FID) of 32 k data points were collected using a spectral width of 6000Hz. The FIDs were multiplied by an exponential weighting function corresponding to a line broadening of 0.3Hz and zero-filled once prior to the Fourier transformation. Subsequently, the spectra were phased and baseline corrected manually and calibrated to the alanine methyl signal ($\delta=1.47$ ppm). To facilitate NMR signal assignment, 2D NMR experiments using ¹H-¹H TOCSY, ¹H-¹³C HSQC and online databases (Human Metabolome Database, Wishart et al, 2013) were employed. The ¹H 1D NMR spectra were directly exported to the AMIX 3.8 software (Bruker Biospin GmbH, Karlsruhe, Germany) and divided into buckets with a width of 0.001 ppm. To remove the effects of variations in the water suppression efficiency, the region between 4.70 and 5.20 ppm was discarded. The obtained NMR dataset X-matrix (40 observations x 8001 buckets) was then normalized to the total spectral intensity and subjected to multivariate statistical analysis using SIMCA-P + v.16 software (Umetrics, Umea, Sweden).

Initially, principal component analysis (PCA) of the ¹H NMR spectral data was performed to check the homogeneity of the dataset, group clustering and detect potential outliers. Following PCA, a supervised orthogonal partial least squares discriminant analysis (OPLSDA) was applied to the X-matrix, in which we defined a Y-matrix as that of sample classes to target metabolic differences between the groups of interest. The resulting score and loading plots were used to visualize the discriminant features. Leave-one-out internal cross-validation was performed to calculate R²_Y and Q² values representing, the explained variance of the Y matrix and the predictive ability of the model, respectively. Model validation was performed by random permutation of the Y matrix with n=999 times and using a CV-ANOVA p value from SIMCA-P + v.16 (analysis of variance in the cross-validated residuals of a Y variable).

Seahorse

The oxygen consumption rate of *in vitro* grown MCA205 cells *in vitro* was measured using a Seahorse XF-24 Metabolic Flux Analyzer. 1.10⁵ cells were seeded on XF-24 V7 multi-well plates, then treated or not with 100μM Pant for 16 h at 37°C. The OCR was evaluated using an XF Cell Mito Stress Kit (Agilent). 5.10⁴ CD8 TILS isolated from control or Pant-treated murine tumors were analyzed using the T cell Metabolic Profiling kit on Seahorse HS Mini Xfp.i

MitoSox

1.10⁵ MCA205 cells were seeded on 24-well plates in RPMI medium supplemented with 10% FBS and stimulated with 1mM Pant for 4h. A 20 min incubation with Antimycin A (5μg.mL⁻¹) was used as a positive control for mitochondrial ROS production. MitoSox probes were used at 5μM for 20 min in pre-warmed HBSS1X. Cells were harvested and MitoSox fluorescence was analyzed by flow cytometry.

Lactate Assay

Lactate concentration was quantified according to the manufacturer's instructions (Sigma-Aldrich). Briefly, the tissues were homogenized in four volumes of lactate assay buffer and centrifuged at 13000 g for 10 min to remove insoluble material. Samples were deproteinized using a 10-kD cut-off spin filter. A master reaction mix containing 46μL lactate assay buffer, 2μL lactate enzyme mix, and 2μL lactate probe was added to 50μL sample solution. The reactions were incubated at RT for 30 min and the absorbance of the sample was measured at 570 nm on a microplate reader.

Flow Cytometry and antibodies

For cytometric analysis, tumors were harvested at the indicated time points in DMEM F12 medium, mechanically dissociated before dissociation using a GENTLEMACS

OctoDissociator with heaters from Miltenyi Biotech, according to the manufacturer's protocol. TDLNs were scratched, and mechanically dissociated. After filtration and red blood cell lysis using eBiosciences reagents, the tumor and TDLN cell suspensions were labeled with LiveDead Fixable Blue and CD16/CD32 in PBS EDTA for 30 min. Cell surface labelling was performed in FACS Buffer for 1 h at 4°C with the indicated antibodies. If needed, streptavidin was incubated after cell surface labelling for 15 min at 4°C. For intracellular staining, cells were permeabilized using a FoxP3 staining kit from eBiosciences and antibodies were incubated 45 min at 4°C. Cells were resuspended in FACS Buffer before analysis on BD LSR Symphony or Fortessa. Mitotracker Deep Red and MitroTracker Green were used following the manufacturer's protocol to assess the membrane mitochondrial potential and mitochondrial mass, respectively. The OVA-tetramer (SIINFEKL – H2-K^b) was purchased from the NIH tetramer core facility and incubated with cell suspension prior to cell surface labelling for 1 h at 4°C. Beads were added to the cell suspension for calibration and normalization. Flow cytometry data were analyzed using FlowJo 10.8. The gating strategies for the analysis of myeloid and lymphoid cells are indicated in FigS1E and S4C, respectively.

Single Cell RNA sequencing

Tumors from MCA-205 bearing mice treated with PBS or Pant were harvested on D20 or D28 in DMEM F12 medium. After dissociation and RBC lysis, cell suspensions from the four experimental conditions were tagged using the TotalSeq B anti-mouse Hashtag Antibody. CD45 positive Live Dead negative cells were sorted on ARIA SORP, collected in SVF-coated tubes and pooled at equivalent ratios. The cell suspensions were immediately processed according to the Chromium Next GEM Single Cell v3.1 GEM protocols. HTO and DNA libraries were sequenced at the CIML genomic facility using a P2 flowcell on an Illumina NextSeq 1000/2000 platform. Two independent experiments (one control versus one Pant representative tumor per experiment) were performed and analyzed separately. FASTQ raw files were aligned to the mouse genome reference (mm10) using 10x Genomics Cell Ranger 6.0.1 (Zheng et al., 2017), which performs filtering, barcode counting, and unique molecular identifier (UMI) counting. After QC, all count matrices were loaded and processed together using the R package Seurat (6.1.0) (Hao et al., 2021). A second QC was performed to evaluate potential batch-related biases, perform HTO demultiplexing, and identify poor-quality cells to be excluded before downstream analyses. Cells with less than 1000 counted UMIs or more than 5000 detected genes (potential doublets), and cells with more than 10% mitochondrial gene expression (apoptotic cells) or less than 5% ribosomal genes were excluded from the analyses. Datasets from two independent experiments were pooled and analyzed. Five metaclusters were identified: Myeloid cells, Lymphoid cells, APC cells including DC cells and B cells and an undefined metacluster call "Others" which include tumor cell, fibroblasts and

stromal cells. For subsequent analyses, the metaclusters of the four immune cell types were recomputed separately. After normalization (lognormalize) and centering, the 2000 most variable features were identified and used for dimensionality reduction by PCA (50 PCs). Further dimensionality reduction was performed using uniform manifold approximation, projection (UMAP) embedding, and cell clustering using the Louvain algorithm (McInnes et al., 2020). Marker genes for each cluster were extracted using the Wilcoxon method with the Seurat function 'FindMarkers'. Functional enrichment analyses were performed using the clusterprofiler (Yu et al., 2012) and fgsea (Korotkevich et al., 2021) R packages, and the external database KEGG (Kanehisa et al., 2022). GSEA enrichment analyses and figures were performed with the 'fgsea' R package against selected reference gmt files from MSigDB (Liberzon et al., 2015; Subramanian et al., 2005). Heatmaps were generated using the R package complex heatmap (Gu et al., 2016) and other custom figures were generated using ggplot2 (ggplot2, 2022). RNA velocity analysis was performed using scVeloAll (Bergen et al., 2020) (detailed parameters for analyses are available in technical reports). For further characterization of NK cells, the results of a differential expression analysis from a previous study (Vienne et al., 2021) comparing ILC and NK cells were downloaded. The top 20 upregulated and down-regulated genes (sorted by p-value) from this study were used to create gene module scores in Seurat, projected on the previously computed uMAP for the NK cell population.

Cytokine array

Frozen tumors were directly homogenized in PBS containing protease inhibitors and 1% Triton. After debris removal, protein concentrations were assessed using the BCA Assay. Tissue lysates (200 µg) were processed using the Mouse XL Cytokine Array Kit (R&D Systems). The membranes were scanned with a Samsung Digital Presenter with a 720P HD document camera with a 14x optical zoom and 3x digital zoom image and quantified by Image J.

CBA

Tumor cell suspensions were centrifuged. TME cytokines were determined in the supernatant using mouse CCL2 and CXCL9 cytometric bead array (CBA) flex set kits (BD Biosciences). Samples were analyzed on a BD LSR II flow cytometer with FCAP Array TM Software V3 (BD Bioscience) to determine cytokine concentrations.

In vivo Depletion

CD8 mAb-based depletion (Clone 53-5.8) was obtained after intraperitoneal injections of 200µg and 150µg per mouse from day 10 and every three-day onwards, respectively. A rat IgG1 anti-horseradish mAb (Clone HRPN) was used as an isotype CTRL. NK1.1/ILC depletion

was achieved by two injections of anti-NK1.1 mAb (Clone PK136) at 100 µg per mouse two days prior to MCA205 cell injection and maintained by injections on days 12 and 24. A mouse IgG2a mAb (Clone C1.18.4) was used as the isotype control. The neutralizing IFN γ Ultra-LEAF™ purified antibody was intraperitoneally injected at D20 and D23 at 200 µg per mouse.

HSV-1 infection

For HSV-1 infection, the KOS strain of HSV-1 was used (Filtjens et al., 2021). Briefly, HSV-1 was grown and titrated on confluent Vero cells in minimal essential medium containing 10% FCS, 50µM 2-mercaptoethanol, 2 mM L-glutamine, 100 U/mL penicillin, and 100 µg/mL streptomycin. Mice were inoculated with HSV-1 by flank scarification (98). Female mice (8 weeks old) were anesthetized by i.p. injection (10 µL/g body weight) of ketamine (2%) / Rompun (5%) in saline solution. The left flank of each mouse was clipped and depilated with Veet hair remover cream. A small area of the skin was abraded with a MultiPro power tool (Dremel, Racine, WI), and 10 µL of viral suspension containing 10⁶ PFU was applied to the skin lesion. Skin samples were harvested using a 12x12 mm skin punch biopsy and immune infiltrate was analyzed on D8 post HSV-1 infection by flow cytometry. To study the virus-specific CD8⁺ T cell response, we used a tetramer H-2K(b) composed of the HSV-1-derived peptide of the SSIEFARL sequence encoding glycoprotein B (NIH tetramer core facilities).

DC-OT-1 co-culture

TDLNs from control PBS and Pant mice were collected and CD11c⁺ cells were sorted using the CD11c Microbeads UltraPure mouse kit (Miltenyi Biotec). CD11c⁺ cells were incubated in a 96-well plate for 1 h at 37 °C with or without the OVA peptide (SIINFEKL). T cells were isolated and purified from the spleens of transgenic OT-1 mice by negative selection using the CD8 α ⁺ cell Isolation Kit from Miltenyi Biotec, according to the manufacturer's instructions, and stained with the Cell Trace Violet Cell Proliferation Kit (Invitrogen), according to the manufacturer's instructions. CD11c⁺ cells and T cells were co-cultured (ratio of 1:10) for three days. Cells were stained with a fixable blue dead-cell staining kit (Invitrogen) and anti-mouse CD8 antibody (PE-Cy5, 53-6.7, 55304 BD). T cell proliferation was assessed using flow cytometry.

Immunofluorescence

For immunofluorescence experiments, tumors were harvested, washed and fixed in Antigenfix solution (Diapath) for 2h with agitation. After several steps of PBS 1X washing, samples were placed in PBS containing 30% sucrose overnight and included in OCT. After saturation with PBS 2% BSA, samples were stained by overnight incubation at 4°C with anti-CD8b (BioXcell - Clone 53-5.8) and MHC-II (BD-Pharmingen – 2G9) mAbs. After incubation with donkey anti-

rabbit Cy3 serum and streptavidin Alexa488 (BioLegend), samples were mounted in mounting medium. Images were acquired using a Zeiss LSM780 confocal microscope and analyzed using ZEN 2.3 software.

Immunohistology

Histological analysis of osteosarcoma, and MCA tumors was realized on 5µm-thick slice mounted in SuperFrost-Plus (VWR, Radnor, Pennsylvania, USA). After deparaffinization and rehydration, hematoxylin-phlowin-safran (HPS) staining was performed to discriminate between the tumor and surrounding tissues. CD8, CD3, and CD31 were stained by immunohistochemistry on the Lyon-Est Research Anatomopathology platform on an automated staining system Ventana Discovery XT (Ventana Medical Systems, Roche, Tucson, Arizona, USA). Slides were digitized using Histech 3D slide scanner. The slide scans were analyzed using QuPath v0.3.0 software (Bankhead et al., 2017). After manual annotation of the tumor area, a specific script for IHC and HPS staining detection was created to quantify the labeled immune cells and the rate of necrotic tissue present in the tumors. The immune infiltration score displayed in Fig4B was calculated for each section as follows: 0, cold tumors; 1, peri-infiltrated tumors; 2-3, weak or strong infiltration by TILs in the tumor mass.

Analysis of VNN1 expression in TCGA Database and Cibersort

The TCGA-SARC dataset was retrieved using the TCGA Biolinks package. Raw HTSeq counts were normalized using DESeq2 variance stabilizing transformation. Co-expression unsigned networks were produced using WGCNA with biweight mid-correlation and soft power =13. Each module was further 2-means clustered to separate correlated and anticorrelated patterns, and their gene sets were queried for functional enrichment against the MSigDB Hallmark (Yu et al., 2012; Liberzon et al., 2015).

Analysis of VNN1 expression in soft tissue sarcoma clinical samples

We analyzed our database (Bertucci et al., 2022) including 1.377 cases of clinically annotated STS clinical samples with available normalized gene expression profiles. Data were gathered from 15 public data sets (Fig.S8C), all samples were from operative specimens of previously untreated primary tumors, and the gene expression profiles were generated using DNA microarrays or RNA-sequencing. VNN1 mRNA expression was analyzed as discrete variable (high vs. low) using the mean expression level of the whole series as a cut-off. As we found a link between VNN1 and immunity in our mouse model, we searched for correlations between VNN1 tumor expression and several immunity-related variables. The latter included the following multigene classifiers/scores: the 3 Gatza's immune pathway activation scores (Gatza et al., 2010), the 24 Bindea's innate and adaptive immune cell subpopulations (Bindea et al.,

2013), two signatures associated with anti-tumor cytotoxic immune response (the Immunologic Constant of Rejection (ICR) classifier (Bertucci et al., 2022), and Rooney's cytolytic activity score (Rooney et al., 2015)), two metagenes associated with response to immune checkpoint inhibitors ICI (the Ayers' T-cell-inflamed signature (TIS) (Ayers et al., 2017), and the Coppola's tertiary lymphoid structures (TLS) signature, the Ballot's Tumor Infiltrating Lymphocytes Signature (TILS) along with both of its inner lymphoid and myeloid signatures (Ballot et al., 2020) and the Thompson's Antigen Processing and presenting Machinery Score (APMS) (Thompson et al., 2020). The correlations between VNN1 expression-based classes and clinicopathological variables were measured using Fisher's exact test or Student's t-test when appropriate. The correlations of immune variables with VNN1-based classes were assessed using logistic regression analysis with the glm function (R statistical package; significance estimated by specifying a binomial family for models with a logit link). The endpoint of the prognostic analysis was the metastasis-free survival (MFS), which was calculated from the date of diagnosis to the date of metastatic relapse or death from any cause, whichever occurred first. Follow-up was measured from the date of diagnosis to the date of last news for event-free patients. Survival was estimated using the Kaplan-Meier method, and curves were compared with the log-rank test. Univariate and multivariate prognostic analyses were performed using the Cox regression analysis (Wald test). The variables tested in the univariate analysis were the patients' age and sex, pathological grade (2-3, 1), pathological size (pT1, pT2), tumor depth (deep, superficial), tumor site (extremities, head and neck, internal trunk, superficial trunk), and VNN1-based classification (high, low). Multivariate analysis incorporated all variables with a p-value < 5% in the univariate analysis. All statistical tests were two-sided, and the significance threshold was set at 5%. Analyses were performed using the survival package (version 2.43) in the R software (version 3.5.2).

Statistical analysis

The sample sizes were designed to minimize the number of individual experimental units (mice or samples) and obtain informative results and appropriate material for downstream analysis. This represents five mice per group and experiments were typically performed twice, unless otherwise stated in the figure legends. GraphPad Prism 7 software was used for the statistical significance assessment. The Gaussian distribution was tested using the D'Agostino–Pearson omnibus normality test. When passing the normality test, the Student's t test was used. Otherwise, the Mann–Whitney U test was used. Differences were considered statistically significant when **** $p < 0.0001$, *** $p < 0.001$, ** $p < 0.01$, * $p < 0.05$.

Acknowledgments

The ANR PLBIO19-015 grant supported the work realized in the PN, JC, LS and JYB teams and RM funding. We thank the core facilities involved in this project: CIML Flow cytometry, CIML Genomics Platform, CIML Animal facilities, and Imagimm. BM and SH were supported by the DCBIOL LabEx (grants ANR-11-LABEX-0043 and ANR-10-IDEX-0001-02 PSL). AR and SU were supported by the European Research Council (ERC) under the European Union's Horizon 2020 research and innovation program, under grant agreement No. 648768, from the Agence Nationale de la Recherche (ANR) (No. ANR-14-CE14-00 09-01), and the Fondation pour la Recherche Médicale (FRM). This work was also supported by institutional grants from INSERM, CNRS, Aix-Marseille University and Marseille-Immunopole to CIML. Guillaume Charbonnier performed bioinformatics analysis of TCGA database. We thank Thomas Vannier from the CENTURI Multi-Engineering Platform for preliminary work on the datamining of the cancer databases. The project leading to this publication has received funding from France 2030, the French Government program managed by the French National Research Agency (ANR-16-CONV-0001) and from Excellence Initiative of Aix-Marseille University - A*MIDEX ". JYB is supported by funds from NetSARC, LYRIC (INCA-DGOS 4664), LYon Recherche Innovation contre le CANcer, European Clinical trials in Rare Sarcomas (FP7-278742), and the European network for Rare Adult Solid Cancer. We thank A. Carrier and T. Nguyen for their assistance with the use of the Cell Culture Platform facility (Centre de Recherche contre le Cancer de Marseille, U1068) in charge of the Seahorse platform.

Abbreviations

APM, antigen-processing molecules; Arg1, arginase 1; Bnip3, BCL2/adenovirus E1B 19 kDa protein-interacting protein 3; CBA, cytometric bead assay; CD74, invariant chain; CEA, cysteamine; CCL or CXCL, CC or CXC chemokines; CCR, CXCR or XCR, CC, CXC or XC chemokine receptors; CFSE, carboxyfluorescein-succinidimyl ester; CoA, coenzyme A; CTLA4, cytotoxic T-lymphocyte associated protein 4; DC, dendritic cell; DCA, dichloroacetate; DDIT, DNA damage induced transcript; ECAR, extracellular acidification rate; ER, endoplasmic reticulum; Flt3, Fms Related Receptor Tyrosine Kinase 3; GZMB, granzyme B; ICI, immune checkpoint inhibitors; GSEA, geneset enrichment analysis; HSV, herpes simplex virus; ICR, Immunologic Constant of Rejection; IFN, interferon; ILC, innate lymphoid cell; KEGG, Kyoto Encyclopedia of Genes and Genomes pathways; LDHA, lactic acid-dehydrogenase; MCA, 3-methylcholanthrene; MDR, mitotracker deep red; MG, mitotracker green; MFS, metastasis-free survival; MHC, major histocompatibility complex; MMP9, metalloprotease 9; MSigDB, Molecular Signatures Database; mtDNA, mitochondrial DNA; mtROS, mitochondrial reactive oxygen species; NK, natural killer cell; NMR, nuclear magnetic

resonance; OCR, oxygen consumption rate; OsA, osteosarcoma; OT, ovalbumin-specific T cell; Pant, pantethine; Pan, pantothenate; PCA, principal component analysis; PD1, Programmed cell death protein-1; Pgam, Phosphoglycerate Mutase 1; PGC1 α , peroxisome-proliferator-activated receptor γ coactivator-1 α ; PRF1, perforin 1; QC, quality control; STS, soft tissue sarcomas; TAM, tumor-associated macrophages; TCGA, The Cancer Genome Atlas; TDLNs, tumor and draining lymph nodes; TILS, tumor-infiltrating lymphocytes; TIM3, TIM immunoregulatory protein 3; TLR, Toll-like receptor; TIS, tumor inflammation signature; TME, tumor microenvironment; TNF, tumor necrosis factor; Treg, regulatory CD4+ T lymphocyte; UMAP, uniform manifold approximation; VEGF, vascular endothelium growth factor; vitB5, vitamin B5; VNN, VANIN; WGCNA, weighted correlation network analysis.

Availability of data and materials

The data used for the bioinformatics analysis were obtained from the publicly available TCGA database. The source code for all the analyses is available at <https://github.com/guillaumecharbonnier/mw-miallot2022> and a compiled version of the Bookdown report is available at <https://guillaumecharbonnier.github.io/mw-miallot2022>

Author contribution

RM, VM, AR, CT, PB, and JSL performed experiments. JC, LS, BM, SH, and SU provided technical assistance, expertise and mice. Single-cell analysis was performed by RF. AD and PF contributed to the bioinformatic analysis of data from sarcoma patients, collected and supervised by JYB and FB. RM, VM and PN analyzed the data and prepared the figures. FG contributed to the manuscript corrections and coaching. PN conceptualized and supervised the project, and RM and PN prepared the manuscript.

Conflict of interest

The authors declare that they have no conflict of interest.

BIBLIOGRAPHY

- Abdi, K., and N.J. Singh. 2015. Making many from few: IL-12p40 as a model for the combinatorial assembly of heterodimeric cytokines. *Cytokine*. 76:53–57. doi:10.1016/j.cyto.2015.07.026.
- Abeshouse, A., C. Adebamowo, S.N. Adebamowo, R. Akbani, T. Akeredolu, A. Ally, M.L. Anderson, P. Anur, E.L. Appelbaum, J. Armenia, J.T. Auman, M.H. Bailey, L. Baker, M. Balasundaram, S. Balu, F.P. Barthel, J. Bartlett, S.B. Baylin, M. Behera, D. Belyaev, J. Bennett, C. Benz, R. Beroukhim, M. Birrer, T. Bocklage, T. Bodenheimer, L. Boice, M.S. Bootwalla, J. Bowen, R. Bowlby, J. Boyd, A.S. Brohl, D. Brooks, L. Byers, R. Carlsen, P. Castro, H.-W. Chen, A.D. Cherniack, F. Chibon, L. Chin, J. Cho, E. Chuah, S. Chudamani, C. Cibulskis, L.A.D. Cooper, L. Cope, M.G. Cordes, D. Crain, E. Curley, L. Danilova, F. Dao, I.J. Davis, L.E. Davis, T. Defreitas, K. Delman, J.A. Demchok, G.D. Demetri, E.G. Demicco, N. Dhalla, L. Diao, L. Ding, P. DiSaia, P. Dottino, L.A. Doyle, E. Drill, M. Dubina, J. Eschbacher, K. Fedosenko, I. Felau, M.L. Ferguson, S. Frazer, C.C. Fronick, V. Fulidou, L.A. Fulton, R.S. Fulton, S.B. Gabriel, J. Gao, Q. Gao, J. Gardner, J.M. Gastier-Foster, C.M. Gay, N. Gehlenborg, M. Gerken, G. Getz, A.K. Godwin, E.M. Godwin, E. Gordienko, J.E. Grilley-Olson, D.A. Gutman, D.H. Gutmann, D.N. Hayes, A.M. Hegde, D.I. Heiman, Z. Heins, C. Helsel, A.J. Hepperla, K. Higgins, K.A. Hoadley, et al. 2017. Comprehensive and Integrated Genomic Characterization of Adult Soft Tissue Sarcomas. *Cell*. 171:950-965.e28. doi:10.1016/j.cell.2017.10.014.
- Almeida, L., A. Dhillon-LaBrooy, G. Carriche, L. Berod, and T. Sparwasser. 2021. CD4+ T-cell differentiation and function: Unifying glycolysis, fatty acid oxidation, polyamines NAD mitochondria. *Journal of Allergy and Clinical Immunology*. 148:16–32. doi:10.1016/j.jaci.2021.03.033.
- Ayers, M., J. Lunceford, M. Nebozhyn, E. Murphy, A. Loboda, D.R. Kaufman, A. Albright, J.D. Cheng, S.P. Kang, V. Shankaran, S.A. Piha-Paul, J. Yearley, T.Y. Seiwert, A. Ribas, and T.K. McClanahan. 2017. IFN- γ -related mRNA profile predicts clinical response to PD-1 blockade. *J Clin Invest*. 127:2930–2940. doi:10.1172/JCI91190.
- Bailis, W., J.A. Shyer, J. Zhao, J.C.G. Canaveras, F.J. Al Khazal, R. Qu, H.R. Steach, P. Bielecki, O. Khan, R. Jackson, Y. Kluger, L.J. Maher, J. Rabinowitz, J. Craft, and R.A. Flavell. 2019. Distinct modes of mitochondrial metabolism uncouple T cell differentiation and function. *Nature*. 571:403–407. doi:10.1038/s41586-019-1311-3.
- Ballot, E., S. Ladoire, B. Routy, C. Truntzer, and F. Ghiringhelli. 2020. Tumor Infiltrating Lymphocytes Signature as a New Pan-Cancer Predictive Biomarker of Anti PD-1/PD-L1 Efficacy. *Cancers (Basel)*. 12:E2418. doi:10.3390/cancers12092418.
- Bankhead, P., M.B. Loughrey, J.A. Fernández, Y. Dombrowski, D.G. McArt, P.D. Dunne, S. McQuaid, R.T. Gray, L.J. Murray, H.G. Coleman, J.A. James, M. Salto-Tellez, and P.W. Hamilton. 2017. QuPath: Open source software for digital pathology image analysis. *Sci Rep*. 7:16878. doi:10.1038/s41598-017-17204-5.
- Barry, K.C., J. Hsu, M.L. Broz, F.J. Cueto, M. Binnewies, A.J. Combes, A.E. Nelson, K. Loo, R. Kumar, M.D. Rosenblum, M.D. Alvarado, D.M. Wolf, D. Bogunovic, N. Bhardwaj, A.I. Daud, P.K. Ha, W.R. Ryan, J.L. Pollack, B. Samad, S. Asthana, V. Chan, and M.F. Krummel. 2018. A natural killer-dendritic cell axis defines checkpoint therapy-responsive tumor microenvironments. *Nat Med*. 24:1178–1191. doi:10.1038/s41591-018-0085-8.

- Bengsch, B., A.L. Johnson, M. Kurachi, P.M. Odorizzi, K.E. Pauken, J. Attanasio, E. Stelekati, L.M. McLane, M.A. Paley, G.M. Delgoffe, and E.J. Wherry. 2016. Bioenergetic Insufficiencies Due to Metabolic Alterations Regulated by the Inhibitory Receptor PD-1 Are an Early Driver of CD8(+) T Cell Exhaustion. *Immunity*. 45:358–373. doi:10.1016/j.immuni.2016.07.008.
- Bergen, V., M. Lange, S. Peidli, F.A. Wolf, and F.J. Theis. 2020. Generalizing RNA velocity to transient cell states through dynamical modeling. *Nat Biotechnol*. 38:1408–1414. doi:10.1038/s41587-020-0591-3.
- Bertucci, F., V. Niziers, A. de Nonneville, P. Finetti, L. Mescam, O. Mir, A. Italiano, A. Le Cesne, J.-Y. Blay, M. Ceccarelli, D. Bedognetti, D. Birnbaum, and E. Mamessier. 2022. Immunologic constant of rejection signature is prognostic in soft-tissue sarcoma and refines the CINSARC signature. *J Immunother Cancer*. 10:e003687. doi:10.1136/jitc-2021-003687.
- Bindea, G., B. Mlecnik, M. Tosolini, A. Kirilovsky, M. Waldner, A.C. Obenauf, H. Angell, T. Fredriksen, L. Lafontaine, A. Berger, P. Bruneval, W.H. Fridman, C. Becker, F. Pagès, M.R. Speicher, Z. Trajanoski, and J. Galon. 2013. Spatiotemporal Dynamics of Intratumoral Immune Cells Reveal the Immune Landscape in Human Cancer. *Immunity*. 39:782–795. doi:10.1016/j.immuni.2013.10.003.
- Blank, C.U., W.N. Haining, W. Held, P.G. Hogan, A. Kallies, E. Lugli, R.C. Lynn, M. Philip, A. Rao, N.P. Restifo, A. Schietinger, T.N. Schumacher, P.L. Schwartzberg, A.H. Sharpe, D.E. Speiser, E.J. Wherry, B.A. Youngblood, and D. Zehn. 2019. Defining “T cell exhaustion.” *Nat Rev Immunol*. 19:665–674. doi:10.1038/s41577-019-0221-9.
- Bonifaz, L., M. Cervantes-Silva, E. Ontiveros-Dotor, E. López-Villegas, and F. Sánchez-García. 2014. A Role For Mitochondria In Antigen Processing And Presentation. *Immunology*. doi:10.1111/imm.12392.
- Brewitz, A., S. Eickhoff, S. Dähling, T. Quast, S. Bedoui, R.A. Kroczeck, C. Kurts, N. Garbi, W. Barchet, M. Iannacone, F. Klauschen, W. Kolanus, T. Kaisho, M. Colonna, R.N. Germain, and W. Kastanmüller. 2017. CD8+ T Cells Orchestrate pDC-XCR1+ Dendritic Cell Spatial and Functional Cooperativity to Optimize Priming. *Immunity*. 46:205–219. doi:10.1016/j.immuni.2017.01.003.
- Broz, M.L., M. Binnewies, B. Boldajipour, A.E. Nelson, J.L. Pollack, D.J. Erle, A. Barczak, M.D. Rosenblum, A. Daud, D.L. Barber, S. Amigorena, L.J. Van’t Veer, A.I. Sperling, D.M. Wolf, and M.F. Krummel. 2014. Dissecting the tumor myeloid compartment reveals rare activating antigen-presenting cells critical for T cell immunity. *Cancer Cell*. 26:638–652. doi:10.1016/j.ccell.2014.09.007.
- Chamoto, K., P.S. Chowdhury, A. Kumar, K. Sonomura, F. Matsuda, S. Fagarasan, and T. Honjo. 2017. Mitochondrial activation chemicals synergize with surface receptor PD-1 blockade for T cell-dependent antitumor activity. *Proc. Natl. Acad. Sci. U.S.A.* 114. doi:10.1073/pnas.1620433114.
- Chang, C.-H., J.D. Curtis, L.B. Maggi, B. Faubert, A.V. Villarino, D. O’Sullivan, S.C.-C. Huang, G.J.W. van der Windt, J. Blagih, J. Qiu, J.D. Weber, E.J. Pearce, R.G. Jones, and E.L. Pearce. 2013. Posttranscriptional control of T cell effector function by aerobic glycolysis. *Cell*. 153:1239–1251. doi:10.1016/j.cell.2013.05.016.
- Chang, C.-H., J. Qiu, D. O’Sullivan, M.D. Buck, T. Noguchi, J.D. Curtis, Q. Chen, M. Gindin, M.M. Gubin, G.J.W. van der Windt, E. Tonc, R.D. Schreiber, E.J. Pearce, and E.L. Pearce. 2015. Metabolic Competition in the Tumor Microenvironment Is a Driver of Cancer Progression. *Cell*. 162:1229–1241. doi:10.1016/j.cell.2015.08.016.

- Chen, X., E. Stewart, A.A. Shelat, C. Qu, A. Bahrami, M. Hatley, G. Wu, C. Bradley, J. McEvoy, A. Pappo, S. Spunt, M.B. Valentine, V. Valentine, F. Krafcik, W.H. Lang, M. Wierdl, L. Tsurkan, V. Tolleman, S.M. Federico, C. Morton, C. Lu, L. Ding, J. Easton, M. Rusch, P. Nagahawatte, J. Wang, M. Parker, L. Wei, E. Hedlund, D. Finkelstein, M. Edmonson, S. Shurtleff, K. Boggs, H. Mulder, D. Yergeau, S. Skapek, D.S. Hawkins, N. Ramirez, P.M. Potter, J.A. Sandoval, A.M. Davidoff, E.R. Mardis, R.K. Wilson, J. Zhang, J.R. Downing, and M.A. Dyer. 2013. Targeting Oxidative Stress in Embryonal Rhabdomyosarcoma. *Cancer Cell*. 24:710–724. doi:10.1016/j.ccr.2013.11.002.
- Choi, J.H., and J.Y. Ro. 2021. The 2020 WHO Classification of Tumors of Bone: An Updated Review. *Advances in Anatomic Pathology*. 28:119–138. doi:10.1097/PAP.0000000000000293.
- Chow, M.T., A.J. Ozga, R.L. Servis, D.T. Frederick, J.A. Lo, D.E. Fisher, G.J. Freeman, G.M. Boland, and A.D. Luster. 2019. Intratumoral Activity of the CXCR3 Chemokine System Is Required for the Efficacy of Anti-PD-1 Therapy. *Immunity*. 50:1498-1512.e5. doi:10.1016/j.immuni.2019.04.010.
- Chowdhury, P.S., K. Chamoto, A. Kumar, and T. Honjo. 2018. PPAR-Induced Fatty Acid Oxidation in T Cells Increases the Number of Tumor-Reactive CD8+ T Cells and Facilitates Anti-PD-1 Therapy. *Cancer Immunol Res*. 6:1375–1387. doi:10.1158/2326-6066.CIR-18-0095.
- Cooper, A.M., and S.A. Khader. 2007. IL-12p40: an inherently agonistic cytokine. *Trends Immunol*. 28:33–38. doi:10.1016/j.it.2006.11.002.
- de la Cruz-López, K.G., L.J. Castro-Muñoz, D.O. Reyes-Hernández, A. García-Carrancá, and J. Manzo-Merino. 2019. Lactate in the Regulation of Tumor Microenvironment and Therapeutic Approaches. *Frontiers in Oncology*. 9.
- Cueto, F.J., and D. Sancho. 2021. The Flt3L/Flt3 Axis in Dendritic Cell Biology and Cancer Immunotherapy. *Cancers*. 13:1525. doi:10.3390/cancers13071525.
- Dangaj, D., M. Bruand, A.J. Grimm, C. Ronet, D. Barras, P.A. Duttagupta, E. Lanitis, J. Duraiswamy, J.L. Tanyi, F. Benencia, J. Conejo-Garcia, H.R. Ramay, K.T. Montone, D.J. Powell, P.A. Gimotty, A. Facciabene, D.G. Jackson, J.S. Weber, S.J. Rodig, S.F. Hodi, L.E. Kandalaft, M. Irving, L. Zhang, P. Foukas, S. Rusakiewicz, M. Delorenzi, and G. Coukos. 2019. Cooperation between Constitutive and Inducible Chemokines Enables T Cell Engraftment and Immune Attack in Solid Tumors. *Cancer Cell*. 35:885-900.e10. doi:10.1016/j.ccell.2019.05.004.
- D'Angelo, S.P., W.D. Tap, G.K. Schwartz, and R.D. Carvajal. 2014. Sarcoma Immunotherapy: Past Approaches and Future Directions. *Sarcoma*. 2014:1–13. doi:10.1155/2014/391967.
- Doedens, A.L., A.T. Phan, M.H. Stradner, J.K. Fujimoto, J.V. Nguyen, E. Yang, R.S. Johnson, and A.W. Goldrath. 2013. Hypoxia-inducible factors enhance the effector responses of CD8(+) T cells to persistent antigen. *Nat Immunol*. 14:1173–1182. doi:10.1038/ni.2714.
- Dorner, B.G., M.B. Dorner, X. Zhou, C. Opitz, A. Mora, S. Güttler, A. Hutloff, H.W. Mages, K. Ranke, M. Schaefer, R.S. Jack, V. Henn, and R.A. Kroccek. 2009. Selective expression of the chemokine receptor XCR1 on cross-presenting dendritic cells determines cooperation with CD8+ T cells. *Immunity*. 31:823–833. doi:10.1016/j.immuni.2009.08.027.
- Du, K., J. Hyun, R.T. Premont, S.S. Choi, G.A. Michelotti, M. Swiderska-Syn, G.D. Dalton, E. Thelen, B.S. Rizi, Y. Jung, and A.M. Diehl. 2018. Hedgehog-YAP Signaling Pathway Regulates Glutaminolysis to Control Activation of Hepatic Stellate Cells. *Gastroenterology*. 154:1465-1479.e13. doi:10.1053/j.gastro.2017.12.022.

- Elefantova, K., B. Lakatos, J. Kubickova, Z. Sulova, and A. Breier. 2018. Detection of the Mitochondrial Membrane Potential by the Cationic Dye JC-1 in L1210 Cells with Massive Overexpression of the Plasma Membrane ABCB1 Drug Transporter. *IJMS*. 19:1985. doi:10.3390/ijms19071985.
- Eulo, V., and B.A. Van Tine. 2022. Immune checkpoint inhibitor resistance in soft tissue sarcoma. *Cancer Drug Resistance*. 5:328–338. doi:10.20517/cdr.2021.127.
- Farrand, K.J., N. Dickgreber, P. Stoitzner, F. Ronchese, T.R. Petersen, and I.F. Hermans. 2009. Langerin+CD8 α + Dendritic Cells Are Critical for Cross-Priming and IL-12 Production in Response to Systemic Antigens. *The Journal of Immunology*. 183:7732–7742. doi:10.4049/jimmunol.0902707.
- Field, C.S., F. Baixauli, R.L. Kyle, D.J. Puleston, A.M. Cameron, D.E. Sanin, K.L. Hippen, M. Loschi, G. Thangavelu, M. Corrado, J. Edwards-Hicks, K.M. Grzes, E.J. Pearce, B.R. Blazar, and E.L. Pearce. 2020. Mitochondrial Integrity Regulated by Lipid Metabolism Is a Cell-Intrinsic Checkpoint for Treg Suppressive Function. *Cell Metab*. 31:422–437.e5. doi:10.1016/j.cmet.2019.11.021.
- Filtjens, J., A. Roger, L. Quatrini, E. Wieduwild, J. Gouilly, G. Hoeffel, R. Rossignol, C. Daher, G. Debroas, S. Henri, C.M. Jones, B. Malissen, L.K. Mackay, A. Moqrich, F.R. Carbone, and S. Ugolini. 2021. Nociceptive sensory neurons promote CD8 T cell responses to HSV-1 infection. *Nat Commun*. 12:2936. doi:10.1038/s41467-021-22841-6.
- Fletcher, C.D.M. 2014. The evolving classification of soft tissue tumours - an update based on the new 2013 WHO classification. *Histopathology*. 64:2–11. doi:10.1111/his.12267.
- Gao, Y., F. Souza-Fonseca-Guimaraes, T. Bald, S.S. Ng, A. Young, S.F. Ngiow, J. Rautela, J. Straube, N. Waddell, S.J. Blake, J. Yan, L. Bartholin, J.S. Lee, E. Vivier, K. Takeda, M. Messaoudene, L. Zitvogel, M.W.L. Teng, G.T. Belz, C.R. Engwerda, N.D. Huntington, K. Nakamura, M. Hölzel, and M.J. Smyth. 2017. Tumor immunoevasion by the conversion of effector NK cells into type 1 innate lymphoid cells. *Nat Immunol*. 18:1004–1015. doi:10.1038/ni.3800.
- Gatza, M.L., J.E. Lucas, W.T. Barry, J.W. Kim, Q. Wang, M.D. Crawford, M.B. Datto, M. Kelley, B. Mathey-Prevot, A. Potti, and J.R. Nevins. 2010. A pathway-based classification of human breast cancer. *Proc Natl Acad Sci U S A*. 107:6994–6999. doi:10.1073/pnas.0912708107.
- Gebhardt, T., P.G. Whitney, A. Zaid, L.K. Mackay, A.G. Brooks, W.R. Heath, F.R. Carbone, and S.N. Mueller. 2011. Different patterns of peripheral migration by memory CD4+ and CD8+ T cells. *Nature*. 477:216–219. doi:10.1038/nature10339.
- ggplot2. 2022.
- Giessner, C., V. Millet, K.J. Mostert, T. Gensollen, T.-P. Vu Manh, M. Garibal, B. Dieme, N. Attaf-Bouabdallah, L. Chasson, N. Brouilly, C. Laprie, T. Lesluyes, J.Y. Blay, L. Shintu, J.C. Martin, E. Strauss, F. Galland, and P. Naquet. 2018. Vnn1 pantetheinase limits the Warburg effect and sarcoma growth by rescuing mitochondrial activity. *Life Sci Alliance*. 1:e201800073. doi:10.26508/lsa.201800073.
- Gropper, Y., T. Feferman, T. Shalit, T.-M. Salame, Z. Porat, and G. Shakhar. 2017. Culturing CTLs under Hypoxic Conditions Enhances Their Cytolysis and Improves Their Anti-tumor Function. *Cell Rep*. 20:2547–2555. doi:10.1016/j.celrep.2017.08.071.

- Gu, Z., R. Eils, and M. Schlesner. 2016. Complex heatmaps reveal patterns and correlations in multidimensional genomic data. *Bioinformatics*. 32:2847–2849. doi:10.1093/bioinformatics/btw313.
- Hao, Y., S. Hao, E. Andersen-Nissen, W.M. Mauck, S. Zheng, A. Butler, M.J. Lee, A.J. Wilk, C. Darby, M. Zager, P. Hoffman, M. Stoeckius, E. Papalexi, E.P. Mimitou, J. Jain, A. Srivastava, T. Stuart, L.M. Fleming, B. Yeung, A.J. Rogers, J.M. McElrath, C.A. Blish, R. Gottardo, P. Smibert, and R. Satija. 2021. Integrated analysis of multimodal single-cell data. *Cell*. 184:3573-3587.e29. doi:10.1016/j.cell.2021.04.048.
- Harel, M., R. Ortenberg, S.K. Varanasi, K.C. Mangalhara, M. Mardamshina, E. Markovits, E.N. Baruch, V. Tripple, M. Arama-Chayoth, E. Greenberg, A. Shenoy, R. Ayasun, N. Knafo, S. Xu, L. Anafi, G. Yanovich-Arad, G.D. Barnabas, S. Ashkenazi, M.J. Besser, J. Schachter, M. Bosenberg, G.S. Shadel, I. Barshack, S.M. Kaeck, G. Markel, and T. Geiger. 2019. Proteomics of Melanoma Response to Immunotherapy Reveals Mitochondrial Dependence. *Cell*. 179:236-250.e18. doi:10.1016/j.cell.2019.08.012.
- Jackson, C.M., J. Choi, and M. Lim. 2019. Mechanisms of immunotherapy resistance: lessons from glioblastoma. *Nat Immunol*. 20:1100–1109. doi:10.1038/s41590-019-0433-y.
- Jha, A.K., S.C.-C. Huang, A. Sergushichev, V. Lampropoulou, Y. Ivanova, E. Loginicheva, K. Chmielewski, K.M. Stewart, J. Ashall, B. Everts, E.J. Pearce, E.M. Driggers, and M.N. Artyomov. 2015. Network integration of parallel metabolic and transcriptional data reveals metabolic modules that regulate macrophage polarization. *Immunity*. 42:419–430. doi:10.1016/j.immuni.2015.02.005.
- Jones, A.E., and A.S. Divakaruni. 2020. Macrophage activation as an archetype of mitochondrial repurposing. *Molecular Aspects of Medicine*. 71:100838. doi:10.1016/j.mam.2019.100838.
- Kamiński, M.M., S.W. Sauer, M. Kamiński, S. Opp, T. Ruppert, P. Grigaravičius, P. Grudnik, H.-J. Gröne, P.H. Krammer, and K. Gülow. 2012. T cell activation is driven by an ADP-dependent glucokinase linking enhanced glycolysis with mitochondrial reactive oxygen species generation. *Cell Rep*. 2:1300–1315. doi:10.1016/j.celrep.2012.10.009.
- Kanehisa, M., M. Furumichi, Y. Sato, M. Kawashima, and M. Ishiguro-Watanabe. 2022. KEGG for taxonomy-based analysis of pathways and genomes. *Nucleic Acids Res*. gkac963. doi:10.1093/nar/gkac963.
- Kavian, N., S. Mehlal, W. Marut, A. Servettaz, C. Giessner, C. Bourges, C. Nicco, C. Chéreau, H. Lemaréchal, M.-F. Dutilh, O. Cerles, P. Guilpain, V. Vuiblet, S. Chouzenoux, F. Galland, I. Quere, B. Weill, P. Naquet, and F. Batteux. 2016. Imbalance of the Vanin-1 Pathway in Systemic Sclerosis. *The Journal of Immunology*. 197:3326–3335. doi:10.4049/jimmunol.1502511.
- Klein Geltink, R.I., R.L. Kyle, and E.L. Pearce. 2018. Unraveling the Complex Interplay Between T Cell Metabolism and Function. *Annu. Rev. Immunol*. 36:461–488. doi:10.1146/annurev-immunol-042617-053019.
- Korotkevich, G., V. Sukhov, N. Budin, B. Shpak, M.N. Artyomov, and A. Sergushichev. 2021. Fast gene set enrichment analysis. 060012. doi:10.1101/060012.
- Kratchmarov, R., S. Viragova, M.J. Kim, N.J. Rothman, K. Liu, B. Reizis, and S.L. Reiner. 2018. Metabolic control of cell fate bifurcations in a hematopoietic progenitor population. *Immunology & Cell Biology*. 96:863–871. doi:10.1111/imcb.12040.

- LeBleu, V.S., J.T. O'Connell, K.N. Gonzalez Herrera, H. Wikman, K. Pantel, M.C. Haigis, F.M. de Carvalho, A. Damascena, L.T. Domingos Chinen, R.M. Rocha, J.M. Asara, and R. Kalluri. 2014. PGC-1 α mediates mitochondrial biogenesis and oxidative phosphorylation in cancer cells to promote metastasis. *Nat Cell Biol.* 16:992–1003. doi:10.1038/ncb3039.
- Liberti, M.V., and J.W. Locasale. 2016. The Warburg Effect: How Does it Benefit Cancer Cells? *Trends Biochem Sci.* 41:211–218. doi:10.1016/j.tibs.2015.12.001.
- Liberzon, A., C. Birger, H. Thorvaldsdóttir, M. Ghandi, J.P. Mesirov, and P. Tamayo. 2015. The Molecular Signatures Database Hallmark Gene Set Collection. *cels.* 1:417–425. doi:10.1016/j.cels.2015.12.004.
- van Lint, A., M. Ayers, A.G. Brooks, R.M. Coles, W.R. Heath, and F.R. Carbone. 2004. Herpes simplex virus-specific CD8⁺ T cells can clear established lytic infections from skin and nerves and can partially limit the early spread of virus after cutaneous inoculation. *J Immunol.* 172:392–397. doi:10.4049/jimmunol.172.1.392.
- Liu, Y., and X. Cao. 2015. The origin and function of tumor-associated macrophages. *Cell Mol Immunol.* 12:1–4. doi:10.1038/cmi.2014.83.
- Ma, E.H., M.J. Verway, R.M. Johnson, D.G. Roy, M. Steadman, S. Hayes, K.S. Williams, R.D. Sheldon, B. Samborska, P.A. Kosinski, H. Kim, T. Griss, B. Faubert, S.A. Condotta, C.M. Krawczyk, R.J. DeBerardinis, K.M. Stewart, M.J. Richer, V. Chubukov, T.P. Roddy, and R.G. Jones. 2019. Metabolic Profiling Using Stable Isotope Tracing Reveals Distinct Patterns of Glucose Utilization by Physiologically Activated CD8⁺ T Cells. *Immunity.* 51:856-870.e5. doi:10.1016/j.immuni.2019.09.003.
- Marcovecchio, P.M., G. Thomas, and S. Salek-Ardakani. 2021. CXCL9-expressing tumor-associated macrophages: new players in the fight against cancer. *J Immunother Cancer.* 9:e002045. doi:10.1136/jitc-2020-002045.
- Masoud, R., G. Reyes-Castellanos, S. Lac, J. Garcia, S. Dou, L. Shintu, N. Abdel Hadi, T. Gicquel, A. El Kaoutari, B. Diémé, F. Tranchida, L. Cormareche, L. Borge, O. Gayet, E. Pasquier, N. Dusetti, J. Iovanna, and A. Carrier. 2020. Targeting Mitochondrial Complex I Overcomes Chemoresistance in High OXPHOS Pancreatic Cancer. *Cell Reports Medicine.* 1:100143. doi:10.1016/j.xcrm.2020.100143.
- McInnes, L., J. Healy, and J. Melville. 2020. UMAP: Uniform Manifold Approximation and Projection for Dimension Reduction. doi:10.48550/arXiv.1802.03426.
- Meghari, S., C. Berruyer, H. Lepidi, F. Galland, P. Naquet, and J.-L. Mege. 2007. Vanin-1 controls granuloma formation and macrophage polarization in *Coxiella burnetii* infection. *Eur. J. Immunol.* 37:24–32. doi:10.1002/eji.200636054.
- Miallot, R., F. Galland, V. Millet, J.-Y. Blay, and P. Naquet. 2021. Metabolic landscapes in sarcomas. *J Hematol Oncol.* 14:114. doi:10.1186/s13045-021-01125-y.
- Miallot, R., V. Millet, Y. Groult, A. Modelska, L. Crescence, S. Roulland, S. Henri, B. Malissen, N. Brouilly, L. Panicot-Dubois, R. Vincentelli, G. Sulzenbacher, P. Finetti, A. Dutour, J.-Y. Blay, F. Bertucci, F. Galland, and P. Naquet. 2023. An OMA1 redox site controls mitochondrial homeostasis, sarcoma growth, and immunogenicity. *Life Sci. Alliance.* 6:e202201767. doi:10.26508/lsa.202201767.

- Michelakis, E.D., L. Webster, and J.R. Mackey. 2008. Dichloroacetate (DCA) as a potential metabolic-targeting therapy for cancer. *Br J Cancer*. 99:989–994. doi:10.1038/sj.bjc.6604554.
- Millet, V., T. Gensollen, M. Maltese, M. Serrero, N. Lesavre, C. Bourges, C. Pitaval, S. Cadra, L. Chasson, T.P. Vu Man, M. Masse, J.J. Martinez-Garcia, F. Tranchida, L. Shintu, K. Mostert, E. Strauss, P. Lepage, M. Chamillard, A. Broggi, L. Peyrin-Biroulet, J.-C. Grimaud, P. Naquet, and F. Galland. 2022. Harnessing the Vnn1 pantetheinase pathway boosts short chain fatty acids production and mucosal protection in colitis. *Gut*. gutjnl-2021-325792. doi:10.1136/gutjnl-2021-325792.
- Naquet, P., C. Giessner, and F. Galland. 2016. Metabolic adaptation of tissues to stress releases metabolites influencing innate immunity. *Current Opinion in Immunology*. 38:30–38. doi:10.1016/j.coi.2015.10.005.
- Naquet, P., E.W. Kerr, S.D. Vickers, and R. Leonardi. 2020. Regulation of coenzyme A levels by degradation: the ‘Ins and Outs.’ *Progress in Lipid Research*. 78:101028. doi:10.1016/j.plipres.2020.101028.
- Naquet, P., G. Pitari, S. Duprè, and F. Galland. 2014. Role of the Vnn1 pantetheinase in tissue tolerance to stress. *Biochemical Society Transactions*. 42:1094–1100. doi:10.1042/BST20140092.
- Paul, M.S., and P.S. Ohashi. 2020. The Roles of CD8+ T Cell Subsets in Antitumor Immunity. *Trends in Cell Biology*. 30:695–704. doi:10.1016/j.tcb.2020.06.003.
- Penet, M.-F., B. Krishnamachary, F. Wildes, Y. Mironchik, D. Mezzanzanica, F. Podo, M. de Reggi, B. Gharib, and Z.M. Bhujwalla. 2016. Effect of Pantethine on Ovarian Tumor Progression and Choline Metabolism. *Front. Oncol*. 6. doi:10.3389/fonc.2016.00244.
- Petitprez, F., A. de Reyniès, E.Z. Keung, T.W.-W. Chen, C.-M. Sun, J. Calderaro, Y.-M. Jeng, L.-P. Hsiao, L. Lacroix, A. Bougoüin, M. Moreira, G. Lacroix, I. Natario, J. Adam, C. Lucchesi, Y. Laizet, M. Toulmonde, M.A. Burgess, V. Bolejack, D. Reinke, K.M. Wani, W.-L. Wang, A.J. Lazar, C.L. Roland, J.A. Wargo, A. Italiano, C. Sautès-Fridman, H.A. Tawbi, and W.H. Fridman. 2020. B cells are associated with survival and immunotherapy response in sarcoma. *Nature*. 577:556–560. doi:10.1038/s41586-019-1906-8.
- Phan, A.T., A.L. Doedens, A. Palazon, P.A. Tyrakis, K.P. Cheung, R.S. Johnson, and A.W. Goldrath. 2016. Constitutive Glycolytic Metabolism Supports CD8+ T Cell Effector Memory Differentiation during Viral Infection. *Immunity*. 45:1024–1037. doi:10.1016/j.immuni.2016.10.017.
- Porporato, P.E. 2018. Mitochondrial metabolism and cancer. *Cell Research*. 28:16.
- Reinfeld, B.I., M.Z. Madden, M.M. Wolf, A. Chytil, J.E. Bader, A.R. Patterson, A. Sugiura, A.S. Cohen, A. Ali, B.T. Do, A. Muir, C.A. Lewis, R.A. Hongo, K.L. Young, R.E. Brown, V.M. Todd, T. Huffstater, A. Abraham, R.T. O’Neil, M.H. Wilson, F. Xin, M.N. Tantawy, W.D. Merryman, R.W. Johnson, C.S. Williams, E.F. Mason, F.M. Mason, K.E. Beckermann, M.G. Vander Heiden, H.C. Manning, J.C. Rathmell, and W.K. Rathmell. 2021. Cell-programmed nutrient partitioning in the tumour microenvironment. *Nature*. 593:282–288. doi:10.1038/s41586-021-03442-1.
- Rongvaux, A. 2018. Innate immunity and tolerance toward mitochondria. *Mitochondrion*. 41:14–20. doi:10.1016/j.mito.2017.10.007.
- Rooney, M.S., S.A. Shukla, C.J. Wu, G. Getz, and N. Hacohen. 2015. Molecular and genetic properties of tumors associated with local immune cytolytic activity. *Cell*. 160:48–61. doi:10.1016/j.cell.2014.12.033.

- Salerno, F., A. Guislain, D. Cansever, and M.C. Wolkers. 2016. TLR-Mediated Innate Production of IFN- γ by CD8⁺ T Cells Is Independent of Glycolysis. *The Journal of Immunology*. 196:3695–3705. doi:10.4049/jimmunol.1501997.
- Scharping, N.E., A.V. Menk, R.S. Moreci, R.D. Whetstone, R.E. Dadey, S.C. Watkins, R.L. Ferris, and G.M. Delgoffe. 2016. The Tumor Microenvironment Represses T Cell Mitochondrial Biogenesis to Drive Intratumoral T Cell Metabolic Insufficiency and Dysfunction. *Immunity*. 45:374–388. doi:10.1016/j.immuni.2016.07.009.
- Scharping, N.E., D.B. Rivadeneira, A.V. Menk, P.D.A. Vignali, B.R. Ford, N.L. Rittenhouse, R. Peralta, Y. Wang, Y. Wang, K. DePeaux, A.C. Poholek, and G.M. Delgoffe. 2021. Mitochondrial stress induced by continuous stimulation under hypoxia rapidly drives T cell exhaustion. *Nat Immunol*. 22:205–215. doi:10.1038/s41590-020-00834-9.
- Semenza, G.L. 2013. HIF-1 mediates metabolic responses to intratumoral hypoxia and oncogenic mutations. *J Clin Invest*. 123:3664–3671. doi:10.1172/JCI67230.
- Sena, L.A., S. Li, A. Jairaman, M. Prakriya, T. Ezponda, D.A. Hildeman, C.-R. Wang, P.T. Schumacker, J.D. Licht, H. Perlman, P.J. Bryce, and N.S. Chandel. 2013. Mitochondria are required for antigen-specific T cell activation through reactive oxygen species signaling. *Immunity*. 38:225–236. doi:10.1016/j.immuni.2012.10.020.
- Senyilmaz, D., and A.A. Teleman. 2015. Chicken or the egg: Warburg effect and mitochondrial dysfunction. *F1000Prime Rep*. 7. doi:10.12703/P7-41.
- Soto-Herederó, G., G. Desdín-Micó, and M. Mittelbrunn. 2021. Mitochondrial dysfunction defines T cell exhaustion. *Cell Metabolism*. 33:470–472. doi:10.1016/j.cmet.2021.02.010.
- Srivastava, R., A.A. Khan, S. Chilukuri, S.A. Syed, T.T. Tran, J. Furness, E. Bahraoui, and L. BenMohamed. 2017. CXCL10/CXCR3-Dependent Mobilization of Herpes Simplex Virus-Specific CD8⁺ T_{EM} and CD8⁺ T_{RM} Cells within Infected Tissues Allows Efficient Protection against Recurrent Herpesvirus Infection and Disease. *J Virol*. 91:e00278-17. doi:10.1128/JVI.00278-17.
- St. Paul, M., S.D. Saibil, S. Han, K. Israni-Winger, S.C. Lien, R.C. Laister, A. Sayad, S. Penny, R.N. Amaria, L.E. Haydu, C.R. Garcia-Batres, M. Kates, D.T. Mulder, C. Robert-Tissot, M.J. Gold, C.W. Tran, A.R. Elford, L.T. Nguyen, T.J. Pugh, D.M. Pinto, J.A. Wargo, and P.S. Ohashi. 2021. Coenzyme A fuels T cell anti-tumor immunity. *Cell Metabolism*. 33:2415-2427.e6. doi:10.1016/j.cmet.2021.11.010.
- Subramanian, A., P. Tamayo, V.K. Mootha, S. Mukherjee, B.L. Ebert, M.A. Gillette, A. Paulovich, S.L. Pomeroy, T.R. Golub, E.S. Lander, and J.P. Mesirov. 2005. Gene set enrichment analysis: a knowledge-based approach for interpreting genome-wide expression profiles. *Proc Natl Acad Sci U S A*. 102:15545–15550. doi:10.1073/pnas.0506580102.
- Tataranni, T., and C. Piccoli. 2019. Dichloroacetate (DCA) and Cancer: An Overview towards Clinical Applications. *Oxid Med Cell Longev*. 2019:8201079. doi:10.1155/2019/8201079.
- Tawbi, H.A., M. Burgess, V. Bolejack, B.A. Van Tine, S.M. Schuetze, J. Hu, S. D'Angelo, S. Attia, R.F. Riedel, D.A. Priebat, S. Movva, L.E. Davis, S.H. Okuno, D.R. Reed, J. Crowley, L.H. Butterfield, R. Salazar, J. Rodriguez-Canales, A.J. Lazar, I.I. Wistuba, L.H. Baker, R.G. Maki, D. Reinke, and S. Patel. 2017. Pembrolizumab in advanced soft-tissue sarcoma and bone sarcoma (SARC028): a multicentre, two-cohort, single-arm, open-label, phase 2 trial. *The Lancet Oncology*. 18:1493–1501. doi:10.1016/S1470-2045(17)30624-1.

- Thompson, J.C., C. Davis, C. Deshpande, W.-T. Hwang, S. Jeffries, A. Huang, T.C. Mitchell, C.J. Langer, and S.M. Albelda. 2020. Gene signature of antigen processing and presentation machinery predicts response to checkpoint blockade in non-small cell lung cancer (NSCLC) and melanoma. *J Immunother Cancer*. 8:e000974. doi:10.1136/jitc-2020-000974.
- Timblin, G.A., K.M. Tharp, J. ten Hoeve, I. Baydemir, C. Khantwal, J.N. Farahzad, J. Domínguez-Andrés, R.E. Vance, and V.M. Weaver. 2022. Coenzyme A governs proinflammatory macrophage metabolism. 2022.08.30.505732. doi:10.1101/2022.08.30.505732.
- Vienne, M., M. Etiennot, B. Escalière, J. Galluso, L. Spinelli, S. Guia, A. Fenis, E. Vivier, and Y.M. Kerdiles. 2021. Type 1 Innate Lymphoid Cells Limit the Antitumoral Immune Response. *Frontiers in Immunology*. 12.
- Wang, B., Q. Li, L. Qin, S. Zhao, J. Wang, and X. Chen. 2011. Transition of tumor-associated macrophages from MHC class IIhi to MHC class IIlow mediates tumor progression in mice. *BMC Immunol*. 12:43. doi:10.1186/1471-2172-12-43.
- Wei, S.C., C.R. Duffy, and J.P. Allison. 2018. Fundamental Mechanisms of Immune Checkpoint Blockade Therapy. *Cancer Discov*. 8:1069–1086. doi:10.1158/2159-8290.CD-18-0367.
- Whitehouse, S., R.H. Cooper, and P.J. Randle. 1974. Mechanism of activation of pyruvate dehydrogenase by dichloroacetate and other halogenated carboxylic acids. *Biochemical Journal*. 141:761–774. doi:10.1042/bj1410761.
- van der Windt, G.J.W., and E.L. Pearce. 2012. Metabolic switching and fuel choice during T-cell differentiation and memory development. *Immunol Rev*. 249:27–42. doi:10.1111/j.1600-065X.2012.01150.x.
- Wohn, C., V. Le Guen, O. Voluzan, F. Fiore, S. Henri, and B. Malissen. 2020. Absence of MHC class II on cDC1 dendritic cells triggers fatal autoimmunity to a cross-presented self-antigen. *Sci Immunol*. 5:eaba1896. doi:10.1126/sciimmunol.aba1896.
- Yang, M., W. Du, L. Yi, S. Wu, C. He, W. Zhai, C. Yue, R. Sun, A.V. Menk, G.M. Delgoffe, J. Jiang, and B. Lu. 2020. Checkpoint molecules coordinately restrain hyperactivated effector T cells in the tumor microenvironment. *Oncol Immunology*. 9:1708064. doi:10.1080/2162402X.2019.1708064.
- Yin, M., and L.A.J. O'Neill. 2021. The role of the electron transport chain in immunity. *The FASEB Journal*. 35:e21974. doi:10.1096/fj.202101161R.
- Yu, G., L.-G. Wang, Y. Han, and Q.-Y. He. 2012. clusterProfiler: an R Package for Comparing Biological Themes Among Gene Clusters. *OMICS: A Journal of Integrative Biology*. 16:284–287. doi:10.1089/omi.2011.0118.
- Yu, Y.-R., H. Imrichova, H. Wang, T. Chao, Z. Xiao, M. Gao, M. Rincon-Restrepo, F. Franco, R. Genolet, W.-C. Cheng, C. Jandus, G. Coukos, Y.-F. Jiang, J.W. Locasale, A. Zippelius, P.-S. Liu, L. Tang, C. Bock, N. Vannini, and P.-C. Ho. 2020. Disturbed mitochondrial dynamics in CD8+ TILs reinforce T cell exhaustion. *Nat Immunol*. 21:1540–1551. doi:10.1038/s41590-020-0793-3.
- Zheng, G.X.Y., J.M. Terry, P. Belgrader, P. Ryvkin, Z.W. Bent, R. Wilson, S.B. Ziraldo, T.D. Wheeler, G.P. McDermott, J. Zhu, M.T. Gregory, J. Shuga, L. Montesclaros, J.G. Underwood, D.A. Masquelier, S.Y. Nishimura, M. Schnall-Levin, P.W. Wyatt, C.M. Hindson, R. Bharadwaj, A. Wong, K.D. Ness, L.W. Beppu, H.J. Deeg, C. McFarland, K.R. Loeb, W.J. Valente, N.G. Ericson, E.A. Stevens, J.P.

Radich, T.S. Mikkelsen, B.J. Hindson, and J.H. Bielas. 2017. Massively parallel digital transcriptional profiling of single cells. *Nat Commun.* 8:14049. doi:10.1038/ncomms14049.

Zorov, D.B., M. Juhaszova, and S.J. Sollott. 2014. Mitochondrial Reactive Oxygen Species (ROS) and ROS-Induced ROS Release. *Physiol Rev.* 94:909–950. doi:10.1152/physrev.00026.2013.

Figure Legends:

Figure 1: VNN1 expression has prognostic value in soft tissue sarcomas.

A. Box plot showing the distribution of mRNA expression levels of VNN1 in 1377 tumor samples.

B. Correlations of VNN1 expression-based classes (high vs. low) and immune variables. Forest plots of correlations with the following immune features: immune pathways activation (Gatza), innate and adaptive immune cell subpopulations (Bindea), ICR score and cytolytic activity score associated with anti-tumor cytotoxic immune response, TIS signature and TLS signature associated with response to ICI, and antigen-processing machinery score. The p-values are for the logit link test. N= 1377 or 1152 (*).

C. Kaplan-Meier MFS curves according to VNN1 expression. The p-value is for the log-rank test.

D. Uni- and multivariate prognostic analyses for MFS. The p-values are for the Wald test.

Figure 2: Pantethine inhibits sarcoma growth.

A. Enzymatic reaction catalyzed by the Vanin1 pantetheinase: pantetheine is hydrolyzed by Vanin1 into cysteamine and vitamin B5 or pantothenic acid, the latter being the Coenzyme A biosynthetic precursor.

B. Schematic representation of the experimental design of murine MCA sarcoma model

C-D. MCA205 tumor growth scored after daily injections of Pant in C57BL/6 mice (n=88) (B) or Nude mice (n=18) (C). Two-way ANOVA with Šídák's multiple comparisons test. Data are shown with SEM.

E-F. Effect of Pant therapy in MCA tumor-bearing mice receiving anti-CTLA4 (n=7 per condition) (D); or anti-PD1 (n=6 per condition) mAbs (E).

G. Growth of OsA orthotopic tumors receiving independent or combined doxorubicine or Pant therapy or vehicle control (n=6 per condition).

H. Therapeutic effect of Pant therapy, alone (D) or combined with PD1 blockade (E) on B16F10 melanoma growth (n=10 per condition).

Figure 3: Analysis of the myeloid compartment.

A. Kinetic evaluation of the CD11b⁺/CD11b⁻ ratio by flow cytometry analysis of immune infiltrating cells in PBS or Pant tumors (n=6-8 per condition). Mann-Whitney test; **p-value < 0.01.

B-C. Quantification of monocyte (**B**) and TAM (**C**) clusters among CD45⁺ cells by flow cytometry on D20 tumors.

D. Proportion of MHCII^{low} and MHCII^{high} TAMs in total TAM (Ly6C^{low} F4/80⁺ CD64⁺) PBS and Pant-treated D20 tumors (n=12).

E. Volcano plot representation of myeloid cell transcripts showing differential expression between Pant and PBS samples at D20. Dot colors refer to average log₂FC: positive in red, negative in blue, below the threshold in black.

F. Individual uMAP projection, clustering, and population identification computed for the myeloid metacluster delineated 11 clusters: neutrophils, monocytes, Mono-TAM A-C, inflammatory TAM, TAM TNF α /NF κ B, moDC, CAF, M2 and Ki67 TAM.

G, H. Pearson's residuals of TAM and APC cell clusters from single-cell dataset obtained from CD45 enriched cells from tumors harvested at day 20 and D28 of PBS or Pant-treated mice (n=2).

I. Quantification of cell contacts between CD8 β ⁺ and MHC II⁺ cells on D24 tumor sections shown in **FigS5E**. Mann-Whitney test; ****p-value < 0.0001.

J. Proteomic profiling of tumor lysates represented by enrichment in Pant versus PBS condition (n=4).

Figure 4: Analysis of the lymphoid compartment.

A. Kinetic evaluation of the CD8⁺ / CD4⁺ Treg cell ratio by flow cytometry among immune infiltrated cells in tumor from PBS or Pant samples (n=5 per condition). Mann-Whitney test; * p-value<0.05. Gating strategy shown in FigS6B.

B. Relative numbers of TILs per mg of PBS and Pant tumors

C. Quantification of OVA-specific CD8 T cells in TDLN evaluated by flow cytometry using a SIINFEKL tetramer.

D. Flow cytometry analysis of effector molecule expression by CD8 T cells isolated from day 20 tumors and *in vitro* restimulated in the presence of PMA / Ionomycin / Brefeldin A (n=6) (**C**). Mann-Whitney test; **p-value < 0.01; * p-value<0.05.

E. Pearson's residuals of lymphoid cell clusters from single-cell dataset obtained from CD45 enriched cells from tumors harvested at day 20 and D28 of PBS or Pant samples (n=2).

F. Graphic representation of GSEA analyses performed in the proliferating CD8 T cell subset as indicated in Table 1.

G. Flow cytometry analysis of immune checkpoint expression by TILs from PBS and Pant-treated mice at day 28 (n=6). Mann-Whitney test; **p-value < 0.01; * p-value<0.05.

H. Projection of individual cell velocity as determined by scVelo analysis performed on each subset of lymphoid cells from D20 samples.

Figure 5: Requirements for Pant anti-tumor efficacy.

A-D. MCA growth curves in *Ifnrgr1*-deficient (n=7-8 per condition) (**A**), cDC1 cell-deficient *XCR1^{DTA}* (n=10-11 per condition) (**E**), anti CD8- (n=10-11 per condition) or anti NK1.1-treated (n=8 per condition) (**F**) control or Pant-treated mice. Two-way ANOVA with Šídák's multiple comparisons test; ****p-value < 0.0001, **p-value < 0.01, * p-value<0.05.

E-F. PFU quantifying viral load (**G**) and numbers of CD8⁺ T cell subpopulations (**H**) in the draining lymph nodes of HSV1-infected mice after 8 days of PBS or Pant treatment.

G. Immunohistochemistry analysis of PBS and Pant tumor sections using anti-CD3 and anti-CD8 mAbs on D24.

H. Quantification of the absolute number of positive cells per field (top panel) and of the immune infiltration score (bottom panel). n=10. Mann-Whitney test; ****p-value < 0.0001, * p-value<0.05.

Figure 6: Metabolic changes induced by Pant administration.

A. Metabolomics quantification of VitB5-related metabolites with or without Pant administration in tumor masses (n=7 per condition).

B. MCA205 tumor growth scored after daily injections of Pant, dichloroacetate (DCA) combined with Pant or not in C57BL/6 mice (n=24). Two-way ANOVA with Šídák's multiple comparisons test; ****p-value < 0.0001, ***p-value < 0.001, **p-value < 0.01, * p-value<0.05. Data are shown with SEM.

C. Metabolomics analysis of total tumors from mice treated with PBS, Pant, DCA, Pant + DCA by LC-MS (n=10) showing the hierarchical cluster of metabolic pathways according to treatment conditions. Scaling is in unit of variance (mean/squared root of SD).

D. Geometric mean fluorescence intensity (MFI) of MitoSox-stained MCA cells incubated or not for 4 hours in Pant-enriched medium *in vitro* (n=6 per condition). Mann-Whitney test; **p-value < 0.01.

E. Seahorse analysis of an energetic map integrating OCR and ECAR measurements of *in vitro* Pant-treated MCA205 or PBS control cells (n=2).

- F.** MDR/MG ratio of CD45⁺ cells at D24 and D28 from Pant-treated or PBS control mice (n=7).
- G.** Lactate concentration quantified in whole tumor masses from PBS or Pant-treated mice at day 20 post engraftment (n=8 per condition).
- H.** Energetic map of CD8⁺ TILs isolated from tumor mass D20 post cell engraftment. Mice were treated with PBS or Pant starting on day 10 (n=3).
- I.** MDR/MG ratio of CD8⁺ and CD4⁺ TILs at D20 and D28 from Pant-treated or PBS control mice (n=7). Mann-Whitney test; * p-value<0.05.

Supplementary Figure Legends

Figure S1: VNN1 expression in human soft tissue sarcomas and correlation with immune signatures and clinicopathological characteristics.

- A.** Pathway analysis using the WGCNA tool of Vanin1-coexpressed genes based on the analysis of the TCGA Database highlighting overexpressed MSigDB hallmarks.
- B.** Cibersort analysis of deconvoluting immune cell subsets enriched in VNN1-high tumors.
- C.** List of soft tissue sarcoma data sets included in our analysis.
- D.** Clinicopathological characteristics of patients and samples in the whole population and according to VNN1-based classification.

Figure S2: Absence of prognostic value for MFS of VNN1 expression in human bone sarcomas and osteosarcomas.

- A.** List of bone sarcoma and osteosarcoma data sets included in analysis.
- B.** Kaplan-Meier MFS curves according to *VNN1* mRNA expression in a cohort of 326 patients with bone sarcoma (left), and a subcohort of 94 patients with osteosarcoma (right). The p-values are for the log-rank test.

Figure S3: Effect of pantethine metabolites on growth.

- A-B.** Effect of administration of pantetheinase products CEA and Pan on MCA growth (A). Effect of *Vnn1*-expression on MCA growth (n=8) (B).
- C-D.** Immunohistochemistry analysis (C) and quantification (D) of paraffin-embedded OsA tumor samples using CD8, CD31 labelling and necrosis scoring; n=5-8.

Figure S4: Single cell analysis of myeloid cells.

- A.** uMAP representation of the 4 metaclusters identified after analysis of the pooled single-cell experimental data: myeloid, APC, lymphoid and non-immune cells called others.

B. Volcano plot highlighting the results of differential expression analysis in PBS versus Pant sample at day 28. The name of the top 10 up- and down-regulated genes sorted by p value are highlighted.

C-D. Density plot representation of the myeloid metacluster for each experimental condition (**C**) showing the definition of 11 cell subsets (**D**) based on the preferential expression of cell-specific markers (Fig3F) defining neutrophils (*Ly6g*, cluster 8), monocytes (*Ly6c2*, cluster 7), TAM subsets (*Adgre1*, clusters 2, 4-6, 10, 11), proliferating cells (*mKi67*, cluster 9) or cell signatures linked with activation or polarization pathways (cluster 11, TNF/NF- κ B; cluster 10 and 2 for M1- versus M2-like phenotypes) (Fig3F). Transitional stages of TAM maturation were annotated mono-TAM A to C (clusters 4-6) as described (Liu and Cao, 2015). The color of circles represents the averaged normalized expression values across relevant cells, and their size is proportional to the proportion of corresponding cells.

E. KEGG graph representation of the pathway “Antigen processing and presentation” for myeloid cells at D20. Colored boxes show the relative logFC ratio computed during differential expression analysis (red = enriched in Pant; blue = enriched in PBS).

Figure S5: Single cell analysis of APCs.

A-B. Projection on an individual uMAP (**A**) and identification of dendritic cell clusters (**B**) based on the enhanced expression of specific markers for cDC1, cDC2, regulatory-like DC, proliferating DC, IFN-responsive monoDC, pDC and B cells.

C. Density plot representation of the APC metacluster for each experimental condition

D. Geometric MFI of MHC II staining on tumor infiltrating APC at day 20 from PBS and Pant-treated mice evaluated by flow cytometry. (n=5-7 per condition). Mann-Whitney test; **p-value < 0.01.

E. Immunofluorescence analysis of CD8 β and MHC II staining on PBS and Pant tumors sections (n=10) at day 20. The contact points between CD8 β ⁺ cells and MHC II⁺ cells were quantified and normalized by the number of CD8 β ⁺ cells present in the field.

F. CBA quantification of CCL2 and CXCL9 concentrations in tumor lysates at day 20 from PBS and Pant-treated mice (n=7 per condition). Mann-Whitney test; **p-value < 0.01. * p-value<0.05.

G. Normalized expression values as modulescore (Seurat) of previously defined anti-tumoral and protumoral genesets in different clusters from Day 20 and 28 from PBS and Pant-treated tumors. Values are centered-scaled for each row.

Figure S6: Flow cytometric analysis of immune cells.

- A.** Gating strategy for the analysis of CD45⁺ cells by flow cytometry shown in Fig3A.
- B.** Gating strategy for the flow cytometry analysis of lymphoid populations.
- C-D.** Quantification of immune cells in lymph nodes and spleen at steady state or in the presence of a tumor, with or without Pant administration at D24.

Figure S7: Single cell analysis of lymphoid cells.

- A.** Identification on individual uMAP projection of the 8 clusters segregating the lymphoid metacluster: NK1.1/ILC1, CD8⁺, Activated CD8⁺, CD4⁺, Treg and Ki67 CD4⁺ T cell, Tregs and NK cells, represented in the uMAP.
- B-C.** Density plot representation of the lymphoid metacluster for each experimental condition (**B**) and cell-specific marker-based identification of cell subset (**C**).
- D.** Representation of the number of coexpressed activation-associated genes (defined as positive) in CD8⁺ or CD4⁺ T cells under various experimental conditions.
- E.** Module score representation of normalized expression values averaged across cells for activation and exhaustion genesets in CD4⁺ and CD8⁺ T cells from D20-D28 tumors. Values are centered-scaled for each row.
- F.** Relative expression of top 20 ILC (left) and NK (right) cells markers genes as described in the method section.
- G.** Graphic representation of the GSEA performed on NK1.1+ cells.

Figure S8: Control experiments.

- A-B.** Flow cytometry control of CD8 (A) and NK1.1+ (B) cell depletion in peripheral blood lymphocytes.
- C-D.** Absolute numbers (**C**) and CFSE quantification (**D**) of OT1+ cells present in the culture with DC extracted for TDLNs in the presence or absence of OVA SIINFEKL peptide (n=5 per condition).

Figure S9: Metabolic analysis.

- A.** NMR PCA analysis of PBS, Pant, DCA, DCA + Pant samples showing the top 5 enriched metabolites detected in samples. Correlation coefficients were calculated for each metabolite (n=10 per condition).
- B.** Plot representation of MDR versus MG staining of CD45⁻ cells from PBS- or Pant-tumors harvested at day 20 and 28 post engraftment.

C. qRT-PCR quantification of metabolic gene transcripts from CD45 negative cells enriched from tumors harvested at day 20 from PBS or Pant-treated mice (n=5 per condition).

Figure 1

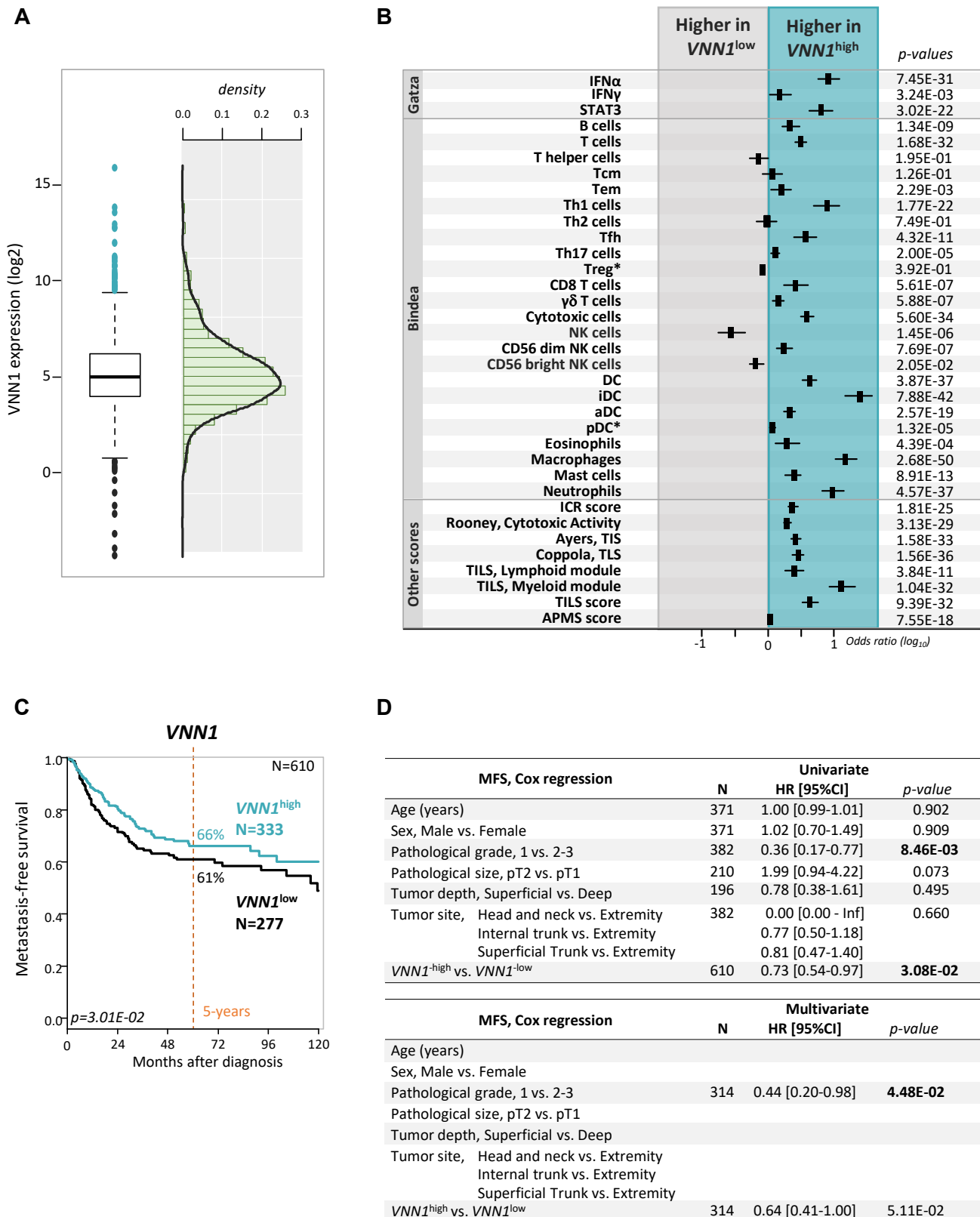


Figure 1: VNN1 expression has prognostic value in soft tissue sarcomas.

A. Box plot showing the distribution of mRNA expression levels of VNN1 in 1377 tumor samples. **B.** Correlations of VNN1 expression-based classes (high vs. low) and immune variables. Forest plots of correlations with the following immune features: immune pathways activation (Gatza), innate and adaptive immune cell subpopulations (Bindea), ICR score and cytolytic activity score associated with anti-tumor cytotoxic immune response, TIS signature and TLS signature associated with response to ICI, and antigen-processing machinery score. The *p*-values are for the logit link test. N= 1377 or 1152 (*). **C.** Kaplan-Meier MFS curves according to VNN1 expression. The *p*-value is for the log-rank test. **D.** Uni- and multivariate prognostic analyses for MFS. The *p*-values are for the Wald test.

Figure 2

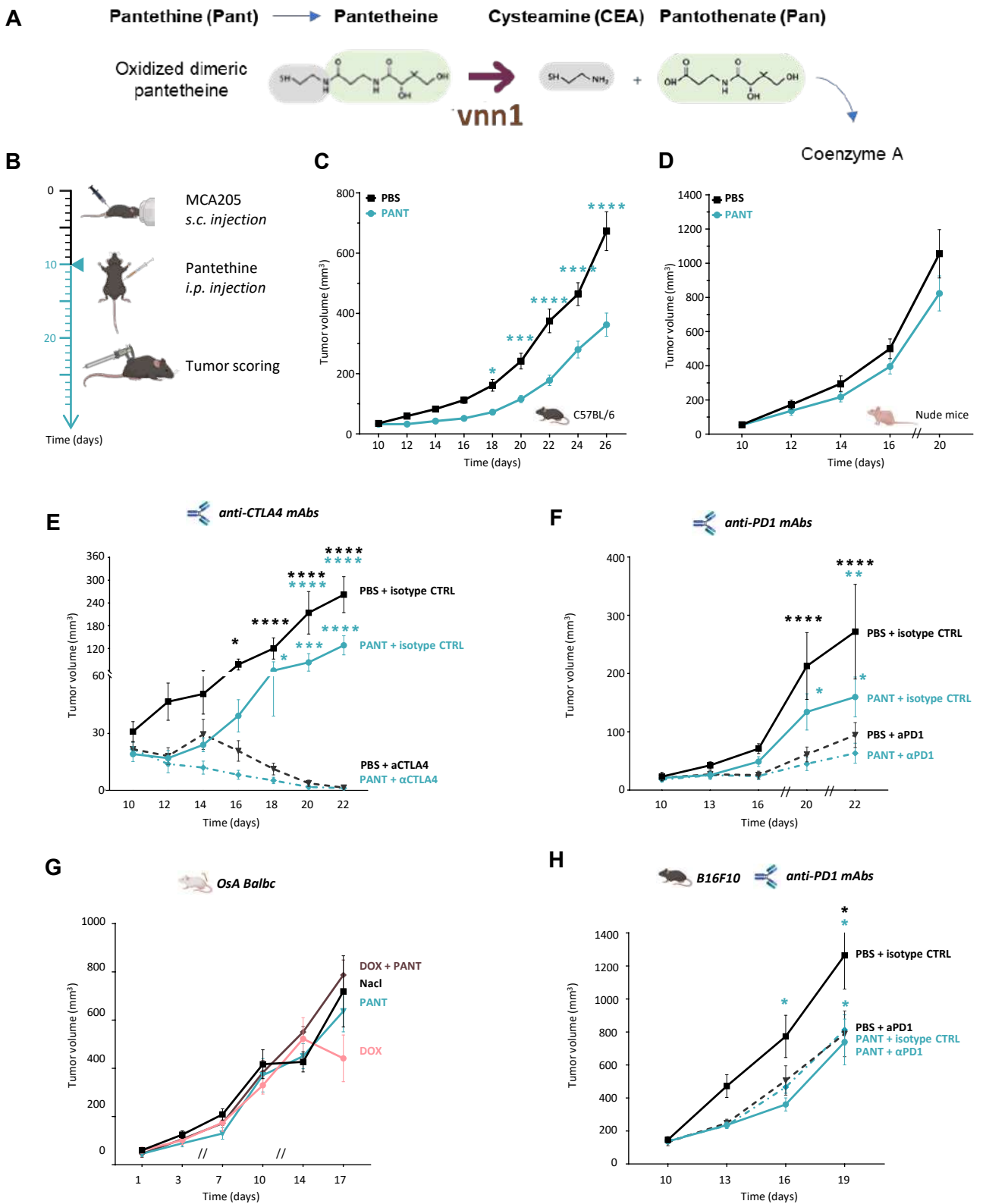


Figure 2: Pantethine inhibits sarcoma growth.

A. Enzymatic reaction catalyzed by the Vanin1 pantetheinase: pantetheine is hydrolyzed by Vanin1 into cysteamine and vitamin B5 or pantothenic acid, the latter being the Coenzyme A biosynthetic precursor.

B. Schematic representation of the experimental design of murine MCA sarcoma model

C-D. MCA205 tumor growth scored after daily injections of Pant in C57BL/6 mice (n=88) (B) or Nude mice (n=18) (C). Two-way ANOVA with Šidák's multiple comparisons test. Data are shown with SEM.

E-F. Effect of Pant therapy in MCA tumor-bearing mice receiving anti-CTLA4 (n=7 per condition) (D), or anti-PD1 (n=6 per condition) mAbs (E).

G. Growth of OsA orthotopic tumors receiving independent or combined doxorubicine or Pant therapy or vehicle control (n=6 per condition).

H. Therapeutic effect of Pant therapy, alone (D) or combined with PD1 blockade (E) on B16F10 melanoma growth (n=10 per condition).

Figure 3

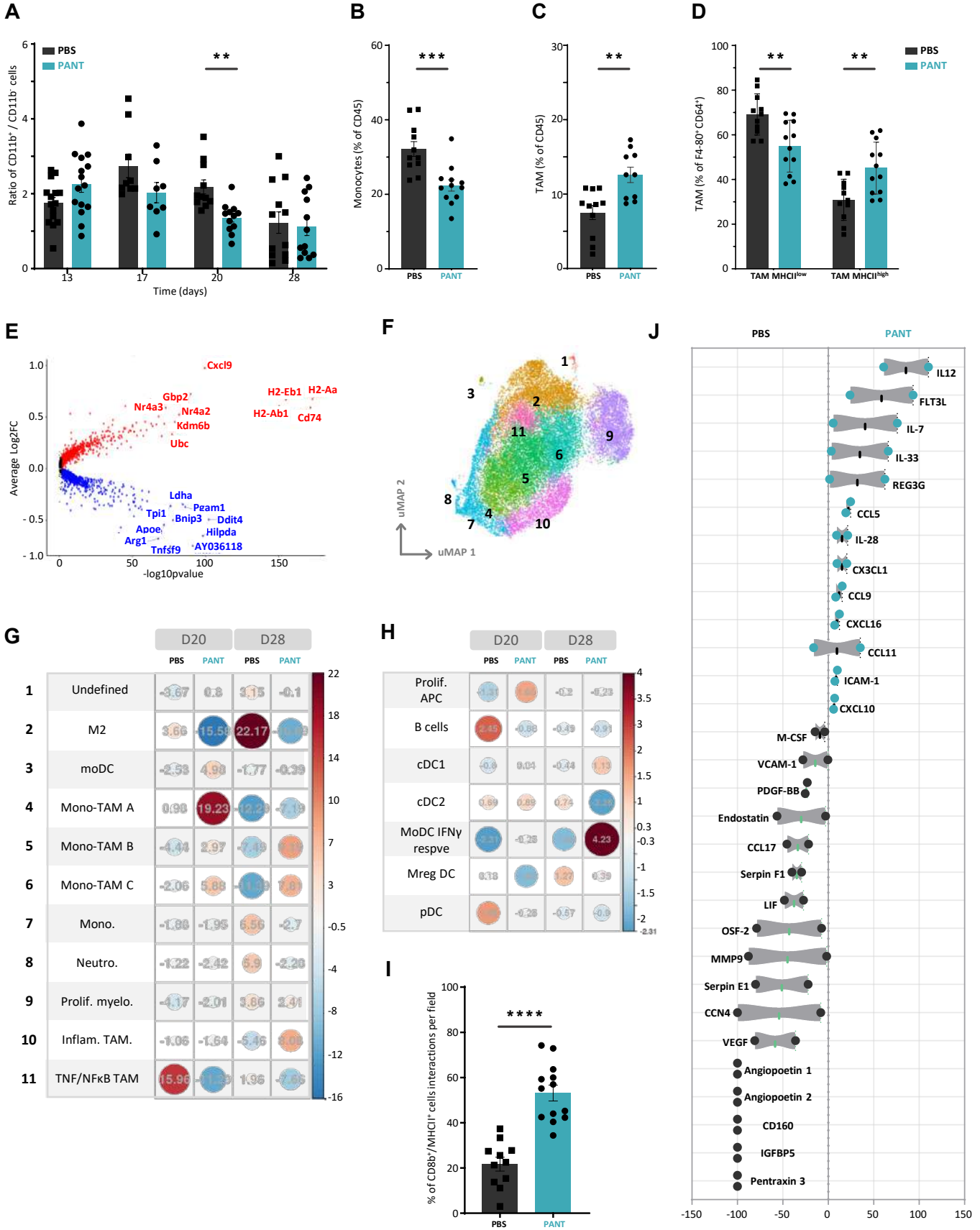


Figure 3: Analysis of the myeloid compartment.

A. Kinetic evaluation of the CD11b⁺/CD11b⁻ ratio by flow cytometry analysis of immune infiltrating cells in PBS or Pant tumors (n=6-8 per condition). Mann-Whitney test; **p-value < 0.01. **B-C.** Quantification of monocyte (**B**) and TAM (**C**) clusters among CD45⁺ cells by flow cytometry on D20 tumors. **D.** Proportion of MHCII^{low} and MHCII^{high} TAMs in total TAM (Ly6C^{low} F4/80⁺ CD64⁺) PBS and Pant-treated D20 tumors (n=12). **E.** Volcano plot representation of myeloid cell transcripts showing differential expression between Pant and PBS samples at D20. Dot colors refer to average log2FC: positive in red, negative in blue, below the threshold in black. **F.** Individual uMAP projection, clustering, and population identification computed for the myeloid metacluster delineated 11 clusters: neutrophils, monocytes, Mono-TAM A-C, inflammatory TAM, TAM TNF α /NF κ B, moDC, CAF, M2 and Ki67 TAM. **G, H.** Pearson's residuals of TAM and APC cell clusters from single-cell dataset obtained from CD45 enriched cells from tumors harvested at day 20 and D28 of PBS or Pant-treated mice (n=2). **I.** Quantification of cell contacts between CD8 β ⁺ and MHC II⁺ cells on D24 tumor sections shown in **FigS5E**. Mann-Whitney test; ****p-value < 0.0001. **J.** Proteomic profiling of tumor lysates represented by enrichment in Pant versus PBS condition (n=4).

Figure 4

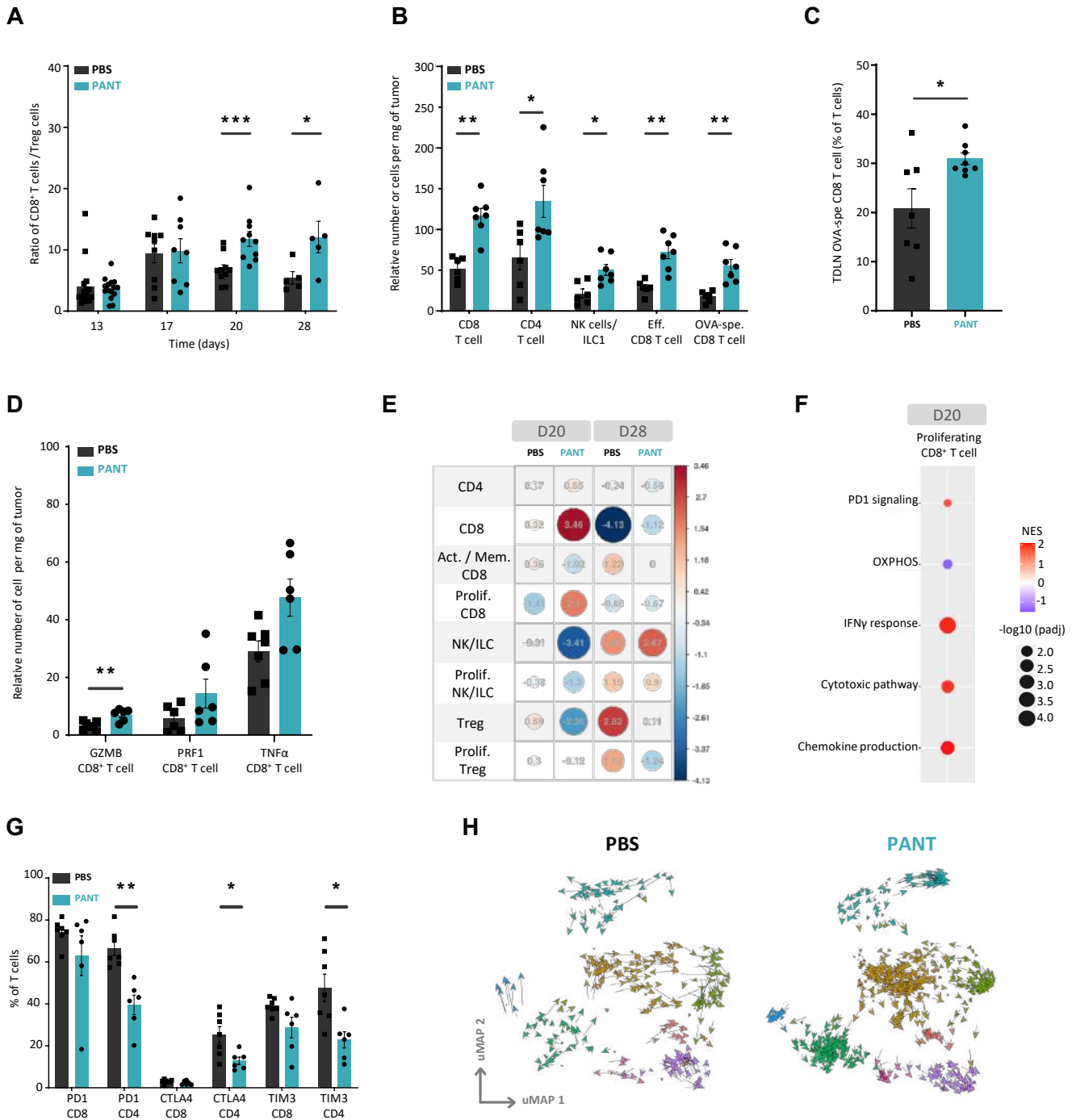


Figure 4: Analysis of the lymphoid compartment.

A. Kinetic evaluation of the CD8⁺ / CD4⁺ Treg cell ratio by flow cytometry among immune infiltrated cells in tumor from PBS or Pant samples (n=5 per condition). Mann-Whitney test; * p-value<0.05. Gating strategy shown in FigS6B. **B.** Relative numbers of TILs per mg of PBS and Pant tumors **C.** Quantification of OVA-specific CD8 T cells in TDLN evaluated by flow cytometry using a SIINFEKL tetramer. **D.** Flow cytometry analysis of effector molecule expression by CD8 T cells isolated from day 20 tumors and *in vitro* restimulated in the presence of PMA / Ionomycin / Brefeldin A (n=6) (**C**). Mann-Whitney test; **p-value < 0.01; * p-value<0.05. **E.** Pearson's residuals of lymphoid cell clusters from single-cell dataset obtained from CD45 enriched cells from tumors harvested at day 20 and D28 of PBS or Pant samples (n=2). **F.** Graphic representation of GSEA analyses performed in the proliferating CD8 T cell subset as indicated in Table 1. **G.** Flow cytometry analysis of immune checkpoint expression by TILs from PBS and Pant-treated mice at day 28 (n=6). Mann-Whitney test; **p-value < 0.01; * p-value<0.05. **H.** Projection of individual cell velocity as determined by scVelo analysis performed on each subset of lymphoid cells from D20 samples.

Figure 5

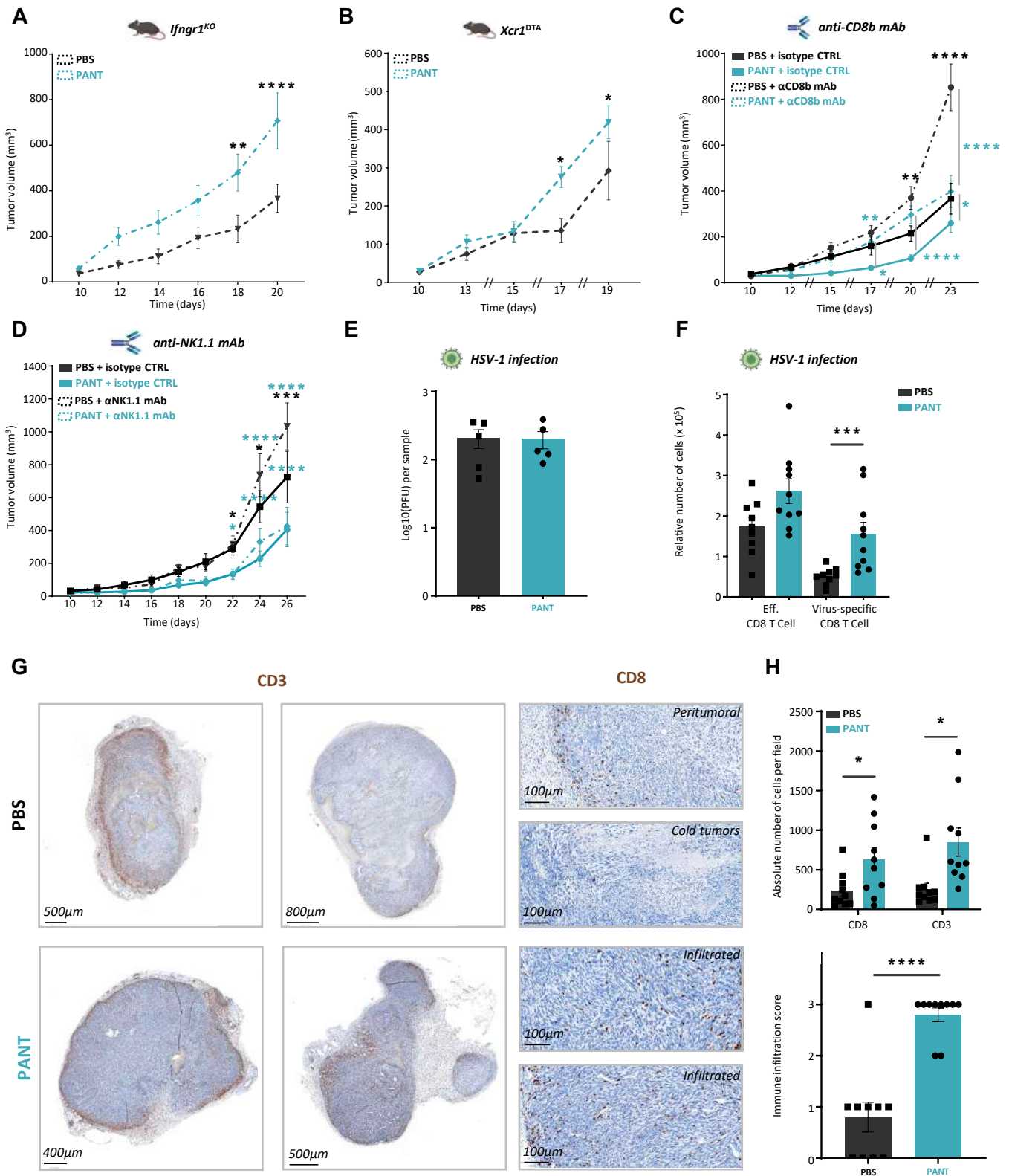


Figure 5: Requirements for Pant anti-tumor efficacy.

A-D. MCA growth curves in *lfng1*-deficient (n=7-8 per condition) (**A**), cDC1 cell-deficient *XCR1^{DTA}* (n=10-11 per condition) (**E**), anti CD8- (n=10-11 per condition) or anti NK1.1-treated (n=8 per condition) (**F**) control or Pant-treated mice. Two-way ANOVA with Šídák's multiple comparisons test; ****p-value < 0.0001, **p-value < 0.01, * p-value<0.05. **E-F.** PFU quantifying viral load (**G**) and numbers of CD8⁺ T cell subpopulations (**H**) in the draining lymph nodes of HSV1-infected mice after 8 days of PBS or Pant treatment. **G.** Immunohistochemistry analysis of PBS and Pant tumor sections using anti-CD3 and anti-CD8 mAbs on D24. **H.** Quantification of the absolute number of positive cells per field (top panel) and of the immune infiltration score (bottom panel). n=10. Mann-Whitney test; ****p-value < 0.0001, * p-value<0.05.

Figure 6

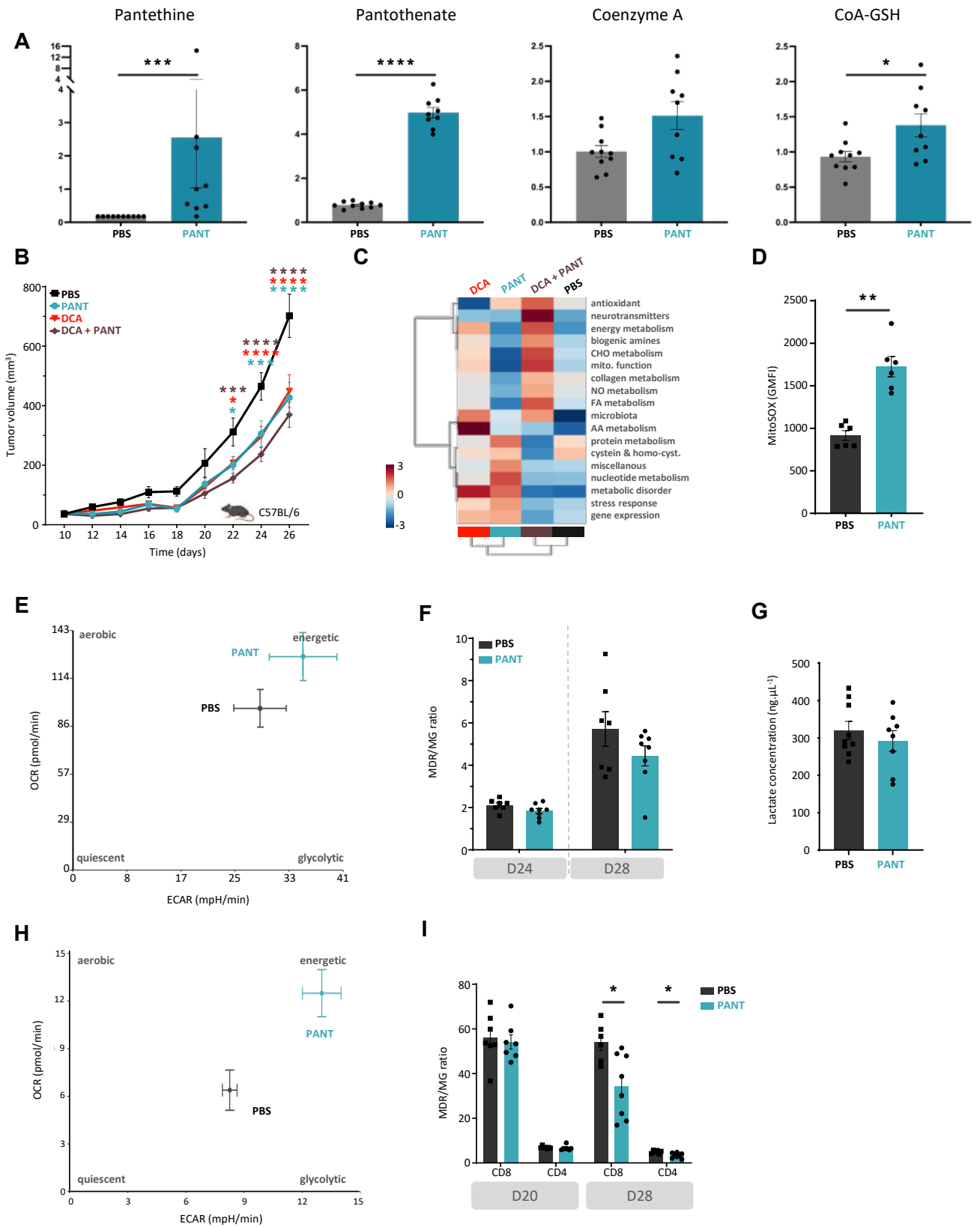
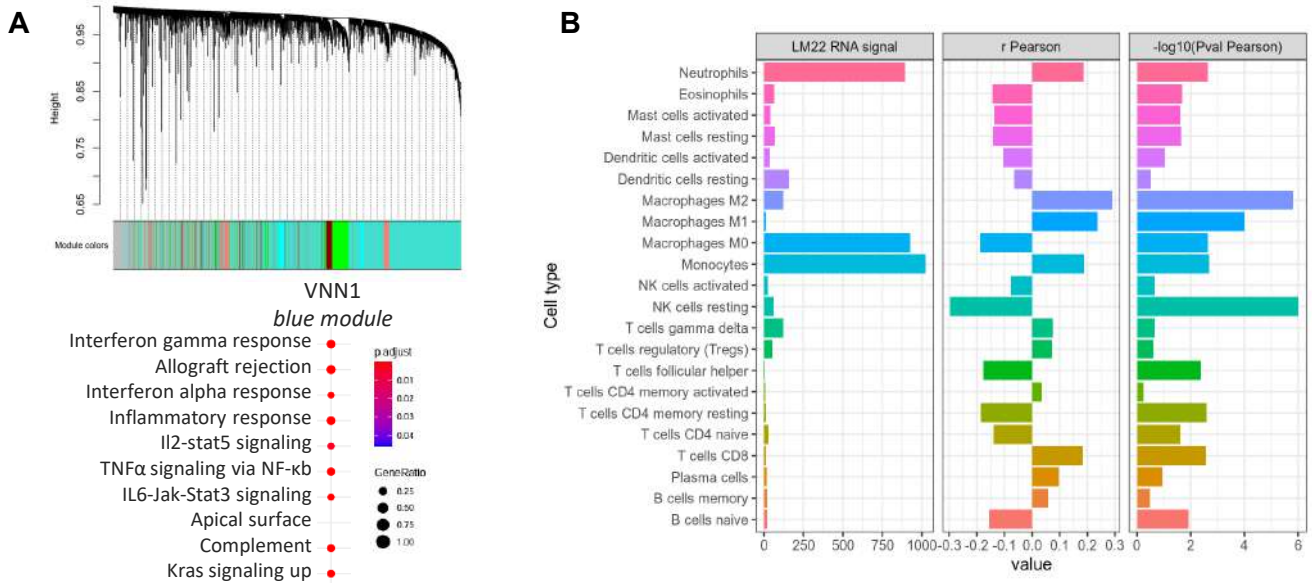


Figure 6: Metabolic changes induced by Pant administration.

A. Metabolomics quantification of VitB5-related metabolites with or without Pant administration in tumor masses (n=7 per condition). **B.** MCA205 tumor growth scored after daily injections of Pant, dichloroacetate (DCA) combined with Pant or not in C57BL/6 mice (n=24). Two-way ANOVA with Šídák's multiple comparisons test; ****p-value < 0.0001, ***p-value < 0.001, **p-value < 0.01, * p-value<0.05. Data are shown with SEM. **C.** Metabolomics analysis of total tumors from mice treated with PBS, Pant, DCA, Pant + DCA by LC-MS (n=10) showing the hierarchical cluster of metabolic pathways according to treatment conditions. Scaling is in unit of variance (mean/squared root of SD). **D.** Geometric mean fluorescence intensity (MFI) of MitoSox-stained MCA cells incubated or not for 4 hours in Pant-enriched medium *in vitro* (n=6 per condition). Mann-Whitney test; **p-value < 0.01. **E.** Seahorse analysis of an energetic map integrating OCR and ECAR measurements of *in vitro* Pant-treated MCA205 or PBS control cells (n=2). **F.** MDR/MG ratio of CD45⁺ cells at D24 and D28 from Pant-treated or PBS control mice (n=7). **G.** Lactate concentration quantified in whole tumor masses from PBS or Pant-treated mice at day 20 post engraftment (n=8 per condition). **H.** Energetic map of CD8⁺ TILs isolated from tumor mass D20 post cell engraftment. Mice were treated with PBS or Pant starting on day 10 (n=3). **I.** MDR/MG ratio of CD8⁺ and CD4⁺ TILs at D20 and D28 from Pant-treated or PBS control mice (n=7). Mann-Whitney test; * p-value<0.05.

Supplementary Data 1



C List of soft tissue sarcoma data sets included in our analysis

Reference	Source of data	Technological platform	N° of probe sets/genes	All samples	STS primary tumor samples included in the present analysis
Baird K et al., Cancer Res 2005	GEO database, GSE2553	Homemade, spotted DNA/cDNA	12K	181	146
Barretina J et al., Nat Genet 2010	GEO database, GSE21124	Affymetrix, array U133 A	22K	158	126
Beck A et al., Oncogene 2010	GEO database, GSE17555	Stanford, spotted DNA/cDNA	24K	51	25
Chibon F et al., Nat. Med. 2010	GEO database, GSE21050	Affymetrix, array U133 Plus 2.0	54K	310	310
Detwiller K et al., Cancer Res 2005	GEO database, GSE2719	Affymetrix, array U133 A	22K	54	37
Gibault L et al., J Pathol 2011	GEO database, GSE23980	Affymetrix, array U133 Plus 2.0	54K	171	34
Gobble R et al., Cancer Res 2011	GEO database, GSE30929	Affymetrix, array U133 A	22K	140	140
Hadju M et al., J Pathol 2010	http://cbio.mskcc.org/public/SFT/	Affymetrix, array U133 Plus 2.0	54K	56	30
Henderson S et al., Genome Biology 2005	Array Express database, E-MEXP-353	Affymetrix, array U133 A	22K	96	42
Nakayama R et al., Modern Pathol 2007	GEO database, GSE6481	Affymetrix, array U133 A	22K	105	99
Nielsen TO et al., Lancet 2002	GEO database, GSE3443	Stanford, spotted DNA/cDNA	24K	46	25
Renner M et al., Genome Biol 2013	GEO database, GSE52392	Illumina, array Human HT-12 V3.0	48K	94	79
TCGA, Cell 2017	TCGA portal, https://tcga-data.nci.nih.gov	Illumina, RNA sequencing V2	25K	265	224
West R et al., PLoS Biology 2005	http://microarray-pubs.stanford.edu/tma-portal/DTF_SFTbreast	Stanford, spotted DNA/cDNA	24K	57	29
Ylipää A et al., Cancer 2011	http://www3.mdanderson.org/~genomics/sarcoma_data_matrix_for_suppl_emental.zip	Agilent, array 44K G4112A (012391)	44K	68	31
Total					1,377

D Clinicopathological characteristics of patients and samples in the whole population and according to VNN1-based classification

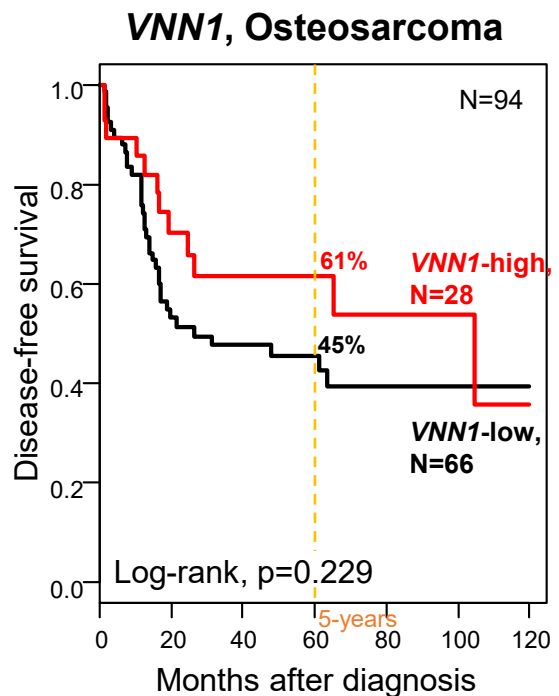
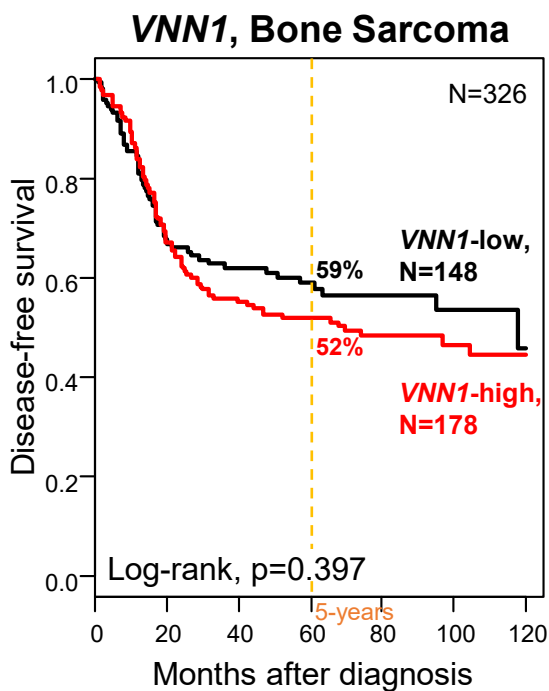
Characteristics	All patients		VNN1		p-value
	N	N (%)	low	high	
Age (years), median (range)	532	61.25 (2-92.12)	532	63.53 (16.16-91)	0,000
Sex					0,056
Female	303	303 (50%)	303	172 (54%)	
Male	306	306 (50%)	306	149 (46%)	
Pathological grade					0,000
1	62	366 (86%)	62	10 (5%)	
2-3	366	62 (14%)	366	176 (95%)	
Pathological size (pT)					0,462
pT1	29	29 (17%)	29	10 (14%)	
pT2	141	141 (83%)	141	62 (86%)	
Tumor depth					0,088
Deep	144	144 (89%)	144	70 (95%)	
Superficial	17	17 (11%)	17	4 (5%)	
Tumor site					0,005
Extremity	208	208 (42%)	208	94 (38%)	
Head and neck	9	9 (2%)	9	2 (1%)	
Internal trunk	195	195 (39%)	195	97 (39%)	
Superficial Trunk	84	84 (17%)	84	55 (22%)	
Follow-up (months), median (range)	610	30 (1-222)	610	26 (1-222)	0,106
MFS event	610	183 (30%)	610	87 (26%)	0,026
5-year MFS [95%CI]	610	64% [59-69]	610	61% [54-68]	0,030

Supplementary Data 2

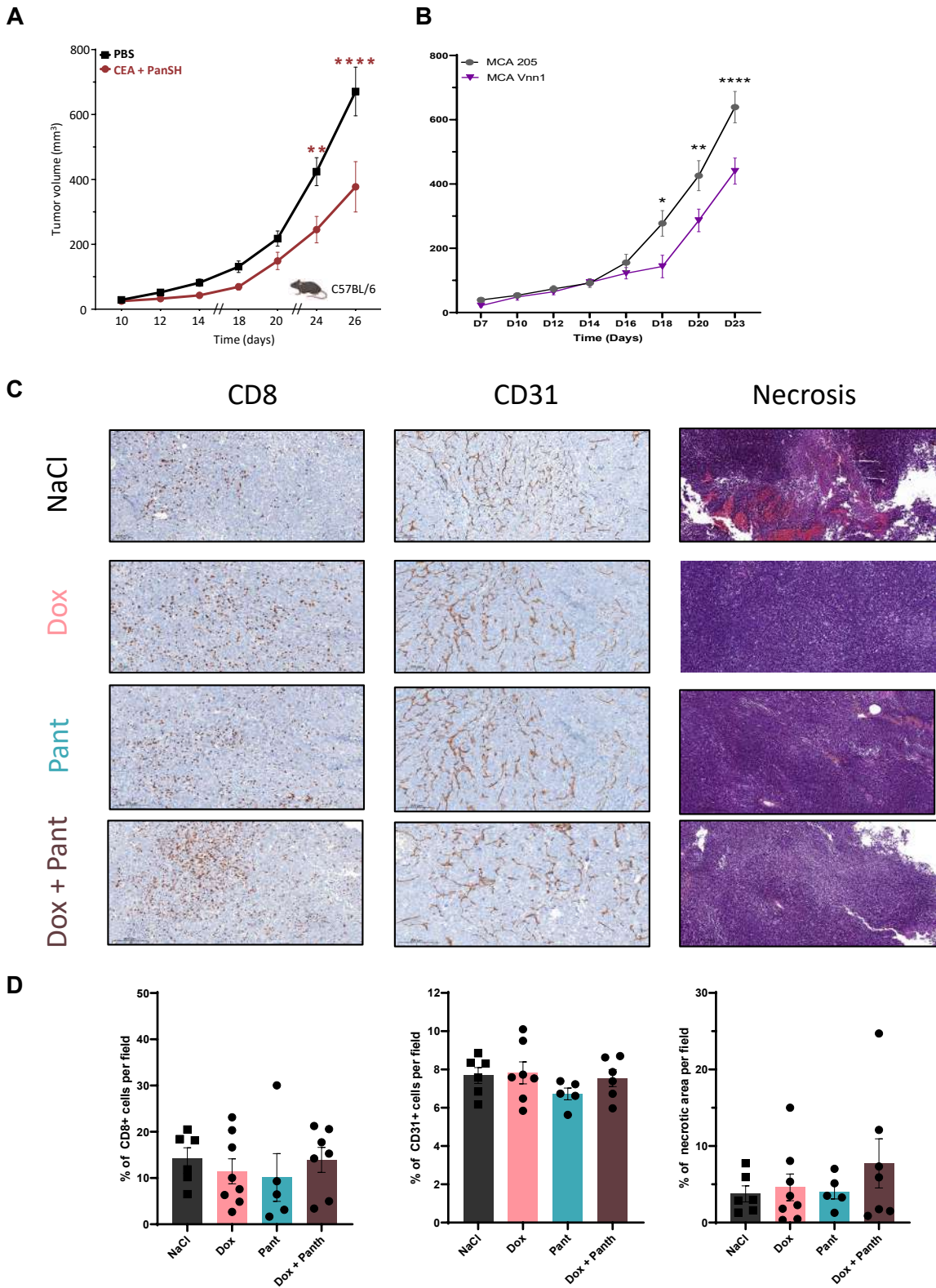
A

List of bone sarcoma data sets included in our analysis					
Reference	Source of data	Technological platform	N° of probe sets/genes	All samples	Bone sarcoma primary tumor samples included in the present analysis
Nicolle R et al., Nat Commun 2019	Array Express database, E-MTAB-7264	Affymetrix, array HuGene 2.0 st	54K	164	83
Savola S et al., ISRN Oncol 2011	GEO database, GSE17679	Affymetrix, array U133 Plus 2.0	54K	117	64
Therapeutically Applicable Research to Generate Effective Treatments (TARGET) database	TARGET portal, https://target-data.nci.nih.gov/Public/OS/	Illumina, RNA sequencing V2	60K	101	94
Volchenboum S et al., J Pathol Clin Res 2015	GEO database, GSE63157	Affymetrix, array U133 Plus 2.0	22K	85	85
				Total	326

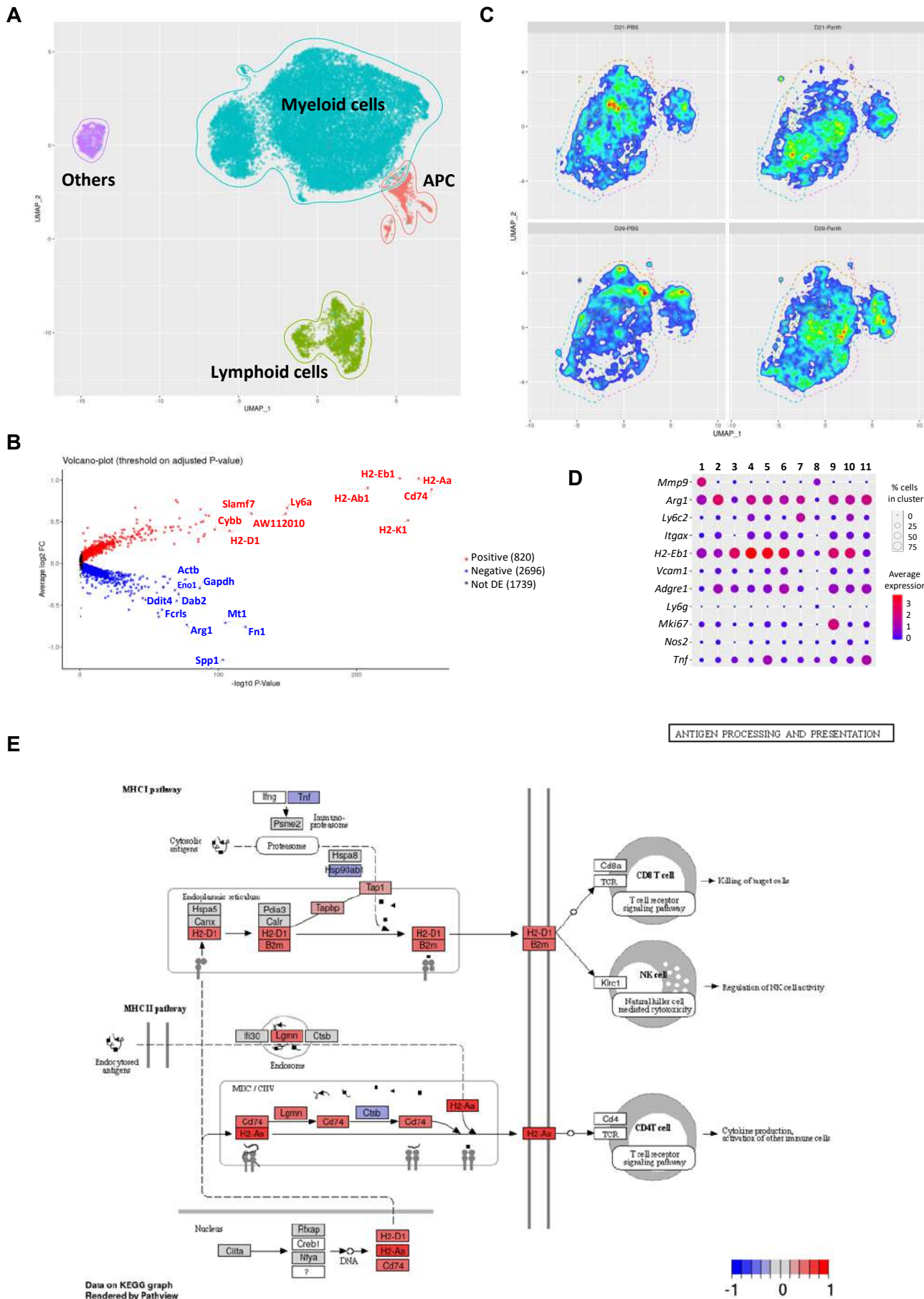
B



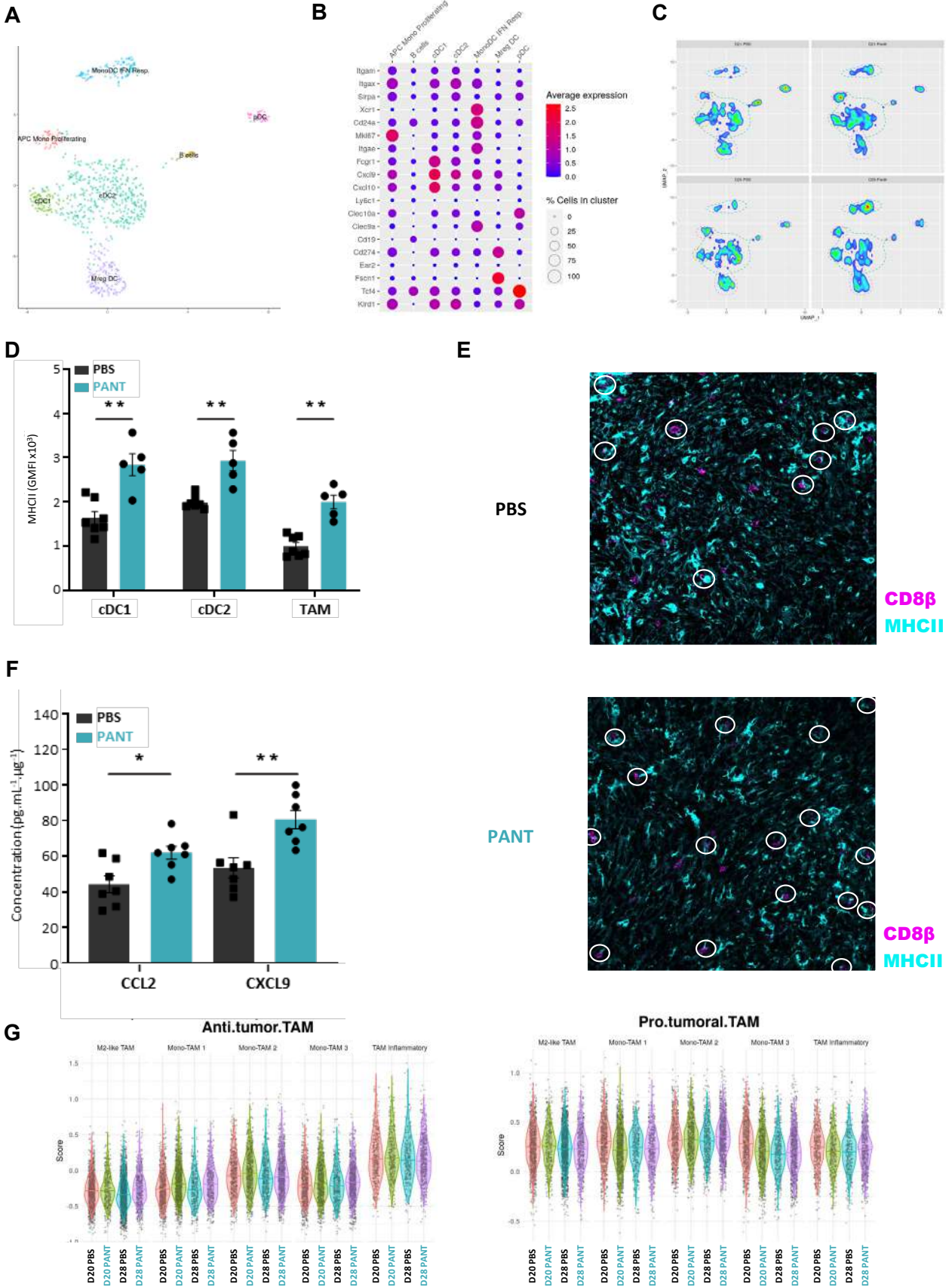
Supplementary Data 3



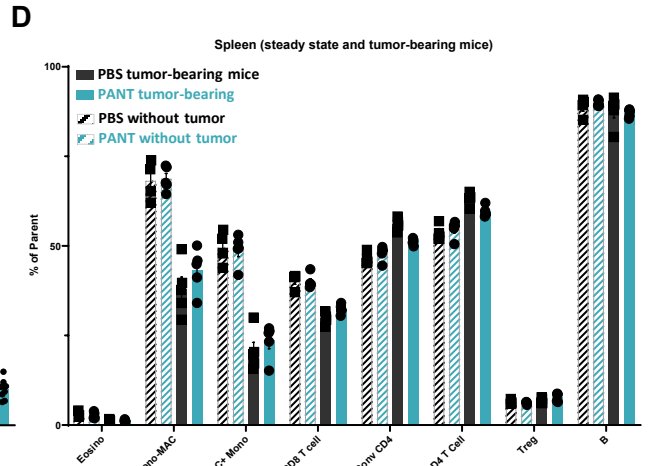
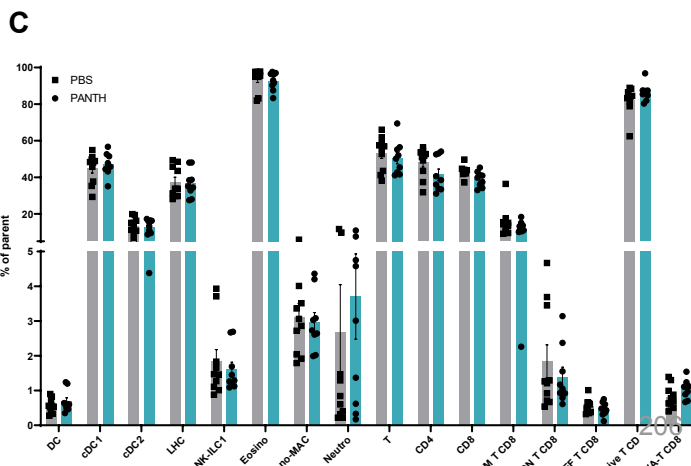
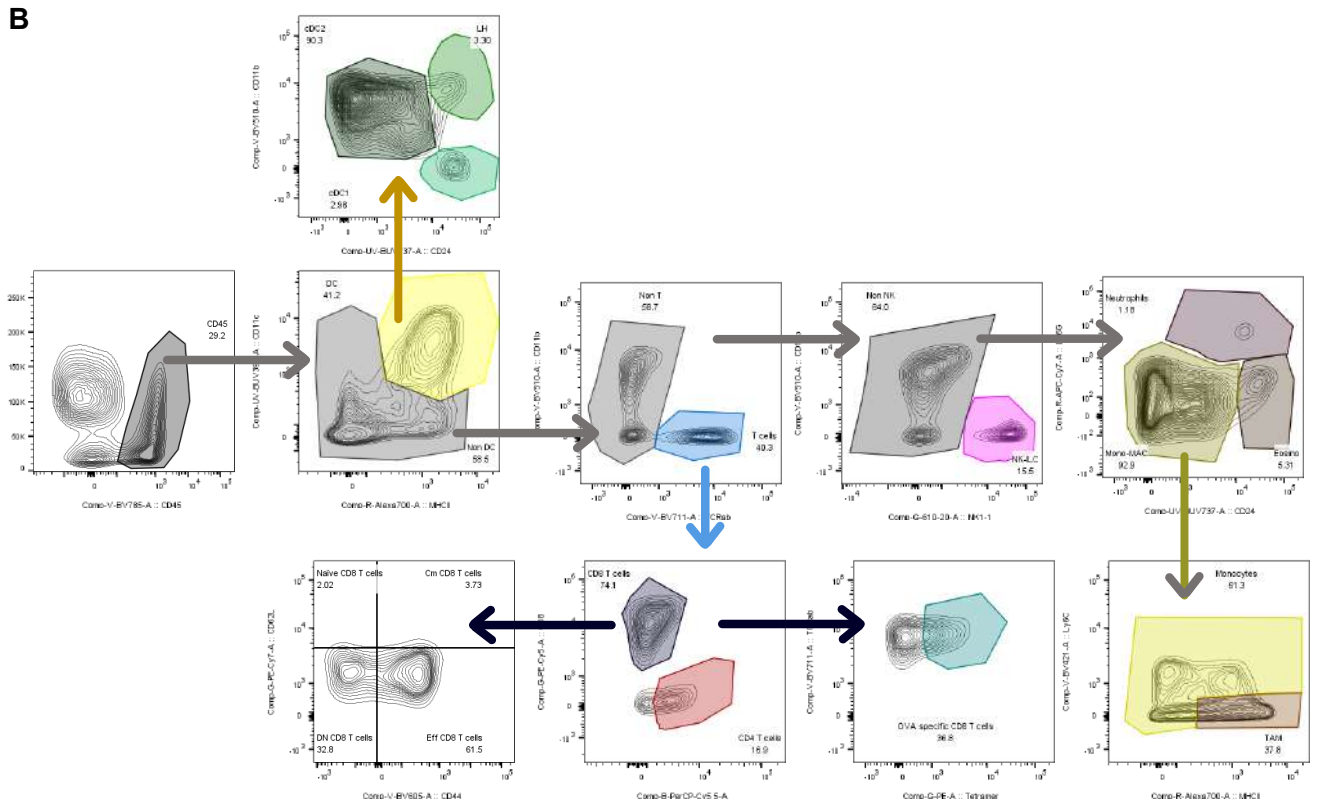
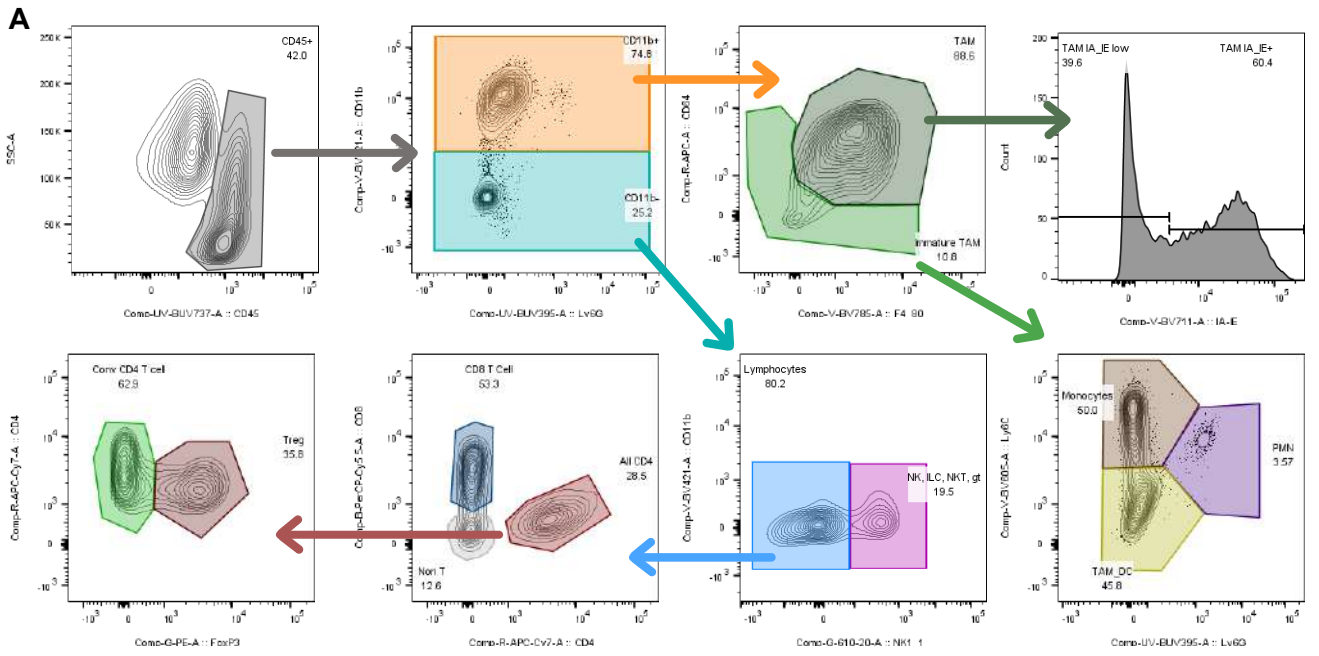
Supplementary Data 4



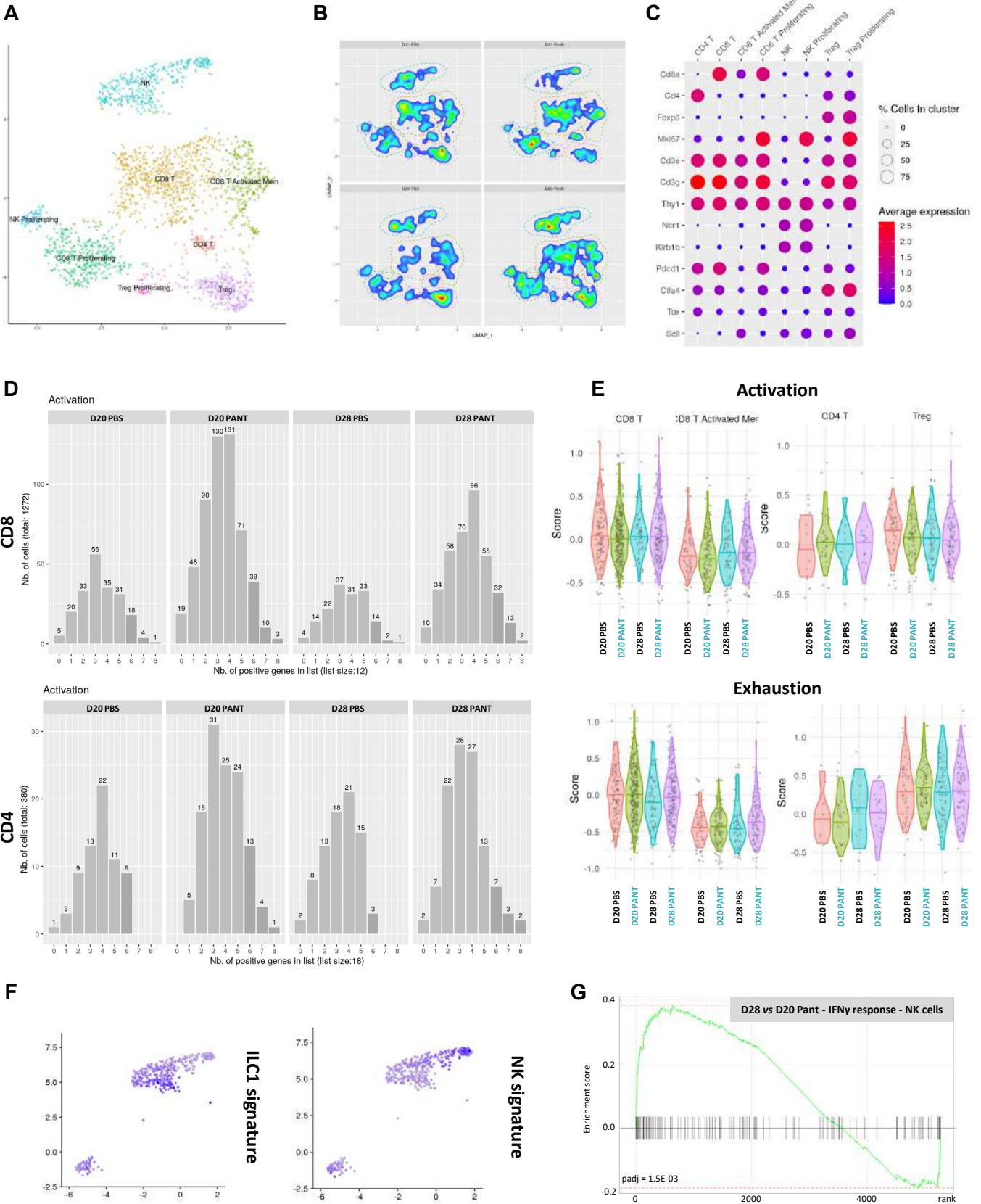
Supplementary Data 5



Supplementary Data 6

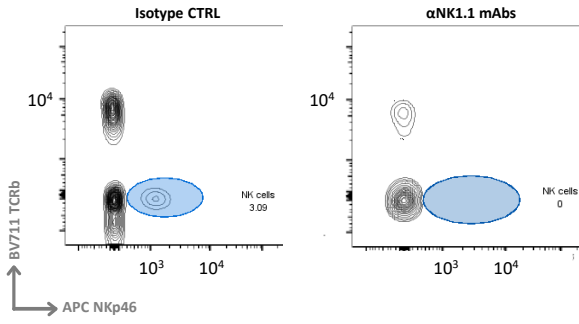


Supplementary Data 7

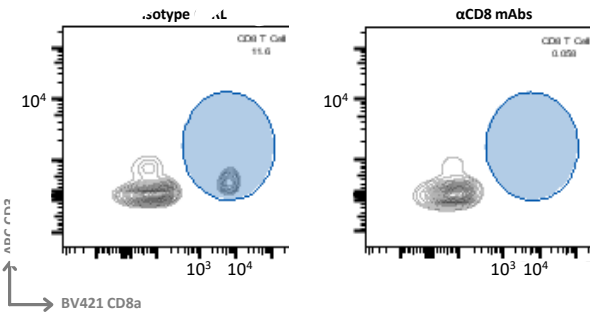


Supplementary Data 8

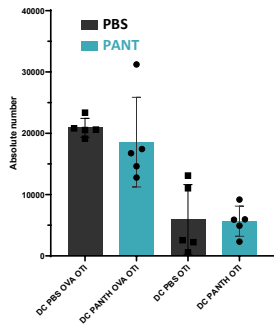
A



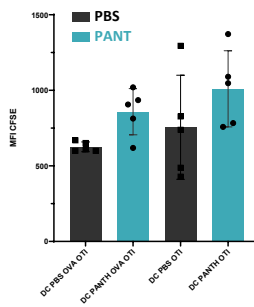
B



C



D

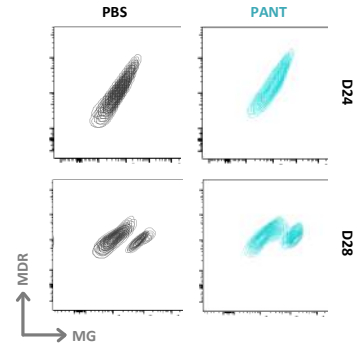


Supplementary Data 9

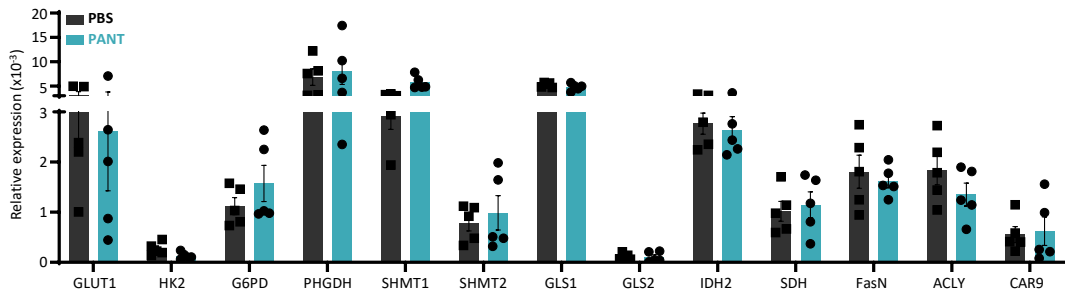
A

	Pant vs PBS	DCA vs PBS	DCA + Pant vs PBS
PCA analysis	p-value = 0.45	p-value = 0.31	p-value = 0.04
Up		Formate - p=0.49	Fumarate - p=0.82 Formate - p=0.68
Down	Uracile - p=0.44 Phenylalanine - p=0.46 Tyrosine - p=0.46 Lysine - p=0.58 Alanine - p=0.45	Fatty acids (F.A.) - p=0.61 Unsaturated F.A. - p=0.55 Hypoxanthine - p = 0.45 Uracile - p=0.40 Phenylalanine - p=0.45 Tyrosine - p=0.44	Lactate - p=0.42 Tyrosine - p=0.43

B



C



VI) Discussion et perspectives

« Rien ne se perd, rien ne se crée, tout se transforme »

Cette phrase, chacun de nous la connaît depuis son enfance. Elle retranscrit les travaux d'Antoine Lavoisier dans son *Traité élémentaire de chimie*. Cette réflexion mènera des années plus tard à la première loi de la thermodynamique sur la conservation de l'énergie dans un système fermé défini par Julius Robert von Mayer. J'ai choisi ces quelques mots pour débiter ma discussion car ils véhiculent l'idée que tout est interdépendant. Au niveau d'un organisme, chaque cellule partage les mêmes ressources et les mêmes éléments fondamentaux qui la constituent ainsi la vie se joue sur l'équilibre parfait entre ressources et besoins. Le cancer provoque une dérégulation notable de cet équilibre mais, en gardant à l'esprit l'interconnexion d'une tumeur avec son environnement et l'organisme, nous pouvons comprendre qu'une action sur un processus peut en impacter d'autres comme dans un engrenage. Au cours de mes travaux de recherche, mon équipe et moi, nous nous sommes intéressés à la question du métabolisme dans les sarcomes pour comprendre comment les modulations de processus mitochondriaux pouvaient impacter la progression tumorale en agissant à la fois sur les cellules cancéreuses, le système immunitaire et le microenvironnement tumoral. Pour cela nous avons développé deux axes de recherche principaux. Le premier se centre sur la manipulation de la voie de signalisation du coenzyme A dans les sarcomes *via* l'activité Vanin1. L'autre concerne le rôle de la régulation des processus de fusion et fission mitochondriale en lien avec la progression tumorale.

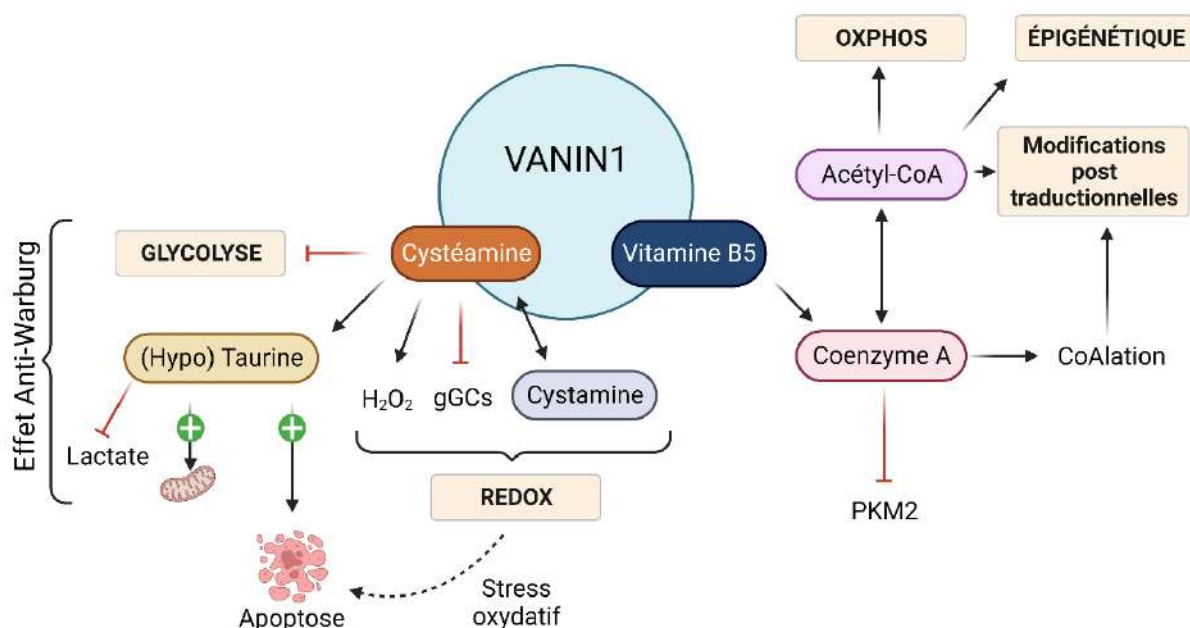


Figure 26 : Reprogrammation métabolique par la cystéamine et la vitamine B5

A) La voie de signalisation du coenzyme A : perspective thérapeutique

1) Reprogrammation métabolique des cellules cancéreuses

L'administration systémique de pantéthine permet la génération de cystéamine et de pantothénate, précurseur biosynthétique du coenzyme A (162). Dans un modèle agressif de fibrosarcome murin, nous avons étudié l'impact de la pantéthine sur le métabolisme tumoral. Par analyse métabolomique, nous savons que le taux relatif de ces deux métabolites est augmenté au sein des tumeurs et nous avons souhaité en évaluer les conséquences au sein des tumeurs. Cependant, dissocier l'effet de la cystéamine et de la vitamine B5 sur le métabolisme tumoral est assez complexe. Cependant, voici quelques pistes de discussion.

La cystéamine est un aminothiols qui peut être oxydé en cystamine en condition de stress (**Figure 27**). Les deux sont des senseurs du stress oxydant et contribuent aux échanges thiols/disulfides sur des cibles enzymatiques principalement (gGCS, PKe, transglutaminases, certaines enzymes glycolytiques et la caspase 3 (163). À forte concentration, la cystamine va inhiber l'activité de la gGCS qui contrôle la synthèse de glutathion. De plus, la cystéamine pourrait être impliquée dans la génération d' H_2O_2 (164). La potentielle cytotoxicité de ces deux mécanismes est à double tranchant dans un contexte tumoral. L'accumulation de ROS et l'altération des mécanismes de résistance au stress oxydant peut être bénéfique aux cellules cancéreuses par l'augmentation du taux de mutations de l'ADN, favorable à la plasticité cellulaire mais aussi dommageable par le risque de déclenchement d'une mort cellulaire induite. Par son action notamment sur la régulation des enzymes redox sensibles de la glycolyse, la cystéamine semble pouvoir exercer un effet de type anti-Warburg. Dans le cancer du pancréas humain transplanté, la cystéamine possède un bénéfice thérapeutique en inhibant l'activité des métalloprotéinases de la matrice extracellulaire, diminuant ainsi les capacités d'invasion et de métastases (165). La cystéamine est également un précurseur de la synthèse de l'hypotaurine et donc de la taurine, deux composés augmentés dans les tumeurs du groupe de souris traitées à la pantéthine. Des études ont révélé le potentiel antitumoral de la taurine. En effet, dans le cancer du sein, la taurine conduit à l'apoptose par régulation de la protéine PUMA (166,167). La taurine peut également diminuer le potentiel métastatique du cancer du sein dans le poumon et diminuer les niveaux de relargage de lactate (**Figure 27**) (168). Enfin, la taurine peut avoir une action antioxydante et améliorer les fonctions mitochondriales (169). La cystéamine semble être une molécule aux propriétés multiples pouvant avoir une action sur le métabolisme des cellules cancéreuses.

Certains processus régulés par le coenzyme A et ses dérivés peuvent avoir une importance dans un contexte tumoral. Par exemple, le coenzyme A inhibe certaines isoformes de PKC comme la PKC ϵ . Cette enzyme est la cible de plusieurs thérapies anticancéreuses car elle favorise la prolifération, la différenciation, la mobilité et la survie des cellules cancéreuses (170,171). Le coenzyme A agit également sur les modifications post-traductionnelles par acétylation, acylation ou encore CoAlation, et donc régule les processus de dégradation des protéines ou de modulation de l'expression génique par épigénétique. Dans des cellules, il peut se fixer sur l'enzyme glycolytique PKM2, sans réelle preuve d'une possible CoAlation.

(144). Enfin, le coenzyme A peut posséder des fonctions extracellulaires notamment dans la communication extracellulaire (144). Les multiples implications du coenzyme A et de ses dérivés dans les processus biologiques rendent difficile de comprendre par quel mécanisme la vitamine B5 peut réguler le métabolisme tumoral et freiner la progression des tumeurs. Les données obtenues dans l'équipe sur un modèle de cellule génétiquement modifiée (p16, p19 déficientes + RAS oncogénique) mais sans anomalie des fonctions mitochondriales ont clairement montré par des approches transcriptomiques, métaboliques et d'imagerie que l'effet le plus concret était l'amélioration générale de la respiration mitochondriale (161).

Ainsi, les mécanismes décrits ci-dessus participent à une reprogrammation métabolique tumorale mais dépendent nécessairement du type d'altérations portées par les cellules cancéreuses, de leur localisation dans l'organisme et des facteurs environnementaux présents dans le microenvironnement. Cependant, la prévalence de l'effet de la pantéthine sur des mécanismes intrinsèques à la cellule tumorale est probablement réduite dans notre modèle. Le potentiel effet antitumoral de la vitamine B5 et de la cystéamine nous conduit à l'hypothèse que l'activité pantéthénase et l'expression de la Vanin1, qui catalyse leur formation, pourrait posséder une valeur pronostique dans les cancers.

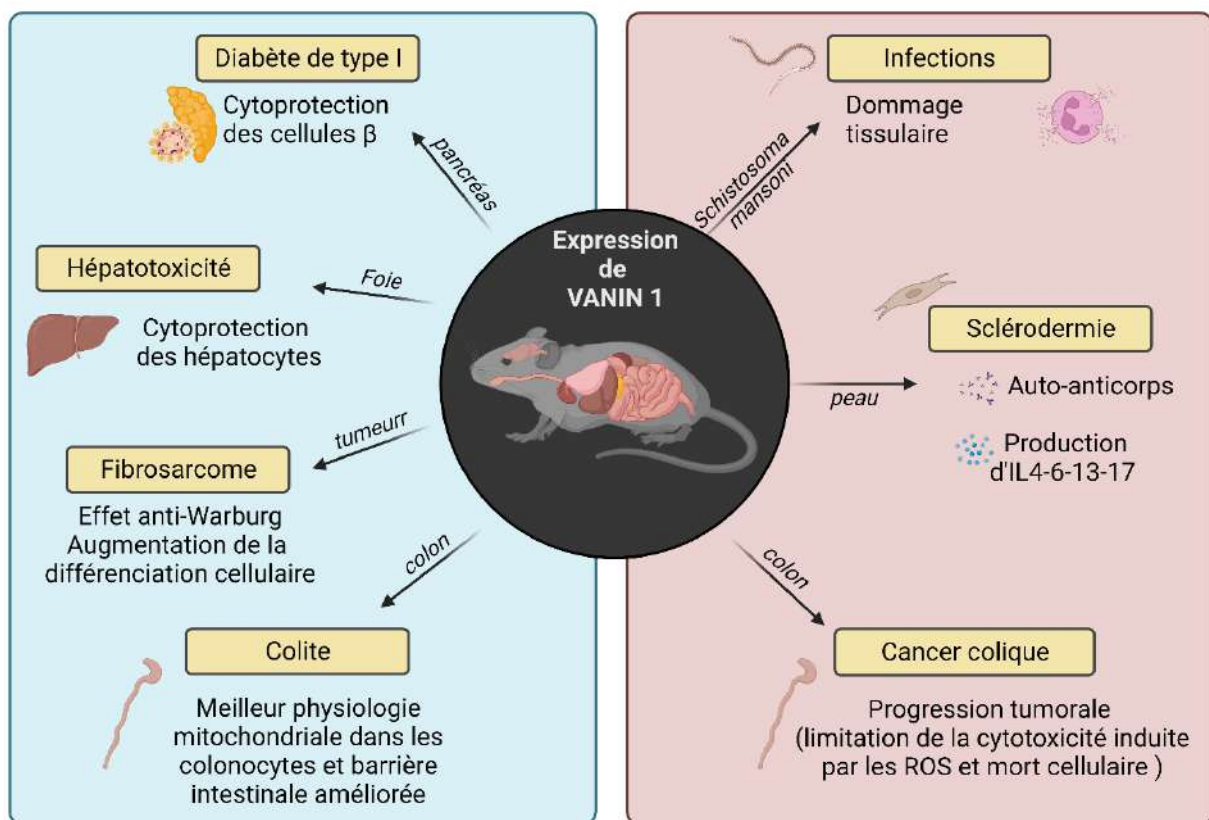


Figure 27 : Expression de Vanin1 en contexte pathologique

2) L'expression de VNN1 a une valeur pronostique

Nous avons montré que l'expression de la *VNN1* est associée à une signature $IFN\gamma$ et une réponse inflammatoire à partir de banques de données de patients atteints de sarcomes. Les tumeurs avec des niveaux élevés de Vanin1 présentent une forte infiltration par le système immunitaire, potentiellement assorti d'une amplification des mécanismes de présentation antigénique et de fonctions cytolytiques. Enfin, cette expression corrèle modestement avec une meilleure survie sans métastase. Nos résultats démontrent également que l'expression de *VNN1* est fortement hétérogène selon les sous types de sarcomes mais qu'elle ne corrèle pas toujours avec un meilleur pronostic notamment dans le cas des sarcomes osseux. Il est intéressant de noter que dans d'autres types de cancers (pancréas, ovaire, estomac), l'expression de Vanin1 est plutôt associée à un mauvais pronostic. Alors, quelle est la valeur pronostique et signification de l'association entre niveau élevé de *VNN1* et pronostic de sarcomes ? Que connaît-on de l'implication de la Vanin1 lors de dérégulation métabolique en contexte pathologique et comment expliquer de telles différences entre les cancers selon les tissus qu'ils touchent ?

La Vanin1 possède un rôle dans le stress oxydant et l'inflammation en condition physiologique. Dans différentes maladies, l'activité pantéthénase portée par la Vanin1 a été associée soit à des mécanismes protecteurs soit à des effets sensibilisateurs selon le modèle d'étude testé et en fonction de l'organe touché. Ces résultats doivent prendre en considération le fait que dans certains cas, le modèle repose sur l'analyse de souris déficientes pour le gène *Vnn1* alors que dans d'autres cas, l'effet observé dépend de la surexpression spécifique de *Vnn1* dans un modèle cellulaire précis. Par ailleurs, certains phénotypes sont directement liés à un impact sur des cellules épithéliales ou fibroblastiques qui peuvent exprimer *VNN1*, alors que dans d'autres situations, c'est le phénotype immunitaire qui est affecté alors que ces cellules n'expriment pas *VNN1* de manière générale. Dans ces modèles, le phénotype est probablement conditionné par l'effet du pantothénate et/ou de la cystéamine, produits d'une activité *VNN1* sur des cellules tissulaires. De manière intéressante, dans la plupart des cas évoqués, les phénotypes obtenus dans des modèles murins récapitulaient assez fidèlement les observations faites en pathologie humaine.

Des effets cytoprotecteurs sur des cellules épithéliales ont été observés dans trois contextes. Dans un modèle de diabète de type 1, l'expression de *VNN1*, par les cellules β des îlots de Langerhans, exerce un effet cytoprotecteur en renforçant la résistance au stress cellulaire (172). Un résultat similaire a été observé après intoxication hépatique par l'acétaminophène. Par ailleurs, une forte activité Vanin1 dans le sang confère une protection contre le stress oxydant pour les érythrocytes et une augmentation de la résistance à la malaria (173). Enfin et plus précisément, la surexpression de *VNN1* par transgénèse dans l'épithélium intestinal s'associe d'une part à une dysbiose génératrice d'acides gras à courte chaîne (SCFA) au potentiel immunorégulateur, et d'autre part à une amélioration de l'état énergétique des colonocytes, dépendant de la respiration mitochondriale, consommatrice du butyrate notamment (174). Le cumul de ces deux effets augmente le niveau de vitamine B5

et de coenzyme A colique, renforce la fonctionnalité des colonocytes et l'efficacité de la barrière intestinale.

Des effets immunomodulateurs ont été observés dans divers modèles auto-immuns ou infectieux principalement. Dans un modèle d'infection *Schistosoma mansoni*, l'expression de Vanin1 est associée à une augmentation des dommages tissulaires induits notamment par les neutrophiles dans l'intestin (175). Dans un modèle tumoral induit dans un contexte inflammatoire (cancer colique induit par le DSS) où les niveaux de génération de ROS et le stress oxydant sont élevés, l'expression de Vanin1 peut favoriser la progression tumorale en limitant l'effet cytotoxique des ROS sur la cellule tumorale et la mort cellulaire. Dans un modèle de sclérodémie, l'expression de VNN1 par les myofibroblastes associés aux zones de fibrose est corrélée à une augmentation des auto-anticorps et de cytokines sériques comme l'IL4, IL6, IL13 ou encore l'IL17 (176). Cela suggère, que directement ou indirectement, la Vanin1 est promotrice des réponses Th2 et plus modestement Th17 et d'une inflammation médiée par les cellules B, le tout aggravant la maladie. Ce type de réponse dans un contexte tumoral pourrait être associé à un mauvais pronostic. Globalement dans tous ces modèles, l'effet améliorant ou aggravant est lié à un effet amplificateur des réponses immunitaires induit par le contexte pathologique : il est délétère car générateur de dégâts tissulaires dans la schistosomiase ou la sclérodémie. Il est protecteur dans une colite en augmentant le taux des SCFA cytoprotecteurs et immunorégulateurs. Il est donc difficile a priori de prédire l'impact de la surexpression de Vnn1 dans un modèle tumoral compte des nombreux niveaux d'impact sur le métabolisme cellulaire et le phénotype immunitaire associé aux tumeurs. L'effet sera-t-il prédominant sur les cellules tumorales, les cellules stromales fibroblastiques ou adipocytaires associées aux tumeurs ou sur les différents sous types de cellules de l'immunité ?

Force est de constater que l'ensemble de ces observations ne semble pas vraiment pouvoir répondre à la question d'une corrélation de l'expression de la Vanin1 et le pronostic médical. Pourtant, elles permettent de mettre en évidence que plusieurs éléments sont à prendre en compte pour établir une corrélation.

Dans le cancer du pancréas où l'expression de *VNN1* est de mauvais pronostic et n'est pas associée à une signature immunitaire, on sait que le niveau d'infiltration et d'activation du système immunitaire est insuffisant pour permettre l'éradication de la tumeur. Nos résultats ont également montré que la pantéthine n'avait aucun effet dans un modèle d'ostéosarcome murin, ce type de sarcome étant un exemple de désert immunitaire. Ainsi, la variable « système immunitaire » semble avoir son importance. Dans les analyses des banques transcriptomiques humaines disponibles, nous avons pu corréliser le bon pronostic associé à un niveau élevé de VNN1 à la présence de signatures immunitaires. Il serait intéressant d'étendre ces études à d'autres modèles et de tenter de corréliser les données humaines avec des modèles murins.

Les corrélations décrites chez l'Homme sont principalement basées sur l'étude de l'expression génique de VNN1. Cette expression varie selon les tissus à l'état basal, et il serait intéressant de connaître comment elle évolue au cours de la transformation tumorale. Les données

obtenues chez la souris dans le modèle des souris double *knock-out* pour les gènes p16 et p19 montrent que les rares fibrosarcomes qui se développaient chez ces souris exprimaient des niveaux très faibles de *Vnn1* alors que des myofibroblastes activés expriment de hauts taux de *Vnn1* (161). Dans ce modèle, l'évolution des tumeurs s'accompagnerait d'une perte d'expression de *Vnn1* et donc de vitamine B5 puis de coenzyme A. C'est dans ce type de modèles que la supplémentation en pantéthine a eu un effet thérapeutique indirect en dopant les réponses immunitaires. Il resterait à vérifier cette hypothèse dans d'autres types de tumeurs exprimant des niveaux variables de VNN1 en phase initiale ou terminale de la maladie. La Vanin1 existe aussi sous forme sérique, et l'activité pantéthénase dans les fluides mériterait d'être investiguée en parallèle avec la progression tumorale.

D'autre part, l'expression de Vanin1 est contrôlée par la prise alimentaire, notamment pendant les périodes de jeûne. Dans la majorité des cas, les biopsies sont réalisées chez les patients à jeun, nous pouvons donc nous interroger sur la pertinence des niveaux de Vanin1 mesurés dans les échantillons. De plus, les patients atteints de cancer présentent fréquemment une altération de leur prise alimentaire ou de dysbioses qui peuvent altérer les effets bénéfiques portés par la Vanin1. En effet, le niveau d'expression de *Vnn1* modifie l'équilibre du microbiote intestinal et la présence de bactéries peut moduler le niveau de *Vnn1* intestinale, notamment dans le colon (174).

Enfin, l'action de l'activité Vanin1 est liée à l'augmentation de la respiration mitochondriale et à une amélioration de l'état redox cellulaire. Dans un contexte tumoral où l'effet Warburg est prédominant, le fonctionnement mitochondrial est souvent altéré et les intermédiaires du cycle de Krebs en amont de la chaîne de transports des électrons, ou encore la conversion du pyruvate en lactate, limitent l'utilisation de la respiration. Ainsi, l'effet suppresseur de tumeur observé dans le premier modèle de sarcome étudié a pu être lié à la capacité de la VNN1 à réinduire un fonctionnement mitochondrial normal (161). Un tel effet devient improbable quand la phosphorylation oxydative ne fonctionne plus, à moins que cela ne contribue à augmenter la fuite d'électrons par le complexe I susceptibles de produire plus d'espèces réactives de l'oxygène et d'induire la mort cellulaire ou l'activation de l'immunité. Dans le modèle de sarcome dépendant de la cellule MCA, le métabolisme de la cellule tumorale est resté peu affecté par l'administration de pantéthine dont l'effet a surtout concerné les cellules immunitaires infiltrantes notamment de type 1, aboutissant à une amélioration du pronostic.

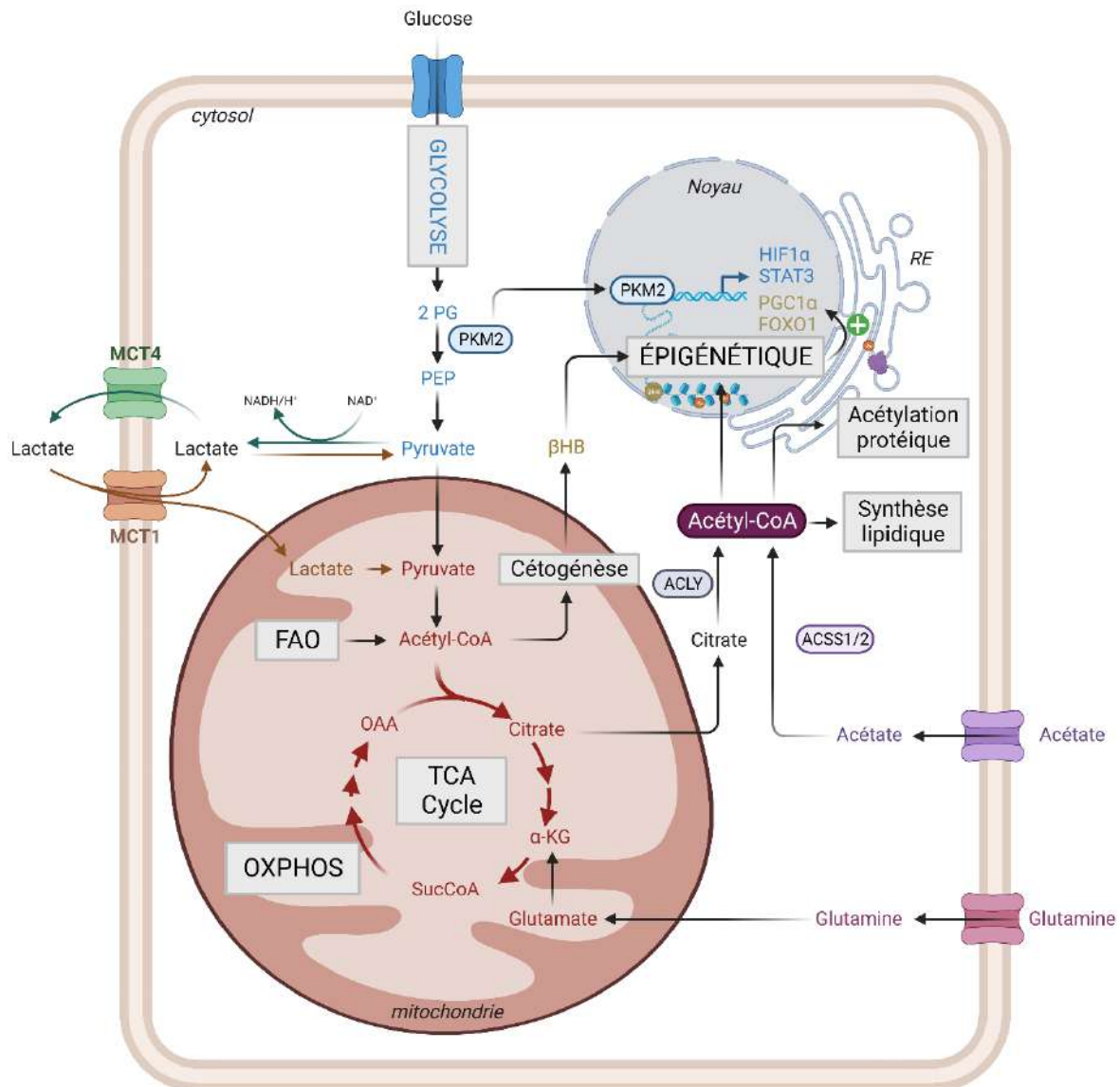


Figure 28 : Rôle de la vitamine B5 et du coenzyme A dans l'immunométabolisme

3) Coenzyme A, B5 et immunoréactivité

Dans le modèle MCA, nos résultats mettent en avant un effet prédominant sur le compartiment immunitaire, notamment une augmentation des processus de présentation antigénique, l'augmentation de la voie de signalisation de l'IFN γ , l'augmentation de l'infiltration des cellules T et NK dans les tumeurs détentrices des fonctions cytolytiques.

L'une des hypothèses est que la vitamine B5 favorise l'augmentation de l'activité mitochondriale dans les lymphocytes T CD8 augmentant leur potentiel antitumoral et/ou le développement des cellules mémoires qui dépendent pour leur survie du maintien de phosphorylation oxydative. Celle-ci est aussi requise en phase initiale d'activation ou réactivation de fonctions effectrices dans un contexte de glycolyse accrue (130). D'une manière intéressante, l'oxydation du glucose dans le cycle de Krebs est l'une des

caractéristiques de la polarisation des cellules T CD8 sécrétant l'IL22 (177). Ces lymphocytes CD8 de type Tc22 possèdent une forte activité cytotoxique antitumorale et augmentent la sensibilité des tumeurs aux immunothérapies. Il a été montré que la production d'IL22 était dépendante de la signalisation HIF et AhR et que l'augmentation du succinate contribuait à la stabilisation de HIF. Cependant, une autre étude a montré que l'accumulation de succinate pouvait inhiber l'activité synthase du SuccinylCoA et donc interrompre le cycle de Krebs (178).

Dans un contexte d'obésité, les cellules T CD4 de type Th17 acquièrent un phénotype inflammatoire qui requiert une augmentation de la glycolyse et de PKM2. Dans ce contexte, il a été montré que la vitamine B5 pouvait reprogrammer le métabolisme des Th17 par augmentation du coenzyme A (179). Ce processus implique l'isoforme PKM2 connue pour avoir une activité réduite par rapport à la PK mais dotée de la possibilité de réguler la transcription de certains gènes après translocation nucléaire (180). Le coenzyme A se fixe à la PKM2 et prévient sa translocation nucléaire conduisant à une réduction de la production de l'IL17 dépendante de STAT3 (181). La vitamine B5 est aussi associée à un meilleur pronostic dans l'EAE et la colite, pathologie en inhibant les réponses Th17 impliquées dans la pathogénicité (174,182).

L'implication du coenzyme A dans l'oxydation des acides gras et l'activité mitochondriale pourrait être favorable à une immunité de type Th2 en optimisant le métabolisme oxydatif des macrophages M2 (183) et les fonctions des cellules T CD4 régulatrices dont le maintien homéostatique dépend d'OXPPOS (184). Dans les tumeurs traitées à la pantéthine, les cellules myéloïdes infiltrantes possèdent une signature de présentation antigénique dépendante de l'action de l'IFN γ et associée à une signature OXPPOS. Le lien entre phosphorylation oxydative et présentation antigénique reste discuté au sein de la communauté scientifique. Plusieurs travaux montrent que l'implication de la chaîne de transports des électrons est envisagée par sa capacité à augmenter l'inflammation *via* son rôle dans les fonctions immunitaires. Dans un modèle de mélanome, la réponse aux immunothérapies dépend de la β -oxydation mitochondriale et de la présentation antigénique (55). Dans les macrophages, l'administration de coenzyme A oriente l'utilisation du glucose pour alimenter le cycle de Krebs, augmentant l'activation de gènes pro-inflammatoires par régulation épigénétique médiée par l'acétyl-CoA. Ceci favorise l'activité antitumorale dans un modèle de cancer du sein (185). Dans le même ordre d'idée, il a été montré que la vitamine B5 augmente les fonctions des macrophages lors d'une infection bactérienne (186). L'acquisition des capacités de présentation antigénique et la réponse à l'IFN γ dans les cellules présentatrices d'antigènes nécessite l'augmentation de l'activité mitochondriale (187,188). Nos résultats sont en phase avec ces observations en montrant que l'efficacité thérapeutique de la pantéthine nécessite l'implication des cellules cDC1 et des cellules T CD8. En effet, la mise en place d'une réponse effectrice des lymphocytes CD8 requiert la présentation croisée des cDC1. De manière intéressante, les cellules dendritiques CD8⁺ utilisent la voie de signalisation Hippo Mst kinase pour augmenter les ressources énergétiques consommées par les mitochondries et nécessaires au maintien de la présentation croisée et de la production de l'IL12. Nous avons trouvé que la quantité d'IL12 était fortement augmentée dans les tumeurs

de souris traitées à la pantéthine. Enfin, l'activité mitochondriale est essentielle durant l'activation, la production de cytokine et la différenciation des cellules T (189–191). Le complexe I de la chaîne de transport d'électrons est requis lors de la prolifération des cellules Th1 et le remodelage épigénétique, alors que le complexe II sera nécessaire à la maintenance des fonctions effectrices (192). L'acétyl-CoA peut augmenter la synthèse lipidique, la production d'IFN γ et l'activité cytolytique des cellules T CD8 (193,194). L'acétyl-CoA mitochondrial peut également participer à la cétogénèse et à la production d'hydroxybutyrate qui vont modifier la lysine 9 de l'histone 3 par un mécanisme épigénétique. Cela va conduire en aval à l'augmentation de régulation des gènes FOXO1 et PGC1s qui conduisent à l'augmentation de l'expression de PCK1. Par conséquent, la gluconogénèse et la voie des pentoses phosphates vont augmenter améliorant le contrôle redox dans les CD8 mémoires (195). Ainsi, il serait intéressant d'approfondir l'immunométabolisme des cellules à différentes étapes de la cinétique de progression tumorale après un traitement à la pantéthine et comprendre par quel mécanisme la respiration et les fonctions des mitochondries sont améliorés dans les lymphocytes T CD8.

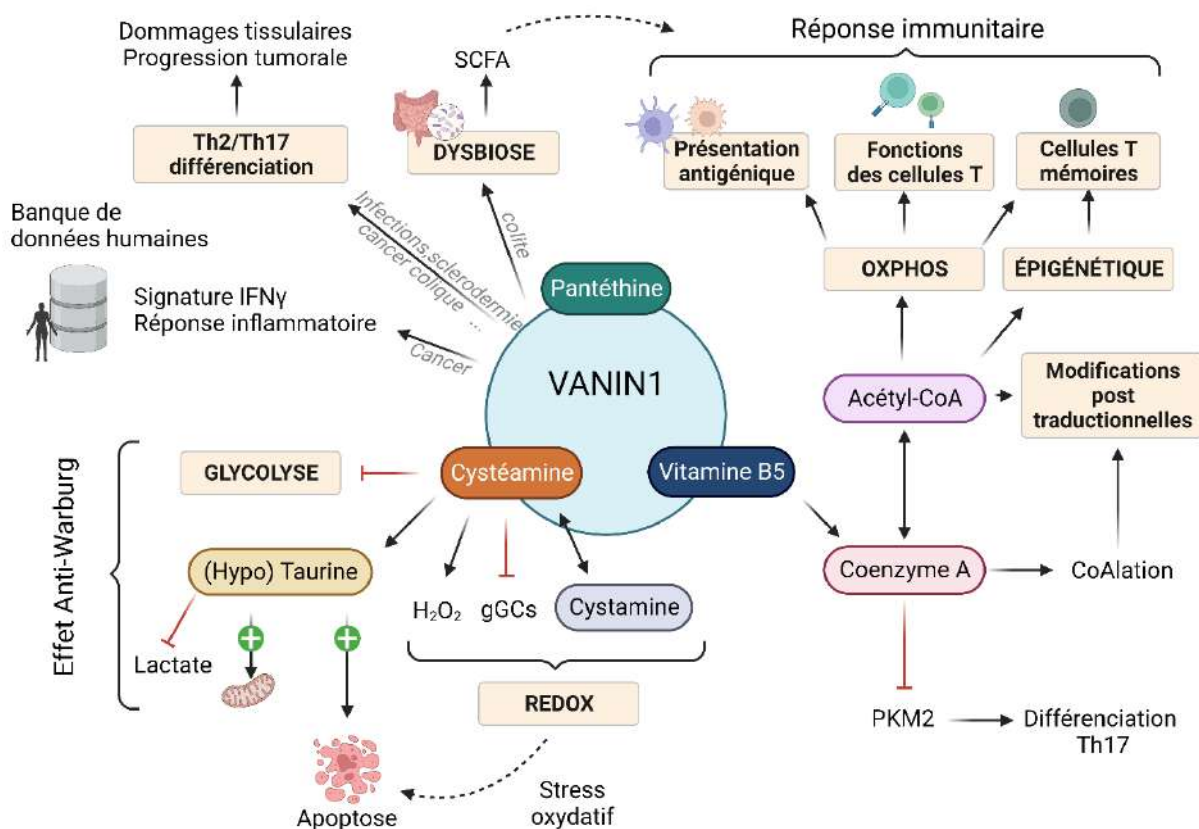


Figure 29 : Bilan de l'effet thérapeutique dépendant de la voie de signalisation Vanin1

4) Perspectives et limites du traitement à la pantéthine

La voie de signalisation du coenzyme A, qu'il s'agisse de l'activité pantéthéinase de la Vanin1, de la cystéamine ou du pantothénate reste une cible thérapeutique de choix par la multiplicité des processus dans lesquels elles interviennent. Cependant, il est nécessaire que les protocoles thérapeutiques soient adaptés pour que son bénéfice thérapeutique soit observable. Il faudrait pouvoir identifier des marqueurs prédictifs de son efficacité thérapeutique associés à l'activité mitochondriale ou à la présence d'un infiltrat immunitaire. Plusieurs limites peuvent être discutées : i) l'épuisement des cellules T conduit à des altérations mitochondriales irréversibles qui peuvent limiter l'action bénéfique de la pantéthine sur le compartiment lymphocytaire ; ii) dans le cadre d'une utilisation en combinaison thérapeutique, il est nécessaire que les drogues utilisées n'agissent pas sur des mécanismes analogues. Par exemple, nos résultats ne montrent pas d'effet synergique de la pantéthine avec le dichloroacétate ou avec les anticorps bloquants l'axe PD1 sur la croissance tumorale. En effet, l'activité des anti-PD1 et l'administration de pantéthine agissent d'une manière similaire sur l'augmentation des fonctions mitochondriales et la production de ROS dans les cellules T CD8 (196).

Le pantothénate est présent en concentration variable dans tous les milieux de culture utilisés. Le transfert adoptif de cellules T portant un récepteur chimérique, appelée CAR T, nécessite une période de mise en culture et d'expansion *in vitro* avant d'être retransférés aux patients. Il serait intéressant de connaître l'impact d'une supplémentation en vitamine B5 dans le milieu de culture sur l'activité cytolytique *in vivo* des CD8 CAR T ainsi que la mise en place de fonction mémoire.

L'un de nos résultats sur les données métabolomiques tend à suggérer que la pantéthine pourrait modifier la composition et/ou l'activité du microbiote, déjà prouvé dans un modèle d'IBD (174). Nous avons observé que sous traitement antibiotique déplaçant le microbiote, l'effet thérapeutique de la pantéthine était perdu. Compte tenu des multiples rôles du microbiote dans la résistance aux immunothérapies (116), il serait intéressant de voir si l'influence de la pantéthine sur le microbiote peut avoir un effet bénéfique sur la réponse anti-tumorale. Enfin, comme nous l'avons montré dans le modèle HSV1, la supplémentation en pantéthine pourrait améliorer l'efficacité de traitements antiviraux ou de vaccination par promotion des réponses antivirales des cellules T.

Ainsi, la reprogrammation de la mitochondrie lorsqu'elle est possible peut favoriser les réponses antitumorales de cellules de l'immunité. Cet effet aurait un intérêt dans des modèles tels que celui développé à partir de la lignée MCA qui possède une faible capacité respiratoire mitochondriale. Par ailleurs, dans un modèle ayant une forte capacité mitochondriale, l'effet de l'expression de la Vanin1 pourrait cibler à la fois le compartiment tumoral par un effet anti Warburg et le compartiment immunitaire.

B) Dynamiques mitochondriales et thérapies ciblées

Dans notre second axe de travail, nous avons cherché à manipuler l'activité mitochondriale des cellules tumorales. Pour cela, nous avons choisi de cibler l'un des processus dynamiques de la mitochondrie en réponse à un stress cellulaire : la fusion et la fission, régi par les protéines OMA1 et OPA1. Nous avons étudié comment une mutation d'OMA1 pouvait avoir des conséquences directes sur les fonctions mitochondriales dans une cellule cancéreuse, influencer sa croissance et potentiellement moduler l'immunoréactivité de la tumeur.

1) OMA1 et OPA1 marqueurs pronostiques ?

Nous avons interrogé des banques de données humaines pour connaître la valeur pronostique d'OMA1 et d'OPA1 en termes de survie sans métastase et de corrélation avec une infiltration immunitaire. Les analyses réalisées suggèrent que l'expression d'OPA1 est significativement corrélée à une diminution de la survie sans métastase et l'expression d'OMA1 suit la même tendance. L'expression d'OPA1 est associée à un score CINSARC à haut risque (CINSARC est un acronyme pour *Complexity INdex in SARComas*). La faible expression d'OPA1 est associée à une bonne infiltration immunitaire, à une présentation antigénique augmentée et à une activité cytolytique présente. Le niveau d'expression d'OMA1 ne semble pas influencer la qualité de l'infiltrat immunitaire. La littérature possède également quelques exemples où la valeur pronostique d'OMA1 et d'OPA1 a été évaluée dans différents types de cancer. La surexpression d'OMA1 favorise la reprogrammation métabolique dépendante de l'hypoxie dans le cancer colorectal (127) et est de mauvais pronostic dans les carcinomes gastriques, carcinome du sein et des cellules squameuses du poumons (197). Au contraire, son expression peut être associée à une survie améliorée dans un type de cancer du sein et dans les adénocarcinomes du poumon (197,198). Comme pour la Vanin1, nous pouvons émettre l'hypothèse d'une utilisation différentielle des mitochondries dans les types de cancer limitant l'implication des voies de signalisation mitochondriales dans la progression tumorale.

2) Cibler les fonctions d'OPA1 et OMA1 dans un contexte tumoral

Les données que nous avons obtenues chez l'Homme et les données montrant la contribution d'OPA1 dans la régulation de l'angiogenèse et de l'apoptose (199) confortent l'hypothèse que moduler sa fonction pourrait avoir un intérêt thérapeutique. Nos résultats montrent que la perte de la formation d'un pont disulfure impliqué dans la fonction de perception du stress oxydant par la protéine OMA1 abroge sa fonction catalytique, et en empêchant le clivage d'OPA1 en situation de stress à une détérioration des fonctions mitochondriales. Ainsi, ce site redox d'OMA1 serait une cible pharmacologique. *In vivo*, nous n'avons pas pu démontrer ce point en administrant des métabolites comme la N-acétylcystéine ou la cystéamine qui ne semblaient pas altérer l'état redox d'OMA1 dans les

conditions utilisées. Le développement d'inhibiteurs d'OMA1 est complexe compte tenu de l'absence de structure tridimensionnelle et du manque de moyens d'évaluation de l'activité d'OMA1 *in vivo* (200).

Dans nos expériences, l'inhibiteur d'OPA1, MYLS22, ne semble pas apporter de bénéfice thérapeutique sur la croissance tumorale des sarcomes. Pourtant, son utilisation dans un modèle d'adénocarcinome en réduit la croissance (128). L'une des difficultés pour développer une thérapie efficace est de comprendre les mécanismes de régulation et l'intersection avec d'autres voies de signalisation des potentielles cibles thérapeutiques. La compréhension de la régulation d'OMA1 possède de nombreuses lacunes, notamment sur son mécanisme d'activation. Certaines études semblent montrer l'effet d'une variation des niveaux d'ATP (201) sur le mécanisme d'autoclivage (202) ou sur sa localisation dans la membrane interne des mitochondries (203). La contribution d'OMA1 ou d'OPA1 au complexe MICOS qui régule le fonctionnement des crêtes mitochondriales reste trop parcellaire. Enfin, la molécule DELE1 a été identifiée comme cible d'OMA1 en réponse au stress et lie le fonctionnement mitochondrial au fonctionnement du réticulum endoplasmique. Ce mécanisme pourrait aussi contribuer aux phénotypes observés dans notre modèle d'étude (204).

La régulation de la dynamique mitochondriale a pourtant permis le développement de plusieurs thérapies ciblant principalement DRP1. En effet, DRP1 est souvent surexprimé dans de nombreux types de cancer comme le cancer du poumon, du colon, du sein ou le mélanome par exemple (205). Ces tumeurs présentent un niveau élevé de fission mitochondriale associée à la reprogrammation métabolique, à la progression du cycle cellulaire, à l'augmentation de la migration et à l'invasion métastatique. Dans un modèle de tumeur du cerveau, l'inhibition de DRP1 augmente l'apoptose et inhibe la croissance tumorale (206). Dans un modèle de cancer du sein, l'inhibition de DRP1 limite les capacités métastatiques (207). Dans cette même étude, la surexpression de MFN1, protéine promotrice de la fusion conduit aux mêmes effets. Le blocage des processus de fusion par déplétion de l'expression d'OPA1, favorise la désorganisation du réseau mitochondrial, la dissipation du potentiel de membrane, le relargage du cytochrome c et l'apoptose dans des cellules de tumeurs ovariennes (208). Ces résultats sont cohérents avec ceux que nous avons obtenus où les mutants OMA1 perdant les capacités de clivage d'OPA1 ne poussent plus dans une souris immunocompétente mais ont une croissance normale chez une souris Nude. Ceci nous a conduit à explorer l'impact de la mutation d'OMA1 sur le déclenchement d'une réponse immunitaire.

3) OMA1/OPA1 et l'immunité

L'absence de prise de greffe des mutants OMA1 dans un modèle immunocompétent suggère un rejet par le système immunitaire. Nous avons exclu l'hypothèse d'un défaut d'implantation des cellules par l'utilisation d'un modèle chimérique comportant à la fois des cellules mutées et des cellules non mutées. Par ailleurs, la présence du clone présentant la mutation d'OMA1 était suffisante pour diminuer la croissance des clones non mutés. Nous avons donc cherché à identifier des signaux activateurs de l'immunité de type DAMPs. La

contribution de la production de ROS mitochondriaux n'étant pas différentielle, nous avons pu corrélérer le déclenchement de la réponse immunitaire au relargage d'ADN mitochondrial. Les conséquences du relargage d'ADN mitochondrial dépendent de la nature de l'infiltrat immunitaire. Il peut favoriser la progression tumorale en augmentant l'activité des neutrophiles (209) ou au contraire augmenter la présentation croisée par les cDC1 et promouvoir le développement d'une réponse antitumorale des cellules T cytotoxiques (210). Dans un modèle génétique murin dépourvu de cellules cDC1, la croissance des clones tumoraux mutés est de nouveau observée renforçant la contribution de ces cellules dans le rejet des tumeurs. L'impact de la mutation sur l'activation des cDC1 peut également avoir une portée plus directe. Effectivement, il a été montré que l'inhibition de la fission mitochondriale est associée à une augmentation de l'expression du CMHI à la surface des cellules cancéreuses. Ainsi, l'altération du clivage d'OPA1 par la mutation d'OMA1 pourrait limiter la fusion mitochondriale dans les tumeurs et potentialiser la réponse antitumorale en favorisant la reconnaissance par le système immunitaire (93).

Les mécanismes de mort induite *in vivo* restent à étudier. En effet, l'activation d'OMA1 *in vitro* est dépendante de l'utilisation de l'agent découplant CCCP. Cependant, l'activation d'OMA1 au sein d'une tumeur peut dépendre de plusieurs paramètres. Étudier l'impact de la mutation d'OMA1 sur la mort *in vivo* pourrait permettre de mieux comprendre nos résultats. En effet, la perméabilisation de la membrane externe de la mitochondrie est un point de bascule lors des processus apoptotiques et nombreux processus inflammatoires activés lors de la mort cellulaire en dépendent. Le relargage d'ADN mitochondrial et autres DAMPs mitochondriaux peut avoir un effet immunostimulant. Une étude récente a démontré que le relargage d'ADN mitochondrial dans le cytosol se fait progressivement par l'élargissement des pores BAX/BAK (211). La présence d'ADN mitochondrial peut déclencher la voie de signalisation cGAS et la génération des messagers secondaires cGAMP, déclenchant ainsi l'activation et la translocation de STING dans le Golgi. STING va activer TBK1 qui va le phosphoryler et cibler également IRF3 favorisant l'expression des gènes stimulés par l'IFN. Il peut également favoriser la voie NF- κ B. Le relargage d'ADN mitochondrial peut également être détecté par TLR9 et l'inflammasome NLRP3. Cependant, les mécanismes inflammatoires engendrés après perméabilisation de la membrane externe mitochondriale et le relargage d'ADN mitochondrial est étroitement lié à l'activité des caspases. En effet, les caspases peuvent cliver et inactiver certains DAMPs ou des régulateurs clefs de l'inflammation : l'IL33 (212), cGAS, MAVS, IRF3, NEMO ou encore I κ B (213–216). Ainsi, pour promouvoir une mort cellulaire immunogénique suite à la reconnaissance de l'ADN mitochondrial, il est essentiel de connaître l'activité des caspases voire de l'inhiber, point qu'il resterait à caractériser dans les cellules OMA1 mutées. Une approche de l'inhibition d'OMA1 pourrait être envisagée à des inhibiteurs des caspases pour augmenter l'immunogénicité et la réponse antitumorale.

4) Perspectives et limites

L'une des limites du ciblage de l'activité dépendante d'OMA1 et OPA1 est le risque d'altérer les fonctions des autres cellules composant le microenvironnement tumoral. Comme nous l'avons vu précédemment, la dynamique mitochondriale est essentielle lors de la différenciation, l'activation et la production de cytokines par le système immunitaire (51). Ainsi, l'utilisation systémique ou locale d'inhibiteur d'OMA1 ou d'OPA1 pourrait fortement impacter les fonctions du système immunitaire et favoriser la progression tumorale. En effet, OPA1 joue un rôle dans la maturation des thymocytes notamment au stade du précurseur DN3 où la respiration oxydative joue un rôle majeur. La déplétion d'OPA1 mène à une susceptibilité des thymocytes à la mort cellulaire et à une forte signalisation du TCR. Les T matures ayant perdu l'expression d'OPA1 présentent un phénotype mémoire effecteur en l'absence de stimulation antigénique (217). D'une manière similaire, la déplétion d'OPA1 dans les cellules myéloïdes empêche la différenciation en macrophage de type M1. La déplétion d'OPA1 dans ces cellules conduit à l'accumulation des métabolites du cycle de Krebs et à une voie de signalisation NF- κ B dysfonctionnelle. Dans un modèle de régénération musculaire, les macrophages ayant perdu OPA1 persistent dans le tissu endommagé causant un excès de collagène et empêche la cicatrisation musculaire.

5) Conclusion

Mon travail de thèse m'a convaincu que cibler la mitochondrie est essentielle dans le développement des futures combinaisons thérapeutiques en oncologie. Elle offre de nombreux avantages pouvant freiner la croissance intrinsèque des cellules cancéreuses et favoriser le développement d'une réponse immunitaire durable tout en prévenant les différentes altérations du système immunitaire induites par les cellules cancéreuses. Cibler la mitochondrie apporte également l'avantage de réorienter les flux métaboliques et d'assurer une bonne répartition des ressources au sein du microenvironnement, favorisant le rétablissement et/ou la réactivation du système immunitaire. Ainsi, de nombreuses thérapies ciblant la mitochondrie ont été approuvées pour une exploitation thérapeutique, avec des usages et finalités différentes. Nous retrouvons ainsi différents inhibiteurs de la chaîne de transport des électrons comme la metformine et la roténone, inhibiteurs du complexe I, la doxorubicine, inhibiteur du complexe IV ou encore l'oligomycine, inhibiteur de l'ATP synthase parmi les plus connus (218). Certaines thérapies vont promouvoir la perméabilisation de la mitochondrie (219), d'autres l'augmentation de la production de ROS comme la menadione, la motefaxin ou l'imexon pour en citer quelques-uns. Les recherches futures devraient permettre d'approfondir cette piste thérapeutique.

VII) Bibliographie

1. Ekhtiari S, Chiba K, Popovic S, Crowther R, Wohl G, Wong AKO, et al. First case of osteosarcoma in a dinosaur: a multimodal diagnosis. *Lancet Oncol.* Elsevier; 2020;21:1021–2.
2. Hanahan D. Hallmarks of Cancer: New Dimensions. *Cancer Discov.* 2022;12:31–46.
3. Hanahan D, Weinberg RA. The Hallmarks of Cancer. *Cell.* 2000;100:57–70.
4. Hanahan D, Weinberg RA. Hallmarks of Cancer: The Next Generation. *Cell.* 2011;144:646–74.
5. Kandoth C, McLellan MD, Vandin F, Ye K, Niu B, Lu C, et al. Mutational landscape and significance across 12 major cancer types. *Nature.* 2013;502:333–9.
6. Danaher P, Warren S, Lu R, Samayoa J, Sullivan A, Pekker I, et al. Pan-cancer adaptive immune resistance as defined by the Tumor Inflammation Signature (TIS): results from The Cancer Genome Atlas (TCGA). *J Immunother Cancer.* 2018;6:63.
7. Rheinbay E, Nielsen MM, Abascal F, Wala JA, Shapira O, Tiao G, et al. Analyses of non-coding somatic drivers in 2,658 cancer whole genomes. *Nature.* 2020;578:102–11.
8. Steele CD, Abbasi A, Islam SMA, Bowes AL, Khandekar A, Haase K, et al. Signatures of copy number alterations in human cancer. *Nature.* 2022;606:984–91.
9. Hogg SJ, Beavis PA, Dawson MA, Johnstone RW. Targeting the epigenetic regulation of antitumour immunity. *Nat Rev Drug Discov.* Nature Publishing Group; 2020;19:776–800.
10. Warmoes MO, Locasale JW. Heterogeneity of glycolysis in cancers and therapeutic opportunities. *Biochem Pharmacol.* 2014;92:12–21.
11. Seth Nanda C, Venkateswaran SV, Patani N, Yuneva M. Defining a metabolic landscape of tumours: genome meets metabolism. *Br J Cancer.* Nature Publishing Group; 2020;122:136–49.
12. Rosario SR, Long MD, Affronti HC, Rowsam AM, Eng KH, Smiraglia DJ. Pan-cancer analysis of transcriptional metabolic dysregulation using The Cancer Genome Atlas. *Nat Commun.* 2018;9:5330.
13. Rihan M, Nalla LV, Dharavath A, Shard A, Kalia K, Khairnar A. Pyruvate Kinase M2: a Metabolic Bug in Re-Wiring the Tumor Microenvironment. *Cancer Microenviron Off J Int Cancer Microenviron Soc.* 2019;12:149–67.
14. Chang C-H, Qiu J, O’Sullivan D, Buck MD, Noguchi T, Curtis JD, et al. Metabolic Competition in the Tumor Microenvironment Is a Driver of Cancer Progression. *Cell.* 2015;162:1229–41.

15. Kawai S, Murata K. Structure and function of NAD kinase and NADP phosphatase: key enzymes that regulate the intracellular balance of NAD(H) and NADP(H). *Biosci Biotechnol Biochem.* 2008;72:919–30.
16. DeBerardinis RJ, Chandel NS. We need to talk about the Warburg effect. *Nat Metab.* 2020;2:127–9.
17. Vander Heiden MG, Cantley LC, Thompson CB. Understanding the Warburg Effect: The Metabolic Requirements of Cell Proliferation. *Science.* 2009;324:1029–33.
18. Warburg O, Wind F, Negelein E. THE METABOLISM OF TUMORS IN THE BODY. *J Gen Physiol.* 1927;8:519–30.
19. Koppenol WH, Bounds PL, Dang CV. Otto Warburg's contributions to current concepts of cancer metabolism. *Nat Rev Cancer.* 2011;11:325–37.
20. Martínez-Reyes I, Chandel NS. Cancer metabolism: looking forward. *Nat Rev Cancer.* Nature Publishing Group; 2021;21:669–80.
21. Moreira JDV, Hamraz M, Abolhassani M, Bigan E, Pérès S, Paulevé L, et al. The Redox Status of Cancer Cells Supports Mechanisms behind the Warburg Effect. *Metabolites.* Multidisciplinary Digital Publishing Institute; 2016;6:33.
22. Hui S, Ghergurovich JM, Morscher RJ, Jang C, Teng X, Lu W, et al. Glucose feeds the TCA cycle via circulating lactate. *Nature.* 2017;551:115–8.
23. de la Cruz-López KG, Castro-Muñoz LJ, Reyes-Hernández DO, García-Carrancá A, Manzo-Merino J. Lactate in the Regulation of Tumor Microenvironment and Therapeutic Approaches. *Front Oncol [Internet].* 2019 [cited 2022 Dec 26];9. Available from: <https://www.frontiersin.org/articles/10.3389/fonc.2019.01143>
24. Caslin HL, Ababayehu D, Pinette JA, Ryan JJ. Lactate Is a Metabolic Mediator That Shapes Immune Cell Fate and Function. *Front Physiol [Internet].* 2021 [cited 2023 Mar 2];12. Available from: <https://www.frontiersin.org/articles/10.3389/fphys.2021.688485>
25. Hayes C, Donohoe CL, Davern M, Donlon NE. The oncogenic and clinical implications of lactate induced immunosuppression in the tumour microenvironment. *Cancer Lett.* 2021;500:75–86.
26. Feng Q, Liu Z, Yu X, Huang T, Chen J, Wang J, et al. Lactate increases stemness of CD8 + T cells to augment anti-tumor immunity. *Nat Commun.* Nature Publishing Group; 2022;13:4981.
27. Hyun D-H. Insights into the New Cancer Therapy through Redox Homeostasis and Metabolic Shifts. *Cancers.* 2020;12:1822.
28. Guzy RD, Schumacker PT. Oxygen sensing by mitochondria at complex III: the paradox of increased reactive oxygen species during hypoxia. *Exp Physiol.* 2006;91:807–19.

29. Brunelle JK, Bell EL, Quesada NM, Vercauteren K, Tiranti V, Zeviani M, et al. Oxygen sensing requires mitochondrial ROS but not oxidative phosphorylation. *Cell Metab.* 2005;1:409–14.
30. Courtney R, Ngo DC, Malik N, Ververis K, Tortorella SM, Karagiannis TC. Cancer metabolism and the Warburg effect: the role of HIF-1 and PI3K. *Mol Biol Rep.* 2015;42:841–51.
31. Ke Q, Costa M. Hypoxia-inducible factor-1 (HIF-1). *Mol Pharmacol.* 2006;70:1469–80.
32. Semenza GL. HIF-1 mediates metabolic responses to intratumoral hypoxia and oncogenic mutations. *J Clin Invest. American Society for Clinical Investigation;* 2013;123:3664–71.
33. Frey TG, Mannella CA. The internal structure of mitochondria. *Trends Biochem Sci.* 2000;25:319–24.
34. Guo R, Gu J, Zong S, Wu M, Yang M. Structure and mechanism of mitochondrial electron transport chain. *Biomed J.* 2018;41:9–20.
35. Nelson DL, Cox MM. *Lehninger Principles of Biochemistry.* 007 edition. New York: W H FREEMAN & CO; 2017.
36. Martínez-Reyes I, Chandel NS. Mitochondrial TCA cycle metabolites control physiology and disease. *Nat Commun.* 2020;11:102.
37. Vercellino I, Sazanov LA. The assembly, regulation and function of the mitochondrial respiratory chain. *Nat Rev Mol Cell Biol. Nature Publishing Group;* 2022;23:141–61.
38. Inigo M, Deja S, Burgess SC. Ins and Outs of the TCA Cycle: The Central Role of Anaplerosis. *Annu Rev Nutr.* 2021;41:19–47.
39. Spinelli JB, Haigis MC. The multifaceted contributions of mitochondria to cellular metabolism. *Nat Cell Biol. Nature Publishing Group;* 2018;20:745–54.
40. Eniafe J, Jiang S. The functional roles of TCA cycle metabolites in cancer. *Oncogene. Nature Publishing Group;* 2021;40:3351–63.
41. Schmidt C, Sciacovelli M, Frezza C. Fumarate hydratase in cancer: A multifaceted tumour suppressor. *Semin Cell Dev Biol.* 2020;98:15–25.
42. Salminen A, Kauppinen A, Kaarniranta K. 2-Oxoglutarate-dependent dioxygenases are sensors of energy metabolism, oxygen availability, and iron homeostasis: potential role in the regulation of aging process. *Cell Mol Life Sci.* 2015;72:3897–914.
43. Marquez J, Flores, Kim SY, Nyamaa B, Nguyen, Park, et al. Rescue of TCA Cycle Dysfunction for Cancer Therapy. *J Clin Med.* 2019;8:2161.
44. Luo Y, Ma J, Lu W. The Significance of Mitochondrial Dysfunction in Cancer. *Int J Mol Sci.* 2020;21:5598.

45. Sabharwal SS, Schumacker PT. Mitochondrial ROS in cancer: initiators, amplifiers or an Achilles' heel? *Nat Rev Cancer*. 2014;14:709–21.
46. Valavanidis A, Vlachogianni T, Fiotakis K. Tobacco Smoke: Involvement of Reactive Oxygen Species and Stable Free Radicals in Mechanisms of Oxidative Damage, Carcinogenesis and Synergistic Effects with Other Respirable Particles. *Int J Environ Res Public Health*. 2009;6:445–62.
47. Wu D, Zhai Q, Shi X. Alcohol-induced oxidative stress and cell responses. *J Gastroenterol Hepatol*. 2006;21 Suppl 3:S26-29.
48. de Jager TL, Cockrell AE, Du Plessis SS. Ultraviolet Light Induced Generation of Reactive Oxygen Species. *Adv Exp Med Biol*. 2017;996:15–23.
49. Ehses S, Raschke I, Mancuso G, Bernacchia A, Geimer S, Tondera D, et al. Regulation of OPA1 processing and mitochondrial fusion by m-AAA protease isoenzymes and OMA1. *J Cell Biol*. 2009;187:1023–36.
50. Gomes LC, Di Benedetto G, Scorrano L. During autophagy mitochondria elongate, are spared from degradation and sustain cell viability. *Nat Cell Biol*. 2011;13:589–98.
51. Rambold AS, Pearce EL. Mitochondrial Dynamics at the Interface of Immune Cell Metabolism and Function. *Trends Immunol*. 2018;39:6–18.
52. Saita S, Ishihara T, Maeda M, Iemura S, Natsume T, Mihara K, et al. Distinct types of protease systems are involved in homeostasis regulation of mitochondrial morphology via balanced fusion and fission. *Genes Cells*. 2016;21:408–24.
53. Youle RJ, van der Bliek AM. Mitochondrial Fission, Fusion, and Stress. *Science*. 2012;337:1062–5.
54. Twig G, Shirihai OS. The Interplay Between Mitochondrial Dynamics and Mitophagy. *Antioxid Redox Signal*. 2011;14:1939–51.
55. Song Z, Chen H, Fiket M, Alexander C, Chan DC. OPA1 processing controls mitochondrial fusion and is regulated by mRNA splicing, membrane potential, and Yme1L. *J Cell Biol*. 2007;178:749–55.
56. Glytsou C, Calvo E, Cogliati S, Mehrotra A, Anastasia I, Rigoni G, et al. Optic Atrophy 1 Is Epistatic to the Core MICOS Component MIC60 in Mitochondrial Cristae Shape Control. *Cell Rep*. 2016;17:3024–34.
57. Hu C, Shu L, Huang X, Yu J, Li L, Gong L, et al. OPA1 and MICOS Regulate mitochondrial crista dynamics and formation. *Cell Death Dis*. Nature Publishing Group; 2020;11:1–17.
58. Schreiber RD, Old LJ, Smyth MJ. Cancer immunoediting: integrating immunity's roles in cancer suppression and promotion. *Science*. 2011;331:1565–70.
59. Smyth MJ, Dunn GP, Schreiber RD. Cancer Immunosurveillance and Immunoediting: The Roles of Immunity in Suppressing Tumor Development and Shaping Tumor

- Immunogenicity. *Adv Immunol* [Internet]. Elsevier; 2006 [cited 2022 Nov 22]. page 1–50. Available from: <https://linkinghub.elsevier.com/retrieve/pii/S0065277606900017>
60. Cui C, Wang J, Fagerberg E, Chen P-M, Connolly KA, Damo M, et al. Neoantigen-driven B cell and CD4 T follicular helper cell collaboration promotes anti-tumor CD8 T cell responses. *Cell*. 2021;184:6101-6118.e13.
 61. Böttcher JP, Reis e Sousa C. The Role of Type 1 Conventional Dendritic Cells in Cancer Immunity. *Trends Cancer*. 2018;4:784–92.
 62. Dhatchinamoorthy K, Colbert JD, Rock KL. Cancer Immune Evasion Through Loss of MHC Class I Antigen Presentation. *Front Immunol* [Internet]. 2021 [cited 2022 Dec 1];12. Available from: <https://www.frontiersin.org/articles/10.3389/fimmu.2021.636568>
 63. Balasubramanian A, John T, Asselin-Labat M-L. Regulation of the antigen presentation machinery in cancer and its implication for immune surveillance. *Biochem Soc Trans*. 2022;50:825–37.
 64. Finetti F, Travelli C, Ercoli J, Colombo G, Buoso E, Trabalzini L. Prostaglandin E2 and Cancer: Insight into Tumor Progression and Immunity. *Biology*. 2020;9:434.
 65. Jhunjhunwala S, Hammer C, Delamarre L. Antigen presentation in cancer: insights into tumour immunogenicity and immune evasion. *Nat Rev Cancer*. Nature Publishing Group; 2021;21:298–312.
 66. Burnet M. IMMUNOLOGICAL FACTORS IN THE PROCESS OF CARCINOGENESIS. *Br Med Bull*. 1964;20:154–8.
 67. Lethé B, Lucas S, Michaux L, De Smet C, Godelaine D, Serrano A, et al. LAGE-1, a new gene with tumor specificity. *Int J Cancer*. 1998;76:903–8.
 68. Boon T, Cerottini JC, Van den Eynde B, van der Bruggen P, Van Pel A. Tumor antigens recognized by T lymphocytes. *Annu Rev Immunol*. 1994;12:337–65.
 69. Blankenstein T, Coulie PG, Gilboa E, Jaffee EM. The determinants of tumour immunogenicity. *Nat Rev Cancer*. Nature Publishing Group; 2012;12:307–13.
 70. Peixoto A, Relvas-Santos M, Azevedo R, Santos LL, Ferreira JA. Protein Glycosylation and Tumor Microenvironment Alterations Driving Cancer Hallmarks. *Front Oncol* [Internet]. 2019 [cited 2022 Nov 22];9. Available from: <https://www.frontiersin.org/articles/10.3389/fonc.2019.00380>
 71. Prota G, Gileadi U, Rei M, Lechuga-Vieco AV, Chen J-L, Galiani S, et al. Enhanced Immunogenicity of Mitochondrial-Localized Proteins in Cancer Cells. *Cancer Immunol Res*. 2020;8:685–97.
 72. Prota G, Lechuga-Vieco AV, De Libero G. Mitochondrial Proteins as Source of Cancer Neoantigens. *Int J Mol Sci*. 2022;23:2627.

73. Hunder NN, Wallen H, Cao J, Hendricks DW, Reilly JZ, Rodmyre R, et al. Treatment of metastatic melanoma with autologous CD4+ T cells against NY-ESO-1. *N Engl J Med.* 2008;358:2698–703.
74. Leone RD. Metabolism of immune cells in cancer. :16.
75. Dugnani E, Pasquale V, Bordignon C, Canu A, Piemonti L, Monti P. Integrating T cell metabolism in cancer immunotherapy. *Cancer Lett.* 2017;411:12–8.
76. Scharping NE, Rivadeneira DB, Menk AV, Vignali PDA, Ford BR, Rittenhouse NL, et al. Mitochondrial stress induced by continuous stimulation under hypoxia rapidly drives T cell exhaustion. *Nat Immunol.* 2021;22:205–15.
77. Blank CU, Haining WN, Held W, Hogan PG, Kallies A, Lugli E, et al. Defining “T cell exhaustion.” *Nat Rev Immunol.* 2019;19:665–74.
78. Chen Z, Ji Z, Ngiow SF, Manne S, Cai Z, Huang AC, et al. TCF-1-Centered Transcriptional Network Drives an Effector versus Exhausted CD8 T Cell-Fate Decision. *Immunity.* 2019;51:840-855.e5.
79. Guo Y, Xie Y-Q, Gao M, Zhao Y, Franco F, Wenes M, et al. Metabolic reprogramming of terminally exhausted CD8+ T cells by IL-10 enhances anti-tumor immunity. *Nat Immunol.* Nature Publishing Group; 2021;22:746–56.
80. Khan O, Giles JR, McDonald S, Manne S, Ngiow SF, Patel KP, et al. TOX transcriptionally and epigenetically programs CD8+ T cell exhaustion. *Nature.* 2019;571:211–8.
81. Beltra J-C, Manne S, Abdel-Hakeem MS, Kurachi M, Giles JR, Chen Z, et al. Developmental Relationships of Four Exhausted CD8+ T Cell Subsets Reveals Underlying Transcriptional and Epigenetic Landscape Control Mechanisms. *Immunity.* 2020;52:825-841.e8.
82. Yu Y-R, Imrichova H, Wang H, Chao T, Xiao Z, Gao M, et al. Disturbed mitochondrial dynamics in CD8+ TILs reinforce T cell exhaustion. *Nat Immunol.* 2020;21:1540–51.
83. Franco F, Jaccard A, Romero P, Yu Y-R, Ho P-C. Metabolic and epigenetic regulation of T-cell exhaustion. *Nat Metab.* Nature Publishing Group; 2020;2:1001–12.
84. Montacchiesi G, Pace L. Epigenetics and CD8+ T cell memory*. *Immunol Rev.* 2022;305:77–89.
85. Weng N, Araki Y, Subedi K. The molecular basis of the memory T cell response: differential gene expression and its epigenetic regulation. *Nat Rev Immunol.* Nature Publishing Group; 2012;12:306–15.
86. McPherson RC, Konkel JE, Prendergast CT, Thomson JP, Ottaviano R, Leech MD, et al. Epigenetic modification of the PD-1 (*Pdcd1*) promoter in effector CD4+ T cells tolerized by peptide immunotherapy. *eLife.* 3:e03416.

87. Vodnala SK, Eil R, Kishton RJ, Sukumar M, Yamamoto TN, Ha N-H, et al. T cell stemness and dysfunction in tumors are triggered by a common mechanism. *Science*. 2019;363:eaau0135.
88. Quinn WJ, Jiao J, TeSlaa T, Stadanlick J, Wang Z, Wang L, et al. Lactate Limits T Cell Proliferation via the NAD(H) Redox State. *Cell Rep* [Internet]. Elsevier; 2020 [cited 2023 Jan 12];33. Available from: [https://www.cell.com/cell-reports/abstract/S2211-1247\(20\)31489-3](https://www.cell.com/cell-reports/abstract/S2211-1247(20)31489-3)
89. Kim M, Mahmood M, Reznik E, Gammage PA. Mitochondrial DNA is a major source of driver mutations in cancer. *Trends Cancer*. 2022;8:1046–59.
90. Krysko O, Løve Aaes T, Bachert C, Vandenabeele P, Krysko DV. Many faces of DAMPs in cancer therapy. *Cell Death Dis*. Nature Publishing Group; 2013;4:e631–e631.
91. Rodríguez-Nuevo A, Zorzano A. The sensing of mitochondrial DAMPs by non-immune cells. *Cell Stress*. 2019;3:195–207.
92. Hernandez C, Huebener P, Schwabe RF. Damage-associated molecular patterns in cancer: a double-edged sword. *Oncogene*. 2016;35:5931–41.
93. Lei X, Lin H, Wang J, Ou Z, Ruan Y, Sadagopan A, et al. Mitochondrial fission induces immunoescape in solid tumors through decreasing MHC-I surface expression. *Nat Commun*. Nature Publishing Group; 2022;13:3882.
94. Kroemer G, Galluzzi L, Kepp O, Zitvogel L. Immunogenic cell death in cancer therapy. *Annu Rev Immunol*. 2013;31:51–72.
95. Wu J, Waxman DJ. Immunogenic chemotherapy: Dose and schedule dependence and combination with immunotherapy. *Cancer Lett*. 2018;419:210–21.
96. Pfirschke C, Engblom C, Rickelt S, Cortez-Retamozo V, Garris C, Pucci F, et al. Immunogenic Chemotherapy Sensitizes Tumors to Checkpoint Blockade Therapy. *Immunity*. 2016;44:343–54.
97. Aspeslagh S, Morel D, Soria J-C, Postel-Vinay S. Epigenetic modifiers as new immunomodulatory therapies in solid tumours. *Ann Oncol*. 2018;29:812–24.
98. Barr LC. The encapsulation of tumours. *Clin Exp Metastasis*. 1989;7:277–82.
99. Hamzah J, Jugold M, Kiessling F, Rigby P, Manzur M, Marti HH, et al. Vascular normalization in Rgs5-deficient tumours promotes immune destruction. *Nature*. Nature Publishing Group; 2008;453:410–4.
100. Buckanovich RJ, Facciabene A, Kim S, Benencia F, Sasaroli D, Balint K, et al. Endothelin B receptor mediates the endothelial barrier to T cell homing to tumors and disables immune therapy. *Nat Med*. Nature Publishing Group; 2008;14:28–36.

101. Fu T, Dai L-J, Wu S-Y, Xiao Y, Ma D, Jiang Y-Z, et al. Spatial architecture of the immune microenvironment orchestrates tumor immunity and therapeutic response. *J Hematol Oncol* *J Hematol Oncol*. 2021;14:98.
102. Saltz J, Gupta R, Hou L, Kurc T, Singh P, Nguyen V, et al. Spatial Organization and Molecular Correlation of Tumor-Infiltrating Lymphocytes Using Deep Learning on Pathology Images. *Cell Rep*. 2018;23:181-193.e7.
103. Tredan O, Galmarini CM, Patel K, Tannock IF. Drug Resistance and the Solid Tumor Microenvironment. *JNCI J Natl Cancer Inst*. 2007;99:1441–54.
104. Baghban R, Roshangar L, Jahanban-Esfahlan R, Seidi K, Ebrahimi-Kalan A, Jaymand M, et al. Tumor microenvironment complexity and therapeutic implications at a glance. *Cell Commun Signal*. 2020;18:59.
105. Ping Q, Yan R, Cheng X, Wang W, Zhong Y, Hou Z, et al. Cancer-associated fibroblasts: overview, progress, challenges, and directions. *Cancer Gene Ther*. Nature Publishing Group; 2021;28:984–99.
106. Hanahan D, Coussens LM. Accessories to the Crime: Functions of Cells Recruited to the Tumor Microenvironment. *Cancer Cell*. Elsevier; 2012;21:309–22.
107. Zelenay S, van der Veen AG, Böttcher JP, Snelgrove KJ, Rogers N, Acton SE, et al. Cyclooxygenase-Dependent Tumor Growth through Evasion of Immunity. *Cell*. 2015;162:1257–70.
108. Maleki Vareki S. High and low mutational burden tumors versus immunologically hot and cold tumors and response to immune checkpoint inhibitors. *J Immunother Cancer*. 2018;6:157, s40425-018-0479–7.
109. Raj S, Miller LD, Triozzi PL. Addressing the Adult Soft Tissue Sarcoma Microenvironment with Intratumoral Immunotherapy. *Sarcoma*. 2018;2018:1–10.
110. Raj SKS, Routh ED, Chou JW, Votanopoulos KI, Triozzi PL, Miller LD. Prognostic attributes of immune signatures in soft tissue sarcomas show differential dependencies on tumor mutational burden. *Cancer*. 2022;128:3254–64.
111. Xie L, Yang Y, Guo W, Che D, Xu J, Sun X, et al. The Clinical Implications of Tumor Mutational Burden in Osteosarcoma. *Front Oncol* [Internet]. 2021 [cited 2022 Nov 22];10. Available from: <https://www.frontiersin.org/articles/10.3389/fonc.2020.595527>
112. Park EM, Chelvanambi M, Bhutiani N, Kroemer G, Zitvogel L, Wargo JA. Targeting the gut and tumor microbiota in cancer. *Nat Med*. Nature Publishing Group; 2022;28:690–703.
113. Egeblad M, Nakasone ES, Werb Z. Tumors as organs: complex tissues that interface with the entire organism. *Dev Cell*. 2010;18:884–901.

114. Geller LT, Barzily-Rokni M, Danino T, Jonas OH, Shental N, Nejman D, et al. Potential role of intratumor bacteria in mediating tumor resistance to the chemotherapeutic drug gemcitabine. *Science*. 2017;357:1156–60.
115. Bachem A, Makhoulouf C, Binger KJ, de Souza DP, Tull D, Hochheiser K, et al. Microbiota-Derived Short-Chain Fatty Acids Promote the Memory Potential of Antigen-Activated CD8+ T Cells. *Immunity*. 2019;51:285-297.e5.
116. Bullman S, Eggermont A, Johnston CD, Zitvogel L. Harnessing the microbiome to restore immunotherapy response. *Nat Cancer*. Nature Publishing Group; 2021;2:1301–4.
117. Vétizou M, Pitt JM, Daillère R, Lepage P, Waldschmitt N, Flament C, et al. Anticancer immunotherapy by CTLA-4 blockade relies on the gut microbiota. *Science*. 2015;350:1079–84.
118. Pardoll DM. The blockade of immune checkpoints in cancer immunotherapy. *Nat Rev Cancer*. Nature Publishing Group; 2012;12:252–64.
119. Patsoukis N, Bardhan K, Chatterjee P, Sari D, Liu B, Bell LN, et al. PD-1 alters T-cell metabolic reprogramming by inhibiting glycolysis and promoting lipolysis and fatty acid oxidation. *Nat Commun*. Nature Publishing Group; 2015;6:6692.
120. Bengsch B, Johnson AL, Kurachi M, Odorizzi PM, Pauken KE, Attanasio J, et al. Bioenergetic Insufficiencies Due to Metabolic Alterations Regulated by the Inhibitory Receptor PD-1 Are an Early Driver of CD8(+) T Cell Exhaustion. *Immunity*. 2016;45:358–73.
121. Franklin RA, Liao W, Sarkar A, Kim MV, Bivona MR, Liu K, et al. The cellular and molecular origin of tumor-associated macrophages. *Science*. 2014;344:921–5.
122. Meulmeester E, Ten Dijke P. The dynamic roles of TGF- β in cancer. *J Pathol*. 2011;223:205–18.
123. Donkor MK, Sarkar A, Savage PA, Franklin RA, Johnson LK, Jungbluth AA, et al. T cell surveillance of oncogene-induced prostate cancer is impeded by T cell-derived TGF- β 1 cytokine. *Immunity*. 2011;35:123–34.
124. Mandai M, Hamanishi J, Abiko K, Matsumura N, Baba T, Konishi I. Dual Faces of IFN γ in Cancer Progression: A Role of PD-L1 Induction in the Determination of Pro- and Antitumor Immunity. *Clin Cancer Res Off J Am Assoc Cancer Res*. 2016;22:2329–34.
125. Li H, Zhao A, Li M, Shi L, Han Q, Hou Z. Targeting T-cell metabolism to boost immune checkpoint inhibitor therapy. *Front Immunol [Internet]*. 2022 [cited 2023 Jan 13];13. Available from: <https://www.frontiersin.org/articles/10.3389/fimmu.2022.1046755>
126. Cheng M, Yu H, Kong Q, Wang B, Shen L, Dong D, et al. The Mitochondrial PHB2/OMA1/DELE1 Pathway Cooperates with Endoplasmic Reticulum Stress to Facilitate the Response to Chemotherapeutics in Ovarian Cancer. *Int J Mol Sci*. 2022;23:1320.

127. Wu Z, Zuo M, Zeng L, Cui K, Liu B, Yan C, et al. OMA1 reprograms metabolism under hypoxia to promote colorectal cancer development. *EMBO Rep* [Internet]. 2021 [cited 2021 Dec 8];22. Available from: <https://onlinelibrary.wiley.com/doi/10.15252/embr.202050827>
128. Zamberlan M, Boeckx A, Muller F, Vinelli F, Ek O, Vianello C, et al. Inhibition of the mitochondrial protein Opa1 curtails breast cancer growth. *J Exp Clin Cancer Res*. 2022;41:95.
129. Lau AN, Vander Heiden MG. Metabolism in the Tumor Microenvironment. *Annu Rev Cancer Biol*. 2020;4:17–40.
130. Pearce EL, Poffenberger MC, Chang C-H, Jones RG. Fueling immunity: insights into metabolism and lymphocyte function. *Science*. 2013;342:1242454.
131. O’Sullivan D, Pearce EL. Targeting T cell metabolism for therapy. *Trends Immunol*. 2015;36:71–80.
132. Ho P-C, Bihuniak JD, Macintyre AN, Staron M, Liu X, Amezquita R, et al. Phosphoenolpyruvate Is a Metabolic Checkpoint of Anti-tumor T Cell Responses. *Cell*. 2015;162:1217–28.
133. Naquet P, Kerr EW, Vickers SD, Leonardi R. Regulation of coenzyme A levels by degradation: the ‘Ins and Outs.’ *Prog Lipid Res*. 2020;78:101028.
134. Depeint F, Bruce WR, Shangari N, Mehta R, O’Brien PJ. Mitochondrial function and toxicity: Role of the B vitamin family on mitochondrial energy metabolism. *Chem Biol Interact*. 2006;163:94–112.
135. Cai L, Tu BP. On Acetyl-CoA as a Gauge of Cellular Metabolic State. *Cold Spring Harb Symp Quant Biol*. Cold Spring Harbor Laboratory Press; 2011;76:195–202.
136. Pietrocola F, Galluzzi L, Bravo-San Pedro JM, Madeo F, Kroemer G. Acetyl Coenzyme A: A Central Metabolite and Second Messenger. *Cell Metab*. 2015;21:805–21.
137. Neess D, Bek S, Engelsby H, Gallego SF, Færgeman NJ. Long-chain acyl-CoA esters in metabolism and signaling: Role of acyl-CoA binding proteins. *Prog Lipid Res*. 2015;59:1–25.
138. Grevengoed TJ, Klett EL, Coleman RA. Acyl-CoA Metabolism and Partitioning. *Annu Rev Nutr*. 2014;34:1–30.
139. Choudhary C, Weinert BT, Nishida Y, Verdin E, Mann M. The growing landscape of lysine acetylation links metabolism and cell signalling. *Nat Rev Mol Cell Biol*. Nature Publishing Group; 2014;15:536–50.
140. Hirschey MD, Zhao Y. Metabolic Regulation by Lysine Malonylation, Succinylation, and Glutarylation *. *Mol Cell Proteomics*. Elsevier; 2015;14:2308–15.

141. Resh MD. Fatty acylation of proteins: The long and the short of it. *Prog Lipid Res.* 2016;63:120–31.
142. Daniotti JL, Pedro MP, Valdez Taubas J. The role of S-acylation in protein trafficking. *Traffic.* 2017;18:699–710.
143. Sabari BR, Zhang D, Allis CD, Zhao Y. Metabolic regulation of gene expression through histone acylations. *Nat Rev Mol Cell Biol.* Nature Publishing Group; 2017;18:90–101.
144. Gout I. Coenzyme A, protein CoAlation and redox regulation in mammalian cells. *Biochem Soc Trans.* 2018;46:721–8.
145. Tsuchiya Y, Peak-Chew SY, Newell C, Miller-Aidoo S, Mangal S, Zhyvoloup A, et al. Protein CoAlation: a redox-regulated protein modification by coenzyme A in mammalian cells. *Biochem J.* 2017;474:2489–508.
146. Said HM. Intestinal absorption of water-soluble vitamins in health and disease. *Biochem J.* 2011;437:357–72.
147. Skrede S. The Degradation of CoA: Subcellular Localization and Kinetic Properties of CoA-and Dephospho-CoA Pyrophosphatase. *Eur J Biochem.* 1973;38:401–7.
148. Decker K, Bischoff E. Purification and properties of nucleotide pyrophosphatase from rat liver plasma membranes. *FEBS Lett.* 1972;21:95–8.
149. Franklin JE, Trams EG. Metabolism of coenzyme A and related nucleotides by liver plasma membranes. *Biochim Biophys Acta BBA - Gen Subj.* 1971;230:105–16.
150. Shibata K, Gross CJ, Henderson LM. Hydrolysis and Absorption of Pantothenate and Its Coenzymes in the Rat Small Intestine. *J Nutr.* 1983;113:2107–15.
151. Duprè S, Cavallini D. [47] Purification and properties of pantetheinase from horse kidney. *Methods Enzymol* [Internet]. Academic Press; 1979 [cited 2023 Jan 17]. page 262–7. Available from: <https://www.sciencedirect.com/science/article/pii/0076687979622279>
152. Boersma YL, Newman J, Adams TE, Cowieson N, Krippner G, Bozaoglu K, et al. The structure of vanin 1: a key enzyme linking metabolic disease and inflammation. *Acta Crystallogr D Biol Crystallogr.* International Union of Crystallography; 2014;70:3320–9.
153. Ono S, Kameda K, Abiko Y. Metabolism of Pantethine in the Rat. *J Nutr Sci Vitaminol (Tokyo).* 1974;20:203–13.
154. Turner JB, Hughes DE. The Absorption of Some B-Group Vitamins by Surviving Rat Intestine Preparations. *Q J Exp Physiol Cogn Med Sci.* 1962;47:107–23.
155. Wang H, Huang W, Fei Y-J, Xia H, Yang-Feng TL, Leibach FH, et al. Human Placental Na+-dependent Multivitamin Transporter: CLONING, FUNCTIONAL EXPRESSION, GENE STRUCTURE, AND CHROMOSOMAL LOCALIZATION *. *J Biol Chem.* Elsevier; 1999;274:14875–83.

156. Quick M, Shi L. Chapter Three - The Sodium/Multivitamin Transporter: A Multipotent System with Therapeutic Implications. In: Litwack G, editor. *Vitam Horm* [Internet]. Academic Press; 2015 [cited 2023 Jan 17]. page 63–100. Available from: <https://www.sciencedirect.com/science/article/pii/S0083672914000168>
157. Domschke W, Liersch M, Decker K. Lack of Permeation of Coenzyme A from Blood into Liver Cells. *De Gruyter*; 1971;352:85–8.
158. Kropf M, Rey G, Glauser L, Kulangara K, Johnsson K, Hirling H. Subunit-specific surface mobility of differentially labeled AMPA receptor subunits. *Eur J Cell Biol*. 2008;87:763–78.
159. Srinivasan B, Baratashvili M, van der Zwaag M, Kanon B, Colombelli C, Lambrechts RA, et al. Extracellular 4'-phosphopantetheine is a source for intracellular coenzyme A synthesis. *Nat Chem Biol*. Nature Publishing Group; 2015;11:784–92.
160. van Diepen JA, Jansen PA, Ballak DB, Hijmans A, Hooiveld GJ, Rommelaere S, et al. PPAR-alpha dependent regulation of vanin-1 mediates hepatic lipid metabolism. *J Hepatol*. 2014;61:366–72.
161. Giessner C, Millet V, Mostert KJ, Gensollen T, Vu Manh T-P, Garibal M, et al. Vnn1 pantetheinase limits the Warburg effect and sarcoma growth by rescuing mitochondrial activity. *Life Sci Alliance*. 2018;1:e201800073.
162. Wittwer CT, Schweitzer C, Pearson J, Song WO, Windham CT, Wyse BW, et al. Enzymes for liberation of pantothenic acid in blood: use of plasma pantetheinase. *Am J Clin Nutr*. 1989;50:1072–8.
163. Naquet P, Pitari G, Duprè S, Galland F. Role of the Vnn1 pantetheinase in tissue tolerance to stress. *Biochem Soc Trans*. 2014;42:1094–100.
164. Jeitner TM, Lawrence DA. Mechanisms for the cytotoxicity of cysteamine. *Toxicol Sci Off J Soc Toxicol*. 2001;63:57–64.
165. Fujisawa T, Rubin B, Suzuki A, Patel PS, Gahl WA, Joshi BH, et al. Cysteamine suppresses invasion, metastasis and prolongs survival by inhibiting matrix metalloproteinases in a mouse model of human pancreatic cancer. *PloS One*. 2012;7:e34437.
166. Zhang X, Lu H, Wang Y, Liu C, Zhu W, Zheng S, et al. Taurine induces the apoptosis of breast cancer cells by regulating apoptosis-related proteins of mitochondria. *Int J Mol Med*. 2015;35:218–26.
167. Ma N, He F, Kawanokuchi J, Wang G, Yamashita T. Taurine and Its Anticancer Functions: In Vivo and In Vitro Study. *Adv Exp Med Biol*. 2022;1370:121–8.
168. Chen W, Li Q, Hou R, Liang H, Zhang Y, Yang Y. An integrated metabolomics study to reveal the inhibitory effect and metabolism regulation of taurine on breast cancer. *J Pharm Biomed Anal*. 2022;214:114711.

169. Jong CJ, Sandal P, Schaffer SW. The Role of Taurine in Mitochondria Health: More Than Just an Antioxidant. *Mol Basel Switz*. 2021;26:4913.
170. Isakov N. Protein kinase C (PKC) isoforms in cancer, tumor promotion and tumor suppression. *Semin Cancer Biol*. 2018;48:36–52.
171. Deka SJ, Trivedi V. Potentials of PKC in Cancer Progression and Anticancer Drug Development. *Curr Drug Discov Technol*. 2019;16:135–47.
172. Roisin-Bouffay C, Castellano R, Valéro R, Chasson L, Galland F, Naquet P. Mouse vanin-1 is cytoprotective for islet beta cells and regulates the development of type 1 diabetes. *Diabetologia*. 2008;51:1192–201.
173. Rommelaere S, Millet V, Rihet P, Atwell S, Helfer E, Chasson L, et al. Serum Pantetheinase/Vanin Levels Regulate Erythrocyte Homeostasis and Severity of Malaria. *Am J Pathol*. 2015;185:3039–52.
174. Millet V, Gensollen T, Maltese M, Serrero M, Lesavre N, Bourges C, et al. Harnessing the Vnn1 pantetheinase pathway boosts short chain fatty acids production and mucosal protection in colitis. *Gut* [Internet]. BMJ Publishing Group; 2022 [cited 2022 Oct 24]; Available from: <https://gut-bmj-com.proxy.insermbiblio.inist.fr/content/early/2022/09/29/gutjnl-2021-325792>
175. JCI - Vanin-1^{-/-} mice show decreased NSAID- and Schistosoma-induced intestinal inflammation associated with higher glutathione stores [Internet]. [cited 2023 Jan 17]. Available from: <https://www.jci.org/articles/view/19557>
176. Naquet P, Giessner C, Galland F. Metabolic adaptation of tissues to stress releases metabolites influencing innate immunity. *Curr Opin Immunol*. 2016;38:30–8.
177. Coenzyme A fuels T cell anti-tumor immunity. *Cell Metab*. Cell Press; 2021;33:2415-2427.e6.
178. Gudgeon N, Munford H, Bishop EL, Hill J, Fulton-Ward T, Bending D, et al. Succinate uptake by T cells suppresses their effector function via inhibition of mitochondrial glucose oxidation. *Cell Rep* [Internet]. Elsevier; 2022 [cited 2023 Jan 16];40. Available from: [https://www.cell.com/cell-reports/abstract/S2211-1247\(22\)01010-5](https://www.cell.com/cell-reports/abstract/S2211-1247(22)01010-5)
179. Moreno-Fernandez ME, Giles DA, Oates JR, Chan CC, Damen MSMA, Doll JR, et al. PKM2-dependent metabolic skewing of hepatic Th17 cells regulates pathogenesis of non-alcoholic fatty liver disease. *Cell Metab*. Elsevier; 2021;33:1187-1204.e9.
180. Steták A, Veress R, Ovádi J, Csermely P, Kéri G, Ullrich A. Nuclear Translocation of the Tumor Marker Pyruvate Kinase M2 Induces Programmed Cell Death. *Cancer Res*. 2007;67:1602–8.
181. Chen C, Zhang W, Zhou T, Liu Q, Han C, Huang Z, et al. Vitamin B5 rewires Th17 cell metabolism via impeding PKM2 nuclear translocation. *Cell Rep* [Internet]. Elsevier; 2022

- [cited 2023 Jan 17];41. Available from: [https://www.cell.com/cell-reports/abstract/S2211-1247\(22\)01619-9](https://www.cell.com/cell-reports/abstract/S2211-1247(22)01619-9)
182. Kono M, Maeda K, Stocton-Gavanescu I, Pan W, Umeda M, Katsuyama E, et al. Pyruvate kinase M2 is requisite for Th1 and Th17 differentiation. *JCI Insight* [Internet]. American Society for Clinical Investigation; 2019 [cited 2023 Jan 18];4. Available from: <https://insight.jci.org/articles/view/127395>
 183. Jha AK, Huang SC-C, Sergushichev A, Lampropoulou V, Ivanova Y, Loginicheva E, et al. Network integration of parallel metabolic and transcriptional data reveals metabolic modules that regulate macrophage polarization. *Immunity*. 2015;42:419–30.
 184. Field CS, Baixauli F, Kyle RL, Puleston DJ, Cameron AM, Sanin DE, et al. Mitochondrial Integrity Regulated by Lipid Metabolism Is a Cell-Intrinsic Checkpoint for Treg Suppressive Function. *Cell Metab*. 2020;31:422-437.e5.
 185. Timblin GA, Tharp KM, Hoeve J ten, Baydemir I, Khantwal C, Farahzad JN, et al. Coenzyme A governs proinflammatory macrophage metabolism [Internet]. *bioRxiv*; 2022 [cited 2022 Oct 29]. page 2022.08.30.505732. Available from: <https://www.biorxiv.org/content/10.1101/2022.08.30.505732v1>
 186. He W, Hu S, Du X, Wen Q, Zhong X-P, Zhou X, et al. Vitamin B5 Reduces Bacterial Growth via Regulating Innate Immunity and Adaptive Immunity in Mice Infected with *Mycobacterium tuberculosis*. *Front Immunol*. 2018;9:365.
 187. Møller SH, Wang L, Ho P-C. Metabolic programming in dendritic cells tailors immune responses and homeostasis. *Cell Mol Immunol*. Nature Publishing Group; 2022;19:370–83.
 188. Kiritsy MC, McCann K, Mott D, Holland SM, Behar SM, Sasseti CM, et al. Mitochondrial respiration contributes to the interferon gamma response in antigen-presenting cells. Horng T, Garrett WS, Zanoni I, editors. *eLife*. eLife Sciences Publications, Ltd; 2021;10:e65109.
 189. Chang C-H, Curtis JD, Maggi LB, Faubert B, Villarino AV, O’Sullivan D, et al. Posttranscriptional control of T cell effector function by aerobic glycolysis. *Cell*. 2013;153:1239–51.
 190. Sena LA, Li S, Jairaman A, Prakriya M, Ezponda T, Hildeman DA, et al. Mitochondria are required for antigen-specific T cell activation through reactive oxygen species signaling. *Immunity*. 2013;38:225–36.
 191. Almeida L, Dhillon-LaBrooy A, Carriche G, Berod L, Sparwasser T. CD4+ T-cell differentiation and function: Unifying glycolysis, fatty acid oxidation, polyamines NAD mitochondria. *J Allergy Clin Immunol*. 2021;148:16–32.
 192. Bailis W, Shyer JA, Zhao J, Canaveras JCG, Al Khazal FJ, Qu R, et al. Distinct modes of mitochondrial metabolism uncouple T cell differentiation and function. *Nature*. Nature Publishing Group; 2019;571:403–7.

193. Chowdhury S, Kar A, Bhowmik D, Gautam A, Basak D, Sarkar I, et al. Intracellular Acetyl CoA Potentiates the Therapeutic Efficacy of Antitumor CD8⁺ T Cells. *Cancer Res.* 2022;82:2640–55.
194. Wenes M, Jaccard A, Wyss T, Maldonado-Pérez N, Teoh ST, Lepez A, et al. The mitochondrial pyruvate carrier regulates memory T cell differentiation and antitumor function. *Cell Metab.* 2022;34:731-746.e9.
195. Zhang H, Tang K, Ma J, Zhou L, Liu J, Zeng L, et al. Ketogenesis-generated β -hydroxybutyrate is an epigenetic regulator of CD8⁺ T-cell memory development. *Nat Cell Biol.* 2020;22:18–25.
196. Chamoto K, Chowdhury PS, Kumar A, Sonomura K, Matsuda F, Fagarasan S, et al. Mitochondrial activation chemicals synergize with surface receptor PD-1 blockade for T cell-dependent antitumor activity. *Proc Natl Acad Sci [Internet]*. 2017 [cited 2022 Oct 29];114. Available from: <https://pnas.org/doi/full/10.1073/pnas.1620433114>
197. Alavi MV. Targeted OMA1 therapies for cancer. *Int J Cancer.* 2019;145:2330–41.
198. Daverey A, Levytskyy RM, Stanke KM, Viana MP, Swenson S, Hayward SL, et al. Depletion of mitochondrial protease OMA1 alters proliferative properties and promotes metastatic growth of breast cancer cells. *Sci Rep.* 2019;9:14746.
199. Herkenne S, Ek O, Zamberlan M, Pellattiero A, Chergova M, Chivite I, et al. Developmental and Tumor Angiogenesis Requires the Mitochondria-Shaping Protein Opa1. *Cell Metab. Elsevier*; 2020;31:987-1003.e8.
200. Alavi MV. Recent advances in, and challenges of, designing OMA1 drug screens. *Pharmacol Res.* 2022;176:106063.
201. Rainbolt TK, Lebeau J, Puchades C, Wiseman RL. Reciprocal Degradation of YME1L and OMA1 Adapts Mitochondrial Proteolytic Activity during Stress. *Cell Rep.* 2016;14:2041–9.
202. Baker MJ, Lampe PA, Stojanovski D, Korwitz A, Anand R, Tatsuta T, et al. Stress-induced OMA1 activation and autocatalytic turnover regulate OPA1-dependent mitochondrial dynamics. *EMBO J.* 2014;33:578–93.
203. Alavi MV. OMA1—An integral membrane protease? *Biochim Biophys Acta BBA - Proteins Proteomics.* 2021;1869:140558.
204. Guo X. Mitochondrial stress is relayed to the cytosol by an OMA1–DELE1–HRI pathway. :29.
205. Rodrigues T, Ferraz LS. Therapeutic potential of targeting mitochondrial dynamics in cancer. *Biochem Pharmacol.* 2020;182:114282.
206. Xie Q, Wu Q, Horbinski CM, Flavahan WA, Yang K, Zhou W, et al. Mitochondrial control by DRP1 in brain tumor initiating cells. *Nat Neurosci. Nature Publishing Group*; 2015;18:501–10.

207. Zhao J, Zhang J, Yu M, Xie Y, Huang Y, Wolff DW, et al. Mitochondrial dynamics regulates migration and invasion of breast cancer cells. *Oncogene*. Nature Publishing Group; 2013;32:4814–24.
208. Olichon A, Baricault L, Gas N, Guillou E, Valette A, Belenguer P, et al. Loss of OPA1 Perturbates the Mitochondrial Inner Membrane Structure and Integrity, Leading to Cytochrome c Release and Apoptosis*. *J Biol Chem*. 2003;278:7743–6.
209. Singel KL, Grzankowski KS, Khan ANMNH, Grimm MJ, D’Auria AC, Morrell K, et al. Mitochondrial DNA in the tumour microenvironment activates neutrophils and is associated with worse outcomes in patients with advanced epithelial ovarian cancer. *Br J Cancer*. 2019;120:207–17.
210. Xu MM, Pu Y, Han D, Shi Y, Cao X, Liang H, et al. Dendritic cells but not macrophages sense tumor mitochondrial DNA for cross-priming through signal regulatory protein α signaling. *Immunity*. 2017;47:363-373.e5.
211. Vringer E, Tait SWG. Mitochondria and cell death-associated inflammation. *Cell Death Differ*. Nature Publishing Group; 2022;1–9.
212. Lüthi AU, Cullen SP, McNeela EA, Duriez PJ, Afonina IS, Sheridan C, et al. Suppression of interleukin-33 bioactivity through proteolysis by apoptotic caspases. *Immunity*. 2009;31:84–98.
213. Ning X, Wang Y, Jing M, Sha M, Lv M, Gao P, et al. Apoptotic Caspases Suppress Type I Interferon Production via the Cleavage of cGAS, MAVS, and IRF3. *Mol Cell*. 2019;74:19-31.e7.
214. Frelin C, Imbert V, Bottero V, Gonthier N, Samraj AK, Schulze-Osthoff K, et al. Inhibition of the NF- κ B survival pathway via caspase-dependent cleavage of the IKK complex scaffold protein and NF- κ B essential modulator NEMO. *Cell Death Differ*. Nature Publishing Group; 2008;15:152–60.
215. Tang G, Yang J, Minemoto Y, Lin A. Blocking caspase-3-mediated proteolysis of IKKbeta suppresses TNF-alpha-induced apoptosis. *Mol Cell*. 2001;8:1005–16.
216. Clemens MJ, Bushell M, Jeffrey IW, Pain VM, Morley SJ. Translation initiation factor modifications and the regulation of protein synthesis in apoptotic cells. *Cell Death Differ*. Nature Publishing Group; 2000;7:603–15.
217. Corrado M, Samardžić D, Giacomello M, Rana N, Pearce EL, Scorrano L. Deletion of the mitochondria-shaping protein Opa1 during early thymocyte maturation impacts mature memory T cell metabolism. *Cell Death Differ*. Nature Publishing Group; 2021;28:2194–206.
218. Sainero-Alcolado L, Liaño-Pons J, Ruiz-Pérez MV, Arsenian-Henriksson M. Targeting mitochondrial metabolism for precision medicine in cancer. *Cell Death Differ*. Nature Publishing Group; 2022;29:1304–17.

219. Fulda S, Galluzzi L, Kroemer G. Targeting mitochondria for cancer therapy. *Nat Rev Drug Discov.* Nature Publishing Group; 2010;9:447–64.

